Nonlinear Systems and Complexity
Series Editor: Albert C. J. Luo

Dimitri Volchenkov
Xavier Leoncini *Editors*

Regularity and Stochasticity of Nonlinear Dynamical Systems

Springer

Nonlinear Systems and Complexity

Volume 21

Series editor

Albert C.J. Luo
Southern Illinois University
Edwardsville, IL, USA

Nonlinear Systems and Complexity provides a place to systematically summarize recent developments, applications, and overall advance in all aspects of nonlinearity, chaos, and complexity as part of the established research literature, beyond the novel and recent findings published in primary journals. The aims of the book series are to publish theories and techniques in nonlinear systems and complexity; stimulate more research interest on nonlinearity, synchronization, and complexity in nonlinear science; and fast-scatter the new knowledge to scientists, engineers, and students in the corresponding fields. Books in this series will focus on the recent developments, findings and progress on theories, principles, methodology, computational techniques in nonlinear systems and mathematics with engineering applications. The Series establishes highly relevant monographs on wide ranging topics covering fundamental advances and new applications in the field. Topical areas include, but are not limited to: Nonlinear dynamics Complexity, nonlinearity, and chaos Computational methods for nonlinear systems Stability, bifurcation, chaos and fractals in engineering Nonlinear chemical and biological phenomena Fractional dynamics and applications Discontinuity, synchronization and control.

More information about this series at http://www.springer.com/series/11433

Dimitri Volchenkov · Xavier Leoncini
Editors

Regularity and Stochasticity of Nonlinear Dynamical Systems

Springer

Editors
Dimitri Volchenkov
Department of Mathematics and Statistics
Texas Tech University
Lubbock, TX
USA

Xavier Leoncini
Centre de Physique Théorique
Aix-Marseille Université
Marseille
France

ISSN 2195-9994 ISSN 2196-0003 (electronic)
Nonlinear Systems and Complexity
ISBN 978-3-319-58061-6 ISBN 978-3-319-58062-3 (eBook)
DOI 10.1007/978-3-319-58062-3

Library of Congress Control Number: 2017939318

Printed on acid-free paper

This Springer imprint is published by Springer Nature
The registered company is Springer International Publishing AG
The registered company address is: Gewerbestrasse 11, 6330 Cham, Switzerland

Our book is dedicated to the 70th Anniversary of Prof. Afraimovich, whose soul and mind forever remain youthful

Preface

This book is based on the conference on *Lie groups and computation methods in nonlinear problems of mathematical modeling,* Shenyang, Liaoning, China, July 27–August 5, 2015. This conference provided a place to exchange recent developments, discoveries, and progress on lie groups and computation methods in nonlinear problems of mathematical modeling. The aims of the conference were to present the fundamental and frontier theories and techniques for modern science and technology; to stimulate more research interest for exploration of nonlinear physical science and mathematical modeling; to directly pass the new knowledge to the young generation of engineers, including the developments, findings and progress on fundamental theories and principles, analytical and symbolic approaches, and computational techniques in nonlinear physical science and nonlinear mathematics.

Through this conference, a celebration of Prof. Valentin Afraimovich's 70th birthday was held. Special invited papers were extended to the book chapters. This book provides recent theoretical developments and new techniques to solve nonlinear dynamical systems, and hopes to help one understand complexity, stochasticity, and regularity in nonlinear dynamical systems. This book covers integro-differential equation solvability, Poincare recurrences in ergodic systems, orientable horseshoe structure, analytical routes of periodic motions to chaos, grazing on impulsive differential equations, from chaos to order in coupled oscillator and differential-invariant solutions for automorphic systems, and inequality under uncertainty. All the materials are placed into 12 book chapters. All the materials dedicated to Prof. Valentin Afraimovich are for his achievements and accomplishments on nonlinear dynamics and complexity. We hope the community of nonlinear dynamics will benefit from this edited book.

We would also like to express our gratitude to Shenyang Aerospace University which took care of all of the necessary arrangements for the conference and special events in China.

Lubbock, TX, USA — Dimitri Volchenkov
Marseille, France — Xavier Leoncini

Contents

Chapter 1
Solvability of Some Integro-Differential Equations with Anomalous Diffusion

Vitali Vougalter and Vitaly Volpert

1.1 Introduction

The present article deals with the existence of stationary solutions of the following nonlocal reaction-diffusion equation

$$\frac{\partial u}{\partial t} = -D\Big(-\frac{\partial^2}{\partial x^2}\Big)^s u + \int_{-\infty}^{\infty} K(x-y)g(u(y,t))dy + f(x), \quad 0 < s < \frac{1}{4}, \tag{1.1}$$

which appears in cell population dynamics. The space variable x here corresponds to the cell genotype and $u(x,t)$ stands for the cell density as a function of their genotype and time. The right side of this equation describes the evolution of cell density via cell proliferation, mutations, and cell influx. The anomalous diffusion term here corresponds to the change of genotype due to small random mutations, and the nonlocal term describes large mutations. Function $g(u)$ designates the rate of cell birth which depends on u (density-dependent proliferation), and the kernel $K(x-y)$ gives the proportion of newly born cells changing their genotype from y to x. We assume that it depends on the distance between the genotypes. Finally, the last term in the right side of this equation stands for the influx of cells for different genotypes.

V. Vougalter (✉)
Department of Mathematics, University of Toronto, Toronto, ON M5S 2E4, Canada
e-mail: vitali@math.toronto.edu

V. Volpert
Institute Camille Jordan, UMR 5208 CNRS, University Lyon 1, 69622 Villeurbanne, France
e-mail: volpert@math.univ-lyon1.fr

D. Volchenkov and X. Leoncini (eds.), *Regularity and Stochasticity of Nonlinear Dynamical Systems*, Nonlinear Systems and Complexity 21,
DOI 10.1007/978-3-319-58062-3_1

The operator $\left(-\frac{\partial^2}{\partial x^2}\right)^s$ in problem (1.1) describes a particular case of anomalous diffusion actively treated in the context of different applications in plasma physics and turbulence [7, 16], surface diffusion [12, 14], semiconductors, [15] and so on. Anomalous diffusion can be described as a random process of particle motion characterized by the probability density distribution of jump length. The moments of this density distribution are finite in the case of normal diffusion, but this is not the case for superdiffusion. Asymptotic behavior at infinity of the probability density function determines the value s of the power of the Laplacian [13]. The operator $\left(-\frac{\partial^2}{\partial x^2}\right)^s$ is defined by virtue of the spectral calculus. In our work, we will treat the case of $0 < s < 1/4$. A similar equation in the case of the standard Laplacian in the diffusion term was investigated recently in [26].

We set $D = 1$ and prove the existence of solutions of the equation

$$-\left(-\frac{d^2}{dx^2}\right)^s u + \int_{-\infty}^{\infty} K(x-y)g(u(y))dy + f(x) = 0, \quad 0 < s < \frac{1}{4}. \tag{1.2}$$

We will consider the case where the linear part of this operator does not satisfy the Fredholm property. Consequently, conventional methods of nonlinear analysis may not be applicable. We use solvability conditions for non-Fredholm operators along with the method of contraction mappings.

Consider the problem

$$-\Delta u + V(x)u - au = f, \tag{1.3}$$

where $u \in E = H^2(\mathbb{R}^d)$ and $f \in F = L^2(\mathbb{R}^d)$, $d \in \mathbb{N}$, a is a constant and the scalar potential function $V(x)$ is either zero identically or converges to 0 at infinity. For $a \geq 0$, the essential spectrum of the operator $A : E \to F$ corresponding to the left side of Eq. (1.3) contains the origin. Consequently, such operator does not satisfy the Fredholm property. Its image is not closed, for $d > 1$ the dimension of its kernel and the codimension of its image are not finite. The present article deals with the studies of certain properties of the operators of this kind. Note that elliptic equations with non-Fredholm operators were treated actively in recent years. Approaches in weighted Sobolev and Hölder spaces were developed in [1, 3–6]. The non-Fredholm Schrödinger-type operators were studied with the methods of the spectral and the scattering theory in [17, 20, 21]. The Laplace operator with drift from the point of view of non-Fredholm operators was treated in [23] and linearized Cahn–Hilliard equations in [19, 24]. Nonlinear non-Fredholm elliptic problems were studied in [22, 25]. Important applications to the theory of reaction-diffusion equations were developed in [9, 10]. Non-Fredholm operators arise also when studying wave systems with an infinite number of localized traveling waves (see [2]). In particular, when $a = 0$, the operator A is Fredholm in some properly chosen weighted spaces (see [1, 3–6]). However, the case of $a \neq 0$ is significantly different and the method developed in

these works cannot be applied. Front propagation equations with anomalous diffusion were treated actively in recent years (see, e.g., [27, 28]).

Let us set $K(x) = \varepsilon \mathcal{K}(x)$ with $\varepsilon \geq 0$ and suppose that the assumption below is satisfied.

Assumption 1.1 Consider $0 < s < \frac{1}{4}$. Let $f(x) : \mathbb{R} \to \mathbb{R}$ be nontrivial, such that $f(x) \in L^1(\mathbb{R}) \cap L^2(\mathbb{R})$ and $\left(-\frac{d^2}{dx^2} \right)^{\frac{1}{2}-s} f(x) \in L^2(\mathbb{R})$. Assume also that $\mathcal{K}(x) : \mathbb{R} \to \mathbb{R}$ and $\mathcal{K}(x) \in L^1(\mathbb{R})$. In addition, $\left(-\frac{d^2}{dx^2} \right)^{\frac{1}{2}-s} \mathcal{K}(x) \in L^2(\mathbb{R})$, such that

$$Q := \left\| \left(-\frac{d^2}{dx^2} \right)^{\frac{1}{2}-s} \mathcal{K}(x) \right\|_{L^2(\mathbb{R})} > 0.$$

We choose the space dimension $d = 1$, which is related to the solvability conditions for the linear Poisson-type problem (1.31) proved in Lemma 1.6. From the perspective of applications, the space dimension is not restricted to $d = 1$ because the space variable corresponds to cell genotype but not to the usual physical space. Let us use the Sobolev spaces

$$H^{2s}(\mathbb{R}) := \left\{ u(x) : \mathbb{R} \to \mathbb{R} \mid u(x) \in L^2(\mathbb{R}),\ \left(-\frac{d^2}{dx^2} \right)^s u \in L^2(\mathbb{R}) \right\},\quad 0 < s \leq 1$$

equipped with the norm

$$\|u\|^2_{H^{2s}(\mathbb{R})} := \|u\|^2_{L^2(\mathbb{R})} + \left\| \left(-\frac{d^2}{dx^2} \right)^s u \right\|^2_{L^2(\mathbb{R})}. \tag{1.4}$$

By virtue of the standard Sobolev inequality in one dimension (see, e.g., Sect. 8.5 of [11]), we have

$$\|u\|_{L^\infty(\mathbb{R})} \leq \frac{1}{\sqrt{2}} \|u\|_{H^1(\mathbb{R})}. \tag{1.5}$$

When the nonnegative parameter ε vanishes, we arrive at the linear Poisson-type equation (1.31). By means of Lemma 1.6 below along with Assumption 1.1, problem (1.31) admits a unique solution

$$u_0(x) \in H^{2s}(\mathbb{R}),\quad 0 < s < \frac{1}{4},$$

such that no orthogonality relations are required. By virtue of Lemma 1.6, when $\frac{1}{4} \leq s < 1$, certain orthogonality conditions (1.33) and (1.34) are required to be able to solve Eq. (1.31) in $H^{2s}(\mathbb{R})$. By virtue of Assumption 1.1, since

$$\left(-\frac{d^2}{dx^2}\right)^{\frac{1}{2}} u(x) = \left(-\frac{d^2}{dx^2}\right)^{\frac{1}{2}-s} f(x) \in L^2(\mathbb{R}),$$

we have for the unique solution of linear problem (1.31) that $u_0(x) \in H^1(\mathbb{R})$. Let us seek the resulting solution of nonlinear equation (1.2) as

$$u(x) = u_0(x) + u_p(x). \tag{1.6}$$

Evidently, we obtain the perturbative equation

$$\left(-\frac{d^2}{dx^2}\right)^s u_p = \varepsilon \int_{-\infty}^{\infty} \mathcal{K}(x-y) g(u_0(y) + u_p(y)) dy, \quad 0 < s < \frac{1}{4}. \tag{1.7}$$

Let us introduce a closed ball in the Sobolev space

$$B_\rho := \{u(x) \in H^1(\mathbb{R}) \mid \|u\|_{H^1(\mathbb{R})} \leq \rho\}, \quad 0 < \rho \leq 1. \tag{1.8}$$

We look for the solution of problem (1.7) as the fixed point of the auxiliary nonlinear equation

$$\left(-\frac{d^2}{dx^2}\right)^s u = \varepsilon \int_{-\infty}^{\infty} \mathcal{K}(x-y) g(u_0(y) + v(y)) dy, \quad 0 < s < \frac{1}{4} \tag{1.9}$$

in ball (1.8). For a given function $v(y)$, this is an equation with respect to $u(x)$. The left side of (1.9) involves the non-Fredholm operator

$$\left(-\frac{d^2}{dx^2}\right)^s : H^{2s}(\mathbb{R}) \to L^2(\mathbb{R}).$$

Its essential spectrum fills the nonnegative semi-axis $[0, +\infty)$. Therefore, such operator has no bounded inverse. The similar situation appeared in works [22, 25], but as distinct from the present situation, the equations studied there required orthogonality conditions. The fixed point technique was used in [18] to estimate the perturbation to the standing solitary wave of the Nonlinear Schrödinger (NLS) equation when either the external potential or the nonlinear term in the NLS was perturbed but the Schrödinger operator involved in the nonlinear equation there had the Fredholm property (see Assumption 1.1 of [18], also [8]). Let us define the interval on the real line

$$I := \left[-\frac{1}{\sqrt{2}}\|u_0\|_{H^1(\mathbb{R})} - \frac{1}{\sqrt{2}}, \ \frac{1}{\sqrt{2}}\|u_0\|_{H^1(\mathbb{R})} + \frac{1}{\sqrt{2}}\right] \tag{1.10}$$

along with the closed ball in the space of $C_2(I)$ functions, namely

$$D_M := \{g(s) \in C_2(I) \mid \|g\|_{C_2(I)} \leq M\}, \quad M > 0. \tag{1.11}$$

Here, the norm

$$\|g\|_{C_2(I)} := \|g\|_{C(I)} + \|g'\|_{C(I)} + \|g''\|_{C(I)}, \tag{1.12}$$

where $\|g\|_{C(I)} := max_{s\in I}|g(s)|$. We make the following assumption on the nonlinear part of equation (1.2).

Assumption 1.2 Let $g(z) : \mathbb{R} \to \mathbb{R}$, such that $g(0) = 0$ and $g'(0) = 0$. It is also assumed that $g(z) \in D_M$ and it does not vanish identically on the interval I.

Let us explain why we impose condition $g'(0) = 0$. If $g'(0) < 0$, then the essential spectrum of the corresponding operator is in the left half plane. The operator satisfies the Fredholm property, and conventional methods of nonlinear analysis are applicable here. If $g'(0) \geq 0$, then the operator does not satisfy the Fredholm property, and the goal of this work is to prove the existence of solutions in this case where usual methods are not applicable. The method developed in this paper can be used for $g'(0) = 0$ but not for $g'(0) > 0$. Therefore, we impose this condition on the nonlinearity.

We introduce the operator T_g, such that $u = T_g v$, where u is a solution of Eq. (1.9). Our first main statement is as follows.

Theorem 1.3 *Let Assumptions 1.1 and 1.2 hold. Then, Eq. (1.9) defines the map $T_g : B_\rho \to B_\rho$, which is a strict contraction for all $0 < \varepsilon < \varepsilon*$ for some $\varepsilon* > 0$. The unique fixed point $u_p(x)$ of this map T_g is the only solution of problem (1.7) in B_ρ.*

Clearly, the resulting solution of Eq. (1.2) given by (1.6) will be nontrivial because the source term $f(x)$ is nontrivial and $g(0) = 0$ due to our assumptions. We make use of the following elementary lemma.

Lemma 1.4 *For $R \in (0, +\infty)$, consider the function*

$$\varphi(R) := \alpha R^{1-4s} + \frac{\beta}{R^{4s}}, \quad 0 < s < \frac{1}{4}, \quad \alpha, \beta > 0.$$

It attains the minimal value at $R^* := \dfrac{4\beta s}{\alpha(1-4s)}$, which is given by

$$\varphi(R^*) = \frac{(1-4s)^{4s-1}}{(4s)^{4s}} \alpha^{4s} \beta^{1-4s}.$$

Our second main result is about the continuity of the fixed point of the map T_g in which existence was established in Theorem 1.3 above with respect to the nonlinear function g.

Theorem 1.5 *Let $j = 1, 2$, the assumptions of Theorem 1.3 hold, such that $u_{p,j}(x)$ is the unique fixed point of the map $T_{g_j} : B_\rho \to B_\rho$, which is a strict contraction for all $0 < \varepsilon < \varepsilon_j^*$ and $\delta := min(\varepsilon_1^*, \varepsilon_2^*)$. Then, for all $0 < \varepsilon < \delta$, the inequality*

$$\|u_{p,1} - u_{p,2}\|_{H^1(\mathbb{R})} \leq C\|g_1 - g_2\|_{C_2(I)} \tag{1.13}$$

holds, where $C > 0$ is a constant.

We proceed to the proof of our first main result.

1.2 The Existence of the Perturbed Solution

Proof of Theorem 3. Let us choose arbitrarily $v(x) \in B_\rho$ and denote the term involved in the integral expression in the right side of problem (1.9) as

$$G(x) := g(u_0(x) + v(x)).$$

Let us use the standard Fourier transform

$$\widehat{\phi}(p) := \frac{1}{\sqrt{2\pi}} \int_{-\infty}^{\infty} \phi(x) e^{-ipx} dx. \tag{1.14}$$

Evidently, we have the inequality

$$\|\widehat{\phi}(p)\|_{L^\infty(\mathbb{R})} \leq \frac{1}{\sqrt{2\pi}} \|\phi(x)\|_{L^1(\mathbb{R})}. \tag{1.15}$$

We apply (1.14) to both sides of problem (1.9) and arrive at

$$\widehat{u}(p) = \varepsilon\sqrt{2\pi} \frac{\widehat{\mathcal{K}}(p)\widehat{G}(p)}{|p|^{2s}}.$$

Hence, for the norm, we obtain

$$\|u\|^2_{L^2(\mathbb{R})} = 2\pi\varepsilon^2 \int_{-\infty}^{\infty} \frac{|\widehat{\mathcal{K}}(p)|^2 |\widehat{G}(p)|^2}{|p|^{4s}} dp. \tag{1.16}$$

As distinct from works [22, 25] including the standard Laplace operator in the diffusion term, here, we do not try to control the norm

$$\left\| \frac{\widehat{\mathcal{K}}(p)}{|p|^{2s}} \right\|_{L^\infty(\mathbb{R})}.$$

Instead, let us estimate the right side of (1.16) using the analog of inequality (1.15) applied to functions $\mathcal{K}$ and G with $R > 0$ as

$$2\pi\varepsilon^2 \int_{|p|\le R} \frac{|\widehat{\mathcal{K}}(p)|^2 |\widehat{G}(p)|^2}{|p|^{4s}} dp + 2\pi\varepsilon^2 \int_{|p|>R} \frac{|\widehat{\mathcal{K}}(p)|^2 |\widehat{G}(p)|^2}{|p|^{4s}} dp \le$$

$$\le \varepsilon^2 \|\mathcal{K}\|^2_{L^1(\mathbb{R})} \left\{ \frac{1}{\pi} \|G(x)\|^2_{L^1(\mathbb{R})} \frac{R^{1-4s}}{1-4s} + \frac{1}{R^{4s}} \|G(x)\|^2_{L^2(\mathbb{R})} \right\}. \tag{1.17}$$

Since $v(x) \in B_\rho$, we have

$$\|u_0 + v\|_{L^2(\mathbb{R})} \le \|u_0\|_{H^1(\mathbb{R})} + 1.$$

Sobolev inequality (1.5) yields

$$|u_0 + v| \le \frac{1}{\sqrt{2}} (\|u_0\|_{H^1(\mathbb{R})} + 1).$$

Formula $G(x) = \int_0^{u_0+v} g'(z)dz$ with the interval I defined in (1.10) implies

$$|G(x)| \le sup_{z\in I} |g'(z)| |u_0 + v| \le M|u_0 + v|.$$

Thus,

$$\|G(x)\|_{L^2(\mathbb{R})} \le M\|u_0 + v\|_{L^2(\mathbb{R})} \le M(\|u_0\|_{H^1(\mathbb{R})} + 1).$$

Obviously, $G(x) = \int_0^{u_0+v} dy \Big[\int_0^y g''(z)dz \Big]$. This gives us

$$|G(x)| \le \frac{1}{2} sup_{z\in I} |g''(z)| |u_0 + v|^2 \le \frac{M}{2} |u_0 + v|^2,$$

$$\|G(x)\|_{L^1(\mathbb{R})} \le \frac{M}{2} \|u_0 + v\|^2_{L^2(\mathbb{R})} \le \frac{M}{2} (\|u_0\|_{H^1(\mathbb{R})} + 1)^2. \tag{1.18}$$

Thus, we obtain the estimate from above for the right side of (1.17) as

$$\varepsilon^2 \|\mathcal{K}\|^2_{L^1(\mathbb{R})} M^2 (\|u_0\|_{H^1(\mathbb{R})} + 1)^2 \left\{ \frac{(\|u_0\|_{H^1(\mathbb{R})} + 1)^2 R^{1-4s}}{4\pi(1-4s)} + \frac{1}{R^{4s}} \right\},$$

where $R \in (0, +\infty)$. By means of Lemma 1.4, we obtain the minimal value of the expression above. Thus,

$$\|u\|^2_{L^2(\mathbb{R})} \le \varepsilon^2 \|\mathcal{K}\|^2_{L^1(\mathbb{R})} (\|u_0\|_{H^1(\mathbb{R})} + 1)^{2+8s} \frac{M^2}{(1-4s)(16\pi s)^{4s}}. \tag{1.19}$$

Obviously, via (1.9), we have

$$\left(-\frac{d^2}{dx^2}\right)^{\frac{1}{2}} u(x) = \varepsilon \left(-\frac{d^2}{dx^2}\right)^{\frac{1}{2}-s} \int_{-\infty}^{\infty} \mathcal{K}(x-y) G(y) dy.$$

By virtue of the analog of inequality (1.15) applied to function G along with (1.18), we arrive at

$$\left\| \frac{du}{dx} \right\|^2_{L^2(\mathbb{R})} \le \varepsilon^2 \|G\|^2_{L^1(\mathbb{R})} Q^2 \le \varepsilon^2 \frac{M^2}{4} (\|u_0\|_{H^1(\mathbb{R})} + 1)^4 Q^2. \tag{1.20}$$

Hence, by means of the definition of the norm (1.4) with $s = \frac{1}{2}$ along with inequalities (1.19) and (1.20), we obtain the estimate from above for $\|u\|_{H^1(\mathbb{R})}$ as

$$\varepsilon (\|u_0\|_{H^1(\mathbb{R})} + 1)^2 M \left[\frac{\|\mathcal{K}\|^2_{L^1(\mathbb{R})} (\|u_0\|_{H^1(\mathbb{R})} + 1)^{8s-2}}{(1-4s)(16\pi s)^{4s}} + \frac{Q^2}{4} \right]^{\frac{1}{2}} \le \rho$$

for all $\varepsilon > 0$ small enough. Thus, $u(x) \in B_\rho$ as well. If for some $v(x) \in B_\rho$, there exist two solutions $u_{1,2}(x) \in B_\rho$ of problem (1.9), and their difference $w(x) := u_1(x) - u_2(x) \in L^2(\mathbb{R})$ satisfies

$$\left(-\frac{d^2}{dx^2}\right)^s w = 0.$$

Since the operator $\left(-\frac{d^2}{dx^2}\right)^s$ considered on the whole real line does not have nontrivial square-integrable zero modes, $w(x)$ vanishes a.e. on $\mathbb{R}$. Therefore, problem (1.9) defines a map $T_g : B_\rho \to B_\rho$ for all $\varepsilon > 0$ sufficiently small.

Our goal is to prove that this map is a strict contraction. We choose arbitrarily $v_{1,2}(x) \in B_\rho$. The argument above yields $u_{1,2} := T_g v_{1,2} \in B_\rho$ as well. By virtue of (1.9), we have

$$\left(-\frac{d^2}{dx^2}\right)^s u_1 = \varepsilon \int_{-\infty}^{\infty} \mathcal{K}(x-y) g(u_0(y) + v_1(y)) dy, \tag{1.21}$$

$$\left(-\frac{d^2}{dx^2}\right)^s u_2 = \varepsilon \int_{-\infty}^{\infty} \mathcal{K}(x-y) g(u_0(y) + v_2(y)) dy, \tag{1.22}$$

$0 < s < \frac{1}{4}$. Let us introduce

$$G_1(x) := g(u_0(x) + v_1(x)), \quad G_2(x) := g(u_0(x) + v_2(x))$$

and apply the standard Fourier transform (1.14) to both sides of problems (1.21) and (1.22). We arrive at

$$\widehat{u_1}(p) = \varepsilon\sqrt{2\pi}\frac{\widehat{\mathcal{K}}(p)\widehat{G_1}(p)}{|p|^{2s}}, \quad \widehat{u_2}(p) = \varepsilon\sqrt{2\pi}\frac{\widehat{\mathcal{K}}(p)\widehat{G_2}(p)}{|p|^{2s}}.$$

Evidently,

$$\|u_1 - u_2\|^2_{L^2(\mathbb{R})} = \varepsilon^2 2\pi \int_{-\infty}^{\infty} \frac{|\widehat{\mathcal{K}}(p)|^2|\widehat{G_1}(p) - \widehat{G_2}(p)|^2}{|p|^{4s}}dp.$$

Apparently, it can be bounded from above by means of inequality (1.15) by

$$\varepsilon^2\|\mathcal{K}\|^2_{L^1(\mathbb{R})}\left\{\frac{1}{\pi}\|G_1(x) - G_2(x)\|^2_{L^1(\mathbb{R})}\frac{R^{1-4s}}{1-4s} + \|G_1(x) - G_2(x)\|^2_{L^2(\mathbb{R})}\frac{1}{R^{4s}}\right\},$$

with $R \in (0, +\infty)$. Let us use the formula

$$G_1(x) - G_2(x) = \int_{u_0+v_2}^{u_0+v_1} g'(z)dz.$$

Thus,

$$|G_1(x) - G_2(x)| \le sup_{z\in I}|g'(z)||v_1 - v_2| \le M|v_1 - v_2|.$$

Therefore,

$$\|G_1(x) - G_2(x)\|_{L^2(\mathbb{R})} \le M\|v_1 - v_2\|_{L^2(\mathbb{R})} \le M\|v_1 - v_2\|_{H^1(\mathbb{R})}.$$

Obviously,

$$G_1(x) - G_2(x) = \int_{u_0+v_2}^{u_0+v_1} dy\Big[\int_0^y g''(z)dz\Big].$$

We derive the upper bound for $G_1(x) - G_2(x)$ in the absolute value as

$$\frac{1}{2}sup_{z\in I}|g''(z)||(v_1 - v_2)(2u_0 + v_1 + v_2)| \le \frac{M}{2}|(v_1 - v_2)(2u_0 + v_1 + v_2)|.$$

The Schwarz inequality implies the estimate from above for the norm $\|G_1(x) - G_2(x)\|_{L^1(\mathbb{R})}$ as

$$\frac{M}{2}\|v_1 - v_2\|_{L^2(\mathbb{R})}\|2u_0 + v_1 + v_2\|_{L^2(\mathbb{R})} \leq M\|v_1 - v_2\|_{H^1(\mathbb{R})}(\|u_0\|_{H^1(\mathbb{R})} + 1). \tag{1.23}$$

Hence, we obtain the upper bound for the norm $\|u_1(x) - u_2(x)\|^2_{L^2(\mathbb{R})}$ given by

$$\varepsilon^2\|\mathcal{K}\|^2_{L^1(\mathbb{R})}M^2\|v_1 - v_2\|^2_{H^1(\mathbb{R})}\left\{\frac{1}{\pi}(\|u_0\|_{H^1(\mathbb{R})} + 1)^2\frac{R^{1-4s}}{1-4s} + \frac{1}{R^{4s}}\right\}.$$

Lemma 1.4 enables us to minimize the expression above over $R \in (0, +\infty)$ to derive the estimate from above for $\|u_1(x) - u_2(x)\|^2_{L^2(\mathbb{R})}$ as

$$\varepsilon^2\|\mathcal{K}\|^2_{L^1(\mathbb{R})}M^2\|v_1 - v_2\|^2_{H^1(\mathbb{R})}\frac{(\|u_0\|_{H^1(\mathbb{R})} + 1)^{8s}}{(1-4s)(4\pi s)^{4s}}. \tag{1.24}$$

Formulas (1.21) and (1.22) yield

$$\left(-\frac{d^2}{dx^2}\right)^{\frac{1}{2}}(u_1 - u_2) = \varepsilon\left(-\frac{d^2}{dx^2}\right)^{\frac{1}{2}-s}\int_{-\infty}^{\infty}\mathcal{K}(x-y)[G_1(y) - G_2(y)]dy.$$

Inequalities (1.15) and (1.23) imply

$$\left\|\frac{d}{dx}(u_1 - u_2)\right\|^2_{L^2(\mathbb{R})} \leq \varepsilon^2 Q^2\|G_1 - G_2\|^2_{L^1(\mathbb{R})} \leq$$

$$\leq \varepsilon^2 Q^2 M^2\|v_1 - v_2\|^2_{H^1(\mathbb{R})}(\|u_0\|_{H^1(\mathbb{R})} + 1)^2. \tag{1.25}$$

By means of (1.24) and (1.25), the norm $\|u_1 - u_2\|_{H^1(\mathbb{R})}$ can be bounded from above by the expression

$$\varepsilon M(\|u_0\|_{H^1(\mathbb{R})} + 1)\left\{\frac{\|\mathcal{K}\|^2_{L^1(\mathbb{R})}(\|u_0\|_{H^1(\mathbb{R})} + 1)^{8s-2}}{(1-4s)(4\pi s)^{4s}} + Q^2\right\}^{\frac{1}{2}}\|v_1 - v_2\|_{H^1(\mathbb{R})}. \tag{1.26}$$

This implies that our map $T_g : B_\rho \to B_\rho$ defined by problem (1.9) is a strict contraction for all values of $\varepsilon > 0$ sufficiently small. Its unique fixed point $u_p(x)$ is the only solution of Eq. (1.7) in the ball B_ρ. The resulting $u(x) \in H^1(\mathbb{R})$ given by (1.6) is a solution of problem (1.2).

Then, we turn our attention to the proof of the second main result of our work.

1.3 The Continuity of the Fixed Point of the Map T_g

Proof of Theorem 5. Clearly, for all $0 < \varepsilon < \delta$, we have

$$u_{p,1} = T_{g_1} u_{p,1}, \quad u_{p,2} = T_{g_2} u_{p,2},$$

such that

$$u_{p,1} - u_{p,2} = T_{g_1} u_{p,1} - T_{g_1} u_{p,2} + T_{g_1} u_{p,2} - T_{g_2} u_{p,2}.$$

Hence,

$$\|u_{p,1} - u_{p,2}\|_{H^1(\mathbb{R})} \le \|T_{g_1} u_{p,1} - T_{g_1} u_{p,2}\|_{H^1(\mathbb{R})} + \|T_{g_1} u_{p,2} - T_{g_2} u_{p,2}\|_{H^1(\mathbb{R})}.$$

By virtue of estimate (1.26), we have

$$\|T_{g_1} u_{p,1} - T_{g_1} u_{p,2}\|_{H^1(\mathbb{R})} \le \varepsilon\sigma \|u_{p,1} - u_{p,2}\|_{H^1(\mathbb{R})},$$

where $\varepsilon\sigma < 1$ due to the fact that the map $T_{g_1} : B_\rho \to B_\rho$ under our assumptions is a strict contraction. Here, the positive constant

$$\sigma := M(\|u_0\|_{H^1(\mathbb{R})} + 1)\left\{ \frac{\|\mathcal{K}\|^2_{L^1(\mathbb{R})}(\|u_0\|_{H^1(\mathbb{R})} + 1)^{8s-2}}{(1-4s)(4\pi s)^{4s}} + Q^2 \right\}^{\frac{1}{2}}.$$

Thus, we arrive at

$$(1 - \varepsilon\sigma)\|u_{p,1} - u_{p,2}\|_{H^1(\mathbb{R})} \le \|T_{g_1} u_{p,2} - T_{g_2} u_{p,2}\|_{H^1(\mathbb{R})}. \tag{1.27}$$

Note that for our fixed point $T_{g_2} u_{p,2} = u_{p,2}$ and denote $\xi(x) := T_{g_1} u_{p,2}$. We obtain

$$\left(-\frac{d^2}{dx^2} \right)^s \xi(x) = \varepsilon \int_{-\infty}^{\infty} \mathcal{K}(x-y) g_1(u_0(y) + u_{p,2}(y)) dy, \tag{1.28}$$

$$\left(-\frac{d^2}{dx^2} \right)^s u_{p,2}(x) = \varepsilon \int_{-\infty}^{\infty} \mathcal{K}(x-y) g_2(u_0(y) + u_{p,2}(y)) dy, \tag{1.29}$$

with $0 < s < \frac{1}{4}$. Let $G_{1,2}(x) := g_1(u_0(x) + u_{p,2}(x))$ and $G_{2,2}(x) := g_2(u_0(x) + u_{p,2}(x))$. By applying the standard Fourier transform (1.14) to both sides of Eqs. (1.28) and (1.29) above, we easily arrive at

$$\widehat{\xi}(p) = \varepsilon\sqrt{2\pi} \frac{\widehat{\mathcal{K}}(p)\widehat{G}_{1,2}(p)}{|p|^{2s}}, \quad \widehat{u}_{p,2}(p) = \varepsilon\sqrt{2\pi} \frac{\widehat{\mathcal{K}}(p)\widehat{G}_{2,2}(p)}{|p|^{2s}}.$$

Obviously,

$$\|\xi(x)-u_{p,2}(x)\|^2_{L^2(\mathbb{R})}=\varepsilon^2 2\pi\int_{-\infty}^{\infty}\frac{|\widehat{\mathcal{K}}(p)|^2|\widehat{G}_{1,2}(p)-\widehat{G}_{2,2}(p)|^2}{|p|^{4s}}dp.$$

Evidently, it can be estimated from above by virtue of (1.15) by

$$\varepsilon^2\|\mathcal{K}\|^2_{L^1(\mathbb{R})}\left\{\frac{1}{\pi}\|G_{1,2}-G_{2,2}\|^2_{L^1(\mathbb{R})}\frac{R^{1-4s}}{1-4s}+\|G_{1,2}-G_{2,2}\|^2_{L^2(\mathbb{R})}\frac{1}{R^{4s}}\right\},$$

where $R\in(0,+\infty)$. Let us use the formula

$$G_{1,2}(x)-G_{2,2}(x)=\int_0^{u_0(x)+u_{p,2}(x)}[g_1'(s)-g_2'(s)]ds.$$

Hence,

$$|G_{1,2}(x)-G_{2,2}(x)|\le sup_{s\in I}|g_1'(s)-g_2'(s)||u_0(x)+u_{p,2}(x)|\le$$

$$\le\|g_1-g_2\|_{C_2(I)}|u_0(x)+u_{p,2}(x)|,$$

such that

$$\|G_{1,2}-G_{2,2}\|_{L^2(\mathbb{R})}\le\|g_1-g_2\|_{C_2(I)}\|u_0+u_{p,2}\|_{L^2(\mathbb{R})}\le$$

$$\le\|g_1-g_2\|_{C_2(I)}(\|u_0\|_{H^1(\mathbb{R})}+1).$$

Another useful representation formula is

$$G_{1,2}(x)-G_{2,2}(x)=\int_0^{u_0(x)+u_{p,2}(x)}dy\Big[\int_0^y(g_1''(z)-g_2''(z))dz\Big].$$

Thus,

$$|G_{1,2}(x)-G_{2,2}(x)|\le\frac{1}{2}sup_{z\in I}|g_1''(z)-g_2''(z)||u_0(x)+u_{p,2}(x)|^2\le$$

$$\le\frac{1}{2}\|g_1-g_2\|_{C_2(I)}|u_0(x)+u_{p,2}(x)|^2.$$

Therefore,

$$\|G_{1,2}-G_{2,2}\|_{L^1(\mathbb{R})}\le\frac{1}{2}\|g_1-g_2\|_{C_2(I)}\|u_0+u_{p,2}\|^2_{L^2(\mathbb{R})}\le$$

$$\leq \frac{1}{2}\|g_1 - g_2\|_{C_2(I)}(\|u_0\|_{H^1(\mathbb{R})} + 1)^2. \tag{1.30}$$

This enables us to estimate the norm $\|\xi(x) - u_{p,2}(x)\|^2_{L^2(\mathbb{R})}$ from above by

$$\varepsilon^2\|\mathcal{K}\|^2_{L^1(\mathbb{R})}(\|u_0\|_{H^1(\mathbb{R})} + 1)^2\|g_1 - g_2\|^2_{C_2(I)}\left[\frac{1}{4\pi}(\|u_0\|_{H^1(\mathbb{R})} + 1)^2\frac{R^{1-4s}}{1-4s} + \frac{1}{R^{4s}}\right].$$

This expression can be easily minimized over $R \in (0, +\infty)$ by means of Lemma 1.4. We arrive at the inequality

$$\|\xi(x) - u_{p,2}(x)\|^2_{L^2(\mathbb{R})} \leq \varepsilon^2\|\mathcal{K}\|^2_{L^1(\mathbb{R})}(\|u_0\|_{H^1(\mathbb{R})} + 1)^{2+8s}\frac{\|g_1 - g_2\|^2_{C_2(I)}}{(1-4s)(16\pi s)^{4s}}.$$

By virtue of (1.28) and (1.29), we have

$$\left(-\frac{d^2}{dx^2}\right)^{\frac{1}{2}}\xi(x) = \varepsilon\left(-\frac{d^2}{dx^2}\right)^{\frac{1}{2}-s}\int_{-\infty}^{\infty}\mathcal{K}(x-y)G_{1,2}(y)dy,$$

$$\left(-\frac{d^2}{dx^2}\right)^{\frac{1}{2}}u_{p,2}(x) = \varepsilon\left(-\frac{d^2}{dx^2}\right)^{\frac{1}{2}-s}\int_{-\infty}^{\infty}\mathcal{K}(x-y)G_{2,2}(y)dy,$$

such that via (1.15) and (1.30), the norm $\|\xi'(x) - u'_{p,2}(x)\|^2_{L^2(\mathbb{R})}$ can be bounded above by

$$\varepsilon^2\|G_{1,2} - G_{2,2}\|^2_{L^1(\mathbb{R})}Q^2 \leq \frac{\varepsilon^2Q^2}{4}(\|u_0\|_{H^1(\mathbb{R})} + 1)^4\|g_1 - g_2\|^2_{C_2(I)}.$$

Therefore, $\|\xi(x) - u_{p,2}(x)\|_{H^1(\mathbb{R})} \leq$

$$\leq \varepsilon\|g_1 - g_2\|_{C_2(I)}(\|u_0\|_{H^1(\mathbb{R})} + 1)^2\left[\frac{\|\mathcal{K}\|^2_{L^1(\mathbb{R})}(\|u_0\|_{H^1(\mathbb{R})} + 1)^{8s-2}}{(1-4s)(16\pi s)^{4s}} + \frac{Q^2}{4}\right]^{\frac{1}{2}}.$$

By means of inequality (1.27), the norm $\|u_{p,1} - u_{p,2}\|_{H^1(\mathbb{R})}$ can be estimated from above by

$$\frac{\varepsilon}{1-\varepsilon\sigma}(\|u_0\|_{H^1(\mathbb{R})} + 1)^2\left[\frac{\|\mathcal{K}\|^2_{L^1(\mathbb{R})}(\|u_0\|_{H^1(\mathbb{R})} + 1)^{8s-2}}{(1-4s)(16\pi s)^{4s}} + \frac{Q^2}{4}\right]^{\frac{1}{2}}\|g_1 - g_2\|_{C_2(I)},$$

which completes the proof of the theorem.

1.4 Auxiliary Results

Below, we derive the solvability conditions for the linear Poisson-type equation with a square-integrable right side

$$\left(-\frac{d^2}{dx^2}\right)^s u = f(x), \quad x \in \mathbb{R}, \quad 0 < s < 1. \tag{1.31}$$

Let us denote the inner product as

$$(f(x), g(x))_{L^2(\mathbb{R})} := \int_{-\infty}^{\infty} f(x)\bar{g}(x)dx, \tag{1.32}$$

with a slight abuse of notations when the functions involved in (1.32) are not square integrable, like for instance the one present in orthogonality condition (1.33) of Lemma 1.6 below. Indeed, if $f(x) \in L^1(\mathbb{R})$ and $g(x) \in L^\infty(\mathbb{R})$, then the integral in the right side of (1.32) is well defined. The left side of relation (1.34) makes sense as well under the given conditions. We have the following technical statement.

Lemma 1.6 *Let $f(x) : \mathbb{R} \to \mathbb{R}$ and $f(x) \in L^2(\mathbb{R})$.*

(1) When $0 < s < \frac{1}{4}$ and in addition $f(x) \in L^1(\mathbb{R})$, Eq. (1.31) admits a unique solution $u(x) \in H^{2s}(\mathbb{R})$.

(2) When $\frac{1}{4} \le s < \frac{3}{4}$ and additionally $|x| f(x) \in L^1(\mathbb{R})$, problem (1.31) possesses a unique solution $u(x) \in H^{2s}(\mathbb{R})$ if and only if the orthogonality relation

$$(f(x), 1)_{L^2(\mathbb{R})} = 0 \tag{1.33}$$

holds.

(3) When $\frac{3}{4} \le s < 1$ and in addition $x^2 f(x) \in L^1(\mathbb{R})$, Eq. (1.31) has a unique solution $u(x) \in H^{2s}(\mathbb{R})$ if and only if orthogonality conditions (1.33) and

$$(f(x), x)_{L^2(\mathbb{R})} = 0 \tag{1.34}$$

hold.

Proof First, we observe that by means of norm definition (1.4) along with the square integrability of the right side of (1.31), it would be sufficient to prove the solvability of problem (1.31) in $L^2(\mathbb{R})$. The solution $u(x) \in L^2(\mathbb{R})$ will obviously belong to $H^{2s}(\mathbb{R})$, $0 < s < 1$ as well.

Let us establish the uniqueness of solutions for Eq. (1.31). If $u_{1,2}(x) \in H^{2s}(\mathbb{R})$ both satisfy (1.31), then the difference $w(x) := u_1(x) - u_2(x) \in L^2(\mathbb{R})$ solves the homogeneous problem

$$\left(-\frac{d^2}{dx^2}\right)^s w = 0.$$

Since the operator $\left(-\frac{d^2}{dx^2}\right)^s$ on $\mathbb{R}$ does not have nontrivial square-integrable zero modes, $w(x)$ vanishes a.e. on the real line.

Let us apply (1.14) to both sides of Eq. (1.31). This gives us

$$\widehat{u}(p) = \frac{\widehat{f}(p)}{|p|^{2s}}\chi_{\{p\in\mathbb{R}\mid |p|\le 1\}} + \frac{\widehat{f}(p)}{|p|^{2s}}\chi_{\{p\in\mathbb{R}\mid |p|> 1\}}, \tag{1.35}$$

where χ_A is the characteristic function of a set $A \subseteq \mathbb{R}$. Obviously, for all $0 < s < 1$, the second term in the right side of (1.35) is square integrable by virtue of the bound

$$\int_{-\infty}^{\infty} \frac{|\widehat{f}(p)|^2}{|p|^{4s}}\chi_{\{p\in\mathbb{R}\mid |p|>1\}}dp \le \|f\|^2_{L^2(\mathbb{R})} < \infty.$$

To prove the square integrability of the first term in the right side of (1.35) when $0 < s < \frac{1}{4}$, we apply estimate (1.15), which gives

$$\int_{-\infty}^{\infty} \frac{|\widehat{f}(p)|^2}{|p|^{4s}}\chi_{\{p\in\mathbb{R}\mid |p|\le 1\}}dp \le \frac{\|f(x)\|^2_{L^1(\mathbb{R})}}{\pi(1-4s)} < \infty,$$

which completes the proof of part (1) of the lemma.

To establish the solvability of equation (1.31) when $\frac{1}{4} \le s < \frac{3}{4}$, we use the formula

$$\widehat{f}(p) = \widehat{f}(0) + \int_0^p \frac{d\widehat{f}(s)}{ds}ds.$$

This allows us to express the first term in the right side of (1.35) as

$$\frac{\widehat{f}(0)}{|p|^{2s}}\chi_{\{p\in\mathbb{R}\mid |p|\le 1\}} + \frac{\int_0^p \frac{d\widehat{f}(s)}{ds}ds}{|p|^{2s}}\chi_{\{p\in\mathbb{R}\mid |p|\le 1\}}. \tag{1.36}$$

By virtue of definition (1.14)

$$\left|\frac{d\widehat{f}(p)}{dp}\right| \le \frac{1}{\sqrt{2\pi}}\||x|f(x)\|_{L^1(\mathbb{R})} < \infty$$

due to one of our assumptions. Hence,

$$\left|\frac{\int_0^p \frac{d\widehat{f}(s)}{ds}ds}{|p|^{2s}}\chi_{\{p\in\mathbb{R}\mid |p|\le 1\}}\right| \le \frac{1}{\sqrt{2\pi}}\||x|f(x)\|_{L^1(\mathbb{R})}|p|^{1-2s}\chi_{\{p\in\mathbb{R}\mid |p|\le 1\}} \in L^2(\mathbb{R}).$$

The remaining term in (1.36) $\frac{\widehat{f}(0)}{|p|^{2s}}\chi_{\{p\in\mathbb{R}\ |\ |p|\leq 1\}} \in L^2(\mathbb{R})$ if and only if $\widehat{f}(0)=0$, which implies orthogonality relation (1.33) in case (2) of the lemma.

Finally, it remains to investigate the situation when $\frac{3}{4}\leq s<1$. For that purpose, we use the representation

$$\widehat{f}(p)=\widehat{f}(0)+p\frac{d\widehat{f}}{dp}(0)+\int_0^p\Big(\int_0^r\frac{d^2\widehat{f}(q)}{dq^2}dq\Big)dr,$$

which enables us to write the first term in the right side of (1.35) as

$$\Big[\frac{\widehat{f}(0)}{|p|^{2s}}+\frac{p\frac{d\widehat{f}}{dp}(0)}{|p|^{2s}}+\frac{\int_0^p\Big(\int_0^r\frac{d^2\widehat{f}(q)}{dq^2}dq\Big)dr}{|p|^{2s}}\Big]\chi_{\{p\in\mathbb{R}\ |\ |p|\leq 1\}}. \tag{1.37}$$

Definition (1.14) yields

$$\Big|\frac{d^2\widehat{f}(p)}{dp^2}\Big|\leq\frac{1}{\sqrt{2\pi}}\|x^2f(x)\|_{L^1(\mathbb{R})}<\infty$$

as assumed. This enables us to estimate

$$\Big|\frac{\int_0^p\Big(\int_0^r\frac{d^2\widehat{f}(q)}{dq^2}dq\Big)dr}{|p|^{2s}}\chi_{\{p\in\mathbb{R}\ |\ |p|\leq 1\}}\Big|\leq\frac{1}{2\sqrt{2\pi}}\|x^2f(x)\|_{L^1(\mathbb{R})}|p|^{2-2s}\chi_{\{p\in\mathbb{R}\ |\ |p|\leq 1\}},$$

which clearly belongs to $L^2(\mathbb{R})$. The sum of the first and the second terms in (1.37) is not square integrable unless both $\widehat{f}(0)$ and $\frac{d\widehat{f}}{dp}(0)$ vanish, which gives us orthogonality relations (1.33) and (1.34), respectively.

Notably for the lower values of the power of the negative second derivative operator $0<s<\frac{1}{4}$ under the assumptions given above, no orthogonality conditions are required to solve the linear Poisson-type equation (1.31) in $H^{2s}(\mathbb{R})$.

References

1. Amrouche, C., Bonzom, F.: 'Mixed exterior Laplace's problem. J. Math. Anal. Appl. **338**, 124–140 (2008)
2. Alfimov, G.L., Medvedeva, E.V., Pelinovsky, D.E.: Wave systems with an infinite number of localized traveling waves. Phys. Rev. Lett. **112**, 054103, 5 pp (2014)
3. Amrouche, C., Girault, V., Giroire, J.: Dirichlet and Neumann exterior problems for the n-dimensional Laplace operator: an approach in weighted Sobolev spaces. J. Math. Pures Appl. **76**(1), 55–81 (1997)

4. Bolley, P., Pham, T.L.: Propriété d'indice en théorie Holderienne pour des opérateurs différentiels elliptiques dans R^n. J. Math. Pures Appl. **72**(1), 105–119 (1993)
5. Bolley, P., Pham, T.L.: Propriété d'indice en théorie Hölderienne pour le problème extérieur de Dirichlet. Commun. Partial Differ. Equations **26**(1–2), 315–334 (2001)
6. Benkirane, N.: Propriété d'indice en théorie Holderienne pour des opérateurs elliptiques dans R^n. CRAS, Série **I**(307), 577–580 (1988)
7. Carreras, B., Lynch, V., Zaslavsky, G.: Anomalous diffusion and exit time distribution of particle tracers in plasma turbulence model. Phys. Plasmas **8**, 5096–5103 (2001)
8. Cuccagna, S., Pelinovsky, D., Vougalter, V.: Spectra of positive and negative energies in the linearized NLS problem. Commun. Pure Appl. Math. **58**(1), 1–29 (2005)
9. Ducrot, A., Marion, M., Volpert, V.: Systemes de réaction-diffusion sans propriété de Fredholm. CRAS **340**, 659–664 (2005)
10. Ducrot, A., Marion, M., Volpert, V.: Reaction-diffusion problems with non Fredholm operators. Adv. Differ. Equations **13**(11–12), 1151–1192 (2008)
11. Lieb, E., Loss, M.: Analysis. Graduate Studies in Mathematics, vol. 14. American Mathematical Society, Providence (1997)
12. Manandhar, P., Jang, J., Schatz, G.C., Ratner, M.A., Hong, S.: Anomalous surface diffusion in nanoscale direct deposition processes. Phys. Rev. Lett. **90**, 4043–4052 (2003)
13. Metzler, R., Klafter, J.: The random walk's guide to anomalous diffusion: a fractional dynamics approach. Phys. Rep. **339**, 1–77 (2000)
14. Sancho, J., Lacasta, A., Lindenberg, K., Sokolov, I., Romero, A.: Diffusion on a solid surface: anomalous is normal. Phys. Rev. Lett. **92**, 250601 (2004)
15. Scher, H., Montroll, E.: Anomalous transit-time dispersion in amorphous solids. Phys. Rev. B **12**, 2455–2477 (1975)
16. Solomon, T., Weeks, E., Swinney, H.: Observation of anomalous diffusion and Lévy flights in a two-dimensional rotating flow. Phys. Rev. Lett. **71**, 3975–3978 (1993)
17. Volpert, V.: Elliptic Partial Differential Equations, Volume 1: Fredholm Theory of Elliptic Problems in Unbounded Domains. Birkhauser, Boston (2011)
18. Vougalter, V.: On threshold eigenvalues and resonances for the linearized NLS equation. Math. Model. Nat. Phenom. **5**(4), 448–469 (2010)
19. Volpert, V., Vougalter, V.: On the solvability conditions for a linearized Cahn-Hilliard equation. Rend. Istit. Mat. Univ. Trieste **43**, 1–9 (2011)
20. Vougalter, V., Volpert, V.: Solvability relations for some non Fredholm operators. Int. Electron. J. Pure Appl. Math. **2**(1), 75–83 (2010)
21. Vougalter, V., Volpert, V.: Solvability conditions for some non-Fredholm operators. Proc. Edinb. Math. Soc. (2) **54**(1), 249–271 (2011)
22. Vougalter, V., Volpert, V.: On the existence of stationary solutions for some non-Fredholm integro-differential equations. Doc. Math. **16**, 561–580 (2011)
23. Vougalter, V., Volpert, V.: On the solvability conditions for the diffusion equation with convection terms. Commun. Pure Appl. Anal. **11**(1), 365–373 (2012)
24. Vougalter, V., Volpert, V.: Solvability conditions for a linearized Cahn-Hilliard equation of sixth order. Math. Model. Nat. Phenom. **7**(2), 146–154 (2012)
25. Vougalter, V., Volpert, V.: Solvability conditions for some linear and nonlinear non-Fredholm elliptic problems. Anal. Math. Phys. **2**(4), 473–496 (2012)
26. Vougalter, V., Volpert, V.: Existence of stationary solutions for some nonlocal reaction-diffusion equations. Dyn. Partial Differ. Equations **12**(1), 43–51 (2015)
27. Volpert, V.A., Nec, Y., Nepomnyashchy, A.A.: Exact solutions in front propagation problems with superdiffusion. Phys. D **239**(3–4), 134–144 (2010)
28. Volpert, V.A., Nec, Y., Nepomnyashchy, A.A.: Fronts in anomalous diffusion-reaction systems. Philos. Trans. R. Soc. Lond. Ser. A Math. Phys. Eng. Sci. **371** (1982); 20120179, 18 pp (2013)

Chapter 2
Poincaré Recurrences in Ergodic Systems Without Mixing

Vadim Anishchenko, Nadezhda Semenova, Elena Rybalova and Galina Strelkova

2.1 Introduction

The Poincaré recurrence is one of the fundamental features pertaining to the time evolution of dynamical systems. Recurrence, according to Poincaré, implies that practically any phase trajectory of a set with given probability measure, which leaves a point x_0 of the phase space, will pass infinitely many times arbitrarily close to its initial state as it evolves in time. Poincaré termed this type of motion in dynamical systems as Poisson stable [1].

The statistics of Poincaré recurrences in the global approach has been a topic of research in recent years [2–4]. The local approach idea of the Poincaré recurrence theory consists in calculating Poincaré recurrences in a certain ε-vicinity of a given initial state [5, 6]. In the framework of the global approach, recurrence times are considered in all covering elements of the whole set and their statistics is then analyzed. The main characteristic of the Poincaré recurrence statistics in the global approach is the dimension of return times, which has been introduced in [4] and called as the Afraimovich–Pesin dimension (AP dimension).

V. Anishchenko (✉) · N. Semenova · E. Rybalova · G. Strelkova
Saratov State University, 83, Astrakhanskaya street, Saratov, Russia
e-mail: wadim@info.sgu.ru

N. Semenova
e-mail: semenovani@info.sgu.ru

E. Rybalova
e-mail: eska1706@gmail.com

G. Strelkova
e-mail: strelkovagi@info.sgu.ru

D. Volchenkov and X. Leoncini (eds.), *Regularity and Stochasticity of Nonlinear Dynamical Systems*, Nonlinear Systems and Complexity 21,
DOI 10.1007/978-3-319-58062-3_2

It has been established that the statistics of recurrences in the global approach depends on the topological entropy h_T. Poincaré recurrences have been studied theoretically for mixing sets with $h_T > 0$ [2–4] and the theoretical results have been confirmed by numerical simulation [7–9]. The situation is different in the case of ergodic sets without mixing, i.e., when $h_T = 0$. There are practically no works devoted to studies of the properties of Poincaré recurrences for this case. Some important theoretical results have been obtained in [2–4] for the shift circle (the linear circle map) with an irrational rotation number. In our present work, we aim to study numerically the Poinaré recurrence statistics in the linear and nonlinear circle map with different irrational rotation numbers and to reveal new peculiarities of Poincaré recurrences. The circle map is widely used in nonlinear dynamics to study quasiperiodic oscillations with two independent frequencies.

In the global approach, the whole set of phase trajectories of a dynamical system is covered with cubes (or balls) of size $\varepsilon \ll 1$. A minimal time of the first recurrence of a phase trajectory in the u_i-vicinity $\tau_{\inf}(u_i)$ is calculated for each covering element u_i $(i = 1, 2, \ldots, N)$. Then, the mean minimal return time is defined over the whole set of covering elements u_i [9–11] as follows:

$$\langle \tau_{\inf}(\varepsilon) \rangle = \frac{1}{N} \sum_{i=1}^{m} \tau_{\inf}(u_i). \tag{2.1}$$

It has been shown in [2] that in the general case

$$\langle \tau_{\inf}(\varepsilon) \rangle \sim \phi^{-1}(\varepsilon^{\frac{d}{\alpha_c}}) \tag{2.2}$$

where d is the fractal dimension of the considered set, and α_c is the AP dimension of a return time sequence. The gauge function $\phi(t)$ in (2.2) can be given by one of the following forms:

$$\phi(t) \sim \frac{1}{t}, \quad \phi(t) \sim \exp(-t), \quad \phi(t) \sim \exp(-t^2), \ldots, \phi(t) \sim \exp(-t^n). \tag{2.3}$$

The appropriate choice of $\phi(t)$ depends on the topological entropy h_T as well as on the multifractality of the considered set if such a property exists. It has been shown in [2, 4] that for $h_T = 0$, the gauge function has an asymptotic form $\phi(t) \sim 1/t$ and the following expression holds

$$\langle \tau_{\inf}(\varepsilon) \rangle \sim \varepsilon^{-\frac{d}{\alpha_c}}, \quad \varepsilon \ll 1\,. \tag{2.4}$$

For chaotic systems, we have $h_T > 0$ and $\phi(t) \sim \exp(-t)$, and thus, the following law is valid [10]:

$$\langle \tau_{\inf}(\varepsilon) \rangle \sim -\frac{d}{\alpha_c} \ln \varepsilon, \quad \varepsilon \ll 1. \tag{2.5}$$

2.2 Model Under Study

We consider a particular example of a minimal set that is produced by the circle map:

$$\theta_{n+1} = \theta_n + \Delta + K \sin\theta_n, \quad \mod 2\pi \tag{2.6}$$

where Δ and K are the parameters of the map. The circle map of type (2.6) is a reference model of a wide class of dynamical systems with quasiperiodic behavior.

The trajectories of (2.6) are characterized by the rotation number which is defined as the mean increment of angle θ over one iteration of the map with respect to the total angle:

$$\rho = \lim_{n\to\infty} (\theta_n - \theta_0)/2\pi n. \tag{2.7}$$

We start by studying the map (2.6) with $K = 0$. In this case, the trajectory rotates by a constant angle Δ per iteration and thus the rotation number can be defined as $\rho = \Delta/2\pi$. An irrational value of ρ is associated with quasiperiodic trajectories which are everywhere dense on a circle, and the distribution $p(\theta)$ is uniform on the interval $0 \le \theta_n \le 2\pi$ (Fig. 2.1). If ρ takes a rational value, i.e., $\rho = k/m$, the trajectory makes k rotations around the circle over m iterations, being a periodic one. In the nonlinear case when $K > 0$, the map cannot already be reduced to rigid rotations of the point on the circle and $p(\theta)$ is no longer uniform (Fig. 2.1).

It has been shown in [2, 4] that the AP dimension of the set $\{\theta_n\}$ which is generated by (2.6) essentially depends on ρ and the methods of its definition.

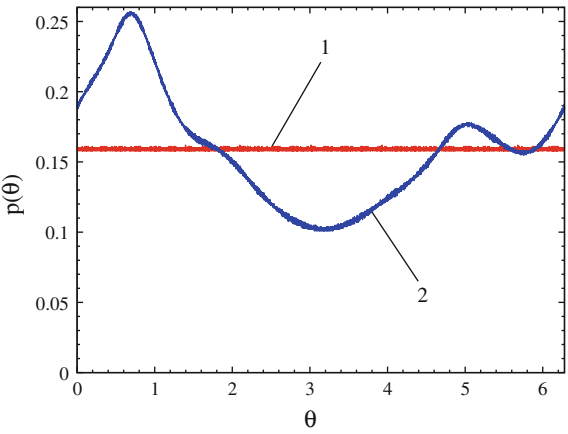

Fig. 2.1 Distribution density $p(\theta)$ on the circle (2.6) for the golden ratio and with $K = 0.0$ (*curve* 1) and $K = 0.6$ (*curve* 2)

All irrational numbers can be divided into transcendental and algebraic numbers. The latter are the numbers that are roots of the equation:

$$C_N \rho^N + \cdots + C_1 \rho + C_0 = 0. \tag{2.8}$$

They can be exemplified by $\sqrt[i]{2}, \sqrt[i]{3}$, and others where i are natural numbers. The numbers that are not algebraic are said to be transcendental. They include π, e, and $\ln 2$.

Any number can be represented as a continued fraction. In the case of an irrational number, this fraction is infinite and can be written in the form [12]:

$$\rho = a_0 + \cfrac{1}{a_1 + \cfrac{1}{a_2 + \cfrac{1}{\ddots}}}. \tag{2.9}$$

The sequence of coefficients $\{a_i\}, i > 0$, which is written as $[a_0; a_1, a_2, a_3, \ldots]$, is called a continued fraction. Irrational values of ρ can be approximated by the ratio of two integers k_i/m_i. That method is said to be the method of rational approximations and the ratio itself is called the ith convergent of a continued fraction. Sequences $\{k_i\}$ and $\{m_i\}$ are increasing, the numerators and denominators are defined using the recursive relations and the coefficients of the continued fraction:

$$\begin{aligned} k_{-1} = 1, \quad k_0 = a_0, \quad k_i = a_i k_{i-1} + k_{i-2}, \\ m_{-1} = 0, \quad m_0 = 1, \quad m_i = a_i m_{i-1} + m_{i-2} \end{aligned} \tag{2.10}$$

where $\{a_i\}$ is a sequence of natural coefficients of the continued fraction, k_i and m_i are numerators and denominators of the convergent.

In terms of the convergence rate of rational approximations, irrational numbers can be divided into Diophantine and Liouvillian numbers. The approximation error obeys the inequality:

$$\left| \rho - \frac{k}{m} \right| < \frac{C}{m^\mu} \tag{2.11}$$

where k/m is a convergent from a set of pairs of integers k_i and m_i, $2 \leq \mu < \infty$ is the measure of irrationality, and C is a constant. An irrational rotation number ρ is said to be Diophantine if the upper bound of values of μ for each of which the inequality (2.11) has infinitely many solutions is finite. Otherwise, ρ is a Liouvillian number.

We consider the case of Diophantine approximations of ρ. Following [2, 4], we obtain

$$\left| \rho - \frac{k}{m} \right| \geq \frac{1}{n^{[\nu(\rho)+1+\xi]}} \tag{2.12}$$

where $\nu(\rho) = \sup\{\nu(\rho)\}$ is the maximal rate of Diophantine approximations of an irrational number over all possible pairs of k and m, and $\xi > 0$. It has been proven analytically for (2.12) [2, 4] that

$$\langle \tau_{\inf}(\varepsilon) \rangle \sim \varepsilon^{-\frac{1}{\nu(\rho)}}, \quad \ln \langle \tau_{\inf}(\varepsilon) \rangle \sim -\frac{1}{\nu(\rho)} \ln \varepsilon. \tag{2.13}$$

Here, the fractal dimension of the set $\{\theta_n\}$, which is generated by (2.6), is $d = 1$. Comparing (2.5) and (2.13), we can obtain that $\nu(\rho) = \alpha_c$ in the considered case. This implies that the AP dimension coincides with the approximation rate of the irrational rotation number ρ. Furthermore, the gauge function is $\phi(t) \sim 1/t$. In the following section, we introduce several features of the dependence $\ln \langle \tau_{\inf}(\varepsilon) \rangle$, which are obtained by numerical simulation.

2.3 Main Properties of Return Time Dependence for the Linear Circle Map

We calculate the dependence $\langle \tau_{\inf}(\varepsilon) \rangle$ on the set $\{\theta_n\}$ of the map (2.6) for $K = 0$ and ρ which is equal to the golden ratio:

$$\rho = \frac{1}{2}(\sqrt{5} - 1) \approx 0.618\ldots, \quad \Delta = 2\pi\rho = \pi(\sqrt{5} - 1). \tag{2.14}$$

Since a point rotates uniformly on the circle when $K = 0$, for any interval of ε, there is a single value $\tau_{\inf}(\varepsilon)$ which is independent of the initial point $\theta = \theta_0$. Therefore, we do not need to calculate the mean value (2.1). Numerical results for $\tau_{\inf}(\varepsilon)$ are shown in Fig. 2.2. As shown in the figure, this dependence looks like a step function, which can be referred to as the "Fibonacci stairs." We have established that it has several features which are as follows.

1. When $\ln \varepsilon$ decreases, the sequence of $\tau_{\inf}(\varepsilon)$ values grows and strictly corresponds to the basic Fibonacci series $(\ldots, 8, 13, 21, 34, 55, 89, 144, \ldots)$: Each subsequent number is the sum of the previous two. The values of $\tau_{\inf}$ which relate to the steps of the Fibonacci stairs are indicated in Fig. 2.2.
2. When ε changes within any step of the Fibonacci stairs, three return times $\tau_1 < \tau_2 < \tau_3$ can be distinguished. This property follows from Slater's theorem [13]. These three return times correspond to the basic Fibonacci series.
3. It has been shown numerically and proven theoretically that lengths and heights of the steps (Fig. 2.2) of the Fibonacci stairs possess a universal property for the golden and silver ratios. The length of the ith step can be defined as follows:

$$D_i = \ln \varepsilon_i - \ln \varepsilon_{i+1} = \text{const} = |\ln \rho|, \quad i \gg 1 \tag{2.15}$$

where ε_i and ε_{i+1} are values of ε at the boundaries of the relevant step. From (2.15), it follows that $\varepsilon_{i+1} = \varepsilon_i \cdot \rho$.
Similarly, for the height of the ith step, we have

$$\ln \tau_{\text{inf}}(\varepsilon_{i+1}) - \ln \tau_{\text{inf}}(\varepsilon_i) = |\ln \rho|, \quad i \gg 1. \tag{2.16}$$

The index i in (2.15) and (2.16) increases as ε decreases (Fig. 2.2). The lengths and the heights of the steps are universal and equal to $|\ln \rho|$ where ρ is the rotation number.

As follows from property 2, when ε changes "within a step," three return times $\tau_1 < \tau_2 < \tau_3$ can be registered. Its sequence corresponds to the sequence of denominators of convergents, i.e., $\tau_1 = m_i$, $\tau_2 = m_{i+1}$, and $\tau_3 = m_{i+2}$. This implies the appearance of the Fibonacci number sequence in return times. Calculations of probability distributions of return times in different regions of an arbitrary step in the Fibonacci stairs show three different situations. These results are illustrated in Fig. 2.3. We first have $P(\tau_3) < P(\tau_2) < P(\tau_1)$ for the return vicinity which is chosen in the right side of the step (Fig. 2.3a). The change between the three distributions occurs in the middle of the step, i.e., $P(\tau_1) = P(\tau_3) < P(\tau_2)$ (Fig. 2.3b). Finally, $P(\tau_1) < P(\tau_3) < P(\tau_2)$ is observed when the return vicinity is taken in the left half of the step (Fig. 2.3c). At the end of the step the probability $P(\tau_1) \to 0$ (Fig. 2.3d), a new return time $\tau_4 = m_{i+3}$ is appeared, and the transition to the next step takes place. The distribution in this case is $P(\tau_3) < P(\tau_2) < P(\tau_1)$ (Fig. 2.3e). The minimal return time is already $\tau_{\text{inf}} = \tau_2$ within the next step, and so on.

Now, we try to prove the third property of the Fibonacci stairs which is expressed by the relations (2.15) and (2.16). The validity of (2.15) and (2.16) can be proven by several methods [14–16]. We give one of them.

The structure of Fibonacci stairs is closely related to the theory of convergents and continued fractions. An irrational number is a real number which cannot be written as a fraction k/m where k and m are natural numbers, 1, 2, ...

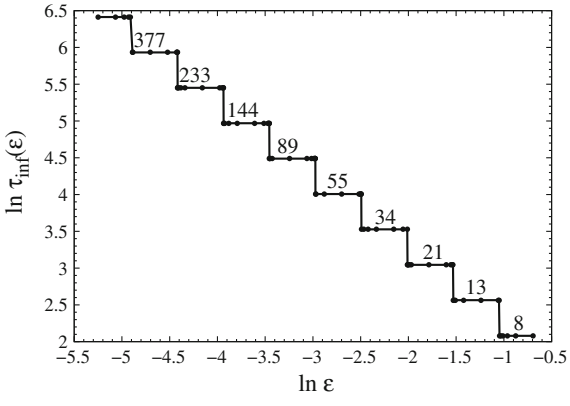

Fig. 2.2 Dependence of the minimal return time $\tau_{\text{inf}}(\varepsilon)$ for the map (2.6) with the golden ratio and for $K = 0$ and $\Delta = 2\pi\rho$

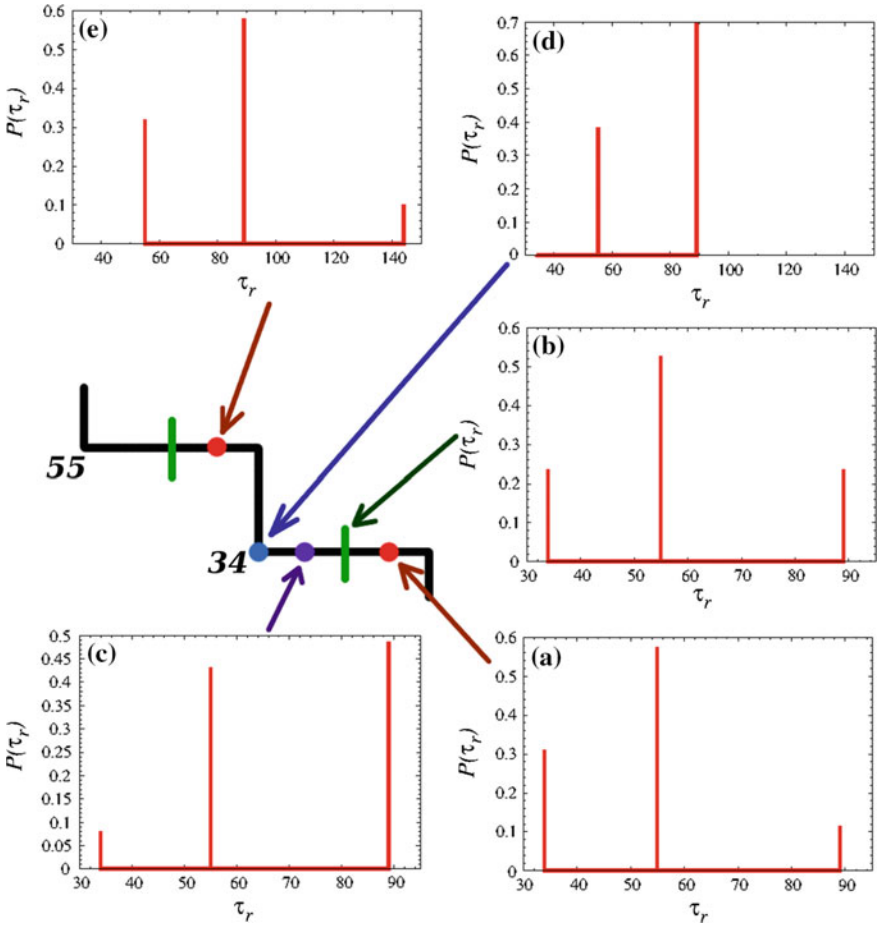

Fig. 2.3 Distributions of return times in the ε-vicinity chosen in different regions of a step of the Fibonacci stairs: **a** at the *right* side, **b** in the *middle*, **c** at the *left* side, **d** at the *left* boundary, and **e** transition to the next step

In the general case, an irrational rotation number can be presented in the form of a continued fraction (2.9). This produces a sequence of approximation coefficients $\{a_i\}$, $i \geq 0$. The notation $[a_0; a_1, a_2, a_3, \ldots]$ is an infinite continued fraction representation of the irrational number.

As mentioned in the previous section, the irrational rotation number ρ can be approximated by the fraction of two integers k_i/m_i. This is the method of rational approximations. The ith convergent of the continued fraction $\rho = [a_0; a_1, a_2, a_3 \ldots]$ is a finite continued fraction $[a_0; a_1, a_2, \ldots, a_i]$, which value is equal to the rational number k_i/m_i. The increasing sequences of numerators $\{k_i\}$ and denominators $\{m_i\}$ are called continuants of the ith convergent (2.9) and can be found using fundamental recurrence formulas (2.11).

It has been found [15, 17] that for any rotation number, the dependence $\tau_{\text{inf}}(\varepsilon)$ is a step function and each value $\tau_{\text{inf}i}$, which corresponds to the ith step, is equal to the denominators of the ith convergent k_i/m_i of the rotation number ρ. Using the equality $\tau_{\text{inf}i}(\varepsilon) = m_i$, we obtain the minimal vicinity size which corresponds to this return time $\tau_{\text{inf}i}$. As noted in Introduction, after one iteration of the linear circle map (2.6), the position of the point on the circle changes by $2\pi\rho$. The expression $\tau_{\text{inf}}(\varepsilon) = m_i$ means that the point returns in the neighborhood of its initial state after m_i iterations, shifting by $2\pi\rho m_i$. During these iterations, the point can make several complete circles and appear to the left or right of the initial state. To take this fact into account, we introduce the modulus and subtract the convergent numerator k_i which defines the number of complete circles. Thus, the return in the neighborhood of the initial state θ_0 takes place at the distance of $2\pi|\rho m_i - k_i|$ from the point θ_0 [14].

Let us consider the case when we start not from the point θ_0 but from the right boundary of its neighborhood, i.e., from the point $\theta_0' = \theta_0 + \varepsilon_c/2$. The return in ε_c after the minimal number of iterations m_i happens near the left boundary of this neighborhood, i.e., at the point $\theta_0 - \varepsilon_c/2$. In such a case, as mentioned above, the point shifts by $2\pi|\rho m_i - k_i|$ from the initial position θ_0' (see Fig. 2.4). This means that

$$\theta_0' - 2\pi|\rho m_i - k_i| = \theta_0 - \varepsilon_c/2. \tag{2.17}$$

$$\theta_0 + \varepsilon_c/2 - 2\pi|\rho m_i - k_i| = \theta_0 - \varepsilon_c/2. \tag{2.18}$$

This enables one to derive the expression for calculating the value ε_i, which corresponds to the left boundary of the stairs step with the minimal return time $\tau_{\text{inf}} = m_i$ for any irrational rotation number ρ:

$$\varepsilon_i = \varepsilon_c = 2\pi|\rho m_i - k_i| \tag{2.19}$$

where ρ is the rotation number, m_i is convergent denominator, and k_i is the convergent numerator. As discussed above, the golden (silver) ratio represents a special case.

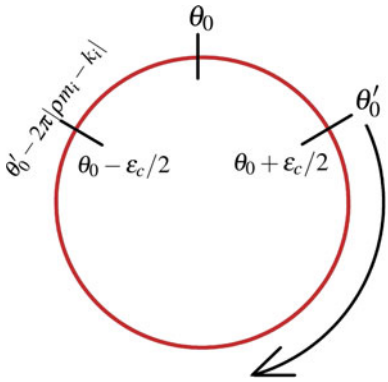

Fig. 2.4 Schematic representation of the neighborhood ε and initial and return points on the *circle*

The universal feature of the staircase dependence is due to the fact that numerators and denominators of convergents have the same definition rules and are elements of the Fibonacci (Pell) series. Thus, for the golden ratio, (2.19) can be rewritten as follows:

$$\varepsilon_i = 2\pi|\rho F_i - F_{i-1}|, \quad \text{or}$$
$$\varepsilon_i \approx \frac{2\pi}{L_i} \tag{2.20}$$

where F_i is the ith Fibonacci number, $\rho = (\sqrt{5}-1)/2$ is the golden ratio, and L_i is the ith Lucas number.

Following the same motivation, for the silver ratio we can find

$$\varepsilon_i = 2\pi|\rho P_i - P_{i-1}| \quad \text{or}$$
$$\varepsilon_i \approx \frac{2\pi}{Q_i} \tag{2.21}$$

where P_i is the ith Pell number, $\rho = \sqrt{2}-1$ is the silver ratio, and Q_i is the ith Pell–Lucas number.

We confirm our analytical results (2.19)–(2.21) by numerical simulation for the golden and silver ratios (Fig. 2.5) as well as for more complex Diophantine numbers $\sqrt[3]{2}$, e, and $\lg(5)$, which correspond to the absence of universal geometry of the step dependence (Fig. 2.6). Using (2.19), we can find the dependence of each step length D_i (Figs. 2.5 and 2.6) on its number in general.

For the golden and silver ratios, the length of stairs steps is constant and independent of the step number but is defined by the rotation number:

$$D_i = \text{const} = |\ln \rho|. \tag{2.22}$$

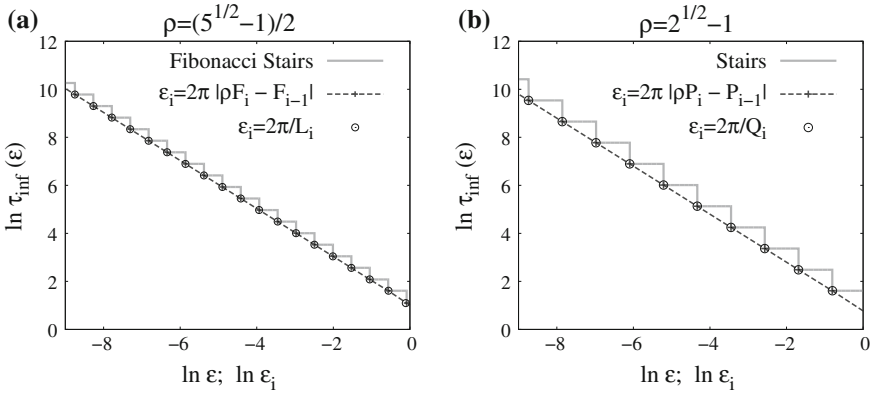

Fig. 2.5 Dependences $\ln \tau_{\text{inf}}(\ln \varepsilon)$ for **a** the golden ratio ($\rho = (\sqrt{5}-1)/2$) and **b** the silver ratio ($\rho = \sqrt{2}-1$) are indicated by *solid lines*; *dashed lines* with *plus points* and *circle points* represent the corresponding approximations using (2.20) for the golden ratio and (2.21) for the silver ratio

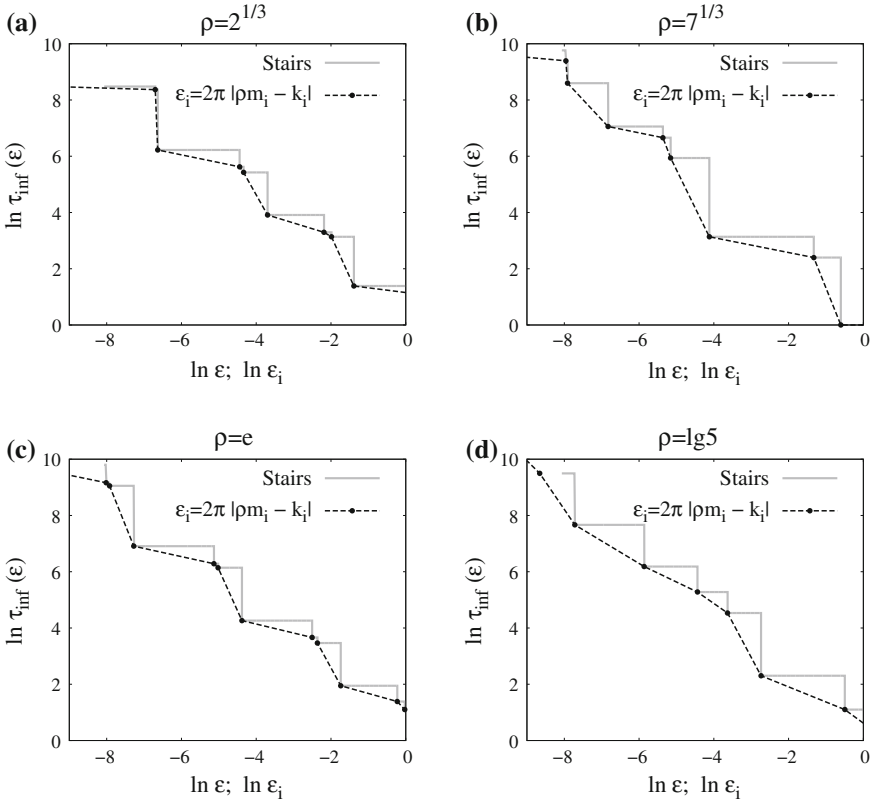

Fig. 2.6 Dependences $\ln \tau_{\text{inf}}(\ln \varepsilon)$ for four values of the rotation number: **a** $\rho = \sqrt[3]{2}$, **b** $\rho = \sqrt[3]{7}$, **c** $\rho = e$, and **d** $\rho = \lg(5)$ (*solid lines*). *Dashed lines* with *circle points* show the corresponding approximations using (2.19)

Figure 2.7 illustrates dependences of the step length on the step number for the golden ratio (the universal geometry is valid) and for two different values of the rotation number, namely $\rho = \sqrt[3]{2}$ and $\lg 5$ (no universal geometry is observed). Figure 2.7a corresponds to the golden ratio and shows that all step lengths are equal. Figure 2.7b, c indicates that the universal geometry fails for the other rotation numbers. As shown in Fig. 2.7, analytical and numerical results are in full agreement. This means that the universal geometry can be obtained only in cases of the golden and silver ratios for which the step length does not depend on the step number (Fig. 2.7a).

Golden ratio.

In the case of the golden ratio ($\rho = (\sqrt{5} - 1)/2$), denominators and numerators of the convergents of ρ can be found as $m_i = F_i$ and $k_i = F_{i-1}$ where $\{F_i\}$ is the Fibonacci sequence. The golden ratio is a special case when numerators and denominators have the same determination rule and are elements of the same sequence. Thus, we can simplify the expression (2.19).

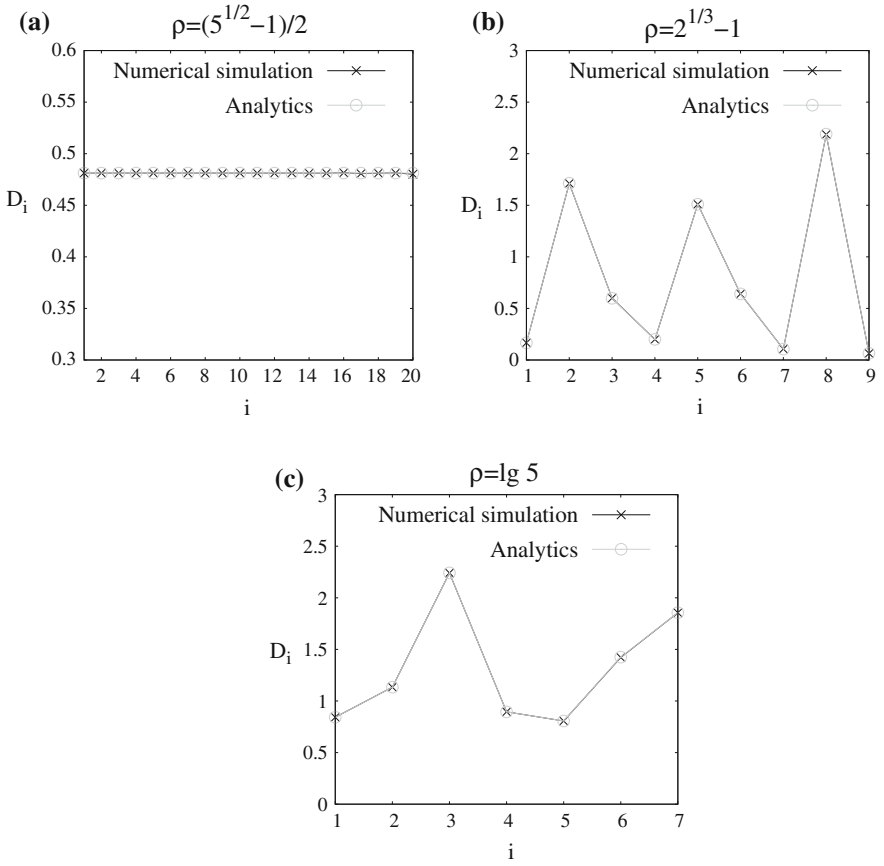

Fig. 2.7 Dependences of the step length on the step number for three values of the rotation number: **a** the golden ratio, **b** $\rho = \sqrt[3]{2}$, and **c** $\rho = \lg 5$

Each ith Fibonacci number is defined by the following recurrence relation:

$$F_i = F_{i-1} + F_{i-2} \tag{2.23}$$

with the set values $F_0 = 1$, $F_1 = 1$. The ith Fibonacci number can also be found using Binet's formula:

$$F_i = \frac{\varphi^i - (-\varphi)^{-i}}{2\varphi - 1} \tag{2.24}$$

where $\varphi = (\sqrt{5} + 1)/2$ is the root of the equation $\varphi^2 - \varphi - 1 = 0$ and depends on ρ as follows:

$$\rho = \varphi - 1 \quad <=> \quad \varphi = 1 + \rho. \tag{2.25}$$

The value of ε which corresponds to the emergence of a new stairs step and relates to the left boundary of the step with the minimal return time $\tau_{\text{inf}} = F_i$ is

$$\varepsilon_i = 2\pi|\rho F_i - F_{i-1}|\,. \tag{2.26}$$

Using (2.24) and (2.25), this expression can be rewritten as follows:

$$\begin{gathered}
\varepsilon_i = 2\pi|(\varphi-1)F_i - F_{i-1}| = 2\pi|\varphi F_i - (F_i + F_{i-1})| = \\
= 2\pi|\varphi F_i - F_{i+1}| = 2\pi\left|\frac{\varphi^i-(-\varphi)^{-i}}{2\varphi-1}\varphi - \frac{\varphi^{i+1}-(-\varphi)^{-i-1}}{2\varphi-1}\right| = \\
= 2\pi\left|\frac{\varphi^{i+1}+(-\varphi)^{-i+1}-\varphi^{i+1}+(-\varphi)^{-i-1}}{2\varphi-1}\right| = \\
= 2\pi\left|\frac{(-1)^{-i-1}(\varphi^{-i+1}+\varphi^{-i-1})}{2\varphi-1}\right| = 2\pi\left|(-1)^{-i-1}\right|\times \\
\times\frac{\varphi^2+1}{2\varphi-1}\varphi^{-i-1} = 2\pi\frac{\varphi^2+1}{2\varphi-1}\varphi^{-i-1} = 2\pi\varphi^{-i}\frac{\varphi^2+1}{2\varphi^2-\varphi} = \\
= 2\pi\varphi^{-i}\frac{\varphi^2-\varphi-1+\varphi+2}{2\varphi^2-\varphi-\varphi-2+2+\varphi} = 2\pi\varphi^{-i}\frac{\varphi+2}{\varphi+2} = 2\pi\varphi^{-i} = \\
= \frac{2\pi\varphi^{-i}(\varphi^i+(-\varphi)^{-i})}{\varphi^i+(-\varphi)^{-i}} = \frac{2\pi}{\varphi^i+(-\varphi)^{-i}}\left(1+(-1)^{-i}\varphi^{-2i}\right).
\end{gathered} \tag{2.27}$$

Since $\varphi > 1$, the second term between the brackets tends to zero when $i \to \infty$. Thus,

$$\lim_{i\to\infty}\varepsilon_i(\tau_{\text{inf}} = F_i) = \frac{2\pi}{\varphi^i+(-\varphi)^{-i}} = \frac{2\pi}{L_i} \tag{2.28}$$

where L_i is the ith Lucas number. It is defined by the same recurrence relation as the Fibonacci numbers (2.23) but with another set values $L_0 = 2$, $L_1 = 1$. The Lucas numbers can be approximately defined by the following formula:

$$L_i = \varphi^i + (-\varphi)^{-i}. \tag{2.29}$$

Calculation of the step length.

The size of the neighborhood ε_i, which corresponds to the left boundary of a step with the minimal return time $\tau_{\text{inf}} = m_i$, for any irrational rotation number ρ can be found as follows:

$$\varepsilon_{Li} = \varepsilon_i = 2\pi|\rho m_i - k_i|\,. \tag{2.30}$$

Similarly, we can obtain the value ε_{i-1}. Since the dependence $\tau_{\text{inf}}(\varepsilon)$ is a steplike function, ε_{i-1} is simultaneously the left boundary of the step with the minimal return time $\tau_{\text{inf}} = m_{i-1}$ and the right boundary of the step with $\tau_{\text{inf}} = m_i$:

$$\varepsilon_{Ri} = \varepsilon_{i-1} = 2\pi|\rho m_{i-1} - m_{i-1}|\,. \tag{2.31}$$

Hence, the length of the ith step of the dependence $\ln\tau_{\text{inf}}(\ln\varepsilon)$ can be calculated as follows:

$$\begin{aligned} D_i &= \ln \varepsilon_{Li} - \ln \varepsilon_{Ri} = \ln \tfrac{\varepsilon_{Li}}{\varepsilon_{Ri}} = \\ &= \ln \tfrac{2\pi|\rho m_i - k_i|}{2\pi|\rho m_{i-1} - k_{i-1}|} = \ln \tfrac{|\rho m_i - k_i|}{|\rho m_{i-1} - k_{i-1}|} = \\ &= \ln \tfrac{q_i|\rho - m_i/k_i|}{m_{i-1}|\rho - k_{i-1}/m_{i-1}|} \approx \ln \tfrac{m_i}{m_{i-1}} . \end{aligned} \tag{2.32}$$

Thus, in general the length of stairs steps depends on denominators of convergents of rotation numbers. For the golden ratio, the denominators and numerators of the convergents are related to the Fibonacci series as $k_{i-1} = m_i = F_i$. It follows that for the golden ratio,

$$D_i \approx \ln \frac{m_i}{m_{i-1}} \approx \ln \frac{k_{i-1}}{k_{i-2}} \approx |\ln \rho| . \tag{2.33}$$

The same motivation can be used for the silver ratio. In this case, the numerators and denominators are connected with the Pell series: $k_{i-1} = m_i = P_i$. For this reason, the step lengths for the golden and silver ratios are constant and independent of the step number. They are defined only by the rotation number $|\ln \rho|$.

2.4 Afraimovich–Pesin Dimension for Different Rotation Numbers

The dependence $\tau_{\text{inf}}(\varepsilon)$ obtained analytically enables one to define α_c more precisely. From (2.4) and (2.13), it follows that

$$\nu(\rho) = \alpha_c = 1. \tag{2.34}$$

Therefore, the AP dimension and the rate of approximation of the rotation number coincide and are equal to 1 in the case of the golden ratio.

All the features described above are also valid in the case of the silver ratio. The dependence $\tau_{\text{inf}}(\varepsilon)$ for the silver ratio is presented in Fig. 2.5b. The universal properties (2.15) and (2.16) of the Fibonacci stairs are also observed in this case. However, for the silver ratio, the sequence of minimal return times obeys the Pell law $m_{i+1} = 2m_i + m_{i-1}$ and forms the series: ..., 29, 70, 169, 408, 985, ... [18]. Calculating the sequence of neighborhoods (2.21), we plot the dependence $\ln \tau_{\text{inf}}(\varepsilon_i)$ which is also a straight line with slope -1 (Fig. 2.5b). Thus, in the case of the silver ratio, the AP dimension and the rate $\nu(\rho)$ are also equal to 1 as for the golden ratio.

The golden and silver ratios are algebraic Diophantine numbers with the measure of irrationality $\mu = 2$. It has been proven that any algebraic irrational number has $\mu = 2$ [19]. This means that (2.12), (2.13), and (2.34) hold for these numbers.

The universal geometry of the Fibonacci stairs is observed only for the golden and silver ratios and is attested to the peculiarities of their expansion in a continued fraction. This universal property is violated for other irrational rotation numbers.

Numerical results obtained for $\rho = \sqrt[3]{2}$ and $\rho = \sqrt[3]{7}$ are similar to the previous cases, but the Fibonacci stairs demonstrates a more complex structure.

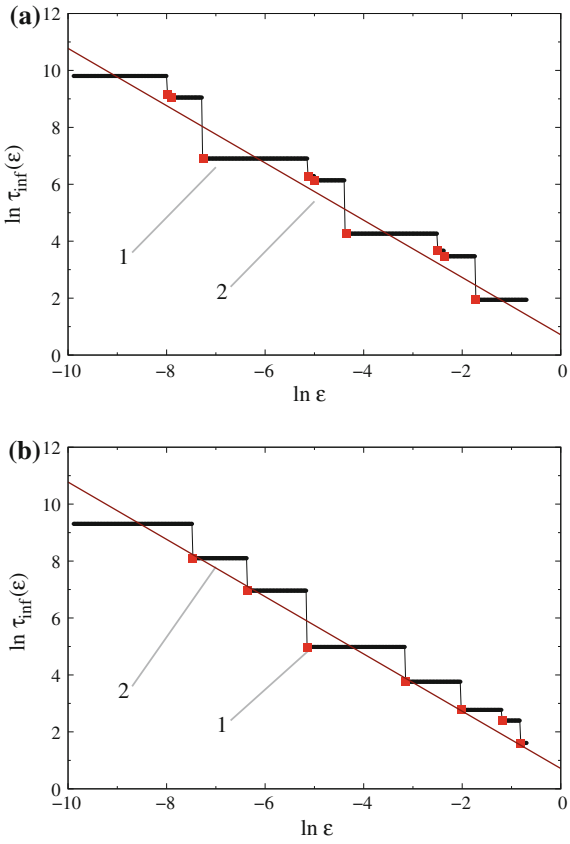

Fig. 2.8 Calculation results for $\tau_{\text{inf}}(\varepsilon)$ in the map (2.6) for $K = 0$ and **a** $\rho = e$ and **b** $\rho = \pi/\sqrt{3}$. The Fibonacci stairs (*curve* 1), its linear approximation (*curve* 2). Plot 2 has slope 1

We now describe in detail transcendental numbers. It is known that any Liouvillian number is transcendental, but the opposite is not true, i.e., there are numbers that can be both Diophantine and transcendental simultaneously. These numbers have the measure of irrationality $\mu \geq 2$. Diophantine transcendental numbers can be exemplified by π, $\pi/\sqrt{3}$, $\pi/100$, e, $\ln 2$, $\ln 10$, and others. It has been proven that the number e has $\mu = 2$. There is only a theoretical estimation from above for the measure of the other numbers, e.g., $\mu(\pi) \leq 7.6063$, $\mu(\pi/\sqrt{3}) \leq 4.6016$, $\mu(\ln 2) \leq 3.57455391$. Figure 2.8 illustrates numerical results for $\pi/\sqrt{3}$ and e. Calculating the slope of the Fibonacci stairs by both averaging and theoretically gives $\nu(\rho) = \alpha_c = 1.0$. From a numerical viewpoint, this implies that both $\pi/\sqrt{3}$ and e are Diophantine numbers with the measure of irrationality $\mu = 2$.

It can be shown that the measure of irrationality for the irrational numbers considered takes exactly the values indicated above. Let us denote $\delta = |\rho - \frac{k}{m}|$ where k/m is a convergent of a continued fraction. In this case, (2.11) can be rewritten in the form

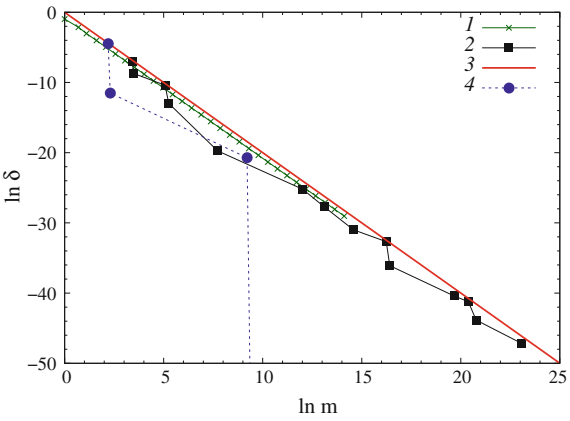

Fig. 2.9 Numerical data for the measure of irrationality μ for different numbers: $\rho = (\sqrt{5}-1)/2$ (*curve* 1), $\rho = \pi/\sqrt{3}$ (*curve* 2), the theoretical approximation $\ln\delta = -2\ln m$ (*curve* 3), and $\rho = \lambda$ (*curve* 4)

$$\delta < \frac{C}{m^{\mu}}, \quad \text{or} \quad \ln\delta < \ln C - \mu \ln m. \tag{2.35}$$

The measure of irrationality can be determined as a slope of the dependence of $\ln\delta$ on $\ln m$ by calculating a sequence of nominators and denominators of convergents. Calculation results are shown in Fig. 2.9 for different irrational values of the rotation number. It is shown in the figure that $\mu = 2$ as in the previously considered cases of the golden and silver ratios, $\rho = e$, and $\rho = \pi/\sqrt{3}$. It follows that

$$\nu(\rho) = \mu(\rho) - 1. \tag{2.36}$$

This means that $\nu(\rho) = 1$ for $\mu = 2$. This fact confirms the numerical data for the unit AP dimension which are obtained for all the aforementioned values of the rotation number.

Transcendental Liouvillian numbers form a last subgroup of irrational numbers. They have a very high rate of convergence of rational approximations. In other words, their measure of irrationality is $\mu \to \infty$. We have considered several Liouvillian numbers, one of which is

$$\rho = \lambda = \sum_{i=0}^{\infty} 10^{-i!}. \tag{2.37}$$

The numerical results presented in Fig. 2.9 (curve 4) attest that $\mu \to \infty$ for $\rho = \lambda$. In this case, $\phi(t) \sim 1/t$ cannot be considered as a gauge function (Fig. 2.10). Unfortunately, we were not able to find an appropriate form for $\phi(t)$ in this case because of the finite computer accuracy. We have only found that (2.12) and (2.13) do not hold for Liouvillian irrational numbers and this fact corroborates the theoretical results [2, 4].

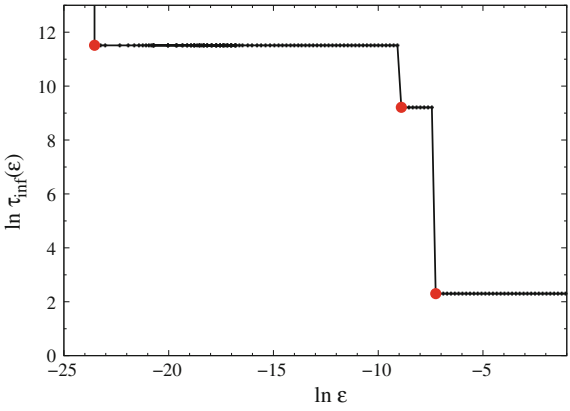

Fig. 2.10 Dependence of $\tau_{\text{inf}}(\varepsilon)$ for the Liouvillian rotation number $\rho = \lambda$

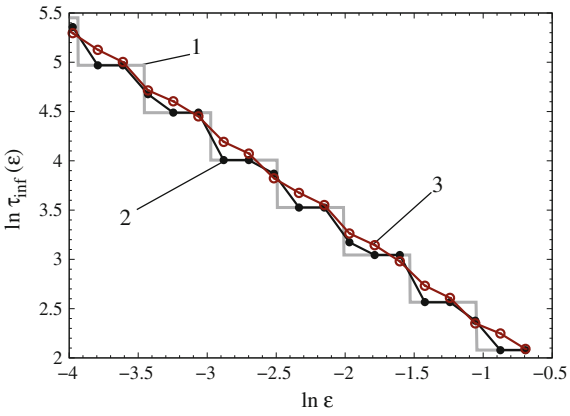

Fig. 2.11 Calculation results for $\ln\langle\tau_{\text{inf}}(\varepsilon)\rangle$ in the map (2.6) for $\rho = (\sqrt{5}-1)/2$ and three different values of K: $K = 0$ (*curve* 1), $K = 0.1$ (*curve* 2), and $K = 0.6$ (*curve* 3)

2.5 Impact of Nonlinearity

We now study the map (2.6) for $0 < K < 1$, i.e., when the system is nonlinear. For $K > 0$, the distribution density $p(\theta)$ is not uniform on the interval $0 \le \theta \le 2\pi$ (see Fig. 2.1). Therefore, to find $\langle\tau_{\text{inf}}(\varepsilon)\rangle$, one needs to divide the whole region on intervals of ε values and to calculate the mean value (2.1). We restrict ourselves to the case when the rotation number ρ is equal to the golden ratio. If K is varied in (2.6), ρ is also changed. Therefore, for fixed values of K, we select Δ in (2.6) so that $\rho = (\sqrt{5}-1)/2$. Calculation data are shown in Fig. 2.11 for three different values of K.

Analysis of the data shown in Fig. 2.11 attests that when K grows, the Fibonacci stairs is gradually smoothing and practically tends to a straight line at $K = 0.6$. Calculations of the mean slope of the plots in Fig. 2.11 show that it is equal to -1 for $K = 0$, 0.1, and 0.6. Thus, in the nonlinear case of the circle map (2.6), the AP dimension coincides with the rate $\nu(\rho)$ and is equal to $\nu(\rho) = \alpha_c = 1$. These

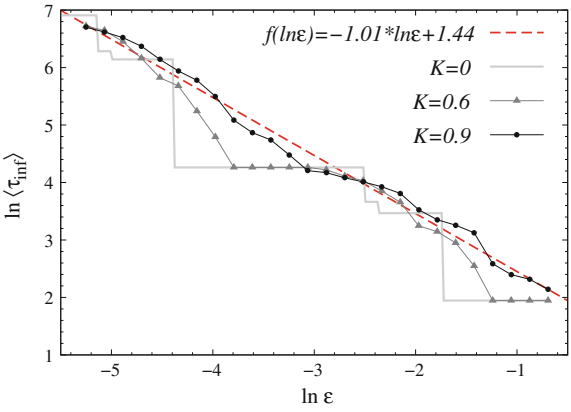

Fig. 2.12 Calculation results for $\ln\langle\tau_{\inf}(\varepsilon)\rangle$ in the map (2.6) for $\rho = e$ and three different values of K: $K = 0$, $K = 0.6$, and $K = 0.9$

conclusions have been confirmed by numerical simulation with other values of the rotation number and for $0 < K < 1$. This is exemplified in Fig. 2.12 for $\rho = e$. It shows that the dependence $\ln\langle\tau_{\inf}(\varepsilon)\rangle$ for $K = 0.9$ is a straight line with unit slope. It means that the AP dimension is equal to 1, $\alpha_c \approx 1.0$.

We note an important point. It is known that in the case of an irrational rotation number, the nonlinear circle map (2.6) can be transformed (or reduced) to the linear circle map $\psi_{n+1} = \psi_n + \Delta$ by using a suitable nonlinear change of variable $\psi = g(\theta)$ [6, 20]. This change must satisfy the property $g(\theta + 2\pi) = 2\pi + g(\theta)$. The result described above for the AP dimension $\alpha_c = 1$, which has been obtained both for the linear and the nonlinear circle map, testifies that the AP dimension is an invariant with respect to the nonlinear change of variables.

2.6 Fibonacci Stairs and the Afraimovich–Pesin Dimension for a Stroboscopic Section of a Nonautonomous van der Pol Oscillator

In addition to periodic oscillations, so-called quasiperiodic oscillations are widely and frequently encountered in nature and technology. Such oscillations are described by functions of the following form:

$$x(t) = \Phi[\gamma_1(\omega_1 t), \gamma_2(\omega_2 t) \ldots \gamma_n(\omega_n t)] \tag{2.38}$$

where each function $f_n(\omega_n t)$ is periodic with period $T_n = 2\pi/\omega_n$. We are interested in quasiperiodic oscillations with two frequencies ω_1 and ω_2. They are associated with a two-dimensional torus in the phase space. When the frequencies ω_1, ω_2 are rationally related, a resonance takes place on the torus and a limit cycle is realized. If the frequencies become irrationally related, the motion on the torus will be nonperiodic

or ergodic. The phase trajectory covers the torus surface everywhere densely and does not close as $t \to \infty$.

If we introduce a Poincaré secant plane which intersects a torus transversally, the points that appear when a trajectory intersects the plane generate a discrete sequence ψ_n lying on the closed curve. This sequence is described by the following equation [21, 22]:

$$\psi_{n+1} = \psi_n + \Delta + f(\psi_n) \tag{2.39}$$

where Δ is a shift of each subsequent point relative to the previous one and $f(\psi_n)$ is a certain periodic function. If only the first term of the expansion of $f(\psi_n)$ in a Fourier series is taken into account, the following discrete equation can be derived:

$$\psi_{n+1} = \psi_n + \Delta + K \sin \psi_n, \quad \mod 2\pi. \tag{2.40}$$

The variable ψ_n can be treated as the coordinate of a point on the circle in the torus section, the parameter $\Delta = 2\pi\rho$ includes the rotation number ρ and characterizes the frequency detuning, and the parameter $0 < K < 1$ is related to the amplitude of oscillations at one of the independent frequencies. Equation (2.40) describes the circle map and serves as a classical model of nonlinear dynamics for modeling the dynamics of two-frequency quasiperiodic oscillations [21–25]. If the nonlinear term in (2.40) is neglected, one can come to the model of a linear circle shift

$$\psi_{n+1} = \psi_n + \Delta, \quad \mod 2\pi, \quad \Delta = 2\pi\rho. \tag{2.41}$$

The circle map (2.40) is frequently used to study effects of synchronization and the transition to chaos via two-frequency oscillation destruction [26, 27].

The regime of two-frequency oscillations can be realized in several ways. For example, one can use two coupled self-sustained oscillatory systems with different basic frequencies. The simplest way consists in considering a self-sustained oscillatory system subjected to an external periodic force. Introducing the Poincaré secant plane of a two-dimensional torus results in a discrete set which must correspond to the circle map (2.40) for small values of the external amplitude. Alternatively, the circle map can be obtained by constructing a discrete set in the stroboscopic section of a phase trajectory through the period of the external force [21]. If the integration step $\Delta t = T/j$ where j is an integer, the set of points in this cross section is computed with maximum accuracy. This method is often known as the stroboscopic technique.

We consider a periodically driven van der Pol oscillator and apply the stroboscopic method to obtain a discrete set which is equivalent to the circle map. The next objective of our work is to show that the features of recurrence statistics established for the circle shift in the framework of the global theory can be reliably observed for the set in the stroboscopic section of the driven van der Pol oscillator. With this purpose, we construct the Fibonacci stairs and calculate the Afraimovich–Pesin dimension for different irrational values of the rotation number. In conclusion, we compare the theoretical results formulated for the circle shift (2.41) with our numerical data for the driven van der Pol oscillator.

2.6.1 System Under Study

The classical periodically driven van der Pol oscillator is described by the following equation:

$$\ddot{x} - (\alpha - x^2)\dot{x} + \omega_0^2 x = A \sin \Omega t. \tag{2.42}$$

We rewrite (2.42) in the form of a system of three first-order differential equations:

$$\begin{cases} \dot{x} = y\,, \\ \dot{y} = (\alpha - x^2)y - \omega_0^2 x + A \sin \Theta\,, \\ \dot{\Theta} = \Omega \end{cases} \tag{2.43}$$

where α is the excitation parameter, ω_0 is the basic frequency of the self-sustained oscillations, A is the amplitude of the external force, $\Theta = \Omega t$ is the phase, and Ω is the frequency of the external force.

In contrast to the work [28], we do not pass to the equations for the amplitude and phase. Numerical simulation has shown that the calculation accuracy can be significantly increased by using the system (2.43) directly. This enables us to compare the theoretical and numerical results in more detail.

For $A \approx 0$ and $\alpha > 0$ in (2.42), a limit cycle is born with amplitude $2\sqrt{\alpha}$. In the three-dimensional system (2.43) for $A > 0$, we have quasiperiodic oscillations corresponding to a two-dimensional torus in the phase space. The torus can be ergodic or resonant depending on the ratio of frequencies ω_0 and Ω. We are interested in the case of an ergodic torus when the ratio of the frequencies (rotation number) is irrational.

We apply the stroboscopic technique to the system (2.43). This means that we observe the driven system at the times $t_j = j \cdot T$ where $T = \frac{2\pi}{\Omega}$ is the period of the external force and $j = 1, 2, \ldots$. This observation results in the set of points shown in Fig. 2.13 together with a two-dimensional torus in the system (2.43). It is clearly shown in the figure that the map is quite equivalent to the circle shift.

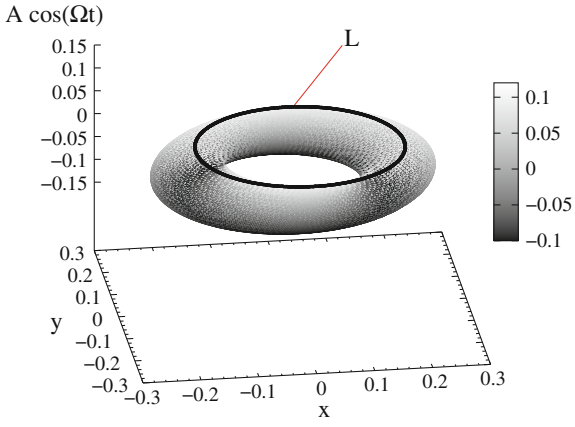

Fig. 2.13 A two-dimensional torus and its stroboscopic section L in the system (2.43) for $\alpha = 0.01$, $\omega_0 = 1.0$, $\Omega = 1.1835944$, and $A = 0.1$

2.6.2 Numerical Results

In the general case of finite values of the external force amplitude $A > 0$, the set in the stroboscopic section corresponds to the nonlinear circle map (2.40):

$$\psi_{n+1} = \psi_n + \Delta + K(A)\sin\psi_n. \tag{2.44}$$

One can expect that for small $A \ll 1$, the coefficient $K(A)$ also satisfies the condition $K(A) \ll 1$, and in this case, the map (2.44) is similar to (2.41). Therefore, we are going to consider the cases of small and relatively large values of the amplitude of the external force A.

In order to compare the presented results with the theoretical data [2] and the calculations carried out in [15, 28], one needs to clarify the way of definition of the rotation number ρ.

The rotation number ρ can be defined as the mean increment of the angle ψ per one iteration of the circle map in relation to the total angle:

$$\rho = \lim_{n\to\infty} \frac{\psi_n - \psi_0}{2\pi n}. \tag{2.45}$$

It is easy to see that for $K(A) \to 0$, the parameter Δ in (2.44) represents a linear phase shift on a circle and is related to the rotation number as $\Delta = 2\pi\rho$. Moreover, in this case, the rotation number depends on the basic frequency ω_0 of the van der Pol oscillator and the frequency of the external force Ω. The dependence $\rho(\Omega)$ is shown in Fig. 2.14 for the fixed parameter values $\alpha = 0.01$, $\omega_0 = 1$, $A = 0.1$. As shown, the plot corresponds to the relation

$$\rho = \omega_0/\Omega \tag{2.46}$$

with the accuracy of $\pm 0.1\%$.

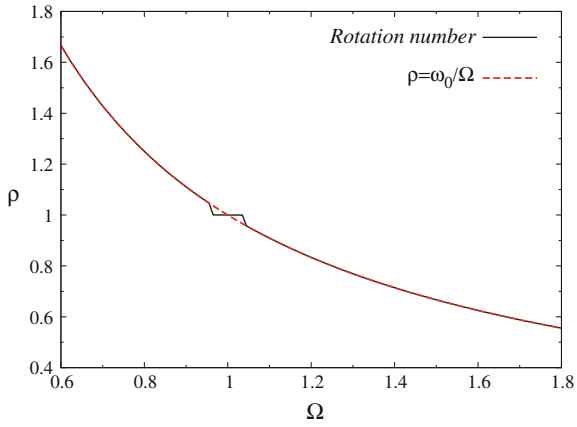

Fig. 2.14 Dependence of the rotation number ρ on the external frequency Ω in the system (2.43) for $\omega_0 = 1$, $\alpha = 0.01$, and $A = 0.01$

When $\omega_0 = \Omega = 1$, the resonance $1:1$ can be observed in Fig. 2.14. The theoretical curve must have an infinite number of "plateus" which correspond to resonances $\omega_0/\Omega = l/q$ where $l, q = 1, 2, \ldots$. This curve is called the "devil's staircase" [29]. However, high-order resonances ($q > 1$) are not visible in the scale of Fig. 2.14 because they can be observed only within the narrow intervals with respect to Ω, and the external amplitude is much less than the amplitude of oscillations in the van der Pol oscillator.

2.6.2.1 The Case of Small Values of the External Amplitude

We now consider the case of small values of the external amplitude ($A = 10^{-5}$). The set in the stroboscopic section of the system (2.43) is shown in Fig. 2.15a on the plane of variables (x_s, y_s). It looks like a circle with radius $r = \sqrt{x_s^2 + y_s^2}$. Since for $\alpha = 0.01$ the amplitude $r = 0.2$ is constant, the sequence of phase shifts ψ_n can be analyzed in the polar system of coordinates: $x_{sn} = r\cos\psi_n$, $y_{sn} = r\sin\psi_n$.

The set of values ψ_n must satisfy the circle map (2.44). Let us consider the case of small values of the external amplitude $A \ll 1$. Figure 2.15b shows the probability distribution density $p(x_s, y_s)$ of points on the circle (Fig. 2.15a) for the golden ratio $\rho = (\sqrt{5} - 1)/2$. As shown in the figure, $p(x_s, y_s)$ is rather uniform and corresponds to the linear circle shift (2.41). If this is true, then only local approach can be used to calculate $\langle \tau_{\text{inf}}(\varepsilon) \rangle$ by varying ε in a certain interval (for any point on the circle). This is related to the fact that for a uniform distribution, $\tau_{\text{inf}}(\varepsilon)$ is independent of the choice of ε on the circle length. The calculation results for $\tau_{\text{inf}}(\varepsilon)$ are presented in Fig. 2.16 for the golden ratio. In contrast to the results of [28], in a wide range of ε values, the numerical plot in Fig. 2.16 is qualitatively and quantitatively consistent with the calculation data for the linear circle map (2.41), which are presented in Fig. 2.2a. This is due to an increase of the calculation accuracy of the stroboscopic section.

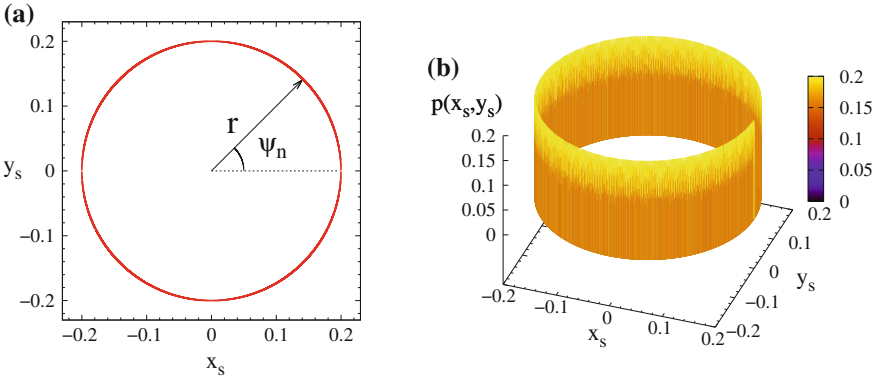

Fig. 2.15 The stroboscopic section (**a**) and the probability distribution density $p(x_s, y_s)$ on the *circle* (**b**) for $\alpha = 0.01$, $\omega_0 = 1$, $A = 10^{-5}$. The value $\Omega = 1.6180141526367187$ corresponds to the golden ratio $\rho = (\sqrt{5} - 1)/2$

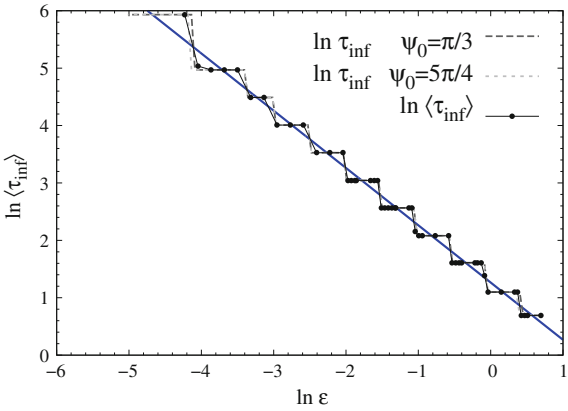

Fig. 2.16 The Fibonacci stairs for the stroboscopic section of phase trajectories in the system (2.43) for $\alpha = 0.01$, $\omega_0 = 1.0$, $A = 10^{-5}$, $\rho = \omega_0/\Omega$, and $\Omega = 1.6180141526367187$. The curve with points corresponds to the global approach; *dashed lines* are constructed by using the local approach when recurrences are calculated in neighborhoods of the points $\psi_0 = \pi/3$ and $\psi_0 = 5\pi/4$. All curves are approximated by a *straight line* with slope $\alpha_c = 1$

Comparing Figs. 2.2a and 2.16 reveals that all the dependences coincide in the range $-4 < \ln \varepsilon < 1$. The sequence of τ_{inf} on the steps of the Fibonacci stairs in Fig. 2.16 strictly complies with the basic Fibonacci series. The height and width of the stairs steps are $D_i \simeq |\ln \rho|$. The average slope of the linear approximation is equal to -1 and gives the AP dimension $\alpha_c = 1$. When $\ln \varepsilon < -4$, the Fibonacci stairs is gradually destroyed. This is due to the accuracy of calculations and to the fact that the distribution density $p(x_s, y_s)$ becomes inhomogeneous for sufficiently small ε. Nearly identical results have been obtained for the external amplitude taken in the range $10^{-8} \leq A \leq 10^{-3}$. One may say that for small values of $A \leq 10^{-3}$, the map in the stroboscopic section has the properties of the circle shift (2.41) with a rather high degree of accuracy.

To confirm the results described above, we consider the case of the silver ratio $\rho = \sqrt{2} - 1$. The corresponding numerical results are shown in Fig. 2.17. In this case, the frequency of the external force is set to be $\Omega = 0.414209134578705$.

Since the external amplitude $A = 10^{-8}$ is very small, the numerical data in Fig. 2.17a, b demonstrate their good qualitative and quantitative agreement. The sequence of $\tau_{\text{inf}}(\varepsilon)$ on the stairs steps corresponds to the basic Pell series. The height and width of the steps are $D_i \simeq |\ln \rho|$.

2.6.2.2 The Case of Relatively Large Values of the External Amplitude

We now turn to relatively large values of the external amplitude $A > 10^{-3}$. In this case, the nonlinear item $K(A)$ in the circle map (2.44) may effect the results. The numerical data are shown in Fig. 2.18 for $A = 10^{-2}$. The distribution density

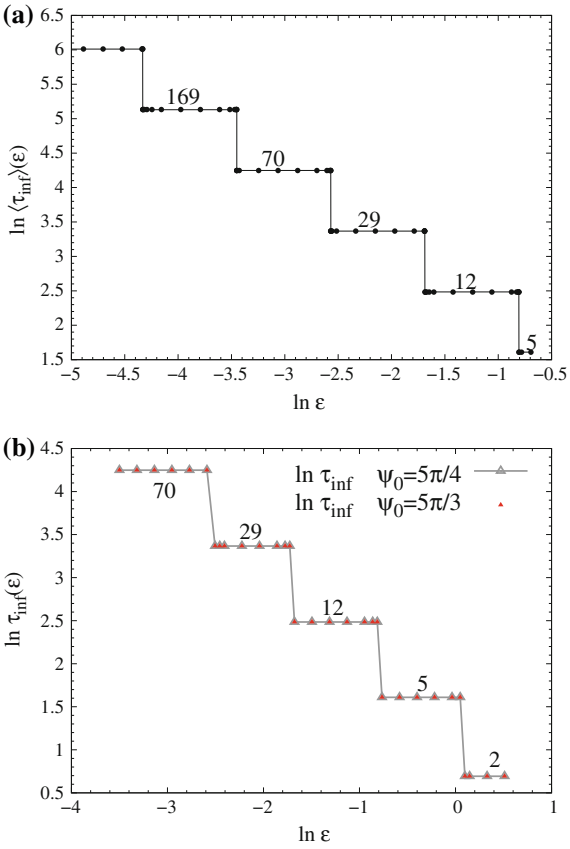

Fig. 2.17 The Fibonacci stairs **a** for the linear circle map (2.41) with $\Delta = 2\pi\rho$, $\rho = \sqrt{2} - 1$ and **b** for the map in the stroboscopic section of the system (2.43) for $\alpha = 0.01$, $\omega_0 = 1$, $A = 10^{-8}$, $\rho = \omega_0/\Omega$, and $\Omega = 0.414209134578705$

$p(x_s, y_s)$ becomes nonuniform (Fig. 2.18a), and $\langle \tau_{\inf}(\varepsilon) \rangle$ must be found by covering the whole set with intervals of size ε and then averaging the calculation data. As shown in Fig. 2.18b, if the external amplitude A increases, the Fibonacci stairs begins to break down. The average slope of the graph is approximately equal -1, i.e., the AP dimension retains the value of $\alpha_c = 1$. When A is further increased, the plot in Fig. 2.18b tends to a straight line with slope $\simeq -1$, as in the case of the nonlinear circle map (2.44) studied in [28].

We have also carried out numerical calculations for another values of the rotation number ρ by varying the external frequency Ω. The obtained results fully comply with the data described in [28], namely the Fibonacci stairs for another Diophantine rotation numbers loses its universal properties established for the golden and silver ratios. However, the AP dimension remains close to 1 ($\alpha_c \simeq 1.0$) both for small and relatively large values of the external amplitude $10^{-8} \leq A \leq 10^{-2}$. Figure 2.19 exemplifies the Fibonacci stairs calculated for the Diophantine rotation number $\rho = \sqrt[3]{2}$.

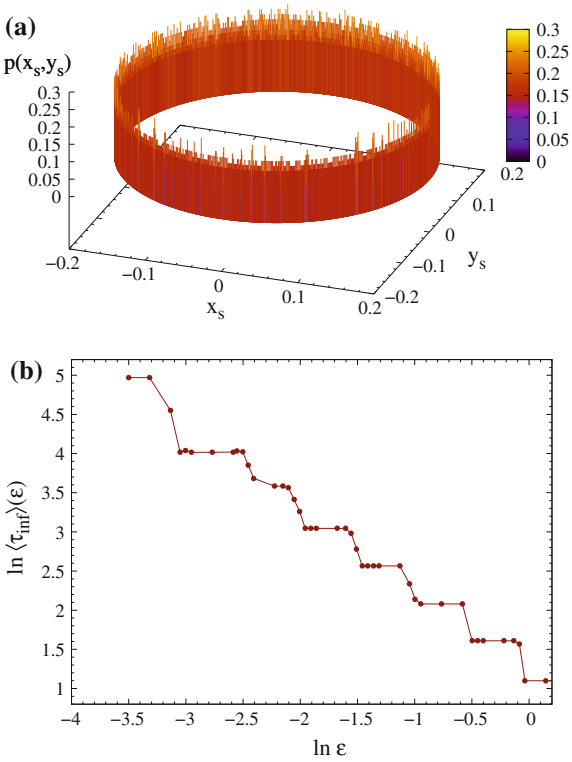

Fig. 2.18 The probability distribution density (**a**) and the Fibonacci stairs (**b**) for the map in the stroboscopic section of the system (2.43) for $\alpha = 0.01$, $\omega_0 = 1$, $A = 10^{-2}$, and $\rho = (\sqrt{5} - 1)/2$

Comparison of the plots in Fig. 2.19a, b testifies a good correspondence of the results. The average value of the slope of these graphs is close to -1 (-0.98 ± 0.01).

In this section, the results of the global analysis of Poincaré recurrence statistics have been presented for the set in the stroboscopic section of the driven van der Pol oscillator through the period of the external force. It has been established that this set can be described by the circle map (2.44) with the irrational rotation number $\rho = \omega_0/\Omega$. It has been shown that the stroboscopic map is close to the linear circle shift (2.41) in the case of small values of the external amplitude $A \ll 1$, while for relatively large values of A, it corresponds to the nonlinear circle map (2.44) due to the nonlinearity. The AP dimension is $\alpha_c \simeq 1$ in both cases. Our numerical simulation has confirmed the universal nature of the Fibonacci stairs (Figs. 2.16 and 2.17) for the golden and silver ratios. The height and width of the stairs steps have been numerically obtained to be equal to $D_i = |\ln \rho|$. The universality of the Fibonacci stairs is violated for other values of the rotation number (see Fig. 2.19). These results completely confirm the data obtained numerically for the map (2.44). The fact that the AP dimension remains equal to 1 both in the linear and nonlinear cases is caused by the invariance of the AP dimension with respect to a nonlinear change of coordinates. As discussed in [28], the map (2.44) can be reduced to the circle shift (2.41) by a suitable change of variables [21].

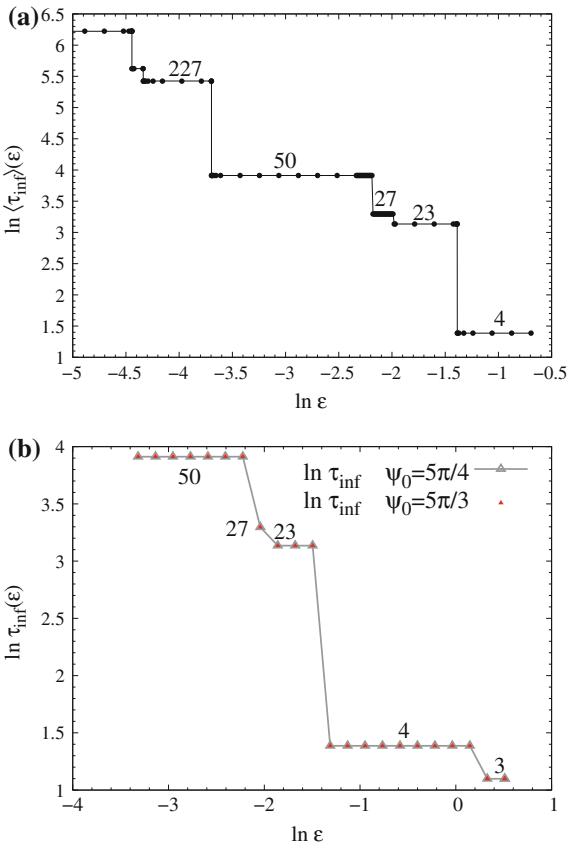

Fig. 2.19 The Fibonacci stairs **a** for the linear circle map (2.41) with $\Delta = 2\pi\rho$, $\rho = \sqrt[3]{2}$ and **b** for the map in the stroboscopic section of (2.43) for $\alpha = 0.01$, $\omega_0 = 1$, $A = 10^{-8}$, and $\rho = \sqrt[3]{2}$

2.7 Poincaré Recurrences in Hamiltonian Systems

Different fractal objects can be observed in the phase space of Hamiltonian systems. They have a complex structure which indicates the complexity in the system behavior [4]. For this reason, this type of systems can be rather interesting to analyze in terms of description of Poincaré recurrence statistics. From the standpoint of Poincaré recurrence theory, Hamiltonian systems were explored long ago [30], while they have only been recently studied in the framework of multifractal analysis [3, 4, 31–33]. The cited works are mainly based on the study of the probability distribution of recurrences which are obtained by using the method of multifractal analysis [4]. Hamiltonian systems can be exemplified by the Hénon–Heiles model [34], scattering billiards (Sinai billiards), a periodically kicked rotator, a double pendulum [35], and several discrete-time systems [3, 4, 36].

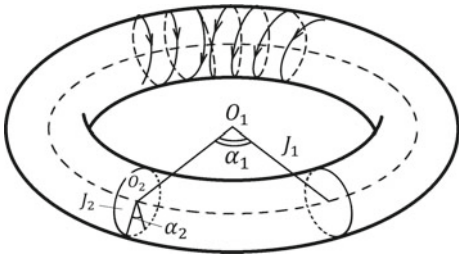

Fig. 2.20 Schematic representation of the phase space of a system with two degrees of freedom

Let us consider one of such systems, namely a periodically driven nonlinear conservative oscillator which is described by the following equations:

$$\begin{aligned} \dot{x} &= y, \\ \dot{y} &= -\sin x + b \sin \Theta, \\ \dot{\Theta} &= \Omega \end{aligned} \tag{2.47}$$

where the oscillation amplitude of the autonomous oscillator is equal to 1 and its frequency is $\omega_0 = 1$. The external force is defined by the amplitude b and frequency Ω. When the variables "action—angle" are used (if the canonic transformation $(\vec{q}, \vec{p}) \rightarrow (\vec{\alpha}, \vec{J})$ is possible), the dynamics of such systems can be visibly represented as follows: the circular motion with the center at O_1, which is formed by the α_1, J_1 variables, and simultaneously the rotation along the circle centered at O_2 (lying in the plane which is transversal to the plane of the O_1 circle), which is formed by the α_2, J_2 variables (Fig. 2.20). The superposition of these rotations defines the motion on a two-dimensional torus.

The behavior of phase trajectories depends crucially on the frequency ratio Ω/ω_0. If the ratio is rational, i.e., $\Omega/\omega_0 = k/m$ where k and m are integers, then in a certain time $T = 2\pi(k\Omega + m/\omega_0)$, the trajectory returns to the point which it leaves at the time $t_0 = t - T$. When the frequencies are irrationally related, the phase trajectory does not close on itself and covers the torus surface everywhere densely.

Phase portraits for the system (2.47) are shown in Fig. 2.21 (left column) for several values of the parameter b. Starting with a certain value of b, quasiperiodic and chaotic motions in the phase portrait become indistinguishable, so that we continue analyzing the Hamiltonian dynamics by applying the stroboscopic technique, i.e., we fix a sequence of points through the interval 2π on the phase variable Θ. In this case, periodic motions will be associated with a finite sequence of points, quasiperiodic motions—with closed trajectories, and chaotic behavior—with a random sequence of points. Related sets of points in the stroboscopic section of the system (2.47) are depicted in Fig. 2.21 (right column).

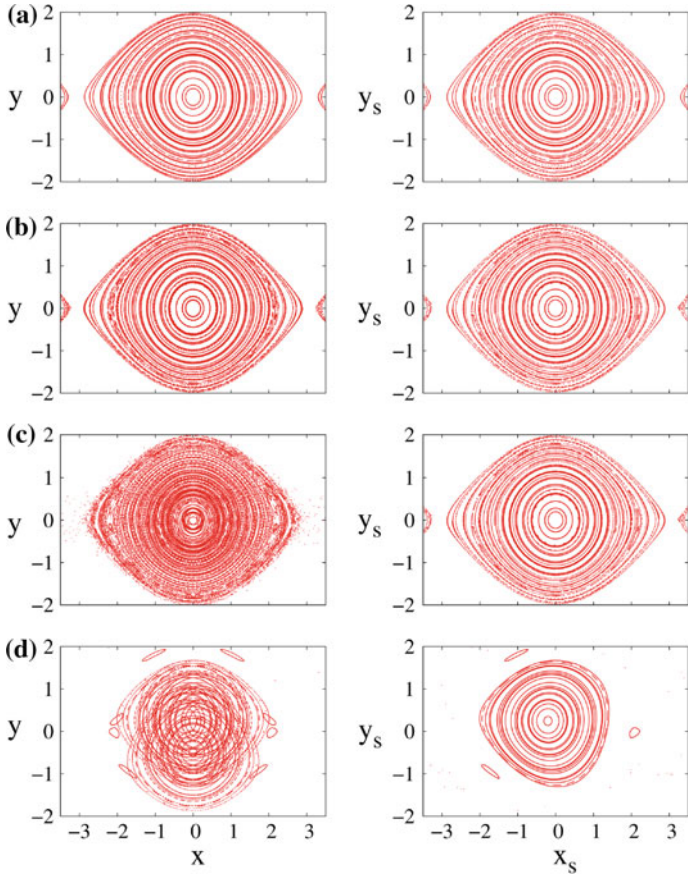

Fig. 2.21 Phase portraits (*left column*) and the corresponding sets of points in the stroboscopic section (*right column*) of the system (2.47) for $\Omega = 2\pi/3$ and different values of the parameter b: (a) $b = 0.001$, (b) $b = 0.01$, (c) $b = 0.1$, and (d) $b = 0.8$

2.7.1 Poincaré Recurrences in a Periodically Driven Nonlinear Conservative Oscillator

Let us consider what happens with the dependence $\ln\langle\tau_{\text{inf}}(\varepsilon)\rangle$ (2.13) in the case of Hamiltonian systems. We first fix $b = 0.001$ that corresponds to Fig. 2.21a. In this case, the phase portrait and the stroboscopic section look like a set of circles and ellipses with different radiuses. Falling on a particular set of points depends on initial conditions, so we fix the initial conditions as $x_0 = 0.44$ and $y_0 = 0$ which correspond to a circle with a constant radius ≈ 0.2. Thus, we can further turn to the polar system of coordinates and consider only one variable—the angle ψ instead of a pair of coordinates (x, y). Figure 2.22 illustrates the dependence of the rotation

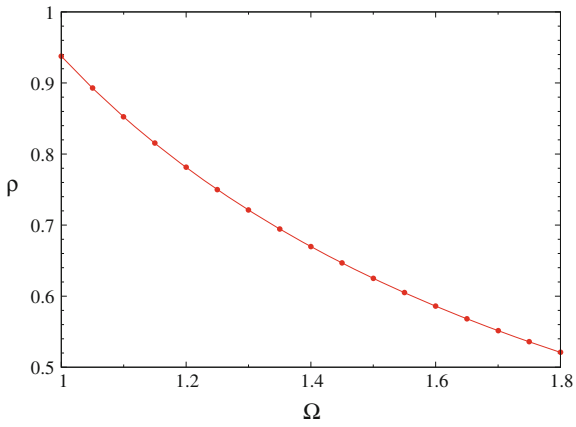

Fig. 2.22 The rotation number ρ as a function of the external frequency Ω in the system (2.47) for $b = 0.001$ and initial conditions $x_0 = 0.44$ and $y_0 = 0$

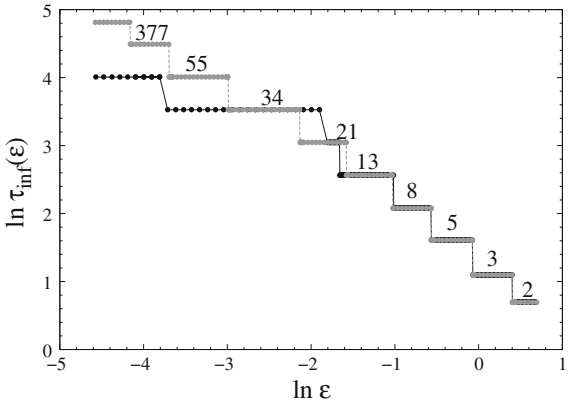

Fig. 2.23 Dependence of the minimal Poincaré return time on the size of the return region (local approach) in the system (2.47) for $b = 0.001$; $\Omega = 1.598233989$; and initial conditions $x_0 = 0.44$ and $y_0 = 0$. The *black curve* corresponds to the return vicinity of the point $\psi_0 = \pi/3$ and the gray curve—to the return region of the point $\psi_0 = 2\pi/3$

number on the external frequency Ω for the system (2.47). This plot is quite similar to that for $\rho = 1/\Omega$. On this basis, one can choose a value of Ω so that the rotation number is close to the golden ratio. However, one must take into account the fact that in Hamiltonian systems, frequencies and, consequently, rotation numbers depend strongly on the radius of a circle. This enables one to set the rotation number only with a certain error.

Figure 2.23 shows the dependence of minimal Poincaré return times (local approach) on the size ε of a return vicinity for two initial states $\psi_0 = 2\pi/3$ and $\psi_0 = \pi/3$. As shown in the figure, the dependences begin to diverge starting from the step with number 13.

Such a difference in the dependences results from the fact that even at $b = 0.001$ the probability distribution density is nonuniform (see Fig. 2.24). This implies that the local approach cannot be applied in the case of $b = 0.001$. Figure 2.25 shows the dependence $\tau_{\text{inf}}(\varepsilon)$ calculated using the global approach. It shows that the stairs

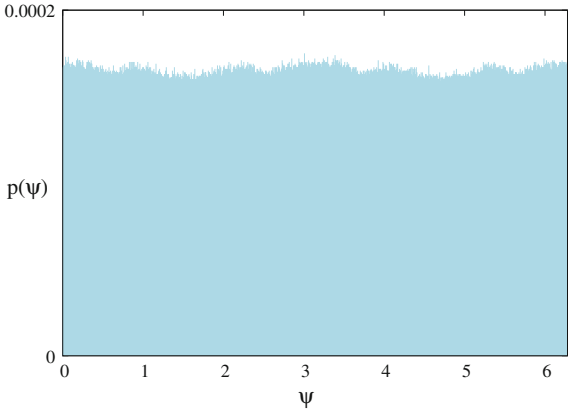

Fig. 2.24 Probability distribution density $p(\psi)$ in the system (2.47) for $b = 0.001$ and initial conditions $x_0 = 0.44$ and $y_0 = 0$

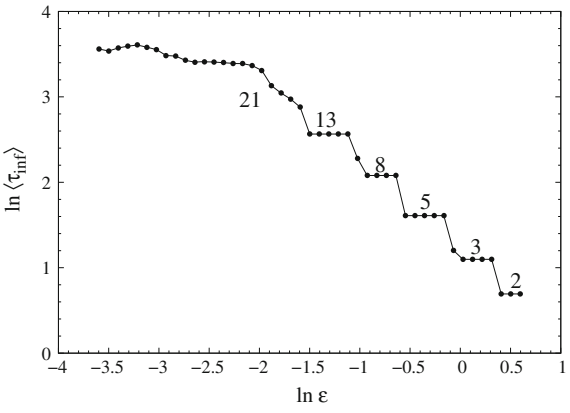

Fig. 2.25 Dependence of the mean minimal Poincaré return time on the vicinity size in the global approach for the system (2.47) at $b = 0.001$ and $\Omega = 1.598233989$

is destroyed also starting form the step $\langle \tau_{\text{inf}}(\varepsilon) \rangle = 13$. This is caused by a too large amplitude of the external force.

Calculation results for the local and global approaches are shown in Fig. 2.26 for $b = 0.00001$. As follows from the figure, when the global approach is applied, the staircase is broken later (from the step with number 34).

We may conclude that the dynamics of points on circles in Hamiltonian systems demonstrate the same regimes as the circle map. For a small external amplitude, the dependence $\tau_{\text{inf}}(\varepsilon)$ represents the Fibonacci stairs which is destroyed when the external amplitude b increases. It should be noted that for different rotation numbers and regardless of the nonlinearity degree of an invariant closed curve in (2.47), the AP dimension α_c turns out to be equal to unity in full compliance with the theory [2, 4]. The AP dimension is defined by the slope of the linear approximation of the step functions (Figs. 2.23, 2.25, and 2.26) in the range of ε values when the Fibonacci stairs is not yet destroyed.

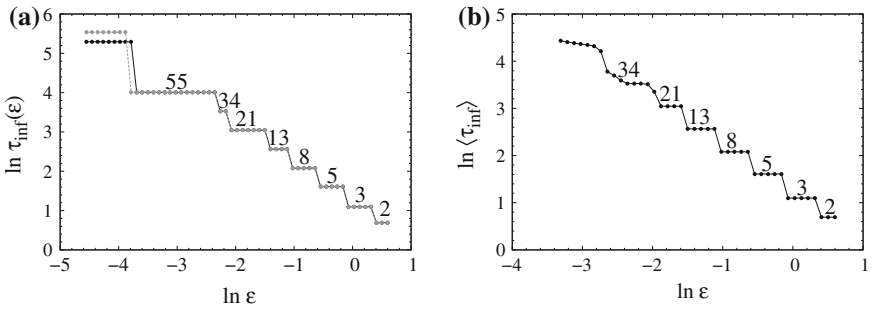

Fig. 2.26 **a** Dependence of the minimal Poincaré recurrence time on the vicinity size (local approach) in the system (2.47) for $b = 0.00001$; $\Omega = 1.598033989$; and initial conditions $x_0 = 0.44$, $y_0 = 0$. The *black curve* corresponds to the return vicinity of the point $\psi_0 = \pi/3$ and the gray curve—to the return region of the point $\psi_0 = 2\pi/3$. **b** Dependence of the mean minimal Poincaré recurrence time on the vicinity size (global approach) in the system (2.47) for $b = 0.00001$ and $\Omega = 1.598033989$

2.8 Conclusion

In the present work, we have described the numerical results for the statistics of Poincaré recurrence sequences in ergodic sets without mixing. We have considered sets in the dissipative circle map and in stroboscopic sections of the nonautonomous van der Pol oscillator and nonautonomous conservative oscillator. It has been found that in all the above examples, regardless of the nonlinearity degree, the Afraimovich–Pesin dimension is $\alpha_c = 1$, that is fully consistent with the theory developed for the linear circle shift [2, 4]. We have established that the dependence of $\ln \tau_{\text{inf}}(\varepsilon)$ on $\ln \varepsilon$ represents a step function and have substantiated theoretically its geometric properties. The universal geometry of the above dependence has been proven for the golden and silver ratios. The length and the height of the Fibonacci stairs steps are defined by $|\ln \rho|$ [15, 16]. The universality of the Fibonacci stairs is violated if rotation numbers are different from the golden and silver ratios as well as in cases caused by the growth of nonlinearity degree of the systems under consideration.

Acknowledgements This work was supported by RFBR (Grants No. 14-52-12002 and No. 15-02-02288) and the Russian Ministry of Education and Science (project code 1008).

References

1. Nemytskii, V.V., Stepanov, V.V.: Dover Books on Mathematics. Dover Publications, New York (1989)
2. Afraimovich, V.: Chaos **7**(1), 12 (1997)
3. Afraimovich, V., Zaslavsky, G.: Phys. Rev. E **55**, 5418 (1997)

4. Afraimovich, V., Ugalde, E., Urias, J.: Fractal Dimension for Poincaré Recurrences. Elsevier, Amsterdam (2006)
5. Kac, M.: Bull. Am. Math. Soc. **53**(10), 1002 (1947)
6. Hirata, M., Saussol, B., Vaienti, S.: Commun. Math. Phys. **206**(1), 33 (1999)
7. Penné, V., Saussol, B., Vaienti, S.: J. de Physique (Paris) Proceedings of the Conference "Disorders and Chaos", Rome **08**(6), 163 (1998)
8. Anishchenko, V., Astakhov, S., Boev, Y., Biryukova, N., Strelkova, G.: Commun. Nonlinear Sci. Numer. Simul. **18**(12), 3423 (2013)
9. Anishchenko, V.S., Astakhov, S.V.: Uspekhi Fizicheskikh Nauk **56**(10), 955 (2013)
10. Afraimovich, V., Lin, W., Rulkov, N.: Int. J. Bifurc Chaos **10**(10), 2323 (2000)
11. Anishchenko, V., Khairulin, M., Strelkova, G., Kurths, J.: Eur. Phys. J. B **82**, 219 (2011)
12. Pettofrezzo, A.J., Byrkit, D.R.: Prentice-Hall (1970)
13. Slater, N.: Proc. Camb. Philos. Soc. **63**(4), 1115 (1967)
14. Buric, N., Rampioni, A., Turchetti, G.: Chaos, Solitons Fractals **23**(5), 1829 (2005)
15. Anishchenko, V., Semenova, N., Vadivasova, T.: Discontinuity, Nonlinearity Complexity **4**(2), 111 (2015)
16. Semenova, N., Rybalova, E., Anishchenko, V.: Discontinuity, Nonlinearity and Complexity (2016)
17. Anishchenko, V.S., Boev, Y.I., Semenova, N., Strelkova, G.: Phys. Rep. **587**, 1 (2015)
18. Bicknell, M.: Fibonacci Q. **13**(4), 345 (1975)
19. Roth, K.: Mathematika **2**(1), 1 (1955)
20. Denjoy, A.: Math. Pures Appl. **11**(9), 333 (1932)
21. Pikovsky, A., Rosenblum, M., Kurths, J.: Synchronization: A Universal Concept in Nonlinear Sciences. Cambridge University Press, Cambridge (2002)
22. Kuznetsov, S.: Dynamical Chaos. Fizmatlit, Moscow (2001)
23. Arnold, V.: Am. Math. Soc. Transl. **2**(46), 213 (1965)
24. Ott, E.: Chaos in Dynamical Systems. Cambridge University Press, Cambridge (1992)
25. Schuster, H.G.: Deterministic Chaos. Physik-Verlag (1984)
26. Boyland, P.: Commun. Math. Phys. **106**(3), 353 (1986)
27. Rand, D., Ostlund, S., Sethna, J., Siggia, E.: Phys. Rev. Lett. **49**, 132 (1982)
28. Semenova, N., Vadivasova, T., Strelkova, G., Anishchenko, V.: Commun. Nonlinear Sci. Numer. Simul. **22**, 1050 (2015)
29. Rasband, S.N.: Chaotic Dynamics of Nonlinear Systems. Willey (1990)
30. Chirikov, B.V., Shepelyansky, D.L.: Physica D **13**, 395 (1984)
31. Chirikov, B.V., Shepelyansky, D.L.: Phys. Rev. Lett. **82**, 528 (1999). doi:10.1103/PhysRevLett.82.528
32. Chirikov, B.V., Shepelyansky, D.L.: Phys. Rev. Lett. **89**, 239402 (2002). doi:10.1103/PhysRevLett.89.239402
33. Shepelyansky, D.L.: Phys. Rev. E **82**, 055202 (2010). doi:10.1103/PhysRevE.82.055202
34. Lichtenberg, A., Liberman, M.: Regular and Stochastic Motion. Applied Mathematical Sciences. Springer, Berlin (1982)
35. Srivastava, N., Kaufman, C., Müller, G.: Comput. Phys. **4**, 549 (1990)
36. Feudel, U., Grebogi, C., Hunt, B.R., Yorke, J.A.: Phys. Rev. E **54**, 71 (1996). doi:10.1103/PhysRevE.54.71

Chapter 3
Success, Hierarchy, and Inequality Under Uncertainty

Dimitri Volchenkov

Domains with a lot of uncertainty have the highest likelihood of skilled people failing. Those that succeed the most under uncertainty are often simply those that tried harder and whose early luck compounded. By fostering hierarchical organization in a group, uncertainty ultimately leads to inequality. Wealth inequality in a population arises from risky decisions being taken under uncertainty by the vital few: The more adventurous traders are, the greater their fortune, and the fewer lucky ones there are. Scarcity also promotes inequality by necessitating competition and fueling conspicuous consumption. Existing econometric data suggest that rising income inequality is a global phenomenon, occurring whenever the national economy is out of step with the world average. Rampant inequality may transform the uncertainty of national economic development into uncertainty of international relations.

3.1 Introduction

Success comes with perseverance and improvements, opposing luck, over which we have zero control.

The probability model of success can be viewed as correlated Bernoulli trials, in which the probability to win in a random experiment with exactly two possible outcomes, "success" and "failure," would depend on the number of trials and previous (successful) outcomes. While the chances of getting lucky might be as small as

D. Volchenkov (✉)
Department of Mathematics & Statistics, Texas Tech University,
Broadway and Boston, Lubbock, TX 79409-1042, USA
e-mail: dr.volchenkov@gmail.com

D. Volchenkov and X. Leoncini (eds.), *Regularity and Stochasticity of Nonlinear Dynamical Systems*, Nonlinear Systems and Complexity 21,
DOI 10.1007/978-3-319-58062-3_3

$p_0 \ll 1$—perhaps, in the same vein as the likelihood of being struck by lightning—success results from the subsequent deliberate actions and skill acquisition with the aim to work on the opportune occasion for boosting its chances of recurrence in the future,

$$p \;\rightarrow\; p + \delta p. \tag{3.1}$$

The positive probability increment $\delta p > 0$ in (3.1) can describe the effectiveness of learning, or the gain of advantageous skill contributing toward a favorable outcome. It can also result from a preferential attachment mechanism where the probability of the next outcome in a series is proportional to the number of previous successful outcomes.

Although being a matter of random chance $p_0 > 0$, the launching phase of success often might be surprisingly controllable. For instance, as the initial phase of a new business is a search for the customer need that has not yet been addressed, the finding of a critical point that would represent a major business opportunity in the future can be accomplished via a predictable process, by identifying a set of market hypothesis and by sequential validating them through controlled experimentation [1].

As soon as the focus point of efforts is identified, it is time to put ourselves in a position to win. There are two factors contributing to the process of success: the number of times (the amount of time) we tried and the magnitude of probability increment δp.

However, the road to success is not that easy.

3.2 Enhancing Success Chances by Persistent Learning and Skill Acquisition

Individuals are capable of continually developing their abilities through persistence and effort. The degree to which early success (characterized by some probability $p_0 > 0$) causes subsequent success may be attributed to a learning process, in which existing knowledge, behaviors, and skills become modified and reinforced. Progress over time does not happen all at once, but builds upon and is shaped by previous knowledge.

We suppose that the efficiency of learning process can be described by the probability gain of getting success in the future, after every successful trial,

$$\delta p \;=\; p_n - p_{n-1} \;=\; \omega \;=\; \text{Const}, \tag{3.2}$$

which we assume a fixed constant $\omega > 0$ for simplicity. We suppose that $p_n = 1$ if $p_{n-1} + \omega > 1$, and $p_n = 0$ if $p_{n-1} + \omega < 0$.

Let us study the distributions of the numbers of successful outcomes in the model (3.2).

The positive probability increment $\omega > 0$ describes a positive feedback on the motivation to perform further trials after the previous success. The modification of the Bernoulli random process that includes a simple component of self-affirmation (3.2) has been introduced and studied in [2] in details.

We consider the trials as a series of N Bernoulli random variables u_i, $i = 1, \ldots, N$, with probabilities $1 - p_i$ and p_i for the outcomes "0" ("failure") and "1" ("success"), respectively. We are interested in the distribution $P_N\left(\sum_{i=1}^{N} u_i = n\right)$ of the n successes over N trials.

With no effect of learning, $p_i = p$, all u_i are independent identically distributed random variables and P_N is given by the binomial distribution

$$P_N\left(\sum_{i=1}^{N} U_i = n\right) = \binom{N}{n} p^n (1-p)^{N-n}. \tag{3.3}$$

The effect of positive feedback (3.2) for the bimodal model (3.3) is revealed by the geometric distribution of distances D_i between sequent success events,

$$P(D_i = d_i) = p_i(1-p_i)^{d_i-1}, \quad i = 0, \ldots, n, \tag{3.4}$$

with respect to the probabilities $1 - p_n$. Therefore, the desired distribution of successes,

$$P_N(n) = \sum_{\{\sum_i u_i = n\}} P(u_1, \ldots, u_N), \tag{3.5}$$

where $P(u_1, \ldots, u_N)$ is the joint probability distribution of the series of random variables $\{u_i\}$, can be calculated as

$$P_N(n) = \sum_{\{\sum_i d_i = N\}} p_0 \ldots p_{n-1}(1-p_0)^{d_0-1} \ldots (1-p_n)^{d_n-1} \tag{3.6}$$

where $1 \le d_i \le N - n$.

This marginal distribution satisfies an intuitively plausible Pascal-type recurrence relation for the probabilities $P_N(n)$, expressing the simple idea of that n successes in N trials can be reached either from n successes in $N - 1$ trials plus a final failure, or from $n - 1$ or from $n - 1$ successes in $N - 1$ trials and a final success:

$$P_N(n) = (1-p_n)\, P_{N-1}(n) + p_{n-1} P_{N-1}(n-1), \tag{3.7}$$

supplied by the boundary conditions $P_0(0) = 1$ and $P_N(n) = 0$, for $n > N$.

Multiplying (3.7) by x^n and summing over all $n = 0, \ldots, \infty$, one arrives at the equation

$$G_N(x) - G_{N-1}(x) = (x-1) H_{N-1}(x), \tag{3.8}$$

for the generating functions,

$$G_N(x) \;=\; \sum_{n=0}^{\infty} x^n P_N(n) \quad \text{and} \quad H_N(x) \;=\; \sum_{n=0}^{\infty} x^n p_n P_N(n). \tag{3.9}$$

Another equation required in order to accomplish the system is taken from the relation $p_n = p_0 + \omega n$ following for the probability gain (3.2),

$$H_N(x) \;=\; p_0 G_N(x) + \omega \cdot x \frac{\partial}{\partial x} G_N(x). \tag{3.10}$$

Combining (3.8) and (3.10), we obtain the following finite difference equation

$$G_N(x) - G_{N-1}(x) \;=\; (x-1)\left[p_0 + \omega \cdot x \frac{\partial}{\partial x}\right] G_N(x). \tag{3.11}$$

For $N\omega < 1$, we can use the continuum approximation $N \mapsto t$ and replace the finite difference in the left hand side of (3.11) by the time derivative that gives

$$\frac{\partial G(x,t)}{\partial t} \;=\; (x-1)\left[p_0 G(x,t) + \omega x \frac{\partial}{\partial x} G(x,t)\right], \tag{3.12}$$

with the following solution,

$$G(x,t) \;=\; \left[e^{\omega t} - x(e^{\omega t} - 1)\right]^{-p_0/\omega}. \tag{3.13}$$

The time continuum analog of the probability function $P_N(n)$ that corresponds to the generating function (3.13) is nothing else but a negative binomial distribution,

$$P_t(n) \;=\; e^{-p_0 t} \frac{\Gamma(p_0/\omega + n)}{n!\,\Gamma(p_0/\omega)} \left(1 - e^{-\omega t}\right)^n = \binom{r+n-1}{n} p^n (1-p)^r, \tag{3.14}$$

with respect to the time-dependent probability function $p = 1 - e^{-\omega t}$, and $r = p_0/\omega$. The derived continuum approximation (3.14) is valid for the total number of trials not exceeding $t_{\max} < \omega^{-1}$ and for the total number of success less than $n_{\max} = (1 - p_0)/\omega$. The probability density plot for the number of successful trials in the process with persistent learning, in which the initial probability of success is $p_0 = 0.1$ and the probability increment $\omega = 0.02$, is given in Fig. 3.1. When learning matters, the number of tries is attributed to skill. The probability gradients shown in Fig. 3.1 by arrows "worsen" the chances for success if the number of trials is small, but "enhance" these chances for longer trial sequences. Driving down cycle time in trials allows for more experiments, which can produce better results for those with early luck compounded.

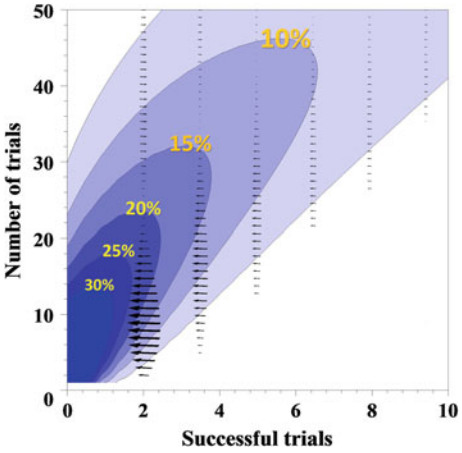

Fig. 3.1 The probability density of successful trials in the process with persistent learning, in which the initial probability of success is $p_0 = 0.1$ and the probability increment is $\omega = 0.02$. The *arrows* show the probability gradients

3.3 Like a Squirrel in a Wheel—Freud's Repetition Compulsion

Factors, over which we have no control, may play an important role in determining performance amidst uncertainty. When cause and effect are not well understood, or the environment is permanently changing the acquired skills do not necessarily pay off over time.

Domains with a lot of uncertainty have the highest likelihood of skilled people failing. The natural mechanism that can help to improve the long-term performance under uncertainty is *diversification of activities*. By getting involved in many different projects, e.g., by making a portfolio of many investments, or by bearing and raising many children, one can dramatically increase the chance of that advantageous skill and persistent efforts will redeem over time.

Let us consider a large group of individuals engaged in many different activities, each being characterized by some probability of initial success $p_0 > 0$ and by some probability increment $\omega > 0$, after every successful trial. The state of getting precisely $n < n_{\max}$ successful outcomes after $t < t_{\max}$ trials in every activity is then characterized by the probability (3.14) where $n_{\max}$ and $t_{\max}$ are precisely determined by p_0 and ω given.

According to the second law of thermodynamics, the equilibrium state of such a group striving for success in a variety of activities can be determined as a state of maximum entropy,

$$H(p_0, \omega) \;=\; -\sum_{n=0}^{n_{\max}} \sum_{t=1}^{t_{\max}} \left[P_t(n) \log_2 P_t(n) + (1 - P_t(n)) \log_2 (1 - P_t(n)) \right], \tag{3.15}$$

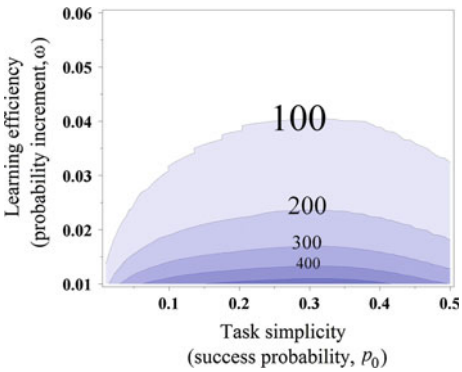

Fig. 3.2 The density plot of entropy (3.15) as a function of the learning efficiency (ω) and the probability of initial success (p_0). The contours correspond to the entropy levels of 100, 200, 300, 400, and 500 bits

which is featured by such a probability distribution $P_t(n)$ that can be achieved in the maximum number of ways, as being the most likely distribution to be observed over all individuals in the group. The phenomenological entropic force driving the group to increase its entropy of success can be expressed as the entropy gradient with respect to the parameters p_0 and ω, determining the chances for success.

It is worth a mention that the number of different (n, t)—states of having precisely n successful outcomes after t trials grows unboundedly when the probability increment tends to zero, $\omega \to 0$, and therefore, entropy of success (3.15) does either.

In Fig. 3.2, we have presented the density plot of entropy (3.15) as a function of the learning efficiency (characterized by the probability increment ω) and the task simplicity (quantified by the probability of initial success p_0). The contours shown in Fig. 3.2 correspond to the rising entropy levels of 100, 200, 300, 400, and 500 bits, respectively. As shown in Fig. 3.2, the value of entropy increases as the number of states grows, as $n_{\max}, t_{\max} \sim \omega^{-1}$ and tends to infinity for reducing probability increments, $\omega \to 0$. The maximum entropy gradient is observed for the initial probability of success $p_0 \approx 1/3$.

When initial success is random, skill does not necessarily play a role over time for improving the future chances for success. Therefore, when success breeds success, but initial success was random, the most likely behavior to be observed over the large enough group of individuals engaged in a variety of activities is to *make things into a matter of routine*, by continuously repeating actions over and over again, *without* searching for any improvement of the future chances for success.

Extreme uncertainty can be a serious distressing factor, indeed. Interestingly, the endless repetition of behavior, or life patterns, which was difficult (or distressing) in previous life was a key concept in Freud's understanding of mental life—*repetition compulsion* [3].

Being in a group in the face of uncertainty, we are forced to repeat always the same behavior pattern, without any improvement—as no lesson can been learnt from the old experience. The essential character traits which remain always the same and which are compelled to find expression in a repetition of the same experience

appeared to Freud as ultimately contradicting with the organism's search for pleasure and thus justified Freud's hypothesis [4]:

> hypothesis of a compulsion to repeat - something that seems more primitive, more elementary, more instinctual than the pleasure principle which it overrides.

In the later editions of his work, Freud had extended this point, by stating that

> such the repetitions are of course the activities of instincts intended to lead to satisfaction; but no lesson has been learnt from the old experience of these activities having led only to unpleasure.

3.4 The Rich Get Richer—Pareto Principle

Sociologist R. Merton first recognized the phenomenon of *accumulated advantage*, emerging when skill does not tell over time and diversification of activities is impossible, and dubbed it "*the Matthew Effect*," quoting a Bible passage in which the rich get richer and the poor get poorer.

The self-reinforcing behavior of certain probability distributions and stochastic processes is known since the early works of Gibrat [5] and Yule [6]. A stochastic urn process—a process in which discrete units of wealth, usually called "balls" (∘), are added continuously as an increasing function of the number of balls already present in a set of cells, usually called "urns" (| |), arranged in linear order,

$$|\circ\circ\circ\circ|\circ||\circ\circ|,$$

is the well-known example [7].

Let the size of the kth cell, t_k, be the number of balls in this cell plus one, i.e., the number of spaces existing in the cell: between two balls, or between two bars, or between a ball and a bar. The steady-state distributions of the cell sizes can be obtained if the number of cells n is increased proportionally as the number of balls is increased.

At each round of the urn process, either a bar or a ball is selected with probability α and $1-\alpha$, respectively.

If a ball is selected, it is thrown in such a way that each space in all cells has an equal chance of receiving it.

If a bar is selected, it is placed next to an existing bar, so that the new cell of unit size emerges at a rate α.

The average size of cells is therefore a random variable with mean $1/\alpha$. It is remarkable that the aggregate size

$$t = \sum_{k=1}^{n} t_k \tag{3.16}$$

of all cells is increased steadily by one at the end of the round, regardless of whether a bar or a ball is selected at any given round, either because the size of one of the cells is increased by one or because a new cell of size 1 is added. Thus, we can use t not only as the aggregate size but also as a counter for the number of rounds, i.e., time in the urn process.

Let $p(x,t)$ be the expected value of the number of cells with size x when the aggregate size of all cells is t. Then, for $x = 1$, we have

$$p(1,t+1) - p(1,t) \;=\; \alpha - \frac{(1-\alpha)}{t} p(1,t) \tag{3.17}$$

where α is the probability that $p(1,t)$ is increased by one and $(1-\alpha)p(1,t)/t$ is the probability that $p(1,t)$ is decreased by one as a result of a ball falling in one of the unit-sized cells.

It is clear that at the steady state, for all $x = 1, 2, ...$, it should be

$$P(x) \;=\; \frac{p(x,t+1)}{\alpha(t+1)} \;=\; \frac{p(x,t)}{\alpha t} \tag{3.18}$$

where αt is the expected value of the total number of cells after t rounds.

Setting $x = 1$, we can use the right-hand side of (3.18) in order to eliminate $p(x,t+1)$ from (3.17),

$$p(1,t) \;=\; \frac{\alpha t}{2-a}. \tag{3.19}$$

For $x > 1$, we have

$$p(xt+1) - p(xt) \;=\; (1-\alpha)\left[\frac{(x-1)p(x-1,t)}{t} - \frac{xp(x,t)}{t}\right]. \tag{3.20}$$

The latter equation assumes that the increase in the number of balls (accumulated wealth) in a cell is proportional to current cell size; it is impossible to make any cell better off (by increasing its wealth), without making at least one cell worse off.

Using (3.18) in (3.20), we then obtain

$$\frac{p(x,t)}{p(x-1,t)} \;=\; \frac{(1-\alpha)(x-1)}{(1+(1-\alpha)x)}. \tag{3.21}$$

If we define

$$\rho \;=\; \frac{1}{1-\alpha}, \tag{3.22}$$

it follows then from (3.21) that

$$\frac{p(x,t)}{p(x-1,t)} = \frac{x-1}{x+\rho}, \tag{3.23}$$

for any time t, and therefore, for the stationary distribution, it will be also true that

$$\frac{P(x)}{P(x-1)} = \frac{x-1}{x+\rho}. \tag{3.24}$$

Moreover, since the stationary probability to obtain a single unit of wealth is

$$P(1) = \frac{p(1,x)}{\alpha t} = \frac{1}{2-\alpha} = \frac{\rho}{1+\rho}, \tag{3.25}$$

this stationary probability distribution can be calculated by the following product:

$$P(x) = \frac{x-1}{x+\rho}\prod_{r=1}^{x}\frac{r-1}{r+\rho}. \tag{3.26}$$

The product formula (3.26) immediately gives the expression for the Yule distribution,

$$P(x) = \rho\frac{\Gamma(x)\Gamma(\rho+1)}{\Gamma(x+\rho+1)} = \rho B(x,\rho+1) \tag{3.27}$$

where $\Gamma(x)$ and $B(x)$ are the Gamma and Beta functions, respectively.

The cumulative distribution function for the Yule distribution (3.27),

$$F(x) = \sum_{i=x}^{\infty}\rho B(i,\rho+1) = \rho B(x,\rho) \tag{3.28}$$

is characterized by the skewed, heavy-tailed asymptote for $x \to \infty$, as

$$B(x,\rho) \to \Gamma(\rho)x^{-\rho}, \tag{3.29}$$

so that the limiting cumulative distribution follows a power law,

$$\lim_{x\to\infty} F(x) = \frac{\Gamma(\rho+1)}{x^{\rho}}. \tag{3.30}$$

According to (3.30), a relative change in the size of a cell (accumulated wealth) always results in a proportional change in the probability of its occurrence over all cells.

The exponent ρ in (3.30) is the inverse probability to add a ball (a unit of wealth) at a round that is nothing else but the average wealth per cell in the urn model.

The processes of accumulated advantage lead to the skewed, heavy-tailed (Pareto) distributions of wealth. The approximate power law distributions similar to (3.30) are observed over a wide range of magnitudes, in a wide variety of physical, biological, and man-made phenomena where an equilibrium is found in the distribution of the "small" to the "large" [8].

In particular, a power law distribution—the well-known Pareto distribution [9]—had been suggested in the context of the distribution of upper incomes and wealth among the population as early as in 1896:

$$F(x) \;=\; 1 - \frac{1}{x^{\rho}}, \quad 1 \le x \le \infty \tag{3.31}$$

where ρ is a fixed parameter called the Pareto coefficient and x is the variable size. It then follows that the probability density function for (3.31) can be described as follows:

$$f(x) \;=\; \frac{\rho}{x^{\rho+1}}, \quad 1 \le x \le \infty, \tag{3.32}$$

so that Zipf's law may be thought of as a discrete counterpart of the Pareto distribution.

The Pareto distribution (3.31) was used to describe the allocation of wealth over a population since a larger portion of the wealth is usually owned by a smaller percentage of individuals in any society. Therefore, it is intuitive that as income becomes larger, the number of observations is expected to decline, following a law dictated by some constant parameter.

This idea is sometimes expressed more simply as the *Pareto principle*, or the "*80-20 rule*"—the law of the vital few—which says that 20% of the population controls 80% of the wealth. Although the 80-20 rule corresponds to a particular value of $\rho \approx 1.161$, it becomes a common rule of thumb in business, e.g., "80% of sales come from 20% of clients." Pareto suggested the negative of the slope ρ might be an indicator of inequality in the underlying population, implying that small values of ρ relates to a high inequality. Under uncertainty, only the vital few accumulates advantage.

3.5 Inequality Rising from Risk Taking Under Uncertainty

An individual is risk averse if he is not willing to accept a fair gamble, with an expected return of zero. "*Anyone who bet any part of his fortune, however small, on a mathematically fair game of chance acts irrationally*," wrote Daniel Bernoulli in 1738 [10]. It is reluctance of a person to accept a bargain with an uncertain payoff rather than another bargain with a more certain, but possibly lower, expected payoff.

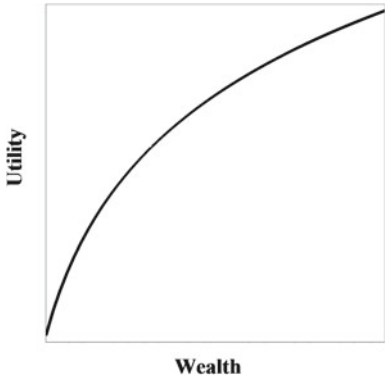

Fig. 3.3 Risk aversion implies that the utility functions are concave

People's preferences with regard to choices that have uncertain outcomes are described by the *expected utility hypothesis* [11]. This hypothesis states that under the quite general conditions the subjective value associated with an uncertain outcome is the statistical expectation of the individual's valuations over all outcomes. In particular, a decision maker could use the expected value criterion as a rule of choice in the presence of risky outcomes. The individual's *risk aversion* is accounted by a mathematical function called the utility function [10]. Utility refers to the perceived value of a good (or wealth), and the utility function (viewed as a continuous function of actual wealth) describes the attitudes toward risky projects of a "rational trader," whose objective is to maximize growth of his wealth in the long term. Such a trader would attach greater weight to losses than he would do to gains of equal magnitude. Thus, risk aversion implies that the utility functions of interest are concave (Fig. 3.3). The plausible example of utility functions is given by

$$U_\lambda(w) \;=\; \frac{w^\lambda - 1}{\lambda} \tag{3.33}$$

where $0 < \lambda < 1$ is the *risk tolerance* parameter—as λ decreases, traders become more risk averse and vice versa. In the limit of maximum risk avoidance, $\lambda \to 0$, and the function (3.33) turns into the Bernoulli logarithmic utility function [10],

$$\lim_{\lambda\to 0} U_\lambda(w) \;=\; \lim_{\lambda\to 0} \frac{\frac{d}{d\lambda}\left(e^{\lambda \ln w} - 1\right)}{\frac{d}{d\lambda}\lambda} \;=\; \ln w. \tag{3.34}$$

Let us consider a population characterized by some distribution of wealth p_w. The expected utility over the population is

$$v \;=\; \langle \ln w \rangle \;=\; \sum_w p_w \ln w. \tag{3.35}$$

According to the maximum entropy principle [12, 13], the system would evolve toward the state of maximum entropy characterized by the probability distribution which can be achieved in the largest number of ways, being the most likely distribution to be observed. We are interested in the probability distribution of wealth over the population p_w with maximum entropy

$$H_w = -\sum_w p_w \ln p_w, \tag{3.36}$$

under the condition of maximum risk avoidance. As soon as the expected logarithmic utility (3.35) is given, it is well known [14] that the maximum entropy (3.36) is attained for the power law distributed wealth.

Pareto distribution of wealth over the population arises under zero risk tolerance. Given expected utility υ, the Lagrangian functional for entropy function H_w subject to two constraints reads as

$$\mathcal{L} = -z\left(\sum_w p_w \ln w - \upsilon\right) - (\ln\zeta - 1)\left(\sum_w p_w - 1\right) - \sum_w p_w \ln p_w, \tag{3.37}$$

Then, the equation for the most likely wealth probability distribution to be observed is

$$-z\ln w - \ln\zeta - \ln p_w = 0. \tag{3.38}$$

The explicit solution of (3.38) is nothing else but the Pareto distribution,

$$p_w = \frac{w^{-z}}{\zeta(z)}, \quad w > 1 \tag{3.39}$$

where $\zeta(z) = \sum_w w^{-z}$ is the appropriate normalization constant. The value of the Lagrange multiplier z, which becomes the exponent in the power law (3.39), can be determined self-consistently as the solution of the equation $\upsilon(z) = -d\ln\zeta(z)/dz$.

In the case of less risk-averse population when $\lambda > 0$, the variation of the corresponding functional leads to the equation

$$-zU_\lambda(w) - \ln\zeta - \ln p_w = 0, \tag{3.40}$$

with the more uneven, exponential solution for the most likely wealth probability distribution,

$$p_w = \frac{1}{\zeta(z)} e^{-\frac{z}{\lambda}\left(w^\lambda + 1\right)}. \tag{3.41}$$

Therefore, we conclude that wealth inequality can be viewed as a direct statistical consequence of *making decisions under uncertainty under the condition of zero risk tolerance*. The more risk is taken by traders investing under uncertainty, and the more

unequal distribution of assets among them is likely to be observed in the long term. Wealth inequality among the population arises from taking risky decisions under uncertainty by the vital few: The more adventurous traders, the more their fortune, the less the number of lucky ones.

3.6 Generalized Mass-Action Principle—Emergence of Hierarchies Under Uncertainty

A graph is a representation of a set of objects (called *vertices*, or *nodes*), in which some pairs of objects may be connected by links (called *edges*). The *degree* of a vertex in a graph is the number of edges incident to it—its valence.

The random graphs with scale–free probability distribution of node degrees are ubiquitous in many real-world networks such as the World Wide Web, social, linguistic, citation, and biochemical networks; an excellent survey on scale–free properties of real-world networks can be found in [15]. Many of them are formed according to the preferential attachment principle, which together with its various modifications, could be seen as a particular case of *degree-mass-action* principle since the degree of a node acts in that as a positive affinity parameter (a *mass*) quantifying the attractiveness of the node for new vertices [16]. "Preferential attachment" is perhaps the most recent of many names that have been given to processes, in which a quantity is distributed over a number of units according to how much they already have.

Our first aim is to construct a family of static random graph models, in which vertex degrees are distributed according to a power law while edges still have a high degree of independence. Our aim is to mimic the community formation process under uncertainty. As usual in random graph theory, we will entirely deal with asymptotic properties in the sense that the graph size goes to infinity.

We consider graphs with the vertex set $V = V_n = \{1, ..., n\}$ where an edge between the vertices x and y (denoted by $x \sim y$) is interpreted as a persistent contact between the two. Given $x \in V$, its degree will be denoted by $d(x)$. We view edges as being generated by a pair-formation process, in which each individual vertex x chooses a set of partners according to a specified x-dependent rule.

The set of individuals which has a contact with the vertex x can be divided into two possibly not disjoint sets:

- the set of nodes which are chosen by x himself;
- the set of nodes which have chosen x as one of their partners.

We call the size of the first set the out-degree $d_{out}(x)$ of x and the size of the second one—the in-degree $d_{in}(x)$ of x. Obviously,

$$d(x) \ \leq \ d_{out}(x) + d_{in}(x), \tag{3.42}$$

and if the choices of partners are sufficiently independent, one can expect the equality in (3.42) to hold almost surely for infinitely large graphs, $n \to \infty$.

We partition the set of vertices V_n into groups $\{C_i(n)\}_{i\geq 1}$ where all members of the group $C_i(n)$ choose exactly i partners by themselves ($d_{out} = i$ on $C_i(n)$).

Let $P_\alpha^1(n, j)$ the probability for x to choose a fixed partner $y \in C_j(n)$, among n partners available for the choice, provided just a single choice will be made,

$$P_\alpha^1(n, j) \;=\; A_\alpha(n)\frac{j^\alpha}{n}. \tag{3.43}$$

Here, $A_\alpha(n)$ is a normalization constant such that

$$A_\alpha(n)\left(\sum_{i\geq 1}|C_i(n)|\frac{i^\alpha}{n}\right) \;=\; 1, \tag{3.44}$$

and α is a real parameter. Since we want $A_\alpha(n) \to A_\alpha$, as $n \to \infty$, we need that the sum $\sum_i |C_i(n)|i^\alpha/n$ to be bounded as a function of n which will impose the constraints on the constant α.

The parameter α in (3.43) acts as the degree of affinity, tuning the tendency to choose a partner with a high out-degree, or with low out-degree. Namely, if $\alpha = 0$, the choice is made without any preference, and $A_\alpha(n) \equiv 1$. For $\alpha > 0$, the "highly active" individuals are preferred, whereas the individuals of "low activity" are favored if $\alpha < 0$.

We then obtain the basic probability of x and y are connected in the graph,

$$\Pr[x \sim y] \;\simeq\; A_\alpha(n)\,\frac{i \cdot j^\alpha}{n}, \quad x \in C_i, \quad y \in C_j. \tag{3.45}$$

Concerning the size of the sets $C_i(n)$, we shall make the following assumption:

$$\frac{|C_i(n)|}{n} \;=\; p_i(n) \;\to\; \frac{c_1}{i^\gamma}, \quad \text{as} \quad n \to \infty. \tag{3.46}$$

With this choice, we have to impose the restriction $\alpha < \gamma - 1$ to ensure the convergence of $A_\alpha(n)$ as $n \to \infty$.

We also require $\gamma > 2$ since otherwise the expected in-degree for individuals from a fixed group would diverge. Note that the fixed out-degree distribution defines a probability distribution on each graph with vertex set V_n and therefore a random graph space $\mathcal{G}_n(\alpha, \gamma)$.

In order to compute the important pairing probabilities, we start with the easier case $\alpha = 0$:

$$\Pr(x \sim y \mid x \in C_i; y \in C_k) \;=\; \frac{i+k}{n} - \frac{ik}{n^2} \sim_{n\to\infty} \frac{i+k}{n} \tag{3.47}$$

Likewise, one can compute the corresponding probabilities for $\alpha \neq 0$. Dropping the details of calculations, we just state the result:

$$\Pr\left(x \sim y \mid x \in C_i\,;\, y \in C_k\right) \;\simeq\; A_\alpha \,\frac{(ki^\alpha + k^\alpha i)}{n}, \quad n \to \infty. \tag{3.48}$$

It turns out that for $\alpha < 2$ the typical community graphs in the model of community formation still have a *power law* distribution for the node degree although being characterized by the different exponents for the in-degree and out-degree components.

For $\alpha > 2$, we obtain a degree distribution, which follows a power law on average.

In order to compare both domains, we will use the integrated tail distribution

$$F_k \;=\; \Pr\left(d\left(x\right) > k\right). \tag{3.49}$$

We show that in both cases, $\alpha < 2$ as well as $\alpha > 2$, we, nevertheless, get the same tail of the degree distribution.

Since the partner choice under uncertainty is sufficiently random and is not strongly biased toward high degree individuals (i.e., the meaning of the condition $\alpha \leq \gamma - 1$), it is easy to see that the in-degree distribution of a vertex from the group C_i converges to a Poisson distribution with mean const $\cdot\, i^\alpha$ for $n \to \infty$,

$$\Pr(X{=}k) \;=\; \frac{\lambda^k e^{-\lambda}}{k!}, \quad \lambda \;=\; \text{const} \cdot i^\alpha. \tag{3.50}$$

Furthermore, there are essentially two regimes of community formation in the parameter space:

- for which the expected in-degree is of smaller order than the out-degree over all groups;
- for which the in-degree is asymptotically of larger order.

In the first case, it is clear that the in-degree is too small to have an effect on the degree distribution exponent. In other words, the set of individuals with degree k consists mainly of individuals whose out-degree is of order k. The further estimation shows that the expected in-degree of individuals from the group i asymptotically equals the power law

$$\langle (d_{in}\left(x\right) \mid x \in C_i) \rangle \;\simeq\; \text{const} \cdot i^\alpha. \tag{3.51}$$

Therefore, the in-degree is of smaller order than the out-degree if $\alpha < 1$. In the case $\gamma - 1 \geq \alpha \geq 1$, the set of individuals with degree k consists mainly of those whose index is of order $k^{1/\alpha}$.

We conclude that under uncertainty when the cumulative advantage is at work, there might be no parity of chances to choose a partner and to be chosen as a partner by other individuals.

In uncertain romantic relationships, love triangles are inevitable. While aiming at exclusive relationships with a partner, we always get an arrangement unsuitable to one or more of the people that might be involved: We either have to compete with

rivals for the love of the beloved, or have to split their attention between many love objects, so that love triangles become inevitable.

Hierarchical organization within large human groups integrated by chains of command would emerge under uncertainty in the pretty same way. As the group size grows, face-to-face interactions among all group members are not required, as the accumulated advantage featuring selection of partners for interactions makes probable only a few interactions between a superior and several subordinates, and this is enough to maintain integrity within the entire group. In the face of uncertainty, the group grows by adding hierarchical levels, and such a process obviously has no physical limit. However, the downside of hierarchical organization is that it inevitably leads to inequality [17].

By fostering hierarchical organization in a group, uncertainty ultimately leads to inequality. An egalitarian social ethos typical for the most of hunter-gatherers is possible only for small enough groups based on kinship and tribe membership, as equality requires active maintenance by means of continuous face-to-face interactions. While hierarchical organization emerges spontaneously amidst uncertainty (as seen among chimpanzees, forming themselves into hierarchies dominated by an alpha male), people living in small-scale societies possess numerous norms and institutions designed to control those individuals who attempt to dominate others [18]. However, such the norms cannot be efficiently implemented within large enough groups and among distantly living individuals. Thus, the side effect of selection for greater societal size was the appearance of permanent leaders and hierarchical organization [19].

3.7 Inverse Mass-Action Principle—Inequality Due to Uniqueness and Scarcity

In the *economics of location theory* introduced in [20] and developed by [21], a city, or a particular city district, may specialize in the production of special goods connected with a unique natural resource, the special education or capabilities of inhabitants, efficient policy, or unusually low expenditures. Cities and city districts can compete among themselves in a market of unique products that is not necessarily connected with the quantity of their inhabitants. The demand for these unique and precious products comes into the city district from everywhere and can be considered as exogenous. The degree of attractiveness of such a place can be specified by a real positive random variable $\omega > 0$ [22]. In the present section, we describe an edge formation principle in a random graph related to some degree of attractiveness a priori imposed on the vertex set in a large graph [16, 23].

Namely, we assume that attractiveness can be described by a real positive random variable ω that quantifies some attractive important property of an individual (such as its wealth or popularity), or beauty and importance of a place. The degree of attractiveness is distributed over the population (or all available places) with a given

probability distribution $\varphi(\omega)$. We shall demonstrate below that the particular form of the function φ is not important for the qualitative understanding of the advantage accumulation process.

Furthermore, we assume that a link between the two individuals (or places), x and y, arises as a result of a directed choice made by either x or y (symbolized by $x \to y$ or $y \to x$, respectively). Although the edge creation is certainly a directed process, in the present section, we consider the resulting graph to be undirected since for the majority of relevant transmission processes defined on the network, the original orientation of an edge is irrelevant.

We suppose that the pairing probability follows an *inverse mass-action principle*: The probability that x decides to connect to y characterized by its affinity value $\omega(y)$ reads as

$$\Pr\{x \to y \mid \omega(y)\} \sim \frac{1}{N} \cdot \frac{1}{\varphi(\omega(y))^{\alpha}}, \quad \alpha \in (0;1) \tag{3.52}$$

where N being the total number of vertices. Let us note that it is not the actual value $\omega(y)$ which plays a decisive role while pairing, but rather its relative frequency of appearance over the population.

The proposed principle captures the essence of antiquity markets: The more rare a property is, the higher is its value, and the more attractive it becomes for others. The paring probability model described above is called the *Cameo-principle*, having in mind the attractiveness, rareness, and beauty of the small medallion with a profiled head in relief called Cameo. And it is exactly their rareness and beauty, which gives them their high value [16, 23].

In practice, it is indeed difficult if ever possible to estimate exactly the actual value of ω for any individual (or a place) since such an assessment is obviously referred to both the economic and cultural factors at once that may vary greatly over the different historical epochs and across the certain population groups.

In the framework of a probabilistic approach, it seems therefore natural to consider the value ω as a real positive independent random variable distributed over the vertex set of the graph uniformly, according to a smooth monotone decreasing probability density function $f(\omega)$.

While introducing the model of Cameo graphs, we assume that

- The parameter ω is independent identically distributed (i.i.d.) over the vertex set with a smooth monotone decreasing density function $\varphi(\omega)$.
- Edges are formed by a sequence of *choices*. By a choice we mean that a vertex x chooses another vertex, say y, to form an edge between y and x. A vertex can make several choices although all choices are assumed to be made independently of each other.
- If x makes a choice, the probability of choosing y as a partner depends only on the relative density of $\omega(y)$ that is of the form (3.52).
- A predefined out-degree distribution determines the number of choices made by the vertices. The total number of choices (and therefore the number of edges) is assumed to be $\propto \text{const} \cdot N$.

We focus on the striking observation that under the above assumptions a scale-free degree distribution emerges independently of the particular choice of the $\omega-$ distribution. Furthermore, it can be shown that the exponent in the degree distribution becomes independent of $\varphi(\omega)$ if the tail of φ decays faster than any power law.

Let $V_N = \{1, ..., N\}$ be the vertex set of a random graph space. We are mainly interested in the asymptotic properties for $N \gg 1$. We assign to each element x from the set V_N a continuous positive real random variable $\omega(x)$ taken from a distribution with density function $\varphi(\omega)$. The variable ω can be interpreted as a parameterization of V_N. For a set

$$C_{\omega_0,\omega_1} = \{x : \omega(x) \in [\omega_0, \omega_1]\}, \tag{3.53}$$

we obtain

$$\left\langle \left(\sharp C_{\omega_0,\omega_1} \right) \right\rangle = N \cdot \int_{\omega_0}^{\omega_1} \varphi(\omega)\, d\omega \tag{3.54}$$

where $\sharp C_{\omega_0,\omega_1}$ denotes the cardinality of the set (3.53). Without loss of generality, we assume that $\varphi > 0$ on $[0, \infty)$ and that the the tail of the distribution for φ is a monotone function of $\omega > \omega_0$.

Edges are created by a directed process in which the basic events are choices made by the vertices. All choices are assumed to be independently identically distributed. The number of times a vertex x makes a choice is itself a random variable which may depend on x. We denote this random variable as $d_{out}(x)$. The number of times a vertex x is chosen in the edge formation process is called the in-degree $d_{in}(x)$. Although each choice generates a directed edge, we are interested in the corresponding undirected graph. In the what following about, we refer just to the original direction in the edge formation process.

Let the probability that a vertex y, with a fixed value of ω, is chosen by x is

$$p_\omega = \Pr\{x \to y \mid \omega = \omega(y)\}. \tag{3.55}$$

For a given realization ξ of the random variable ω, we assume that

$$p_\omega(\xi, N) = \frac{1}{N} \cdot \frac{A(\xi, N)}{[\varphi(\omega)]^\alpha} \tag{3.56}$$

where $\alpha \in (0, 1)$ and $A(\xi, N)$ is a normalization constant. It is easy to see that the condition

$$\int_0^\infty [\varphi(\omega)]^{1-\alpha}\, d\omega < \infty \tag{3.57}$$

is necessary and sufficient in order to get

$$A(\xi, N) \to A > 0, \quad N \to \infty, \tag{3.58}$$

so that it should be $\alpha < 1$.

One might argue that the choice probabilities should depend more explicitly on the actual realization ξ of the random variable ω over V_N, and not only via the normalization constant. The reason not to do so is twofold: First, it is mathematically unpleasant to work with the empirical distribution of ω induced by the realization ξ since one had to use a somehow artificial $N-$dependent coarse graining. Second, the empirical distribution is not really "observed" by the vertices (having in mind for instance individuals in a social network). What seems to be more relevant is the *common believe* about the distribution of ω. In this sense, our setting is a natural one.

The emergence of a power law distribution in the above settings is not a surprise. The situation is best explained by the following example. Let us take

$$\varphi(\omega) = C \cdot e^{-\omega}$$

and define a new variable

$$\omega^* = \frac{1}{[\varphi(\omega)]^\alpha} = \frac{e^{\omega\alpha}}{C^\alpha}.$$

The new variable ω^* can be seen as the effective parameter to which the vertex choice process applies. Then, the induced distribution of ω^* is

$$F(z) = \Pr\left\{\omega^* < z\right\} = \int_0^{\frac{1}{\alpha}\ln C^\alpha \cdot z} \varphi(\omega)\, d\omega = -\frac{1}{z^{1/\alpha}} - C, \tag{3.59}$$

and therefore, the ω^*-distribution is nothing else but a power law,

$$\phi\left(\omega^*\right) = \frac{1}{\alpha} \cdot \frac{1}{(\omega^*)^{1+1/\alpha}},$$

with an exponent depending only on α.

We conclude that a common belief about rarity (or scarcity) of a resource or an item automatically fosters inequality between individuals (or places) (i.e., revealed by the highly skewed distributions of accumulated advantage) with respect to accessibility to (or availability of) the scarce resource, independently of the particular choice of the $\omega-$distribution.

Scarcity always promotes inequality. It is remarkable that by no means an item has to be important for survival, for it to be scarce. However, people have to be ready to make a sacrifice by giving something up, or by making a trade-off in order to obtain more of the resource that is wanted so much (and viewed as scarce).

Thus, scarcity ultimately involves a scarifies for sake of *keeping up with the Joneses* indicating benchmarks for a particular social class and demonstrating the desire of an individual for upward social mobility.

Scarcity necessitates competition and fuel conspicuous consumption. Scarce resources necessitate competition, as "people strive to meet the criteria that are being used to determine who gets what" [24], and fuel conspicuous consumption, as people always care about their standard of living in relation to their peers [25].

3.8 Cross-Database Analysis Suggests the Worldwide Growth-Inequality Relation (U-Curve)

The American economist S. Kuznets had suggested [26] that as an economy develops, market forces first increase and then decrease economic inequality (see Fig. 3.4). Kuznets demonstrated this relationship using cross-sectional data about income inequality [27] collected in the middle of the twentieth century, in the USA. According to Kuznets, as a country develops, more capital is accumulated by the owners of industry, introducing inequality. However, more developed countries move then back to lower levels of inequality through various redistribution mechanisms, such as social welfare programs. Kuznets himself expressed concerns about the "fragility of the data" which underpinned the hypothesis and about that

> even if the data turned out to be valid, they pertained to an extremely limited period of time and to exceptional historical experiences [28].

The recent data show that after the 1970s the level of income inequality began to rise in the USA again [29] although a worldwide pattern of declining inequality had been intact until 1980 [30]. Then, a long and sharp period of increasing inequality has been observed worldwide, starting from 1981 through the end of the century that rather portrayed inequality as a global macroeconomic phenomenon in the globalized world than a net result of the disparate effects of technology, trade in national labor markets, and particular national policy choices [30].

The new databases that have become available recently can help us to understand how economic growth and inequality are related: whether growth produces inequality, and that inequality is a necessity for overall growth [31]. In the present section, we

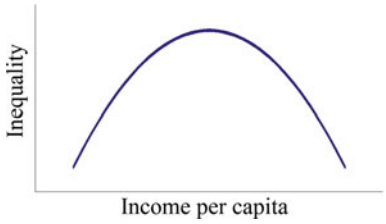

Fig. 3.4 As an economy develops, market forces first increase and then decrease economic inequality, as S. Kuznets suggested

report on the unprecedented cross-database analysis of inequality and economic performance for different world regions and time periods.

First, we have used all existent data series (1870–2014) in the *World Top Incomes Database* [32] as the source of inequality statistics available for the moment for 30 countries,[1] over the long period of time, including scattered and isolated data patches, such as the top income data records for Denmark attributed to 1870. In contrast to existing international databases, generally restricted to the post-1970 or post-1980 period, the top income database covers (although partially) nearly all of the twentieth century—a much longer period, which is important for the analysis because structural changes in income and wealth distributions often span several decades [32]. It is also important that by using data from the income tax records the studies underlying the database [29, 33–36] used similar sources and methods as the pioneering works by Kuznets [26, 27] for the USA.

Second, we have used the GDP historical database of the Maddison Project[2] [37] on the gross domestic product (GDP) per capita (per person) as the main source of data on economic development and evolving living standards. GDP per capita is a measure of product produced within a country's borders (the sum of the gross values added of all resident and institutional units engaged in production) divided by the resident population on a given date, the primary indicator used to gauge the health and size of a country's economy. The major advantage of GDP per capita as an indicator of standard of living is that the data are available for almost every country in the world and the technical definition of GDP per capita is consistent among different countries. The estimates of GDP per capita in the data of Maddison Project are given in the US dollars of 1990. The underlying methodology and main results on the economic growth in the world between AD 1 and 2010 were reported by the Maddison Project in [38].

We have used the *inverted Pareto–Lorenz coefficient* (IPLC) proposed in [29] as the measure of inequality. The IPLC is related to the standard Pareto coefficient for the top income shares,

$$\rho = \frac{1}{1 - \log_{10}\left(\frac{S_{10}}{S_1}\right)}, \tag{3.60}$$

by

$$\text{IPLC} = \frac{\rho}{\rho - 1} = 1/\log_{10}\left(\frac{S_{10}}{S_1}\right) \tag{3.61}$$

[1] The data series for the following countries have been used: Argentina, Australia, Canada, China, Colombia, Denmark, Finland, France, Germany, India, Indonesia, Ireland, Italy, Japan, Korea, Malaysia, Mauritius, the Netherlands, New Zealand, Norway, Portugal, Singapore, South Africa, Spain, Sweden, Switzerland, Taiwan, UK, USA, and Uruguay.

[2] The Maddison Project had been initiated in March 2010 by a group of close colleagues of Angus Maddison.

where S_{10} and S_1 represent the income shares of the top 10% and 1% of the population, respectively.

Larger values of the IPLC correspond to larger top income shares while the opposite is true for the standard Pareto coefficient (3.60), so that the IPLC provides a direct snapshot indication of top incomes. Recent studies on top incomes [29] have shown that the IPLC is effectively stable for any income distribution, in any given year and country, although it can vary over time due to a combination of economic and political factors.

We have presented all existent data series in the *World Top Incomes Database* [32] against the relevant GDP per capita data of the Maddison Project [37] in Fig. 3.5. Since the analyzed historical data on the relation between the economic growth and inequality is attributed to the different countries and covers almost one and a half century of economic development (1870–2014), we think that it might reveal a global trend, independently of short-term national economic miracles and misadventures.

Inequality is closely correlated with low growth, yet with high growth either. The entire data set (including marginal outliers) is best fitted by the parabolic trend line,

$$y = 2.5 - 0.114x + 0.004x^2,$$

or, equally well, by the hyperbolic cosine, $y = 0.72 + \cosh(0.084x - 1.18)$. As shown in Fig. 3.5, the level of inequality is maximum for low as well as for high values of GDP per capita, but is minimum (IPLC ≈ 1.6) for the intermediate GDP levels of approximately US$14,250. Interestingly, the observed GDP level of minimum inequality is very close to the mean GDP level of the world (US$14,402 for 2013) as estimated by the World Bank [39]. The observed trend may partially due to the fact that unprecedented economic growth observed in the last decades in most

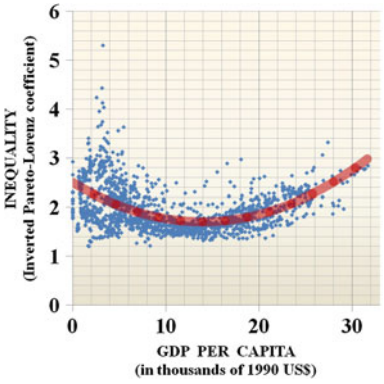

Fig. 3.5 All presently available data series (1870–2014) in the *World Top Incomes Database* [32] are given against the GDP per capita data of the Maddison Project [37]. The parabolic trend line ($y = 2.5 - 0.114x + 0.004x^2$) fits the data best (the goodness of fit of linear regression over the entire data set, including marginal outliers, is $R^2 = 0.26$; the goodness of the parabolic fit for the central part of the U-curve is $R^2 = 0.84$)

countries and expressed by the very high GDP figures goes along with growing inequality. The trend, however, suggests that as the economic growth is a global worldwide phenomenon, rising inequality accompanying that is a global worldwide phenomenon either, occurring once the national economy is out of step with the world average.

It is also remarkable that the observed trend in the relation between the economic performance and inequality is precisely the opposite to Kuznets's hypothesis [26] sketched in Fig. 3.4. As economy had developed, differences in inequality across rich countries were mostly down to the generosity of wealth redistribution. The economic and social policy regimes, providing important social protection for millions of industrial workers in developed countries, had proven to be adequate for a globally dominant industrial economy, underlying three decades of widely shared economic growth [40].

However, then the ever rising need to propel growth through risky entrepreneurship and innovation, into an era of globalization, deindustrialization, and economic dislocation fostered large financial rewards to the very top and bent incentives toward the short-term maximization of share prices rather than planning for long-term growth. The both factors apparently promote the unprecedented rise of inequality during the last 30 years [41, 42]. No surprise the present level of income inequality in the USA is comparable to that in Ghana and Turkmenistan. And, as reported in the *Global Wealth Report 2015* [43], just 0.7% of the world's adult population yet own 45% of all household wealth in 2015.

The empirically observed U-curve in the relationship between the economic performance and income inequality (presented on Fig. 3.5) can be understood in the context of probability models discussed in the present chapter. Namely, a stagnant planned/ command/palace economy aiming at the complete elimination of risks (e.g., by rationing food) engenders scarcity of virtually everything in the society. We have discussed in Sect. 3.7 on that scarcity might fuel ultimate inequality, as just a few redistributing people get the unfettered access to the scarce resources while the shares of others dwindle continuously.

At the opposite end, increasingly risky entrepreneurship and adventurous innovations necessary to propel economic growth foster inequality either, as we have proven in Sect. 3.5. Therefore, the both ends of economic performance—the richest and the poorest alike—are prone to live under conditions of rising inequality. Equality calls for active maintenance, as usual. We might suggest that on average the dynamics of inequality level is apt to obey the *law of pendulum* (Fig. 3.6), as it rises at the both ends of economic performance while is minimum in the middle of span, very close to the estimated mean GDP per capita of the world. The economy is growing there at a pace sufficient to meet fundamental human needs and to avoid shortages although the considerable share of earned income is redistributed among the entire society by means of the various social mechanisms such as taxation, monetary policies, and welfare at the cost of relative economic slowdown. The establishment and efficient functioning of such the redistributive mechanisms naturally require a broad public consensus to be reached about the necessity, harmlessness, and fairness of changes that would take place within the social institutions. However, such a social consensus

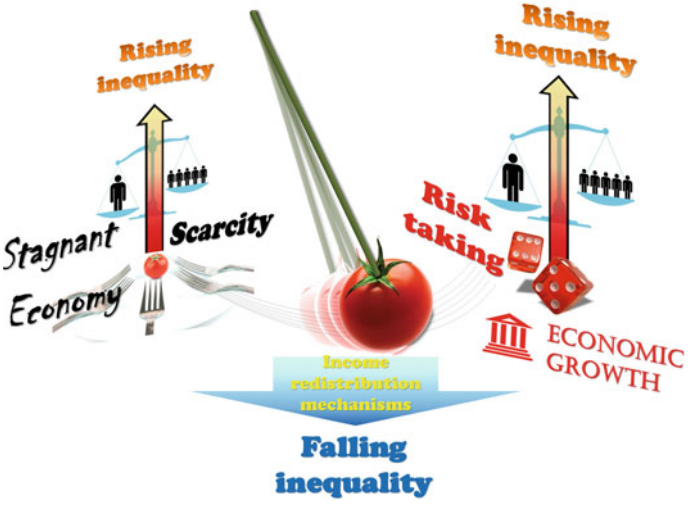

Fig. 3.6 The law of pendulum in inequality-growth relation. The level of inequality experiences rises in both low- and high-performing economies

based on a reciprocal willingness to sacrifice particular interests, including the quest for large domestic production and growth, for the common interest of rising social trust is not that easy to achieve, unless people face an existential threat to their way of life and their ultimate security. Perhaps, wars provide the most vital and compelling motive to gladly embrace the "economy and equality of sacrifice-satisfied"[3] that may open the door to the efficient application of inequality reducing policies.

While running its trail, the pendulum of rising inequality in one country inevitably pushes those in other countries. It is worth a mention that rampant inequality in a "winner-take-all economy" [42] breeds political polarization and boosts social mistrust, with a tendency to distort functioning of democratic institutions and to further erode social capital in the society [40, 41]. For the service economy rewards primarily highly educated and highly skilled elite while leaving displaced workers and unprotected middle class behind, the latter social groups find themselves unable to rely on the state for economic and social protection anymore. As the state fails to carry out its basic social functions, it is not more served and admired by the population majority, but rather endured and tolerated [44]. Rational country leaders facing common dissatisfaction with domestic policies and aggravating economic conditions that prompt their removal from office are likely to gamble on a risky *diversionary war*, as the diversionary war theory (DWT) suggests [45]. The data on the long-term inequality dynamics propose that during the last century the sharp increases of inequality level occur in many countries synchronously (see Fig. 3.7). Therefore, many a government at once may start considering the diversionary foreign

[3]Franklin D. Roosevelt: "A Call for Sacrifice," 28 April, 1942.

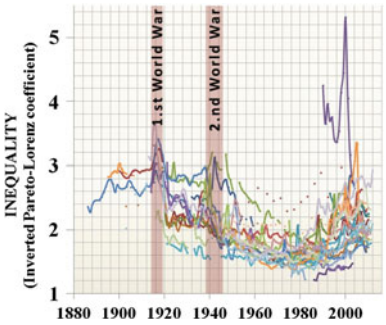

Fig. 3.7 The long-term dynamics of inequality level measured by the inverted Pareto–Lorenz coefficient for 30 countries. The data are taken from the *World Top Incomes Database* [32]

policy as leaving room only for gain essentially when preying on weaker states.[4] The use of modern hybrid warfare tactics that blend conventional warfare, irregular warfare, and subversive efforts, with an intention to avoid attribution and retribution, makes such a temptation almost irresistible.

The primary purpose of diversionary conflicts is to divert attention of the public away from domestic issues, increasing that available time the government has to address the internal troubles [46]. Furthermore, the external threat—either real or illusory—certainly unifies the country through the rally round the flag effect by creating a new out-group, other than the government, for the population to direct its dissatisfaction and by increasing a short-run popular support of the country leader. Moreover, when "*freedom hath fled from the world*"—in the absence of any prospect to improve the well-being and quality of life, to guarantee personal freedom and civil rights, and to promote upward social mobility, it is well known that *"the soldier, alone, is the freeman"*.[5] Taking part in a war as a mercenary or as a volunteer would

[4]The profound commentary on diversionary wars was given by Plato in *The Republic*: "*But when he [tyrant] has disposed of foreign enemies by conquest or treaty, and there is nothing to fear from them, then he is always stirring up some war or other, in order that the people may require a leader. To be sure. Has he not also another object, which is that they may be impoverished by payment of taxes, and thus compelled to devote themselves to their daily wants and therefore less likely to conspire against him? Clearly. And if any of them are suspected by him of having notions of freedom, and of resistance to his authority, he will have a good pretext for destroying them by placing them at the mercy of the enemy; and for all these reasons the tyrant must be always getting up a war. He must.*" (Translated by B. Jowett). Downloaded from *The Internet Classics Archive*, D.C. Stevenson, Web Atomics (C) 1994–2000.

[5]From "The Camp of Wallenstein" by Friedrich Schiller, *Musen-Almanach* für das Jahr 1798, 137–140, Scene **XI**; translated by J. Churchill.

> *Now freedom hath fled from the world, we find*
> *But lords and their bondsmen vile*
> *And nothing holds sway in the breast of mankind*
> *Save falsehood and cowardly guile.*
> *Who looks in death's face with a fearless brow,*
> *The soldier, alone, is the freeman now.*

become a cherished desire and a welcome breath of freedom for most young people vegetating in godforsaken provinces under the conditions of total social despair.

Of course, we may disagree with the general message of DWT, which is hard to prove quantitatively [47]. Nevertheless, the data on the long-term dynamics of inequality over 30 countries presented in Fig. 3.7 show convincingly that the sharp picks of inequality level visible synchronously for many countries at once *do* announce the periods of global conflicts and uncertainty of international relations a good deal in advance. The growing number and scale of international conflicts we are witnessing today apparently confirm this observation.

Rampant inequality may transform uncertainty of national economic development into uncertainty of international relations. In face of common challenges, a moderate economic growth, though might be considered as a relative backwardness, seems to be not such a big disgrace, as well as the rapid economic advancements might not look a source of that strong pride.

3.9 Conclusion

We have introduced and studied the probability model of success. The probability increments of getting success in the future can be maximized over time when the consistent efforts are made in a direction of highest positive impact and when the personal role of an actor within a team is increasingly important. This can be achieved, in particular, with the help of followers and supporters by commitment to the ethic of reciprocity focused on the simultaneous success of those around us.

We have shown that the ones that succeeded the most under uncertainty are simply the ones that tried more. The gradients of probability of getting a success "worsen" the chances for luck if the number of trials is small, but "enhance" these chances for longer trial sequences. Driving down cycle time in trials would allow for more experiments, which can produce better results for those with early luck compounded.

However, domains with a lot of uncertainty have the highest likelihood of skilled people failing. When initial success is random and not highly probable, skill does not necessarily play a role over time for improving the future chances for success. We have also demonstrated that being in a group facing uncertainty, we may be trapped within the repetition compulsion and forced to repeat always the same behavior pattern, without any improvement—as no lesson can been learnt from the old experience.

We have discussed on that the processes of accumulated advantage lead to the highly skewed, heavy-tailed distributions of wealth. In particular, under uncertainty only the vital few would accumulate advantage. When a trader would attach greater weight to losses than he would do to gains of equal magnitude, we say that he is risk averse. We have shown that the Pareto distribution of wealth corresponds to the logarithmic wealth utility. Wealth inequality among the population rises from taking risky decisions under uncertainty by the vital few: The more adventurous traders, the more their fortune, the less the number of lucky ones.

When the cumulative advantage is at work, there might be no parity of chances to choose a partner and to be chosen as a partner by other individuals. By fostering hierarchical organization in a group, uncertainty ultimately leads to inequality. A common belief about rarity (or scarcity) of a resource, or an item automatically fosters inequality between individuals with respect to accessibility to the scarce resource. Scarcity also promotes inequality by necessitating competition and fueling conspicuous consumption.

We have analyzed all existent data series in the *World Top Incomes Database* [32] against the relevant GDP per capita data of the Maddison Project [37] and demonstrated that income inequality is closely correlated with low growth, yet with high growth either. The discovered trend suggests that rising income inequality is a global worldwide phenomenon, occurring once the national economy is out of step with the world average. Finally, we have discussed on how rampant inequality may transform uncertainty of national economic development into uncertainty of international relations.

Acknowledgements We acknowledge the support from the Cluster of Excellence Cognitive Interaction Technology 'CITEC' (EXC 277), Bielefeld University (Germany).

References

1. Smith, R.: Skill, Effort Or Luck: Which Is More Important For Success?, Forbes/Leadership, 18 Aug 2014
2. Bittner, E., Nußbaumer, A., Janke, W., Weigel, M.: Football fever: goal distributions and non-Gaussian statistics. Eur. Phys. J. B **67**, 459–471 (2009)
3. Clark, J., Crawley, J.: Transference and Projection: Mirrors to the self. Open University Press, Buckingham (2002)
4. Freud, S., "Beyond the Pleasure Principle" (1920); in *On Metapsychology*, Middlesex (1987)
5. Gibrat, R.: Les Inégalités économiques. France, Paris (1931)
6. Yule, G.U.: A mathematical theory of evolution, based on the conclusions of Dr. J. C. Willis, F.R.S. Philos. Trans. Royal Soc. B **213**(402–410), 21–87 (1925)
7. Ijiri, Y., Simon, H.A.: Some distributions associated with bose-einstein statistics. Proc. Natl. Acad. Sci. USA **72**(5), 1654–1657 (1975)
8. Newman, M.E.J.: Power laws, Pareto distributions and Zipf's law. Contemp. Phys. **46**(5), 323–351 (2005)
9. Arnold, B.C.: Pareto and Generalized Pareto Distributions. Springer, Berlin (2008)
10. Bernoulli, D.: (1738) Exposition of a new theory on the measurement of risk. Econom.: J. Econ. Soc. **22**(1), 23–36 (1954)
11. Anand, P.: Foundations of Rational Choice Under Risk. Oxford University Press, Oxford (1993)
12. Jaynes, E.T.: Information theory and statistical mechanics. Phys. Rev. Ser. II **106**(4), 620–630 (1957)
13. Jaynes, E.T.: Information theory and statistical mechanics II. Phys. Rev. Ser. II **108**(2), 171–190 (1957)
14. Visser, M.: Zipf's law, power laws and maximum entropy. New J. Phys. **15**, 043021 (2013)
15. Albert, R., Barabási, A.-L.: Statistical mechanics of complex networks. Rev. Mod. Phys. **74**(1), 47–97 (2002)
16. Volchenkov, D., Blanchard, Ph, Krüger, T.: Heavy-tailed distributions in some stochastic dynamical models. Discontin. Nonlinearity Complex. **1**(1), 1–40 (2012)

17. Turchin, P.: Religion and empire in the axial age. Relig. Brain Behav. **2**(3), 256–260 (2012)
18. Boehm, C.: Hierarchy in the Forest: The Evolution of Egalitarian Behavior. Harvard University Press, Cambridge (1999)
19. Turchin, P.: Warfare and the evolution of social complexity: a multilevel selection approach. Struct. Dyn. **4**(3), 1–37 (2011)
20. Lösch, A.: The Economics of Location. Yale University Press, New Haven (1954)
21. Henderson, J.: Economic theory and the cities. Am. Econ. Rev. **LXIV**, 640 (1974)
22. Blanchard, Ph, Volchenkov, D.: Mathematical Analysis of Urban Spatial Networks. Springer Series Understanding Complex Systems. Springer, Berlin (2009)
23. Blanchard, Ph., Krüger, T.: The Cameo principle and the origin of scale-free graphs in social networks. J. Stat. Phys. **114**(5–6), 1399–1416 (2004)
24. Heyne, P., Boettke, P.J., Prychitko, D.L.: The Economic Way of Thinking, 13th edn. Pearson, Upper Saddle River (2014)
25. Galí, J.: Keeping up with the joneses: consumption externalities, portfolio choice, and asset prices. J. Money, Credit Bank. **26**(1), 1–8 (1994)
26. Kuznets, S.: Economic growth and income inequality. Am. Econ. Rev. **45**, 1–28 (1955)
27. Kuznets, S.: Shares of Upper Income Groups in Income and Savings. National Bureau of Economic Research, New York, 707 pp (1953)
28. Fogel, R.W.: Some Notes on the Scientific Methods of Simon Kuznets, pp. 26–7. National Bureau of Economic Research (1987)
29. Atkinson, B.A., Piketty, T., Saez, E.: Top incomes in the long run of history. J. Econ. Lit. **49**(1), 3–71 (2011)
30. Galbraith, J.: Global inequality and global macroeconomics. J. Policy Model. **29**(4), 587–607 (2007)
31. Stiglitz, J.E.: Some lessons from the East Asian miracle. World Bank Res. Obs. **11**(2), 151–177 (1996)
32. Alvaredo, F., Atkinson, A.B., Piketty, Th., Saez, E.: The World Top Incomes Database. http://topincomes.g-mond.parisschoolofeconomics.eu/ 15 Feb 2014
33. Piketty, Th: Les Hauts Revenus en France au 20éme siècle. Grasset, Paris (2001)
34. Piketty, Th: Income inequality in France, 1901–1998. J. Polit. Econ. **111**(5), 1004–1042 (2003)
35. Atkinson, A.B., Piketty, Th: Top Incomes over the Twentieth Century: A Contrast between Continental European and English-Speaking Countries, vol. 1. Oxford University Press, Oxford, 585 pp (2007)
36. Atkinson, A.B., Piketty, Th: Top Incomes over the Twentieth Century: A Global Perspective, vol. 2. Oxford University Press, Oxford, 776 pp (2010)
37. The Maddison-Project (2013). http://www.ggdc.net/maddison/maddison-project/home.htm
38. Bolt, J., van Zanden, J.L.: The maddison project: collaborative research on historical national accounts. Econ. Hist. Rev. **67**(3), 627–651 (2014)
39. GDP per capita, PPP (current international $), World Development Indicators database, World Bank. Database updated on 14 Apr 2015
40. Lieberman, R.C.: Why the Rich Are Getting Richer: American Politics and the Second Gilded Age, Foreign Affairs (2011). https://www.foreignaffairs.com/reviews/review-essay/2011-01-01/why-rich-are-getting-richer
41. Stiglitz, J.E.: The Price of Inequality: How Today's Divided Society Endangers Our Future. W.W. Norton & Company, New York (2013)
42. Hacker, J.S., Pierson, P.: Winner-Take-All Politics. Simon & Schuster, New York City (2010)
43. Global Wealth Report 2015, Credit Suisse Ag, Research Institute (2015). https://publications.credit-suisse.com/tasks/render/file/?fileID=F2425415-DCA7-80B8-EAD989AF9341D47E
44. van Creveld, M.: The Rise and Decline of the State. Cambridge University Press, Cambridge (1999)
45. Smith, A.: Diversionary foreign policy in democratic systems. Int. Stud. Q. **40**(1), 133–153 (1996)
46. Sobek, D.: Rallying around the podesta: testing diversionary theory across time. J. Peace Res. **44**, 1 (2007)
47. Clifton, M.: Domestic support and diversionary external conflict in Great Britain, 1950–1992. J. Polit. **61**(3), 799–814 (1999)

Chapter 4
Functional Differential Equations with Piecewise Constant Argument

M.U. Akhmet

4.1 Introduction and Preliminaries

Differential equations with generalized piecewise constant argument, *EPCAG*, were introduced in [1] and investigated in [2–17]. Extended information about these systems can be found in book [8]. These equations contain a subclass, differential equations with piecewise constant argument, *EPCA*, which were introduced in [22, 23] and deeply analyzed in papers [19, 20, 23, 24, 26, 29, 36, 37, 40–47], and many others.

In paper [1], we not only generalized *EPCA* to *EPCAG*, but, what is most important, propose to investigate newly introduced systems by reduction them to integral equations. This innovation has appeared to be very effective. There are two main reasons for that. Firstly, it is possible to investigate systems, which are essentially nonlinear, more precisely, nonlinear with respect to values of solution at discrete moments of time, while the main and unique method of analysis for *EPCA* [47] is reduction to discrete equation. Hence, only those equations are considered, where values of solutions at the discrete moments appear linearly [47]. Secondly, we analyze existence and stability of solutions not only with specially fixed initial moments, but arbitrarily chosen. Thus, we have deepen the analysis insight significantly. Further our proposals were used not only in theoretical studies, but also in applications [12, 13, 20, 38].

Recently, in papers [41, 45], delay differential equations with piecewise constant argument have been investigated and interesting problems mainly related to the existence of periodic and almost periodic solutions were considered. Investigation in these papers continues to be through reduction to discrete equations, and only *linear* equations have been discussed. Though more general equations with piecewise constant argument were introduced in our papers and the research has been implemented

M.U. Akhmet (✉)
Department of Mathematics, Middle East Technical University, 06800 Ankara, Turkey
e-mail: marat@metu.edu.tr

D. Volchenkov and X. Leoncini (eds.), *Regularity and Stochasticity of Nonlinear Dynamical Systems*, Nonlinear Systems and Complexity 21,
DOI 10.1007/978-3-319-58062-3_4

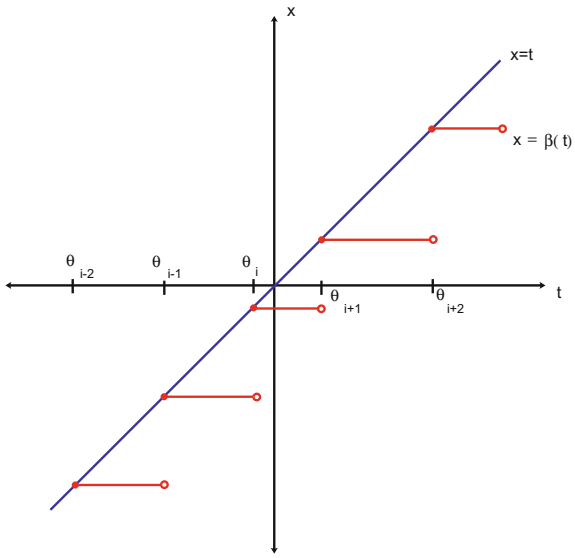

Fig. 4.1 The graph of the argument $\beta(t)$

for *nonlinear* systems. In the present chapter, we suggest to investigate more general functional differential equations with functional response on piecewise constant argument and describe the class.

We start with piecewise constant argument functions.

Let $\theta_i, i \in \mathbb{Z}$ be a strictly ordered sequence of real numbers such that $|\theta_i| \to \infty$ as $|i| \to \infty$. We define the argument function as $\beta(t) = \theta_i$ if $\theta_i \leq t < \theta_{i+1}, i \in \mathbb{Z}$. The greatest integer function $[t]$, which is equal to the maximal among all integers less than t, is a $\beta(t)$ function with $\theta_i = i, i \in \mathbb{Z}$. Similarly, $\beta(t) = 2[t/2]$ if $\theta_i = 2i, i \in \mathbb{Z}$. One can see the graph of a $\beta-$type function in Fig. 4.1.

Let two real-valued sequences $\theta_i, \zeta_i, i \in \mathbb{Z}$, be defined such that $\theta_i < \theta_{i+1}, \theta_i \leq \zeta_i \leq \theta_{i+1}$ for all $i \in \mathbb{Z}$, $|\theta_i| \to \infty$ as $|i| \to \infty$. The argument function $\gamma(t)$ is defined by $\gamma(t) = \zeta_i$, if $\theta_i \leq t < \theta_{i+1}, i \in \mathbb{Z}$. One can easily find, for example, that $2[\frac{t+1}{2}]$ is $\gamma(t)$ function with $\theta_i = 2i - 1, \zeta_i = 2i$. In Fig. 4.2, the typical graph of $\gamma(t)$ function is seen.

Finally, we say that a function is of $\chi-$type and denote it $\chi(t)$, if $\zeta_i = \theta_{i+1}, i \in \mathbb{Z}$. The function $[t + 1]$ is a good example of $\chi(t)$ function with $\theta_i = i, i \in \mathbb{Z}$.

Now, we can introduce the following differential equations,

$$x' = f(t, x_t, x_{\beta(t)}), \tag{4.1}$$

$$x' = f(t, x_t, x_{\gamma(t)}), \tag{4.2}$$

and

$$x' = f(t, x_t, x_{\chi(t)}). \tag{4.3}$$

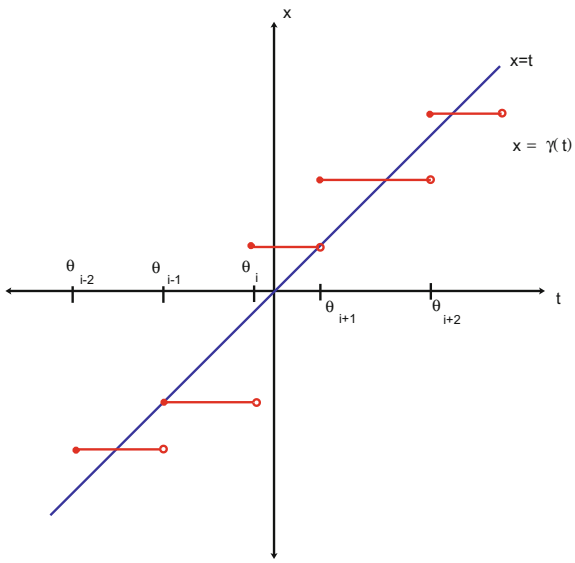

Fig. 4.2 The graph of the argument $\gamma(t)$

In these equations, x_t must be understood as for functional differential equations, *FDE*, [21, 25, 28, 31]. More precise description will be given in next sections. We shall call systems (4.1)–(4.3) functional differential equations with piecewise constant deviation of argument and abbreviate *FDEPCA*. This is a large class of equations and has the following three subclasses: with retarded constancy of argument, *RCA*; with advanced constancy of argument, *ACA*; and with alternate (delay/advanced) constancy of argument, *MCA*. Examples of these equations are provided in Sect. 4.6.

The models (4.1)–(4.3) are much more general than those investigated in [41, 45], where the delay is constant $\tau = 1$ and it is equal to the step of the greatest integer function, $[t]$. Moreover, it is the first time, when we introduce the functional depending of $x_{\gamma(t)}$, when previous authors were busy with at most terms of the form $x_{\gamma(t)}$. Thus, we can say that in this paper we begin to investigate functional differential equations with piecewise constant argument in the most general form.

Let us clarify that $\gamma(t)$ is a function of the alternate constancy. Fix $k \in \mathbb{N}$ and consider $t \in [\theta_k, \theta_{k+1})$. Then, $\gamma(t) = \zeta_k$. If argument t satisfies $\theta_k \leq t < \zeta_k$, then $\gamma(t) > t$ and the piecewise constant argument is advanced. Similarly, if $\zeta_k < t < \theta_{k+1}$, then $\gamma(t) < t$, and the constancy is retarded. Consequently, (4.2) is a retarded functional differential equation with alternate constancy of argument, *RFDEMCA*. Equation (4.1) is a retarded functional differential equation with retarded constancy of argument, *RFDERCA*, and (4.3) is a retarded functional differential equation with advanced constancy of argument, *RFDEACA*. Since there are three types of *FDE*: retarded, advanced, and neutral [31], we submit the following classes: *RFDERCA*, *RFDEMCA*, *RFDEACA*, retarded functional differential equations with piecewise constant argument; *NFDERCA*, *NFDEMCA*, *NFDEACA*, neutral functional differential equations with piecewise constant argument; and

AFDERCA, *AFDEMCA*, *AFDEACA*, advanced functional differential equations with piecewise constant argument. In the present paper, we focus on retarded functional differential equations and neutral functional differential equations both with retarded and alternate constancy of argument. That is, *RFDERCA*, *RFDEMCA*, *NFDERCA*, and *NFDEMCA* are under discussion. It is obvious that they are functional differential equations. Existence and uniqueness of solutions, continuation, continuous dependence, periodic and almost periodic solutions, integral manifolds, and asymptotic properties, that is, the standard list of problems for any theory of differential equations, has to be under investigation for *FDEPCA*. Arguments, to ensure that newly introduced systems can play important role in applications, are the same as for *FDE* [35], since our systems are *FDE* in their generalized form. After all, they are differential equations with piecewise constant argument. Consequently, applications discussed in [8, 24, 47] are also suitable. Moreover, providing *FDEPCA* as a new object for investigation, we are confident that it will provoke modeling activity, since this has been true for any type of differential equations.

In this paper, we have formulated several theorems on existence and uniqueness of solutions, continuous dependence, and continuation of solutions. Simple ideas how to prove these assertions on the basis of their analogues for functional differential equations [31, 35] are provided. Theorems on bounded, periodic, and almost periodic solutions of quasilinear systems and their stability are proved. The important part of the paper is the last section, where we have formulated several real-world problems and consider systems for future investigations.

4.2 Retarded Functional Differential Equations with Retarded Constancy of Argument

Fix a nonnegative real number $\tau \in \mathbb{R}$. Denote by $\mathscr{C} = C([-\tau, 0], \mathbb{R}^n)$ the set of all continuous functions mapping interval $[-\tau, 0]$ into $\mathbb{R}^n$, with the uniform norm $\|\phi\|_0 = \max_{[-\tau,0]} \|\phi\|$. If a function $x(t)$ is defined on intervals $[\sigma - \tau, \sigma]$ and $[\beta(\sigma) - \tau, \beta(\sigma)]$, with fixed $\sigma \in \mathbb{R}$, then we define functions $x_\sigma(t) = x(\sigma + t)$ and $x_{\beta(\sigma)}(t) = x(\beta(\sigma) + t)$, $t \in [-\tau, 0]$, respectively. One can easily see that $x_\sigma(t), x_{\beta(\sigma)}(t) \in \mathscr{C}$, if $x(t)$ is a continuous function.

Consider a subset $\mathscr{D}$ of $\mathbb{R} \times \mathscr{C} \times \mathscr{C}$ and introduce a continuous functional $f : \mathscr{D} \to \mathbb{R}^n$. We may assume that $\mathscr{D} = J \times G \times G$, where $J \subseteq \mathbb{R}$, G is a subset of $\mathscr{C}$ and $G = \{\phi \in \mathscr{C} | \|\phi\|_0 < H\}$ with some positive $H \in \mathbb{R}$.

Let us define initial conditions for (4.1). Fix a number $\sigma \in J$ and two functions $\phi, \psi \in \mathscr{C}$. We shall say that a solution $x(t)$ of Eq. (4.1) satisfies the initial condition and write $x(t) = x(t, \sigma, \phi, \psi)$, $t \geq \sigma$, if $x_\sigma(s) = \phi(s)$, $x_{\beta(\sigma)}(s) = \psi(s)$, $s \in [-\tau, 0]$. We assume, in what follows, that equality $\phi(s) = \psi(s + \sigma - \beta(\sigma))$ is true for all $s \in [-\tau, \beta(\sigma) - \sigma]$, provided that set $[\beta(\sigma) - \tau, \beta(\sigma)] \cap [\sigma - \tau, \sigma]$ is not empty. One can easily see that the last condition is valid, if $\beta(\sigma) = \sigma$, that is, $\sigma = \theta_i$, for some $i \in \mathbb{Z}$. Remember that $\beta(\sigma) \leq \sigma$, and we do not exclude that intervals

$[\beta(\sigma)-\tau, \beta(\sigma)]$ and $[\sigma-\tau, \sigma]$ may be disjoint. Thus, we can write the following initial conditions,

(IC) $x_\sigma(s)=\phi(s), x_{\beta(\sigma)}(s)=\psi(s), s \in [-\tau, 0]$.

Thus, we obtain the following initial value problem, IVP,

$$\begin{aligned} &x'=f(t, x_t, x_{\beta(t)}), \\ &x_\sigma(s)=\phi(s), x_{\beta(\sigma)}(s)=\psi(s), s \in [-\tau, 0]. \end{aligned} \tag{4.4}$$

Now, one can give the following definition.

Definition 1 A function $x(t)=x(t, \sigma, \phi, \psi)$ is a solution of (4.4) on $[\sigma, \sigma+a), a>0$, if:

(i) It satisfies the initial condition (IC);
(ii) $x(t)$ is continuous on $[\sigma, \sigma+a)$;
(iii) The derivative $x'(t)$ exists for $t \geq \sigma$ with possible exception of the points σ and θ_i, where one-sided derivatives exist;
(iv) Equation (4.4) is satisfied by $x(t)$ for all $t>\sigma$, except possibly points θ_i, and it holds for the right derivative of $x(t)$ at the points θ_i.

Remark 1 If $\theta_k \leq \sigma < \theta_{k+1}$ for some fixed $k \in \mathbb{Z}$, then Eq. (4.1) has the form

$$x'=f(t, x_t, x_{\theta_k}). \tag{4.5}$$

Hence, for all $t \in [\theta_k, \theta_{k+1})$, the equation is just a *RFDE* (not *RFDEPCA*), since x_{θ_k} is the fixed function for the interval.

Lemma 1 *Let $\sigma \in J$, $\phi, \psi \in G$ be given. Then, the initial value problem (4.4) is equivalent to the following integral equation,*

$$\begin{aligned} &x_\sigma=\phi, x_{\beta(\sigma)}=\psi, \\ &x(t)=\phi(0)+\int_\sigma^t f(s, x_s, x_{\beta(s)})ds, \quad t \geq \sigma. \end{aligned} \tag{4.6}$$

The necessity for Lemma 1 can be easily proved, if we utilize Lemma 2.1, Chap. 2, [31] on continuity of function x_t, and Remark 1. Sufficiency can be verified very similarly to the proof of Lemma 3.1 from [2] or Lemma 3.2 from [8], for differential equations with piecewise constant argument.

Theorem 1 (Existence and Uniqueness) *Suppose that f is continuous on an open subset $\mathscr{D}$ of $\mathbb{R} \times \mathscr{C} \times \mathscr{C}$, and local Lipschitz condition for the second argument is valid. If $(\sigma, \phi, \psi) \in \mathscr{D}$, then there exists a unique solution of (4.4) passing through (σ, ϕ, ψ).*

Proof Fix an integer $k, \theta_k \leq \sigma < \theta_{k+1}$, and a number α such that $0 < \alpha < \min\{\theta_{k+1} - \sigma, \tau\}$. Consider the space $\mathscr{P}$ of continuous on $[\sigma - \tau, \sigma + \alpha]$ functions π, such that $\pi(\sigma + s) = \phi(s), s \in [-\tau, 0], \|\pi(t) - \phi(0)\| < H, \sigma \leq t \leq \sigma + \alpha$. Denote $M = \sup_{\sigma \leq t \leq \sigma+\alpha, \mathscr{P}} ||f(t, \pi, \psi)||$.

Define the operator T on $\mathscr{P}$ such that

$$T\pi(\sigma + s) = \phi(s), s \in [-\tau, 0], T\pi(t) = \phi(0) + \int_{\sigma}^{t} f(u, \pi_u, \psi(u))du, t \geq \sigma.$$

First verify that $T : \mathscr{P} \to \mathscr{P}$. Indeed,

$$\|T\pi(t) - \phi(0)\| \leq M\alpha < H,$$

if α is sufficiently small.

Moreover, we have that

$$\|T\pi_1(t) - T\pi_2(t)\| \leq L\alpha\|\pi_1(t) - \pi_2(t)\|_\alpha,$$

where $\|\pi(t)\|_\alpha = \max_{\sigma \leq t \leq \sigma+\alpha} \|\pi(t)\|$ is the norm for continuous on $[\sigma, \sigma + \alpha]$ functions.

Assume that $\alpha < 1/L$. Now, apply the contraction mapping theorem to prove that there exists a unique solution of (4.4). The theorem is proved.

Applying Lemma 1, Remark 1, Schauder theorem, and theorems in [31, 35], one can prove the following assertions about existence, continuous dependence [31], and continuation theorems [31, 35] for (4.4). They are very similar to those in [31]. So, let us, formulate them without proof.

Theorem 2 (Existence) *Suppose that f is continuous on an open subset $\mathscr{D}$ of $\mathbb{R} \times \mathscr{C} \times \mathscr{C}$. If $(\sigma, \phi, \psi) \in \mathscr{D}$, then there is a solution of (4.4) passing through (σ, ϕ, ψ).*

Theorem 3 (Continuous dependence) *Suppose that f is continuous on an open subset $\mathscr{D}$ of $\mathbb{R} \times \mathscr{C} \times \mathscr{C}$, and $x(t)$ is a solution of (4.4) through $(\sigma, \phi, \psi) \in \mathscr{D}$, which exists and unique on $[\sigma, a]$. Let $K \subset \mathscr{D}$ be a compact set defined by $K = \{(t, x_t\} : t \in [\sigma, a]\}$, and let W be a neighborhood of K on which f is bounded. If $(\sigma^k, \phi^k, \psi^k, f_k), k \in \mathbb{N}$, satisfies $\sigma^k \to \sigma, \phi^k \to \phi, \psi^k \to \psi$, $\sup_W \|f^k - f\| \to 0$ as $k \to \infty$, then there is a number $N \in \mathbb{N}$, such that, for $k \geq N$, each solution x^k through $(\sigma^k, \phi^k, \psi^k)$ of*

$$x'(t) = f^k(t, x_t, x_{\beta(t)})$$

exists on $[\sigma^k, a]$ and $\max_{[\max(\sigma,\sigma_k),a]} \|x^k - x\| \to 0$ as $k \to \infty$.

Assume that $x(t) = x(t, \sigma, \phi, \psi)$ is a solution of (4.4) on an interval $[\sigma, a), a > \sigma$. A solution $x_1(t) = x(t, \sigma, \phi, \psi)$ of (4.4) is a continuation of $x(t)$, if it is defined on $[\sigma, b)$ with $b > a$ and $x_1(t) = x(t), t \in [\sigma, a)$. A solution x of (4.4) is saturated (non-continuable), if no continuation exists, and interval $[\sigma, a)$ is the maximal interval of

existence of the solution x. The existence of the saturated solution is a consequence of Zorn's lemma. It is obvious that the maximal interval of existence is open from the right.

Theorem 4 *Suppose that f is defined on an open subset $\mathscr{D}$ of $\mathbb{R} \times \mathscr{C} \times \mathscr{C}$, and $x(t) = x(t, \sigma, \phi, \psi)$ is a non-continuable solution of (4.4) on $[\sigma, a)$. Then, for any compact set V in $\mathscr{D}$ there exists a number t_V such that $(t, x_t) \notin V$, if $t_V \leq t < a$.*

4.3 Retarded Functional Differential Equations with Alternate Constancy of Argument

Let us consider equations with alternate constancy of argument (4.2). The initial conditions for equations with *MCA* are more complicated than those for equations with retarded constancy of argument. Namely, if $\theta_i \leq \sigma < \theta_{i+1}$, for some $i \in \mathbb{Z}$, then one has to consider two cases:

1. (IC_1) $x_\sigma(s) = \phi(s), \phi \in G, s \in [-\tau, 0]$ if $\theta_i \leq \sigma \leq \zeta_i < \theta_{i+1}$;
2. (IC_2) $x_\sigma(s) = \phi(s), x_{\gamma(\sigma)}(s) = \psi(s), \phi, \psi \in G, s \in [-\tau, 0]$, if $\theta_i \leq \zeta_i < \sigma < \theta_{i+1}$.

We assume, in what follows, that equality $\phi(s) = \psi(s + \sigma - \gamma(\sigma))$ is true for all $s \in [-\tau, \gamma(\sigma) - \sigma]$, provided that set $[\gamma(\sigma) - \tau, \gamma(\sigma)] \cap [\sigma - \tau, \sigma]$ is not empty.

Considering Eq. (4.2) with these conditions, we shall say about initial value problem, *IVP*, for system (4.2). Thus, we can provide the following definition now.

Definition 2 A function $x(t)$ is a solution of (4.2) with (IC_1) or (IC_2) on $[\sigma, \sigma + a)$ if:

(i) It satisfies the initial condition;
(ii) $x(t)$ is continuous on $[\sigma, \sigma + a)$;
(iii) The derivative $x'(t)$ exists for $t \geq \sigma$ with the possible exception of the points θ_i, where one-sided derivatives exist;
(iv) Equation (4.2) is satisfied by $x(t)$ for all $t > \sigma$, except, possibly, points θ_i, and it holds for the right derivative of $x(t)$ at the points θ_i.

All the discussions made for the retarded constancy argument are valid for also case (IC_2) For example, the local existence and uniqueness theorem proved for *FDE* [31, 35] can be extended. While for (IC_1), the analysis is much more complicated. The following example is a good evidence for that.

Example 1 Consider the following scalar *FDEPCA*,

$$x' = x(t - 1) + x^2([t + 1]). \tag{4.7}$$

Solve this equation with $\sigma = 0, x(t) \equiv x_0$, for $t \leq 0$. We have that $x(t) = x_0 + (x_0 + z^2)t$ for $t \in [0, 1]$, where $z = x(1)$. Then, $z^2 - z + x_0 = 0$. Solution of the

last quadratic equation is $z = \frac{1}{2} \pm \sqrt{\frac{1}{4} - 2x_0}$. One can see that the solution exists not for all x_0 as well that uniqueness is not valid for certain initial values.

The last example shows that more attention to existence and uniqueness theorems is needed, if the constancy of argument is alternate.

Let us make the following assumptions.

(C1) functional f satisfies the Lipschitz condition in the second and third arguments, if

$$\|f(t, \phi_1, \psi_1) - f(t, \phi_2, \psi_2)\| \leq \ell(\|\phi_1 - \phi_2\|_0 + \|\psi_1 - \psi_2\|_0),$$

where (t, ϕ_1, ψ_1) and (t, ϕ_2, ψ_2) are from $\mathscr{D}$.

(C2) There exists a positive number $\bar{\theta}$ such that

$$\theta_{i+1} - \theta_i \leq \bar{\theta}$$

for all $i \in \mathbb{Z}$.

(C3)

$$M = \sup_{\mathscr{D}} \|f\| < \infty.$$

(C4)

$$2\ell\bar{\theta} < 1.$$

Consider the space $\mathscr{P}(\sigma, r, \phi)$ of continuous on $[\sigma - \tau, r]$, $r \geq \sigma$, functions π, such that $\pi(\sigma + s) = \phi(s)$, $s \in [-\tau, 0]$, $\|\pi(t) - \phi(0)\| < M\bar{\theta}$, $\sigma \leq t \leq r$.

Theorem 5 *Assume that conditions* $(C1)$–$(C4)$ *are fulfilled. The initial moment,* σ, *is such that* $\theta_i \leq \sigma < \zeta_i < \theta_{i+1}$, *for some* $i \in \mathbb{Z}$, *and, if* $\pi \in \mathscr{P}(\sigma, \zeta_i, \phi)$, *then* $\pi_t \in G$, *for all* $t \in [\sigma, \zeta_i]$. *Then, the IVP for (4.2) admits a unique solution* $x(t, \sigma, \phi)$ *on interval* $[\sigma, \zeta_i]$.

Proof Construct sequence $x^i(t) \in \mathscr{P}(\sigma, \zeta_i, \phi)$, $i = 0, 1, 2, \ldots$, $x^0(t) = \phi(0)$, $t \geq \sigma$, such that

$$x^{i+1}(t) = \phi(0) + \int_{\sigma}^{t} f(u, x^i_u, x^i_{\gamma(u)})du.$$

By using the contraction mapping theorem for the operator $T : \mathscr{P} \to \mathscr{P}$,

$$T\pi(\sigma + s) = \phi(s), s \in [-\tau, 0], T\pi(t) = \phi(0) + \int_{\sigma}^{t} f(u, \pi_u, \pi_{\gamma(u)})du, t \geq \sigma,$$

one can prove that sequence x^i converges uniformly on $[\sigma, \zeta_i]$ to the unique solution of (4.2). The theorem is proved.

The main peculiarity of the last assertion is that the existence and uniqueness is not local, it is rather global one. We cannot consider the problem locally, since of alternate constancy of argument.

Let us formulate the following Theorems 6–8. Proofs of these assertions can be done by using technique for Theorem 5 similarly to results in [35].

Theorem 6 *Assume that conditions* $(C1)$–$(C3)$ *are fulfilled. Moreover, the initial moment,* σ, *is such that* $\theta_i \le \zeta_i \le \sigma < \theta_{i+1}$, *for some* $i \in \mathbb{Z}$, *there exists a real number* $h > 0$ *such that if* $\pi \in \mathscr{P}(\sigma, \sigma + h, \phi)$, *then* $\pi_t \in G, t \in [\sigma, \sigma + h]$, *and* $2\ell h < 1$. *Then, the IVP for (4.2) admits a unique solution* $x(t)$ *on interval* $[\sigma, \min\{\sigma + h, \theta_{i+1}\}]$.

Theorem 7 *Suppose that* f *is defined on an open subset* $\mathscr{D}$ *of* $\mathbb{R} \times \mathscr{C} \times \mathscr{C}$, *conditions* $(C1)$–$(C4)$ *are fulfilled, and* x *is a non-continuable solution of the IVP for (4.2) on* $[\sigma, a)$. *Then, for any compact set* V *in* $\mathscr{D}$ *there exists a number* t_V *such that* $(t, x_t) \notin V$, *if* $t_V \le t < a$.

Theorem 8 *Assume that* $J = \mathbb{R}^+ = [0, \infty)$, *conditions of the last theorem are valid,* $x(t), \sigma \ge 0$, *is a non-continuable solution of the IVP for (4.2). Moreover, there exists a positive number* $h, 2\ell h < 1$, *such that for all* $\delta \ge \sigma$, *if* $x(t) \in \mathscr{P}(\delta, \delta + h, x_\delta)$ *then* $x_t \in G$ *for all* $t \in [\delta, \delta + h]$. *Then the solution is continuable to* ∞.

The last theorem is useful for stability analysis and theorems on existence of bounded, periodic, and almost periodic solutions.

4.4 Quasilinear Systems: Preliminaries

Let us introduce the following functional differential equations,

$$x'(t) = A_0(t)x(t) + A_1(t)x(\gamma(t)) + f(t, x_t, x_{\gamma(t)}), \tag{4.8}$$

where $t \in \mathbb{R}, x \in \mathbb{R}^n$. In Eq. (4.8), terms $x_t, x_{\gamma(t)}(s)$, must be understood in the way used for *FDE* [31, 35]. That is, $x_t(s) = x(t + s), s \in [-\tau, 0], x_{\gamma(t)}(s) = x(\gamma(t) + s), s \in [-\tau, 0]$. Let us clarify that the argument function $\gamma(t)$ is of the alternate type. Fix $k \in \mathbb{N}$ and consider the function on the interval $[\theta_k, \theta_{k+1})$. Then, the function $\gamma(t)$ is equal to ζ_k. If the argument t satisfies $\theta_k \le t < \zeta_k$, then $\gamma(t) > t$ and it is of advanced type. Similarly, if $\zeta_k < t < \theta_{k+1}$, then $\gamma(t) < t$, and hence, it is of the delayed type. Consequently, it is worth pointing out that the Eq. (4.8) is with *alternate constancy* of argument. If the argument function is of $\beta-$type or $\chi-$type, we shall say about *retarded constancy* and *advanced constancy* of argument, respectively.

Consider a subset $\mathscr{D}$ of the product $\mathbb{R} \times \mathscr{C} \times \mathscr{C}$ and introduce a continuous functional $f : \mathscr{D} \to \mathbb{R}^n$. To be concrete, we assume that $\mathscr{D} = \mathbb{R} \times \mathscr{C} \times \mathscr{C}$. Let $s \in \mathbb{R}$ be a positive number. We denote $\mathscr{C}_s = \{\phi \in \mathscr{C} | \|\phi\|_0 \le s\}$. Let $C_0(\mathbb{R})$ (respectively

$C_0(\mathbb{R} \times \mathscr{C}_H \times \mathscr{C}_H)$ for a given $H \in \mathbb{R},\ H > 0$) be the set of all bounded and continuous functions on $\mathbb{R}$ (respectively on $\mathbb{R} \times \mathscr{C}_H \times \mathscr{C}_H$).

The following assumptions will be needed:

(Q1) A_0, A_1 are $n \times n$ matrices, and their elements are from $C_0(\mathbb{R})$;
(Q2) $f \in C_0(\mathbb{R} \times \mathscr{C}_H \times \mathscr{C}_H)$ for each positive $H \in \mathbb{R}$;
(Q3) f satisfies the Lipschitz condition in the second and third arguments:

$$\|f(t, \phi_1, \psi_1) - f(t, \phi_2, \psi_2)\| \leq L(\|\phi_1 - \phi_2\|_0 + \|\psi_1 - \psi_2\|_0),$$

where (t, ϕ_1, ψ_1) and (t, ϕ_2, ψ_2) are from $\mathscr{D}$, for some positive constant L;
(Q4) $\inf_{\mathbb{R}} \|A_1(t)\| > 0$;
(Q5) There exist positive numbers $\bar{\theta}, \bar{\zeta} > 0$ such that $\theta_{i+1} - \theta_i \leq \bar{\theta}, \zeta_{i+1} - \zeta_i \leq \bar{\zeta}, i \in \mathbb{Z}$.

One can easily see that system (4.8) has the form of a functional differential equation,

$$z'(t) = A_0(t)z(t) + A_1(t)z(\zeta_i) + f(t, z_t(t), z_{\zeta_i}), \tag{4.9}$$

if $t \in [\theta_i, \theta_{i+1}), i \in \mathbb{Z}$. That is, this system has the structure of a functional differential equation with continuous time within intervals $[\theta_i, \theta_{i+1}), i \in \mathbb{Z}$.

Consider the following linear system,

$$z'(t) = A_0(t)z(t) + A_1(t)z(\gamma(t)), \tag{4.10}$$

which corresponds to Eq. (4.1). Systems of type (4.10) have been investigated in [4, 8]. In what follows, we will give a short information from the book.

Let $\mathscr{I}$ be an $n \times n$ identity matrix. Denote by $X(t, s),\ X(s, s) = \mathscr{I},\ t, s \in \mathbb{R}$, the fundamental matrix of solutions of the system

$$x'(t) = A_0(t)x(t) \tag{4.11}$$

which is associated with systems (4.8) and (4.10). We introduce the following matrix function

$$M_i(t) = X(t, \zeta_i) + \int_{\zeta_i}^{t} X(t, s)A_1(s)ds, i \in \mathbb{Z}.$$

This matrix is very useful in what follows.

From now on, we make the assumption:

(Q6) For every fixed $i \in \mathbb{Z}$, $\det[M_i(t)] \neq 0$, $\forall t \in [\theta_i, \theta_{i+1}]$.

We shall call $C(6)$ *the regularity condition*.

Remark 2 It is easily seen that the last condition is equivalent to the following one:

$$\det[\mathscr{I} + \int_{\zeta_i}^{t} X(\zeta_i, s)A_1(s)ds] \neq 0,$$

for all $t \in [\theta_i, \theta_{i+1}]$, $i \in \mathbb{Z}$.

Definition 3 A function $x(t)$ is a solution of (4.8) (4.10) on $\mathbb{R}$ if:

(i) $x(t)$ is continuous;
(ii) The derivative $x'(t)$ exists for all $t \in \mathbb{R}$ with the possible exception of the points θ_i, $i \in \mathbb{Z}$, where one-sided derivatives exist;
(iii) Equations (4.1) (4.3) is satisfied by $x(t)$ for all $t \in \mathbb{R}$, except points of θ, and it holds for the right derivative of $x(t)$ at the points θ_i, $i \in \mathbb{Z}$.

Theorem 9 ([4, 8]) *If condition* $(Q1)$ *is fulfilled, then for every* $(t_0, z_0) \in \mathbb{R} \times \mathbb{R}^n$ *there exists a unique solution* $z(t) = z(t, t_0, z_0)$, $z(t_0) = z_0$, *of (4.3) in the sense of Definition 3 if and only if condition* $(Q6)$ *is valid.*

Using the last theorem, one can easily prove [4, 8] that the set of the solutions of (4.10) is an $n-$dimensional linear space. Hence, for a fixed $t_0 \in \mathbb{R}$, there exists a fundamental matrix of solutions of (4.8), $Z(t) = Z(t, t_0)$, $Z(t_0, t_0) = \mathscr{I}$, such that

$$\frac{dZ}{dt} = A_0(t)Z(t) + A_1(t)Z(\gamma(t)).$$

Let us show how to construct the fundamental matrix. Without loss of generality, assume that $\theta_i < t_0 < \zeta_i$ for a fixed $i \in \mathbb{Z}$ and define the matrix only for increasing t, as the construction is similar for decreasing t.

We have

$$Z(t) = M_l(t)\Big[\prod_{k=l}^{i+1} M_k^{-1}(\theta_k)M_{k-1}(\theta_k)\Big]M_i^{-1}(t_0), \tag{4.12}$$

if $t \in [\theta_l, \theta_{l+1}]$, for arbitrary $l > i$.

Similarly, if $\theta_j \leq t \leq \theta_{j+1} < \ldots < \theta_i \leq t_0 \leq \theta_{i+1}$, then

$$Z(t) = M_j(t)\Big[\prod_{k=j}^{i-1} M_k^{-1}(\theta_{k+1})M_{k+1}(\theta_{k+1})\Big]M_i^{-1}(t_0). \tag{4.13}$$

Next, it is obtained that $Z(t, s) = Z(t)Z^{-1}(s)$, $t, s \in \mathbb{R}$, and a solution $z(t)$, $z(t_0) = z_0$, $(t_0, z_0) \in \mathbb{R} \times \mathbb{R}^n$, of (4.8) is equal to $z(t) = Z(t, t_0)z_0$, $t \in \mathbb{R}$.

One can easily see that $(Q4)$–$(Q7)$ imply the existence of positive constants m, M, and $\bar{M}$ such that $m \leq \|Z(t, s)\| \leq M$, $\|X(t, s)\| \leq \bar{M}$ for $t, s \in [\theta_i, \theta_{i+1}]$, $i \in \mathbb{Z}$.

From now on, we make the assumptions

(Q7) $2\bar{M}L(1+M)\bar{\theta} < 1$.

Lemma 2 *Suppose that conditions* $(Q1)$–$(Q7)$, *hold, and fix* $i \in \mathbb{Z}$. *Then, for every* $(\sigma, \phi, \psi) \in [\theta_i, \theta_{i+1}] \times \mathscr{C} \times \mathscr{C}$, *there exists a unique solution* $x(t) = x(t, \sigma, \phi, \psi)$ *of (4.1) on* $[\theta_i, \theta_{i+1}]$.

Proof Existence. Fix $i \in \mathbb{Z}$. We assume without loss of generality that $\theta_i \le \sigma \le \zeta_i \le \theta_{i+1}$. That is, we consider (IC_1) this time and the solution $x(t, \sigma, \phi)$.

Set $\|x(t)\|_0 = \max_{[\sigma, \theta_{i+1}]} \|x(t)\|$, take $x_0(t) = Z(t, \sigma)\phi(\sigma)$, and define a sequence $\{x^k(t)\}$, $k \ge 0$, by

$$x^k(t) = \phi(t), t \le \sigma,$$
$$x^{k+1}(t) = Z(t, \xi)\Big[\phi(\sigma) + \int_\sigma^{\zeta_i} X(\zeta_i, s) f(s, x_s^k, x_{\zeta_i}^k) ds\Big] + \int_{\zeta_i}^t X(t, s) f(s, x_s^k, x_{\zeta_i}^k) ds, t \ge \sigma.$$

The last expression implies that

$$\|x^{k+1}(t) - x^k(t)\|_0 \le [2\bar{M}L(1+M)\bar{\theta}]^{k+1} M \|\phi(\sigma)\|.$$

Thus, there exists a unique solution $x(t) = x(t, \sigma, \phi)$ of the equation

$$x(t) = Z(t, \xi)\Big[\phi(\sigma) + \int_\sigma^{\zeta_i} X(\zeta_i, s) f(s, x_s, x_{\zeta_i}) ds\Big] \tag{4.14}$$
$$+ \int_{\zeta_i}^t X(t, s) f(s, x_s, x_{\zeta_i}) ds, t \ge \sigma. \tag{4.15}$$

which is a solution of (4.8) on $[\theta_i, \theta_{i+1}]$ as well. This proves the existence.

Uniqueness. Denote by $x^j(t) = x(t, \sigma, \phi)$, $j = 1, 2$, the solutions of (4.8), where $\theta_i \le \sigma \le \theta_{i+1}$. Without loss of generality, we assume that $\sigma \le \zeta_i$.

We have that

$$x^1(t) - x^2(t) = Z(t, \xi)\{\int_\sigma^{\zeta_i} X(\zeta_i, s)[f(s, x_s^1(s), x^1(\zeta_i)) - f(s, x_s^2(s), x^2(\zeta_i))] ds\}$$
$$+ \int_{\zeta_i}^t X(t, s)[f(s, x_s^1(s), x^1(\zeta_i)) - f(s, x_s^2(s), x^2(\zeta_i))] ds.$$

Hence,

$$\|x^1(t) - x^2(t)\| \le \bar{M}L\bar{\theta}(1+M)\|x_{\zeta_i}^1 - x_{\zeta_i}^2\|_0 + \bar{M}L(1+M)\Big|\int_\xi^t \|x_s^1 - x_s^2\|_0 ds\Big|.$$

Let $\|x^1(\eta) - x^2(\eta)\| = \max_{[\theta_i,\theta_{i+1}]} \|x^1(t) - x^2(t)\|$. Then, from the last two inequalities, it follows that

$$\|x^1_\eta - x^2_\eta\|_0 \le 2\bar{M}L\bar{\theta}(1+M)\|x^1_\eta - x^2_\eta\|_0.$$

Since of $(Q7)$, it is possible if only $\|x^1_\eta - x^2_\eta\|_0 = \max_{[\theta_i,\theta_{i+1}]} \|x^1(t) - x^2(t)\| = 0$. The lemma is proved.

The next lemma can be proved exactly in the way that is used to verify Lemma 2.2 from [8], see also [4], if we use Lemma 2.

Lemma 3 *Suppose that conditions* $(Q1)$–$(Q7)$, *hold. Then, for every* $(\sigma, \phi, \psi) \in [\theta_i, \theta_{i+1}] \times \mathscr{C} \times \mathscr{C}$, *there exists a unique solution* $x(t) = x(t, \sigma, \phi, \psi), t \ge \sigma$, *of (4.8), and it satisfies the integral equation*

$$\begin{aligned} x(t) = Z(t,\sigma)[\phi(\sigma) + \int_\sigma^{\zeta_i} X(\sigma, s) f(s, x_s, x_{\gamma(s)})\, ds] \\ + \sum_{k=i}^{j-1} Z(t, \theta_{k+1}) \int_{\zeta_k}^{\zeta_{k+1}} X(\theta_{k+1}, s) f(s, x_s, x_{\gamma(s)})\, ds \\ + \int_{\zeta_j}^{t} X(t, s) f(s, x_s, x_{\gamma(s)})\, ds, \end{aligned} \tag{4.16}$$

where $\theta_i \le \sigma \le \theta_{i+1}$ and $\theta_j \le t \le \theta_{j+1}$, $i < j$.

4.5 Bounded Solutions of Quasilinear Systems

We will make the following assumption,

(Q8) $\|Z(t,s)\| \le K\mathrm{e}^{-\alpha(t-s)}$, $s \le t$, where K, α are positive numbers.

Lemma 4 *Suppose that conditions* $(Q1)$–$(Q8)$, *hold. Then, a bounded on* $\mathbb{R}$ *function* $x(t)$ *is a solution of (4.8) if and only if it satisfies the following integral equation*

$$\begin{aligned} x(t) = \int_{\zeta_j}^{t} X(t, s) f(s, x_s, x_{\gamma(s)})\, ds + \\ \sum_{k=-\infty}^{k=j-1} Z(t, \theta_{k+1}) \int_{\zeta_k}^{\zeta_{k+1}} X(\theta_{k+1}, s) f(s, x_s, x_{\gamma(s)})\, ds, \end{aligned} \tag{4.17}$$

where $\theta_j \le t \le \theta_{j+1}$.

Proof We consider only sufficiency. The necessity can be proved by using (4.16) and $(Q8)$, in very similar way to the ordinary differential equation case. Since the

solution is bounded, one can suppose that there is a positive constant M_x, such that $\sup_{\mathbb{R}} \|f(s, x_s, x_{\gamma(s)})\| = M_x < \infty$. Then,

$$\|\int_{\zeta_j}^{t} X(t,s) f(s, x_s, x_{\gamma(s)})\, ds + \sum_{k=-\infty}^{k=j-1} Z(t, \theta_{k+1}) \int_{\zeta_k}^{\zeta_{k+1}} X(\theta_{k+1}, s) f(s, x_s, x_{\gamma(s)})\, ds\| \leq$$

$$|\int_{\zeta_j}^{t} \bar{M} M_x ds| + \sum_{k=-\infty}^{k=j-1} K \mathrm{e}^{-\alpha(t-\theta_{k+1})} \int_{\zeta_k}^{\zeta_{k+1}} \bar{M} M_x\, ds \leq \bar{M} M_x [\bar{\theta} + \bar{\zeta} \frac{K \mathrm{e}^{\alpha\bar{\theta}}}{1 - \mathrm{e}^{-\alpha\underline{\theta}}}].$$

That is, the series and integral in (4.17) are convergent. Let us differentiate (4.17). We have that

$$x'(t) = \int_{\zeta_j}^{t} A_0(t) X(t,s) f(s, x_s, x_{\gamma(s)})\, ds + f(s, x_s, x_{\gamma(s)})$$

$$\sum_{k=-\infty}^{k=j-1} [A_0(t) Z(t, \theta_{k+1}) + A_1(t) Z(\zeta_j, \theta_{k+1})] \int_{\zeta_k}^{\zeta_{k+1}} X(\theta_{k+1}, s) f(s, x_s, x_{\gamma(s)})\, ds =$$

$$A_0(t) x(t) + A_1(t) x(\gamma(t)) + f(s, x_s, x_{\gamma(s)}).$$

The lemma is proved.

We shall need the following assumptions:

(Q9) $\bar{M} L [\bar{\theta} + \bar{\zeta} \frac{K \mathrm{e}^{\alpha\bar{\theta}}}{1 - \mathrm{e}^{-\alpha\underline{\theta}}}] < 1$;

(Q10) $L \frac{2K\bar{M}(1+\mathrm{e}^{\alpha\bar{\theta}})\mathrm{e}^{\alpha\bar{\theta}}\mathrm{e}^{\alpha\tau}}{\alpha} < 1$;

(Q11) there exist positive numbers $\underline{\theta}, \underline{\zeta} > 0$ such that $\theta_{i+1} - \theta_i \geq \underline{\theta}$, $\zeta_{i+1} - \zeta_i \geq \underline{\zeta}$, $i \in \mathbb{Z}$;

(Q12) $LK\bar{M} \frac{\mathrm{e}^{\bar{\theta}}}{1 - \mathrm{e}^{-\alpha\underline{\theta}}} < 1$;

(Q13) $2M\bar{M}L\bar{\theta} < 1$.

Now, we apply the result of the last lemma to prove the existence of a unique bounded on $\mathbb{R}$ solution of (4.8). Then, we find conditions of its stability. So, we will prove that the following theorem is valid.

Theorem 10 *Suppose that conditions* $(Q1)$–$(Q9)$, *hold. Then, (4.8) admits a unique bounded of* $\mathbb{R}$ *solution. If, additionally, conditions* $(Q10)$–$(Q13)$ *are valid then the solution is exponentially stable.*

Proof Consider the set $C_0(\mathbb{R})$ of continuous functions, uniformly bounded on $\mathbb{R}$. That is, if a continuous function $y(t) \in C_0(\mathbb{R})$, then $\|y\|_1 \equiv \sup_{\mathbb{R}} \|y(t)\| < \infty$. Define on $C_0(\mathbb{R})$ the operator Π such that

$$\Pi y \equiv \int_{\zeta_j}^{t} X(t,s) f(s, y_s, y_{\gamma(s)})\, ds + \sum_{k=-\infty}^{k=j-1} Z(t, \theta_{k+1}) \int_{\zeta_k}^{\zeta_{k+1}} X(\theta_{k+1}, s) f(s, y_s, y_{\gamma(s)})\, ds.$$

One can show that $\|\Pi y\|_1 < \infty$. Let us verify that this operator is contractive. Indeed, if $u, v \in C_0(\mathbb{R})$, then

$$\|\Pi u(t) - \Pi v(t)\| \le | \int_{\zeta_j}^{t} \bar{M} L \|u - v\|_1 ds + \sum_{k=-\infty}^{k=j-1} K \mathrm{e}^{-\alpha(t-\theta_{k+1})} \int_{\zeta_k}^{\zeta_{k+1}} \bar{M} L \|u - v\|_1\, ds \le$$

$$\bar{M} L [\bar{\theta} + \bar{\zeta} \frac{K \mathrm{e}^{\alpha \bar{\theta}}}{1 - \mathrm{e}^{-\alpha \underline{\theta}}}] \|u - v\|_1.$$

Since of $(Q9)$, the operator is contractive. That is, Eq. (4.8) admits a unique solution $u(t)$ from $C_0(\mathbb{R})$.

Let us investigate its stability. We apply representation (4.16) for this. We have that if u, v, are solutions of the equation with initial data (σ, ϕ, ψ), (σ, η, π), then

$$u(t) - v(t) = Z(t, \sigma)[(\phi(\sigma) - \eta(\sigma)) + \int_{\sigma}^{\zeta_i} X(\sigma, s)(f(s, u_s, u_{\gamma(s)}) - f(s, v_s, v_{\gamma(s)}))\, ds] +$$

$$+ \sum_{k=i}^{k=j-1} Z(t, \theta_{k+1}) \int_{\zeta_k}^{\zeta_{k+1}} X(\theta_{k+1}, s)(f(s, u_s, u_{\gamma(s)}) - f(s, v_s, v_{\gamma(s)}))\, ds +$$

$$\int_{\zeta_j}^{t} X(t, s)(f(s, u_s, u_{\gamma(s)}) - f(s, v_s, v_{\gamma(s)}))\, ds.$$

Denote by $w(t)$ the difference $u(t) - v(t)$. Then, w satisfies the following integral equation

$$\begin{aligned} w(t) &= Z(t, \sigma)[(\phi(\sigma) - \eta(\sigma)) + \\ &+ \int_{\sigma}^{\zeta_i} X(\sigma, s)(f(s, u_s, u_{\gamma(s)}) - f(s, u_s + w_s, u_{\gamma(s)} + w_{\gamma(s)}))\, ds] + \\ &+ \sum_{k=i}^{k=j-1} Z(t, \theta_{k+1}) \int_{\zeta_k}^{\zeta_{k+1}} X(\theta_{k+1}, s)(f(s, u_s, u_{\gamma(s)}) - f(s, u_s + w_s, u_{\gamma(s)} + w_{\gamma(s)}))\, ds \\ &+ \int_{\zeta_j}^{t} X(t, s)(f(s, u_s, u_{\gamma(s)}) - f(s, u_s + w_s, , u_{\gamma(s)} + w_{\gamma(s)}))\, ds. \end{aligned} \tag{4.18}$$

We will solve this equation for $\sigma = 0$, and initial function $w_\sigma = \phi(s) - \eta(s)$, $\|\phi(s) - \eta(s)\| < \delta$, where $\delta > 0$, will be given precisely later, assuming that $\gamma(0) \le 0$.

Fix $\varepsilon > 0$ and denote $L(l, \delta) = \frac{K \mathrm{e}^{\alpha\tau} \delta}{1 - L \frac{2K\bar{M}(1 + \mathrm{e}^{\alpha\bar{\theta}}) \mathrm{e}^{\alpha\bar{\theta}} \mathrm{e}^{\alpha\tau}}{\alpha}}$. Take δ so small that $L(l, \delta) < \varepsilon$.

Let Ψ_δ be the set of all continuous functions which are defined on $[-\tau, \infty)$ such that:

1. $\pi_\sigma = \phi(s) - \eta(s)$;
2. $\pi(t)$ is uniformly continuous on $[0, +\infty)$;
3. $||\pi(t)|| \leq L(l, \delta) \exp(-\frac{\alpha}{2}t)$ if $t \geq 0$,

for all $\pi \in \Psi_\delta$.

Define on Ψ_δ an operator $\tilde{\Pi}$ such that

$$\tilde{\Pi}\pi = \begin{cases} \phi(t) - \eta(t), t \in [-\tau, 0] \\ Z(t,0)[(\phi(0) - \eta(0) + \int_0^{\zeta_i} X(0,s)(f(s,u_s,u_{\gamma(s)}) - \\ -f(s,u_s+\pi_s,u_{\gamma(s)}+\pi_{\gamma(s)}))\,ds] + \\ +\sum_{k=i}^{k=j-1} Z(t,\theta_{k+1}) \int_{\zeta_k}^{\zeta_{k+1}} X(\theta_{k+1},s)(f(s,u_s,u_{\gamma(s)}) - \\ -f(s,u_s+\pi_s,u_{\gamma(s)}+\pi_{\gamma(s)}))\,ds + \\ \int_{\zeta_j}^{t} X(t,s)(f(s,u_s,u_{\gamma(s)}) - f(s,u_s+\pi_s,,u_{\gamma(s)}+\pi_{\gamma(s)}))\,ds, t > 0. \end{cases}$$

We shall show that $\tilde{\Pi} : \Psi_\delta \to \Psi_\delta$. Indeed, for $t \geq 0$, it is true that

$$||\tilde{\Pi}\pi|| \leq K \exp(-\alpha t)[\delta + \int_0^{\zeta_i} \bar{M}L(\|\pi_s\|_0 + \|\pi_s\|_{\gamma(s)}\|)ds]$$

$$\sum_{k=i}^{j-1} K \exp(-\alpha(t-\theta_{k+1}) \int_{\zeta_k}^{\zeta k+1} \bar{M}L(\|\pi_s\|_0 + \|\pi_{\gamma(s)}\|_0\|)ds +$$

$$\int_{\zeta_j}^{t} \bar{M}L(\|\pi_s\|_0 + \|\pi_{\gamma(s)}\|_0\|)ds \leq L(l,\delta)\exp(-\frac{\alpha}{2}t).$$

Let $\pi_1, \pi_2 \in \Psi_\delta$. Then,

$$\sup_{t\geq 0} ||\tilde{\Pi}\pi_1 - \tilde{\Pi}\pi_2|| \leq LK\bar{M}\frac{e^{\bar{\theta}}}{1-e^{-\alpha\bar{\theta}}} \sup_{t\geq 0} ||\pi_1 - \pi_2||.$$

Using a contraction mapping argument, one can conclude that there exists a unique fixed point $v(t,\delta)$ of the operator $\tilde{\Pi} : \Psi_\delta \to \Psi_\delta$ which is a solution of (4.18).

To complete the proof, we should show that there is no other solutions of the initial value problem. Consider first the interval $[\theta_0, \theta_1]$. Assume that on this interval, (4.18) has two different solutions v_1, v_2 of the problem. Denote $w = v_1 - v_2$, $\bar{m} = \max_{[\theta_0,\theta_1]} ||w(t)||$ and assume, on contrary, that $\bar{m} > 0$. We have that on the interval

$$||w(t)|| \leq || \int_0^{\zeta_i} M\bar{M}L2\bar{m}ds + \int_{\zeta_i}^{t} \bar{M}L2\bar{m}ds \leq 2M\bar{M}L\bar{\theta}\bar{m}.$$

The last inequality contradicts condition $(Q13)$. Now, using induction, one can easily prove the uniqueness for all $t \geq 0$. The theorem is proved.

4.5.1 Periodic Solutions

Assume that there are two numbers, $\omega \in \mathbb{R}$, $p \in \mathbb{Z}$, such that $\theta_{k+p} = \theta_k + \omega$, $\zeta_{k+p} = \zeta_k + \omega$, $k \in \mathbb{Z}$. Then, denote by Q the product $\prod_{k=1}^{p} G_k$, where matrices G_k are equal to $M_k^{-1}(\theta_k) M_{k-1}(\theta_k)$, $k \in \mathbb{Z}$. The matrix Q is the monodromy matrix, and eigenvalues of the matrix, ρ_j, $j = 1, 2, \ldots, n$, are multipliers. It is clear that system (4.8) admits a periodic solution, if there exists a unit multiplier. Generally, all the results known for linear homogeneous ordinary differential equations based on the unit multipliers can be identically repeated for the present systems. Our main goal in this section is to study the non-critical systems and find formulas for solutions. We assume that the system is $\omega-$ periodic. That is, in addition to the above conditions, $A_j(t + \omega) = A_j(t)$, $j = 1, 2$, $f(t + \omega, \phi, \psi) = f(t, \phi, \psi)$, $t \in \mathbb{R}$. In what follows, we assume without loss of generality that $\zeta_0 = 0$ and consider $t_0 = \zeta_0$.

Consider the solution $z(t) = z(t, 0, z_0)$. We have that

$$z(t) = Z(t, 0)z_0 + \sum_{k=0}^{k=j-1} Z(t, \theta_{k+1}) \int_{\zeta_k}^{\zeta_{k+1}} X(\theta_{k+1}, s) f(s, z_s, z_{\gamma(s)})\, ds + \int_{\zeta_j}^{t} X(t, s) f(s, z_s, z_{\gamma(s)})\, ds, \tag{4.19}$$

and

$$z(\omega) = Z(\omega, 0)z_0 + \sum_{k=0}^{k=p-1} Z(\omega, \theta_{k+1}) \int_{\zeta_k}^{\zeta_{k+1}} X(\theta_{k+1}, s) f(s, z_s, z_{\gamma(s)})\, ds.$$

In papers [15, 16], we proved the Poincaré criterion for EPCAG. According to this, $z(t)$ is a periodic solution if and only if z_0 satisfies

$$[I - Z(\omega, 0)]z_0 = \sum_{k=0}^{k=p-1} Z(\omega, \theta_{k+1}) \int_{\zeta_k}^{\zeta_{k+1}} X(\theta_{k+1}, s) f(s, z_s, z_{\gamma(s)})\, ds.$$

By conditions of non-criticality,

$$\det[I - Z(\omega, 0)] \neq 0, \tag{4.20}$$

and the last equation admits a unique solution,

$$z^* = [I - Z(\omega, 0)]^{-1} \sum_{k=0}^{k=p-1} Z(\omega, \theta_{k+1}) \int_{\zeta_k}^{\zeta_{k+1}} X(\theta_{k+1}, s) f(s, z_s, z_{\gamma(s)})\, ds.$$

Thus, we have obtained that

$$z(t) = Z(t, 0)[I - Z(\omega, 0)]^{-1} \sum_{k=0}^{p-1} Z(\omega, \theta_{k+1}) \int_{\zeta_k}^{\zeta_{k+1}} X(\theta_{k+1}, s) f(s, z_s, z_{\gamma(s)})\, ds +$$
$$\sum_{k=0}^{j-1} Z(t, \theta_{k+1}) \int_{\zeta_k}^{\zeta_{k+1}} X(\theta_{k+1}, s) f(s)\, ds + \int_{\zeta_j}^{t} X(t, s) f(s, z_s, z_{\gamma(s)})\, ds. \tag{4.21}$$

Use formula (4.21) to obtain

$$z(t) = \sum_{k=0}^{k=j-1} Z(t)[I - Z(\omega)]^{-1} Z^{-1}(\theta_{k+1}) \int_{\zeta_k}^{\zeta_{k+1}} X(\theta_{k+1}, s) f(s, z_s, z_{\gamma(s)})\, ds +$$
$$\sum_{k=j}^{k=p-1} Z(t)[I - Z(\omega)]^{-1} Z(\omega) Z^{-1}(\theta_{k+1}) \int_{\zeta_k}^{\zeta_{k+1}} X(\theta_{k+1}, s) f(s, z_s, z_{\gamma(s)})\, ds +$$
$$\int_{\zeta_j}^{t} X(t, s) f(s, z_s, z_{\gamma(s)})\, ds. \tag{4.22}$$

One can easily verify by substitution that (4.22) is a solution, and it is a continuous function. One can construct the following *Green function* for the *periodic solution*, $G_P(t, s), t, s \in [0, \omega]$, [9].

If $t \in [\theta_j, \theta_{j+1})$, $j = 0, 2, \ldots, p-1$, then

$$G_P(t, s) = \begin{cases} Z(t)[I - Z(\omega)]^{-1} Z^{-1}(\theta_{k+1}) X(\theta_{k+1}, s), & s \in [\zeta_k, \zeta_{k+1}), k < j, \\ Z(t)[I - Z(\omega)]^{-1} Z(\omega) Z^{-1}(\theta_{k+1}) X(\theta_{k+1}, s), & s \in [\zeta_k, \zeta_{k+1}) \backslash [\zeta_{\hat{j}}, t], k \geq j, \\ Z(t)[I - Z(\omega)]^{-1} Z(\omega) Z^{-1}(\theta_{k+1}) X(\theta_{k+1}, s) + X(t, s), & s \in [\zeta_{\hat{j}}, t] \end{cases}$$

Now, apply the last formula in (4.22) to see that the periodic solution satisfies

$$z(t) = \int_0^{\omega} G_P(t, s) f(s, z_s, z_{\gamma(s)}) ds.$$

Denote $\tilde{M} = \max_{t,s \in [0,\omega]} \|G(t, s)\| < \infty$. By applying the last integral equation, one can easily verify that the following theorem is valid.

Theorem 11 ([10]) *Suppose that conditions* $(Q1)$–$(Q9)$ *are valid, inequalities (4.20) and* $\tilde{M} L \omega < 1$ *hold. Then, (4.8) admits a unique* $\omega-$ *periodic solution.*

4.5.2 Almost Periodic Solutions

In this section, we will continue study system (4.8), assuming that all notations of the last section are valid. Concerning conditions $(Q1)$–$(Q13)$, we have to say that some of them are consequences of the almost periodicity.

For $f \in C_0(\mathbb{R})$ (respectively $C_0(\mathbb{R} \times \mathscr{C} \times \mathscr{C})$ and $\tau \in \mathbb{R}$, a translation of f by τ is a function $Q_\tau f = f(t+\tau)$, $t \in \mathbb{R}$ (respectively $Q_\tau f(t, \phi, \psi) = f(t+\tau, \phi, \psi)$, $(t, \phi, \psi) \in \mathbb{R} \times \mathscr{C} \times \mathscr{C}$). A number $\tau \in \mathbb{R}$ is called an $\varepsilon-$ translation number of a functional $f \in C_0(\mathbb{R})$ ($C_0(\mathbb{R} \times \mathscr{C} \times \mathscr{C})$) if $||Q_\tau f - f|| < \varepsilon$ for every $t \in \mathbb{R}$ ($(t, \phi, \psi) \in \mathbb{R} \times \mathscr{C} \times \mathscr{C}$). A set $S \subset \mathbb{R}$ is said to be relatively dense if there exists a number $l > 0$ such that $[a, a+l] \cap S \neq \emptyset$ for all $a \in \mathbb{R}$.

Definition 4 ([32]) A function (functional) $f \in C_0(\mathbb{R})(Q_0(\mathbb{R} \times \mathscr{C} \times \mathscr{C}))$ is said to be almost periodic (almost periodic in t uniformly with respect to $\phi, \psi \in \mathscr{C}_H \times \mathscr{C}_H$, $H > 0$) if for, every $\varepsilon \in \mathbb{R}, \varepsilon > 0$, there exists a relatively dense set of $\varepsilon-$ translation numbers of f.

Denote by $\mathscr{A}P(\mathbb{R})$ ($\mathscr{A}P(\mathbb{R} \times \mathscr{C}_H \times \mathscr{C}_H)$) the set of all such functions.

Definition 5 A sequence $a_i, i \in \mathbb{Z}$, is almost periodic, if for any $\varepsilon > 0$ there exists a relatively dense set of its $\varepsilon-$almost periods.

Let $\zeta_i^j = \zeta_{i+j} - \zeta_i, \theta_i^j = \theta_{i+j} - \theta_i$ for all i and j. We call the family of sequences $\{\zeta_i^j\}_i$, $j \in \mathbb{Z}$, equipotentially almost periodic [8, 30, 39] if for an arbitrary positive ε there exists a relatively dense set of $\varepsilon-$almost periods, common for all sequences $\{\zeta_i^j\}_i$, $j \in \mathbb{Z}$.

We assume that the following conditions are valid throughout this section:

(A1) $A_0, A_1 \in \mathscr{A}P(\mathbb{R})$;
(A2) $f \in \mathscr{A}P(\mathbb{R} \times \mathscr{C}_H \times \mathscr{C}_H)$ for each $H > 0$;
(A3) sequences ζ_i^j, $j \in \mathbb{Z}$, as well sequences θ_i^j, $j \in \mathbb{Z}$, are equipotentially almost periodic.

One can easily see that $(A1)$ implies $(Q1)$. From condition $(A3)$, it follows [8, 30, 39] that there exist positive numbers $\bar{\theta}$ and $\bar{\zeta}$ for $(Q5)$, and $|\theta_i|, |\zeta_i| \to \infty$, as $|i| \to \infty$. Let us prove an auxiliary assertion.

Lemma 5 *Let $\omega \in \mathbb{R}$ be a common $\eta-$ almost period of matrices $A_0(t)$, $A_1(t)$, then there exists a function $R(\eta) = \frac{R\tilde{M}e^{\alpha\bar{\theta}}}{\alpha}\eta$ such that*

$$\|Z(t+\omega, s+\omega) - Z(t+\omega, s+\omega)\| < R(\eta)e^{-\frac{\alpha}{2}(t-s)}, s \leq t. \tag{4.23}$$

Proof Set $W(t,s) = Z(t+\omega, s+\omega) - Z(t+\omega, s+\omega)$. Then

$$\frac{\partial W}{\partial t} = A_0(t)W(t,s) + A_1(t)W(\gamma(t), s) + [A_0(t+\omega) - A(t)]W(t+\omega, s+\omega) +$$

$$[A_1(t+\omega) - A(t)]W(\gamma(t)+\omega, s+\omega).$$

Since $W(s,s)=0$, from the last equation it follows that

$$W(t,s)=Z(t,s)\int_s^{\zeta_i}X(s,u)[A_0(u+\omega)-A(u)]Z(u+\omega,s+\omega)+$$

$$[A_1(u+\omega)-A(u)]Z(\gamma(u)+\omega,s+\omega)]\,du+$$

$$\sum_{k=i}^{k=j-1}Z(t,\theta_{k+1})\int_{\zeta_k}^{\zeta_{k+1}}X(\theta_{k+1},u)[A_0(u+\omega)-A(u)]Z(u+\omega,s+\omega)+$$

$$[A_1(u+\omega)-A(u)]Z(\gamma(u)+\omega,s+\omega)]\,du+$$

$$\int_{\zeta_j}^{t}X(t,u)[A_0(u+\omega)-A(u)]Z(u+\omega,s+\omega)+[A_1(u+\omega)-A(u)]Z(\gamma(u)+\omega,s+\omega)]\,du.$$

Then, we have that

$$\|W(t,s)\|\le\int_s^{\zeta_i}R\bar{M}\eta e^{-\alpha(t-s-\bar{\theta})}du+\sum_{k=i}^{k=j-1}\int_{\zeta_k}^{\zeta_{k+1}}R\bar{M}\eta e^{-\alpha(t-s-\bar{\theta})}du+\int_{\zeta_j}^{t}R\bar{M}\eta e^{-\alpha(t-s-\bar{\theta})}du\le$$

$$\int_s^{t}R\bar{M}\eta e^{-\alpha(t-s-\bar{\theta})}du=R\bar{M}\eta e^{-\alpha(t-s-\bar{\theta})}(t-s)\le\frac{R\bar{M}e^{\alpha\bar{\theta}}}{\alpha}\eta e^{-\frac{\alpha}{2}(t-s)}.$$

The lemma is proved.

The following assertion can be proved by the method of common almost periods developed in [18] (see, also, [39]).

Lemma 6 ([30]) *Assume that $f(t,\phi,\psi)$, and $\xi_j(t)$, $j=1,2,\dots,k$, are Bohr almost periodic in t. Conditions $(Q11)$, $(A3)$ are valid. Then, for arbitrary $H,\eta>0, 0<\nu<\eta$, there exist a respectively dense set of real numbers Ω and integers Q, such that for $\omega\in\Omega, q\in Q$, it is true that*

1. $\|f(t+\omega,\phi,\psi)-f(t,\phi,\psi)\|<\eta$, *for all* $\phi,\psi\in\mathscr{C}_H$;
2. $\|\xi_j(t+\omega)-\xi_j(t)\|<\eta$, $j=1,2,\dots,k, t\in\mathbb{R}$;
3. $|\zeta_i^q-\omega|<\nu, i\in\mathbb{Z}$;
4. $|\theta_i^q-\omega|<\nu, i\in\mathbb{Z}$.

Let us formulate the following assertion.

Theorem 12 ([10]) *Assume that conditions $(A1)$–$(A3)$, $(Q3)$, $(Q4)$, $(Q6)$–$(Q9)$, are valid. Then, (4.8) admits a unique almost periodic solution. If, additionally, conditions $(Q10)$–$(Q13)$ are valid then the solution is exponentially stable.*

Proof It follows from Theorem 10 that (4.8) admits a unique bounded on $\mathbb{R}$ solution $u(t)$, which is exponentially stable. We shall show that it is an almost periodic function. Consider the operator

$$\Pi y \equiv \int_{\zeta_j}^{t} X(t,s) f(s, y_s, y_{\gamma(s)})\, ds + \sum_{k=-\infty}^{k=j-1} Z(t, \theta_{k+1}) \int_{\zeta_k}^{\zeta_{k+1}} X(\theta_{k+1}, s) f(s, y_s, y_{\gamma(s)})\, ds,$$

again.

It is sufficient to verify that $\Pi y(t)$ is almost periodic, if $y(t)$ is. Fix positive ε. Suppose that ω and q satisfy conditions of Lemma 6, such that ω is an $\eta-$ translation number for y. We assume that $\theta_j + \eta < t < \theta_{j+1} - \eta$. Then, $t + \omega \in (\theta_i, \theta_{i+1})$ and $i = j + q$ [18, 39]. We have that

$$\Pi y(t+\omega) - \Pi y(t) = \int_{\zeta_i}^{t+\omega} X(t+\omega, s) f(s, y_s, y_{\gamma(s)})\, ds +$$

$$\sum_{k=-\infty}^{k=i-1} Z(t+\omega, \theta_{k+1}) \int_{\zeta_k}^{\zeta_{k+1}} X(\theta_{k+1}, s) f(s, y_s, y_{\gamma(s)})\, ds - \int_{\zeta_j}^{t} X(t,s) f(s, y_s, y_{\gamma(s)})\, ds +$$

$$\sum_{k=-\infty}^{k=j-1} Z(t, \theta_{k+1}) \int_{\zeta_k}^{\zeta_{k+1}} X(\theta_{k+1}, s) f(s, y_s, y_{\gamma(s)})\, ds,$$

Transform the last expression to

$$\Pi y(t+\omega) - \Pi y(t) = \int_{\zeta_i}^{t} X(t+\omega, s+\omega) f(s+\omega, y_{s+\omega}, y_{\gamma(s+\omega)})\, ds +$$

$$\sum_{k=-\infty}^{k=j-1} Z(t+\omega, \theta_{k+1+q}) \int_{\zeta_{k+q}}^{\zeta_{k+1+q}} X(\theta_{k+1+q}, s) f(s, y_s, y_{\gamma(s)})\, ds$$

$$- \int_{\zeta_j}^{t} X(t,s) f(s, y_s, y_{\gamma(s)})\, ds + \sum_{k=-\infty}^{k=j-1} Z(t, \theta_{k+1}) \int_{\zeta_k}^{\zeta_{k+1}} X(\theta_{k+1}, s) f(s, y_s, y_{\gamma(s)})\, ds =$$

$$\int_{\zeta_i}^{t} [X(t+\omega, s+\omega) f(s+\omega, y_{s+\omega}, y_{\gamma(s+\omega)}) - X(t,s) f(s, y_s, y_{\gamma(s)})]\, ds +$$

$$\sum_{k=-\infty}^{k=j-1} \{Z(t+\omega, \theta_{k+1+q}) \int_{\zeta_{k+q}}^{\zeta_{k+1+q}} X(\theta_{k+1+q}, s) f(s, y_s, y_{\gamma(s)})\, ds -$$

$$Z(t, \theta_{k+1}) \int_{\zeta_k}^{\zeta_{k+1}} X(\theta_{k+1}, s) f(s, y_s, y_{\gamma(s)})\, ds\}. \tag{4.24}$$

Let us begin with estimation of the first integral in the last expression, if $|t - s| \leq \bar{\theta}$. We have that

$$\|X(t+\omega,s+\omega)f(s+\omega,y_{s+\omega},y_{\gamma(s+\omega)})-X(t,s)f(s,y_s,y_{\gamma(s)})\|\leq$$

$$\|X(t+\omega,s+\omega)-X(t,s)\|\|f(s+\omega,y_{s+\omega},y_{\gamma(s+\omega)})\|+$$

$$\|X(t,s)\|\|f(s+\omega,y_{s+\omega},y_{\gamma(s+\omega)})-f(s,y_s,y_{\gamma(s)})\|.$$

At first, let us observe that $\|X(t+\omega,s+\omega)-X(t,s)\|<R_1(\eta)$, since of the "diagonal almost periodicity" of the fundamental matrix of solutions [18, 39].

Next, we have that

$$\|f(s+\omega,y_{s+\omega},y_{\gamma(s+\omega)})-f(s,y_s,y_{\gamma(s)})\|\leq\|f(s+\omega,y_{s+\omega},y_{\gamma(s+\omega)})-f(s,y_{s+\omega},y_{\gamma(s+\omega)})\|+$$

$$\|f(s,y_{s+\omega},y_{\gamma(s+\omega)})-f(s,y_s,y_{\gamma(s+\omega)})\|+\|f(s,y_s,y_{\gamma(s+\omega)})-f(s,y_s,y_{\gamma(s)})\|$$

Let us estimate the last three norms. The first one is less than η, since of the almost periodicity of f in t. The second one is less than $L\eta$, since of the almost periodicity of y and the Lipschitz condition. To evaluate the last one, we use again Lemma 6 and consider $\nu>0$ so small such that $|y(t')-y(t'')|<\eta$, if $|t'-t''|<\nu$. Then, we obtain that $\|y_{\gamma(t+\omega)}-y_{\gamma(t)}\|=\|y(\zeta_{i+q}+s)-y(\zeta_i+s)\|\leq\|y(\zeta_{i+q}+s)-y(\zeta_i+\omega+s)\|+\|y(\zeta_i+\omega+s)-y(\zeta_i+s)\|<2\eta$, for all $t\in\mathbb{R}$, $s\in[0,\omega]$, since $|\zeta_{i+q}-\zeta_i-\omega|<\nu$. Thus, the third norm is less than $2L\eta$. Now, from boundedness of $\|f(s+\omega,y_{s+\omega},y_{\gamma(s+\omega)})\|$ and $\|X(t,s)\|$, it implies that

$$\|X(t+\omega,s+\omega)f(s+\omega,y_{s+\omega},y_{\gamma(s+\omega)})-X(t,s)f(s,y_s,y_{\gamma(s)})\|\leq R_2(\eta),$$

and consequently, the first integral is less than $R_2(\eta)\bar{\theta}$, where $R_2\to 0$, as $\eta\to 0$.

Let us now estimate the sum in (4.24),

$$\sum_{k=-\infty}^{k=j-1}\{Z(t+\omega,\theta_{k+1+q})\int_{\zeta_{k+q}}^{\zeta_{k+1+q}}X(\theta_{k+1+q},s)f(s,y_s,y_{\gamma(s)})\,ds-Z(t,\theta_{k+1})\int_{\zeta_k}^{\zeta_{k+1}}X(\theta_{k+1},s)f(s,y_s,y_{\gamma(s)})\,ds\}.$$

We fix k in the sum and consider

$$\|Z(t+\omega,\theta_{k+1+q})\int_{\zeta_{k+q}}^{\zeta_{k+1+q}}X(\theta_{k+1+q},s)f(s,y_s,y_{\gamma(s)})\,ds-Z(t,\theta_{k+1})\int_{\zeta_k}^{\zeta_{k+1}}X(\theta_{k+1},s)f(s,y_s,y_{\gamma(s)})\,ds\|\leq$$

$$\|Z(t+\omega,\theta_{k+1+q})-Z(t,\theta_{k+1})\|\|\int_{\zeta_{k+q}}^{\zeta_{k+1+q}}X(\theta_{k+1+q},s)f(s,y_s,y_{\gamma(s)})\,ds\|+$$

$$\|Z(t,\theta_{k+1})\|\|\int_{\zeta_{k+q}}^{\zeta_{k+1+q}}X(\theta_{k+1+q},s)f(s,y_s,y_{\gamma(s)})\,ds-\int_{\zeta_k}^{\zeta_{k+1}}X(\theta_{k+1},s)f(s,y_s,y_{\gamma(s)})\,ds\|.$$

We have that

$$\|Z(t+\omega,\theta_{k+1+q})-Z(t,\theta_{k+1})\|\le\|Z(t+\omega,\theta_{k+1+q})-Z(t+\omega,\theta_{k+1}+\omega)\|+$$

$$\|Z(t+\omega,\theta_{k+1}+\omega)-Z(t,\theta_{k+1})\|.$$

Then,

$$\|Z(t+\omega,\theta_{k+1+q})-Z(t+\omega,\theta_{k+1}+\omega)\|\le$$

$$\|Z(t+\omega,\theta_{k+1+q})\|\|I-Z(\theta_{k+1+q},\theta_{k+1}+\omega)\|\le KR_3(\eta)\mathrm{e}^{-\alpha(t+\omega-\theta_{k+1+q})},$$

where $R_3\to 0$ as $\eta\to 0$. Moreover,

$$\|Z(t+\omega,\theta_{k+1}+\omega)-Z(t,\theta_{k+1})\|\le R(\eta)\mathrm{e}^{-\frac{\alpha}{2}(t-\theta_{k+1})},$$

since of Lemma 5.

Thus, it is true that

$$\|Z(t+\omega,\theta_{k+1+q})-Z(t,\theta_{k+1})\|\le R_4(\eta)\mathrm{e}^{-\frac{\alpha}{2}(t-\theta_{k+1})}.$$

There exist numbers $\nu_1,\nu_2,|\nu_j|<\eta$, $j=1,2$, such that $\zeta_{k+q+1}=\zeta_{k+1}+\omega+\nu_2$ and $\zeta_{k+q}=\zeta_k+\omega+\nu_1$. Let us make the following transformations,

$$\int_{\zeta_{k+q}}^{\zeta_{k+1+q}}X(\theta_{k+1+q},s)f(s,y_s,y_{\gamma(s)})\,ds-\int_{\zeta_k}^{\zeta_{k+1}}X(\theta_{k+1},s)f(s,y_s,y_{\gamma(s)})\,ds=$$

$$\int_{\zeta_k+\omega+\nu_1}^{\zeta_k+\omega}X(\theta_{k+1+q},s)f(s,y_s,y_{\gamma(s)})\,ds-\int_{\zeta_{k+1}+\omega+\nu_2}^{\zeta_{k+1}+\omega}X(\theta_{k+1+q},s)f(s,y_s,y_{\gamma(s)})\,ds+$$

$$\int_{\zeta_k}^{\zeta_{k+1}}[X(\theta_{k+1+q},s+\omega)f(s+\omega,y_{s+\omega},y_{\gamma(s+\omega)})-X(\theta_{k+1},s)f(s,y_s,y_{\gamma(s)})]\,ds$$

Apply to the last expressions discussion similar to that made above to obtain that

$$\|\int_{\zeta_{k+q}}^{\zeta_{k+1+q}}X(\theta_{k+1+q},s)f(s,y_s,y_{\gamma(s)})\,ds-\int_{\zeta_k}^{\zeta_{k+1}}X(\theta_{k+1},s)f(s,y_s,y_{\gamma(s)})\,ds\|\le R_5(\eta),$$

where $R_5\to 0$, as $\eta\to 0$.

Write $\tilde{M}=\sup_{\mathbb{Z}}\|\int_{\zeta_{k+q}}^{\zeta_{k+1+q}}X(\theta_{k+1+q},s)f(s,y_s,y_{\gamma(s)})\,ds\|<\infty$ and obtain that

$$\|\Pi y(t+\omega)-\Pi y(t)\|\le R_2(\eta)\bar{\theta}+\sum_{k=-\infty}^{k=j-1}\{R_4(\eta)\tilde{M}\mathrm{e}^{-\frac{\alpha}{2}(t-\theta_{k+1})}+R_5(\eta)K\mathrm{e}^{-\alpha(t-\theta_{k+1})}\}\le$$

$$R_2(\eta)\bar{\theta} + R_4(\eta)\tilde{M}\frac{\mathrm{e}^{\frac{\alpha}{2}\bar{\theta}}}{1-\mathrm{e}^{-\frac{\alpha}{2}\underline{\theta}}} + R_5(\eta)K\frac{\mathrm{e}^{\alpha\bar{\theta}}}{1-\mathrm{e}^{-\alpha\underline{\theta}}}.$$

From the properties of functions R_j, it follows that if η is sufficiently small, then

$$\|\Pi y(t+\omega) - \Pi y(t)\| \leq \varepsilon/2,$$

if $\theta_i + \eta < t < \theta_{i+1} - \eta$. Now, use uniform continuity of Πy and take η so small that $\|\Pi y(t') - \Pi Y(t'')\| < \varepsilon/2$, if $|t' - t''| < \eta$. Then, ω is an $\varepsilon-$almost period of $\Pi y(t)$.

The theorem is proved.

4.5.3 Examples

Example 2 Let us give examples of the function $f(t, x_t, x_{\gamma(t)})$ in (4.8).

1. $$\sum_{j=1}^{m} A_j(t)x(t-\tau_j) + \sum_{i=1}^{k} B_i(t)x(\gamma(t)-\omega_j),$$

   where τ_j and ω_i are fixed positive numbers. The linear function is with constant delays and alternate constancy of argument;

2. $$\sum_{j=1}^{m} A_j(t)x(t-\tau_j(t)) + \sum_{i=1}^{k} B_i(t)x(\gamma(t)-\omega_j(t)),$$

   where $\tau_j(t)$ and $\omega_i(t)$ are fixed bounded positive functions. This linear function is with variable delays and alternate constancy of argument;

3. $$\int_{-\tau}^{0} K(s, x(t+s))ds + \int_{-\gamma(t)}^{0} L(s, x(\beta(t)+s))ds.$$

   The function is with bounded distributed delay, and constancy of argument is of two types, alternate and retarded.

4. $$\int_{-\infty}^{0} K(s, x(t+s))ds + \int_{-\infty}^{0} L(s, x(\beta(t)+s))ds.$$

   The function is with unbounded distributed delay and retarded constancy of argument.

One can easily see that the Lipschitz condition is valid for the last examples, if coefficient functions A_j and B_i are bounded, and functions K and L are

Lipschitzian. Finally, one can remark that functions of the form $f(t, x(t), x(\gamma(t)))$ are also particular case of the functional $f(t, x_t, x_{\gamma(t)})$.

Example 3 Consider the system

$$z'(t) = A_0 z(t) + A_1 z(\gamma(t)) + f(t, z_t, z_{\gamma(t)}), \tag{4.25}$$

where $z = \begin{pmatrix} z_1 \\ z_2 \end{pmatrix}$, and $A_0 = \begin{pmatrix} 0 & 0 \\ a & 0 \end{pmatrix}$, $A_1 = \begin{pmatrix} k & 0 \\ 0 & 0 \end{pmatrix}$.

We find that $X(t, s) = \begin{pmatrix} 1 & 0 \\ 0 & \mathrm{e}^{a(t-s)} \end{pmatrix}$, and

$$M_i(\theta_i) = \begin{pmatrix} 1 + k(\theta_i - \zeta_i) & 0 \\ 0 & \mathrm{e}^{a(\theta_i - \zeta_i)} \end{pmatrix}, M_{i-1}(\theta_i) = \begin{pmatrix} 1 + k(\theta_i - \zeta_{i-1}) & 0 \\ 0 & \mathrm{e}^{a(\theta_i - \zeta_{i-1})} \end{pmatrix}, i \in \mathbb{Z}.$$

Next, we have that

$$G = M_i^{-1}(\theta_i) M_{i-1}(\theta_i) = \begin{pmatrix} \frac{1+k(\theta_i - \zeta_{i-1})}{1+k(\theta_i - \zeta_i)} & 0 \\ 0 & \mathrm{e}^{a(\zeta_i - \zeta_{i-1})} \end{pmatrix}.$$

From (4.12), it implies that the zero solution of (4.10) is uniformly exponentially stable, if

$$\sup_i \left| \frac{1 + k(\theta_i - \zeta_{i-1})}{1 + k(\theta_i - \zeta_i)} \right| < 1, \sup_i \mathrm{e}^{a(\zeta_i - \zeta_{i-1})} < 1.$$

Assume that the last two inequalities are correct. Then, system (4.25) admits uniformly asymptotically stable bounded, periodic, or almost periodic solution, if the Lipschitz constant is sufficiently small and sequences θ, ζ and functional f satisfy appropriate properties of periodicity and almost periodicity mentioned for Theorems 10–11.

Let us discuss more specific cases. Assume, first, that $\theta_i = \zeta_i = i, i \in \mathbb{Z}$. Then, matrix

$$G = \begin{pmatrix} 1 + k & 0 \\ 0 & \mathrm{e}^a \end{pmatrix}, i \in \mathbb{Z}.$$

Denote by ρ_j, $j = 1, 2$, eigenvalues of matrix G. They are *multipliers* of system (4.25). From (4.12), it implies that the zero solution of (4.3) is exponentially stable, if and only if absolute values of both multipliers are less than one. Easy to see that $|\rho_1| = |1 + k|$, $|\rho_2| = \mathrm{e}^a$, and sufficient conditions for uniform asymptotic stability of the bounded solution are $a < 0, -2 < k < 0$.

Now, suppose that the piecewise constant argument is advanced, $\theta_{i+1} = \zeta_i = i + 1$. This time $\rho_1 = (1 - k)^{-1}$, $\rho_2 = \mathrm{e}^a$, and sufficient conditions for asymptotic stability are $a < 0, k > 0$ or $k < -2$.

Example 4 Consider the following sequence, $\theta_i = i + a_i$, where $a_i = \frac{1}{4}|\sin(i) - \cos(i\sqrt{2})|$. By repeating proof of [18, 39], one can verify that θ satisfies the conditions of the last theorem. That is, sequences θ_i^j are equipotentially almost periodic, and there are positive numbers $\bar{\theta}$ and $\underline{\theta}$ such that $\underline{\theta} < \theta_{i+1} - \theta_i \leq \bar{\theta}, i \in \mathbb{Z}$. Now, introduce a sequence ζ such that $\zeta_i = \frac{\theta_{i+1}+\theta_i}{2}$. One can easily verify that this sequence also satisfies all conditions of the theorem. Moreover, $\bar{\zeta} = \bar{\theta}, \underline{\zeta} = \underline{\theta}$. So, we fix the chosen sequences and define on this basis the function $\gamma(t)$. Introduce the following *RFDEPCA*,

$$x'(t) = \alpha x(t) + \beta x(\gamma(t)) + f(t, x_t, x_{\gamma(t)}), \tag{4.26}$$

in which α, β are fixed real constants, the identification function $\gamma(t)$ is defined above, and function f can be chosen, for example, as the following one,

$$f(t, x_t, x_{\gamma(t)}) = L\sin(\gamma(t))cos^2(\pi t)\int_{-2}^{0}[x^2(t+s) + x^4(\gamma(t)+s)]ds.$$

It is obvious that it remains to check whether the zero solution of the equation

$$y'(t) = \alpha y(t) + \beta y(\gamma(t)), \tag{4.27}$$

is uniformly exponentially stable.

We investigated the equation in [4, 18] with simple case of $\gamma(t)$. One can evaluate that

$$M_i(t) = \mathrm{e}^{\alpha(t-\zeta_i)} + \int_{\zeta_i}^{t} \mathrm{e}^{\alpha(t-s)}\beta ds = \mathrm{e}^{\alpha(t-\zeta_i)} + \frac{\beta}{\alpha}\left(\mathrm{e}^{\alpha(t-\zeta_i)} - 1\right).$$

Then,

$$M_i(\theta_i) = \mathrm{e}^{-\alpha\frac{\theta_{i+1}-\theta_i}{2}} + \frac{\beta}{\alpha}(\mathrm{e}^{-\alpha\frac{\theta_{i+1}-\theta_i}{2}} - 1),$$

$$M_{i-1}(\theta_i) = \mathrm{e}^{\alpha\frac{\theta_i-\theta_{i-1}}{2}} + \frac{\beta}{\alpha}(\mathrm{e}^{\alpha\frac{\theta_i-\theta_{i-1}}{2}} - 1),$$

and

$$M_i^{-1}(\theta_i)M_{i-1}(\theta_i) = \frac{\mathrm{e}^{\alpha\frac{\theta_i-\theta_{i-1}}{2}} + \frac{\beta}{\alpha}(\mathrm{e}^{\alpha\frac{\theta_i-\theta_{i-1}}{2}} - 1)}{\mathrm{e}^{-\alpha\frac{\theta_{i+1}-\theta_i}{2}} + \frac{\beta}{\alpha}(\mathrm{e}^{-\alpha\frac{\theta_{i+1}-\theta_i}{2}} - 1)}.$$

Now, we assume that $\alpha < 0$, $\beta > 0$, and $\frac{|\beta|}{|\alpha|} < 1$. Then, one can find that

$$\left| \frac{e^{\alpha \frac{\theta_i - \theta_{i-1}}{2}} + \frac{\beta}{\alpha}(e^{\alpha \frac{\theta_i - \theta_{i-1}}{2}} - 1)}{e^{-\alpha \frac{\theta_{i+1} - \theta_i}{2}} + \frac{\beta}{\alpha}(e^{-\alpha \frac{\theta_{i+1} - \theta_i}{2}} - 1)} \right| \leq q < 1, i \in \mathbb{Z},$$

with some positive number q. The last inequality is sufficient for the zero solution of (4.27) to be uniformly exponentially stable, and then, Eq. (4.26) admits a unique almost periodic solution, if the constant L is sufficiently small.

4.6 Further Investigations

In this part of the chapter, we describe some of problems, which can be studied on the basis of our present results. Firstly, several models (population dynamics, optimal control, ship stabilization) will be considered. Secondly, we introduce differential equations, which are much more general, in some sense, than those we investigated in the paper, but they still are *FDEPCA*.

A number of models with piecewise argument are considered in [8, 22, 24]. In what follows, we propose a very short list of models which are *FDEPCA*.

One may investigate the following prey–predator Volterra system with piecewise constant argument,

$$\begin{aligned} x'(t) &= [a_1 - b_1 y(t) - \int_{-\tau}^{0} Q_1(s) y(\beta_1(t) + s) ds] x(t), \\ y'(t) &= [a_2 + b_2 y(t) + \int_{-\tau}^{0} Q_2(s) x(\beta_2(t) + s) ds] y(t). \end{aligned} \tag{4.28}$$

In this equation, we assume that the effect of the species accumulation is seen only near the moments of discontinuity, which can, for example, depend on seasonal behavior of animals. It is natural that two different constancy functions, β_1, β_2, are considered, for each of the two species. The model is *RFDERCA*.

Similar arguments for investigation can be accepted for the following equation of an isolated population [27],

$$x'(t) = -\alpha[\int_{-\tau}^{0} x(\beta(t) + s) d\eta(s)](1 + x(t)). \tag{4.29}$$

More biological arguments for equations with piecewise constant argument can be found in our book [8].

It is obvious that piecewise continuous control is easier to apply than continuous one. The following control problem for *FDE* with *MCA* can be investigated,

$$x'(t) = P(t)x(t) + B(t)u(\gamma(t)),$$
$$y(t) = Q(t)x(t),$$
$$u'(t) = \int_{-\tau}^{0} [d_s\eta(t,s)]y(\gamma(t)+s) + \int_{-\tau}^{0} [d_s\mu(t,s)]u(\gamma(t)+s). \quad (4.30)$$

which is the generalization of the optimal control problem in [34]. One has to emphasis that alternate constancy function γ does not make theoretical investigation more difficult as it is for advanced argument in *FDE* [31, 35].

Consider one technical problem, ship stabilization. The following retarded functional differential equation is discussed in [33],

$$a\phi^{'''}(t) + b\phi^{''}(t) + c\phi'(t-\tau) + d\phi(t-\tau) = 0,$$

In the last equation, ϕ is the ship deviation angle. The time lag τ is utilized, since it is impossible to measure ship deviation instantaneously. Technically, it is easy to use the deviation function $\beta(t)$ for control. So, we obtain the following *FDEPCA*,

$$a\phi^{'''}(t) + b\phi^{''}(t) + c\phi'(t-\tau) + d\phi(t-\tau) + e\phi'(\beta(t)) + f\phi(\beta(t)) = 0.$$

Finally, anticipated deviation one can be considered for control, and we obtain the following *FDEPCA*,

$$a\phi^{'''}(t) + b\phi^{''}(t) + c\phi'(t-\tau) + d\phi(t-\tau) + e\phi'(\beta(t)) + f\phi(\beta(t)) + g\phi'(\chi(t)) + h\phi(\chi(t)) = 0.$$

Thus, *FDE* with *RCA* and *MCA* can be investigated for the ship stabilization.

Next, we consider argument functions of more general type than those have been analyzed in the main body of the paper. Denote by $\theta = \{\theta_i\}$, $i \in \mathbb{Z}$, $\theta \subset \mathbb{R}$, a strictly ordered sequence of real numbers such that $|\theta_i| \to \infty$ as $|i| \to \infty$. Let, also, $\zeta = \{\zeta_i\}$, $i \in \mathbb{Z}$, be another sequence of elements of $\mathbb{R}$. This sequence may be strictly increasing or non-decreasing, and it is not necessary that $\zeta_i \in [\theta_i, \theta_{i+1}]$. We say that a function, which is defined on $\mathbb{R}$, is of the $\eta-$type and denote it $\eta(t)$, if it is equal to ζ_i, whenever $\theta_i \le t < \theta_{i+1}$, $i \in \mathbb{Z}$. This type of functions has been introduced in [8]. Now, we can suggest to consider the following functional differential equation with piecewise constant argument,

$$x'(t) = f(t, x_t, x_{\eta(t)}). \quad (4.31)$$

What is the main difference between the last system and Eqs. (4.1)–(4.3)? Values of function η are not necessary in the interval of constancy, where t lies in. Consequently, one has more interesting opportunities in investigation. For example, one can request that $\eta(t) = \theta_{i+1}$ for $t \in [\theta_i, \theta_{i+1})$. It is of great mathematical interest to investigate these type o equations, as well it provides more opportunities for applications.

Since any differential equation with piecewise constant argument is a differential equation with *deviated argument*, one can suppose that they are functional differential

equations. We, on the basis of our experience, propose to consider two classes of equations, which relate to each other similarly to ordinary differential equations and functional differential equations. That is, there have to be *EPCAG* and *FDEPCA*. If one considers Eqs. (4.1)–(4.3), there is no doubt that they are *FDEPCA*. Let us introduce another example to illustrate our point of view,

$$x' = f(t, x(t), x(\eta_1(t)), x(\eta_2(t)), \ldots, x(\eta_m(t))), \tag{4.32}$$

where $t \in \mathbb{R}$, $x \in \mathbb{R}^n$, function f is continuous in all arguments, η_j, $j = 1, 2, \ldots, m$, are piecewise constant functions of $\eta-$type. We call (4.32) differential equation with piecewise constant argument (EPCAG, and not *FDE*), if the following condition holds,

(A) For each $j = 1, 2, \ldots, m$, and $t \in J$, the values of function $\eta_j(t)$ and t are in the same interval of constancy of $\eta_j(t)$.

If there is a function η_j in (4.32) such that (A) does not hold for all t from the domain, then (4.32) is a *functional differential equation with piecewise constant argument*, *FDEPCA*.

Assume that function f in (4.32) is defined not for all $t \in \mathbb{R}$, but in some subset $J \subset \mathbb{R}$. In this case, one should request that $\eta_j(t) \in J$ for all j and $t \in J$.

Let us provide more concrete examples. Fix strictly increasing sequences of real numbers θ_i^j, $i \in \mathbb{Z}$, $j = 1, 2, \ldots, m$, and sequences ζ_i^j, $\theta_i^j \le \zeta_i^j \le \theta_{i+1}$, $i \in \mathbb{Z}$, $j = 1, 2, \ldots, m$. Define functions $\eta_j(t) = \zeta_i^j$, if $t \in [\theta_i^j, \theta_{i+1}^j)$. One can easily see that (4.32) is *EPCAG*, and this system is not *FDEPCA*. Now, define $\eta_j(t) = \zeta_{i-1}^j$, if $t \in [\theta_i^j, \theta_{i+1}^j)$. In this case, condition (A) is not valid, and (4.32) is *FDEPCA*. One can call it retarded functional differential equation with piecewise constant argument. Nevertheless, this equation is not of the same type as (4.2).

Finally, we suggest a new name for functional differential equations with piecewise constant argument, *functional differential equations with functional response on piecewise constant argument*, *FDEFRPCA*. This class of systems may involve all equations considered in the present paper, and moreover, we suggest to investigate and to apply in modeling of real-world problems the following types of equations,

$$x' = f(t, x_t, x_{\beta(t-\tau(t))}), \tag{4.33}$$

$$x' = f(t, x_t, x_{\gamma(t-\tau(t))}), \tag{4.34}$$

and

$$x' = f(t, x_t, x_{\chi(t-\tau(t))}), \tag{4.35}$$

where $\tau(t)$ is a deviation function, which is positive, negative, or alternate type.

Our proposals that have been formulated just above show that the there are various functional differential equations with piecewise constant argument, and they may provide more theoretical challenges and ways of solutions for real- world problems.

References

1. Akhmet, M.U.: On the integral manifolds of the differential equations with piecewise constant argument of generalized type. In: Agarval, R.P., Perera, K. (eds.) Proceedings of the Conference on Differential and Difference Equations at the Florida Institute of Technology, pp. 11–20. Hindawi Publishing Corporation (2006)
2. Akhmet, M.U.: Integral manifolds of differential equations with piecewise constant argument of generalized type. Nonlinear Anal. **66**, 367–383 (2007)
3. Akhmet, M.U.: On the reduction principle for differential equations with piecewise constant argument of generalized type. J. Math. Anal. Appl. **336**, 646–663 (2007)
4. Akhmet, M.U.: Stability of differential equations with piecewise constant argument of generalized type. Nonlinear Anal. TMA **68**, 794–803 (2008)
5. Akhmet, M.U.: Almost periodic solutions of differential equations with piecewise constant argument of generalized type. Nonlinear Anal. HS **2**, 456–467 (2008)
6. Akhmet, M.U.: Asymptotic behavior of solutions of differential equations with piecewise constant arguments. Appl. Math. Lett. **21**, 951–956 (2008)
7. Akhmet, M.U.: Almost periodic solutions of the linear differential equation with piecewise constant argument. Discret. Impuls. Syst. Ser. A, Math. Anal. **16**, 743–753 (2009)
8. Akhmet, M.U.: Nonlinear Hybrid Continuous/Discrete Time Models. Antlantis Press, Amsterdam (2011)
9. Akhmet, M.U.: Exponentially dichotomous linear systems of differential equations with piecewise constant argument. Discontinuity, Nonlinearity Complex. **1**, 337–352 (2012)
10. Akhmet, M.U.: Quasilinear retarded differential equations with functional dependence on piecewise constant argument. Commun. Pure Appl. Anal. **13**, 929–947 (2014)
11. Akhmet, M.U., Aruğaslan, D.: Lyapunov–Razumikhin method for differential equations with piecewise constant argument. Discrete Contin. Dyn. Syst. **25**, 457–466 (2009)
12. Akhmet, M.U., Aruğaslan, D., Yilmaz, E.: Stability in cellular neural networks with piecewise constant argument. J. Comput. Appl. Math. **233**, 2365–2373 (2010)
13. Akhmet, M.U., Aruğaslan, D., Yilmaz, E.: Stability analysis of recurrent neural networks with piecewise constant argument of generalized type. Neural Netw. **23**, 805–811 (2010)
14. Akhmet, M.U., Aruğaslan, D., Yilmaz, E.: Method of Lyapunov functions for differential equations with piecewise constant delay. J. Comput. Appl. Math. **235**, 4554–4560 (2011)
15. Akhmet, M.U., Buyukadali, C.: Differential equations with a state-dependent piecewise constant argument. Nonlinear Anal. TMA **72**, 4200–4210 (2010)
16. Akhmet, M.U., Buyukadali, C.: Periodic solutions of the system with piecewise constant argument in the critical case. Comput. Math. Appl. **56**, 2034–2042 (2008)
17. Akhmet, M.U., Buyukadali, C., Ergenc, T.: Periodic solutions of the hybrid system with small parameter. Nonlinear Anal. HS **2**, 532–543 (2008)
18. Akhmetov, M. U., Perestyuk, N.A., Samoilenko, A.M. : Almost-periodic solutions of differential equations with impulse action (Russian). Akad. Nauk Ukrain. SSR Inst. Mat. Preprint, no. 26. p. 49 (1983)
19. Alonso, A., Hong, J., Obaya, R.: Almost periodic type solutions of differential equations with piecewise constant argument via almost periodic type sequences. Appl. Math. Lett. **13**, 131–137 (2000)
20. Bao, G., Wen, S., Zeng, Z.: Robust stability analysis of interval fuzzy CohenGrossberg neural networks with piecewise constant argument of generalized type. Neural Netw. **33**, 32–41 (2012)
21. Burton, T.A.: Stability and Periodic Solutions of Ordinary and Functional Differential Equations. Academic Press, Orlando (1985)
22. Busenberg, S., Cooke, K.L.: Models of vertically transmitted diseases with sequential-continuous dynamics. Nonlinear Phenomena in Mathematical Sciences. Academic Press, New York (1982)
23. Cooke, K.L., Wiener, J.: Retarded differential equations with piecewise constant delays. J. Math. Anal. Appl. **99**, 265–297 (1984)

24. Dai, L.: Nonlinear Dynamics of Piecewise Constant Systems and Implementation of Piecewise Constant Arguments. World Scientific, Hackensack (2008)
25. Diekmann, O., van Gils, S.A., Verduyn, L., Sjoerd, M., Walther, H.-O.: Delay Equations. Functional, Complex, and Nonlinear Analysis. Applied Mathematical Sciences, vol. 110. Springer, New York (1995)
26. Dai, L., Singh, M.C.: On oscillatory motion of spring-mass systems subjected to piecewise constant forces. J. Sound Vibration **173**, 217–232 (1994)
27. Dunkel, G.: Single-species model for population growth depending on past history. Seminar of Differential Equations and Dynamical Systems. Lecture Notes in Mathematics, vol. 60. Springer, Berlin (1968)
28. Elsgolts, L.E. : Introduction to the Theory of Differential Equations with Deviating Arguments. Holden-Day, Inc. (1966)
29. Gopalsamy, K., Zhang, B.G.: On a neutral delay logistic equation. Dyn. Stab. Syst. **2**, 183–195 (1988)
30. Halanay, A., Wexler, D.: Qualitative Theory of Impulsive Systems (Russian). Mir, Moscow (1971)
31. Hale, J., Lunel, S.M.V.: Introduction to Functional Differential Equations. Springer, New York (1993). Wiley, New York (1964)
32. Fink, A.M.: Almost-Periodic Differential Equations. Lecture Notes in Mathematics. Springer, Berlin (1974)
33. Kolmanovskii, V.B.: Stability of Functional Differential Equations. Academic Press, Orlando (1986)
34. Krasovskii, N.N.: Certain problems in the theory of stability of motion. (Russian) Gosudarstv. Izdat. Fiz.-Mat. Lit., Moscow (1959)
35. Kuang, Y.: Delay Differential Equations with Applications in Population Dynamics. Academic Press, Boston (1993)
36. Küpper, T., Yuan, R.: On quasi-periodic solutions of differential equations with piecewise constant argument. J. Math. Anal. Appl. **267**, 173–193 (2002)
37. Papaschinopoulos, G.: Some results concerning a class of differential equations with piecewise constant argument. Math. Nachr. **166**, 193–206 (1994)
38. Pinto, M.: Asymptotic equivalence of nonlinear and quasi linear differential equations with piecewise constant arguments. Math. Comput. Modelling **49**, 1750–1758 (2009)
39. Samoilenko, A., Perestyuk, N.: Impulsive Differential Equations. World Scientific, Singapore (1995)
40. Seifert, G.: Almost periodic solutions of certain differential equations with piecewise constant delays and almost periodic time dependence. J. Differ. Equ. **164**, 451–458 (2000)
41. Wang, G.: Periodic solutions of a neutral differential equation with piecewise constant arguments. J. Math. Anal. Appl. **326**, 736–747 (2007)
42. Wang, G.Q., Cheng, S.S.: Note on the set of periodic solutions of a delay differential equation with piecewise constant argument. Int. J. Pure Appl. Math. **9**, 139–143 (2003)
43. Wang, G.Q., Cheng, S.S.: Existence of periodic solutions for a neutral differential equation with piecewise constant argument. Funkcial. Ekvac. **48**, 299–311 (2005)
44. Wang, L., Yuan, R., Zhang, C.: Corrigendum to: "on the spectrum of almost periodic solution of second order scalar functional differential equations with piecewise constant argument" [J. Math. Anal. Appl. 303 (2005), 103–118, by Yuan, R.]. J. Math. Anal. Appl. **349**, 299 (2009)
45. Wang, Y., Yan, J.: Oscillation of a differential equation with fractional delay and piecewise constant argument. Comput. Math. Appl. **52**, 1099–1106 (2006)
46. Wang, Z., Wu, J.: The stability in a logistic equation with piecewise constant arguments. Differ. Equ. Dyn. Syst. **14**, 179–193 (2006)
47. Wiener, J.: Generalized Solutions of Functional Differential Equations. World Scientific, Singapore (1993)

Chapter 5
Grazing in Impulsive Differential Equations

M.U. Akhmet and A. Kıvılcım

5.1 Introduction

Grazing phenomenon is one of the attractive features for nonlinear dynamics [7, 8, 23]. There are two approaches for the definition of grazing in literature. One is presented in the studies of Bernardo, Budd and Champneys [7, 8], Bernardo and Hogan [9], and Luo [17, 18, 20, 21]. In these studies, it is asserted that grazing occurs when a trajectory hits the surface of discontinuity tangentially. In [24–27], Nordmark defines grazing as the approach of the velocity to zero in the neighborhood of the surface of discontinuity which is the case of the studies conducted in [7–9, 17–21]. Our comprehension of grazing in this study is close to that one in [7, 9, 17].

In this study, we model the dynamics with grazing impacts by utilizing differential equations with impulses at variable moments and applying the methods of [1–3]. As a consequence of such methods, the role of the mappings [24–27] is diminished. One can observe that a trajectory at a grazing point may have tangency to the surface of discontinuity, which is parallel to one or several coordinate axises. Particularly, it means the velocity approaches to zero [24–27].

The papers [7–9, 17–21, 24–27] can be combined in the following way; that is, vector field is the function of both time and space variables, and the jump functions and the surfaces are defined only through space variables. Then, it is easy to call these ones non-autonomous systems with stationary impulses. However, there are some systems whose vector fields, surfaces of discontinuity and jump functions are defined only through space variables, then these ones are called autonomous system. Moreover, under certain conditions, some autonomous systems define a discontinuous dynamical system [3]. Eventually, there are some impulsive systems

M.U. Akhmet (✉) · A. Kıvılcım
Department of Mathematics, Middle East Technical University, 06800 Ankara, Turkey
e-mail: marat@metu.edu.tr

A. Kıvılcım
e-mail: kivilcim@metu.edu.tr

D. Volchenkov and X. Leoncini (eds.), *Regularity and Stochasticity of Nonlinear Dynamical Systems*, Nonlinear Systems and Complexity 21,
DOI 10.1007/978-3-319-58062-3_5

whose vector field and the surfaces of discontinuity are the functions of both time and space variables. These systems are called non-autonomous impulsive differential equations.

For investigation of autonomous differential equations, it is convenient to utilize properties of dynamical systems. The studies of discontinuous dynamical systems with transversal intersections of orbits and surfaces, B-smooth discontinuous flows, can be found in [1–3]. In this research, the dynamics is approved for systems with grazing orbits. Moreover, the definitions of orbital stability and asymptotic phase are adapted to grazing cycles. The orbital stability theorem is proved, which cannot be underestimated for theory of impact mechanisms. In the second half of the chapter, we consider grazing in non-autonomous systems with stationary impulsive conditions and give appropriate definitions, obtain the variational system for the grazing periodic solutions, investigate the stability of them and analyze regular perturbations around the grazing periodic solutions.

5.2 Discontinuous Dynamical Systems

Let $\mathbb{R}$, $\mathbb{N}$ and $\mathbb{Z}$ be the sets of all real numbers, natural numbers and integers, respectively. Consider the set $D \in \mathbb{R}^n$ such that $D = \cup D_i$, where D_i, $i = 1, 2, \ldots, k$, components of D, are disjoint open connected subsets of $\mathbb{R}^n$. To describe the surface of discontinuity, we present a two times continuously differentiable function $\Phi : D^r \to \mathbb{R}^n$. The set can be defined as $\Gamma = \Phi^{-1}(0)$ and is a closed subset of $\bar{D}$, where $\bar{D}$ is the closure of D. Denote $\partial\Gamma$ as the boundary of Γ. One can easily see that $\Gamma = \cup_{i=1}^{k} \Gamma_i$, where Γ_i are parts of the surface of discontinuity in the components of D. Denote $\tilde{\Gamma} = J(\Gamma)$, $\tilde{\Phi}(x) = \Phi(J^{-1}(x))$. Denote an r-neighborhood of D in $\mathbb{R}^n$ for a fixed $r > 0$ as D^r. Let Γ^r be the r-neighborhood of Γ in $\mathbb{R}^n$, for a fixed $r > 0$ and define functions $J : \Gamma^r \to D^r$ and $\tilde{J} : \tilde{\Gamma}^r \to D^r$, such that, $J(\Gamma)$, $\tilde{J}(\tilde{\Gamma}) \subset D$. Assume that a function $f(x) : D^r \to \mathbb{R}^n$ is continuously differentiable in D^r. Set the gradient vector of Φ as $\nabla\Phi(x)$.

The following definitions will be utilized in the remaining part of the study. Let $x(t-)$ be the left limit position of the trajectory and $x(t+)$ be the right limit of the position of the trajectory at the moment t. Define $\Delta x(t) := x(t+) - x(t-)$ as the jump operator for a function $x(t)$ such that $x(t) \in \Gamma$ and t is a moment of discontinuity (discontinuity moment). In other words, the discontinuity moment t is the moment when the trajectory meets the surface of discontinuity Γ. The function $I(x)$ will be used in the following part of the chapter which is defined as $I(x) := J(x) - x$, for $x \in \Gamma$.

The following assumptions are needed throughout this study.

(C1) $\nabla\Phi(x) \neq 0$ for all $x \in \Gamma$,

(C2) $J \in C^1(\Gamma^r)$ and $\det\left[\frac{\partial J(x)}{\partial x}\right] \neq 0$, for all $x \in \Gamma^r \setminus \partial\Gamma$,

(C3) $\Gamma \bigcap \tilde{\Gamma} \subseteq \partial\Gamma \cap \partial\tilde{\Gamma}$,

(C4) $\langle \nabla \Phi(x), f(x) \rangle \neq 0$ if $x \in \Gamma \setminus \partial\Gamma$,
(C5) $\langle \nabla \tilde{\Phi}(x), f(x) \rangle \neq 0$ if $x \in \tilde{\Gamma} \setminus \partial\tilde{\Gamma}$,
(C6) $J(x) = x$ for all $x \in \partial\Gamma$,
(C7) $\tilde{J}(x) = x$ for all $x \in \partial\tilde{\Gamma}$.

One can verify that $\tilde{\Gamma} = \{x \in D | \tilde{\Phi}(x) = 0\}$ and $\tilde{J}(x) \neq x$ on $\tilde{\Gamma}$ since of (C2). Condition (C1) implies that for every $x_0 \in \Gamma$, there exist a number j and a function $\phi_{x_0}(x_1, \ldots, x_{j-1}, x_{j+1}, \ldots, x_n)$ such that Γ is the graph of the function $x_j = \phi_{x_0}(x_1, \ldots, x_{j-1}, x_{j+1}, \ldots, x_n)$ in a neighborhood of x_0. Same is true for every $x_0 \in \tilde{\Gamma}$. Moreover, $\nabla\tilde{\Phi}(x) \neq 0$, for all $x \in \tilde{\Gamma}$, can be verified by using the condition (C2). The conditions (C2), (C6), (C7) imply that the equality $\tilde{J}(x) = x$ is true for all $x \in \partial\tilde{\Gamma}$.

Let $\mathscr{A}$ be an interval in $\mathbb{Z}$. We say that the strictly ordered set $\theta = \{\theta_i\}, i \in \mathscr{A}$, is a *B-sequence* [3] if one of the following alternatives holds: (i) $\theta = \emptyset$, (ii) θ is a non-empty and finite set, (iii) θ is an infinite set such that $|\theta_i| \to \infty$ as $i \to \infty$. In what follows, θ is assumed to be a B-sequence.

The main object of our discussion is the following system,

$$\begin{aligned} x' &= f(x), \\ \Delta x|_{x \in \Gamma} &= I(x). \end{aligned} \tag{5.1}$$

In order to define a solution of (5.1), we need the following function and spaces.

A function $\phi(t) : \mathbb{R} \to \mathbb{R}^n$, $n \in \mathbb{N}$, θ is a B-sequence, is from the set $PC(\mathbb{R}, \theta)$ if it: (i) is left continuous, (ii) is continuous, except, possibly, points of θ, where it has discontinuities of the first kind.

A function $\phi(t)$ is from the set $PC^1(\mathbb{R}, \theta)$ if $\phi(t), \phi'(t) \in PC(\mathbb{R}, \theta)$, where the derivative at points of θ is assumed to be the left derivative. If $\phi(t)$ is a solution of (5.1), then it is required that it belongs to $PC^1(\mathbb{R}, \theta)$ [3].

We say that $x(t) : \mathscr{I} \to \mathbb{R}^n$, $\mathscr{I} \subset \mathbb{R}$, is a solution of (5.1) on $\mathscr{I}$ if there exists an extension $\tilde{x}(t)$ of the function on $\mathbb{R}$ such that $\tilde{x}(t) \in PC^1(\mathbb{R}, \theta)$, the equality $x'(t) = f(x(t))$, $t \in \mathscr{I}$, is true if $x(t) \notin \Gamma$, $x(\theta_i+) = J(x(\theta_i))$ for $x(\theta_i) \in \Gamma$ and $x(\theta_i+) \in \tilde{\Gamma}$, $\theta_i \in \mathscr{I}$. If θ_i is a discontinuity moment of $x(t)$, then $x(\theta_i) \in \Gamma$, for $\theta_i > 0$ and $x(\theta_i) \in \tilde{\Gamma}$, for $\theta_i < 0$. If $x(\theta_i) \in \partial\Gamma$ or $x(\theta_i) \in \partial\tilde{\Gamma}$, then $x(\theta_i)$ is a point of discontinuity with zero jump.

Definition 1 A point x^* from $\partial\Gamma$ or $\partial\tilde{\Gamma}$ is a *grazing point* of system (5.1) if $\langle \nabla\Phi(x^*), f(x^*) \rangle = 0$ or $\langle \nabla\tilde{\Phi}(x^*), f(x^*) \rangle = 0$, respectively.

Definition 2 An orbit $\gamma(x^*) = \{x(t, 0, x^*) | x^* \in D, \ t \in \mathbb{R}\}$ of (5.1) is grazing if there exists at least one grazing point on the orbit.

Consider a solution $x(t) : \mathbb{R} \to \mathbb{R}^n$ and $\{\theta_i\}$ be the moments of the discontinuity, they are the moments where solution $x(t)$ intersects Γ as time increases and the moments when the solution it intersects $\tilde{\Gamma}$ as time decreases.

A solution $x(t) = x(t, 0, x_0)$, $x_0 \in D$ of (5.1) locally exists and is unique if the conditions (C1)–(C3) are valid [3].

In what follows, let $\|\cdot\|$ be the Euclidean norm; that is, for a vector $x = (x_1, x_2, \ldots, x_n)$ in $\mathbb{R}^n$, the norm is equal to $\sqrt{x_1^2 + x_2^2 + \ldots + x_n^2}$.

The following condition for (5.1) guarantees that any set of discontinuity moments of the system constitutes a B-sequence and we call the condition *B-sequence condition*.

(C8) $\sup_D \|f(x)\| < +\infty$, and $\inf_{x_0 \in \tilde{\Gamma}} (x_0, y(\zeta, 0, x_0)) > 0$.

In [3], some other B-sequence conditions are provided.

We will request for discontinuous dynamical systems that any sequence of discontinuity moments to be a B-sequence.

Let us set the system

$$y' = f(y) \tag{5.2}$$

for the possible usage in the remaining part of the study.

Consider a solution $y(t, 0, x_0)$, $x_0 \in \tilde{\Gamma}$, of (5.2). Denote the first meeting point of the solution with the surface Γ, provided the point exists, by $y(\zeta, 0, x_0)$. The following conditions are sufficient for the continuation property.

(C9) (a) Every solution $y(t, 0, x_0)$, $x_0 \in D$, of (5.2) is continuable to either ∞ or Γ as time increases,
(b) Every solution $y(t, 0, x_0)$, $x_0 \in D$, of (5.2) is continuable to either $-\infty$ or $\tilde{\Gamma}$ as time decreases.

To verify the continuation of the solutions of (5.1), the following theorems can be applied.

Theorem 1 ([3]) *Assume that conditions (C8) and (C9) are valid. Then, every solution $x(t) = x(t, 0, x_0)$, $x_0 \in D$ of (5.1) is continuable on $\mathbb{R}$.*

Now, we will present a condition which is sufficient for the *group property*.

(C10) For all $x_0 \in D$, the solution $y(t, 0, x_0)$ of (5.2) does not intersect $\tilde{\Gamma}$ before it meets the surface Γ as time increases.

In other words, for each $x_0 \in D$ and a positive number s such that $y(s, 0, x_0) \in \tilde{\Gamma}$, there exists a number r, $0 \leq r < s$, such that $y(r, 0, x_0) \in \Gamma$.

Theorem 2 ([3]) *(The group property) Assume that conditions (C1)–(C10) are valid. Then, $x(t_2, 0, x(t_1, 0, x_0)) = x(t_2 + t_1, 0, x_0)$, for all $t_1, t_2 \in \mathbb{R}$.*

Denote by $\widehat{[a, b]}$, $a, b \in \mathbb{R}$, the interval $[a, b]$, whenever $a \leq b$ and $[b, a]$, otherwise. Let $x_1(t) \in PC(\mathbb{R}_+, \theta^1)$, $\theta^1 = \{\theta_i^1\}$, and $x_2(t) \in PC(\mathbb{R}_+, \theta^2)$, $\theta^2 = \{\theta_i^2\}$, be two different solutions of (5.1).

Definition 3 The solution $x_2(t)$ is in the ε-neighborhood of $x_1(t)$ on the interval $\mathscr{I}$ if

- the sets θ^1 and θ^2 have same number of elements in $\mathscr{I}$;
- $|\theta_i^1 - \theta_i^2| < \varepsilon$ for all $\theta_i^1 \in \mathscr{I}$;
- the inequality $||x_1(t) - x_2(t)|| < \varepsilon$ is valid for all t, which satisfy $t \in \mathscr{I} \setminus \cup_{\theta_i^1 \in \mathscr{I}} (\theta_i^1 - \varepsilon, \theta_i^1 + \varepsilon)$.

The topology defined with the help of ε-neighborhoods is called the B-topology.

5.2.1 B-Equivalence to a System with Fixed Moments of Impulses

In order to facilitate the analysis of the system with variable moments of impulses (5.1), a *B-equivalent system* [3] to the system with variable moments of impulses will be utilized in our study. Below, we will construct the B-equivalent system.

Let $x(t) = x(t, 0, x_0 + \Delta x)$ be a solution of system (5.1) neighbor to $x_0(t)$ with small $\|\Delta x\|$. If the point $x_0(\theta_i)$ is a (β)- or (γ)-type point, then it is a boundary point. For this reason, there exist two different possibilities for the near solution $x(t)$ with respect to the surface of discontinuity. They are:

(N1) The solution $x(t)$ intersects the surface of discontinuity, Γ, at a moment near to θ_i,

(N2) The solution $x(t)$ does not intersect Γ, in a small time interval centered at θ_i.

Consider a solution $x_0(t) : \mathscr{I} \to \mathbb{R}^n$, $\mathscr{I} \subseteq \mathbb{R}$, of (5.1). Assume that all discontinuity points θ_i, $i \in \mathscr{A}$ are interior points of $\mathscr{I}$. There exists a positive number r, such that r-neighborhoods of $D_i(r)$ of $(\theta_i, x_0(\theta_i))$ do not intersect each other. Consider r is sufficiently small and so that every solution of (5.2) which satisfies condition $(N1)$ and starts in $D_i(r)$ intersects Γ in $G_i(r)$ as t increases or decreases. Fix $i \in \mathscr{A}$ and let $\xi(t) = x(t, \theta_i, x)$, $(\theta_i, x) \in D_i(r)$, be a solution of (5.2), $\tau_i = \tau_i(x)$ the meeting time of $\xi(t)$ with Γ and $\psi(t) = x(t, \tau_i, \xi(\tau_i) + J(\xi(\tau_i)))$ another solution of (5.2). Denoting by $W_i(x) = \psi(\theta_i) - x$, one can find that it is equal to

$$W_i(x) = \int_{\theta_i}^{\tau_i} f(\xi(s))ds + J(x + \int_{\theta_i}^{\tau_i} f(\xi(s))ds) + \int_{\tau_i}^{\theta_i} f(\psi(s))ds \qquad (5.3)$$

and maps an intersection of the plane $t = \theta_i$ with $D_i(r)$ into the plane $t = \theta_i$.

Let us present the following system of differential equations with impulses at fixed moments, whose impulse moments, $\{\theta_i\}$, $i \in \mathscr{A}$, are the moments of discontinuity of $x_0(t)$,

$$y' = f(y),$$
$$\Delta y|_{t=\theta_i} = W_i(y(\theta_i)). \tag{5.4}$$

The function f is the same as the function in system (5.1), and the maps W_i, $i \in \mathscr{A}$, are defined by Eq. (5.3). If $\xi(t) = x(t, \theta_i, x)$ does not intersect Γ near θ_i then we take $W_i(x) = 0$.

Let us introduce the sets $F_r = \{(t, x) | t \in I, \|x - x_0(t)\| < r\}$, and $\bar{D}_i(r)$, $i \in \mathscr{A}$, closure of an r-neighborhood of the point $(\theta_i, x_0(\theta_i+))$. Write $D^r = F_r \cup (\cup_{i\in\mathscr{A}} D_i(r)) \cup (\cup_{i\in\mathscr{A}} \bar{D}_i(r))$. Take $r > 0$ sufficiently small so that $D^r \subset \mathbb{R} \times D$. Denote by $D(h)$ an h-neighborhood of $x_0(0)$. Assume that conditions (C1)–(C10) hold. Then systems (5.1) and (5.4) are B-equivalent in D^r for a sufficiently small r [3]. That is, if there exists $h > 0$, such that:

- for every solution $y(t)$ of (5.4) such that $y(0) \in D(h)$, the integral curve of $y(t)$ belongs to D^r and there exists a solution $x(t) = x(t, 0, y(0))$ of (5.1) which satisfies

$$x(t) = y(t), \quad t \in [a, b] \setminus \cup_{i=-k}^{m} \widehat{(\tau_i, \theta_i]}, \tag{5.5}$$

  where τ_i are moments of discontinuity of $x(t)$. One should precise that we assume $\tau_i = \theta_i$, if $x(t)$ satisfies $(N2)$. Particularly,

$$x(\theta_i) = \begin{cases} y(\theta_i), & \text{if } \theta_i \le \tau_i, \\ y(\theta_i^+), \text{ otherwise,} \end{cases}$$
$$y(\tau_i) = \begin{cases} x(\tau_i), & \text{if } \theta_i \ge \tau_i, \\ x(\tau_i^+), \text{ otherwise.} \end{cases}$$

- Conversely, if (5.4) has a solution $y(t) = y(t, 0, y(0))$, $y(0) \in D(h)$, then there exists a solution $x(t) = x(t, 0, y(0))$ of (5.1) which has an integral curve in D^r, and (5.5) holds.

Consider a solution $x_0(t) : \mathbb{R} \to \mathbb{R}^n$, $x_0(t) = x(t, 0, x_0)$, $x_0 \in D$ with discontinuity moments $\{\theta_i\}$. Fix a discontinuity moment θ_i. At this discontinuity moment, the trajectory may be on Γ and $\tilde{\Gamma}$. All possibilities of discontinuity moment should be analyzed. For this reason, we should investigate the following six cases:

(α) $x_0(\theta_i) \in \Gamma \setminus \partial\Gamma$,
(α') $x_0(\theta_i) \in \tilde{\Gamma} \setminus \partial\tilde{\Gamma}$,
(β) $x_0(\theta_i) \in \partial\Gamma$ & $\langle \nabla\Phi(x_0(\theta_i)), f(x_0(\theta_i))\rangle \neq 0$,
(β') $x_0(\theta_i) \in \partial\tilde{\Gamma}$ & $\langle \nabla\tilde{\Phi}(x_0(\theta_i)), f(x_0(\theta_i))\rangle \neq 0$,
(γ) $x_0(\theta_i) \in \partial\Gamma$ & $\langle \nabla\Phi(x_0(\theta_i)), f(x_0(\theta_i))\rangle = 0$,
(γ') $x_0(\theta_i) \in \partial\tilde{\Gamma}$ & $\langle \nabla\tilde{\Phi}(x_0(\theta_i)), f(x_0(\theta_i))\rangle = 0$.

If a discontinuity point $x_0(\theta_i)$ satisfies the case (α), $((\alpha'))$ the case (β), $((\beta'))$ and the case (γ), $((\gamma'))$ we will call it an (α)-type point, a (β)-type point and a (γ)-type point, respectively.

Besides, we present the following definition which is compliant with Definition 2.

Definition 4 If there exists a discontinuity moment, θ_i, $i \in \mathscr{A}$, for which one of the cases (γ) or (γ') is valid, then the solution $x_0(t) = x(t, 0, x_0)$, $x_0 \in \mathbb{R}^n$ of (5.1) is called *a grazing solution*, and $t = \theta_i$ is called a *grazing moment*.

Next, we consider *the differentiability properties of grazing solutions*. The theory for the smoothness of discontinuous dynamical systems' solutions without grazing phenomenon is provided in [3].

Denote by $\bar{x}(t)$, $j = 1, 2, \ldots, n$, a solution of (5.4) such that $\bar{x}(0) = x_0 + \Delta x$, $\Delta x = (\xi_1, \xi_2, \ldots, \xi_n)$, and let η_i be the moments of discontinuity of $\bar{x}(t)$.

The following conditions are required in what follows.

(A) For all $t \in [0, b] \setminus \cup_{i \in \mathscr{A}} \widehat{(\eta_i, \theta_i]}$, the following equality is satisfied

$$\bar{x}(t) - x_0(t) = \sum_{i=1}^{n} u_i(t)\xi_i + O(\|\Delta x\|), \tag{5.6}$$

where $u_i(t) \in PC([0, b], \theta)$.

(B) There exist constants v_{ij}, $j \in \mathscr{A}$, such that

$$\eta_j - \theta_j = \sum_{i=1}^{n} v_{ij}\xi_i + O(\|\Delta x\|); \tag{5.7}$$

(C) The discontinuity moment η_j of the near solution approaches to the discontinuity moment θ_j, $j \in \mathscr{A}$, of grazing one as ξ tends to zero.

The solution $\bar{x}(t)$ has a linearization with respect to solution $x_0(t)$ if the condition (A) is valid and, moreover, if the point $x_0(\theta_i)$ is of (α)- or (β)-type, then the condition (B) is fulfilled. For the case $x_0(\theta_i)$ is of (γ)-type the condition (C) is true.

The solution $x_0(t)$ is K-differentiable with respect to the initial value x_0 on $[0, b]$ if for each solution $\bar{x}(t)$ with sufficiently small Δx the linearization exists. The functions $u_i(t)$ and v_{ij} depend on Δx and uniformly bounded on a neighborhood of x_0.

It is easy to see that the differentiability implies B-continuous dependence on solutions to initial data.

Define the map $\zeta(t, x)$ as $\zeta(t, x) = x(t, 0, x)$, for $x \in D$.

A K-smooth discontinuous flow is a map $\zeta(t, x) : \mathbb{R} \times D \to D$, which satisfies the following properties:

(I) The group property:

(i) $\zeta(0, x) : D \to D$ is the identity;

(ii) $\zeta(t, \zeta(s, x)) = \zeta(t + s, x)$ is valid for all $t, s \in \mathbb{R}$ and $x \in D$.

(II) $\zeta(t, x) \in PC^1(\mathbb{R})$ for each fixed $x \in D$.

(III) $\zeta(t, x)$ is K-differentiable in $x \in D$ on $[a, b] \subset \mathbb{R}$ for each a, b such that the discontinuity points of $\zeta(t, x)$ are interior points of $[a, b]$.

In [3], it was proved that if the conditions of Theorem 1 and (C1)–(C10) are fulfilled, then system (5.1) defines a B-smooth discontinuous flow [3] if there are no grazing points for the dynamics. It is easy to observe that the B-smooth discontinuous flow is a subcase of the K-smooth discontinuous flow. In the next section, we will construct a variational system for (5.1) in the neighborhood of grazing orbits. That is, we will assume that some of the discontinuity points are (γ)-type points. Linearization around a solution and its stability will be taken into account. Thus, analysis of the discontinuous dynamical systems with grazing points will be completed.

5.2.2 *Linearization Around Grazing Orbits and Discontinuous Dynamics*

The objective of this section is to verify K-differentiability of the grazing solution. Consider a grazing solution $x_0(t) = x(t, 0, x_0),\ x_0 \in D$, of (5.1). We will demonstrate that one can write the variational system for the solution $x_0(t)$ as follows:

$$\begin{aligned} u' &= A(t)u, \\ \Delta u|_{t=\theta_i} &= B_i u(\theta_i), \end{aligned} \tag{5.8}$$

where the matrix $A(t) \in \mathbb{R}^{n\times n}$ of the form $A(t) = \frac{\partial f(x_0(t))}{\partial x}$. The matrices B_i, $i = 1, \ldots, n$, will be defined in the remaining part of the study. The matrix B_i is bivalued if θ_i is a grazing moment or of (β)-type.

The right-hand side of the second equation in (5.8) will be described in the remaining part of the study for each type of the points. As the *linearization at a point of discontinuity*, we comprehend the second equation in (5.8).

5.2.2.1 Linearization at Non-grazing Points

Discontinuity points of (α) and (α') types are discussed in [3]. In this subsection, we will outline the results of the book. For non-grazing point, the points are of the form (α) or (β). Let us start with an (α)-type point.

Assume that $x(\theta_i)$ is an (α)-type point. It is clear that the B-equivalent system (5.4) can be applied in the analysis. The functions $\tau_i(x)$ and $W_i(x)$ are described in Sect. 5.2.1. Differentiating $\Phi(x(\tau_i(x))) = 0$, we have

$$\frac{\partial \tau_i(x_0(\theta_i))}{\partial x_j} = -\frac{\Phi_x(x_0(\theta_i))\frac{\partial x_0(\theta_i)}{\partial x_{0j}}}{\Phi_x(x_0(\theta_i))f(x_0(\theta_i))}. \tag{5.9}$$

Then, considering (5.3), we get the following equation,

$$\frac{\partial W_i(x_0(\theta_i))}{\partial x_{0j}} = (f(x_0(\theta_i)) - f(x_0(\theta_i) + J(x_0(\theta_i)))) \frac{\partial \tau_i}{\partial x_{0j}} + \frac{\partial I}{\partial x}\left(e_j + f\frac{\partial \tau_i}{\partial x_{0j}}\right), \tag{5.10}$$

where $e_j = (\underbrace{0, \ldots, 1}_{j}, \ldots, 0)$.

The matrix $B_i \in \mathbb{R}^{n\times n}$ in Eq. (5.8) is defined as $B_i = W_{ix}$, where W_{ix} is the $n \times n$ matrix of the form $W_{ix} = [\frac{\partial W_i(x_0(\theta_i))}{\partial x_1}, \frac{\partial W_i(x_0(\theta_i))}{\partial x_2}, \ldots, \frac{\partial W_i(x_0(\theta_i))}{\partial x_n}]$. Its vector-components $\frac{\partial W_i(x_0(\theta_i))}{\partial x_{0j}}$, $j = 1, \ldots, n$, evaluated by (5.10). Moreover, the components of the gradient $\nabla\tau_i$ have to be evaluated by formula (5.9).

Then, consider $x(\theta_i)$ is an (β)-type point. There exist two different possibilities with respect to the surface of discontinuity for a near solution, such as it intersects it or not. Above, we consider that as $(N1)$ and $(N2)$. In light of $(N1)$ and $(N2)$, the matrix B_i in (5.1) can be expressed as follows:

$$B_i = \begin{cases} O_n, & \text{if} \quad (N1) \text{ is valid,} \\ W_{ix}, & \text{if} \quad (N2) \text{ is valid,} \end{cases} \tag{5.11}$$

where O_n is $n \times n$ zero matrix, W_{ix} is evaluated by formula (5.10) and $\nabla\tau(x)$ evaluated by formula (5.9).

The differentiability properties for the cases (α') and (β') can be investigated similarly.

5.2.2.2 Linearization at a Grazing Point

Fix a discontinuity moment θ_i and assume that one of the cases (γ) or (γ') is satisfied. We will investigate the case (γ). The case (γ') can be considered in a similar way.

Considering condition (C1) with the formula (5.9), it is easy to see that one coordinate of it is infinity at a grazing point. This gives arise singularity in the system, which makes the analysis harder and the dynamics complex. Through the formula (5.9), one can see that the singularity is just caused by the position of the vector field with respect to the surface of discontinuity, and the impact component of the dynamical system does not participate in the appearance of the singularity. To handle with the singularity, we will rely on the following conditions.

(A1) A grazing point is isolated. That is, there is a neighborhood of the point with no other grazing points.
(A2) The map $W_i(x)$ in (5.3) is differentiable at the grazing point $x = x_0(\theta_i)$.
(A3) The function $\tau_i(x)$ does not exceed a positive number less than $\theta_{i+1} - \theta_i$ near a grazing point, $x_0(\theta_i)$, on a set of points which satisfy condition $(N1)$.

In this study, we analyze the case, when the impact functions neutralize the singularity caused by transversality. That is, the triad: impact law, the surface of discontinuity and the vector field is specially chosen, such that condition (A2) is valid.

Presumably, if there is no this type of suppressing, complex dynamics near the grazing motions may appear [8, 18, 24, 25]. In the examples stated in the remaining part of the study, one can see the verification of (A2), in details.

Let us prove the following assertion.

Lemma 1 *If conditions (C1), (C4), (C6), (C8) and (A3) hold, then, $\tau_i(x)$ is continuous near a grazing point $x_0(\theta_i)$, on a set of points, which satisfy condition* $(N1)$.

Proof Let $x_0(\theta_i)$ be a grazing point. If $\bar{x}$ is not a point from the orbit of the grazing solution, the continuity of $\tau_i(x)$ at the point $x = \bar{x}$ can be proven using similar technique presented in [3]. Now, the continuity at $x_0(\theta_i)$ is taken into account. On the contrary, assume that $\tau_i(x)$ is not continuous at the point $x = x_0(\theta_i)$. Then, there exists a positive number ε_0 and a sequence $\{x_n\}_{n\in\mathbb{Z}}$ such that $\tau_i(x_n) > \varepsilon_0$ whenever $x_n \to x_0(\theta_i)$, as $n \to \infty$. Moreover, from condition (A3), one can assert that there exists a subsequence $\tau_i(x_{n_k})$ which converges to a number $\varepsilon_0 \leq \tau_0 < \theta_{i+1} - \theta_i$. Without loss of generality, assume that the subsequence converges the point where the sequence $\{x_n\}_{n\in\mathbb{Z}}$ converges. Because of the continuity of solutions in initial value, $x(\tau_i(x_n), 0, x_n)$ approaches to $x(\tau_0, 0, x(\theta_i))$. But $x(\tau_i(x_n), 0, x_n)$ is on the surface of discontinuity Γ, $x(\tau_0, 0, x_0(\theta_i)) \notin \Gamma$. This contradicts with the closeness of the surface of discontinuity Γ. The continuity at other points of the grazing orbit is valid by the group property.

Due to the B-equivalence of systems (5.1) and (5.4), we will consider linearization around $x_0(t)$ as solution of the system (5.4), consequently, only formula (5.6) will be needed. Finally, the linearization matrix for the grazing point also has to be defined by the formula (5.11), where W_{ix} exists by condition (A2).

5.2.2.3 Linearization Around a Grazing Periodic Solution

Let $\Psi(t) : \mathbb{R} \to D$ be a periodic solution of (5.1) with period $\omega > 0$ and θ_i, $i \in \mathbb{Z}$, are the points of discontinuity which satisfy (ω, p)-property, i.e., $\theta_{i+p} = \theta_i + \omega$, p is a natural number.

Let us fix a solution $x(t) = x(t, 0, \Psi(0) + \Delta x)$ and assume that linearization of $\Psi(t)$ with respect to $x(t)$ exists and is of the form

$$\begin{aligned} u' &= A(t)u, \\ \Delta u|_{t=\theta_i} &= B_i u. \end{aligned} \tag{5.12}$$

The matrix B_i is determined by (5.11). It is known that $A(t + \omega) = A(t)$, $t \in \mathbb{R}$. But, the sequence B_i may not be periodic in general, because of (5.11). This makes the analysis of the neighborhood of $\Psi(t)$ difficult. For this reason, we suggest the following condition.

(A4) For each sufficiently small $\Delta x \in \mathbb{R}^n$, the variational system (5.12) satisfies $B_{i+p} = B_i$, $i \in \mathbb{Z}$. There exist a finite number $m \leq 2^l$, where l is the number of points of (β)- or (γ)-type in the interval $[0, \omega]$, of the periodic sequences B_i.

To distinguish periodic sequences B_i in the assumption (A4), we will apply the notation $B_i = D_i^{(j)}$, $i \in \mathbb{Z}$ and $j = 1, 2, \ldots, m$.

In the next example, we will demonstrate that the system constitutes K-smooth discontinuous flow although it has grazing points in the phase space.

Example 1 Consider an impact model

$$\begin{aligned} y_1' &= y_2, \\ y_2' &= -y_1 + 0.001 y_2, \end{aligned} \tag{5.13a}$$

$$\begin{aligned} \Delta y_2|_{y \in \Gamma_1} &= -y_2 - R_1 y_2^2, \\ \Delta y_2|_{y \in \Gamma_2} &= -(1 + R_2) y_2, \end{aligned} \tag{5.13b}$$

with the domain $D = \mathbb{R}^2$, $R_1 = \exp(-0.0005\pi)$ and $R_2 = 0.9$. In the paper [10], it is stated that the coefficient of restitution for low velocity impact still remains as an open problem. In the study [4], by considering Kelvin–Voigt model for the elastic impact, we derived quadratic terms of the velocity in the impact law. These arguments make the quadratic term for the impulse equation (5.13b) reasonable.

Let us describe the set of discontinuity curves by $\Gamma = \Gamma_1 \cup \Gamma_2$. The components Γ_1 and Γ_2 are intervals of the vertical lines $y_1 = \exp(0.00025\pi)$ and $y_1 = 0$, respectively, and they will be precised next. Fix a point $P = (0, \bar{y}_2) \in D$, with $\bar{y}_2 > 1$. Let $y(t, 0, P)$ be a solution of (5.13a) and it meets with the vertical line $x_1 = \exp(0.00025\pi)$, $x_2 > 0$ at the point $P_2 = (\exp(0.00025\pi), y_2(\theta_1, 0, P))$, where θ_1 is the meeting moment with the line. Consider the point on the $\tilde{\Gamma}_1$ which is $Q_2 = (\exp(0.00025\pi), -R_1 y_2(\theta_1, 0, P_2)^2)$ and denote $Q_1 = (0, y_2(\theta_2, 0, Q_2))$, where θ_2 is the moment of meeting of the solution $y(t, 0, Q_2)$ with the vertical line $x_1 = 0$, $x_2 < 0$. We shall need also the point $P_1 = (0, -R_2 y_2(\theta_2, 0, Q_2))$. Finally, we obtain the region G in yellow and blue between the vertical lines and graphs of the solutions in Fig. 5.1. The region G contains discontinuous trajectories, and outside of this region all trajectories are continuous. Moreover, both region G and its complement are invariant.

Define $\Gamma_1 = \{(y_1, y_2) |\ y_1 = \exp(0.00025\pi), \quad 0 \leq y_2 \leq y_2(\theta_1, 0, (0, \bar{y}_2))\}$, and $\Gamma_2 = \{(y_1, y_2) |\ y_1 = 0,\ y_2(\theta_2, 0, -R_1 y_2((\theta_1, 0, (0, \bar{y}_2)))^2) \leq y_2 \leq 0\}$. The boundary of the curve, $\Gamma = \Gamma_1 \cup \Gamma_2$, has of four points, they are

$$\partial\Gamma = \{(0, 0), (\exp(0.00025\pi), 0), (\exp(0.00025\pi), y_2(\theta_1, 0, (0, \bar{y}_2))),$$

$$(0, y_2(\theta_2, 0, -R_1 y_2(\theta_1, 0, (0, \bar{y}_2))))\}.$$

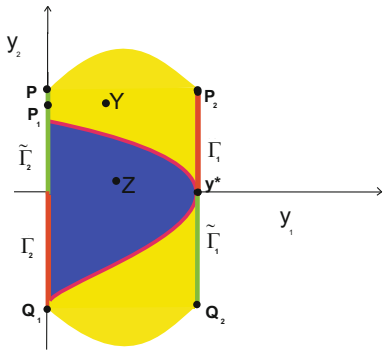

Fig. 5.1 The region G for system (5.13) is depicted in details. The curves of discontinuity $\Gamma = \Gamma_1 \cup \Gamma_2$ and $\tilde{\Gamma} = \tilde{\Gamma}_1 \cup \tilde{\Gamma}_2$ are drawn as *vertical lines* in *red* and *green*, respectively, and the grazing orbit in *magenta*

In the following part of the example, we will show that two of them, $y^* = (y_1^*, y_2^*) = (\exp(0.00025\pi), 0)$ and the origin, $(0, 0)$ are grazing points. Moreover, it can be easily validated that other two points are of β-type.

Issuing from system (5.13), the curve of discontinuity $\tilde{\Gamma}$ consists of two components $\tilde{\Gamma}_1$ and $\tilde{\Gamma}_2$. The components are the following sets

$$\tilde{\Gamma}_1 = \{(y_1, y_2) |\ y_1 = \exp(0.00025\pi),\ -R_1 y_2(\theta_1, 0, (0, \bar{y}_2))^2 \le y_2 \le 0\}$$

and

$$\tilde{\Gamma}_2 = \{(y_1, y_2) |\ y_1 = 0,\ 0 \le -R_2 y_2(\theta_2, 0, Q_2)\}.$$

One can verify that the function

$$\Psi(t) = \begin{cases} \exp(0.0005t)\Big(\sin(t), \cos(t)\Big), & \text{if } t \in [0, \pi), \\ (0, 1), & \text{if } t = \pi, \end{cases} \tag{5.14}$$

is a discontinuous periodic solution of (5.13) with period $\omega = \pi$, whose discontinuity points $(0, 1)$ and $(0, -\exp(0.0005\pi))$ belong to $\tilde{\Gamma}$ and Γ, respectively. The expression

$$\begin{aligned} &\langle \nabla \Phi((\exp(0.00025\pi), 0)),\ f((\exp(0.00025\pi), 0))\rangle \\ &= \langle (1, 0), (0, -\exp(-0.00025\pi))\rangle = 0 \end{aligned}$$

verifies that y^* is a (γ)-type point, i.e., a grazing point of the solution $\Psi(t)$. It is easily seen that the grazing is axial. Now, we can assert that the periodic solution (5.14) is a grazing solution in the sense of Definition 4. Its simulation is depicted in Fig. 5.2.

Since the complement of G is invariant in both directions and consists of continuous trajectories of the linear system (5.13a), one can easily conclude that the complement is a continuous dynamical system [13]. Thus, to verify the dynamics for the whole system, one need to analyze it in the region G. This set is bounded,

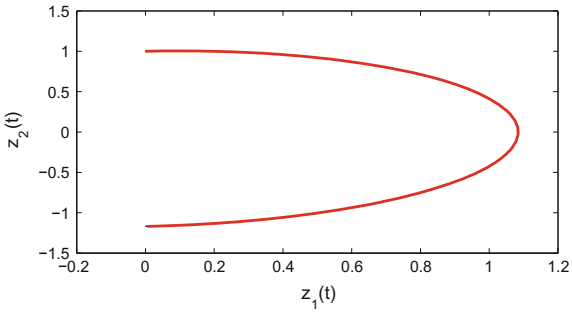

Fig. 5.2 The grazing orbit of system (5.13)

consequently for solutions in it conditions (C8) and (C9) are fulfilled and by Theorem 1, they admit B-sequences and continuation property.

Consider a function

$$\zeta(y_2) : [y_2(\theta_2, 0, Q_2), y_2(\theta_1, 0, P)] \to [y_2(\theta_2, 0, Q_2), y_2(\theta_1, 0, P)]$$

such that it is continuously differentiable, satisfies $\zeta(y_2) = -R_2 y_2$ in a neighborhood of $y_2 = 0$ and is the identity at the boundary points, i.e., $\zeta(y_2(\theta_1, 0, P)) = y_2(\theta_1, 0, P)$ and $\zeta(y_2(\theta_1, 0, P)) = y_2(\theta_1, 0, P)$. It is easily seen that such function exists. On the basis of this discussion, let us introduce the following system,

$$\begin{aligned} y_1' &= y_2, \\ y_2' &= -y_1 + 0.001 y_2, \\ \Delta y_2|_{y \in \Gamma} &= \zeta(y_2) - y_2. \end{aligned} \tag{5.15}$$

It is apparent that system (5.15) is equivalent to (5.13) near the orbit of periodic solution $\Psi(t)$. That is, they have the same trajectories there.

Specifying (5.1) for (5.15), it is easy to obtain that $\Phi(y_1, y_2) = \tilde{\Phi}(y_1, y_2) = (y_1 - \exp(0.00025\pi))y_1$, $f(y_1, y_2) = (y_2, -y_1 + 0.001 y_2)$ and $J(y) = (y_1, \zeta(y_2))$.

Now, we will verify that system (5.15) defines a K-smooth discontinuous flow. First, condition (C1) is verified since $\nabla\Phi_1(y) = \nabla\Phi_2(y) = (1, 0) \neq 0$, for all $y \in D$. The jump function $J(y) = (y_1, \zeta(y_2))$ is continuously differentiable function. So, condition (C2) is valid. It is true that $\Gamma \cap \tilde{\Gamma} \subseteq \partial\Gamma \cap \partial\tilde{\Gamma}$. Inequalities $\langle \nabla\Phi_1(y), f(y)\rangle = \langle (1, 0), (y_2, -y_1 + 0.001 y_2)\rangle = y_2 \neq 0$ and $\langle \nabla\Phi_2(y), f(y)\rangle = \langle (1, 0), (y_2, -y_1 + 0.001 y_2)\rangle = y_2 \neq 0$, if $y \in \Gamma \setminus \partial\Gamma$, validate the condition (C4). Moreover, we have $\langle \nabla\tilde{\Phi}_1(y), f(y)\rangle = \langle (1, 0), (y_2, -y_1 + 0.001 y_2)\rangle = y_2 \neq 0$ and $\langle \nabla\tilde{\Phi}_2(y), f(y)\rangle = \langle (1, 0), (y_2, -y_1 + 0.001 y_2)\rangle = y_2 \neq 0$, if $y \in \tilde{\Gamma} \setminus \partial\tilde{\Gamma}$. Conditions (C6) and (C7) hold as the function ζ is such defined. Thus, conditions (C1)–(C10) have been verified. Consequently, the system (5.13) defines the K-smooth discontinuous flow for all motions except the grazing ones. To complete the discussion, one need to linearize the system near the grazing solutions. First, we proceed with the linearization around the grazing periodic orbit (5.14).

The solution $\Psi(t)$ has two discontinuity moments $\theta_1 = \frac{\pi}{2}$ and $\theta_2 = \omega$ in the interval $[0, \omega]$. The corresponding discontinuity points are of (γ)- and (α)-types, respectively. Next, we will linearize the system at these points. The linearization at the second point exists [3], and the details of this will be analyzed in the next example. This time, we will focus on the grazing point y^*.

First, we assume that $y(t) = y(t, 0, y^* + \Delta y)$, $\Delta y = (\Delta y_1, \Delta y_2)$ is not a grazing solution. Moreover, the solution intersects the line Γ_1 at time $t = \xi$ near $t = \theta_1$ as time increases. The meeting point $\bar{y} = (\bar{y}_1, \bar{y}_2) = (y_1(\xi, 0, (y^* + \Delta y)), y_2(\xi, 0, (y^* + \Delta y))$, is transversal one. It is clear $\bar{y}_1 = \exp(0.00025\pi)$ and $\bar{y}_2 > 0$. In order to find a linearization at the moment $t = \theta_i$, we use formula (5.3) for $y(t)$ and find that

$$\frac{\partial W_i(y)}{\partial y_1^0} = \int_{\theta_i}^{\tau(y)} \frac{\partial f(y(s))}{\partial y} \frac{\partial y(s)}{\partial y_1^0} ds + f(y(s)) \frac{\partial \tau(y)}{\partial y_1^0} + J_y(y)\Big(e_1 + f(y(s)) \frac{\partial \tau(y)}{\partial y_1^0}\Big)$$
$$+ f(y(s) + J(y(s))) \frac{\partial \tau(y)}{\partial y_1^0} + \int_{\tau(y)}^{\theta_i} \frac{\partial f(y(s) + J(y(s)))}{\partial x} \frac{\partial y(s)}{\partial y_1^0} ds, \tag{5.16}$$

where $e_1 = (1, 0)^T$, T denotes the transpose of a matrix. Substituting $y = \bar{y}$ to the formula (5.16), we obtain that

$$\frac{\partial W_i(y(\xi, 0, y^* + \Delta y))}{\partial y_1^0} = f(y(\xi, 0, y^* + \Delta y)) \frac{\partial \tau(y(\xi, 0, y^* + \Delta y))}{\partial y_1^0}$$
$$+ J_y(y(\xi, 0, y^* + \Delta y))\Big(e_1 + f(y(\xi, 0, y^* + \Delta y))) \frac{\partial \tau(y(\xi, 0, y^* + \Delta y)))}{\partial y_1^0}\Big) \tag{5.17}$$
$$+ f(y(\xi, 0, (J(y(\xi, 0, y^* + \Delta y))))) \frac{\partial \tau(J(y(\xi, 0, y^* + \Delta y)))}{\partial y_1^0}.$$

Considering the formula (5.9) for the transversal point $\bar{y} = (\bar{y}_1, \bar{y}_2)$, the first component $\frac{\partial \tau(\bar{y})}{\partial y_1^0}$ can be evaluated as $\frac{\partial \tau(\bar{y})}{\partial y_1^0} = -\frac{1}{\bar{y}_2}$. From the last equality, it is seen how the singularity appears at the grazing point. Finally, we obtain that

$$\frac{\partial W_i(\bar{y})}{\partial y_1^0} = \begin{bmatrix} \bar{y}_2 - R_1(\bar{y}_2)^2 \\ -\bar{y}_1 - 0.001(\bar{y}_2 - R_1(\bar{y}_2)^2) \end{bmatrix} \Big(-\frac{1}{\bar{y}_2}\Big)$$
$$+ \begin{bmatrix} 1 & 0 \\ 0 & -2R_1\bar{y}_2 \end{bmatrix} \begin{bmatrix} 0 \\ \dfrac{\bar{y}_1 + 0.001\bar{y}_2}{\bar{y}_2} \end{bmatrix}. \tag{5.18}$$

Calculating the right-hand side of (5.18), we have

$$\frac{\partial W_i(\bar{y})}{\partial y_1^0} = \begin{bmatrix} -R_1\bar{y}_2 - 1 \\ 0.001(1 - R_1\bar{y}_2) + 2R_1(0.001\bar{y}_2 - \bar{y}_1) \end{bmatrix}. \tag{5.19}$$

The last expression demonstrates that the derivative is a continuous function of its arguments in a neighborhood of the grazing point. Since it is defined and continuous for the points, which are not from the grazing orbit by the last expression and for other points, it can be determined by the limit procedure. Indeed, one can easily show that the derivative at the grazing point y^* is

$$\begin{bmatrix} -1 \\ 0.001 - 1.8\exp(0.00025\pi) \end{bmatrix}. \tag{5.20}$$

Similarly, all other points of the grazing orbit can be discussed.
Next, differentiating (5.3) with $y(t)$ again we obtain that

$$\frac{\partial W_i(y)}{\partial y_2^0} = \int_{\theta_i}^{\tau(y)} \frac{\partial f(y)}{\partial y}\frac{\partial y(s)}{\partial y_2^0}ds + f(y(s))\frac{\partial \tau(y)}{\partial y_2^0} + J_y(y)(e_2 + f(y(s))\frac{\partial \tau(y)}{\partial y_2^0})$$
$$+f(y + J(y))\tfrac{\partial \tau(y)}{\partial y_2^0} + \int_{\tau(y)}^{\theta_i} \frac{\partial f(y(s) + J(y(s)))}{\partial x}\frac{\partial y(s)}{\partial y_2^0}ds, \tag{5.21}$$

where $e_2 = (0, 1)^T$. Calculate the right-hand side of (5.21) at the point $\bar{y} = (\bar{y}_1, \bar{y}_2)$ to obtain

$$\frac{\partial W_i(y(\xi, 0, y^* + \Delta y))}{\partial y_2^0} = f(y(\xi, 0, y^* + \Delta y))\frac{\partial \tau(y(\xi, 0, y^* + \Delta y))}{\partial y_2^0}$$
$$+J_y(y(\xi, 0, y^* + \Delta y))\left(e_2 + f(y(\xi, 0, y^* + \Delta y)))\frac{\partial \tau(y(\xi, 0, y^* + \Delta y))}{\partial y_2^0}\right) \tag{5.22}$$
$$+f(y(\xi, 0, y^* + \Delta y))\frac{\partial \tau(y(\xi, 0, y^* + \Delta y))}{\partial y_2^0}.$$

To calculate the fraction $\dfrac{\partial \tau(y(\xi, 0, y^* + \Delta y))}{\partial y_2^0}$ in (5.22), we apply formula (5.9) for the transversal point $\bar{y} = (\bar{y}_1, \bar{y}_2)$. The second component $\dfrac{\partial \tau(\bar{y})}{\partial y_2^0}$ takes the form $\dfrac{\partial \tau(\bar{y})}{\partial y_2^0} = 0$. This and formula (5.22) imply

$$\frac{\partial W_i(\bar{y})}{\partial y_2^0} = \begin{bmatrix} 0 \\ -2R\bar{y}_2 \end{bmatrix}. \tag{5.23}$$

Similar to (5.20), one can obtain that

$$\frac{\partial W_i(y^*)}{\partial y_2^0} = \begin{bmatrix} 0 \\ 0 \end{bmatrix}. \tag{5.24}$$

Joining (5.20) and (5.24), it can be obtained that

$$W_{iy}(y^*) = \begin{bmatrix} -1 & 0 \\ 0.001 - 1.8\exp(0.00025\pi) & 0 \end{bmatrix}. \tag{5.25}$$

The continuity of the derivatives in a neighborhood of y^* implies that the function W is differentiable at the grazing point $y = y^*$, and the condition (A2) is valid.

Now, on the basis of the discussion made above, one can obtain the bivalued matrix of coefficients for the grazing point as

$$B_1 = \begin{cases} O_2, & \text{if (N1) is valid,} \\ \begin{bmatrix} -1 & 0 \\ 0.001 - 1.8\exp(0.00025\pi) & 0 \end{bmatrix}, & \text{if (N2) is valid.} \end{cases}$$

The matrix $D_1^{(1)} = O_2$ is for near solutions of (5.14) which are in the region where Z in, see Fig. 5.1, and do not intersect the curve of discontinuity Γ_1. The matrix

$$D_1^{(2)} = \begin{bmatrix} -1 & 0 \\ 0.001 - 1.8\exp(0.00025\pi) & 0 \end{bmatrix}$$

is for near solutions of (5.14), which intersects the curve of discontinuity Γ_1. They start in the subregion, where the point Y is placed. Thus, the linearization for $\Psi(t)$ at the grazing point exists. Moreover, since another point of discontinuity $(0, \exp(0.0005\pi))$ is not grazing, the linearization at the point exist as well as linearization at points of continuity [3, 28]. Consequently, there exist linearization around $\Psi(t)$.

To verify condition (A3), consider a near solution $y(t) = y(t, 0, \bar{y})$ to $\Psi(t)$, where $\bar{y} = (0, \bar{y}_2)$, $\bar{y}_2 > \Psi_2(0) = 1$, which satisfy the condition $(N1)$. It is true that $\theta_{i+1} - \theta_i = \dfrac{\pi}{2} = \dfrac{\omega}{2}$. The first coordinate of the near solution to $\Psi(t)$ can be obtained as $y_1(t) = \bar{y}\exp(0.0005t)\sin(t)$ and $y_1(\frac{\omega}{2}) = y_1(\dfrac{\pi}{2}) = \bar{y}\exp(0.00025\pi) > \exp(0.00025\pi) = \Psi_1(\dfrac{\omega}{2})$. Thus, the meeting moment of near solution $y(t)$ with the surface of discontinuity is less than $\frac{\omega}{2}$. So, it implies that $0 < \tau(y) < \frac{\pi}{2} - \varepsilon$ for a small number ε if the first coordinate of $\bar{y}$ is close to $\exp(0.00025\pi)$. This validates condition (A3). Now, Lemma 1 proves the condition (C).

Now, let us consider the point $(0, 0)$. We have that $\langle \nabla\Phi((0,0)), f((0,0))\rangle = \langle (1,0), (0,0)\rangle = 0$. That is the origin is a grazing point. In the same time, it is a fixed point of the system. For this particular grazing point, we can find the linearization directly. Indeed, all the near solutions satisfy the linear impulsive system,

$$\begin{aligned} x_1' &= x_2, \\ x_2' &= -x_1 + 0.001x_2, \\ \Delta x_2|_{x_1=0} &= -(1 + R_2)x_2. \end{aligned} \tag{5.26}$$

Consider a solution $x(t) = x(t, 0, x_0)$, where $x_0 = (x_1^0, x_2^0) \neq (0, 0)$ with moments of discontinuity $\theta_i, i \in \mathbb{Z}$, then the linearization system for the equation around the equilibrium is

$$\begin{aligned} u_1' &= u_2, \\ u_2' &= -u_1 + 0.001u_2, \\ \Delta u_2|_{t=\theta_i} &= -(1 + R_2)u_2. \end{aligned} \tag{5.27}$$

Indeed, if $u_1(t)$, $u_1(0) = e_1$, $u_2(t)$, $u_2(0) = e_2$, are solutions of (5.27), then one can see that $x(t) - (0, 0) = x_1^0 u_1(t) + x_2^0 u_2(t)$, for all $t \in \mathbb{R}$.

We have obtained that linearization exists for both grazing solutions $\Psi(t)$ and the equilibrium at the origin. Moreover, conditions (C1)–(C10) are valid, and all other solutions are B-differentiable in parameters [3]. Thus, the system (5.13) defines a K-smooth discontinuous flow in the plane.

In the next example, we will finalize the linearization around the grazing solution $\Psi(t)$.

Example 2 (*Linearization around the grazing discontinuous cycle*) We continue analysis of the last example and complete the variational system for $\Psi(t)$.

Let us consider this time, the linearization at the non-grazing moment $\omega = \pi$. The discontinuity point is $c = (0, -\exp(0.0005\pi))$ and it is of (α)-type, since

$$\begin{aligned} \langle \nabla \Phi(c), f(c) \rangle &= \langle (1, 0)(-\exp(0.0005\pi), -0.001 \exp(0.0005\pi)) \rangle \\ &= -\exp(0.0005\pi) \neq 0. \end{aligned}$$

Utilizing formula (5.9), the gradient is computed as $\nabla \tau(c) = (\exp(-0.0005\pi), 0)$.

Then, utilizing $\nabla \tau(c)$ and formula (5.10), one can determine that the matrix of linearization at the moment π is

$$B_2 = \begin{bmatrix} \exp(-0.0005\pi) & 0 \\ 0.001 & 0 \end{bmatrix}.$$

From the monotonicity of the jump function, $-R_1 y_2^2$, it follows that the yellow and blue subregions of G are invariant. Consequently, for each solution near to $\Psi(t)$, the sequences B_i are of two types $B_i = D_i^{(j)}$, $i \in \mathbb{Z}$ and $j = 1, 2$, where $D_{2i-1}^{(1)} = O_2$, $D_{2i-1}^{(2)} = D_1^{(2)} = \begin{bmatrix} -1 & 0 \\ 0.001 - 1.8 \exp(0.00025\pi) & 0 \end{bmatrix}$, $D_{2i}^{(1)} = D_{2i}^{(2)} = \begin{bmatrix} \exp(-0.0005\pi) & 0 \\ 0.001 & 0 \end{bmatrix}$, $i \in \mathbb{Z}$. That is, the condition (A4) is valid and the linearization around the periodic solution (5.14) on $\mathbb{R}$ is of two subsystems:

$$\begin{aligned} u_1' &= u_2, \\ u_2' &= -u_1 + 0.001u_2, \\ \Delta u|_{t=\theta_{2i-1}} &= D_{2i-1}^{(1)} u, \\ \Delta u|_{t=\theta_{2i}} &= D_{2i}^{(1)} u, \end{aligned} \tag{5.28}$$

and

$$\begin{aligned} u_1' &= u_2, \\ u_2' &= -u_1 + 0.001u_2, \\ \Delta u|_{t=\theta_{2i-1}} &= D_{2i-1}^{(2)} u, \\ \Delta u|_{t=\theta_{2i}} &= D_{2i}^{(2)} u, \end{aligned} \tag{5.29}$$

where $\theta_{2i-1} = \frac{(2i-1)\pi}{2}$ and $\theta_{2i} = i\pi$.

The sequences $\{D_i^{(j)}\}$, $j = 1, 2$, are 2-periodic. It is appearant that system (5.28) + (5.29) is a $(\omega, 2)$-periodic. Thus, the variational system for the grazing solution is constructed.

5.2.3 *Orbital Stability*

In this section, we proceed investigation of the grazing periodic solution $\Psi(t)$. Analysis of orbital stability will be taken into account. Denote by $B(z, \delta)$, an open ball with center at z and the radius $\delta > 0$ for a fixed point $z \in \Gamma \setminus \partial\Gamma$. By condition (C3), the ball is divided by surface Γ into two connected open regions. Denote $c^+(z, \delta)$, for the region, where solution $x(t) = x(t, 0, z)$ of (5.2) enters as time increases. The region is depicted in Fig. 5.3.

Set the path of the periodic solution $\Psi(t)$ as

$$\eta := \{x \in D : x = \Psi(t), \quad t \in \mathbb{R}\}.$$

Define $dist(A, a) = \inf_{\alpha \in A} \|\alpha - a\|$, where A is a set, and a is a point.

Fig. 5.3 The region $c^+(z, \delta)$

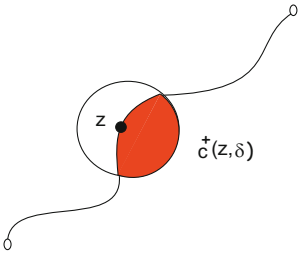

Definition 5 The periodic solution $\Psi(t) : \mathbb{R} \to D$ of (5.1) is said to be orbitally stable if for every $\varepsilon > 0$, there corresponds $\delta = \delta(\varepsilon) > 0$ such that $dist(x(t, 0, x_0), \eta) < \varepsilon$, for all $t \geq 0$, provided $dist(x_0, \eta) < \delta$ and $x_0 \notin \cup_i c^+(\Psi(\theta_i), \delta)$, for $i = 1, \ldots, m$, where m is the number of points $\Psi(\theta_i) \in \Gamma \setminus \partial\Gamma$.

The point x_0 is not considered in regions $c^+(\Psi(\theta_i), \delta)$, $i = 1, \ldots, m$, since solutions which start there move continuously on a finite interval, while $\Psi(t)$ experiences a nonzero jump at $t = \theta_i$ and this violates the continuity in initial value, in general. In the same time, we take into account any region adjoint to points of $\partial\Gamma$, since the jump of $\Psi(t)$ is zero there and, consequently, the continuous dependence in initial value is valid for all near points.

Definition 6 The solution $\Psi(t) : \mathbb{R}_+ \to D$ of (5.1) is said to have asymptotic phase property if a $\delta > 0$ exists such that to each x_0 satisfying $dist(x_0, \eta) < \delta$ and $x_0 \notin \cup_i c^+(\Psi(\theta_i), \delta)$, $for\ i = 1, \ldots, m$, there corresponds an asymptotic phase $\alpha(x_0) \in \mathbb{R}$ with property: for all $\varepsilon > 0$, there exists $T(\varepsilon) > 0$, such that $x(t + \alpha(x_0), 0, x_0)$ is in ε-neighborhood of $\Psi(t)$ in B-topology for $t \in [T(\varepsilon), \infty)$.

Let us consider the following system, which will be needed in the following lemmas and theorem

$$\begin{aligned} x' &= A(t)x, \\ \Delta x|_{t=\zeta_i} &= B_i u, \end{aligned} \tag{5.30}$$

where $A(t)$ and B_i are $n \times n$ function-matrices, $A(t + \omega) = A(t)$, for all $t \in \mathbb{R}$ and there exists an integer p such that $\zeta_{i+p} = \zeta_i + \omega$ and $B_{i+p} = B_i$, for all $i \in \mathbb{Z}$.

Lemma 2 *Assume that system (5.30) has a simple unit characteristic multiplier and the remaining $n - 1$ ones are in modulus less than unity. Then, the system (5.30) has a real fundamental matrix $X(t)$, of the form*

$$X(t) = P(t) \begin{pmatrix} 1 & 0 \\ 0 & \exp(Bt) \end{pmatrix}, \tag{5.31}$$

where $P \in PC^1(\mathbb{R}, \theta)$ is a regular, ω-periodic matrix, and B is an $(n-1) \times (n-1)$ matrix with all eigenvalues have negative real parts.

The proof of above lemma is same as proof of Lemma 5.1.1 in [11].

Throughout this section, we will assume that (A4) is valid. That is, the variational system (5.12) consists of m periodic subsystems. For each of these systems, we find the matrix of monodromy, $U_j(\omega)$ and denote corresponding Floquet multipliers by $\rho_i^{(j)}$, $i = 1, \ldots, n$, $j = 1, \ldots, m$. In the next part of the study, the following assumption is needed.

(A5) $\rho_1^{(j)} = 1$ and $|\rho_i^{(j)}| < 1$, $i = 2, \ldots, n$ for each $j = 1, \ldots, m$.

Lemma 3 *Assume that the assumptions (A4) and (A5) are valid. Then, for each* $j = 1, \ldots, m$, *the system (5.12) admits a fundamental matrix of the form*

$$U_j(t) = P_j(t)[1, \exp(H_j\omega)], \quad t \in \mathbb{R}, \tag{5.32}$$

where $P_j \in PC^1(\mathbb{R}, \zeta)$ is a regular, ω-periodic matrix and H_j is an $(n-1) \times (n-1)$-matrix with all eigenvalues have negative real parts.

The proof of Lemma 3, can be done similar to that of Lemma 2.

Theorem 3 *Assume that conditions (C1)–(C7), (C10), and assumptions (A1)–(A5) hold. Then* ω*- periodic solution* $\Psi(t)$ *of (5.1) is orbitally, asymptotically stable and has the asymptotic phase property.*

Proof According to the group property, we may assume $\Psi(0)$ is not a discontinuity point. Then, one can displace the origin to the point $\Psi(0)$, and the coordinate system can be rotated in such a way that the tangent vector $\Psi_0' = \Psi'(0)$ points in the direction of the positive x_1 axis i.e. the coordinates of this vector are $\Psi_0' = (\Psi_{01}', 0, \ldots, 0)$, $\Psi_{01}' > 0$.

Let $\theta_i, i \in \mathbb{Z}$, be the discontinuity moments of $\Psi(t)$. Denote the path of the solution by $\eta = \{x \in X : x = \Psi(t), t \in \mathbb{R}\}$. There exists a natural number p, such that $\theta_{i+p} = \theta_i + \omega$ for all i. Because of conditions (C1)–(C7) and K-differentiability of $\Psi(t)$, there exists continuous dependence on initial data, and consequently, there exists a neighborhood of η such that any solutions which starts in the set will have moments of discontinuity which constitute a B-sequence with difference between neighbors approximately equal to the distance between corresponding neighbor moments of discontinuity of the periodic solution $\Psi(t)$. Consequently, we can determine variational system for $\Psi(t)$, with points of discontinuity θ_i, $i \in \mathbb{Z}$.

On the basis of discussion in Sect. 5.2.1, one can define in the neighborhood of η a B-equivalent system of type (5.4). The variational system of it takes the form

$$\begin{aligned} z' &= A(t)z + r(t, z), \\ \Delta z|_{t=\theta_i} &= D_i^{(j)} z + q_i(z), \quad j = 1, 2, \ldots, m. \end{aligned} \tag{5.33}$$

The functions in (5.33) have the property that $r(t, z) = [f(\Psi(t) + z) - f(\Psi(t))] - A(t)z$ and $q_i(z) = W_i(\Psi(\theta_i) + z) - W_i(\Psi(\theta_i)) - D_i^{(j)} z$, are continuous functions, and matrices $D_i^{(j)}$ satisfy condition (A4). The functions are continuously differentiable with respect to z. One can verify that $r(t, 0) \equiv q_i(0) \equiv 0$ and $r(t + \omega, z) = r(t, z)$ for $t \in \mathbb{R}$. Moreover, the derivatives satisfy $r'(t, 0) \equiv q_{iz}'(0) \equiv 0$ and the functions $r(t, z) \to 0$, $q_i(z) \to 0$, $r_z'(t, z) \to 0$ and $q_{iz}'(z) \to 0$, as $z \to 0$ uniformly in $t \in [0, \infty)$, $i \geq 0$. Each system (5.33) for $j = 1, 2, \ldots, m$, corresponds to a region adjoint to initial value, x_0 such that these regions cover a neighborhood of x_0.

Fix a number j and denote $Y_j(t)$ the fundamental matrix of adjoint to (5.33) linear homogeneous system

$$\begin{aligned} y' &= A(t)y, \\ \Delta y|_{t=\theta_i} &= D_i^{(j)} y, \end{aligned} \tag{5.34}$$

of the form (5.32). One can verify that

$$Y_j(t)Y_j^{-1}(s) = P_j(t)\begin{pmatrix} 1 & 0 \\ 0 & \exp(H_j(t-s)) \end{pmatrix} P_j^{-1}(s), \tag{5.35}$$

for $-\infty < t, s < \infty$.

We can write

$$\begin{pmatrix} 1 & 0 \\ 0 & \exp(H_j(t-s)) \end{pmatrix} = \begin{pmatrix} 0 & 0 \\ 0 & \exp(H_j(t-s)) \end{pmatrix} + \begin{pmatrix} 1 & 0 \\ 0 & O_{n-1} \end{pmatrix},$$

where O_{n-1} is the $(n-1) \times (n-1)$ zero matrix. Then it can be driven

$$Y_j(t)Y_j^{-1}(s) = G_1^{(j)}(t,s) + G_2^{(j)}(t,s) = G^{(j)}(t,s),$$

where

$$\begin{aligned} G_1^{(j)}(t,s) &= P_j(t)\begin{pmatrix} 0 & 0 \\ 0 & \exp(H_j(t-s)) \end{pmatrix} P_j^{-1}(s), \\ G_2^{(j)}(t,s) &= P_j(t)\begin{pmatrix} 1 & 0 \\ 0 & O_{n-1} \end{pmatrix} P_j^{-1}(s). \end{aligned}$$

Denote the eigenvalues of the matrix H_j by $\lambda_2^{(j)}, \ldots, \lambda_n^{(j)}$. By means of the Lemma 2 and 3, there exits a number $\alpha > 0$, such that $Re(\lambda_k^{(j)}) < -\alpha$, $k = 2, 3, \ldots, n$, where $Re(z)$ means the real part of the number, z. Taking into account that the matrices P_j and P_j^{-1} are regular and periodic, the following estimates can be calculated

$$|G_1^{(j)}(t,s)| \leq K^{(j)} \exp(-\alpha(t-s)), \tag{5.36}$$

$$|G_2^{(j)}(t,s)| \leq K^{(j)}, \tag{5.37}$$

where $K^{(j)}$ is a positive real constant.

Denote the first column of the fundamental matrix Y by χ^1. By the Eq. (5.32), χ^1 is equal to the first column of P_j, this means that it is a ω-periodic solution of (5.12).

By assumptions of the theorem, the variational system (5.33) satisfies the conditions of Lemma 3, and one can verify that the following estimate is true [11]

$$|Y_j(t)| \leq K_1^{(j)} \exp(-\alpha t) \quad for \quad t \geq 0, \tag{5.38}$$

where $K_1^{(j)}$ is a positive constant. Let us setup the following integral equation

$$z^{(j)}(t,a) = Y_j(t)a + \int_0^t G_1^{(j)}(t,s)r(s,z(s))ds - \int_t^\infty G_2^{(j)}(t,s)r(s,z(s))ds$$
$$+ \sum_{0<\theta_k<t} G_1^{(j)}(t,\theta_k+)q_k(z(\theta_k)) - \sum_{t<\theta_k<\infty} G_2^{(j)}(t,\theta_k+)q_k(z(\theta_k)), \tag{5.39}$$

where $a = [0, a_2, \ldots, a_n]$, $a_i \in \mathbb{R}$, $i = 2, 3, \ldots, n$, are orthogonal to $\Psi'(0)$, i.e., with the zero first coordinate.

Let $z_0^{(j)}(t,a) \equiv 0$, and consider the following successive approximations

$$z_k^{(j)}(t,a) = Y_j(t)a + \int_0^\infty G^{(j)}(t,s)r(s,z_{k-1}(s))ds + \sum_{k=1}^\infty G^{(j)}(t,\theta_k+)q_k(z_{k-1}(\theta_k)), \tag{5.40}$$

for $k = 1, 2, \ldots$. By using the approximation (5.40) and estimation (5.38), one can verify that

$$|z_1^{(j)}(t,a)| \le K_1^{(j)}|a|\exp(-\alpha t/2). \tag{5.41}$$

We will show that the bounded solution of (5.39) exists and satisfies (5.33). For arbitrary positive small number L, there exists a number $\delta = \delta(L)$ such that for $|z_1| < \delta$, $|z_2| < \delta$

$$|r(t,z_1) - r(t,z_2)| \le L|z_1 - z_2| \tag{5.42}$$

and

$$|q_i(z_1) - q_i(z_2)| \le L|z_1 - z_2|, \tag{5.43}$$

uniformly in $t \in [0, \infty)$.

Denote by $L_1 = 4K^{(j)}\Big(\dfrac{2}{\alpha} - \dfrac{1}{1-\exp(-\alpha\underline{\theta}/2)}\Big)$.

Next, by using mathematical induction, we are going to show that $z_s^{(j)}(t,a)$, $s = 1, 2, \ldots$, are defined for $t \in [0,\infty)$ and satisfy

$$|z_{s+1}^{(j)}(t,a) - z_s^{(j)}(t,a)| \le K_1^{(j)}|a|\exp(-\alpha t/2)/2^s,\ s = 0, 1, 2, \ldots, \tag{5.44}$$

if $L < L_1$. Utilizing Lemma 3 and inequalities (5.38), (5.42), (5.43) and $\theta_{i+1} - \theta_i \ge \underline{\theta}$, $i \in \mathbb{Z}$, one can verify that

$$|z_{k+1}^{(j)}(t,a) - z_k^{(j)}(t,a)| \le K_1^{(j)}|a|L_1\exp(-\alpha t/2)/(2^k\alpha). \tag{5.45}$$

As a consequence of (5.44), the sequence $z_{k+1}^{(j)}(t,a)$ converges uniformly on $t \in [0,\infty)$, $|a| < \delta/2K_1^{(j)}$, and

$$|z_s^{(j)}(t,a)| \le 2K_1^{(j)}|a|\exp(-\alpha t/2), s = 1, 2, \ldots.$$

Therefore, the limit function $z^{(j)}(t,a)$ exists on the same domain, it is piecewise continuous, satisfies (5.39) and the following estimate

$$|z^{(j)}(t,a)| \leq 2K_1^{(j)}|a|\exp(-\alpha t/2). \tag{5.46}$$

Denote by $z(t) = z^{(j)}(t,a)$, for $j = 1, 2, \ldots, m$. Next, we will verify that $z^{(j)}(t,a)$ satisfies (5.33). For it, differentiate (5.39)

$$\begin{aligned}
z'(t) &= Y_j'(t)a + G_1^{(j)}(t,t)r(t,z(t)) + G_2^j(t,t)r(t,z(t)) + \int_0^t G_{1t}^{(j)}(t,s)r(s,z(s))ds \\
&- \int_t^\infty G_{2t}^{(j)}(t,s)r(s,z(s))ds + \sum_{0<\theta_k<t} G_{1t}^{(j)}(t,\theta_k+)q_k(z(\theta_k)) - \sum_{t<\theta_k<\infty} G_{2t}^{(j)}(t,\theta_k+) \\
&\times q_k(z(\theta_k)) = A(t)Y_j(t)a + G^{(j)}(t,t)r(t,z(t)) + \int_0^\infty A(t)G^{(j)}(t,s)r(s,z(s))ds \\
&+ \sum_{0<\theta_i<t} A(t)G^{(j)}(t,\theta_k+)q_k(z(\theta_k)) = A(t)z(t) + r(t,z(t)).
\end{aligned}$$

Fix θ_k, $k \in \mathbb{Z}$, then

$$\begin{aligned}
z(\theta_k+) - z(\theta_k) &= Y_j(\theta_k+)a + \int_0^{\theta_k} G_1^{(j)}(\theta_k+,s)r(s,z(s))ds - \int_{\theta_k}^\infty G_2^{(j)}(\theta_k+,s) \\
&\times q_k(z(\theta_k)) + \sum_{0\leq\theta_i<\theta_k} G_1^{(j)}(\theta_k+,\theta_i+)q_i(z(\theta_i+)) - \sum_{\theta_k<\theta_i<\infty} G_2^{(j)}(\theta_k+,\theta_i+) \\
&\times q_i(z(\theta_i+)) - Y_j(\theta_k)a - \int_0^{\theta_k} G_1^{(j)}(\theta_k,s)r(s,z(s))ds + \int_{\theta_k}^\infty G_2^{(j)}(\theta_k,s)r(s,z(s))ds \\
&- \sum_{0\leq\theta_i<\theta_k} G_1^{(j)}(\theta_k,\theta_i+)q_i(z(\theta_i)) + \sum_{\theta_k\leq\theta_i<\infty} G_2^{(j)}(\theta_k,\theta_i+)q_i(z(\theta_i+)) \\
&= D_k^{(j)}z(\theta_k) + q_k(z(\theta_k)).
\end{aligned}$$

The above discussion proves that $z^{(j)}(t,a)$, $j = 1,, 2, \ldots, m$, are bounded solutions of system (5.33).

We will determine the initial values of bounded solutions in terms of $(n-1)$ parameters $a_2^{(j)}, \ldots, a_n^{(j)}$, $j = 1,, 2, \ldots, m$. Denote $a^{(j)} = [0, a_2^j, a_3^j, \ldots, a_n^j]$. By using (5.39), we obtain

$$z^{(j)}(0, a^{(j)}) = Y_j(0)a^{(j)} - \int_0^\infty G_2^{(j)}(0, s)r(s, z(s))ds - \sum_{0<\theta_k<\infty} G_2^{(j)}(0, \theta_k+)q_k(z(\theta_k))$$

$$= P_j(0)a^{(j)} - P_j(0)\begin{pmatrix} 1 & 0 \\ 0 & O_{n-1} \end{pmatrix} \int_0^\infty P_j^{-1}(s)r(s, z(s))ds$$

$$- \sum_{0<\theta_k<\infty} P_j^{-1}(s)q_k(z(\theta_k)).$$

In the way utilized in [11], one can show that the coordinates of the initial value $(x_1, \ldots, x_n) \in D$ of the solution $z^{(j)}$ satisfy the equation

$$x_1 + \sum_{i=2}^{n} c_i^j x_i - h_j(x_2, \ldots, x_n) = 0, \tag{5.47}$$

where $h_j \in C^1$, $j = 1, , 2, \ldots, m$.

One can see that Eq. (5.47) determines $(n-1)$ dimensional hypersurfaces $S^j \subset D$, $j = 1, 2, \ldots, m$, in a neighborhood of the origin such that each solution which starts at the surface satisfies inequality (5.46). From the analytical representation, it follows that the equation of the tangent space of S^j at the origin is described by the equation $x_1 + \sum_{i=2}^{n} c_i^j x_i$, and the first coordinate of the gradient of the left-hand side in (5.47) is unity. Moreover, the path η intersects S^j transversely. This and condition (A4) imply that the path of every solution $\phi(t)$ near $\Psi(t)$ intersects one of the manifolds S^j, $j = 1, 2, \ldots, m$, at some $\bar{t} \in [0, 2\omega]$.

Because of the continuous dependence on initial values, a $\delta(\varepsilon) > 0$ exists for a given $\varepsilon > 0$, such that if $dist(x^0, \eta_\delta) < \delta(\varepsilon)$, then the solution $\phi(t, x^0)$ is defined on $[0, 2\omega]$, and $dist(\phi(t, x^0), \eta) < \varepsilon \leq \varepsilon_1$ for $t \in [0, 2T]$. Therefore, the path of $\phi(t, x^0)$ intersects S^j for some $j = 1, 2, \ldots, m$ and $t_1 \in [0, 2\omega]$. The solution $\phi(t, \phi(t_1, x^0)) = \phi(t + t_1, x^0)$ has its initial value in S^j, consequently, satisfies (5.46). In light of the B-equivalence, the corresponding solution $x(t)$, $x(0) = \phi(0) - \Psi(0)$, of (5.33) satisfies the property that for all $\varepsilon > 0$, there exists $T(\varepsilon)$ such that $x(t)$ is in an ε-neighborhood of $\Psi(t)$ for $t \in [T(\varepsilon), \infty)$. That is, the solution $\Psi(t)$ is orbitally, asymptotically stable, and there exists an asymptotical phase.

Because of the continuous dependence on initial values, a $\delta(\varepsilon) > 0$ exists for a given $\varepsilon > 0$, such that if $dist(x^0, \eta_\delta) < \delta(\varepsilon)$, then the solution $\phi(t, x^0)$ is defined on $[0, 2\omega]$, and $dist(\phi(t, x^0), \eta) < \varepsilon \leq \varepsilon_1$ for $t \in [0, 2T]$. Therefore, the path of $\phi(t, x^0)$ intersects S^j for some $j = 1, 2, \ldots, m$ and $t_1 \in [0, 2\omega]$. The solution $\phi(t, \phi(t_1, x^0)) = \phi(t + t_1, x^0)$ has its initial value in S^j, consequently, satisfies (5.46). In light of the B-equivalence, the corresponding solution $x(t)$, $x(0) = \phi(0) - \Psi(0)$, of (5.33) satisfies the property that for all $\varepsilon > 0$, there exists $T(\varepsilon)$ such that $x(t)$ is in an ε-neighborhood of $\Psi(t)$ for $t \in [T(\varepsilon), \infty)$. That is, the solution $\Psi(t)$ is orbitally, asymptotically stable and there exists an asymptotical phase.

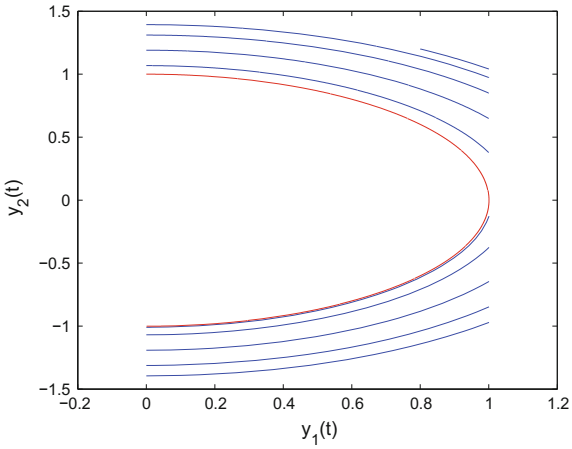

Fig. 5.4 The *red* discontinuous cycle of (5.13) grazes Γ at $(0.00025\pi), 0)$, and $(0, -\exp(-0.0005\pi))$ is an (α)-type point. The *blue arcs* are of the trajectory with initial value (0.8, 1.2). It can be observed that it approaches the grazing one as time increases

Definitions of the orbital stability and an asymptotic phase as well as theorem of orbital stability for non-grazing periodic solutions are also presented in [29]. In our study, we suggest the orbital stability theorem for grazing periodic solutions, its proof and formulate the definitions for the stability. They are different in many aspects from those provided in [29]. It is valuable that they also valid, if the solution is non-grazing.

To shed light on our theoretical results, we will present the following examples.

Example 3 We continue with the system presented in Examples 1 and 2. In Example 1, we verified that system (5.15) defines a K-smooth discontinuous flow in the plane, and the variational system (5.28) + (5.29) around the grazing periodic solution $\Psi(t)$ is approved.

Using systems (5.28) and (5.29), one can evaluate the Floquet multipliers as $\rho_1^{(1)} = 1$, $\rho_2^{(1)} = 0.8551$, $\rho_1^{(2)} = 1$ and $\rho_2^{(2)} = 0$. This verifies condition (A5).

The conditions (C1)–(C7) and (C10) are validated, and the assumptions (A4) and (A5) verified. By using Theorem 3, we can assert that the solution, $\Psi(t)$ is orbitally, asymptotically stable. The stability is illustrated in Fig. 5.4. The red one is for a trajectory of the discontinuous periodic solution (5.14) of (5.13), and the blue one is for the near solution of (5.13) with initial value $y_0 = (0.8, 1.2)$. It can be observed from Fig. 5.4 that the blue trajectory approaches the red one as time increases.

5.2.4 Small Parameter Analysis and Grazing Bifurcation

In this part, we will discuss existence and bifurcation of cycles for perturbed systems, if the generating one admits a grazing periodic solution. In continuous dynamical systems, a small parameter may cause a change in the number of periodic solutions

in critical cases. In this analysis, we will demonstrate that the change may happen in *non-critical* cases, because of the non-transversality. That is why, one can say that *grazing bifurcation* is under discussion. Let us deal with the following system

$$\begin{aligned} x' &= f(x) + \mu g(x, \mu), \\ \Delta x|_{x \in \Gamma(\mu)} &= I(x) + \mu K(x, \mu), \end{aligned} \tag{5.48}$$

where $x \in \mathbb{R}^n$, $t \in \mathbb{R}$, $\Gamma(\mu) = \{x |\ \Phi(x) + \mu\phi(x, \mu) = 0\}$, $\mu \in (-\mu_0, \mu_0)$, and μ_0 is a sufficiently small positive number. Functions $f(x)$, $I(x)$ and $\Phi(x)$ are continuously differentiable up to second order, $g(x, \mu)$, $K(x, \mu)$ are continuously differentiable in x and μ. The function $\phi(x, \mu)$ is continuously differentiable in x up to second order and to first order in μ. We assume that the generating system for (5.48) is the system (5.1) with all conditions assumed for the system, earlier. The main assumption of this section is that (5.1) admits a ω-periodic solution, $\Psi(t)$. Let $\Psi(0) = (\zeta_1^0, \zeta_2^0, \ldots, \zeta_n^0)$ be the initial value of the solution.

Our aim is to find conditions that verify the existence of periodic solutions of (5.48) with a period $\mathscr{T}$ such that for $\mu = 0$, the periodic solutions of (5.48) are turned down to $\Psi(t)$. It is common for the autonomous systems that the period $\mathscr{T}$ does not coincide with ω. Thus, in the remaining part of the study, we will consider the period $\mathscr{T}$ as an unknown variable.

Since $\Psi(0)$ is not an equilibrium, there exists a number $j = 1, 2, \ldots, n$, such that $f_j(\zeta_1^0, \zeta_1^0, \ldots, \zeta_n^0) \neq 0$. In other words, the vector field is transversal to $x_j = \zeta_j^0$ near the point. Hence, to try points near to $\Psi(0)$ for the periodicity, it is sufficient to consider those with j-th coordinate is equal to ζ_j^0, [22]. For the discontinuous dynamics, the choice of the fixed coordinate can be made easier if the surface of discontinuity is provided with a constant coordinate. It will be demonstrated in examples. Denote the initial values of the intended periodic solution by $\zeta_1, \zeta_2, \ldots, \zeta_n$. Assume that one initial value ζ_j is known, i.e., ζ_j^0. Thus, the problem contains n-many unknowns, they can be presented as $\zeta_1, \zeta_2, \ldots, \zeta_{j-1}, \zeta_{j+1}, \ldots, \zeta_n, \mathscr{T}$. Denote the solution of (5.48) by $x_s(t, \zeta_1, \zeta_2, \ldots, \zeta_n, \mu)$ with initial conditions $x_s(0, \zeta_1, \zeta_2, \ldots, \zeta_n, \mu) = \zeta_s$. To determine the unknowns, we will consider the Poincaré criterion, which can be written as

$$\mathscr{S}_k(\mathscr{T}, \zeta_1, \zeta_2, \ldots, \zeta_n, \mu) \equiv x_k(\mathscr{T}, \zeta_1, \zeta_2, \ldots, \zeta_n, \mu) - \zeta_k = 0,\ k = 1, 2, \ldots, n, \tag{5.49}$$

where $\zeta_j = \zeta_j^0$. The Eq. (5.49) is satisfied with $\mu = 0$, $\mathscr{T} = \omega$, $\zeta_i = \zeta_i^0$, $i = 1, 2, \ldots, n$, since $\Psi(t)$ is the periodic solution.

The following condition for the determinant is also needed in the remaining part study.

(A6)

$$\begin{vmatrix} \frac{\partial(\mathscr{S}_1(\omega,\zeta_1^0,\zeta_2^0,\ldots,\zeta_{j-1}^0,\zeta_{j+1}^0,\ldots,\zeta_n^0,0))}{\partial\mathscr{T}} & \cdots & \frac{\partial(\mathscr{S}_1(\omega,\zeta_1^0,\zeta_2^0,\ldots,\zeta_{j-1}^0,\zeta_{j+1}^0,\ldots,\zeta_n^0,0))}{\partial\zeta_n} \\ \frac{\partial(\mathscr{S}_2(\omega,\zeta_1^0,\zeta_2^0,\ldots,\zeta_{j-1}^0,\zeta_{j+1}^0,\ldots,\zeta_n^0,0))}{\partial\mathscr{T}} & \cdots & \frac{\partial(\mathscr{S}_2(\omega,\zeta_1^0,\zeta_2^0,\ldots,\zeta_{j-1}^0,\zeta_{j+1}^0,\ldots,\zeta_n^0,0))}{\partial\zeta_n} \\ \vdots & \ddots & \vdots \\ \frac{\partial(\mathscr{S}_n(\omega,\zeta_1^0,\zeta_2^0,\ldots,\zeta_{j-1}^0,\zeta_{j+1}^0,\ldots,\zeta_n^0,0))}{\partial\mathscr{T}} & \cdots & \frac{\partial(\mathscr{S}_n(\omega,\zeta_1^0,\zeta_2^0,\ldots,\zeta_{j-1}^0,\zeta_{j+1}^0,\ldots,\zeta_n^0,0))}{\partial\zeta_n} \end{vmatrix} \neq 0 \quad (5.50)$$

Theorem 4 *Assume that condition (A6) is valid. Then, (5.48) admits a non-trivial periodic solution, which converges in the B-topology to the non-trivial ω-periodic solution of (5.48) as μ tends to zero.*

We will present the following example to realize our theoretical results.

Example 4 Let us consider the following system with variable moments of impulses and a small parameter

$$\begin{aligned} x_1' &= x_2, \\ x_2' &= -0.0001[x_2^2 + (x_1-1)^2 - (1+\mu)^2]x_2 - x_1 + 1, \\ \Delta x_2|_{x\in\Gamma} &= -(1 + Rx_2 + \mu x_2^3)x_2 + \mu^2, \end{aligned} \quad (5.51)$$

where $R = 0.9$ and $\Gamma = \{x | x_1 = 0, x_2 \leq 0\}$. It is easy to see that system (5.51) is of the form (5.48) and $\Phi(x_1, x_2) = x_1 = 0$. The system has a periodic solution

$$\Psi_\mu(t) = (1 + (1+\mu)\cos(t), -(1+\mu)\sin(t)), \quad (5.52)$$

where $t \in \mathbb{R}$ for $\mu \in (-2, 0]$.

The generating system of (5.51) has the following form

$$\begin{aligned} x_1' &= x_2, \\ x_2' &= -0.0001[x_2^2 + (x_1-1)^2 - 1]x_2 - x_1 + 1, \\ \Delta x_2|_{x\in\Gamma} &= -(1 + Rx_2)x_2, \end{aligned} \quad (5.53)$$

and admits the periodic solution $\Psi_0(t) = (1 + \cos(t), -\sin(t))$. By means of the equality $\langle \nabla\Phi(x^*), f(x^*)\rangle = \langle (1,0), (0,1)\rangle = 0$ with $x^* = (0,0) \in \partial\Gamma$, it is easy to say that x^* is a grazing point of $\Psi_0(t)$.

Considering the same way done in Example 1, it is easy to obtain

$$W_{iy}(y^*) = \begin{bmatrix} -1 & 0 \\ 0.0003R & 0 \end{bmatrix}, \quad (5.54)$$

and

$$B_i = \begin{cases} O_2, & \text{if} \quad (N1) \quad \text{is valid,} \\ \begin{bmatrix} -1 & 0 \\ 0.0003R & 0 \end{bmatrix}, & \text{if} \quad (N2) \quad \text{is valid.} \end{cases} \tag{5.55}$$

By means of the formula (5.55), the linearization system for (5.53) around the grazing cycle $\Psi_0(t)$ consists of the following two subsystems

$$\begin{aligned} u_1' &= u_2, \\ u_2' &= -0.0001\sin(2t)u_1 + 0.0002\sin^2(t)u_2, \end{aligned} \tag{5.56}$$

and

$$\begin{aligned} u_1' &= u_2, \\ u_2' &= -0.0001\sin(2t)u_1 + 0.0002\sin^2(t)u_2, \\ \Delta u|_{2\pi i} &= \begin{bmatrix} -1 & 0 \\ 0.0003R & 0 \end{bmatrix} u. \end{aligned} \tag{5.57}$$

The system (5.56) + (5.57) is $(2\pi, 1)$ periodic. The Floquet multipliers of system (5.56) + (5.57) are $\rho_1^{(1)} = 1$, $\rho_2^{(1)} = 0.939$, $\rho_1^{(2)} = 1$, $\rho_2^{(2)} = 0.912$. Thus, condition (A5) is validated. Moreover, the conditions (C1)–(C7) and (A1)–(A4) can be verified utilizing similar way presented in Example 1. Consequently, Theorem 3 authenticates that the grazing periodic solution (cycle), $\Psi_0(t)$ of the system (5.53) is orbitally stable. The simulation results demonstrating the orbital stability of $\Psi_0(t)$ are depicted in Fig. 5.5.

Next, we will investigate two sorts of periodic solutions of system (5.51) with a period $\mathscr{T}$ near to 2π. The first one is continuous, and the second admits discontinuities once on a period. For those solutions, corresponding linearization systems around the grazing cycle $\Psi_0(t)$ are (5.56) and (5.57), respectively. Let us start with the

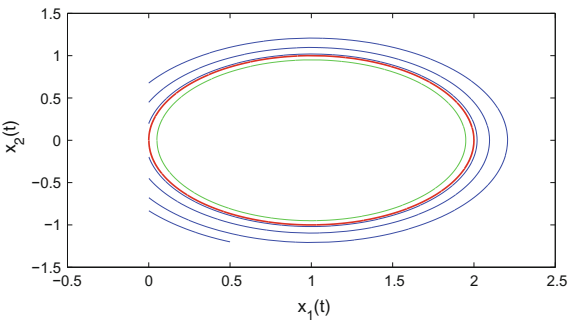

Fig. 5.5 The grazing cycle of system (5.53) is in *red*. The *blue arcs* are the trajectory of the system with initial point (0.5, 1.2), and the *green* continuous orbit is with initial value (0.1, 0). They demonstrate stability of the grazing solution

continuous periodic solutions of (5.51). For continuous periodic solution, we will consider the linearization system (5.56).

To apply Theorem 4, denote $\Psi_0(0) = (\zeta_1^0, 0)$. That is, consider $\zeta_2^0 = 0$. Then, applying the above discussion, obtain that the Poincarè condition admits the form of the following equations,

$$\begin{aligned} \mathscr{S}_1(\mathscr{T}, \zeta_1, \mu) &= x_1(\mathscr{T}, \zeta_1, \mu) - x_1 = 0, \\ \mathscr{S}_2(\mathscr{T}, \zeta_1, \mu) &= x_2(\mathscr{T}, \zeta_1, \mu) = 0. \end{aligned} \tag{5.58}$$

Because solutions of the system (5.53) have continuous derivatives with respect to the time, phase variables and parameters, we can calculate the following determinant

$$\begin{vmatrix} \dfrac{\partial \mathscr{S}_1(\omega, \zeta_1^0, 0)}{\partial \mathscr{T}} & \dfrac{\partial \mathscr{S}_1(\omega, \zeta_1^0, 0)}{\partial x_1^0} \\ \dfrac{\partial \mathscr{S}_2(\omega, \zeta_1^0, 0)}{\partial \mathscr{T}} & \dfrac{\partial \mathscr{S}_2(\omega, \zeta_1^0, 0)}{\partial x_1^0} \end{vmatrix}. \tag{5.59}$$

First, we need the monodromy matrix of the system (5.56). It is

$$\begin{bmatrix} 0.939 & -0.0001407 \\ -0.0003165 & 1 \end{bmatrix}. \tag{5.60}$$

It is easy to see that first column of the determinant (5.59) is computed by utilizing (5.53), and the second column is evaluated by means of the first column of the matrix (5.60). From this discussion, one can obtain that the determinant (5.59) is equal to

$$\begin{vmatrix} 0 & -0.061 \\ 1 & -0.0003165 \end{vmatrix} = 0.061 \neq 0. \tag{5.61}$$

Thus, in light of Theorem 4, we can conclude that for sufficiently small $|\mu|$, there exists a unique periodic solution of the system

$$\begin{aligned} x_1' &= x_2, \\ x_2' &= -0.0001[x_2^2 + (x_1 - 1)^2 - (1 + \mu)^2]x_2 - x_1 + 1. \end{aligned} \tag{5.62}$$

It is exactly the cycle (5.52) with a period $\mathscr{T} = 2\pi$. If $\mu < 0$, the solution is separated from the set Γ. Consequently, it is a periodic continuous solution of the Eq. (5.51). It is orbitally stable by the theorem for continuous dynamics [13], because of the continuous dependence of multipliers on the parameter. The function $\Psi_\mu(t)$, $\mu > 0$, intersects Γ and cannot be a solution of Eq. (5.51). Thus, the system does not admit a continuous periodic solution near to $\Psi_0(t)$, if the parameter is positive.

Considering those solutions which have one moment of discontinuity in a period, one can find that the corresponding linearization of $\Psi_0(t)$ is the system (5.57).

The monodromy matrix of (5.57) can be evaluated as

$$\begin{bmatrix} 0.939 & -0.00052 \\ -0.000427 & 1 \end{bmatrix}. \tag{5.63}$$

It can be easily observed that the discontinuous solution intersects the line $x_1 = 0$. For this reason, one can specify the first coordinate of the initial value as $\zeta_1 = \zeta_1^0 \equiv 0$. In light of these discussions and the formula (5.49), the following equations are obtained:

$$\begin{aligned} \mathscr{S}_1(\mathscr{T}, 0, \zeta_2, \mu) &= x_1(\mathscr{T}, 0, \zeta_2, \mu) = 0, \\ \mathscr{S}_2(\mathscr{T}, 0, \zeta_2, \mu) &= x_2(\mathscr{T}, 0, \zeta_2, \mu) - \zeta_2 = 0. \end{aligned} \tag{5.64}$$

Then, taking the derivative of the system (5.64) with respect to $\mathscr{T}$ and ζ_2, and calculating it at $\mathscr{T} = \omega$, $\zeta_2 = \zeta_2^0 = 0$, and for $\mu = 0$, the following determinant is obtained

$$\begin{vmatrix} \dfrac{\partial \mathscr{S}_1(\omega, 0, \zeta_2^0, 0)}{\partial \mathscr{T}} & \dfrac{\partial \mathscr{S}_1(\omega, 0, \zeta_2^0, 0)}{\partial \zeta_2} \\ \dfrac{\partial \mathscr{S}_2(\omega, 0, \zeta_2^0, 0)}{\partial \mathscr{T}} & \dfrac{\partial \mathscr{S}_2(\omega, 0, \zeta_2^0, 0)}{\partial \zeta_2} \end{vmatrix} = \begin{vmatrix} 0 & -0.0006 \\ 1 & 0.0009 \end{vmatrix} = -0.0006 \neq 0. \tag{5.65}$$

Thus, condition (A6) holds. Then, utilizing Theorem 4, it is easy to conclude that for sufficiently small μ there exists a unique periodic solution of the system (5.51) with a period $\approx 2\pi$. It is true that for positive and negative μ. Moreover, these solutions are orbitally, asymptotically stable because of the continuous dependence of solutions on parameter and initial values, and they meet the discontinuity line transversally.

For each fixed $\mu \neq 0$, solutions near to the periodic ones intersect the line of discontinuity Γ transversally once during the time approximately equal to the period. That is, the smoothness which is requested for the application of the Poincarè condition is valid, since the smoothness for the grazing point has already been verified. It is clear that there can not be another solutions with period close to 2π. Thus, one can make the following conclusion. The original system (5.51) admits two orbitally stable periodic solutions, continuous and discontinuous, if $\mu < 0$. There is a single orbitally stable continuous solution (grazing) if $\mu = 0$. Additionally, there is a unique discontinuous orbitally stable periodic solution for positive values of the parameter. Consequently, grazing bifurcation of cycles appears for the system with small parameter.

We have obtained regular behavior in dynamics near grazing orbits by Poincarè small parameter analysis. Nevertheless, outside the attractors irregular phenomena may be observed.

In Fig. 5.6, the solutions of the system (5.51) with parameter $\mu = -0.2$ are depicted through simulations. The red arcs are the trajectory of the system (5.51) with initial value $(0.7, 0.05)$, and the blue arcs are the trajectory of the system (5.51) with initial value $(0.4, 0.05)$. It is seen that both red and blue trajectories approach the

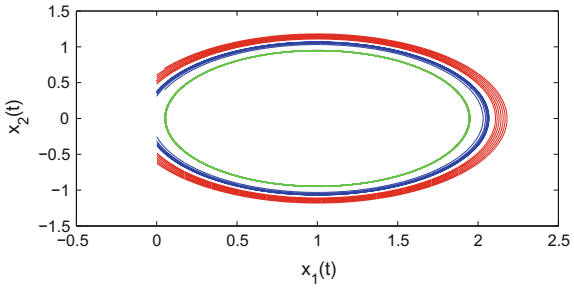

Fig. 5.6 The *blue*, *red* and *green arcs* constitute the trajectories of system (5.51) with $\mu = -0.2$. The first two approach as time increases to the discontinuous limit cycle and the third one is the continuous limit cycle itself

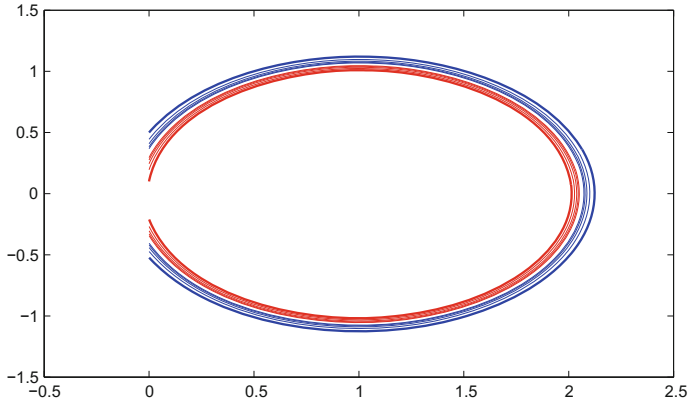

Fig. 5.7 The *red* and *blue arcs* constitute the trajectories of the system (5.51) with $\mu = 0.2$. Both orbits approach to the discontinuous limit cycle, as time increases

discontinuous periodic solution of (5.51), as time increases. So, the discontinuous cycle is orbitally stable trajectory. Moreover, the green one is a continuous periodic trajectory of (5.51) with initial value $(0, 0.05)$ and it is orbitally, asymptotically stable. To sum up, there exists two periodic solutions of (5.51) for the parameter $\mu = -0.2$, one is continuous, the other one is discontinuous, and both solutions are orbitally, asymptotically stable.

In Fig. 5.7, the red arcs are the orbit of the system with initial value $(0, 0.1)$, and the blue arcs are the trajectory of it with initial value $(0, 0.4)$. Both trajectories approach to the discontinuous cycle of system (5.51), as time increases. Thus, Fig. 5.7 illustrates the existence of the orbitally stable discontinuous periodic solution if $\mu = 0.2$.

5.3 The Grazing Solutions of Non-autonomous Systems with Stationary Impulsive Conditions

Let $\Phi : G \to \mathbb{R}$ be a function, differentiable up to second order with respect to x, $S = \Phi^{-1}(0)$ is a closed subset of G. Define a continuously differentiable function $J : G \to G$ such that $J(S) \subset G$. The function $I(x)$ will be used in the following part of the paper which is defined as $I(x) := J(x) - x$, for $x \in S$.

The following definitions will be utilized in the remaining part of the paper. Let $x(\theta-)$ be the left limit of a function $x(t)$ at the moment θ, and $x(\theta+)$ be the right limit of the solution. Define $\Delta x(\theta) := x(\theta+) - x(\theta-)$ as the jump operator for $x(t)$ such that $x(\theta) \in S$ and $t = \theta$ is a moment of discontinuity. Discontinuity moments are the moments when the solution meets the surface of discontinuity.

In this chapter, we take into account the following system

$$\begin{aligned} x' &= f(t, x), \\ \Delta x|_{x \in S} &= I(x), \end{aligned} \tag{5.66}$$

where $(t, x) \in \mathbb{R} \times G$, the functions $f(t, x)$ is continuously differentiable with respect to x up to second order and continuous with respect to time. We will consider the surface of discontinuity as $\Gamma = \{(t, x) | \Phi(x) = 0\} \subseteq \mathbb{R} \times S$. We say that the system is with stationary impulse conditions, since the function $I(x)$ and the surface S do not depend on time.

For the convenience in notation, let us separate the differential equation of the impulse system as

$$y' = f(t, y). \tag{5.67}$$

Assume that the solution $x_0(t) = x(t, t_0, x_0)$, $t_0 \in \mathbb{R}$, $x_0 \in G$ of (5.66) intersects the surface of discontinuity Γ, at the moments $t = \theta_i$, $i \in \mathbb{Z}$.

Set the gradient vector of Φ with respect to x as $\nabla\Phi(x)$. The normal vector of Γ at a meeting moment, $t = \theta_i$, of the solution $x_0(t)$ can be determined as $\overrightarrow{n} = (0, \nabla\Phi(x_0(\theta_i))) \in \mathbb{R}^{n+1}$, where $\langle , \rangle$ means the dot product. For the tangency, the vectors $\overrightarrow{n}$ and $(1, f(\theta_i, x_0(\theta_i)))$ should be perpendicular. That is, $\langle \nabla\Phi(x_0(\theta_i)), f(\theta_i, x_0(\theta_i)) \rangle = 0$.

Consider the function $H(t, x) := \langle \nabla\Phi(x), f(t, x) \rangle$, with $(t, x) \in \mathbb{R} \times S$.

Let us start with the following definitions.

Definition 7 A point $(\theta_i, x_0(\theta_i))$ is a *grazing point* and θ_i a grazing moment for a solution $x_0(t)$ of (5.66) if $H(\theta_i, x_0(\theta_i)) = 0$ and $I(x_0(\theta_i)) = 0$.

Definition 8 A solution $x_0(t)$ of (5.66) is grazing if it has a grazing point $(\theta_i, x_0(\theta_i))$. The moment θ_i is the grazing moment of the solution $x_0(t)$.

Definition 9 A point $(\theta_i, x_0(\theta_i))$ is a *transversal point* and θ_i a transversal moment for a solution $x_0(t)$ if $H(\theta_i, x_0(\theta_i)) \neq 0$.

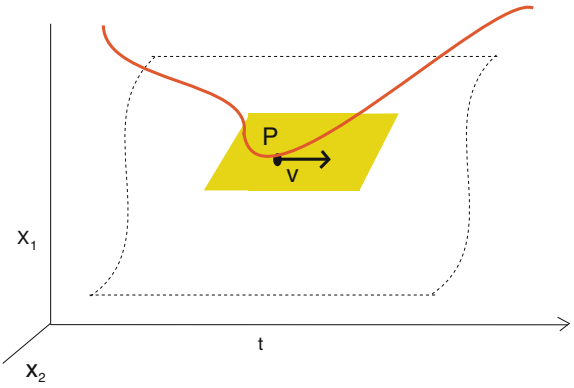

Fig. 5.8 The *red line* is a grazing solution $x_0(t)$ of (5.66) with the grazing point $P = (\theta_i, x_0(\theta_i))$. The *yellow region* is the tangent plane to the surface Γ at the grazing point. Vector v is tangent to the integral curve at P

Figure 5.8 is drawn to illustrate the grazing phenomenon. The red line is a grazing solution $x_0(t)$ of (5.66), and it intersects the surface Γ at the point $P = (\theta_i, x_0(\theta_i))$. The yellow region is the tangent plane to the surface at the point. Vector v is tangent to the integral curve at P. It belongs to the tangent plane. This is why the point is grazing.

In what follows, we will assume that the following condition is valid.

(H1) For each grazing point $(\theta_i, x_0(\theta_i))$, there is a number $\delta > 0$ such that $H(t, x) \neq 0$ and $J(x) \notin S$ if $0 < |t - \theta_i| < \delta$ and $0 < \|x - x_0(\theta_i)\| < \delta$.

It is also clear that function $H(t, x) \neq 0$ near a transversal point.

Consider a solution $x(t) = x(t, \theta_i, x_0 + \Delta x)$ of (5.66) with a small $\|\Delta x\|$. Because of the geometrical reasons caused by the tangency at the grazing point, this solution may not intersect the surface of discontinuity near $(\theta_i, x_0(\theta_i))$. For this reason, there exist two different behaviors of it with respect to the surface of discontinuity, they are:

(N1) The solution $x(t)$ intersects the surface of discontinuity Γ at a moment near to θ_i.
(N2) There is no intersection moments of $x(t)$ close to θ_i.

We say that $\theta = \{\theta_i\}$ is a *B-sequence* if one of the following alternatives holds: (i) $\theta = \emptyset$, (ii) θ is a non-empty and finite set, and (iii) θ is an infinite set such that $|\theta_i| \to \infty$ as $i \to \infty$. In what follows, we will consider B-sequences.

In order to define a solution of (5.66), the following functions and sets are needed.

A function $\phi(t) : \mathbb{R} \to \mathbb{R}^n$, $n \in \mathbb{N}$, is from the set $PC(\mathbb{R}, \theta)$ if it: (i) is left continuous, (ii) is continuous, except, possibly, points of θ, where it has discontinuities of the first kind.

A function $\phi(t)$ is from the set $PC^1(\mathbb{R}, \theta)$ if $\phi(t), \phi'(t) \in PC(\mathbb{R}, \theta)$, where the derivative at points of θ is assumed to be the left derivative. If $\phi(t)$ is a solution of (5.66), then it is required that it belongs to $PC^1(\mathbb{R}, \theta)$. We say that $x(t) : \mathscr{I} \to$

$\mathbb{R}^n$, $\mathscr{I} \subset \mathbb{R}$, is a solution of (5.66) on $\mathscr{I}$ if there exists an extension $\tilde{x}(t)$ of the function on $\mathscr{I}$ such that $\tilde{x}(t) \in PC^1(\mathbb{R}, \theta)$, the equality (5.67) $t \in \mathscr{I}$, is true if $x(t) \notin S$, $x(\theta_i+) = J(x(\theta_i))$ for $x(\theta_i) \in S$ and $\theta_i \in \mathscr{I}$.

5.3.1 B-Equivalence

The system with variable moments of impulses is a difficult task for the investigations. In order to facilitate the analysis, in [3], a powerful instrument was suggested which reduces the systems with variable moments of impulses to those with fixed moments of impulses, which preserves the dynamical properties of (5.66). The system with fixed moment of impulses is called a *B-equivalent system* to the system with variable moments of impulses. The B-equivalent system can be constructed as follows.

Consider a solution $x_0(t) : \mathscr{I} \to \mathbb{R}^n$, $\mathscr{I} \subseteq \mathbb{R}$, of (5.66). Assume that all discontinuity points θ_i of $x_0(t)$, $i \in \mathscr{A}$, are interior points of $\mathscr{I}$. Where $\mathscr{A}$ is an interval in $\mathbb{Z}$. There exists a positive number r, such that r-neighborhoods $G_i(r)$ of $(\theta_i, x_0(\theta_i))$ do not intersect each other. Fix $i \in \mathscr{A}$ and let $\xi(t) = x(t, \theta_i, x)$, $(\theta_i, x) \in G_i(r)$, be a solution of (5.67), which satisfies $(N1)$, and $\tau_i = \tau_i(x)$ the meeting time of $\xi(t)$ with S and $\psi(t) = x(t, \tau_i, \xi(\tau_i) + J(\xi(\tau_i)))$ another solution of (5.67). Denote $W_i(x) = \psi(\theta_i) - x$ and one can define the map $W_i(x)$ as

$$W_i(x) = \int_{\theta_i}^{\tau_i} f(s, \xi(s))ds + J(x + \int_{\theta_i}^{\tau_i} f(s, \xi(s))ds) + \int_{\tau_i}^{\theta_i} f(s, \psi(s))ds \tag{5.68}$$

It is a map of an intersection of the plane $t = \theta_i$ with $G_i(r)$ into the plane $t = \theta_i$. Let us present the following system of differential equations with impulses at fixed moments, whose impulse moments, θ_i, $i \in \mathscr{A}$, correspond to the points of discontinuity of $x_0(t)$,

$$\begin{aligned} y' &= f(t, y), \\ \Delta y|_{t=\theta_i} &= W_i(y(\theta_i)). \end{aligned} \tag{5.69}$$

The function f is the same as the function in system (5.69), and the map W_i, $i \in \mathscr{A}$, is defined by Eq. (5.68) if $x(t)$ satisfies condition $(N1)$. Otherwise, if a solution $x(t)$ satisfies $(N2)$, then we assume that it admits the discontinuity moment θ_i with zero jump such that $W_i(x(\theta_i)) = 0$.

Let us introduce the sets $F_r = \{(t, x) | t \in \mathscr{I}, \|x - x_0(t)\| < r\}$, and $G_i^+(r)$, $i \in \mathscr{A}$, an r-neighborhood of the point $(\theta_i, x_0(\theta_i+))$. Write $G^r = F_1 \cup (\cup_{i \in \mathscr{A}} G_i(r)) \cup (\cup_{i \in \mathscr{A}} G_i^+(r))$. Take r sufficiently small so that $G^r \subset \mathbb{R} \times G$. Denote by $G(h)$ an h-neighborhood of $x_0(0)$.

Definition 10 Systems (5.66) and (5.69) are said to be B-equivalent in G^r if there exists $h > 0$, such that:

- for every solution $y(t)$ of (5.69) such that $y(0) \in G(h)$, the integral curve of $y(t)$ belongs to G^r there exists a solution $x(t) = x(t, 0, y(0))$ of (5.66) which satisfies

$$x(t) = y(t), \quad t \in [a, b] \setminus \cup_{i=-k}^{m} \widehat{(\tau_i, \theta_i]}, \tag{5.70}$$

  where τ_i are moments of discontinuity of $x(t)$. Particularly:

$$\begin{aligned} x(\theta_i) &= \begin{cases} y(\theta_i), & \text{if } \theta_i \le \tau_i, \\ y(\theta_i+), & \text{otherwise,} \end{cases} \\ y(\tau_i) &= \begin{cases} x(\tau_i), & \text{if } \theta_i \ge \tau_i, \\ x(\tau_i+), & \text{otherwise.} \end{cases} \end{aligned} \tag{5.71}$$

- Conversely, if (5.66) has a solution $x(t) = x(t, 0, x(0))$, $x(0) \in G(h)$, then there exists a solution $y(t) = y(t, 0, x(0))$ of (5.69) which has an integral curve in G^r, and (5.70) holds.

5.3.2 *Variational System for Grazing Solutions*

The objective of this section is to investigate the smoothness of the grazing solution. Consider a grazing solution $x_0(t) = x(t, 0, x_0)$, $x_0 \in G$, of (5.66) which was introduced in the last section. We will demonstrate that one can write the variational system for the solution as follows:

$$\begin{aligned} u' &= A(t)u, \\ \Delta u|_{t=\theta_i} &= B_i u(\theta_i), \end{aligned} \tag{5.72}$$

where the matrix $A(t) \in \mathbb{R}^{n\times n}$ of the form $A(t) = \frac{\partial f(t, x_0(t))}{\partial x}$. We call the second equation in (5.72) as the *linearization at a moment of discontinuity or at a point of discontinuity*. It is different for transversal and grazing points. However, the first differential equation in (5.72) is common for all type of solutions. The matrices B_i will be described in the remaining part of the paper for each type of the points.

5.3.2.1 Linearization at a Transversal Moment

Linearization at the transversal point has been analyzed completely in Chap. 6, [3]. Let us demonstrate the results shortly. The B-equivalent system (5.69) is involved in the analysis, since the solution $x_0(t)$ satisfies also the Eq. (5.69) at all moments of time, and near solutions do the same for all moments except small neighborhoods of the discontinuity moment θ_i. Consequently, it is easy to see that the system of variations around $x_0(t)$ for (5.66) and (5.69) is identical. Assume that $x(\theta_i)$ is at a transversal point. We consider the reduced B-equivalent system and use the functions

$\tau_i(x)$ and $W_i(x)$, defined by Eq. (5.68), are presented in Sect. 5.3.1 for linearization. Differentiating $\Phi(x(\tau_i(x))) = 0$, we have

$$\frac{\partial \tau_i(x_0(\theta_i))}{\partial x_{0j}} = -\frac{\langle \Phi_x(x_0(\theta_i)), \frac{\partial x_0(\theta_i)}{\partial x_{0j}} \rangle}{\langle \Phi_x(x_0(\theta_i)), f(\theta_i, x_0(\theta_i)) \rangle}, \ j = 1, \ldots, n. \tag{5.73}$$

The Jacobian $W_{ix}(x_0(\theta_i)) = [\frac{\partial W_i(x_0(\theta_i))}{\partial x_{01}}, \frac{\partial W_i(x_0(\theta_i))}{\partial x_{02}}, \ldots, \frac{\partial W_i(x_0(\theta_i))}{\partial x_{0n}}]$ is evaluated by

$$\begin{aligned}\frac{\partial W_i(x_0(\theta_i))}{\partial x_{0j}} &= (f(\theta_i, x_0(\theta_i)) - f(\theta_i, x_0(\theta_i) + I(x_0(\theta_i)))) \frac{\partial \tau_i}{\partial x_{0j}} \\ &+ \frac{\partial I}{\partial x_0} \left(e_j + f(\theta_i, x_0(\theta_i)) \frac{\partial \tau_i}{\partial x_{0j}} \right),\end{aligned} \tag{5.74}$$

where $e_j = (\underbrace{0, \ldots, 1}_{j}, \ldots, 0)$, $j = 1, 2, \ldots, n$. Next, by considering the second equation in (5.69) and using mean value theorem, one can obtain that

$\Delta(x(\theta_i) - x_0(\theta_i)) = W_i(x(\theta_i) - x_0(\theta_i)) = W_{ix}(x_0(\theta_i))(x(\theta_i) - x_0(\theta_i)) + O(\|x(\theta_i) - x_0(\theta_i)\|)$.

From the last expression, it is seen that the linearization at the transversal moment is determined with the matrix $B_i = W_{ix}(x_0(\theta_i))$.

5.3.2.2 Linearization at a Grazing Moment

Fix a discontinuity moment θ_i and assume that it is of grazing type. Considering Definition 7 with the formula (5.73), it is appearant that at least one coordinate of the gradient, $\nabla\tau(x)$, is infinity at the grazing point. This causes singularity in the system, which makes the analysis harder and the dynamics complex. Through the formula (5.73), one can see that the singularity is just caused by the position of the vector field with respect to the surface of discontinuity, and the impact does not participate in the appearance of the singularity. To get rid of the singularity, we will consider the following conditions.

(A1) The map $W_i(x)$ in (5.68) is differentiable if $x = x_0(\theta_i)$.

(A2) $\tau_i(x) < \theta_{i+1} - \theta_i - \varepsilon$ for some positive ε on a set of points near $x_0(\theta_i)$, which satisfy condition $(N1)$.

The appearance of singularity in (5.73) does not mean that the Jacobian $W_{ix}(x)$ is infinity. Because, in order to find the Jacobian, not only the surface of discontinuity and the vector field are required, but also the jump function is also needed. The regularity of the Jacobian can be arranged by means of the proper choice of the vector field, surface of discontinuity and jump function. In other words, if they are specially chosen, the map can be differentiable, and this validates condition (A1). Thus, in this chapter, we analyze the case, when the impact functions neutralize the singularity. Presumably, if there is no this type of suppressing, complex dynamics

near the grazing motions may appear [8, 18, 24, 25]. In the examples stated in the remaining part of the paper, one can see the verification of (A1), in details.

There are many ways are suggested to investigate the existence and stability of periodic solution of systems with graziness in literature [14, 26]. They investigate them by constructing special maps around the grazing point. In this chapter, we suggest to investigate the existence and stability by using the method of Floquet multipliers for dynamics with continuous time. It is a well-known method in literature [3, 29], but this is not widely applied to the analysis of the stability of grazing solutions because of the tangency of the grazing solution with the surface of discontinuity. This is the main novelty of our chapter.

By means of these discussions, one can conclude that the matrix B_i in (5.72) is the following

$$B_i = \begin{cases} O_n & \text{if} \quad (N1) \quad \text{is valid,} \\ W_{ix} & \text{if} \quad (N2) \quad \text{is valid,} \end{cases} \tag{5.75}$$

where O_n denotes the $n \times n$ zero matrix.

Denote by $\bar{x}(t)$, $j = 1, 2, \ldots, n$, a solution of (5.66) such that $\bar{x}(t_0) = x_0 + \Delta x$, $\Delta x = (\xi_1, \xi_2, \ldots, \xi_n)$, and let η_j be the moments of discontinuity of $\bar{x}(t)$. The solution $\bar{x}(t)$ has a linearization with respect to solution $x_0(t)$ if the condition (A) is valid. Moreover, if $x_0(\theta_i)$ is a grazing point, then the condition (C) is fulfilled and condition (B) is true if $x_0(\theta_i)$ is a transversal point.

The solution $x_0(t)$ is K-differentiable with respect to the initial value x_0 on $\mathscr{I}$, $t_0 \in \mathscr{I}$, if for each solution $\bar{x}(t)$ with sufficiently small Δx the linearization exists. The functions $u_i(t)$ and v_{ij} depend on Δx and uniformly bounded on a neighborhood of x_0.

Lemma 4 *Assume that the conditions (H1) and (A2) are valid. Then, the function $\tau_i(x)$ is continuous on the set of points near a grazing point which satisfy condition $(N1)$.*

Proof of the lemma can be done similarly with that of Lemma 1.

The systems (5.66) and (5.69) are B-equivalent, for this reason it is acceptable to linearize system (5.69) instead of system (5.66) around $x_0(t) = x(t, t_0, x_0)$, which is a solution of both systems. Thus, by applying linearization to (5.69), the system (5.72) is obtained. Additionally, the linearization matrix B_i in (5.72) for the grazing point also has to be defined by the formula (5.75), where W_{ix} exists by condition (A2).

On the basis of the discussion made in Sects. 5.3.2.1–5.3.2.2, one can conclude that the variational system for the solution $x_0(t)$ with the grazing points can be constructed as a system (5.72).

5.3.3 Stability of Grazing Periodic Solutions

In this part of the chapter, by means of the discussions made in the previous part of the chapter, we will investigate the stability of a periodic solution. Consider the system (5.66) again and the function $f(t,x):\mathbb{R}\times D\to\mathbb{R}^n$, where D is open connected subset of $\mathbb{R}^n$. Additionally assume that $f(t,x)$ is T-periodic in time, i.e., $f(t+T,x)=f(t,x)$, for $T>0$.

Let $\Psi(t):\mathbb{R}_+\to D$ be a periodic solution of (5.66) with period T and θ_i, $i\in\mathbb{Z}$, be the points of discontinuity which satisfy (T,p)-property, i.e., $\theta_{i+p}=\theta_i+T$, p is a natural number.

Fix a solution $x(t)=x(t,t_0,\Psi(t_0)+\Delta x)$ and assume that the linearization of that solution around $\Psi(t)$ exists, and there are l many transversal and k many grazing discontinuity moments of $\Psi(t)$ in $[t_0,t_0+T]$. It is easily seen that the matrix $A(t)$ in the variational system (5.72) for $\Psi(t)$ is T-periodic. However, in general, through the formula (5.75), the sequence B_i may not be periodic. For this reason, in what follows we assume the validity of the next condition.

(A3) For each $\Delta x\in\mathbb{R}^n$, the variational system for the near solution $x(t)=x(t,t_0,x_0+\Delta x)$ to $\Psi(t)$ is one of the following m periodic homogeneous linear impulsive systems

$$\begin{aligned} u' &= A(t)u,\\ \Delta u|_{t=\theta_i} &= B_i^{(j)}u, \end{aligned} \tag{5.76}$$

such that $B_{i+p}^{(j)}=B_i^{(j)}$, $i\in\mathbb{Z}$, $j=1,\dots,m$, where the number m cannot be larger than 2^k.

We will call the collection of m systems (5.76) *the variational system around the periodic grazing orbit*. This assumption is valid for many low-dimensional models and those which can be decomposed into two-dimensional subsystems.

So, the variational system (5.76) consists of m periodic subsystems. For each of these systems, we find the matrix of monodromy, $U_j(T)$ and denote corresponding Floquet multipliers by $\rho_i^{(j)}$, $i=1,\dots,n$, $j=1,\dots,m$. Next, we need the following assumption,

(A4) $|\rho_i^{(j)}|<1$, $i=1,\dots,n$, for each $j=1,\dots,m$.

Theorem 5 *Assume that the conditions (H1), (A1)–(A4) are valid. Then T-periodic solution $\Psi(t)$ of (5.66) is asymptotically stable.*

The proof of Theorem can be done in a similar way with that of presented in Sect. 7 as Theorem 7.1.1 in [3]. The next example is presented to authenticate the above theorem.

Example 5 In this example, we consider the following system of differential equation with variable moments of impulses

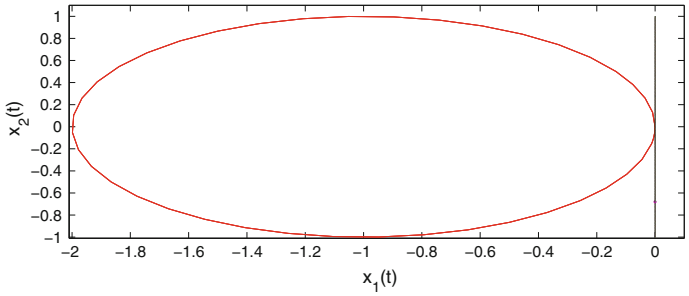

Fig. 5.9 The periodic solution $\Psi(t)$ of (5.78) and the *black vertical line* is the surface of discontinuity S

$$\begin{aligned} x'' + 0.002x' + x &= -1 - 0.002\sin(t), \\ \Delta x'|_{x\in S} &= -(1 + 0.9x')x', \end{aligned} \tag{5.77}$$

where $S = \{(x, x')|\Phi(x, x') = x = 0\}$. Let us rewrite the system (5.77) in the form

$$\begin{aligned} x_1' &= x_2, \\ x_2' &= -0.002x_2 - x_1 - 1 - 0.002\sin(t), \\ \Delta x_2|_{x\in S} &= -(1 + 0.9x_2)x_2, \end{aligned} \tag{5.78}$$

where $x = (x_1, x_2)$ and the discontinuity surface S can be written in the form $S = \{(x_1, x_2)|\Phi(x) = x_1 = 0\}$. It has a periodic solution $\Psi(t) = (-1 + \cos(t), -\sin(t))$. The orbit of which is pictured in Fig. 5.9

The system (5.78) has discontinuity surfaces $S = \{(x_1, x_2)|\ x_1 = 0,\ x_2 > 0\}$. Then, we have $\Phi(x) = x_1^2$. Consider the function $H(t, x)$ at the point $(\theta_i, \Psi(\theta_i)) = (2\pi i, \Psi(2\pi i))$, $i \in \mathbb{Z}$. It is true that $H(2\pi i, \Psi(2\pi i)) = 0$, $J(\Psi(2\pi i)) = 0$ and $H(t, x) \neq 0$ for some number $\delta > 0$, such that $|t - 2\pi i| < \delta$ and $\|x - \Psi(2\pi i)\| < \delta$. So, by means of Definitions 7 and 8, we can say that $(\theta_i, \Psi(\theta_i)) = (2\pi i, \Psi(2\pi i)) = (2\pi i, 0, 0)$ is a grazing point, and the periodic solution $\Psi(t)$ contains the grazing point $(2\pi i, 0, 0)$, then we can say that $\Psi(t)$ is a grazing periodic orbit. Additionally, all points $(2\pi i, \Psi(2\pi i))$, $i \in \mathbb{Z}$ are grazing points. This validates the condition $(H1)$.

In the remaining part, we will investigate the stability of the grazing orbit by the linearization of (5.78) around the solution. Because the point $(2\pi i, 0, 0)$ is a grazing point, we will consider the linearization by applying formulas (5.73) and (5.75). By means of condition (H1), it is true that the solutions intersects the surface of discontinuity transversely near the grazing one. For this reason, consider a point $\bar{x} = (0, \bar{x}_2)$ on the surface of discontinuity Γ near $x^* = (0, 0)$. Because of the transversality of $\bar{x}$, the first component $\frac{\partial\tau(\bar{x})}{\partial x_1}$ of the gradient $\nabla\tau(\bar{x})$ can be determined by formula (5.73), it is obtained as $\frac{\partial\tau(\bar{x})}{\partial x_1} = -\frac{1}{\bar{x}_2}$. At the grazing point, the first component can be evaluated as $\frac{\partial\tau(x^*)}{\partial x_1} = -\infty$.

First, we assume that $x(t) = x(t, 0, x^* + \Delta x)$, $\Delta x = (\Delta x_1, \Delta x_2)$ is not a grazing solution. That is, the point $x^* + \Delta x$ is not an orbit point of $\Psi(t)$. Hence, the meeting point $\bar{x} = (\bar{x}_1, \bar{x}_2) = (x_1(\xi, 0, (x^* + \Delta x)), x_2(\xi, 0, (x^* + \Delta x))$, is transversal one. Moreover, ξ is the meeting moment with Γ.

It is clear $\bar{x}_1 = 0$ and $\bar{x}_2 < 0$. In order to find a linearization at the moment $t = \theta_i$, we use formula (5.3) and find that

$$\frac{\partial W_i(x)}{\partial x_1^0} = \int_{\theta_i}^{\tau(x)} \frac{\partial f(s, x(s))}{\partial x} \frac{\partial x(s)}{\partial x_1^0} ds + f(s, x(s)) \frac{\partial \tau(x)}{\partial x_1^0} + J_x(x)(e_1 + f(s, x(s)) \times \frac{\partial \tau(x)}{\partial x_1^0}) + f(s, x(s) + J(x(s))) \frac{\partial \tau(x)}{\partial x_1^0} + \int_{\tau(x)}^{\theta_i} \frac{\partial f(s, x(s) + J(x(s)))}{\partial x} \frac{\partial x(s)}{\partial x_1^0} ds, \quad (5.79)$$

where $e_1 = (1, 0)^T$, T denotes the transpose of a matrix. Substituting $x = \bar{x}$ to the formula (5.79), we obtain that

$$\frac{\partial W_i(x(\xi, 0, x^* + \Delta x))}{\partial x_1^0} = f(\xi, x(\xi, 0, x^* + \Delta x)) \frac{\partial \tau(x(\xi, 0, x^* + \Delta x))}{\partial x_1^0} + J_x(x(\xi, 0, x^* + \Delta x)) \left(e_1 + f(\xi, x(\xi, 0, x^* + \Delta x))) \frac{\partial \tau(x(\xi, 0, x^* + \Delta x)))}{\partial x_1^0} \right) + f(\xi, x(\xi, 0, (J(x(\xi, 0, x^* + \Delta x))))) \frac{\partial \tau(J(x(\xi, 0, x^* + \Delta x)))}{\partial x_1^0}. \quad (5.80)$$

Considering the formula (5.73) for the transversal point $\bar{x} = (\bar{x}_1, \bar{x}_2)$, the first component $\frac{\partial \tau(\bar{x})}{\partial x_1^0}$ can be evaluated as $\frac{\partial \tau(\bar{x})}{\partial x_1^0} = -\frac{1}{\bar{x}_2}$. From the last equality, it is seen how the singularity appears at the grazing point. By taking into account (5.77) with (5.80), one can obtain that

$$\begin{aligned} \frac{\partial W_i(\bar{x})}{\partial x_1^0} &= \begin{bmatrix} \bar{x}_2 \\ -\bar{x}_1 - 0.002\bar{x}_2 - 1 - 0.002\sin(\xi) \end{bmatrix} \left(-\frac{1}{\bar{x}_2} \right) + \begin{bmatrix} 1 & 0 \\ 0 & -2R\bar{y}_2 \end{bmatrix} \\ &\times \left(e_1 + \begin{bmatrix} \bar{x}_2 \\ -\bar{x}_1 - 0.002\bar{x}_2 - 1 - 0.002\sin(\xi) \end{bmatrix} \left(-\frac{1}{\bar{x}_2} \right) \right) \\ &- \begin{bmatrix} -R(\bar{x}_2)^2 \\ -\bar{x}_1 + 0.002R(\bar{x}_2)^2 - 1 - 0.002\sin(\xi) \end{bmatrix} \left(-\frac{1}{\bar{x}_2} \right) \\ &= \begin{bmatrix} \bar{x}_2 - R(\bar{x}_2)^2 \\ -\bar{x}_1 - 0.002(\bar{x}_2 - R(\bar{x}_2)^2) \end{bmatrix} \left(-\frac{1}{\bar{x}_2} \right) \\ &+ \begin{bmatrix} 1 & 0 \\ 0 & -2R\bar{x}_2 \end{bmatrix} \begin{bmatrix} 1 + \frac{-\bar{x}_2}{\bar{x}_2} \frac{\bar{x}_1 + 0.1\bar{x}_2 - 1 - 0.002\sin(\xi)}{\bar{x}_2} \end{bmatrix}. \end{aligned} \quad (5.81)$$

Calculating the right-hand side of (5.81) we can obtain that

$$\frac{\partial W_i(\bar{x})}{\partial x_1^0} = \begin{bmatrix} R\bar{x}_2 - 1 \\ 0.1(1 - R\bar{x}_2) + 2R(0.1\bar{x}_2 - \bar{x}_1 - 1 - 0.002\sin(\xi)) \end{bmatrix}. \quad (5.82)$$

Similarly, differentiating (5.3) with $x(t)$ one can find that

$$\frac{\partial W_i(x)}{\partial x_2^0} = \int_{\theta_i}^{\tau(x)} \frac{\partial f(s,x)}{\partial x}\frac{\partial x(s)}{\partial x_2^0}ds + f(s,x(s))\frac{\partial \tau(x)}{\partial x_2^0} + J_x(x)(e_2 + f(s,x(s))\frac{\partial \tau(x)}{\partial x_2^0})$$

$$+f(s,x+J(x))\frac{\partial \tau(x)}{\partial x_2^0} + \int_{\tau(x)}^{\theta_i} \frac{\partial f(s,x(s)+J(x(s)))}{\partial x}\frac{\partial x(s)}{\partial x_2^0}ds, \quad (5.83)$$

where $e_2 = (0,1)^T$. Calculate the right-hand side of (5.83) at the point $\bar{x} = (\bar{x}_1, \bar{x}_2)$ to obtain

$$\frac{\partial W_i(x(\xi,0,x^* + \Delta x))}{\partial x_2^0} = f(\xi, x(\xi,0,y^* + \Delta x))\frac{\partial \tau(x(\xi,0,x^* + \Delta x))}{\partial x_2^0}$$

$$+J_x(x(\xi,0,x^* + \Delta x))\left(e_2 + f(\xi, x(\xi,0,x^* + \Delta x)))\frac{\partial \tau(x(\xi,0,x^* + \Delta x))}{\partial x_2^0}\right)$$

$$+f(\xi, x(\xi,0,x^* + \Delta x))\frac{\partial \tau(x(\xi,0,x^* + \Delta x))}{\partial x_2^0}. \quad (5.84)$$

To calculate the fraction $\frac{\partial \tau(x(\xi,0,x^* + \Delta x))}{\partial x_2^0}$ in (5.84), we apply formula (5.73) for the transversal point $\bar{x} = (\bar{x}_1, \bar{x}_2)$. The second component $\frac{\partial \tau(\bar{x})}{\partial x_2^0} = 0$. This and formula (5.84) imply

$$\frac{\partial W_i(\bar{x})}{\partial x_2^0} = \begin{bmatrix} 0 \\ -2R\bar{x}_2 \end{bmatrix}. \quad (5.85)$$

Joining (5.82) and (5.85), the matrix $W_{ix}(\bar{x})$ can be obtained as

$$W_{iy}(\bar{x}) = \begin{bmatrix} R\bar{x}_2 - 1 & 0 \\ 0.1(1 - R\bar{x}_2) + 2R(0.1\bar{x}_2 - \bar{x}_1 - 1 - 0.002\sin(\xi)) & -2R\bar{x}_2 \end{bmatrix}. \quad (5.86)$$

Taking into account formula (5.86), we can assert that the map $W_i(x)$ is differentiable at $x = x^*$. Thus, this verifies the condition (A1). Let consider a near solution to $(\theta_i, \Psi(\theta_i))$, there are two possibilities for the near solution it satisfies $(N1)$ an d $(N2)$. The meeting moment $\tau(x)$ cannot be taken into account whenever it satisfies $(N1)$. So, to validate the condition (A2), we should only consider those which satisfies $(N2)$. To verify it, let us take into account a solution of the first equation in (5.77) which starts at the point $\bar{x} = (0, \bar{x}_2) \in \mathscr{S}$. The solution of (5.77) at $\bar{x}$ is the form $x(t,0,\bar{x}) = \frac{\bar{x}_2}{\sqrt{1-(0.01)^2}}\exp(0.01t)\sin(\sqrt{1-(0.01)^2}t)$. This solution

meets the surface $\mathscr{S}$ at the moment $\bar{t} = \frac{2\pi}{\sqrt{1-(0.01)^2}}$, again. Thus, the meeting moment $\tau_i(x) = \bar{t} < 2\pi - \varepsilon$, where ε is a small positive number and this verifies (A2). Let us come back to the linearization part. The last expression (5.86) demonstrates that the Jacobian is continuous function of its arguments in a neighborhood of the grazing point. Indeed, it is defined and continuous for the points, which are not from the orbit of grazing solution. For the orbit points of the grazing solution, the Jacobian can be determined by the limit procedure. We apply it when $x \to x^*$, as well as $\xi \to 2\pi$, where 2π is the first grazing discontinuity point of periodic solution $\Psi(t)$, then we obtain that

$$W_{iy}(y^*) = \begin{bmatrix} -1 & 0 \\ 0.1 - 2R & 0 \end{bmatrix}. \tag{5.87}$$

Consequently, the function $W_i(x)$ is differentiable at the grazing point $x = x^*$ and (A1) is valid.

Utilizing (5.75) with above discussion, we obtain that

$$B_1 = \begin{cases} O_2, & \text{if (N1) } is\ valid, \\ \begin{bmatrix} -1 & 0 \\ 0.1 - 2R & 0 \end{bmatrix} & \text{if (N2) } is\ valid. \end{cases} \tag{5.88}$$

On the basis of the above discussion, we can assert that the variational system consists of $m = 2$ linear homogenous subsystems:

$$\begin{aligned} z' &= A(t)z, \\ \Delta z|_{t=\theta_i} &= B^{(1)}z, \end{aligned} \tag{5.89}$$

and

$$\begin{aligned} z' &= A(t)z, \\ \Delta z|_{t=\theta_i} &= B^{(2)}z, \end{aligned} \tag{5.90}$$

where $A(t) = \begin{bmatrix} 0 & 1 \\ -1 & -0.02 \end{bmatrix}$, $\theta_i = 2\pi i$, $B^{(1)} = O_2$ and $B^{(2)} = \begin{bmatrix} 0 & 0 \\ -0.6 & 0.4 \end{bmatrix}$. One can check easily that $A(t + 2\pi) = A(t)$, for all $t \in \mathbb{R}$, $B_i^{(1)} = B^{(1)}$, $B_i^{(2)} = B^{(2)}$, and $2\pi(i + 1) = 2\pi i + 2\pi$. Thus, $\{B_i^{(j)}\}$, $j = 1, 2$ are 1-periodic. Moreover, system (5.89) + (5.90) is a $(2\pi, 1)$-periodic system this validates (A3). The monodromy matrices for (5.89) and (5.90) have multipliers $\rho_1^{(1)} = 0.9844$, $\rho_2^{(1)} = 0.9844$, $\rho_1^{(2)} = 0.9844$, $\rho_2^{(2)} = 0.098$. Thus, the condition (A4) is valid. Consequently, the conditions (H1) and (A1)–(A4) are valid, by means of Theorem 5, it is easy to say that the periodic solution $\Psi(t)$ is asymptotically stable. In Fig. 5.10, the red curve corresponds to the periodic solution $\Psi(t)$, the blue line is the discontinuity surfaces S and $\tilde{S}$, and

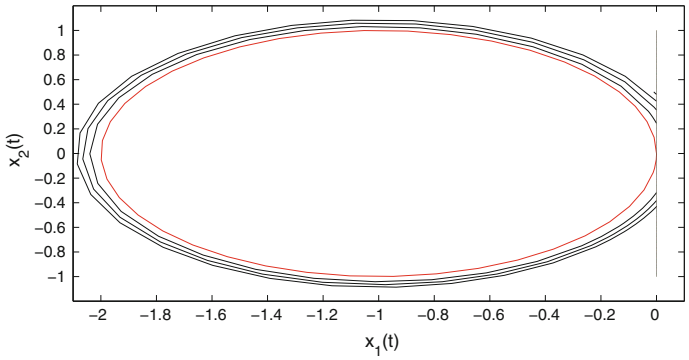

Fig. 5.10 The *red curve* is the periodic solution $\Psi(t)$ of (5.78), the *blue* ones are the phase portrait of the solution of (5.78) with initial value $x_0 = (-0.01, 0.5)$, and the *blue line* is the surface of discontinuity S

the black curves are the phase portrait of a solution of (5.78) with initial value $x_0 = (-0.01, 0.5)$. One can observe that the black curves approach the red one as time increases.

5.3.4 Regular Perturbations Around the Grazing Periodic Solution

In the previous part of the chapter, we analyze the existence and stability of periodic solutions of non-autonomous systems with a stationary impulse condition. In this part, we will investigate the bifurcation of grazing periodic solutions by applying regular perturbation to the system. Under certain conditions, the perturbation gives rise the existence of periodic solution in impulsive systems. Due to the complexity of the grazing behavior, there may be different type of bifurcation scenarios. In this part of the chapter, we will demonstrate the increment in the number of periodic solutions with the variation of the parameter μ.

To make our investigations, we take into account the following perturbed system:

$$\begin{aligned} x' &= f(t,x) + \mu g(x,\mu), \\ \Delta x|_{x\in S(\mu)} &= I(x) + \mu K(x,\mu), \end{aligned} \tag{5.91}$$

where $(t,x) \in \mathbb{R} \times G$, $\mu \in (-\mu_0, \mu_0)$, μ_0 is a fixed positive number. The system (5.91) is T-periodic system, i.e., $f(t+T,x) = f(t,x)$ and $g(t+T,x,\mu) = g(t,x,\mu)$ with some positive number T. Additionally, $f(t,x,\mu)$ is two times differentiable in x, continuous in time and first-order differentiable in μ. The function $K(x,\mu)$ is differentiable in x and μ, and $I(x)$ is differentiable in x. The surface of

discontinuity of (5.91), $S(\mu)$ is defined as $S(\mu) = \{x \in G| \ \ \Phi(x) + \mu\phi(x, \mu) = 0\}$, where $\Phi(x)$ second-order differentiable in x, and $\phi(x, \mu)$ is second- and first-order differentiable in x and μ, respectively.

The generating system of (5.91) is the system (5.66). In the previous section, we assumed that the generating system has a periodic solution $\Psi(t)$. All assumptions and conditions (H1), (A1)–(A4) are also valid in this section.

Let us seek the periodic solutions of (5.91) around the grazing one. Generally, the investigation on the periodic solutions of such systems is carried out by utilizing Poincare map which is based on the values of solutions at the period moment. For this reason, we will analyze the existence of the periodic solution of (5.91) in light of this map. But, it may not be differentiable near a grazing point [6, 19, 24]. To handle with this problem, we make use of the condition (A1). It can be understood from (5.76) that there exist m-many different partition around the grazing periodic solution. Fix some partition j, where $j \in 1, 2, \ldots, m$. Denote a solution of system (5.91) by

$$x_i^{(j)}(t, \gamma_1^{(j)}, \ldots, \gamma_n^{(j)}, \mu), \ i = 1, 2, \ldots, n, \tag{5.92}$$

with initial values

$$x_i^{(j)}(0, \gamma_1^{(j)}, \ldots, \gamma_n^{(j)}, \mu) = \gamma_i^{(j)}, \ i = 1, 2, \ldots, n. \tag{5.93}$$

Moreover, considering the periodic solution $\Psi(t) = (\Psi_1(t), \ldots, \Psi_n(t))$ of the generating system, it is easy to obtain that

$$x_i^{(j)}(t, \Psi_1(0), \ldots, \Psi_n(0), 0) \equiv \Psi_i(t), \ i = 1, 2, \ldots, n. \tag{5.94}$$

In order to verify the existence of such periodic solution of (5.91), it is necessary and sufficient to check the validity of the following equality

$$\mathscr{P}_i^{(j)}(\gamma_1^{(j)}, \ldots, \gamma_n^{(j)}) = x_i^{(j)}(T, \gamma_1^{(j)}, \ldots, \gamma_n^{(j)}, \mu) - \gamma_i^{(j)}, \ i = 1, 2, \ldots, n. \tag{5.95}$$

By means of the Eq. (5.92) conditions (5.93)–(5.95) are satisfied for $\mu = 0$, $\gamma_i = \Psi_i(0)$, since the generating solution is periodic.

The following conditions for the determinant will be needed for the rest of the chapter.

(A5)

$$\begin{vmatrix} \frac{\partial \mathscr{P}_1^{(j)}(\gamma_1, \ldots, \gamma_n)}{\partial \gamma_1} & \cdots & \frac{\partial \mathscr{P}_1^{(j)}(\gamma_1, \ldots, \gamma_n)}{\partial \gamma_n} \\ \vdots & \ddots & \vdots \\ \frac{\partial \mathscr{P}_n^{(j)}(\gamma_1, \ldots, \gamma_n)}{\partial \gamma_1} & \cdots & \frac{\partial \mathscr{P}_n^{(j)}(\gamma_1, \ldots, \gamma_n)}{\partial \gamma_n} \end{vmatrix} \neq 0. \tag{5.96}$$

Assume that the assumptions and conditions (H1) and (A1)–(A5) are valid. Then, (5.66) admits a non-trivial m T-periodic solution, which converges in the B-topology to the T-periodic solution of (5.91) as μ tends to zero.

Let us verify the above assertion. Without loss of generality, assume that the moments of discontinuity of the periodic solution $\Psi(t)$ admits that $0 < \theta_1 < \ldots < \theta_p < T$ Let $x^{(j)}(t) = x(t, 0, x^{(j)}, \mu)$ be a solution of the perturbed system (5.91) with initial values $x^{(j)}(0) = x^{(j)}$. Taking into account the conditions and assumptions (H1) and (A1)–(A4), it is easy to verify that the discontinuity moments of $x^{(j)}(t)$ satisfy that $0 < \eta_1 < \cdots < \eta_p < T$ and there exists a neighborhood $\Psi(0)$ which does not intersect . Applying the formulas (5.92)–(5.95), the following can be obtained

$$\mathscr{P}^{(j)}(y, \mu) = X(T, 0, y, \mu) - y = 0. \tag{5.97}$$

It is satisfied with $y = z^{(j)}$. Now, let us apply implicit function theorem to verify the existence of the periodic solutions of (5.91) with the help of (5.97) in the neighborhood of $(\Psi(0), 0)$. For $\mu = 0$, it is easy to obtain the following variational system

$$\begin{aligned} u' &= A(t)u, \\ \Delta u(\theta_i) &= B_i^{j)} u(\theta_i), \end{aligned} \tag{5.98}$$

where $i \in \mathbb{Z}$ and $j = 1, \ldots, m$. The K-derivatives of the solution $x^{(j)}(t)$ in $x^{(j)}$ form the fundamental matrix $Y^{(j)}(t, x^{(j)}(t), \mu)$, of the variational system (5.98) with $Y^{(j)}(0, x^{(j)}(t), \mu) = I$, where I is an identity matrix. The uniqueness of the periodic solution $\Psi(t)$ implies that

$$\mathscr{P}_y^{(j)}(y, \mu) = Z^{(j)}(T, 0, y, \mu) - I \neq 0. \tag{5.99}$$

Thus, the Eq. (5.97) has a unique solution in the neighborhood of $\Psi(0)$ for sufficiently small $|\mu|$. The suggested periodic solution takes the form $z^{(j)}(t) = z(t, 0, z^{(j)}(\mu), \mu)$, where $z^{(j)}(\mu)$ are the initial values of that solution which are obtained uniquely from the Eq. (5.97). This solution became closer to $\Psi(0)$ as μ tends to zero. Thus, we can conclude that the system (5.66) admits a non-trivial β-many T-periodic solution, which converge in the B-topology to the T-periodic solution of (5.91) as μ tends to zero.

Denote the number of periodic solution by β and it can be vary from 0 to m. The above part is verified only for a fixed j, but it can be done for all possible β-many periodic solutions. This assertion will be realized in the example thoroughly.

Our theoretical results will be exemplified in the following one.

Example 6 Consider the following perturbed system of differential equation with variable moments of impulses:

$$\begin{aligned} x'' + 0.002x' + x &= -(1 + \mu) - 0.002\sin(t), \\ \Delta x'|_{x \in S} &= -(1 + 0.9x')x', \end{aligned} \tag{5.100}$$

where $S = \{(x, x') | \Phi(x, x') = x = 0\}$. The surface of discontinuity is, $S = \{x| \quad x = 0\}$.

Defining the variables as $x_1 = x$, $x_2 = x'$, (5.100) can be rewritten as

$$\begin{aligned} x_1' &= x_2, \\ x_2' &= -0.002x_2 - x_1 - (1+\mu) - 0.002\sin(t), \\ \Delta x_2|_{x\in S} &= -(1+0.9x_2)x_2, \end{aligned} \tag{5.101}$$

where $x = (x_1, x_2)$ and the discontinuity surface S can be written in the form $S = \{(x_1, x_2)|\Phi(x) = x_1 = 0\}$. If $\mu \in (-2, 0]$, the system (5.100) admits periodic solution $\Psi_\mu(t) = (-1 - \mu + \cos(t), -\sin(t))$.

For $\mu = 0$, the system (5.100) is reduced to (5.78). In the remainder, we will seek the periodic solutions of (5.100) for sufficiently small μ.

Two sorts of periodic solutions of (5.100) exist around the grazing one. One of them has no impulse during the period since it does not cross the line of discontinuity. The other sort is the periodic solution which intersects the line $x_1 = 0$ and intersects the line $x_1 = 0$. We will show the existence of both type of periodic solutions if $|\mu|$ sufficiently small.

Let us start with the second type. Denote the initial values of the periodic solution by ζ_1 and ζ_2. By specifying the formula for the system (5.78), it is easy to obtain the following expressions

$$\begin{aligned} \mathscr{P}_1^{(1)}(T, \zeta_1, \zeta_2, \mu) &= x_1(T, \zeta_1, \zeta_2, \mu) - \zeta_1 = 0, \\ \mathscr{P}_2^{(1)}(T, \zeta_1, \zeta_2, \mu) &= x_2(T, \zeta_1, \zeta_2, \mu) - \zeta_2 = 0. \end{aligned} \tag{5.102}$$

Next, taking the derivative of the expressions in (5.102), we can obtain the following

$$\begin{vmatrix} \frac{\partial(\mathscr{P}_1^{(1)}(T,\zeta_1,\zeta_2,\mu)}{\partial\zeta_1} & \frac{\partial(\mathscr{P}_1^{(1)}(T,\zeta_1,\zeta_2,\mu)}{\partial\zeta_2} \\ \frac{\partial(\mathscr{P}_2^{(1)}(T,\zeta_1,\zeta_2,\mu)}{\partial\zeta_1} & \frac{\partial(\mathscr{P}_2^{(1)}(T,\zeta_1,\zeta_2,\mu)}{\partial\zeta_2} \end{vmatrix} = \begin{vmatrix} \frac{\partial x_1(T,\zeta_1,\zeta_2,\mu)}{\partial\zeta_1} & \frac{\partial x_1(T,\zeta_1,\zeta_2,\mu)}{\partial\zeta_2} \\ \frac{\partial x_2(T,\zeta_1,\zeta_2,\mu)}{\partial\zeta_1} & \frac{\partial x_2(T,\zeta_1,\zeta_2,\mu)}{\partial\zeta_2} \end{vmatrix}. \tag{5.103}$$

The determinant (5.103) is calculated by means of the monodromy matrix of (5.78), with the impulse matrix $D_1^{(1)} = O_2$, i.e.,

$$\begin{bmatrix} 1 & -0.0317 \\ 1.0158 & -0.1014 \end{bmatrix}. \tag{5.104}$$

Taking into account the system (5.107) with (5.104) at $\zeta_1 = \zeta_1^0 = 0$ and $\zeta_2 = \zeta_2^0 = 0$ and $\mathscr{T} = \omega$ for $\mu = 0$, one can derive that

$$\begin{vmatrix} \frac{\partial(\mathscr{P}_1^{(1)}(T,\zeta_1^0,\zeta_2^0,0)}{\partial\zeta_1} & \frac{\partial(\mathscr{P}_1^{(1)}(T,\zeta_1^0,\zeta_2^0,0)}{\partial\zeta_2} \\ \frac{\partial(\mathscr{P}_2^{(1)}(T,\zeta_1^0,\zeta_2^0,0)}{\partial\zeta_1} & \frac{\partial(\mathscr{P}_2^{(1)}(T,\zeta_1^0,\zeta_2^0,0)}{\partial\zeta_2} \end{vmatrix} = 0.76\exp(\frac{0.01\pi}{2\sqrt{3.99}}) \neq 0. \tag{5.105}$$

This verifies condition (A5). Thus, condition (A5) is valid, then by utilizing we can assert that the system (5.101) admits a non-trivial periodic solution, which converges in the B-topology to the non-trivial T-periodic solution of (5.78) as μ tends to zero.

Now, let us verify that system (5.78) has a circle which intersects the line $x_1 = 0$ in the neighborhood of $(0, 0)$. So, the periodic solution will attain a discontinuity moments in a period. Denote the initial values of the periodic solution by ζ_1 and ζ_2. In light of the expressions (5.95)

$$\begin{aligned}\mathscr{P}_1^{(2)}(T, \zeta_1, \zeta_2, \mu) &= x_1(T, \zeta_1, \zeta_2, \mu) - \zeta_1 = 0,\\ \mathscr{P}_2^{(2)}(T, \zeta_1, \zeta_2, \mu) &= x_2(T, \zeta_1, \zeta_2, \mu) - \zeta_2 = 0.\end{aligned} \tag{5.106}$$

Taking the derivative of the expressions (5.95) with respect to variables ζ_1 and ζ_2, one can obtain the following

$$\begin{vmatrix} \frac{\partial(\mathscr{P}_1^{(2)}(T, \zeta_1, \zeta_2, \mu)}{\partial \zeta_1} & \frac{\partial(\mathscr{P}_1^{(2)}(T, \zeta_1, \zeta_2, \mu)}{\partial \zeta_2} \\ \frac{\partial(\mathscr{P}_2^{(2)}(T, \zeta_1, \zeta_2, \mu)}{\partial \zeta_1} & \frac{\partial(\mathscr{P}_2^{(2)}(T, \zeta_1, \zeta_2, \mu)}{\partial \zeta_2} \end{vmatrix} = \begin{vmatrix} \frac{\partial x_1(T, \zeta_1, \zeta_2, \mu)}{\partial \zeta_1} & \frac{\partial x_1(T, \zeta_1, \zeta_2, \mu)}{\partial \zeta_2} \\ \frac{\partial x_2(T, \zeta_1, \zeta_2, \mu)}{\partial \zeta_1} & \frac{\partial x_2(T, \zeta_1, \zeta_2, \mu)}{\partial \zeta_2} \end{vmatrix}. \tag{5.107}$$

For $\mu = 0$, the determinant (5.107) can be determined as

$$\begin{vmatrix} \frac{\partial(\mathscr{P}_1^{(2)}(2\pi, 0, 0, 0)}{\partial \zeta_1} & \frac{\partial(\mathscr{P}_1^{(2)}(2\pi, 0, 0, 0)}{\partial \zeta_2} \\ \frac{\partial(\mathscr{P}_2^{(2)}(2\pi, 0, 0, 0)}{\partial \zeta_1} & \frac{\partial(\mathscr{P}_2^{(2)}(2\pi, 0, 0, 0)}{\partial \zeta_2} \end{vmatrix} = -0.02 \exp(0.001/\sqrt{3.99}) \neq 0. \tag{5.108}$$

This verifies condition (A5). So, we can conclude that the perturbed system (5.78) admits a non-trivial periodic solution which converges in the B-topology to the non-trivial T-periodic solution of (5.78) as μ tends to zero.

By taking into account the condition (A5), we can say that (5.100) admits a periodic solution. Consequently, we can say that system (5.78) admits two periodic solutions with the variation of μ around zero. It means that the number of periodic solution increases with the help of the small change in μ. We will call this bifurcation of the grazing periodic solution.

In general, the analysis of periodic solutions by using implicit function theorem is not applicable in systems which have graziness, because grazing point may violate the differentiability of the Poincare map. For this, in literature, many methods have been used such as Nordmark map [24–27] and zero-time discontinuity mapping (ZDM) [5]. By using special assumptions, we investigate the existence and stability of periodic solution of the perturbed system without disrupting the nature of the mechanisms with impacts.

5.4 Conclusion

The Poincare map is a significant method for the investigation of the existence and stability of periodic solutions of autonomous and non-autonomous systems. The stability of them is determined by considering the derivative of the Poincare map with respect to the initial data. However, in some systems, a periodic solution may meet the surface of discontinuity tangentially, this causes the singularity in the derivative of the Poincare map. For this reason, the Poincare method cannot be applied. For them, in literature different mapping approaches are presented such as zero-time discontinuity mapping [5] and Nordmark mapping [24–27]. As distinct from the mapping results, Ivanov [15, 16] analyzed the stability of the grazing periodic solution under a parameter variation in the vector field through the variational system approach. Our approach is different than those in many aspects. They are: We analyze the grazing periodic solutions of the system through the variational system which can be obtained by means of the position of with respect to the grazing periodic solution and through which we can consider such systems more deeply. We provide some examples with simulations to demonstrate the practicability of our theoretical results. In addition, this work can be applied the integrate and fire neuron models which intersects the threshold tangentially. For the first part of our study, we take into account the autonomous system and we propose the sufficient condition for it to be a discontinuous dynamical system. Orbital stability of periodic solution is analyzed, and the small parameter analysis is applied around this solution, and existence of grazing bifurcation is observed in a specific example. In the second half, we consider non-autonomous systems with stationary impulsive conditions. By applying regular perturbations to the autonomous and non-autonomous system, we investigate the existence of periodic solution of the perturbed system. We derive rigorous mathematical method for the analysis of discontinuous trajectories near grazing orbits. If there is no impacts in models, our results can be easily reduced to those for finite-dimensional continuous dynamics. That is why, this method is convenient to investigate infinite-dimensional problems and cycles of functional differential equations and bifurcation theory.

References

1. Akhmet M.U. : On the smoothness of solutions of impulsive autonomous systems. Nonlinear Anal.: TMA. **60**, 311–324 (2005)
2. Akhmet, M.U.: Perturbations and Hopf bifurcation of the planar discontinuous dynamical system. Nonlinear Anal. **60**, 163–178 (2005)
3. Akhmet, M.U.: Principles of Discontinuous Dynamical Systems. Springer, New York (2010)
4. Akhmet, M.U., Kıvılcım, A.: The models with impact deformations. Discontinuity Nonlinearity Complex. **4**, 49–78 (2015)
5. Budd, C.J.: Non-smooth dynamical systems and the grazing bifurcation. Nonlinear Mathematics and its Applications, pp. 219–235. Cambridge University Press, Cambridge (1996)

6. Chin, W., Ott, E., Nusse, E.H., Grebogi, C.: Grazing bifurcations in impact oscillators. Phys. Rev. E **50**, 4427–4444 (1994)
7. di Bernardo, M., Budd, C.J., Champneys, A.R.: Grazing, skipping and sliding: analysis of the nonsmooth dynamics of the DC/DC buck converter. Nonlinearity **11**, 858–890 (1998)
8. di Bernardo, M., Budd, C.J., Champneys, A.R.: Grazing bifurcations in n-dimensional piecewise-smooth dynamical systems. Physica D **160**, 222–254 (2001)
9. di Bernardo, M., Hogan, S.J.: Discontinuity-induced bifurcations of piecewise smooth dynamical systems. Philos. Trans. R. Soc. A **368**, 4915–4935 (2010)
10. Falcon, E., Laroche, C., Fauve, S., Coste, C.: Behavior of one inelastic ball bouncing repeatedly off the ground. Eur. Phys. J. B **3**, 45–57 (1998)
11. Farkas, M.: Periodic Motions. Springer, New York (1994)
12. Hartman, P.: Ordinary Differential Equations. SIAM, Philadelphia (2002)
13. Hirsch, M.W., Smale, S., Devaney, R.L.: Differential Equations, Dynamical Systems, and an Introduction to Chaos. Elsevier, USA (2004)
14. H*ö*s, C., Champneys, A.R.: Grazing bifurcations and chatter in a pressure relief valve model. Physica D **241**, 2068–2076 (2012)
15. Ivanov, A.P.: Impact oscillations: linear theory of stability and bifurcations. J. Sound Vib. **178**, 361–378 (1994)
16. Ivanov, A.P.: Bifurcations in impact systems. Chaos Solitons Fractals **7**, 1615–1634 (1996)
17. Luo, A.C.J.: A theory for non-smooth dynamical systems on connectable domains. Commun. Nonlinear Sci. Numer. Simul. **10**, 1–55 (2005)
18. Luo, A.C.J.: Singularity and Dynamics on Discontinuous Vectorfields. Elsevier, Amsterdam (2006)
19. Luo, G., Xie, J., Zhu, X., Zhang, J.: Periodic motions and bifurcations of a vibro-impact system. Chaos Solitons Fractals **36**, 1340–1347 (2008)
20. Luo, A.C.J.: Discontinuous Dynamical Systems on Time-varying Domains. Higher Education Press, Beijing (2009)
21. Luo, A.C.J., Gegg, B.C.: Grazing phenomena in a periodically forced, friction-induced, linear oscillator. Commun. Nonlinear Sci. Numer. Simul. **11**, 777–802 (2006)
22. Malkin, I.G.: Some Problems in the Theory of Nonlinear Oscillations. State Technical Publishing House, Moscow (1956)
23. Molenaar, J., de Weger, J.G., van de Water, W.: Mappings of grazing-impact oscillators. Nonlinearity **14**, 301–321 (2001)
24. Nordmark, A.B.: Non-periodic motion caused by grazing incidence in an impact oscillator. J. Sound Vib. **145**, 279–297 (1991)
25. Nordmark, A.B.: Universal limit mapping in grazing bifurcations. Phys. Rev. E **55**, 266–270 (1997)
26. Nordmark, A.B.: Existence of periodic orbits in grazing bifurcations of impacting mechanical oscillators. Nonlinearity **14**, 1517–1542 (2001)
27. Nordmark, A.B., Kowalczyk, P.A.: Codimension-two scenario of sliding solutions in grazing-sliding bifurcations. Nonlinearity **19**, 1–26 (2006)
28. Perko, L.: Differential Equations and Dynamical Systems. Springer, New York (2001)
29. Simeonov, P.S., Bainov, D.D.: Orbital stability of the periodic solutions of autonomous systems with impulse effect. Publ. RIMS, Kyoto Univ. **25**, 312–346 (1989)

Chapter 6
On Local Topological Classification of Two-Dimensional Orientable, Non-Orientable, and Half-Orientable Horseshoes

S.V. Gonchenko, A.S. Gonchenko and M.I. Malkin

Mathematical Subject Classification 37Dxx · 37D20

Smale horseshoes of new types, the so called half-orientable horseshoes, have been found in [1]. Such horseshoes can exist as invariant sets for endomorphisms of the disk and for diffeomorphisms of non-orientable two-dimensional manifolds as well. They have many features different from those of the classical orientable and non-orientable horseshoes. In particular, half-orientable horseshoes may have boundary points of arbitrary periods. It follows from this fact that there are infinitely many types of such horseshoes with respect to the local topological conjugacy. To prove this and similar results, an effective geometric construction is proposed.

6.1 Introduction

This chapter is devoted to dynamical and topological properties of Smale horseshoes of new types, the so-called *half-orientable horseshoes*, and also to comparison of these horseshoes with the classical Smale ones. For this, we use mainly the properties

S.V. Gonchenko (✉) · A.S. Gonchenko · M.I. Malkin
Lobachevsky State University of Nizhny Novgorod, Gagarin Avenue 23,
603000 Nizhny Novgorod, Russia
e-mail: sergey.gonchenko@mail.ru

A.S. Gonchenko
e-mail: agonchenko@mail.ru

M.I. Malkin
e-mail: malkin@unn.ru

D. Volchenkov and X. Leoncini (eds.), *Regularity and Stochasticity of Nonlinear Dynamical Systems*, Nonlinear Systems and Complexity 21,
DOI 10.1007/978-3-319-58062-3_6

of boundary points of hyperbolic basic sets. The boundary points of basic sets of two-dimensional diffeomorphisms have been introduced and applied in the papers by V. Afraimovich, V. Grines, R. Plykin, and A. Zhirov for classification and dynamical behavior problems of diffeomorphisms.

Half-orientable horseshoes have been discovered quite recently (Refs. [1, 2]) while studying the hyperbolic dynamics of *generalized Hénon maps* of the form

$$\bar{x} = y, \quad \bar{y} = \gamma y(1 - y) - bx + \alpha xy, \quad (x, y) \in \mathbb{R}^2, \tag{6.1}$$

with b and α small enough and γ large enough. We will use often the abbreviation GHM (Generalized Hénon Map) when we refer to the map (6.1). As shown in [1], for any fixed $\gamma > 4$ and sufficiently small α and b, GHM has the so called *geometric Smale horseshoe*. The latter means that there exists a square $Q_\beta = [-\beta, 1 + \beta] \times [-\beta, 1 + \beta]$ with $\beta = \beta(\alpha, b) \to +0$ as $(\alpha, b) \to 0$, which is mapped under (6.1) to a figure that resembles the horseshoe shape, but unlike the classical horseshoes, the horseshoes considered in [1] have a degenerate point ("the collapse point", compare Fig. 6.1 with Fig. 6.6). Such a geometry implies that on Q_β, there is an invariant set $\Lambda = \Lambda(\alpha, b)$ and that the map (6.1) has no non-wandering points outside Q_β.

It seems that people think of Smale horseshoes as of the simplest non-trivial (zero-dimensional) hyperbolic sets which are completely understood. In fact, all horseshoes

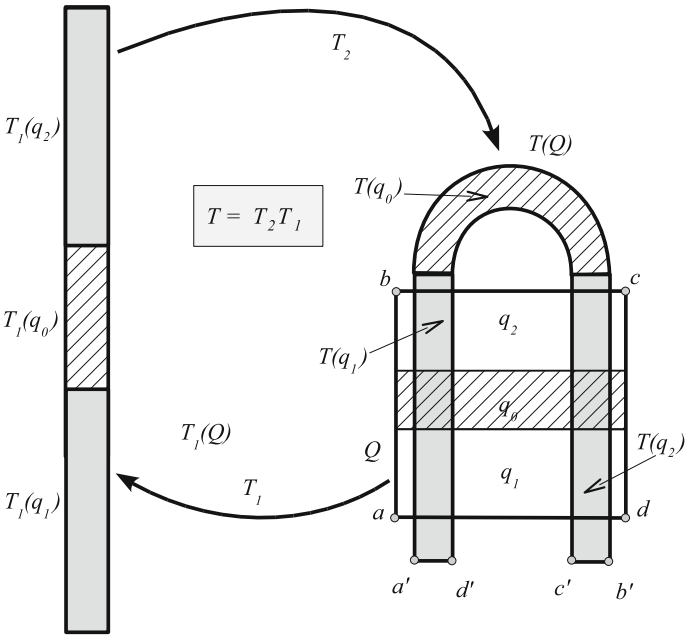

Fig. 6.1 Geometric construction of the linear Smale horseshoe *Source* (figures of this paper are borrowed from our paper [2])

are the same from the point of view of Ω-conjugacy, i.e., topological conjugacy on Λ, the set of non-wandering orbits. Remark that for any horseshoe (on two-dimensional manifold), the topological (and, in fact) the geometric structure of Λ is the direct product of two interval Cantor sets, while the restriction of the map on Λ is conjugate to the topological Bernoulli shift $\mathcal{B}_2$ with two symbols. However, if one is interested not only in trajectories from Λ, but also in trajectories from some neighborhood, i.e., if one studies horseshoes from the point of view of the *local topological conjugacy*, then the horseshoes can be distinguished. Even linear horseshoes (see Sect. 6.2 below) may differ, and, moreover, there are 10 different types of linear horseshoes (see Figs. 6.2, 6.3, and Proposition 6.1). Six of them (such as in Fig. 6.2) may occur for plane diffeomorphisms. Four types of linear horseshoes, which are represented in Fig. 6.3, may occur for diffeomorphisms on two-dimensional non-orientable manifolds or for two-dimensional endomorphisms (smooth non-invertible maps). In nonlinear case, there are much more types of different horseshoes but if one considers only the plane diffeomorphisms (more precisely, the diffeomorphisms of the disk), then the six types indicated in Fig. 6.2 represent all the possibilities.

On the other hand, if one considers endomorphisms instead of diffeomorphisms, or if one considers diffeomorphisms on non-orientable manifolds, then, as has been

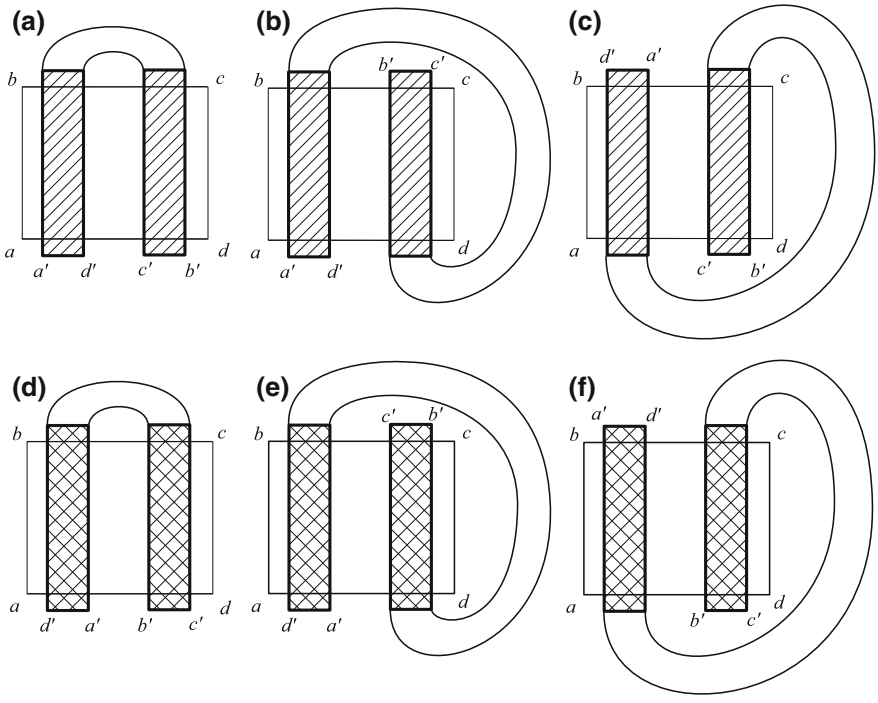

Fig. 6.2 Types of horseshoes for plane diffeomorphisms **a–c** in orientable case, **d–f** in non-orientable case

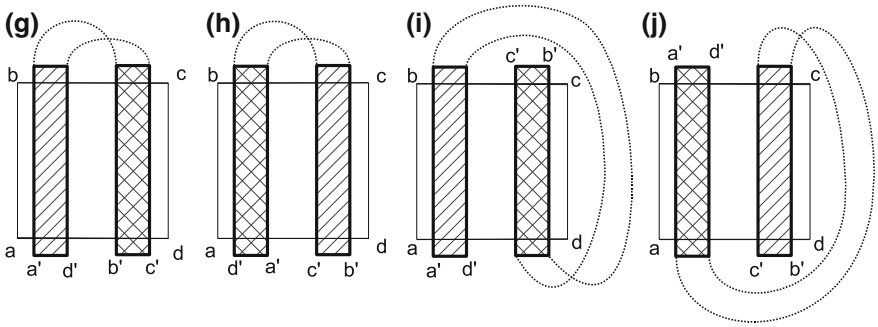

Fig. 6.3 Types of linear half-orientable horseshoes

shown in [1], there exist infinitely many types of horseshoes; more precisely, almost all of them (with the exception of two types: orientable and non-orientable ones) belong to the class of the so called *half-orientable horseshoes*.

Note that while studying the (non-trivial) hyperbolic basic sets of two-dimensional maps, one can get very important information from the structure of the set of *boundary points*, see Definition 6.2. It is known (see [3]) that in two-dimensional case, the boundary points are periodic, and their stable and/or unstable manifold form the natural invariant border of the hyperbolic set, so that from one side of this manifold, there are no points of this set, while from the other side of the manifold there are such points.

In the present chapter, we study the problem on topological classification of Smale horseshoes in terms of the boundary points. As mentioned above, linear horseshoes will be represented by 10 different types (their boundary points are described in Proposition 6.1), and, in contrast, for half-orientable hyperbolic horseshoes, the classification provides countably many types.

Unlike the well-known *orientable* and *non-orientable* Smale horseshoes (see Fig. 6.2), half-orientable horseshoes are not so popular (some examples of linear half-orientable horseshoes are shown in Fig. 6.3, and of nonlinear ones in Figs. 6.6 and 6.11). It seems that their study begins from [1], in which paper such horseshoes were discovered for GHM.

The structure of the chapter is as follows. In Sect. 6.1, we consider mainly linear Smale horseshoes and classify them in terms of the type of their boundary periodic points (see Statement 1). Main attention in Sect. 6.2 is paid to the problems of hyperbolic of GHM (6.1). We show that dynamical behavior of GHM is related to existence of both the usual orientable/non-orientable horseshoes and also of half-orientable ones. The regions where such horseshoes exist are described in Theorem 6.1 (we cite the result from [1]), and in Lemma 6.1. Then in Sect. 6.2, we prove Theorem 6.2 on existence of countably many different types (with respect to the local topological conjugacy) of half-orientable horseshoes. This fact is known from [1], but we give here totally different proof, which is geometric and constructive. By using similar

geometric construction, we prove Theorem 6.3 on existence of boundary points of arbitrary (given) period. Since the proof of Theorem 6.3 is constructive, it is actually a realization theorem.

6.2 Linear Smale Horseshoes and Their Boundary Points

From the geometrical point of view, the construction of the horseshoe map T can be easily described; see Fig. 6.1 for the linear horseshoe construction. Indeed, the map T here is constructed as the composition of two maps T_1 T_2, i.e., $T = T_2 T_1$. First, the square Q is mapped under T_1 (which can be linear) into the long narrow rectangle $T_1(Q)$, so that T_1 contracts Q in the horizontal direction and expands it in the vertical one. Then under the map T_2 (which always is essentially nonlinear), the rectangle $T_1(Q)$ is bent into the horseshoe shape and laid onto the square Q, with the horseshoe vertexes being outside Q. The geometric properties of the horseshoe are as follows (see Fig. 6.1)

(i) $T(Q) \cap Q$ consists of two components: $T(q_1) \cap Q$ and $T(q_2) \cap Q$;
(ii) $T(q_0) \cap Q = \emptyset$;
(iii) the segments $[a', d'] = T([a, d])$ and $[b', c'] = T([b, c])$ are outside Q.

The conditions above are sufficient for the horseshoe to exist in the case when the maps T_1 and $T_2\big|_{T_1(q_i)}$, $i = 1, 2$ are linear, and in this case we have the *linear horseshoe*. However, in the general situation, one needs not only conditions (i), (ii), and (iii) but also some contraction and expansion estimates in order to provide hyperbolicity of the invariant set

$$\Lambda = \bigcap_{n=-\infty}^{+\infty} T^n(Q) \tag{6.2}$$

Actually, the set Λ itself is called by many authors the *Smale horseshoe*, for example, it is defined in this way in [4]. This set is a locally maximal (on Q), uniformly hyperbolic, invariant set, and besides, it is zero-dimensional and homeomorphic to the direct product of two Cantor interval sets. Moreover, for any horseshoe, the corresponding dynamical system restricted on it, i.e., $T\big|_{\Lambda}$, is conjugate to the topological Bernoulli shift $\mathcal{B}_2$ with two symbols. The latter fact along with hyperbolicity of Λ is considered often as the definition of the horseshoe. This is why one may say that all the horseshoes are the same with respect to such equivalence relation as Ω-conjugacy, i.e., conjugacy on the non-wandering set.

However, if one considers stronger equivalence relations, then it is possible to distinguish Smale horseshoes. There is well-known equivalence relation in the theory of dynamical systems which is called *local topological equivalence*.

Definition 6.1 Let T and T' be two maps that have closed invariant sets Λ and Λ', respectively. One says that T and T' are locally topologically equivalent on

Λ and Λ' if for any their neighborhoods $V = V(\Lambda)$ and $V' = V'(\Lambda')$ there exist smaller neighborhoods $U \subset V$, $U' \subset V'$, and a homeomorphism $\tilde{h} : U \to U'$ such that $\tilde{h}(\Lambda) = \Lambda'$ with commutative diagram

$$\begin{array}{ccc} U(\Lambda) & \xrightarrow{T} & U(\Lambda) \\ \downarrow \tilde{h} & & \downarrow \tilde{h} \\ U'(\Lambda') & \xrightarrow{T'} & U'(\Lambda') \end{array} \tag{6.3}$$

Local topological equivalence is also called *local topological conjugacy*. Thus, the homeomorphism $\tilde{h}$ provides not only correspondence between trajectories of the systems (restrictions) $T\big|_{\Lambda}$ and $T'\big|_{\Lambda'}$ but also between trajectories from some their neighborhoods (more precisely, between (possibly finite) parts of trajectories which belong to these neighborhoods).

Evidently, local topological conjugacy implies Ω-conjugacy, but the inverse statement is not true in general, even for the Smale horseshoes (which can be thought of as the simplest hyperbolic sets). Moreover, there are different types of linear horseshoes with respect to local topological equivalence.[1] Let us remind that for a linear horseshoe, the map T_1 is (by its definition) a saddle linear map of the form (for appropriate coordinates) $\bar{x} = \lambda x + \alpha_1$, $\bar{y} = \gamma y + \alpha_2$ with $|\lambda| < 1/2$, $|\gamma| > 2$, while the vector (α_1, α_2) provides some translation. The map T_2 is always nonlinear; however, for a linear horseshoe, it is nonlinear only on the middle part $T_1(q_0)$ of the rectangle $T_1(Q)$, and it is linear on two other parts, i.e., on rectangles $T_1(q_1)$ and $T_1(q_2)$, see Fig. 6.1. For a linear horseshoe, the conditions $|\lambda| < 1/2$ and $|\gamma| > 2$ guarantee that $T(Q)$ intersects Q correctly.

It is not hard to find certain invariants of local topological conjugacy. Such invariants are, in particular, the signs of multiplicators of horseshoe fixed points. Note that any horseshoe contains precisely two fixed points O_1 and O_2. Assume, without loss of generality, that $O_1 \in q_1$, $O_2 \in q_2$. Then, the point O_1 corresponds to the sequence $(\dots, 0, \dots, 0, \dots)$, and the point O_2 corresponds to the sequence $(\dots, 1, \dots, 1, \dots)$ in Bernoulli shift $\mathcal{B}_2$. By using this notation, we can easily represent 10 different types of linear horseshoes (with respect to local topological conjugacy).

Six types of them can appear for plane diffeomorphisms, see Fig. 6.2. Here three cases (a), (b), and (c) correspond to orientable horseshoes, i.e., when the map T is an orientable diffeomorphism, in which cases every fixed point has both multiplicators (eigenvalues) of the same sign. In the case (a), the point O_1 has positive multiplicators, while the point O_2 has negative ones. We denote this case as $\{O_1(+,+), O_2(-,-)\}$, where the first sign in brackets is the sign of the stable multiplicator (which is less than one in absolute value) and the second sign is the sign of unstable multiplicator

[1] To be precise, the linear property is not very important in the case when one has two horseshoes with the same geometry, in which case those two horseshoes are just topologically equivalent. The fact is that some types of geometry are impossible for linear horseshoes; for example, there are no linear horseshoes such as in Fig. 6.6a, c, d, f or in Fig. 6.11 below.

(bigger than one in absolute value). For these notations, the horseshoe in case (b) will be denoted as $\{O_1(+,+), O_2(+,+)\}$, and in case (c) as $\{O_1(-,-), O_2(-,-)\}$. The cases (d)–(f) in Fig. 6.2 correspond to non-orientable horseshoes of different types (here both fixed points have multiplicators of different signs), namely case (d) is denoted as $\{O_1(-,+), O_2(+,-)\}$; case (e) is denoted as $\{O_1(-,+), O_2(-,+)\}$; and case (f) as $\{O_1(+,-), O_2(+,-)\}$.

However, one may assume that the horseshoe map T is "half-orientable," i.e., it has different orientations on the components $T(q_i) \cap Q$, $i = 1, 2$ (this means that either the map $T : q_1 \to Q$ is orientable and the map $T : q_2 \to Q$ non-orientable or vice versa). In fact, this may happen even for linear horseshoes in the situations when T is a plane endomorphism (rather than diffeomorphism) or when T is a diffeomorphism on non-orientable two-dimensional manifold (one can imagine that the square Q lies in the Moebius band and the image $T(Q)$ passes round this band). It is not hard to see that in this situation, there are four essentially different combinations of signs for multiplicators of the points O_1 and O_2; these combinations correspond to four different types of half-orientable linear horseshoes, see Fig. 6.3. More precisely, the horseshoe (g) corresponds to the type $\{O_1(+,+), O_2(+,-)\}$; the horseshoe (h) to the type $\{O_1(-,+), O_2(-,-)\}$; the horseshoe (i) to the type $\{O_1(+,+), O_2(-,+)\}$; and, at last, the horseshoe (j) to the type $\{O_1(+,-), O_2(-,-)\}$. Hence, one has that in cases (g) and (i), the map T is orientable on q_1 and non-orientable on q_2; conversely, in cases (h) and (j), the map T is non-orientable on q_1 and orientable on q_2.

There are other invariants that can be used to classify horseshoes. We will use for this purpose the set of *boundary periodic points*. It is known (see [3]) that boundary points serve as invariants of topological conjugacy for transitive hyperbolic sets on two-dimensional manifolds (and the Smale horseshoes surely satisfy these conditions).[2]

We will use the following definition of boundary periodic points.

Definition 6.2 Let Λ be a closed invariant transitive hyperbolic set of two-dimensional map. A saddle periodic point $P \in \Lambda$ is called an s-boundary point, if segment $W^s_{loc}(P)$ of its stable manifold divides any sufficiently small neighborhood $V = V(P)$ of P into two open disks V_1 and V_2 (i.e., $V = V_1 \cup V_2 \cup (W^s_{loc} \cap V)$) with $V_1 \cap \Lambda = \emptyset$ and $V_2 \cap \Lambda \neq \emptyset$. Similarly, $P \in \Lambda$ is called a u-boundary point, if such division takes place for W^u_{loc}. If P is simultaneously s-boundary and u-boundary, we will call it an (s, u)-boundary point.

Classification of linear horseshoes (orientable, non-orientable, and half-orientable) in terms of their boundary periodic points has been done in [1, 2]. In some cases not only fixed points O_1 and O_2 are used as boundary points but also points P_1 and P_2

[2]Remark that the problem on classification of hyperbolic diffeomorphisms and hyperbolic sets on two-dimensional manifolds is one of the most important and well known in the hyperbolic theory. For this classification, the boundary points have been applied essentially as principal invariants in [3] (see also [5]). However, to our knowledge, this problem was not considered for horseshoes (perhaps, because of seemingly trivial setting from usual point of view, such a view is not correct as we will show).

of period-2 cycle, i.e., $T(P_1) = P_2, T(P_2) = P_1$ with $P_1 \neq P_2$. It is well known that for any horseshoe such a cycle exists and is unique.

The following statement from [1, 2] characterizes boundary periodic points for all 10 types of linear horseshoes.

Proposition 6.1 *For each of ten types of linear horseshoes (plotted and listed in Figs. 6.2 and 6.3), the set of boundary periodic points* Γ *can be classified as follows:*

(a) $\Gamma = \{O_1\}$, *where* O_1 *is an* (s, u)*-boundary point;*
(b) $\Gamma = \{O_1, O_2\}$, *where both points* O_1 *and* O_2 *are* (s, u)*-boundary;*
(c) $\Gamma = \{P_1, P_2\}$, *where* P_1 *and* P_2 *are* (s, u)*-boundary points which form 2-cycle;*
(d) $\Gamma = \{O_1, O_2\}$, *where* O_1 *is* s*-boundary and* O_2 *is* u*-boundary;*

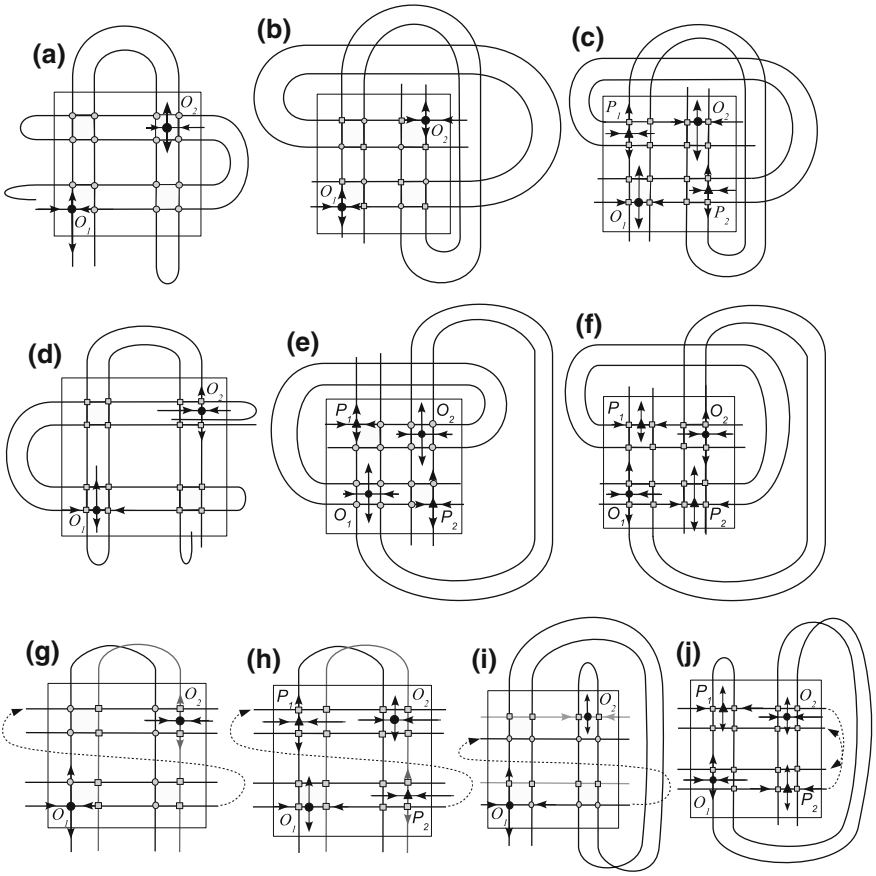

Fig. 6.4 Figure shows for each of the ten cases, the boundary periodic points along with the parts of their invariant manifolds. The *bold points* here are the fixed points O_1 and O_2, *light circles* denote homoclinic points, and *black small triangles* denote the points P_1 *и* P_2 of the 2-cycle

(e) $\Gamma = \{O_1, O_2, P_1, P_2\}$, *where* O_1 *and* O_2 *are s-boundary, while* P_1 *and* P_2 *are u-boundary points;*
(f) $\Gamma = \{O_1, O_2, P_1, P_2\}$, *where* O_1 *and* O_2 *are u-boundary, while* P_1 *and* P_2 *are s-boundary points;*
(g) $\Gamma = \{O_1, O_2\}$, *where* O_1 *is* (s, u)*-boundary, and* O_2 *is u-boundary;*
(h) $\Gamma = \{O_1, P_1, P_2\}$, *where* O_1 *is an s-boundary point, while* (P_1, P_2) *are u-boundary points which form 2-cycle;*
(i) $\Gamma = \{O_1, O_2\}$, *where* O_1 *is* (s, u)*-boundary, and* O_2 *is s-boundary;*
(j) $\Gamma = \{O_1, P_1, P_2\}$, *where* O_1 *is u-boundary and* P_1, P_2 *are s-boundary points.*

The above proposition is illustrated in Fig. 6.4 which shows for each of the 10 cases that boundary periodic points and their stable and unstable manifolds are responsible for creating the principal geometry of the horseshoe Λ.

6.3 Horseshoes in Generalized Hénon Maps and Their Topological Properties

Smale horseshoes as hyperbolic sets appear in any system which admits rough (transverse) homoclinic Poincaré trajectories. This fundamental result goes back to works by Smale [6] and Shilnikov [7]. In their papers, Smale and Shilnikov have described the set N of trajectories which lie entirely in a neighborhood of rough homoclinic orbit.[3] It was also shown in [7] that in dynamical systems under consideration, the Smale horseshoe may exist as a part (non-trivial invariant subset) of N. Note that Smale horseshoes (even infinitely many of them) may exist in dynamical systems with homoclinic loops to a fixed point of the saddle-focus type (see [8, 9]), in systems with homoclinic tangencies (see [10]), etc. Note also that horseshoes appear often via non-local bifurcations. In particular, there are bifurcations of this type that start from Morse-Smale systems and lead to systems with complicated dynamics. All these bifurcations can be united by the common term "homoclinic Ω-explosion." The characteristic property of these bifurcations is that they result in countably many horseshoes which appear immediately (by "explosion") at the moment when the system reaches the bifurcation border (see surveys [11, 12] and refereces therein concerning these bifurcations).

Among many specific models which contain Smale horseshoes, the original Hénon map seems to be the most popular. However, this map cannot have half-orientable horseshoes: Its horseshoes can be either orientable or non-orientable (depending on parameter b in its Eq. (6.4) below), see also Fig. 6.5. On the other hand, in [1] it has been shown that even small perturbation of the original Hénon map (so that the Jacobian of the map becomes non-constant) may create half-orientable horseshoes,

[3] Note that in [7] such a result was obtained without additional technical assumption on smooth reducibility to the linear form in a neighborhood of the saddle, while in [6] such reducibility was assumed. Of course, this improvement has expanded the scope of applications including important classes of dynamical systems (e.g., Hamiltonian, conservative, and invertible systems.).

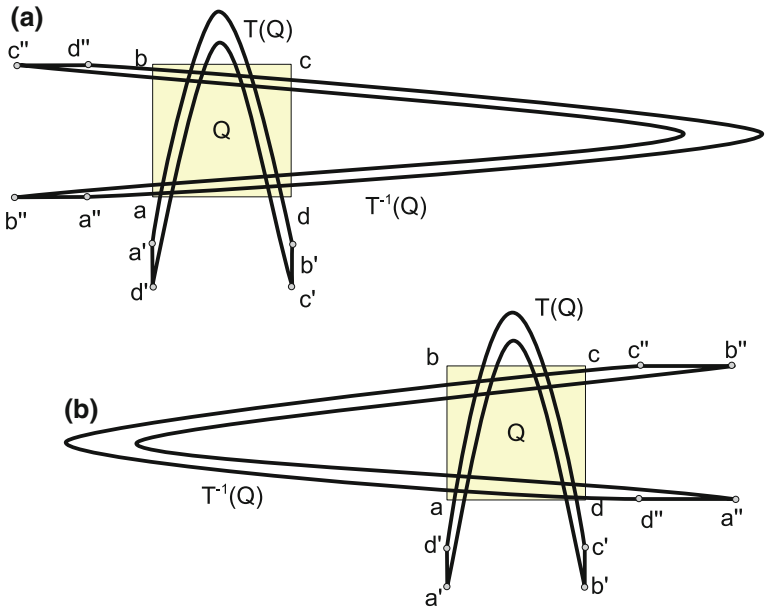

Fig. 6.5 Geometry of the original Hénon map (6.4) in the hyperbolicity region when M is big enough and b is small enough **a** orientable (for $b > 0$) and **b** non-orientable (for $b < 0$)

such as those from Sect. 6.1 and besides, many others as well. Moreover, with respect to the local topological equivalence, there are infinitely many types of half-orientable horseshoes. It is remarkable that any such horseshoe can be realized as a (half-orientable) horseshoe of a diffeomorphism on two-dimensional manifold (actually, non-orientable). We will observe these results below.

The original (classical) Hénon map is of the form

$$\bar{x} = y,\ \bar{y} = 1 - bx - ay^2,\quad (x, y) \in \mathbb{R}^2,$$

where a and b are parameters (b being the Jacobian determinant). The equation above can be given (if $a \neq 0$) in the equivalent form

$$\bar{x} = y,\ \bar{y} = M - bx - y^2, \tag{6.4}$$

(where $M = -a$) which is usually called the standard form of the Hénon map. Note that in homoclinic dynamics, the Hénon map usually appears in the standard form (6.4) (see [10, 13, 14]).

It is well known that for M big enough, e.g. for

$$M > 1/4(5 + 2\sqrt{5})(1 + |b|)^2,\quad b \neq 0 \tag{6.5}$$

the Hénon map (6.4) has hyperbolic dynamics which can be described precisely as the Smale horseshoe (orientable for $b > 0$ and non-orientable for $b < 0$), see [15–18]) and Fig. 6.5.

If the Hénon map (6.4) has two fixed points, i.e., if $M > -\dfrac{(b+1)^2}{4}$, its equation can be rewritten also in the following form (sometimes called the parabolic form)

$$\bar{x} = y, \quad \bar{y} = \gamma y(1-y) - bx, \tag{6.6}$$

where $\gamma = b + 1 + \sqrt{(b+1)^2 + 4M}$. This form of the Hénon map is convenient for further investigations because after rescaling above the whole non-wandering set of (6.6) is contained in the square $Q_\beta = [-\beta, 1+\beta] \times [-\beta, 1+\beta]$, where β is independent of γ, and β tends to 0 as $b \to 0$ (see [19]). Here the hyperbolicity condition (6.5) will be rewritten as $\gamma > (|b| + 1)(2 + \sqrt{5})$.

For $b = 0$ the Hénon map (6.6) degenerates to the following form

$$\bar{x} = y, \quad \bar{y} = \gamma y(1-y), \tag{6.7}$$

whose dynamics is one-dimensional: Any point from $\mathbb{R}^2$ after one iteration lies on the invariant curve (invariant parabola) $y = \gamma x(1-x)$ and then its movement is governed by the parabola map $\bar{y} = \gamma y(1-y)$. It is well known that the non-wandering set $\tilde{\Lambda}(\gamma)$ of this map is contained in the interval $[0, 1]$. If $\gamma > 4$, then $\tilde{\Lambda}(\gamma)$ is a Cantor set and the restriction of the map on $\tilde{\Lambda}(\gamma)$ is conjugate to one-sided Bernoulli shift $\mathcal{B}_{2+}$ with two symbols. One may say that hyperbolicity here takes place merely in one-dimensional setting (due to definitions from one-dimensional dynamics). Note that in general, by embedding of one-dimensional map (like (6.7)) into a family of two-dimensional maps, the hyperbolicity could be lost. Fortunately, in the case of the family (6.6) of Hénon maps, the hyperbolic set $\tilde{\Lambda}(\gamma)$ (which is one-dimensional at $b = 0$) transforms for $b \neq 0$ into a genuine hyperbolic set, the Smale horseshoe, which is orientable for $b > 0$ and non-orientable for $b < 0$ (see Fig. 6.5).

The hyperbolic dynamics of generalized Hénon maps (6.1) have been studied in [1]. Note that the form (6.1) for GHM (as well as its analogs) was introduced in [20, 21] as the normal form for the Poincaré map near homoclinic tangency. Unlike the original (standard) Hénon map, GHM (6.1) undergoes non-degenerate bifurcations of periodic trajectories with multiplicators $e^{\pm i\varphi}$, and thus it may help in studying corresponding bifurcations in numerous classes of dynamical systems with non-rough homoclinic and heteroclinic trajectories.

From now on, we will denote the map (6.1) by T, assuming that b and α are small enough, while γ is big enough (actually, we assume that $\gamma > 4$). It is worth noting that the generalized Hénon map (6.1) is not a diffeomorphism on $\mathbb{R}^2$. Its Jacobian determinant $J(T)$ is equal to $J = b - \alpha y$, and, hence, it vanishes on the line $y = b/\alpha$. It is easy to see that the image of this line under T is just one singular point

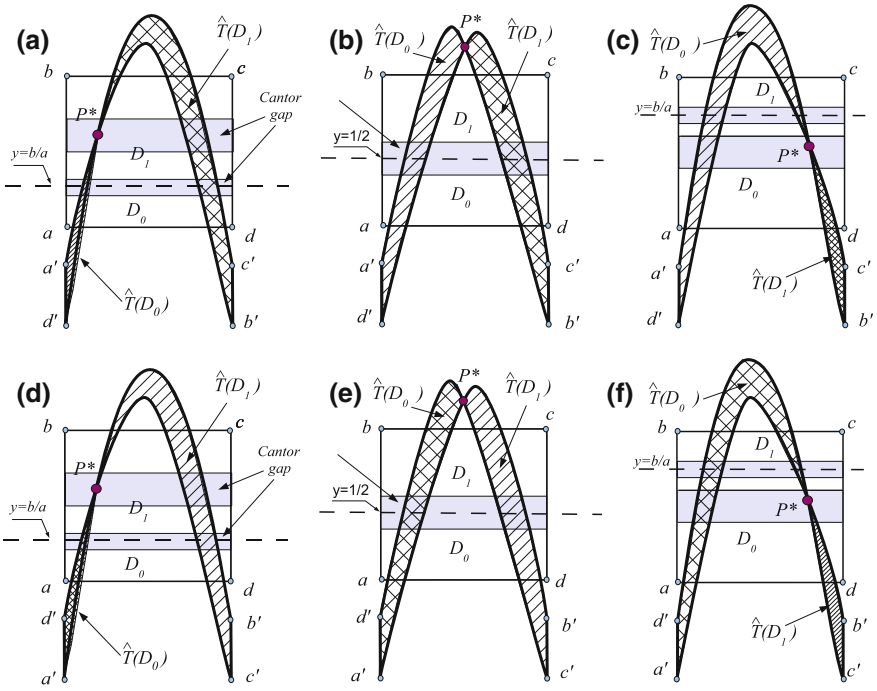

Fig. 6.6 **a**–**c** left-orientable horseshoes; **d**–**f** right-orientable horseshoes. D_0 and D_1 are the regions on Q which lie, respectively, below and above the line $y = b/\alpha$ (on this line, the Jacobian determinant of T vanishes)

$$P^* = \left(\frac{b}{\alpha}, \frac{\gamma b}{\alpha}(1 - \frac{b}{\alpha}\right),$$

We will call this point the *collapse point*.[4] The presence of this singularity is a crucial factor in dynamical properties of the map (6.1) in a whole. The influence of the collapse point manifests itself even in the case when one has hyperbolic dynamics, in which case one may have usually a singular hyperbolicity. However, if the line $y = b/\alpha$ does not intersect Q_β, the hyperbolic dynamics is proper, and one has either orientable (for $b > 0$), or non-orientable (for $b < 0$) horseshoe. Otherwise (when the line $y = b/\alpha$ does intersect Q_β) there appears a new hyperbolic dynamics related to existence of half-orientable horseshoes. Some examples of them see in Figure 6.6.

The following result from [1] describes the parameter regions for which GHM (6.1) has horseshoes of different types.

Theorem 6.1 *Let $\gamma > 4$ be fixed. Then in any small neighborhood V of the origin in the plane (α, b), there is a cone-like region $\hat{D}$ (adjoint to the point $(0, 0)$)*

[4] In the theory of non-invertible smooth maps there is another term for such a point, namely, the "knot point" [22].

$$0 < \frac{b}{\alpha} < 1 + \rho(\alpha, b), \tag{6.8}$$

with $\rho(\alpha, b) \to 0$ *as* $\alpha, b \to 0$ *and such that*

(1) if $(\alpha, b) \in V \setminus \hat{D}$ *then the non-wandering set* $\Lambda(T)$ *is the Smale horseshoe, which is either orientable (for* $b > 0$*) or non-orientable (for* $b < 0$*);*
(2) the region $\hat{D}$ *contains infinitely many open cone-like domains adjoint to the point* $(0, 0)$*, and for any parameters from these domains,* $\Lambda(T)$ *is a half-orientable horseshoe;*
(3) the border $b = 0$ *of the region* $\hat{D}$ *is responsible for the first bifurcation at which moment the point* P^* *coincides with the fixed point* O_1 *(and* O_1 *has got zero multiplicator at this moment));*
(4) the border $b = \alpha(1 + \rho(\alpha, b))$ *is responsible for the last bifurcation, at which moment the point* P^* *becomes (at the last time) homoclinic to* O_1*.*

Figure 6.7 illustrates the above theorem. Here the important bifurcation moments have been indicated: for first bifurcation at $b = 0$ see Fig. 6.7, items (d) and (h), and for the last bifurcation at $b/\alpha = 1 + \rho(\alpha, b)$ see Fig. 6.7, items (b) and (f).

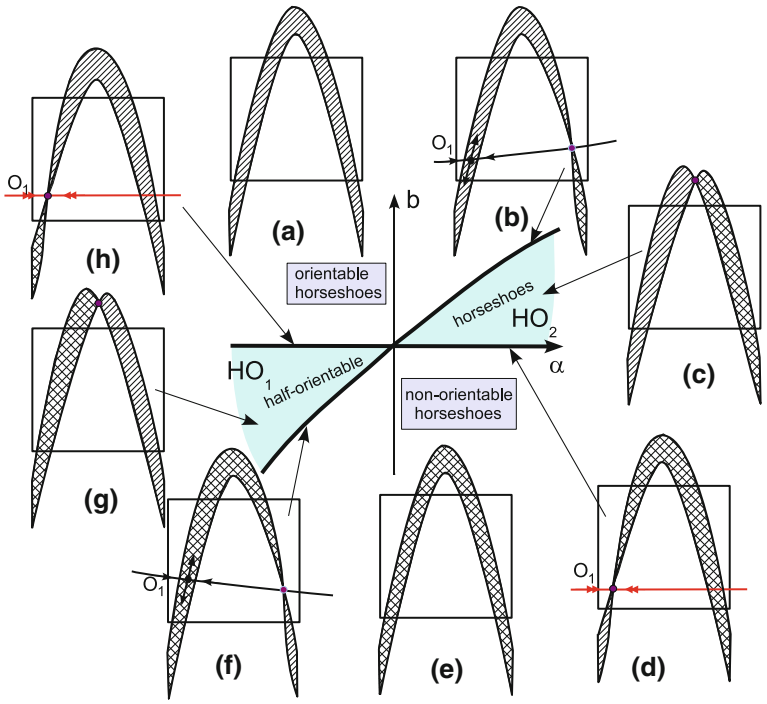

Fig. 6.7 An illustration to Theorem 6.1: the partition of a neighborhood of the origin of (α, b)-plane (for fixed $\gamma > 4$) is shown. The cone-like region adjoint to the point (0, 0) corresponds to the existence of half-orientable horseshoes in Q; other two regions correspond to existence of orientable and non-orientable Smale horseshoes

The following result represents an improved version of statement 2 of Theorem 6.1.

Lemma 6.1 *The region $\hat{D}$ contains countably many open cone-like domains g_i, $i = 1, ..., \infty$, whose borders correspond to the situations when $P^* \in W^s(O_1)$. If $(\alpha, b) \in \mathcal{G} = \bigcup g_i$, then the non-wandering set $\Lambda(T)$ is a half-orientable hyperbolic horseshoe. The closed set $\mathcal{K} = \hat{D} \setminus \mathcal{G}$ is a one-dimensional cone over Cantor set, and if one has in addition that $(\alpha, b) \in \mathcal{K}$, then $\Lambda(T)$ is a singular horseshoe.*

Proof First we show that the point O_1 is always s-boundary for the non-wandering set $\Lambda(T)$. Indeed, let l_s be that curve (connected component) of the set $W^s(O_1) \cap Q$ which contains the point O_1. Then by using the properties of horseshoe geometry for GHM, we have that all the points on Q below the curve l_s are wandering. That is why the process of constructing the horseshoe involves construction which indicates the gaps, i.e., open horizontal domains on Q which do not contain non-wandering points. In our case, the set of invariant borders of such gaps is the countable set $W^s(O_1) \cap Q$ of horizontal curves (segments) on Q. These gaps can be enumerated in accordance with the following standard algorithm.

Let $\hat{G} \subset T(Q) \cap Q$ be the upper part of $T(Q)$, i.e., the part of the horseshoe that lies above the square Q, see Fig. 6.8a. Let $G \subset Q$ be the band on the square Q, which is mapped into $\hat{G}$, i.e., $T(G) = \hat{G}$. In its turn, the set G has two preimages G_0 and G_1 such that $T(G_i) = G, i = 0, 1$, where G_0 lies above G while G_1 lies below it, see Fig. 6.8a.

Next, we define the bands G_{00}, G_{01} such that $T(G_{0i}) = G_0$, $i = 0, 1$, and the bands G_{10}, G_{11} such that $T(G_{1i}) = G_1, i = 0, 1$. As before, we assume that G_{j0} lies

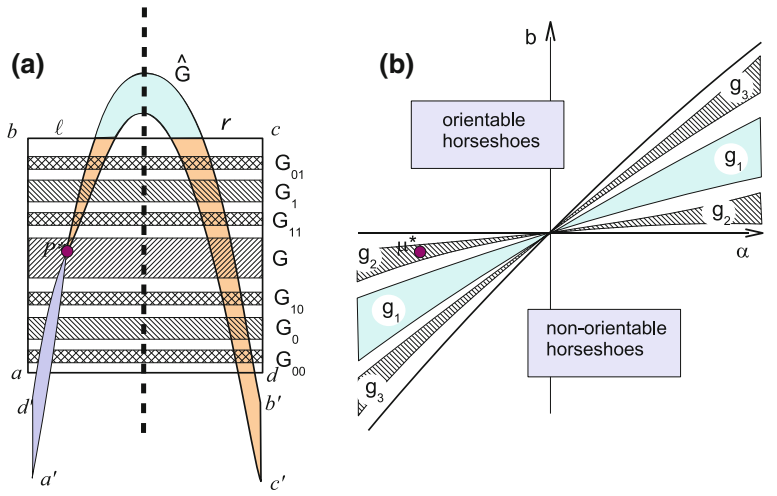

Fig. 6.8 An illustration to Lemma 6.1. The cone-like region contains infinitely many "cones" g_i such that if $(\alpha, \beta) \in g_i$, then the collapse point P^* is wandering (it belongs to some gap $G_\beta \subset Q$ that leave Q under iterations of T). Then, if $(\alpha, \beta) \in g_i$ the map T has a half-orientable hyperbolic horseshoe

below G_{j1}, see Fig. 6.8a. With proceeding by induction, we will get countable set of bands $G_{\beta 0}$, $G_{\beta 1}$, and corresponding set of indexes $\beta = [\beta_1, ..., \beta_n]$, $n = 1, 2...$, with $\beta_i \in \{0, 1\}$, such that $T(G_{\beta 0}) = T(G_{\beta 1}) = G_\beta$ and $G_{\beta 0}$ lies below $G_{\beta 1}$. At last, we divide each of the bands G_β into two parts: G^l_β and G^r_β which lie in Q left and right from the line $x = 1/2$, respectively.

Definitely, we may assume that all the bands G_β have invariant borders (upper and lower ones) which correspond to appropriate parts of the stable manifold $W^s(O_1)$.

Now the correspondence between cone-like domains g_i from Theorem 6.1 and the domains $\hat{G}$, G, and $G^{l,r}_\beta$ can be easily established. Indeed, those parameters (α, b) for which $P^* \in \hat{G}$ correspond to domain g_1; parameters for which $P^* \in G^l$ and $P^* \in G^r$ correspond to domains g_2 and g_3; parameters for which $P^* \in G^l_0$ and $P^* \in G^r_0$ correspond to domains g_4 and g_5; parameters for which $P^* \in G^l_1$ and $P^* \in G^r_1$ correspond to domains g_6 and g_7, etc., see Fig. 6.8b. This completes the proof. □

Next by using the geometric construction from Lemma 6.1, we prove the following result which has been also established in [1] by another (non-constructive) method.

Theorem 6.2 *There exist countably many types of half-orientable horseshoes with respect to the local topological conjugacy.*

The proof easily comes after the following lemma.

Lemma 6.2 *Let T and T' be GHM maps with half-orientable horseshoes Λ and Λ', respectively, such that $P^* \in G_\beta$ and $P^{*\prime} \in G_{\beta'}$. The restrictions $T|\Lambda$ $T'|\Lambda'$ are not locally topologically conjugate provided that one of the following conditions holds:*

(i) $\beta \neq \beta'$, or
(ii) $\beta = \beta'$, and $P^* \in G^l_\beta$, $P^{*\prime} \in G^r_\beta$ (or $P^* \in G^r_\beta$, $P^{*\prime} \in G^l_\beta$).

Proof Consider first the case when $\beta \neq \beta'$ and let $S_{\beta\beta'}$ be the band between G_β and $G_{\beta'}$, see Fig. 6.9a, b. Evidently, it contains periodic points because it follows from the

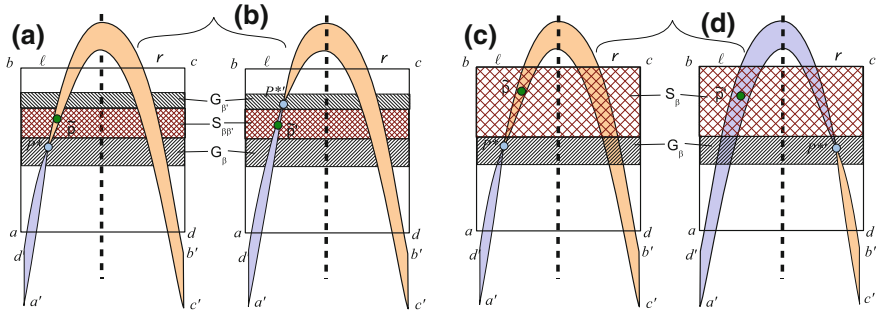

Fig. 6.9 An illustration to Lemma 6.2. **a** and **b** If the collapse points belong to different gaps G_β of Q, then the corresponding half-orientable horseshoes have periodic points $\tilde{p}$ and $\tilde{p}'$ with the same coding but with different type of orientability. **c** and **d** the same is true when the collapse points belong to G^l_β and G^r_β, respectively

horseshoe construction that any band is not contained completely in some domain G_β (conversely, such a band contains infinitely many smaller gaps). Also, due to the horseshoe properties, among these periodic trajectories, there is a trajectory whose point (or, more precisely, odd number of points) belongs to $S_{\beta\beta'}$. Denote this point $\tilde{p}$ for the map T and let $\tilde{p}'$ be the corresponding point for the map T' (here corresponding means that periodic trajectories $O(\tilde{p})$ and $O(\tilde{p}')$ have the same coding. However, it is evident that the trajectories $O(\tilde{p})$ and $O(\tilde{p}')$ have different type of orientation. Since the codes are invariants of topological conjugacy, it follows that $T|\Lambda$ and $T'|\Lambda'$ cannot be conjugate.

Now let $\beta = \beta'$ and let P^* and $P^{*\prime}$ belong to G^l_β and G^r_β, respectively (or $P^* \in G^r_\beta$, $P^{*\prime} \in G^l_\beta$). Then, we can adjust the above proof if we consider in the capacity of $S_{\beta\beta'}$ the band S_β that lies in Q over G_β, see Figure 6.9c, d. After this, the proof becomes similar to that in the previous case. □

Let us revisit the Theorem 6.1 and Fig. 6.7, where the cone-like regions HO_1 and HO_2 are indicated. We will call the half-orientable horseshoes, corresponding to the region HO_1 of parameters (α, b), the *right-orientable horseshoes*, and those corresponding to the region HO_2, the *left-orientable horseshoes* (see also Fig. 6.6). Obviously left- and right-orientable horseshoes cannot be locally conjugate to each other while two horseshoes of the same type (i.e., left- or right-orientable both) can be locally conjugate. Let HG^* be the set consisting of countably many disjoint open domains $\hat{G}, G^l, G^r$ along with domains G^l_β and G^r_β for arbitrary finite symbolic segments β compiled by two symbols ("0" and "1"). Then, by using the proof of Lemma 6.2 we get the following result.

Theorem 6.3 *Two half-orientable hyperbolic horseshoes Λ and Λ' of the same type (left- or right-orientable both) are locally topologically conjugate if and only if the collapse points P^* and $P^{*\prime}$ belong to the same connected component of the set HG^*.*

Now it is evident that if we know the position of the collapse point P^*, then we have the whole information about topological properties of the corresponding half-orientable horseshoe Λ. Though it is not always a simple problem to determine the position of the collapse points in the domains under consideration, nevertheless we can describe one result of this kind which illustrates the non-trivial dynamics (even for hyperbolic horseshoes).

Theorem 6.4 *Let Λ be a right-orientable horseshoe.*

(1) *If $P^* \in G^l_\beta$, where $\beta = [\overbrace{0, \ldots, 0}^{n}]$, then u-boundary point of Λ is periodic with period $(n+3)$ and has periodic coding $\{[\overbrace{0, 0, \ldots, 0}^{n+2}, 1]\}$.*

(2) *If $P^* \in G^l$, then u-boundary point of Λ is periodic with period three and has coding $\{[\overbrace{0, 0, 1}^{3}]\}$.*

(3) *If $P^* \in \hat{G}$, then u-boundary point of Λ is periodic with period two.*

(4) *If $P^* \in G^r$ or $P^* \in G^r_\beta$ and moreover, G_β lies below G, then u-boundary point of Λ is the fixed point O_2.*

Proof The statement (3) concerning the point of period two has been proved in [1] (see Theorem 6.2 there).

We prove now the statement (2). Since the collapse point P^* lies in the band G^l, it follows that this point is the image under the map T of the whole line $l_0 \subset G_0$. Due to geometry of the horseshoe, any (curvilinear) segment in the square Q connecting a point from the side $[a, d]$ of Q with a point from the line l_0 and lying in the domain $\hat{q}_0$ below l_0 is mapped into a segment which intersects $[a, d]$ and contains P^* as the end point. First in the capacity of these segments, we choose invariant ones, actually we choose some parts of unstable manifolds of horseshoe points. Since Λ is a hyperbolic basic set, it has a periodic point which is a u-boundary point. Then among the parts of the unstable manifold connecting the side $[a, d]$ with the line l_0, one can choose the rightmost. Denote it by $\hat{q}_0$. Since the map T is non-orientable on $\hat{q}_0$, it follows that the image $T(\hat{S}_0)$ is the leftmost part among the invariant segments connecting P^* with $[a, d]$. As $P^* \in G$, we have that $T(P^*) \in \hat{G}$ and also that the invariant segment $T^2(\hat{S}_0)$ intersects vertically the square Q. Note that the segment $T^2(\hat{S}_0)$ consists of two parts with the common point P^*, namely the lower part is the rightmost on $T_l(Q)$, while the upper part is the leftmost on $T_l(Q)$ and contains the point p_3. The T-image of this segment is the rightmost invariant curve on $T_r(Q)$, whose end points are $T(P^*) \in \hat{G}$ and $T^2(P^*)$, the second end point being below the side $[a, d]$. This implies that the curve $T^3(\hat{S}_0)$ contains $\hat{S}_0$. Since the map T is expanding on $\hat{S}_0$, it follows that on $\hat{S}_0$ there is (a unique) point of period three, namely the point p_1. The prescribed symbol for this point is "1" because it belongs to Q^r, the right-hand part of Q. The points $p_2 = T(p_1)$ and $p_3 = T(p_2)$ lie in Q^l, the left-hand part of Q, that

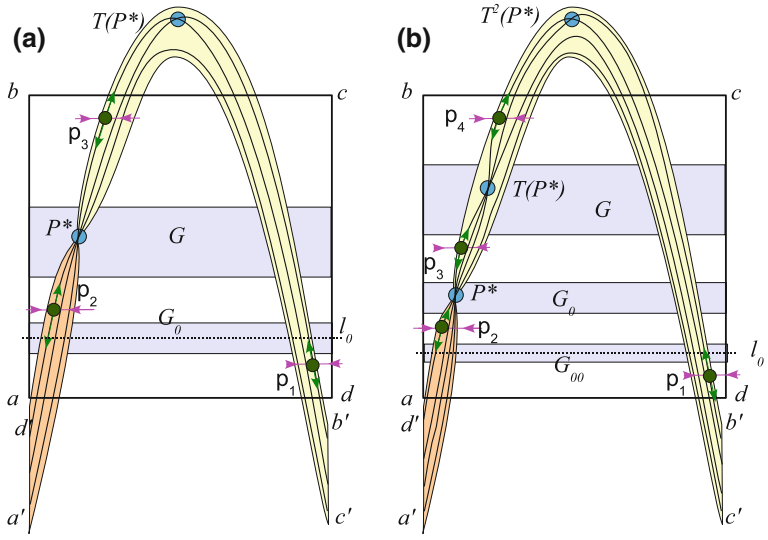

Fig. 6.10 Examples of half-orientable horseshoes with **a** the boundary point of period 3; **b** the boundary point of period 4

is why the prescribed symbol for them is "0." So, the cycle $\{p_1, p_2, p_3\}$ of period three has periodic coding $\{[0, 0, 1]\}$ (see Fig. 6.10a which illustrates right-orientable horseshoe with a boundary point of period three).

To prove the statement (1), we use the same arguments. Let $P^* \in G^l_\beta$, where $\beta = [\overbrace{0, \ldots, 0}^{n}]$. Consider the segment $l_n \in G_{\beta 0}$ such that $T(l_n) = P^*$. Let us choose in the domain $\hat{q}_n$ on Q below l_n, the rightmost invariant part of $W^u(\Lambda)$. Denote this segment by S_n. Its T-image, $T(\hat{S}_n)$, is a segment from the invariant curve, and, moreover, it is the leftmost segment among invariant curves connecting P^* with $[a, d]$. Under iterates of T, this segment becomes longer and longer (due to expansion property). Since $P^* \in G^l_\beta$, it follows from the definition of the band G_β, that after $(n + 1)$ iterations of the map T, the image $T^{n+1}(T(\hat{S}_n))$ intersects Q vertically. And then just the next iteration will cover $\hat{S}_n$. This implies that in $\hat{S}_n$, there exists a point of period $(n + 3)$, and this point is u-boundary by the construction (see Fig. 6.10b which shows right-orientable horseshoe which has boundary point of period four).

At last, we prove statement (4). Let $\hat{L}_1$ be a segment on Q_r which is the rightmost invariant segment among those connected parts of $W^u(\Lambda)$ on Q_r whose first end point is P^* and the second end point lies on the side $[b, c]$. Then, the end points of the segment $T(\hat{L}_1)$ will be $T(P^*) \in \hat{G}$ and also another point which lies on $[b', c']$ below $[a, d]$. It is obvious that the part of the segment $T(\hat{L}_1)$ from the point $T(P^*)$ to the collapse point P^* is the rightmost segment among parts of $W^u(\Lambda)$ with lower end point P^*. This means that $T(\hat{L}_1) \supset L_1$ and, in its turn, the segment L_1 contains fixed point. More precisely, this fixed point is obviously O_2. □

Let us remark that half-orientable horseshoes of different types can be realized as horseshoes for diffeomorphisms on non-orientable manifolds. Indeed, with any

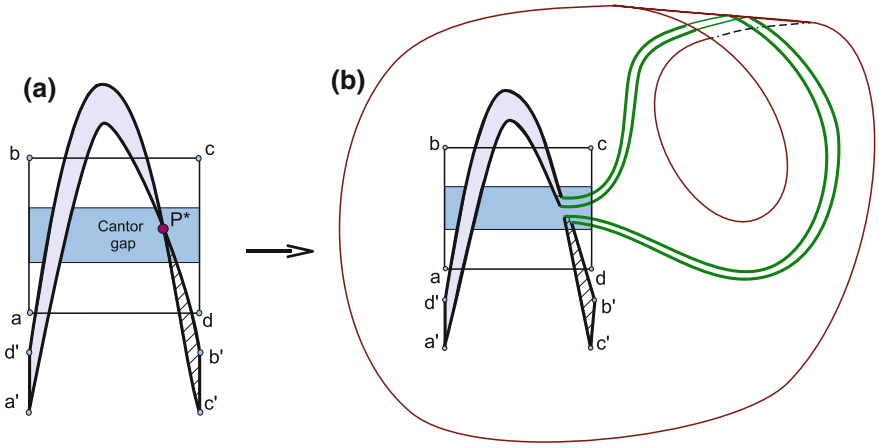

Fig. 6.11 **a** a half-orientable horseshoe for a plane endomorphism; **b** the same horseshoe for a diffeomorphism on a non-orientable surface (Moebius band)

half-orientable horseshoe of the map T, one can associate (by using the "surgery operation" on the wandering set) a horseshoe of the same type on the manifold (see Fig. 6.11 for such construction on the Moebius band). In principle, the above results concerning generalized Hénon maps can be adjusted for this case. However, the description of horseshoes for GHM given in Theorem 6.1 will not (in general) take place here (there will be only finitely many hyperbolicity regions, and transitions between them will correspond to regions of non-rough systems having homoclinic tangencies).

Acknowledgements The work is partially supported by the RSF grant 14-41-00044. The authors thank the RFBR (grants No. 16-01-00364, No. 16-51-10005 KO-a, No. 15-01-03687) and the Russian Ministry of Science and Education (project 1.3287.2017, target part) for supporting scientific researches.

References

1. Gonchenko, S., Li, M.-C., Malkin, M.: Generalized Henon maps and Smale horseshoes of new types. Int. J. Bifurc. Chaos **18**(10), 3029–3052 (2008)
2. Gonchenko, S., Gonchenko, A., Malkin, M.: On classification of classical and half-orientable horseshoes in terms of boundary points. Rus. Nonlinear Dyn. **6**(3), 549–566 (2010) [in Russian]
3. Grines, V.Z.: The topological conjugacy of diffeomorphisms of a two-dimensional manifold on one-dimensional orientable basic sets I, II, vol. 32, pp. 35–60 (1975); Trudy MMO, vol. 34, pp. 243–252 (1977) (in Russian) Translation in Trans. Moscow Math. Soc. **32**, 31–56 (1975); Trans. Moscow Math. Soc. **34**, 237–246 (1977)
4. Dynamical Systems-9. (Ed. D.V. Anosov) Modern mathematical problems. Fundamental directions, vol. 66. VINITI (1991)
5. Anosov, D.V., Aranson, S.Kh., Bronshtein, I.U., Grines, V.Z.: Smooth Dynamical Systems, Modern mathematical problems, Fundamental directions, Dynamical Systems-1, vol. 1. VINITI (1985)
6. Smale, S.: Diffeomorphisms with many periodic points. Diff. and Comb. Topology, pp. 63–80. Princeton University Press, Princeton (1965)
7. Shilnikov, L.P.: On a Poincare–Birkhoff problem. Mat. Sb. **74**(116), 378–397 (1967)
8. Shilnikov, L.P.: A case of the existence of a countable number of periodic motions. DAN SSSR (Soviet Mathematics) **160**(3), 558–561 (1965)
9. Shilnikov, L.P.: A contribution to the problem of the structure of an extended neighborhood od a rough equilibrium state of saddle-focus type. Mat. Sb. **81**, 92–103 (1970)
10. Gavrilov, N.K., Shilnikov, L.P.: On three-dimensional dynamical systems close to a system with nonrough homoclinic curve, Part 1 – Mat. sb. **88**(4), 475–492 (1972); Part 2 – Mat. sb. **90**(1), 139–157 (1973)
11. Arnold, V.I., Afraimovich, V.S., Ilyashenko, Yu.S., Shilnikov, L.P.: Theory of bifurcations, Modern mathematical problems. Fundamental directions, vol. 5. VINITI (1986)
12. Homoclinic tangencies: Collection of papers. Editors S.V. Goncheko and L.P. Shilnikov, Moscow-Izhevsk (2007)
13. Tedeshini-Lalli, L., Yorke, J.A.: How often do simple dynamical processes have infinitely many coexisting sinks. Comm. Math. Phys. **106**, 635–657 (1986)
14. Gonchenko, S.V., Turaev, D.V., Shilnikov, L.P.: Dynamical phenomena in multidimensional systems with non-rough Poincaré homoclinic curve. Dokl. Ross. Akad. Nauk **330**(2), 144–147 (1993)
15. Afraimovich, V., Hsu, S.-B.: Lectures on Chaotic Dynamical Systems. Studies in Advanced Mathematics, vol. 28. AMS-International Press, Providence

16. Afraimovich, V.S., Shilnikov, L.P.: Strange attractors and quasiattractors. Nonlinear Dynamics and Turbulence, pp. 336–339. Pitman, Boston (1982)
17. Afraimovich, V.S.: Strange attractors and quasiattractors. In: Sagdeev, R.Z. (ed.) Nonlinear and Turbulent Processes in Physics, vol. 3, pp. 1133–1138. Gordon and Breach, Harwood Academic Publishers (1984)
18. Devaney, R., Nitecki, Z.: Shift automorphisms in the Hénon mapping. Comm. Math. Phys. **67**, 137–146 (1979)
19. Li, M.-C., Malkin, M.: Bounded nonwandering sets for polinomial mappings. J. Dyn. Control Syst. **10**, 377–389 (2004)
20. Gonchenko, S.V., Gonchenko, V.S.: On Andronov-Hopf Bifurcations of Two-Dimensional Diffeomorphisms with Homoclinic Tangencies. WIAS-preprint No. 556, Berlin (2000)
21. Gonchenko, S.V., Gonchenko, V.C.: On bifurcation of the birth of closed invariant curves for two-dimensional diffeomorphisms with homoclinic tangencies. In: MIAN Proceedings, vol. 244, pp. 87–114 (2004)
22. Bischi, G.I., Gardini, L., Mira, C.: Plane maps with denominator part I: some generic properties. Int. J. Bifurc. Chaos **9**(1), 119–153 (1999)

Chapter 7
From Chaos to Order in a Ring of Coupled Oscillators with Frequency Mismatch

Alexander N. Pisarchik and Mariano Alberto García-Vellisca

7.1 Introduction

Synchronization is commonly understood as a dynamical process to reach a collective state of coupled oscillatory systems. Generally, synchronization requires some relation between the functionals of different processes due to their interaction [1, 2]. As a result of synchronization, coupled systems adjust their individual frequencies in a certain ratio. Numerous examples of synchronization can be found in almost all fields of science and in nature, from mechanics and electronics to physics, chemistry, and biology. Therefore, the study of synchronization of coupled oscillators is of extreme importance for understanding the dynamical processes underlying this phenomenon. The mechanisms behind the cooperative synchronous behavior are different for each system and determined by its properties. The knowledge of these mechanisms will allow the understanding of the principles of self-organization of the matter.

The notion of synchronization was first used to describe the cooperative behavior of periodic systems, such as the Huygens's clocks, but it was later extended to chaotic systems [3] able to adjust their individual behaviors from uncorrelated oscillations to a completely identical motion as the coupling strength increases. The ever-present demand for secure communication was one of the primary motivations for studying the synchronization of chaotic systems. This demand, especially in military applications, led Louis Pecora and Thomas Carroll [4] to develop a method for synchronizing two chaotic systems that continue to be a reason for innovation in this field nowadays [5, 6]. They revealed the necessary conditions needed for synchronization and indicated that secure communication using a chaotic carrier was possible. If a receiver synchronizes with a transmitter, a message can be extracted from the mask. Although their simple method for encrypting a signal in chaos is easily defeated by cryptanalysis, such as synchronization attacks [7], synchronous chaotic oscillators continue to

A.N. Pisarchik (✉) · M.A. García-Vellisca
Center for Biomedical Technology, Technical University of Madrid,
Campus Montegancedo, 28223 Pozuelo de Alarcon, Madrid, Spain
e-mail: alexander.pisarchik@ctb.upm.es

D. Volchenkov and X. Leoncini (eds.), *Regularity and Stochasticity of Nonlinear Dynamical Systems*, Nonlinear Systems and Complexity 21,
DOI 10.1007/978-3-319-58062-3_7

stimulate many researchers in developing new increasingly sophisticated methods to improve communication security [8].

Synchronization of simple systems composed by two identical chaotic oscillators has been extensively studied (see, e.g., [1, 9] and references therein) and is now relatively well understood. Many types of chaos synchronization have been identified and characterized using typical synchronization measures, such as synchronization error, cross-correlation, similarity function, and phase difference. Among them, it is worth mentioning complete synchronization [4], phase synchronization [10], antiphase synchronization [11], lag synchronization [12], anticipating synchronization [13], and generalized synchronization [14]. A route to synchronization depends on both type of coupling and the coupling configuration. In the simplest case of two identical chaotic oscillators, the most common synchronization scenario from asynchronous motion to complete synchronization, as the coupling strength is increased, is as follows: imperfect phase synchronization → perfect phase synchronization → complete synchronization [1]. A different scenario occurs in the presence of a mismatch between natural frequencies of coupled oscillators. When the natural frequency of the slave oscillator is smaller than the natural frequency of the master oscillator, the oscillators synchronize with lag; in the opposite case, the slave oscillator anticipates the master oscillator dynamics [15, 16].

More sophisticated routes to synchronization occur in systems with three and more coupled chaotic oscillators, especially in the presence of frequency mismatch. The synchronization of such systems is not well understood yet. Complex networks formed by many oscillators exhibit other, more interesting types of synchronization, e.g., chimera states [17] and explosive synchronization [18]. Even three coupled oscillators can display synchronous states not observed in two coupled oscillators. For example, three chaotic oscillators unidirectionally coupled in a ring exhibit stabilization of a periodic orbit, when their natural frequencies are detuned. The study of synchronization of three coupled oscillators is very important for understanding the dynamics of complex networks, because three coupled oscillators represent the simplest *network motif*, where each oscillator is nothing more than a node. The network motifs were explored by Uri Alon and his colleagues [19] in the gene regulation (transcription) network of the bacteria *Escherichia coli*, and then they were found in a large set of natural networks [20]. Network motifs repeat themselves in a specific network or even among various networks and can be responsible for particular functions. Synchronization in network motifs is one of the hottest research topics, still poorly explored. In addition to biological applications, network motifs are also used in computational graphs [21].

In this chapter, we describe the route to synchronization in three chaotic oscillators unidirectionally coupled in a ring. We will show how synchronization emerges in this system as the coupling strength increases. We also address the important question of how the distance (frequency mismatch) between the oscillators affects synchronization. Numerical simulations and electronic experiments with Rössler oscillators allow us to answer these questions.

The rest of the chapter is organized as follows: In Sect. 7.2, we introduce the model and present the results of numerical simulations. In Sect. 7.3, we describe the experimental setup, analyze experimental results, and compare them with numerical ones. Finally, in Sect. 7.4, we summarize the content of the chapter.

7.2 Theory

7.2.1 General Equation

The system of three oscillators in the ring configuration shown in Fig. 7.1 can be described in the following general form

$$\dot{\mathbf{x}}_i = \mathbf{F}(\mathbf{x}_i, \omega_i) + \sigma_{ji}(\mathbf{x}_j - \mathbf{x}_i), \tag{7.1}$$

where $\mathbf{x}_{j,i}$ are vectors of state variables of the j-th and i-th oscillators, respectively, $\mathbf{F}$ is a vector function, and σ_{ji} is a coupling strength. For simplicity, we consider almost identical oscillators. The oscillators are only distinct by their natural frequencies ($\omega_j \neq \omega_i$). Due to nonlinearity, the dominant frequency Ω_j in the chaotic power spectrum of an uncoupled j-th oscillator usually does not coincide with its natural frequency ($\Omega_j \neq \omega_j$). When the oscillators are unidirectionally coupled, the j-th oscillator drives the i-th oscillator. Thus, the former acts as a master, while the latter acts as a slave. For sufficiently strong coupling, the master oscillator j entrains the dominant frequency Ω_i of the slave oscillator i that results in phase synchronization [10]. The time-averaged difference between the oscillators' phases $\delta_{ij} = \langle \varphi_i - \varphi_j \rangle$ is negative if the frequency mismatch is $\Delta_{ij} = \omega_i - \omega_j < 0$ and positive if $\Delta_{ij} > 0$. In the former case, the phase of the slave oscillator is locked by the master oscillator with lag, whereas in the latter case with anticipation [15].

7.2.2 Rössler Model

Without loss of generality, we focus on the Rössler model, the prototypical system frequently used for studying synchronization of chaotic oscillators [1]. The dynamics

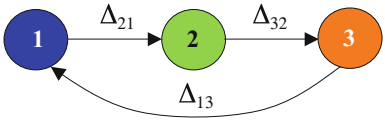

Fig. 7.1 Ring of three coupled oscillators i, $j = 1, 2, 3$. Δ_{ij} ($i \neq j$) is the distance between i and j oscillators in units of frequency mismatch

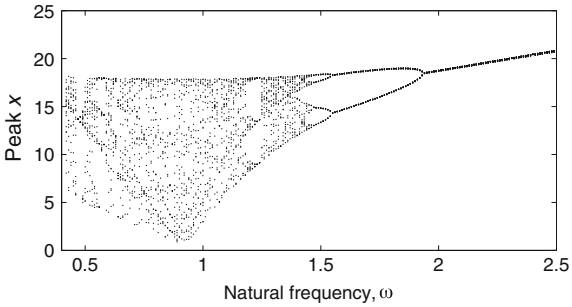

Fig. 7.2 Numerical bifurcation diagram of peak x with respect to natural frequency of the uncoupled Rössler oscillator Eq. (7.2)

of the ring-coupled oscillators shown in Fig. 7.1 are described by the following system of equations

$$\begin{aligned} \dot{x_i} &= -\omega_i y_i - z_i, \\ \dot{y_i} &= \omega_i x_i + a y_i + \sigma_{ji}(y_j - y_i), \\ \dot{z_i} &= b + z_i(x_i - c), \end{aligned} \tag{7.2}$$

where $i, j = 1, 2, 3$ $(i \neq j)$ is the oscillator number, and x_i, y_i, z_i are the state variables of the ith oscillator. Slave oscillator i is coupled to neighboring master oscillator j through variable y_j. When uncoupled ($\sigma = 0$), the oscillators, Eq. (7.2), are chaotic for $a = 0.165$, $b = 0.2$, and $c = 10$. In the configuration shown in Fig. 7.1, the coupling strength between each pair of oscillators is the same, $\sigma_{21} = \sigma_{32} = \sigma_{13} = \sigma$ and $\sigma_{12} = \sigma_{23} = \sigma_{31} = 0$, i.e., the oscillator 1 acts as a master for the oscillator 2 and as a slave for the oscillator 3.

In Fig. 7.2, we plot the bifurcation diagram of the solitary oscillator using its natural frequency ω as a control parameter. One can see from the bifurcation diagram that the oscillator is chaotic in a wide range of its natural frequency ω. This allows us to vary significantly the distance Δ (frequency mismatch) between the oscillators so that it is inside the chaotic range.

Let the natural frequencies be $\omega_1 = 0.95$, $\omega_2 = 0.97$, and $\omega_3 = 0.99$. Starting from different initial conditions, the uncoupled oscillators with different natural frequencies exhibit asynchronous motion as seen from the time series in Fig. 7.3a. The power densities of the chaotic power spectra of the system variables, shown in Fig. 7.3b, exhibit maxima at dominant frequencies $\Omega_1^0 \approx 0.975$, $\Omega_2^0 \approx 0.998$, and $\Omega_3^0 \approx 1.02$. These frequencies are a little different from the natural frequencies of the corresponding oscillators, because nonlinearity relates the amplitude with the frequency of oscillations [22].

Quantitatively, phase synchronization between a pair of oscillators i and j can be characterized by the difference between their instantaneous phases [1]

$$\theta_{ij} = \phi_i - \phi_j, \tag{7.3}$$

where

$$\phi_{i,j} = \arctan(y_{i,j}/x_{i,j}). \tag{7.4}$$

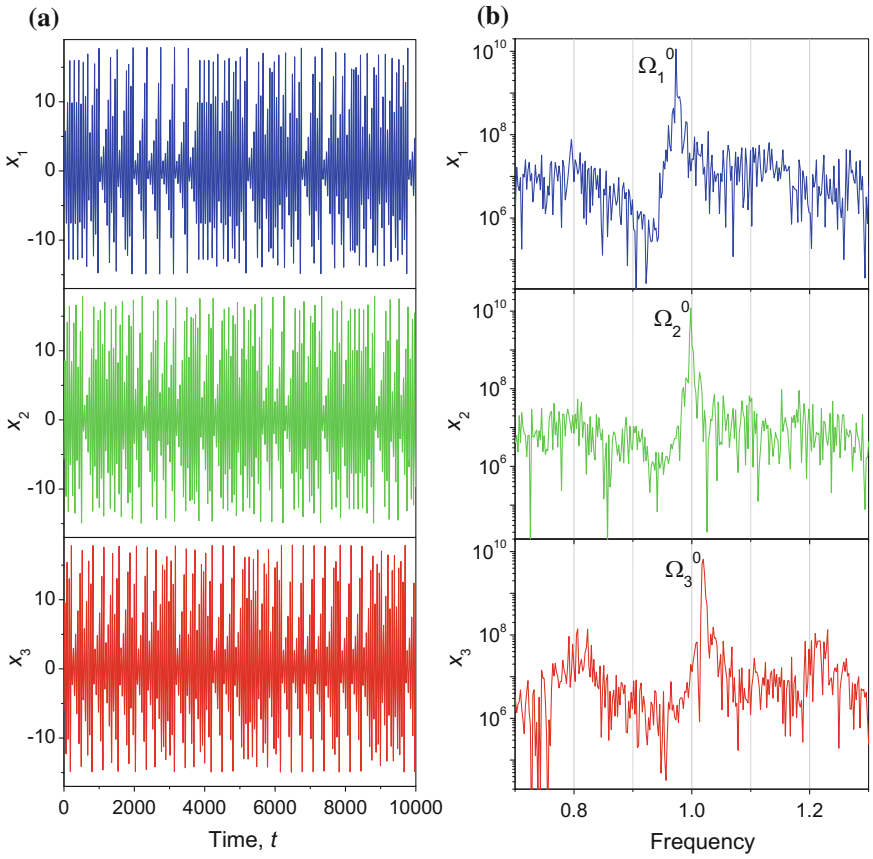

Fig. 7.3 **a** Time series and **b** power spectra of x variables of uncoupled Rössler oscillators with natural frequencies $\omega_1 = 0.95$, $\omega_2 = 0.97$, and $\omega_3 = 0.99$. The oscillators exhibit asynchronous chaotic behavior with dominant frequencies Ω_1^0, Ω_2^0, and Ω_3^0 in the power spectra

Since the oscillators have different natural frequencies, θ_{ij} of the uncoupled oscillators either monotonically increases or decreases in time depending on a sign of the frequency mismatch. The oscillators interact already for a very small coupling strength $\sigma > 5 \times 10^{-3}$. The interaction manifests itself in the form of irregular windows of phase synchronization. Within these windows, a master oscillator locks the phase of a slave oscillator so that both have the same dominant frequency in their power spectra. The windows intermittently appear and disappear in the time series, and therefore this regime is called *intermittent phase synchronization*.

This situation is illustrated in Fig. 7.4, where we plot the time dependences of θ_{21} for three different coupling strengths. When the oscillators' phases are not well synchronized, the phase difference θ_{ij} increases or decreases monotonically depending on its sign. The horizontal intervals in these dependences result from the windows

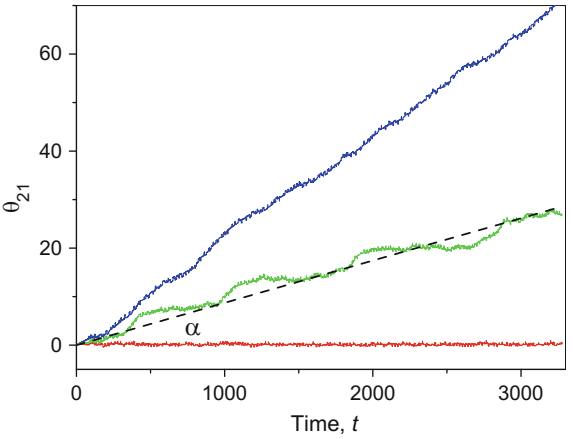

Fig. 7.4 Time-dependent phase difference θ_{21} between oscillators 2 and 1 for $\sigma = 6.6 \times 10^{-3}$ (*upper blue line*), 2.6×10^{-2} (*middle green line*), and 4.6×10^{-2} (*lower red line*). The *dashed line* is a linear fit of the middle dependence with slope α. The horizontal parts of these dependences correspond to the regions of intermittent phase synchronization

of phase synchronization, where the dominant frequency of the slave oscillator is locked by the corresponding master oscillator. Within these windows, θ_{ij} increases or decreases monotonically in time but fluctuates around a certain value, similar to a Brownian motion. As the coupling σ is increased, these windows enlarge leading finally, for sufficiently strong σ, to permanent phase synchronization.

Intermittent phase synchronization can be quantitatively characterized by the slope α of the fitting straight line, determined by the phase difference averaged over the whole time series. The smaller α the lager the duration of the phase synchronization windows. When the slope $\alpha = 0$, as in the lowest red horizontal line, we deal with permanent phase synchronization, i.e., the dominant frequency of the slave oscillator is always entrained by the corresponding master oscillator.

In the following subsections, we will describe the synchronization scenarios with respect to the coupling strength and frequency mismatch.

7.2.3 *Route to Synchronization with Respect to Coupling Strength*

We have already shown in the previous subsection that, as the coupling strength is increased, the oscillators, on the route from asynchronous motion to lag or anticipating synchronization, first represent intermittent phase synchronization and then permanent phase synchronization. We will consider these two types of synchronization in detail.

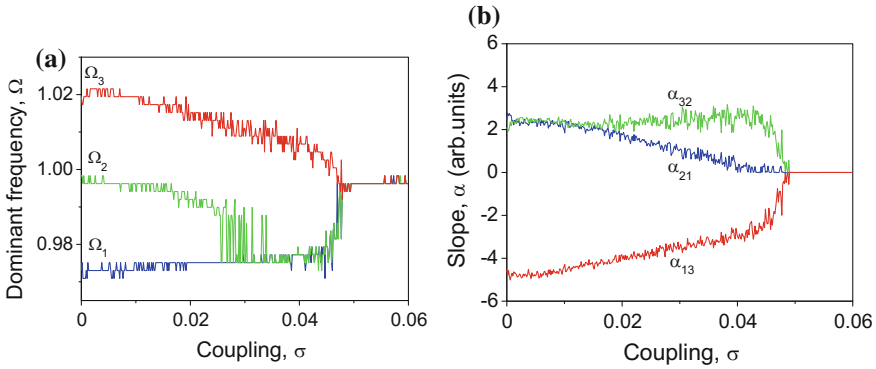

Fig. 7.5 **a** Time-averaged dominant frequencies $\langle\Omega_i\rangle$ and **b** slopes α_{ij} of time-dependent phase differences as a function of the coupling strength

7.2.3.1 Intermittent Phase Synchronization

Due to frequency locking in the phase synchronization windows, the dominant frequency of a slave oscillator is equal to the dominant frequency of its master oscillator, whereas out of these windows, the oscillators have distinct dominant frequencies. In other words, the locking of the dominant frequency of the slave oscillator by its master oscillator leads to phase synchronization. To characterize intermittent phase synchronization, we use the time-averaged dominant frequency $\langle\Omega\rangle$ in the chaotic power spectrum and the slope α of the time dependence of the phase difference θ_{ij} (time-averaged θ_{ij}). The closer $\langle\Omega_i\rangle$ to $\langle\Omega_j\rangle$, the better the synchronization.

Figure 7.5a shows how time-averaged dominant frequencies $\langle\Omega_i\rangle$ of every oscillator depend on the coupling strength σ. The corresponding slopes α_{ij} of the time-dependent phase differences are plotted in Fig. 7.5b. One can see that these two characteristics of intermittent phase synchronization are strongly correlated.

As the coupling σ increases, both $\langle\Omega_2\rangle$ and $\langle\Omega_3\rangle$ of the slave oscillators 2 and 3, respectively, slowly decreases because the duration of intermittent frequency-locked windows increases (Fig. 7.5a). However, almost no changes occur in $\langle\Omega_1\rangle$ because the distance (frequency mismatch) between the oscillators 3 and 1 is too large. Only as σ approaches 0.048, the oscillator 1 adjusts very fast its time-averaged dominant frequency $\langle\Omega_1\rangle$ to the arithmetic average of the dominant frequencies of the uncoupled oscillators $\left(\sum_{i=1}^{3}\Omega_i^0/3\right)$.

The oscillators begin to interact already for a very small coupling strength ($\sigma > 5\times10^{-3}$) giving rise to the irregular windows of phase-synchronized oscillations in the time series. Within these windows, a master oscillator locks the phase of the corresponding slave oscillator so that their dominant frequencies match. As a consequence, within these windows, θ_{ij} neither increases nor decreases monotonically in time but fluctuates near a certain average value. This regime is known as

intermittent phase synchronization. The slopes α_{ij} in Fig. 7.5b reflect changes in the time-averaged dominant frequencies. One can see that oscillators 1 and 2 synchronize first, and then they all synchronize with the remaining oscillator 3.

7.2.3.2 From Phase to Lag (or Anticipating) Synchronization

As soon as the oscillators' phases have synchronized, synchronization quality can be characterized by comparing amplitudes of coupled oscillators. The commonly used measures for lag and anticipating synchronization are cross-correlation function C and similarity function S defined, respectively, as [12]

$$C_{ij}(\tau) = \frac{\langle [x_j(t) - \langle x_j \rangle][x_i(t+\tau) - \langle x_i \rangle] \rangle}{\sqrt{[x_j(t) - \langle x_j \rangle]^2 [x_i(t) - \langle x_i \rangle]^2}} \tag{7.5}$$

and

$$S_{ij}^2(\tau) = \frac{\left\langle [x_j(t) - x_i(t+\tau)]^2 \right\rangle}{\sqrt{\left\langle x_j(t)^2 \right\rangle \left\langle x_i(t)^2 \right\rangle}}, \tag{7.6}$$

where τ is the time shift between two signals and $\langle ... \rangle$ denotes time average. The higher the maximum of cross-correlation $C_{\max}$ and the lower the minimum of similarity function $S_{\min}$, the better synchronization.

Figure 7.6 shows how these two characteristics vary with the coupling strength. At the coupling strength $\sigma = 0.18$, intermittent phase synchronization becomes permanent that results in increasing $C_{\max}$ and decreasing $S_{\min}$. The phase difference θ drifts around its average value but never exceeds the modulation period, i.e., $\theta \in [-\pi, \pi]$.

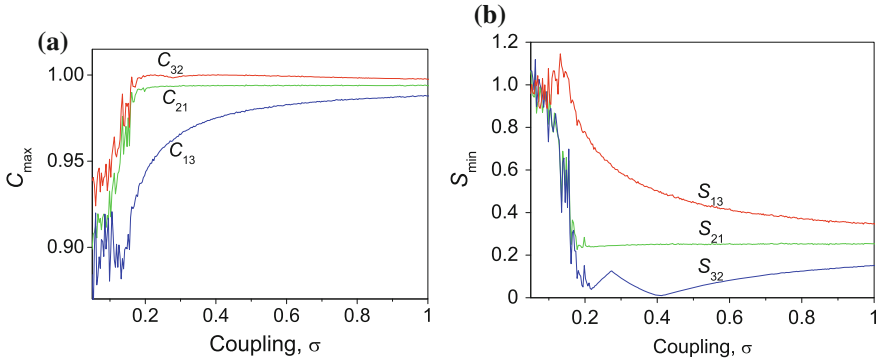

Fig. 7.6 **a** Maximum cross-correlation function and **b** minimum similarity function via coupling strength for every pair of oscillators

As σ is further increased, the amplitude of these fluctuations decreases resulting in perfect phase synchronization.

On the route from phase to lag (anticipating) synchronization, the oscillators adjust their amplitudes, as σ increases. The best synchronization occurs between the oscillators 3 and 2, for $\sigma = 0.4$, these oscillators display identical dynamics with anticipation because $C_{\max} = 1$ and $S_{\min} = 0$. Evidently, the oscillators 1 and 3 are worse synchronized because the mismatch between their natural frequencies is higher. Complete synchronization cannot be achieved in this system, because the oscillators are not identical; however, for strong enough coupling, the amplitudes are highly correlated (when the time lag is compensated). The time shift between the waveforms of the slave and master oscillators is always equal to $2\pi(1/\omega_i - 1/\omega_j)$, where ω_i and ω_j are the natural frequencies of the slave and master oscillators, respectively.

Interestingly, for a certain coupling strength, the oscillators' dynamics become more coherent. The coherence enhancement in a chaotic Rössler oscillator subjects to a chaotic input from another, almost identical Rössler oscillator has been first demonstrated in Ref. [23]. The coherence enhancement has a resonance character with respect to both the coupling strength and the mismatch between the natural frequencies of the slave and master oscillators. A similar effect occurs in the ring of the chaotic oscillators. The coherence enhancement can be seen in Fig. 7.7, where we plot the bifurcation diagrams versus the coupling strength. The shrink of the bifurcation diagrams indicates the increasing amplitude coherence referred to as *deterministic coherence resonance*. One can see that such resonances occur at $\sigma \approx 0.08$ and 0.18 for $\Delta = 0.03$ and 0.07, respectively. One can see in the right-hand column of Fig. 7.7 that for large mismatch ($\Delta = 0.25$) and strong coupling ($\sigma > 0.18$) the oscillators behave periodically.

We should note that this synchronization scenario is almost independent of the coupling direction. In the other words, it does not matter whether $\omega_1 < \omega_2 < \omega_3$ or $\omega_1 > \omega_2 > \omega_3$. The only difference is that in the former (forward) coupling the oscillators synchronize with anticipation, whereas in the latter (backward) coupling with lag. For very strong coupling, the oscillators 3 and 2 for forward and 1 and 2 for backward coupling completely synchronize, when the time shift is compensated.

7.2.4 *Route to Synchronization with Respect to Frequency Mismatch*

We consider, for simplicity, a symmetric case when the distances between the oscillators 1 and 2 and the oscillators 2 and 3 are the same, i.e., $\Delta_{21} = \Delta_{32} = \Delta_{13}/2 = \Delta$. To study the influence of the distance on synchronization, we fix the natural frequency of the oscillator 2 to $\omega_2 = 0.9$ and vary Δ.

In Fig. 7.8, we plot the times series, phase portraits, and power spectra of the x variable of the uncoupled (Fig. 7.8a, c) and coupled (Fig. 7.8b, d) oscillators.

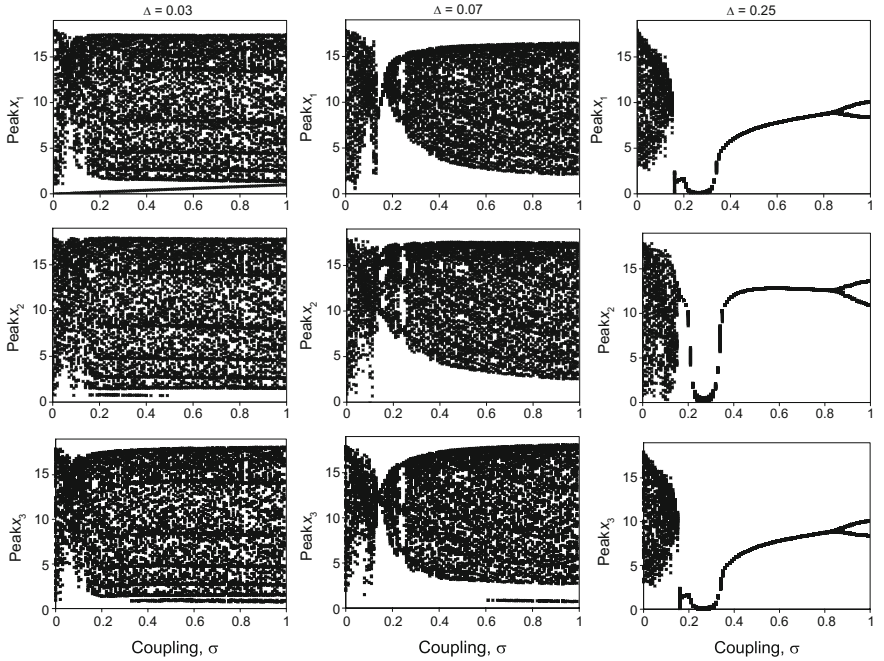

Fig. 7.7 Bifurcation diagrams of peak x of three oscillators with the coupling strength as a control parameter for (*left-hand column*) $\Delta = 0.03$, (*middle column*) $\Delta = 0.07$, and (*right-hand column*) $\Delta = 0.25$

The uncoupled oscillators have different dominant frequencies in their power spectra (Fig. 7.8c). As the coupling strength σ is increased, the oscillators adjust their dominant frequencies (Fig. 7.8d) that result in phase synchronization. A further increase in the coupling results in stabilization of a period-2 orbit as seen from Fig. 7.8b.

The system stability is analyzed by calculating the Lyapunov exponents. In Fig. 7.9, we plot nonzero Lyapunov exponents in the parameter space of the coupling strength σ and frequency mismatch Δ.

When the oscillators' frequencies are very close to each other, they are chaotic for any coupling strength, whereas for larger distances their dynamics become more regular. However, for large distances ($\Delta > 0.1$) and intermediate coupling ($0.1 < \sigma > 0.4$), the leading (largest) Lyapunov exponent takes a negative value; in this parameter region, a period-2 orbit is stable.

The route to phase and lag synchronization is clearly shown in Fig. 7.10, where we plot the maximum cross-correlation $C_{\max}$ and minimum similarity function $S^2_{\min}$ for each pair of the oscillators as a function of mismatch Δ and coupling σ.

One can see that the weakly coupled oscillators ($\sigma < 0.1$) synchronize only when their natural frequencies are very close ($\Delta < 0.05$), whereas stronger coupling ($\sigma > 0.2$) makes them synchronized for any frequency mismatch in the considered

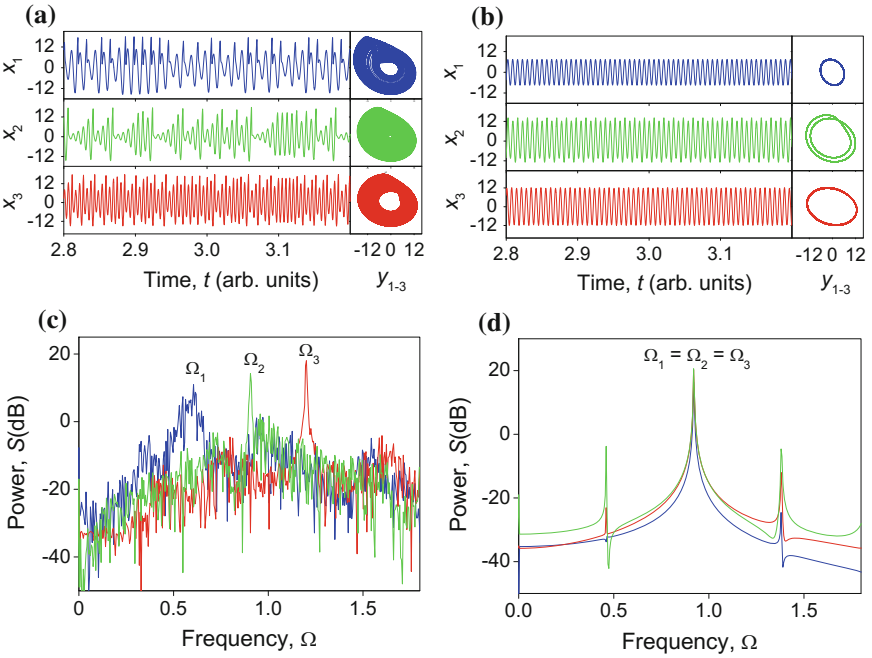

Fig. 7.8 Numerical (**a**, **b**) time series, phase portraits, and (**c**, **d**) power spectra of three (**a**, **c**) uncoupled and (**b**, **d**) coupled Rössler oscillator for $\sigma = 0.33$ and $\Delta = 0.2$, respectively. The coupled oscillators become periodic

range. The blue dark regions in right-hand column of Fig. 7.10 bound the regime of perfect phase synchronization where $S_{\min} = 0$. One can see that the best synchronization is observed for the oscillator 2 and 3, while the oscillators 1 and 3 are worse synchronized. It is quite evident because the distance between the oscillator 1 and 3 is double of the distance between 2 and 3. By comparing Fig. 7.10 with Fig. 7.9, it can be seen that in the periodic regime (for $\Delta > 0.1$ and $0.1 < \sigma > 0.4$) the oscillators reach perfect phase synchronization, i.e., $S_{\min} = 0$.

7.3 Experimental Implementation

7.3.1 Electronic Circuits

The experimental setup is constructed on the base of the electronic circuits shown in Fig. 7.11. These circuits are analog implementations of the Rössler oscillators and the unidirectional coupling.

The Kirchhoff's mesh analysis yields the following equations:

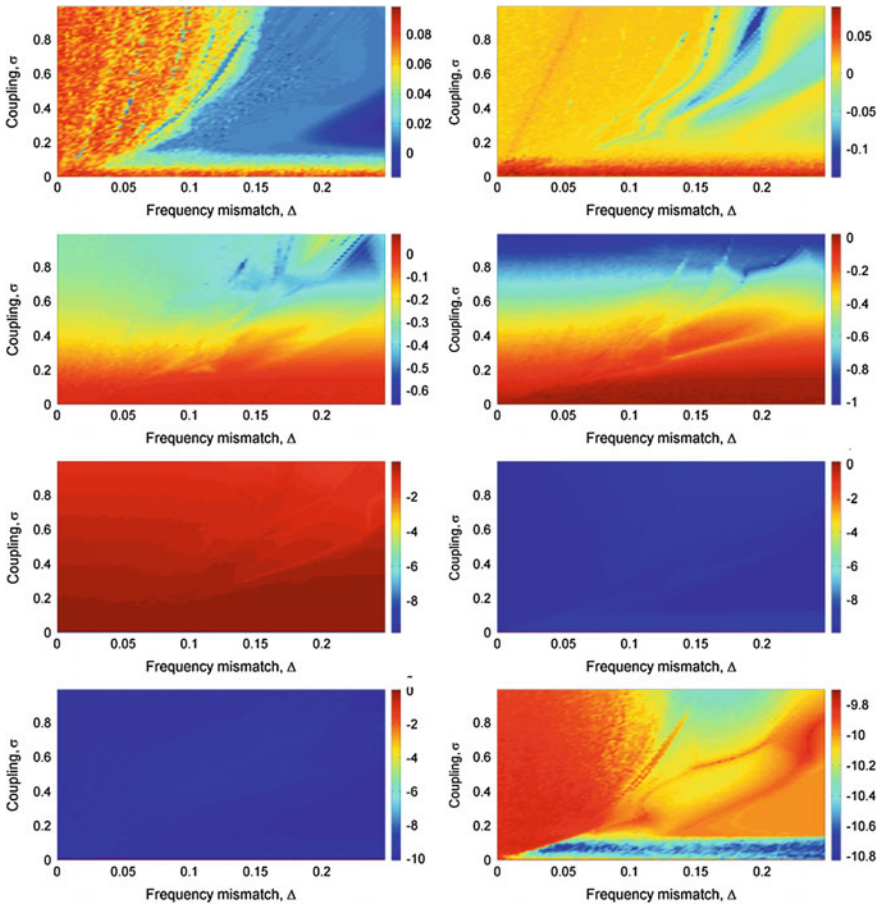

Fig. 7.9 Lyapunov exponents in (Δ, σ)-parameter space. The *blue* (*dark*) tongue indicates the region of periodicity for large Δ and intermediate σ

$$\begin{aligned}
\dot{V}_{xj} &= -\alpha A(V_{yj} + V_{zj}),\\
\dot{V}_{yj} &= \alpha[BV_{xj} + CV_{yj} + \sigma_{ji}(V_{yi} - V_{yj})],\\
\dot{V}_{zj} &= \alpha[D + EV_{zj}(V_{xj} - F)],
\end{aligned} \tag{7.7}$$

where V_{xj}, V_{yj}, and V_{zj} are the output voltages of the three meshes, $\alpha = 10^3$ s^{-1} is the time scale coefficient, σ_{ji} is the coupling strength between the oscillators j and i defined by the parameters of the coupler (Fig. 7.11b), and A, B, C, D, E, and F are the parameters expressed in terms of electronic components as

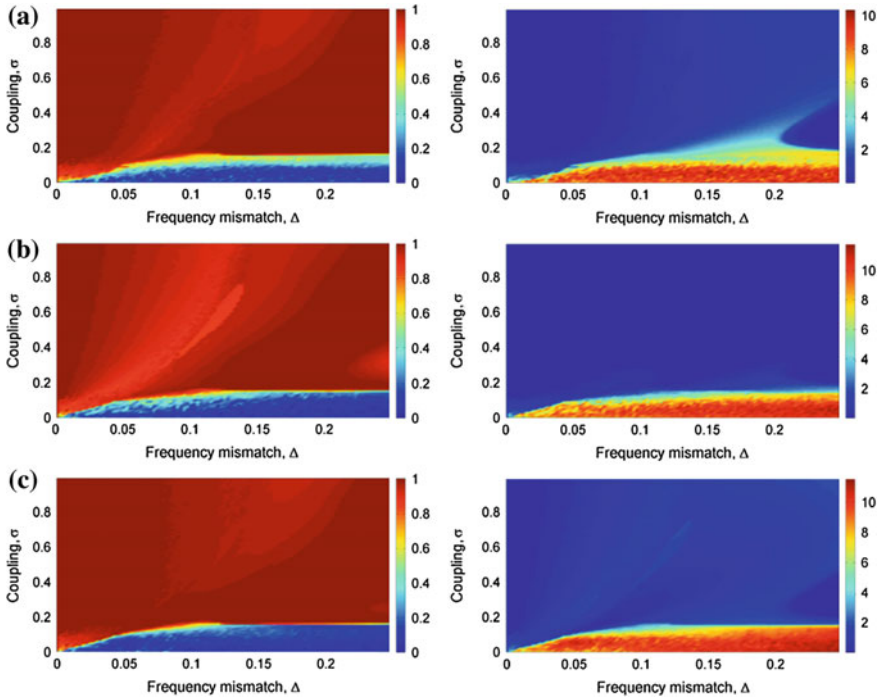

Fig. 7.10 (*Left column*) maximum cross-correlation $C_{\max}$ and (*right column*) minimum similarity $S^2_{\min}$ for oscillators **a** 1 and 2, **b** 2 and 3, and **c** 1 and 3 in (Δ, σ)-parameter space for unidirectionally coupled oscillators

$$
\begin{aligned}
&A = C_1 R_1,\ B = \frac{R_5}{C_1 R_2 R_6} = 1,\ C = \frac{R_5}{C_1 R_2 R_7},\\
&D = \frac{V_0}{10 C_3 R_3}\left(\frac{1 - 2R_{10}}{R_8 + R_9 + R_{10}}\right),\ E = \frac{15}{V_0} = 1,\\
&F = \frac{V_0}{10 C_3 R_3}\left(1 - \frac{2R_8}{R_8 + R_9 + R_{10}}\right),
\end{aligned}
\tag{7.8}
$$

where $V_0 = 15\,\mathrm{V}$ is the power voltage of each mesh.

Although in Eq. (7.7) the coupling is realized through variable V_y, our experiments show that there is no principal difference if the oscillators are coupled through variable V_x. Since, we observe coherence resonance in both cases, here we will only present the results for the coupling given by Eq. (7.7).

We consider three chaotic Rössler oscillators unidirectionally coupled in a ring. The natural frequencies of the oscillators are determined by resistors R1 and R6, different for every oscillator. Since these resistors are not variable in the experiments, we do not use the natural frequencies as control parameters because variable resistors with the required variation step are not available. The full experimental process

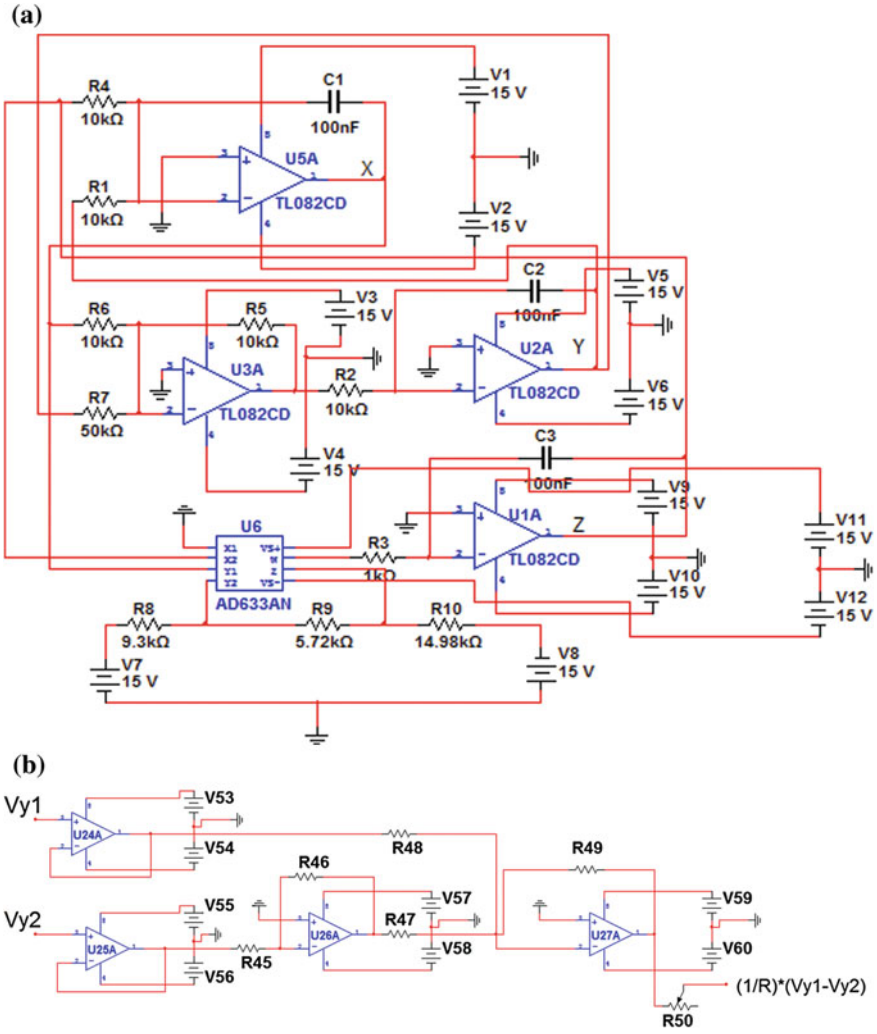

Fig. 7.11 Electronic schemes of **a** Rössler oscillator and **b** coupler

is controlled with a virtual interface developed in LABVIEW 8.5, which can be considered as a state machine. The coupling strength is regulated by variable resistor $R_{50} = 3 \div 300\,k\Omega$ with a step of $3\,k\Omega$. Since $\sigma_{ji} \sim 1/R_{50}$, the oscillators can be considered to be uncoupled, when R_{50} is high ($R_{50} = 300\,k\Omega$).

The experimental procedure is realized as follows: First, the coupling is set to the minimum value ($R_{50} = 300\,k\Omega$). After a waiting time of 500 ms (roughly corresponding to 60 cycles of the autonomous system), the output signals from all circuits are acquired by analog ports. Once the dynamics of the whole system is recorded,

the value of R_{50} is decreased by one step (3 kΩ), and the signals are again stored in the PC for further analysis. This process is repeated until the maximum coupling ($R_{50} = 3\,k\Omega$) is reached.

7.3.2 Experimental Results

In the ring of three unidirectionally coupled chaotic Rössler oscillators, each oscillator acts simultaneously as a master for one oscillator and a slave for another. All oscillators are coupled with the same coupling strength $\sigma_{21} = \sigma_{32} = \sigma_{13} = \sigma$. Since the coupling is unidirectional, $\sigma_{12} = \sigma_{23} = \sigma_{31} = 0$. The resistors R1 and R6 in each of the three circuits are chosen so that the dominant frequencies in the chaotic power spectra of the uncoupled oscillators are in an ascending order, i.e., $f_1 < f_2 < f_3$, where $f_1 = 152\,Hz$, $f_2 = 168\,Hz$, and $f_3 = 177\,Hz$. The time series and power spectra of the uncoupled oscillators are shown in Fig. 7.12.

As the coupling is increased (R_c decreases), the oscillators adjust their dominant frequencies as shown in Fig. 7.13. First, all three frequencies decrease, then, the frequencies of the oscillators 1 and 2 are locked at $R_c \approx 200\,k\Omega$, and finally, the frequencies of all oscillators are entrained at $R_c \approx 125\,k\Omega$. This means that for sufficiently strong coupling, the oscillators are in phase synchronization.

While being uncoupled or weakly coupled, the oscillators are chaotic; for certain intermediate coupling, their dynamics become more coherent. This situation is illustrated in Fig. 7.14, where we plot the bifurcation diagrams and the normalized standard deviations of the peak amplitude of the x variable. As soon as the oscillators' phases synchronize (for $1/R_c > 0.8 \times 10^{-5}\,\Omega^{-1}$), the bifurcation diagrams shrink, meaning partial stabilization of a periodic orbit (in our case, a period 2). Such coherence enhancement has a resonant character as can be seen in the lower panels,

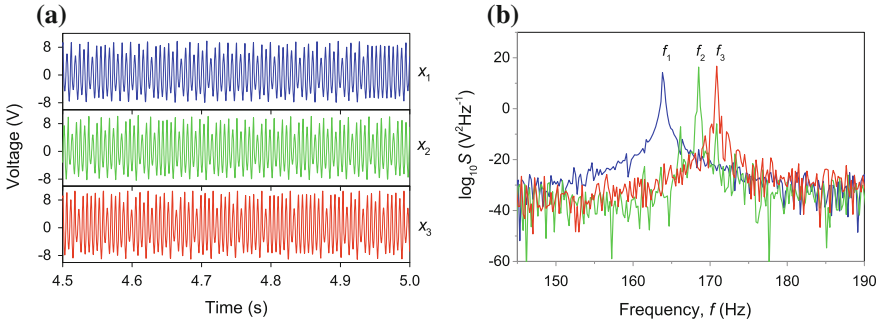

Fig. 7.12 Experimental (a,b) time series, phase portraits, and (c,d) power spectra of three (a,c) uncoupled and (b,d) coupled Rössler oscillators at $1/R_{50} \approx 2 \times 10^{-5}\,\Omega^{-1}$

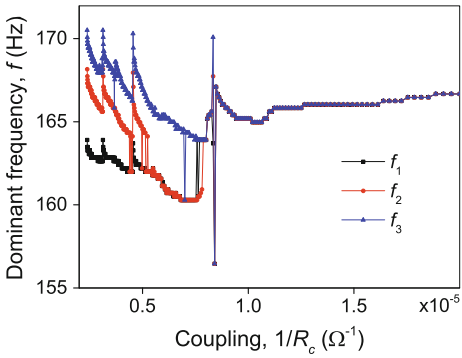

Fig. 7.13 Dominant frequencies as a function of the coupling strength between three ring-coupling oscillators. For relatively strong coupling, all oscillators have the same dominant frequency close to the dominant frequency of the oscillator with highest energy (in our case this is the oscillator 3)

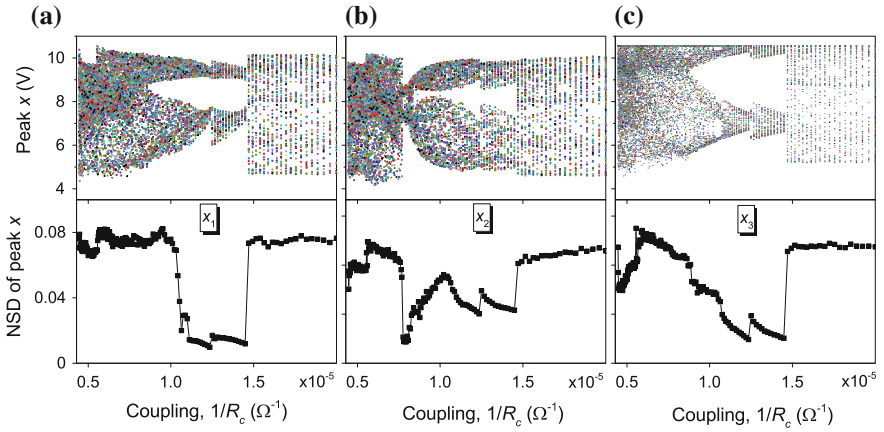

Fig. 7.14 (*Upper row*) bifurcation diagrams and (*lower row*) normalized standard deviations (NSD) of peak x as a function of the coupling strength. Certain coupling makes the oscillators more periodic

where the minima indicate the location of the deterministic coherence resonance. As the coupling is further increased, all oscillators again behave chaotically in the crisis bifurcation at $1/R_c \approx 1.5 \times 10^{-5}\,\Omega^{-1}$.

7.4 Conclusion

We have demonstrated the route to synchronization in a ring of three unidirectionally coupled Rössler oscillators with small mismatch between their natural frequencies $\omega_1 < \omega_2 < \omega_3$ for the forward coupling direction ($1 \to 2 \to 3 \to 1$). As the

coupling strength increases, the oscillators first synchronize their phases intermittently and then adjust their amplitudes. We have quantitatively characterized intermittent phase synchronization by the time-averaged dominant frequency of the power spectrum of every oscillator and the linearly approximated slope of the time-dependent phase difference for every pair of the coupled oscillators. The route to synchronization is as follows: intermittent phase synchronization → imperfect phase synchronization → perfect phase synchronization → lag or anticipating synchronization. The lag or anticipation depends on the frequency mismatch sign.

As the coupling strength increases, the oscillator with lowest natural frequency ω_1 first entrains dominant frequency Ω_2 of the oscillator with middle natural frequency ω_2 so that its time-averaged dominant frequency becomes equal to approximately the dominant frequency of uncoupled oscillator 1 (i.e., $\langle\Omega_2\rangle \approx \Omega_1^0$), while their phases remain synchronized, and then their common time-averaged dominant frequency slowly increases until being rapidly adjusted (within a narrow range of the coupling strengths) to the arithmetic average frequency of all three oscillators. At the same time, $\langle\Omega_3\rangle$ decreases almost linearly with the coupling strength.

It should be noted that in the case of the backward coupling direction, i.e., when $\omega_1 < \omega_2 < \omega_3$, the route to synchronization is very similar. First, the oscillators 2 and 3 synchronize their phases and adjust their time-averaged dominant frequencies $\langle\Omega_2\rangle$ and $\langle\Omega_3\rangle$ to average frequency $(\Omega_2^0 + \Omega_3^0)/2$, and then their common time-averaged dominant frequency slowly decreases to the arithmetic average frequency of all three oscillators, while $\langle\Omega_1\rangle$ first slowly increases and then rapidly adjusts its value, within a very narrow range of the coupling strength, to the arithmetic average dominant frequency of all oscillators. Interestingly, for this configuration, phase synchronization occurs for lower coupling strengths, i.e., the backward coupling is more favorable than the forward one. In other words, phase synchronization is more easily achieved when a master is faster than a slave. The reason for such asymmetry is still unclear.

As soon as the oscillators start to oscillate with the same dominant frequency, their phases synchronize, and as the coupling further increases, they adjust their amplitudes going to almost synchronization. Since in our system, the oscillators are not identical, complete synchronization is never achieved. However, for large enough coupling, the oscillations are strongly correlated being shifted in time with either lag or anticipation depending on the sign of the frequency mismatch. As expected, the oscillators with closer natural frequencies synchronize better than the oscillators with larger mismatch.

A surprising behavior occurs for intermediate distances between the oscillators, when the oscillators are in phase synchronization. For certain coupling strength, the oscillators exhibit regular dynamics, i.e., they behave periodically. The analysis of the Lyapunov exponent spectra has shown that all Lyapunov exponents take negative values in a certain range of the frequency mismatch and coupling strength. This is the evidence of how an order appears in chaotic systems due to their interaction.

References

1. Pikovsky, A., Rosenblum, M., Kurths, J.: Synchronization: A Universal Concept in Nonlinear Science. Cambridge University Press, New York (2001)
2. Boccaletti, S., Kurths, J., Osipov, G., Valladares, D.L., Zhou, C.S.: Phys. Rep. **366**, 1 (2002)
3. Fujisaka, H., Yamada, T.: The control of chaos: theory and applications. Prog. Theor. Phys. **69**, 32 (1983)
4. Pecora, L.M., Carroll, T.L.: Synchronization in chaotic system. Phys. Rev. Lett. **64**, 821 (1990)
5. Fotsin, H., Bowong, S., Daafouz, J.: Adaptive synchronization of two chaotic systems consisting of modified Van der Pol-Duffing and Chua oscillators. Chaos Solitons Fractals **26**, 215 (2005)
6. Pisarchik, A.N., Ruiz-Oliveras, F.R.: Nonlinear Dynamics New Directions: Models and Applications. Nonlinear Systems and Complexity, vol. 12. Springer, Berlin (2014)
7. Zanin, M., Sevilla-Escoboza, R., Jaimes-Reátegui, R., García-Lopez, J.H., Pisarchik, A.N.: Synchronization attack of chaotic communication systems. Discontinuity Nonlinearity Complex. **2**(4), 333–343 (2013)
8. Pisarchik, A.N., Jiménez-Rodríguez, M., Jaimes-Reátegui, R.: How to resist synchronization attacks. Discontinuity Nonlinearity Complex. **4**(1), 1–9 (2015)
9. González-Miranda, J.M.: Synchronization and Control of Chaos. Imperial College Press, London (2004)
10. Rosenblum, M.G., Pikovsky, A.S., Kurths, J.: Phase synchronization of chaotic oscillators. Phys. Rev. Lett. **76**, 1804 (1996)
11. Liu, W., Xia, J., Qian, X., Yang, J.: Antiphase synchronization in coupled chaotic oscillators. Phys. Rev. E **73**, 057203 (2006)
12. Rosenblum, M.G., Pikovsky, A.S., Kurths, J.: From phase to lag synchronization in coupled chaotic oscillator. Phys. Rev. Lett. **78**, 4193 (1997)
13. Voss, H.U.: Anticipating chaotic synchronization. Phys. Rev. E **61**, 5115 (2000)
14. Rulkov, N.F., Sushchik, M.M., Tsimring, L.S., Abarbanel, H.D.I.: Generalized synchronization of chaos in directionally coupled chaotic systems. Phys. Rev. E **51**, 980 (1995)
15. Pyragienė, T., Pyragas, K.: Anticipating spike synchronization in nonidentical chaotic neurons. Nonlinear Dyn. **74**, 297 (2013)
16. Sausedo-Solorio, J.M., Pisarchik, A.N., Sausedo-Solorio, J.M., Pisarchik, A.N.: Phys. Lett. A **378**, 2108 (2014)
17. Abrams, D.M., Strogatz, S.H.: Chimera states for coupled oscillators. Phys. Rev. Lett. **93**, 174102 (2004)
18. Zhang, X., Zou, Y., Boccaletti, S., Liu, Z.: Explosive synchronization as a process of explosive percolation in dynamical phase space. Sci. Rep. **4**, 5200 (2014)
19. Shen-Orr, S.S., Milo, R., Mangan, S., Alon, U.: Network motifs in the transcriptional regulation network of Escherichia coli. Nat. Genet. **31**, 64 (2002)
20. Alon, U.: Network motifs: theory and experimental approaches. Nat. Rev. Genet. **8**, 450–461 (2007)
21. Valverde, S., Solé, R.V.: Network motifs in computational graphs: a case study in software architecture. Phys. Rev. E **72**, 026107 (2005)
22. Nayfeh, A., Mook, D.: Nonlinear Oscillations. Wiley-Interscience, New York (1979)
23. Pisarchik, A.N., Jaimes-Reátegui, R.: Deterministic coherence resonance in coupled chaotic oscillators with frequency mismatch. Phys. Rev. E **92**, 050901(R) (2015)

Chapter 8
Dynamics of Some Nonlinear Meromorphic Functions

P. Domínguez, M.A. Montes de Oca and G.J.F. Sienra

8.1 Introduction

In many situations, we need to iterate a function in order to solve a problem. For example, in certain conditions, the logistic function $L_\lambda(x) = \lambda x(1-x)$ models the behaviour of the population in the following manner: if x is the initial population, then $L_\lambda(x)$ indicates the total population at the end of one unit of time u (could be a second, a day, a year, etc.). The parameter λ depends on initial conditions. So $L_\lambda(L_\lambda(z)) = L_\lambda^2(z)$ indicates the total population at the end of $2u$. In order to predict the behaviour of the population, we need to iterate the function, and the *n-th* iteration tells us the total population at nu units of time. Also, the Newton's method which is used to find roots requires an iterative process.

Discrete dynamical systems are very useful for modelling different phenomena and also for a wide variety of problems in mathematics. Usually, we only need an endomorphism of a space X to define the discrete dynamical system, $f : X \to X$. As we will see further, we need to work with functions that are not endomorphism, so

P. Domínguez (✉) · M.A. Montes de Oca
Benemérita Universidad Autónoma de Puebla, FCFM, Ciudad Universitaria, Puebla, Mexico
e-mail: pdsoto@fcfm.buap.mx

M.A. Montes de Oca
e-mail: mobm791223@yahoo.com

G.J.F. Sienra
Facultad de Ciencias, Ciudad Universitaria, Universidad Nacional Autónoma de México, Mexico City, Mexico
e-mail: guillermo.sienra@gmail.com

D. Volchenkov and X. Leoncini (eds.), *Regularity and Stochasticity of Nonlinear Dynamical Systems*, Nonlinear Systems and Complexity 21,
DOI 10.1007/978-3-319-58062-3_8

some special situations have to be considered. When the behaviour of an element in X depends on its size and there is a rotation involved, we expect to have a holomorphic function involved.

The theory of iteration of rational holomorphic functions began in the early twentieth century with P. Fatou and G. Julia. Once the computer became a powerful tool, many more researchers got involved in field and the Mandelbrot set became an icon.

The tools in complex analysis are very important to understand the dynamics of holomorphic functions. Although we will try to focus on the dynamical definitions and results, we expect that readers with basic concepts on complex analysis and topology will be able to understand this work. Also we expect that readers familiarized with holomorphic discrete dynamical systems to find this text useful, since we want to show some differences between transcendental meromorphic functions with at least one non-omitted pole and other kind of meromorphic functions.

Meromorphic functions are divided into two disjoint subclasses:

1. the class of rational functions ***Rat*** and
2. the class of transcendental meromorphic functions ***Mer***.

We recall that rational functions are quotient of polynomial functions. The functions in ***Mer*** without poles define the class of transcendental entire functions, denoted by $\mathscr{E}$. Such kind of functions are analytic on $\mathbb{C}$, which means that its Taylor series converges uniformly on every compact set of $\mathbb{C}$, some examples are e^z and $\sin z$. A transcendental meromorphic function is a quotient of a rational function and transcendental entire functions, the result should not be a rational function. Examples of transcendental meromorphic functions not in class $\mathscr{E}$ are $-e^z + 1/z$, $\sin z + 1/z$ and $\tan z$. For further reading concerning the complex analysis, see [1, 29].

Since we are interested in functions from the complex plane $\mathbb{C}$ to the Riemann sphere $\overline{\mathbb{C}}$, we are mainly interested in singularities with the Picard property:

Definition 8.1 Let $f \in \boldsymbol{Mer}$. We say that $z_0 \in \overline{\mathbb{C}}$ has the Picard property if every punctured neighbourhood of z_0 is mapped into the Riemann sphere infinitely many times except for at most two points.

If $f^{-1}(w)$ is empty, we say that w is an *omitted value* of f; if $f^{-1}(w)$ is finite, we say that w is a *Picard exceptional value* of f.

Functions in ***Mer*** have only one singularity at ∞, and functions in ***Rat*** have none. By the Picard's Property, functions in ***Mer*** may have at most two omitted values or two Picard exceptional values. For example, (i) the exponential map e^z has two omitted values, zero and ∞; (ii) for the function e^z/z, zero is an omitted value and ∞ is a Picard exceptional value, but is not an omitted value and, (iii) the function $-e^z + 1/z$ has no omitted values but ∞ is a Picard exceptional value.

Some dynamical aspects in class ***Mer*** depend on how many points are eventually mapped to ∞, such points are called *pre-poles* of the function. Some dynamical properties of the following subclasses in class ***Mer*** will be presented in this chapter.

1. $\mathscr{E} = \{f \in \textbf{\textit{Mer}}$ has no poles$\}$,
2. $\mathscr{P} = \{f \in \textbf{\textit{Mer}}$ has only one pole and it is an omitted value$\}$ and
3. $\mathscr{M} = \{f \in \textbf{\textit{Mer}}$ has at least one pole which is not an omitted value$\}$.

These three classes are disjoint and the union is ***Mer***. Examples of functions in classes defined above are $e^z \in \mathscr{E}$, $e^z/z \in \mathscr{P}$ and $-e^z + 1/z \in \mathscr{M}$. Observe that $\tan z$ has infinitely many poles, so infinitely many of them are not omitted. In fact, functions with two or more poles are in class $\mathscr{M}$.

A point w is an *asymptotic value* of $f \in$ ***Mer*** if there is a curve $\gamma : [0, \infty) \to \mathbb{C}$ such that $\lim_{t\to\infty} \gamma(t) = \infty$ and $\lim_{t\to\infty} f(\gamma(t)) = w$.

Definition 8.2 The *set of finite singular values* of $f \in$ ***Mer*** denoted by $SV(f)$ is the closure in $\mathbb{C}$ of the set of critical values and finite asymptotic values. The set $SV(f)$ is also known as the set of singularities of the inverse function f^{-1}.

For instance, zero and ∞ are asymptotic values of e^z, since $\gamma_1(t) = -t$ and $\gamma_2(t) = t$ are the corresponding curves mentioned above, so $SV(e^z) = \{0\}$.

It can be proved that all omitted values and Picard exceptional values are asymptotic values. See [12] for the classification of this kind of singularities. The following classes of functions in ***Mer*** can be defined in terms of the set $SV(f)$.

1. $\mathscr{S} = \{f \in \textbf{\textit{Mer}}$ such that $SV(f)$ is finite$\}$.
2. $\mathscr{B} = \{f \in \textbf{\textit{Mer}}$ such that $SV(f)$ is bounded$\}$.

Observe that $\mathscr{S}$ is contained in $\mathscr{B}$. Functions in these classes have special dynamical properties that will be mentioned further. Some examples of functions in class $\mathscr{S}$ are:

(a) $e^z \in \mathscr{S} \cap \mathscr{E}$, where $SV(e^z) = \{0\}$;
(b) $e^z/z \in \mathscr{S} \cap \mathscr{P}$, where $SV(e^z/z) = \{0\}$ and
(c) $\tan z \in \mathscr{S} \cap \mathscr{M}$, where $SV(\tan z) = \{\pm i\}$.
Observe that the functions $\sin z + 1/z$ and $-e^z + 1/z$ are in class $\mathscr{B} - \mathscr{S}$.

From now on, when we mention a function f without specifying in which class it belongs, we mean it belongs to class ***Mer***. In the following sections, we will study the dynamics of some families in class $\mathscr{M} \subset$ ***Mer*** and their Stable and Chaotic sets related to them.

8.2 Holomorphic Discrete Dynamical Systems

As we mentioned before, Fatou and Julia developed the theory of iteration of holomorphic functions at the beginning of the XXth century, and they focused on functions in ***Rat***. For our interests, constant and linear functions are not considered when

rational functions are mentioned. Fatou extended some results of functions in ***Rat*** to functions in class $\mathscr{E}$. At the end of the century, when many researchers recovered interest in the area, the theory was extended by Baker, Kotus and Lü for functions in $\mathscr{M}$. For further reading concerning the dynamics of all the classes of functions mentioned above, see [4, 6]–[9–11, 13, 16, 20, 25, 28].

Let be $f : \mathbb{C} \to \overline{\mathbb{C}}$ a transcendental meromorphic function. We refer to $f^n = f \circ f \circ ... \circ f$ n times as the *n-th iterate* of f. When $n = 0$, we define $f^0(z) = z$ and $f^1(z) = f(z)$. We denote by $\{f^n\}_{n\geq 1}$ the *set of iterations* of f. The sequence $O^+(z, f) = \{z, f(z), \ldots, f^n(z), \ldots\}$ is the *(forward) orbit* of z under f; while $O^-(z, f) = \bigcup_{n\geq 0} f^{-n}(z)$ is the *backward orbit* of z under f. The *full orbit* of z under f is $O(z, f) = O^+(z, f) \cup O^-(z, f)$.

Remark The class ***Rat*** is a semi-group under composition, as well as the class $\mathscr{E}$, while $\mathscr{P}$ or $\mathscr{M}$ is not. However, all the iterations of functions in $\mathscr{P}$ are holomorphic in the punctured plane, $\mathbb{C} - \{0\}$.

Proposition 8.1 *For functions in $\mathscr{M}$, the backward orbit of ∞ is infinite.*

Proof If $f \in \mathscr{M}$, there is a non-omitted pole p. Since f have at most two Picard exceptional values, there are three cases: (a) $f^{-1}(\infty)$ is infinite, (b) $f^{-1}(p)$ is infinite and (c) $f^{-1}(\infty)$ and $f^{-1}(p)$ are finite, then there is $z \in \mathbb{C}$ such that $f(z) = p$ and z is not a Picard exceptional value, so $f^{-3}(\infty)$ is infinite. If $p \in O^-(\infty, f)$, we say that p is a pre-pole of f; therefore, in all cases the set of pre-poles is infinite.

If $f(z) = z$, we say that z a *fixed point* of f. If there is $n \geq 1$ such that $f^n(z) = z$, we say that z is a *periodic point*, when n is the less positive integer for which this happens, we say that the *period* of z is n. If for some $n \geq 1$ the point $f^n(z)$ is periodic and z is not periodic, then we say that z is *pre-periodic*.

The classification of a periodic point z of a holomorphic function is as follows: (a) when $|(f^n)'(z)| < 1$, z is called an *attracting periodic* point, in the case that $|(f^n)'(z)| = 0$, z is a *super-attracting periodic* point; (b) when $|(f^n)'(z)| > 1$, then z is a *repelling periodic* point and (c) when $|(f^n)'(z)| = 1$, then z is an *indifferent periodic* point. Additionally if $(f^n)'(z)$ is a root of the unit, we say that z is *rationally indifferent* or a *parabolic periodic* point, while if it is not a root of the unit and indifferent, it is called *irrationally indifferent*.

The basic problem on discrete dynamical systems is to understand the behaviour of the orbits of a function f. There are many other ways that an orbit may behave, for instance, either it can converge to a point or it can be dense in $\mathbb{C}$. The problem to predict the behaviour of the orbits leads us to define the Stable and the Chaotic sets of a meromorphic function f.

Definition 8.3 Let be $f \in$ ***Mer***. The *Chaotic set* $J(f)$ is the closure of the repelling periodic points and the *Stable set* $F(f)$ is its complement.

In holomorphic dynamical systems, $J(f)$ is known as the Julia set of f and $F(f)$ is known as the Faotu set of f.

In what follows we shall explain what a chaotic behaviour means. Following the idea of Devaney in [13], the chaotic behaviour of f in $J(f)$ is because it satisfies two conditions: (a) the set of repelling points is dense in $J(f)$ and (b) f has topological transitivity on $J(f)$. We say that the function f has *topological transitivity* on $J(f)$ if for any two non-empty open sets U and V in $J(f)$, there is $n \in \mathbb{N}$ such that, $f^n(U) \cap V \neq \emptyset$.

The density of periodic points in $J(f)$ and the topological transitivity imply that f has *sensitivity to initial conditions*. The sensitivity means that for any point $z \in J(f)$, there is an arbitrarily close point w such that eventually their orbits are very different. On the other hand, for every point z in the Stable set, there is a neighbourhood of z where all points behave essentially the same.

We can predict the behaviour of an orbit if we have an initial condition in the Stable set, otherwise we cannot because of the uncertainty to determine with precision the initial conditions when we are modelling a phenomenon. A clear example on how different the orbits behave in $J(f)$ is that in every open set of $J(f)$, on one side, we have points with an orbit dense in the Chaotic set, and on the other hand, we have periodic points.

Equivalently to the Definition 8.3, we have that z is in the Stable set $F(f)$ if $\{f^n\}$ is a normal family of functions on a neighbourhood of z. The Chaotic set $J(f)$ is its complement. For the case when $f \in \mathscr{M}$, as we have discussed before, $O^-(\infty, f)$ has infinite cardinality, therefore the following Proposition is another characterization of $J(f)$ for such functions.

Proposition 8.2 *Let $f \in \mathscr{M}$. The Chaotic set $J(f)$ is the closure of the set of pre-poles.*

We can think of the Stable set as the bigger open set where all the iterates of f are well defined, and the behaviour of the orbits is predictable. Depending on the context, the Stable and Chaotic sets are in the complex plane or in the Riemann sphere. In the latter case, ∞ is always in the Chaotic set for $f \in \boldsymbol{Mer}$.

The Stable and Chaotic sets have the following basic properties:

1. $F(f)$ is open and $J(f)$ is closed,
2. $J(f)$ is non-empty and perfect,
3. $F(f)$ and $J(f)$ are completely invariant (see below),
4. $F(f) = F(f^n)$ and $J(f) = J(f^n)$ for all $n \in \mathbb{N}$.

A set $U \subseteq \mathbb{C}$ is *(forward) invariant* for f if $f(U) \subseteq U$, it is *backward invariant* if $f^{-1}(U) \subseteq U$ and U is *completely invariant* if it is both. For all functions, the set of periodic points $Per(f)$ is invariant, but if a function f has pre-periodic points, then $Per(f)$ is not backward invariant. The union of $Per(f)$ with the set of pre-periodic points is completely invariant, while the set of pre-periodic points is backward invariant but not invariant.

All orbits in one connected component U of the Stable set behave essentially the same. We usually refer to these components as domains of the Stable set.

Definition 8.4 Let $f \in \boldsymbol{Mer}$ and U a component in $F(f)$. We say that U is a *periodic component* if there is $n \geq 1$ such that $f^n(U) \subseteq U$; U is a *pre-periodic component* if there is $n \geq 0$ such that $f^n(U)$ is contained in a periodic component and U is *wandering component* if it is not pre-periodic. U is a wandering component if and only if for all $n < m$, $f^n(U)$ is not contained in $f^m(U)$.

Definition 8.5 Let $f \in \boldsymbol{Mer}$ and U, U_1 be periodic components in $F(f)$.

(a) If n is the smallest positive integer for which $f^n(U) \subseteq U$, we say that U has period n.

(b) Let U_1 with period n, consider the set $C = \{U_1, U_2, \ldots, U_n\}$, where $f(U_i) \subseteq U_{i+1}$ for all $i \in \{1, \ldots, n-1\}$ and $f(U_n) \subseteq U_1$ and all U_i are components in $F(f)$, we say that C is a *cycle* of period n of components in $F(f)$.

The dynamics in periodic components of the Stable set is classified by the following theorem.

Theorem 8.1 ([6]) *Classification of periodic components in the Stable set*

Let $f \in \boldsymbol{Mer}$ and U be a periodic component in $F(f)$ of period n. Then U satisfies one of the following options:

1. *U contains an attracting periodic point z_0 of period n, then $f^{kn}(z) \to z_0$ for all $z \in U$ as $n \to \infty$. U is called the immediate attracting basin of z_0.*
2. *∂U contains a parabolic periodic point z_0 of period n, then $f^{kn}(z) \to z_0$ for all $z \in U$ as $n \to \infty$ and $(f^n)'(z_0) = 1$. U is called either a Leau domain or a parabolic component.*
3. *U is called a Siegel disc if there exists an analytic homeomorphism $\varphi : U \to D$, where D is the unit disc such that $\varphi(f^n(\varphi^{-1}(z))) = e^{2\pi i\alpha} z$ for some $\alpha \in \mathbb{R} - \mathbb{Q}$.*
4. *U is called a Herman ring if there exists an analytic homeomorphism $\varphi : U \to A$, where A is an annulus $A = \{z : 1 < |z| < r\}$, $r > 1$, such that $\varphi(f^n(\varphi^{-1}(z))) = e^{2\pi i\alpha} z$ for some $\alpha \in \mathbb{R} - \mathbb{Q}$.*
5. *U is called a Baker domain if there exists $z_0 \in \partial U$ such that $f^{kn}(z) \to z_0$, for all $z \in U$ as $n \to \infty$, but $f^n(z_0)$ is not defined.*

Let us call z_0 an *absorbing point* of U in the previous theorem in any of the three cases 1, 2 or 5. Using this concept, we are able now to explain more about the previous theorem. In a periodic domain U of the Stable set, there are two possibilities: (a) there is an absorbing point z_0 to which all orbits in U converge under f^n or, (b) U has no absorbing point so f^n behaves essentially as an irrationally rotation. Now if U has an absorbing point z_0, then we have three possibilities: (1) z_0 is in U, (2) $z_0 \in \partial U$ and $f^n(z_0)$ is well defined and (3) $z_0 \in \partial U$ or z_0 is a pre-pole. When U has no absorbing point, then f^n is a rotation on U, and there are two options: U can be either simply connected or U has connectivity 2.

8.2.1 Dynamical Differences Between Classes of Functions in Class Mer

In each class of functions described in the introduction, there are functions which have attracting, parabolic or a Siegel disc component. But there are classes without Herman rings or Baker domains.

By the Maximum Principle Theorem in complex analysis, functions in class $\mathscr{E} \cup \mathscr{P}$ do not have Herman rings. In [18], several examples are presented of functions in class $\mathscr{M}$ with Herman rings.

In [21], Fatou gave the first example for $f \in \mathscr{E}$ of a Baker domain, by this time it was called indetermination domain. For functions in this class, the absorbing point of Baker domains is ∞. Functions in class $\mathscr{M}$ may have a Baker domain with finite absorbing point, for instance, the function $-e^z + 1/z$, see [8]. This is a very important difference between functions in class $\mathscr{E}$ and class $\mathscr{M}$.

Concerning the connectivity of periodic domains in $F(f)$, there is the following Theorem.

Theorem 8.2 ([11]) *If $f \in \boldsymbol{Mer}$, the connectivity of a periodic component in $F(f)$ is 1, 2 or ∞. For invariant components, it is 2 only for Herman rings.*

In contrast to the connectivity of periodic components, it is known that wandering domains may have any connectivity for functions in class $\mathscr{M}$, [7]. For further reading concerning wandering domains, we refer to [3, 5, 23, 30].

Periodic components of functions in class $\mathscr{E}$ are simply connected, so the Chaotic set is never totally disconnected, see [2], but it may contain a totally disconnected subset as the following theorem shows.

Theorem 8.3 ([16]) *Let $f \in \mathscr{M} \cup \mathscr{E}$ and U a component of $F(f)$. If U has connectivity at least five, then the set of singleton components of $J(f)$ is dense in $J(f)$. In particular, if $f \in \mathscr{M}$, this result remains valid if the connectivity of U is three.*

We define the post-critical set of $f \in \boldsymbol{Mer}$ by $SV^+(f) = \bigcup_{n\in\mathbb{N}} f^n(SV(f))$. The relation between singular values of f and the periodic components is as follows.

Theorem 8.4 ([11]) *Let $f \in \boldsymbol{Mer}$ and $C = \{U_1, \ldots, U_{n-1}\}$ a cycle of periodic components in $F(f)$.*

1. *If the domains in C are attracting basins or parabolic domains, then some U_i contains one singular value, say z_0, of f. The point z_0 is not pre-periodic, and if z_0 is periodic, then it is a super-attracting periodic point.*
2. *If the domains in C are Siegel discs or Herman rings, then for all i, ∂U_i is contained in the closure of $SV^+(f)$.*

The relation between $SV(f)$ and Baker domains as well with wandering domains is more complicated, although there is the following result.

Theorem 8.5 ([11]) *If $f \in \mathscr{S}$, then f has no Baker or wandering domains.*

As we mentioned before, all Baker domains for functions in class $\mathscr{E}$ have ∞ as the absorbing point, so they are unbounded, while functions in class $\mathscr{E} \cap \mathscr{B}$ do not have Baker domains. As we will see in Sect. 8.4, in class $\mathscr{M}$, there are functions with bounded Baker domains, with a finite absorbing point even when the functions are in $\mathscr{B}$.

8.3 The Escaping Set in Class *Mer*

In [20], the *escaping set* $I(f)$ of a function f in class $\mathscr{E}$ was defined and in [16] it was generalized to transcendental meromorphic functions as follows.

$$I(f) = \{z \in \mathbb{C} | \lim_{n\to\infty} f^n(z) = \infty \text{ and } f^n(z) \neq \infty \text{ for all } n \in \mathbb{N}\}.$$

If $z \in I(f)$, we say that z is an *escaping point* of f. Observe that escaping points are not pre-poles.

Theorem 8.6 ([16]) *For $f \in$ **Mer**, $I(f)$ satisfies the three following properties:*

1. $I(f) \neq \emptyset$;
2. $I(f) \cap J(f) \neq \emptyset$ *and,*
3. $\partial I(f) = J(f)$.

We refer to these as the basic properties of the escaping set. The third property is very useful in programming the computer to visualize the Chaotic set as we will see in the following section. Observe that $I(f)$ is neither a closed set nor an open set, since periodic points and escaping points in the Chaotic set accumulate on each other.

If f has no Baker or wandering domains (as it is the case for functions in $\mathscr{S}$), then $I(f) \subset J(f)$ and then $\overline{I(f)} = J(f)$. If U is an invariant Baker domain of f, then $U \subset I(f)$. Baker domains of entire functions are contained in the escaping set. Also wandering domains may be contained in $I(f)$ or not.

There are examples for which the components of $I(f)$ may be points or curves. We will show some examples in the following section.

Theorem 8.7 ([31]) *Let $f \in$ **Mer** of finite order.*

1. *If f has finitely many poles and $f \in \mathscr{B}$, then every escaping point of f can be connected with ∞ or to a pre-pole of f by a curve contained in $I(f)$.*
2. *If f has a logarithmic singularity over ∞, then $J(f)$ contains uncountable many curves to ∞ contained in $I(f)$.*

The set of escaping curves contained in $J(f)$ connected with the same pre-pole p is called an *escaping bouquet* at p. We call its closure a *bouquet* of the Chaotic set at p. As an example of these definitions, for the exponential family $E_\lambda(z) = \lambda e^z$

for $0 < \lambda < 1/e$, we have that $J(f)$ is one bouquet at ∞ and it is a Cantor bouquet; this kind of set has special topological and dynamical properties. For more about Cantor bouquets, see [14]. In the next section, we will show more examples involving escaping bouquets.

8.4 Three Families of Functions in Class $\mathscr{M} \subset Mer$

In this section, we present some results concerning the dynamics of three families in class $\mathscr{M}$; these are some examples known in this class. In what follows we introduce the families which has been investigated in [19, 22, 26, 27]. In all the families below, λ and μ are nonzero complex numbers and k is a nonzero integer.

(a) $T_\lambda(z) = \lambda \tan z$,
(b) $S_{\lambda,\mu,k}(z) = \lambda \sin z + \frac{\mu}{z-k\pi}$, and
(c) $E_{\lambda,\mu}(z) = \lambda e^z + \frac{\mu}{z}$.

We recall that when we study the dynamics of functions $f \in \mathscr{M}$, we are interested in the behaviour of the orbits and also in special sets; some examples are the Stable set $F(f)$, the Chaotic set $J(f)$, the escaping set $I(f)$ and their components. When we identify special sets from a dynamical point of view in the domain of a function, we call it a *dynamical plane* of f. As the dynamics of a function f become more complicated to describe, the computer helps us to visualize the dynamical plane of f. So they are very helpful for explaining the dynamics of the function for a broader public, as well as for research and artistic purposes, since many of them are visually interesting.

In order to get the dynamical plane with the computer, we can use the set $I(f)$ to depict $J(f)$ and $F(f)$. Colours in the dynamical plane mean that such points have an iteration with its modulus bigger than a selected value, and we refer to this value as the escaping value of the dynamical plane.

In Sects. 8.4.1, 8.4.2 and 8.4.3, in all the dynamical planes, the colour discs show where are some pre-poles. Usually $F(f)$ is on black, otherwise it is pointed out, $J(f)$ is on colour and the points on white show an orbit (the white lines show the order of the iteration). Naturally, these are approximations, remember that the Chaotic set is either the whole complex plane or its interior is empty.

8.4.1 The Tangent Family

For the family $T_\lambda(z) = \lambda \tan z$, in the context of complex analysis, ∞ is not an isolated singularity since it is an accumulation point of poles. For us, the only singularity is ∞. It is in class $\mathscr{S}$, so it has no Baker or wandering domains. It has no critical points, and $\pm\lambda i$ are the only asymptotic values. Since T_λ is symmetric respect the origin, the

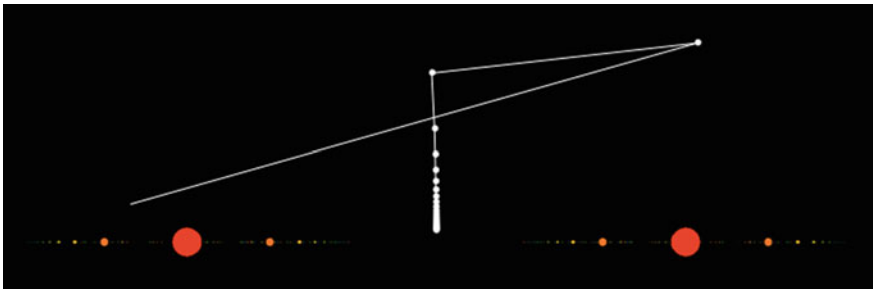

Fig. 8.1 Dynamical plane of $0.9 \tan z$

behaviour of these singular values is the same. So T_λ may have at most two periodic cycles in the Stable set. Also because of this symmetry, the Stable and Chaotic sets are symmetric respect to zero.

As mentioned before, in class $\mathscr{M}$ there are functions for which the Chaotic set is totally disconnected. The following result shows that the family T_λ presents a dichotomy. The Chaotic set is either a totally disconnected or a connected set.

Theorem 8.8 ([22]) *For T_λ either*

1. $|\lambda| < 1$, *the Chaotic set of T_λ is a Cantor set in the Riemann sphere and the Stable set is a single completely invariant component infinitely connected U, or*
2. $|\lambda| \geq 1$, *the Chaotic set of T_λ is connected and the Stable set consists of either exactly two components or infinitely many simply connected components.*

Observe that for all λ, zero is a fixed point and its derivative is λ. Thus, if $|\lambda| < 1$, then U is the immediate attracting basin of zero.

In Fig. 8.1, for the function $T_{0.9}$, the Chaotic set is a Cantor set in the Riemann sphere (a perfect and totally disconnected set) contained in the real line. Zero is an attracting fixed point, and the Stable set is a single completely invariant component U, the orbits of all points in U converge to zero. So U is an attracting basin with connectivity ∞ (U has an uncountable set of holes).

When $\lambda = 1$, zero is a parabolic fixed point and $F(T_1)$ is the union of the upper and the lower half planes, which are completely invariant simply connected parabolic domains, and $J(T_1)$ is the real line.

In Fig. 8.2, we consider the function $2 \tan z$, the Chaotic set is the real line, so it is a connected set. The Stable set is the union of two completely invariant components, each one is an attracting basin simply connected.

In Fig. 8.3, for the function $2i \tan z$, the Chaotic set is also connected, so all the stable components are simply connected, but in this case the Stable set has infinitely many of them. Experimentally we find that this function has two attracting cycles of period two $\{A, B\}$ and $\{U, V\}$. The orbit depicted in the Figure starts in a preimage of V.

In contrast to Fig. 8.3, if we use a bigger escaping value to compute the dynamical plane, the Chaotic set begins to shade away, see Fig. 8.4. If we use even bigger

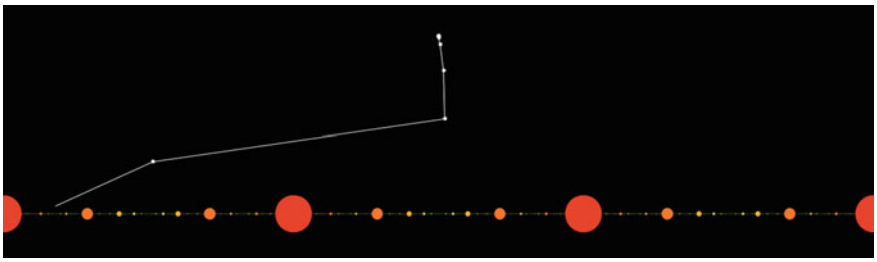

Fig. 8.2 Dynamical plane of $2\tan z$

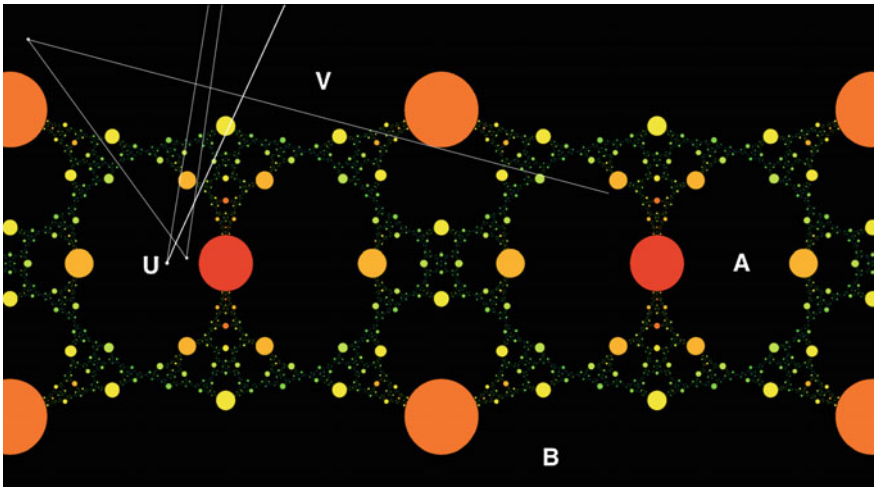

Fig. 8.3 Dynamical plane of $2i\tan z$

escaping values, $J(f)$ seems to vanish completely. One reason for this is that in some cases, it is bigger the number of iterations needed for a escaping point to grow more than the escaping value. On the other hand, for a small escaping value M, there are points that in the first iterations they grow bigger than M, but they are not really escaping points of f.

8.4.2 The Sine Family with One Pole

The function $S_{\lambda,\mu,k}(z) = \lambda \sin z + \frac{\mu}{z-k\pi}$, for nonzero λ and μ complex numbers has only one pole which is not an omitted value. It has no finite asymptotic values, but it has infinitely many critical values which accumulate at $\pm\lambda$. So $S_{\lambda,\mu,k}$ is in class $\mathscr{B}$ and it is not in class $\mathscr{S}$.

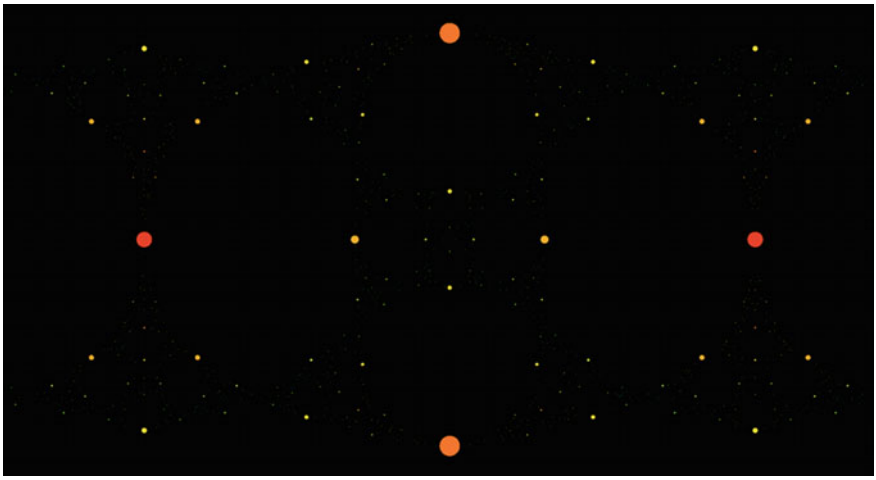

Fig. 8.4 Dynamical plane of $2i \tan z$ computed with a bigger escaping value

Theorem 8.9 ([19]) *Let λ, μ be real, $0 < |\lambda| < 1$ or $\lambda = 1$, $0 < \mu$ sufficiently small and k a nonzero integer. The family $S_{\lambda,\mu,k}$ has an attracting completely invariant component in the Stable set which is multiply connected.*

The region T, which is a horizontal strip intersecting the complement of a disc containing the pole, is invariant and contains all the critical values and an attracting fixed point. Therefore, T is contained in an attracting component A. So the functions do not have more periodic Stable components. Also in [19], it is proved that the functions do not have wandering domains. Since A is invariant and not simply connected, because of Theorem 8.2, the connectivity is ∞.

As a consequence of Theorem 8.3, the components of the Chaotic set with one point are dense in $J(S_{\lambda,\mu,k})$.

If $\lambda = 0.75$, $\mu = 0.75\pi^2/(16\sqrt{2})$ and $k = 2$, then $J(S_{\lambda,\mu,k})$ is disconnected but not totally disconnected. From Theorem 8.7, we know that the escaping set contains an uncountable set of curves attached to any pre-pole; these curves are contained in the Chaotic set. The Stable set is a single completely invariant attracting basin A depicted in Fig. 8.5. Also in its dynamical plane, we can see the bouquet containing the pole, which is the small orange decoration on the right side surrounded by A. We expect that the big orange decorations are part of the bouquet at ∞.

8.4.3 The Exponential Family with One Pole

The function $E_{\lambda\mu}(z) = \lambda e^z + \mu/z$ has one non-omitted pole at zero and has infinitely many critical values accumulating at zero; zero is the only finite asymptotic value. So this function is in classes $\mathscr{M}$ and $\mathscr{B}$ but not in $\mathscr{S}$. The preimages of zero are

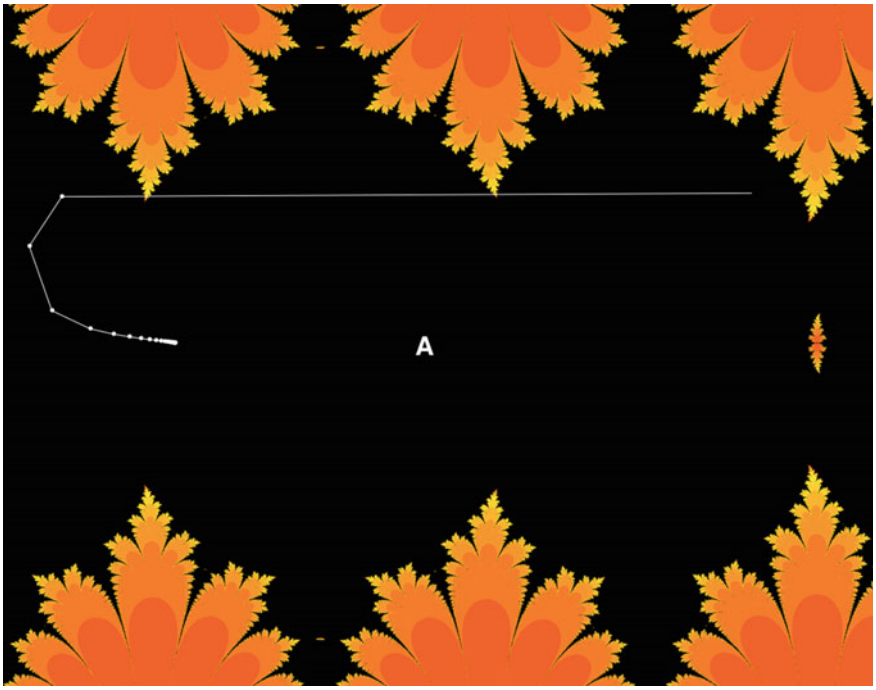

Fig. 8.5 Dynamical plane of $0.75 \sin z + \frac{0.75\pi^2}{16\sqrt{2}(z-2\pi)}$

contained in a left-hand semi-plane. This exponential with one pole has infinitely many fixed points, and only a finite number of them are non-repelling. The repelling fixed points are contained in a right-hand semi-plane.

In [8], it is shown that the function $E_{-1,1}$ has a cycle of period two of Baker domains. So the following result is a generalization for a family of this kind of exponentials with one pole.

Theorem 8.10 ([26]) *If $Re(\lambda) < 0$ and $|Im(\lambda)| < \frac{1}{2}|Re(\lambda)|$, then $E_{\lambda,\mu}$ has a cycle of period two of Baker domains. For one of them ∞ is the absorbing point and the other one has zero as the absorbing point.*

To prove it, a non-empty open set W is shown to be $E^2_{\lambda,\mu}$-$invariant$. This happens because the distance from $E^2_{\lambda,\mu}(z)$ to $z + \lambda$ is sufficiently small. W is not empty since it contains $(-\infty, a]$ for some negative real number a. All points in W converge to ∞ with the even iterations of $E_{\lambda,\mu}$, so W is contained in a Baker domain, and all points in W converge to zero with the odd iterations of the function. Therefore, the Baker domain A is of period two with ∞ as its absorbing point, and there is B a Baker domain with zero as its absorbing point.

Even more, if $Re(\lambda) < 0$ and $|Im(\lambda)| < \frac{1}{2}|Re(\lambda)| - 4$, then A has infinitely many critical points and B has infinitely many critical values.

Concerning the connectivity of these Baker domains, there is the following result.

Theorem 8.11 ([27]) *For all* (λ, μ) *in a neighbourhood of* $(-20, 1/4)$*, the Baker domains of* $E_{\lambda,\mu}$ *are infinitely connected.*

The proof consists in showing that a closed simple curve γ is contained in one of the Baker domains B. One of the preimages of γ in A contains a simple closed curve surrounding a region with a preimage of zero and no asymptotic values, so A is not simply connected. Using the following result, we conclude that A and B have at least connectivity three.

Theorem 8.12 ([27]) *Let* f *be a meromorphic function with finitely many asymptotic values. If* U *and* W *are components of the Fatou set such that* $f(U) \subseteq W$ *and* W *has connectivity* ∞*, then* U *is multiply connected.*

Since the connectivity of periodic components is 1, 2 or ∞ and the connectivity of A and B is at least three, then their connectivity is ∞. Again, as a consequence of Definition 8.3, the components of the Chaotic set with one point are dense in $J(E_{\lambda,\mu})$.

The function $E_{-20,1/4}$ has a cycle of period two of Baker domains with connectivity ∞, one of them with infinitely many critical points and the other one with infinitely many critical values. Also from Theorem 8.7, we know that the escaping set contains an uncountable set of curves attached to any pre-pole; these curves are contained in the Chaotic set.

In Fig. 8.6, the cycle is $\{A, B\}$, the points in A converge to ∞ with the second iteration of the function and points in B converge to zero. So the modulus of points

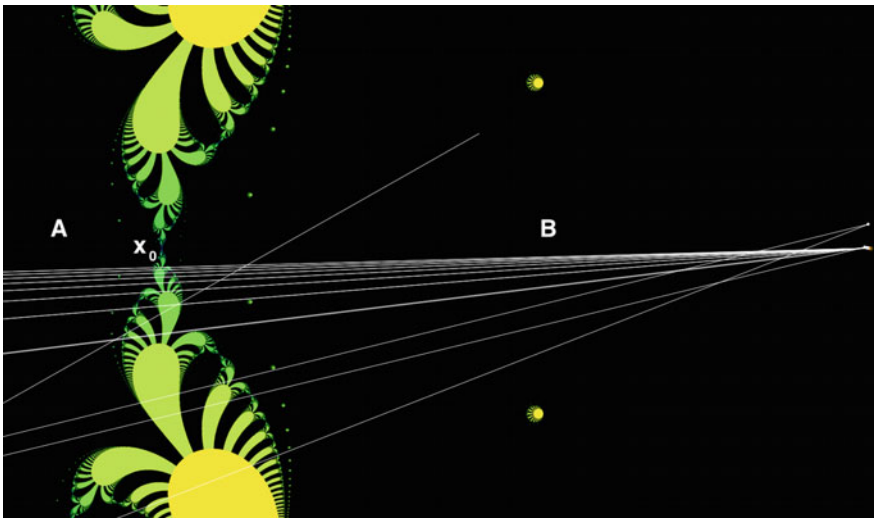

Fig. 8.6 Dynamical plane of $-20e^z + \frac{1}{4z}$

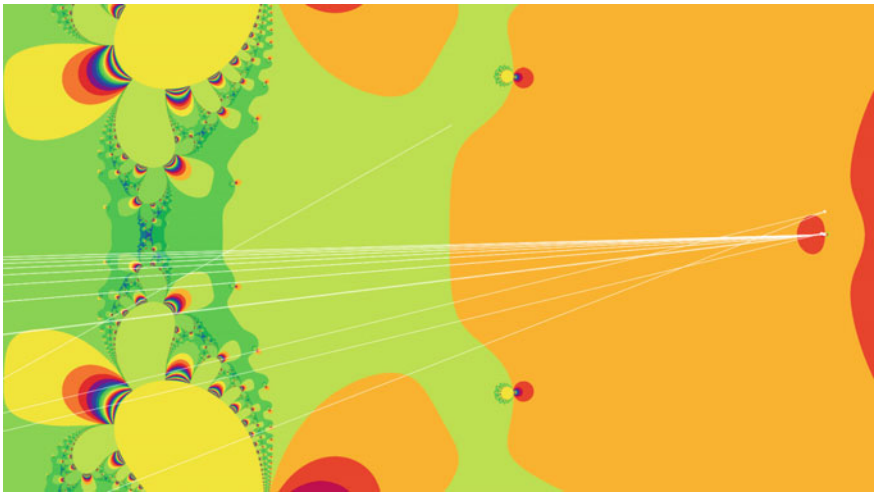

Fig. 8.7 Dynamical plane of $-20e^z + \frac{1}{4z}$ with a smaller escaping value

in A and B eventually grow bigger than any selected escaping value, fortunately for this kind of functions the orbits in Baker domains grow slow, so with an appropriate escaping value the computer choose black for points in these domains. Observe that points in these Baker domains are not in the escaping set of the function since its orbits do not converge to ∞. See [24] for more about the dynamics in the Baker domains.

Also there is a negative repelling fixed point x_0 in the real line, $(-\infty, x_0)$ is contained in A and $(x_0, 0)$ is contained in B. Using this, it is shown that B is unbounded. Also in the dynamical plane of $E_{-20,1/4}$, we can see small decorations which are the bouquets of different pre-poles. We expect that the big ones are part of the bouquet at ∞.

In Fig. 8.7, the dynamical plane of $-20e^z + 1/(4z)$ is displayed again but changing the escaping value for a smaller one, so points in Baker domains are in colour.

The family $E_{\lambda,\mu}$ has a bifurcation concerning the connectivity of the Baker domains. There is a function in this family with a cycle of period two of Baker domains simply connected. Also the Baker domain B in Fig. 8.8 is bounded and is surrounded by an attracting basin U which has connectivity ∞. Remember that entire transcendental functions do not have bounded Baker domains.

8.5 Bifurcation Diagrams

For any one family of functions, we want to understand the locus of the bifurcations, it means, the set of parameters for which the functions change their dynamics. It is

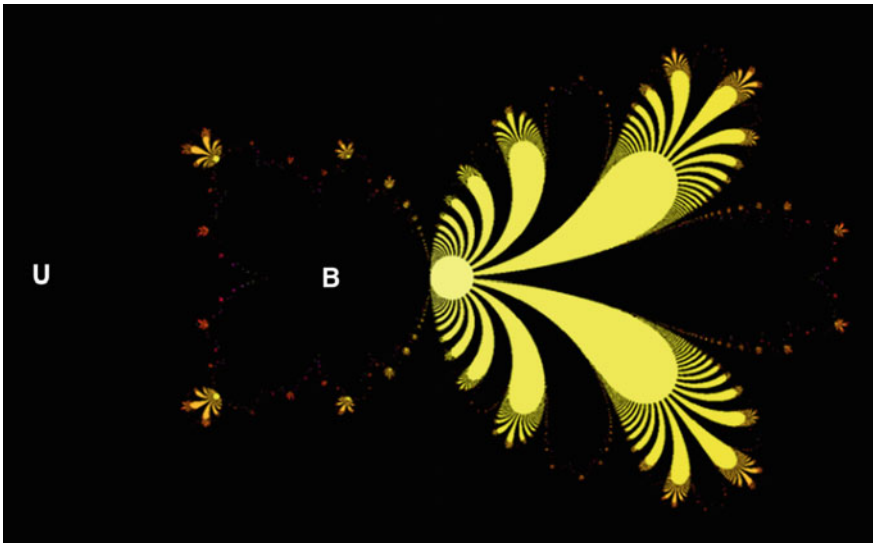

Fig. 8.8 Dynamical plane of a function $\lambda e^z + \frac{\mu}{z}$ for small values λ and μ

beyond the scope of this text to precise the meaning of it, but for instance, there is a bifurcation in the family if the number of attracting cycles change, or their period or their classification. Now we are dealing with the second main type of problem when we study dynamics; it is how the dynamics change when a function is perturbed.

When the family has one complex parameter, the family is the parameter plane. So when we find special sets from a dynamical point of view and their properties, we are studying the dynamics of the family. Sometimes the computer is very helpful to depict those sets, we refer to such figures as parameter planes.

With Theorem 8.8, we can say that the unit circle centred at zero is contained in the locus of bifurcations of $T_\lambda(z) = \lambda \tan z$. Observe that for any λ_0 such that $|\lambda_0| = 1$, there is λ arbitrarily close to λ_0 such that T_{λ_0} and T_λ have different dynamics. That is why we say that the family has a bifurcation at λ_0.

The dynamics of the exponential family $E_\lambda(z) = \lambda e^z$ has been studied by several authors. The family $E_{\lambda,\mu}(z) = \lambda e^z + \mu/z$ can be thought as a singular perturbation of E_λ, in the same way that a function like $z^2 + c/z$ is a singular perturbation of z^2. For such kind of perturbations, see [15]. So $S_{\lambda,\mu,k}(z) = \lambda \sin z + \mu/(z - k\pi)$ is a singular perturbation of $S_\lambda(z) = \lambda \sin z$, for the dynamics of the latter family see [17]. The problem is that the singular perturbed families have more than one complex parameter, so the parameter set is no longer a subset of the plane.

To study the bifurcations of such kind of families is more complicated. Not only because of the dimension of the parameter set but also the families E_λ, S_λ and T_λ have either one singular value or have two. In the latter case, the functions behave symmetrically, so it is necessary to follow the orbit of only one singular value to study the dynamics of the families. The problem to understand the bifurcations of

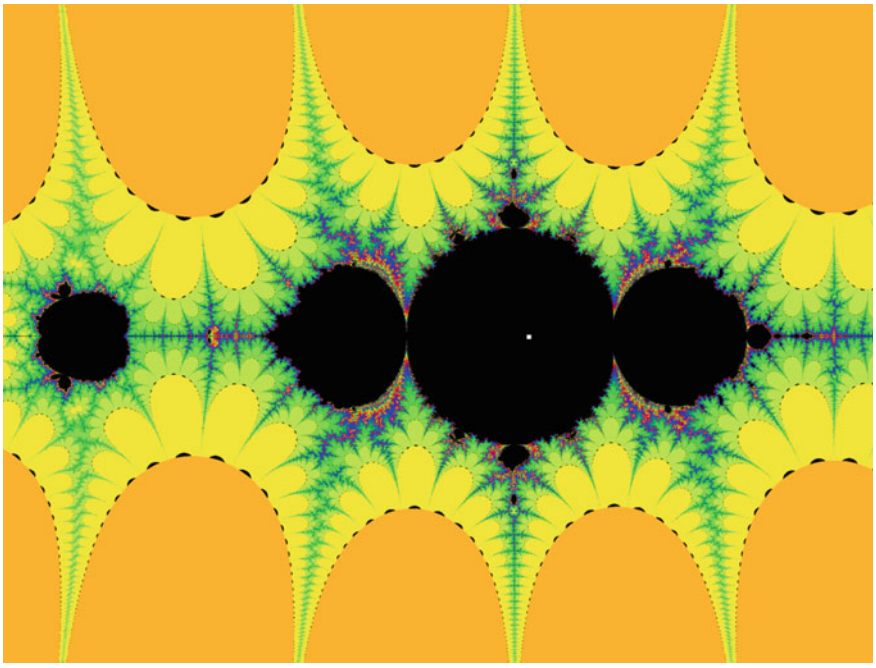

Fig. 8.9 A cut of the parameter set of the family $S_{\lambda,\mu,k}$

$E_{\lambda,\mu}$ and $S_{\lambda,\mu,k}$ is much more complicated because $SV(f)$ is infinite. Despite the difficulties, below we present some cuts of the parameter sets of the families $E_{\lambda,\mu}$ and $S_{\lambda,\mu,k}$.

If in the family $S_{\lambda,\mu,k}$ we set the critical point to be $z_0 = \frac{7}{4}\pi$, the pole to be 2π and $k = 2$, we have $\mu = \frac{\pi^2\lambda}{16\sqrt{2}}$. Thus, we obtain the sub-family $S_{\lambda,z_0,2}(z) = \lambda \sin z + \frac{\pi^2\lambda}{16\sqrt{2}(z-2\pi}$. Figure 8.9 is the parameter plane of this sub-family, which is a cut of the parameter set of $S_{\lambda,\mu,k}$. On colour are the parameters for this sub-family for which the orbit of the critical point is unbounded. Therefore, the region on black shows the parameters for which the orbit of z_0 is bounded. The boundary is the bifurcation locus for this sub-family, which is contained in the locus of the original family. The white point indicates the parameter $\lambda = 0.75$, for which we obtained the dynamical plane in the previous section.

The following parameter plane is a special cut of the parameter space of $E_{\lambda,\mu}$, since the axis is for real parameters λ and μ. Instead of fixing a critical point, follow its orbit. In Fig. 8.10, the curves show for which parameters the family has a real fixed point with real parameters. The blue line L_{-1} is for which the fixed point has derivative -1, for the black curve L_1 the derivative of the fixed point is 1, so in both cases, the family has an indifferent real fixed point. The red curve L_0 are the parameters for which the family has a super-attracting fixed point. Then the regions

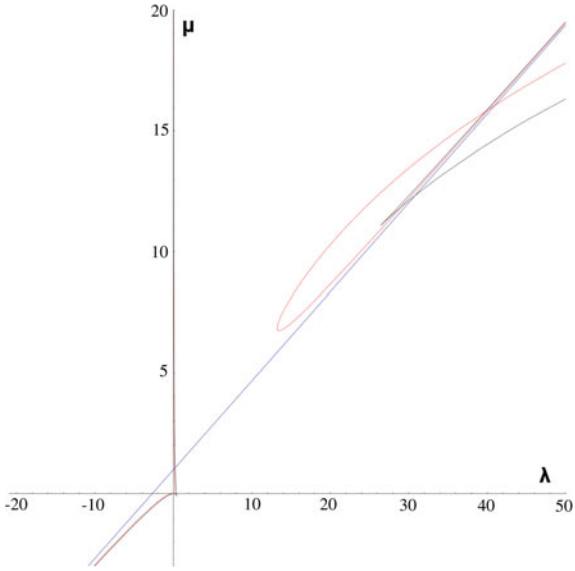

Fig. 8.10 A real section of the parameter set of the family $\lambda e^z + \mu/z$

delimited by L_{-1} and L_1 containing L_0 is the set of real parameters for which the family has a real-attracting fixed point. We call this parameter plane a real section of the parameter set of the family $E_{\lambda,\mu}$.

Open Problems

While this chapter was under preparation, the following interesting questions arise.

- Is there non-invariant components of connectivity 2 which are not Herman rings in class $\mathscr{M}$?
- Let $\{U_1, \ldots, U_n\}$ is a cycle of components in the Stable set. Are all U_i of the same dynamical type?
- Let $S_{\lambda,\mu,p} = \lambda \sin z + \frac{\mu}{z-p}$, p any complex number. How can we compute the set of parameters for which the function $S_{\lambda,\mu,p}$ has a completely invariant multiply connected attracting basin?
- Let $E_{\lambda,\mu}$ the family as in Sect. 8.5. For which parameters the Baker domains are completely invariant for the second iteration of the function?
- How can we compute the set of parameters for which the function $E_{\lambda,\mu}$ has a cycle of multiply connected Baker domains?
- Find dynamical planes for functions in class $\mathscr{M}$ with either multiply connected parabolic domain, a Siegel disc, Herman ring or wandering domain.
- Is there a non-invariant Baker domain with connectivity 2 for a function in class $\mathscr{M}$?
- Is there a non-invariant attracting basin with connectivity 2 in class $\mathscr{M}$?
- Is there a non-invariant parabolic domain with connectivity 2 in class $\mathscr{M}$?

References

1. Ahlfors, L.: Complex Analysis, 2nd edn (International Student Edition). McGraw-Hill, New York (1966)
2. Baker, N.: The domains of normality of an entire function. Ann. Acad. Sci. Fenn. Ser. A I Math. **1**, 277–283 (1975)
3. Baker, N.: An entire function which has wandering domains. J. Aust. Math. Soc. Ser. A **22**, 173–176 (1976)
4. Baker, N.: Iteration of meromorphic functions: an introductory survey. Lectures on Complex Analysis, pp. 1–17. World Scientific, Singapore (1987)
5. Baker, N.: 'Wandering domains for maps of a punctured plane. Ann. Acad. Sci. Fenn. **12**, 191–198 (1987)
6. Baker, N., Kotus, J., Lü, Y.: Iterates of meromorphic functions I. Ergod. Theory Dyn. Syst. **11**, 241–248 (1991)
7. Baker, N., Kotus, J., Lü, Y.: Iterates of meromorphic functions II: examples of wandering domains. J. Lond. Math. Soc. **42**, 267–278 (1990)
8. Baker, N., Kotus, J., Lü, Y.: Iterates of meromorphic functions III: preperiodic domains. Ergod. Theory Dyn. Syst. **11**, 603–618 (1991)
9. Baker, N., Kotus, J., Lü, Y.: Iterates of meromorphic functions IV: critically finite functions. Results Math. **22**, 651–656 (1992)
10. Beardon, A.F.: Iteration of Rational Functions. Springer, New York (1991)
11. Bergweiler, W.: Iteration of meromorphic functions. Bull. Am. Math. Soc. (N. S.) **29**, 151–188 (1993)
12. Bergweiler, W., Eremenko, A.: On the singularities of the inverse to a meromorphic function of finite order. Rev. Mat. Iberoam. **11**(2), 355–373 (1995)
13. Devaney, R.: An Introduction to Chaotic Dynamical Systems, 2nd edn. Addison-Wesley, Reading (1989)
14. Devaney, R.: Complex Exponential Dynamics, preprint. Published in (Broer et al. 2010) (2006)
15. Devaney, R., Holzer, M., Look, D., Moreno, M., Uminsky, D.: Singular perturbations of z^n. Lond. Math. Soc. Lect. Note Ser. **348**, 111–137 (2008)
16. Domínguez, P.: Dynamics of transcendental meromorphic functions. Ann. Acad. Sci. Fenn. Math. **23**, 225–250 (1998)
17. Domínguez, P., Sienra, G.: A study of the dynamics of the family $\lambda sen z$. Int. J. Bifurc. Chaos **12**, 2869–2883 (2002)
18. Domínguez, P., Fagella, N.: Existance of Herman rings for meromorphic functions. Complex Var. Theory Appl. **49**(12), 851–870 (2004)
19. Domínguez, P., Vázquez, J., Montes de Oca, M.A.: A study of the dynamics of the family $f_{\lambda,\mu} = \lambda \sin z + \frac{\mu}{z-k\pi}$ where $\lambda, \mu \in \mathbb{R} - \{0\}$ and $k \in \mathbb{Z} - \{0\}$. Disc., Nonlinearity, and Com. (2016)
20. Eremenko, A.E.: On the iteration of entire functions. Dyn. Syst. Ergod. Theory Banach Center Publ. **23**, 339–345 (1989)
21. Fatou, P.: Sur le équations fonctionelles. Bull. Soc. Math. Fr. **47**, 161–271 (1919); **48**, 33–94, 208–314 (1920)
22. Keen, L., Kotus, J.: Dynamics of the family $\lambda \tan z$. Conform. Geom. Dyn. **1**, 28–57 (1997)
23. Kisaka, M., Shishikura, M.: On multiply connected wandering domains of entire functions. In: Rippon, P., Stallard, G. (eds.) Trascendental Dynamics and Complex Analysis. LMS Lecture Note Series, vol. 348, pp. 217–250. Cambridge University Press, Cambridge (2008)
24. König, H.: Conformal conjugacies in Baker domains. J. Lond. Math. Soc. **59**, 153–170 (1999)
25. Milnor, J.: Dynamics in One Complex Variable. Annals of Mathematics Studies, vol. 160, 3rd edn. Princeton University Press, Princeton (2006)
26. Montes de Oca, M., Sienra, G., King, J.: Baker domains of period two for the family $f_{\lambda,\mu}(z) = \lambda e^z + \mu/z$. Int. J. Bifurc. Chaos **25**(5), 1–8 (2014)
27. Montes de Oca, M.: Aspectos dinámicos de la familia $f_{\mu,\lambda}(z) = \lambda e^z + \frac{\mu}{z}$, PhD thesis Universidad Naciona Autónoma de México (2015)

28. Morosawa, S., Nishimura, Y., Taniguchi, M., Ueda, T.: Holomorphic Dynamics. Cambridge University Press, Cambridge (2000)
29. Remmert, R.: Theory of Complex Functions, 2nd edn. Springer, Berlin (1991)
30. Rippon, P., Stallard, G.: On Multiply Connected Wandering Domains of Meromorphic Functions. arXiv:0711.2582v1 [math.CV] (2007)
31. Rottenfusser, G., Rückert, J., Rempe, L., Schleicher, D.: Dynamics Rays of Bounded-Type Entire Functions, pp. 1–42. arXiv:0704.3213.v2 [math.DS] (2009)

Chapter 9
Dynamics of Oscillatory Networks with Pulse Delayed Coupling

Vladimir Klinshov, Dmitry Shchapin, Serhiy Yanchuk and Vladimir Nekorkin

Introduction

The networks of pulse-coupled oscillators have been widely studied as models for various physical and biological systems such as spiking neurons [1–3], fireflies communicating by short light pulses [3–5], impacting mechanical oscillators [6], electronic oscillators [7–10], optical systems [11–13], cardiac [14–18], respiratory [19, 20] or circadian [21] rhythms. In all these cases, the common feature is that the oscillators exchange signals which have the duration much smaller than the intrinsic period of the oscillations.

A common approach to describe the interaction between the oscillators in such networks is to use the so-called phase resetting curves (PRC) [3, 5, 22–27]. In the framework of this concept, each oscillator is characterized by its phase only, and the PRC describes how the input pulse advances or delays the oscillator depending upon in what phase it is applied. In its representation as a phase oscillator, each oscillatory system possesses a characteristic PRC corresponding to a particular stimulus. Hence, parameter changes in the neuron or the stimulus are reflected by changes in the shape of the PRC. Pulse-coupled systems can be considered either as stand-alone models, or as approximations of more complex systems. Among the advantages of such models is their simple numerical implementation, their lower dimension, as well as the possibility to adjust the PRC numerically and measure it experimentally [28–32]. A number of important results have been obtained for the model of pulse-coupled

V. Klinshov · D. Shchapin · V. Nekorkin (✉)
Institute of Applied Physics of the Russian Academy of Sciences,
46 Ul'yanov Street, 603950 Nizhny Novgorod, Russia
e-mail: vnekorkin@neuron.appl.sci-nnov.ru

S. Yanchuk
Institute of Mathematics, Technical University of Berlin, Straße des 17. Juni 136,
10623 Berlin, Germany

D. Volchenkov and X. Leoncini (eds.), *Regularity and Stochasticity of Nonlinear Dynamical Systems*, Nonlinear Systems and Complexity 21,
DOI 10.1007/978-3-319-58062-3_9

oscillators. The stability of synchronous [5, 26, 33–35] and asynchronous [36] states has been studied, as well as stable clusters [22, 37–39] and splay states [40].

In realistic networks of various physical nature, pulses propagate with finite speed leading to nonzero coupling time delays. The influence of delays has been proven significant in many cases and may result in new dynamical phenomena, such as multi-stability [33, 41–43], oscillations death [44], strong and weak chaos [45], and other complicated regimes [46–50]. The particular attention was paid to the influence of the delay on synchronization of oscillatory networks, especially neural networks. Synchronization of brain areas is believed to be crucial for cognitive functions and to act as an integrative mechanism bringing a widely distributed set of neurons together into a coherent ensemble for a cognitive act [51]. For example, synchronous γ-rate activity of various areas in visual cortex underlies binding of numerous features of an object for its perception [52]. Synchronization is also assumed to be involved in memory and learning [53], motor control [54], and, on the opposite site, in pathologies such as Parkinson's disease or schizophrenia [55].

In this chapter, we present our results on networks of phase oscillators with pulse delayed coupling. This chapter is organized as follows. In Sect. 9.1, we introduce the general model of a network of phase oscillators with pulse delayed coupling. We also introduce the approach which allows to reduce such the system to a finite-dimensional map. Further, we utilize this technique to study networks of various configurations. We study the so-called jittering regimes of one oscillator with pulse delayed feedback, in Sect. 9.2, and jittering waves in rings of oscillators in Sect. 9.3. Then, we investigate mutual synchronization of two oscillators, for the case of small frequency detuning in Sect. 9.4 and large detuning in Sect. 9.5. In Sect. 9.6, we illustrate the richness of the dynamics of even small networks on the example of four oscillators with heterogeneous coupling. Section 9.7 is devoted to global synchronization of large networks with all-to-all coupling.

9.1 General Model and the Reduction Technique

In the most general form, such a network is described by the following system:

$$\frac{d\varphi_j(t)}{dt} = \omega_j + \sum_{k=1}^{N} \left(f_{jk}(\varphi_j(t)) \sum_{t_k^p} \delta(t - t_k^p - \tau_{jk})) \right). \tag{9.1.1}$$

Here, $j = \overline{1, N}$, φ_j, and ω_j are the phase and the intrinsic frequencies of the jth oscillator. When the jth oscillator reaches the threshold $\varphi_j = 1$, it emits a pulse and resets its phase to zero. The functions $f_{jk}(\varphi)$ are the phase resetting curves describing the interaction between the kth and the jth oscillators. When a pulse comes from the kth oscillator to the jth oscillator, it causes the instant shift of the phase of the latter one $\Delta\varphi_j = f_{jk}(\varphi_j)$. Note that the topology of the network is reflected by these functions as well: If there is no link from the kth oscillator to the jth one, the

function f_{jk} is set to zero. The values τ_{jk} are the delays for pulses to come from the kth oscillator to the jth one. The first sum in the right part of (9.1.1) runs over all the oscillators and the second sum runs over all the moments t_k^p when the kth oscillator produces pulses.

The common approach to study the networks of pulse-coupled oscillators is the construction of maps from one discrete event to the next event. In the case of zero delays, these discrete events are related to emitting of the pulse by one on the oscillators which causes immediate perturbation of the phases of the other oscillators. In this case, all information which is necessary to predict the dynamics of the network in future is contained in the instant values of the phases $\varphi_j(t)$. In other words, the values of $\varphi_j(t)$ fully characterize the state of the system. These values allow to define which of the oscillators emits pulse next and to calculate what phase shifts it causes in the other oscillators [5, 22, 23, 26, 56–58].

In the presence of delays, the situation becomes more complicated. The information about the instant values of the phases is now not enough to predict the future dynamics which is influenced by the signals produced in the past. Thus, the information on the past activity of the network is required to describe the full state of the system and to construct the map. The larger the delays, the longer the time interval in the past has to be considered. Because of the pulsatile nature of the coupling, the only important information about the past activity of the network is the timing of the produced pulses. The question is what exact number of the recently produced pulses past have to be taken into account and if this number is finite or not.

In [59], we have defined the conditions under which just a finite number of the recent pulses influence the future dynamics of the network. Under these conditions, system (9.1.1) can be characterized by the current phases φ_j and the timing t_k^p of the last P pulses of each oscillator. The conditions are as follows:

1. The coupling is not very strong, namely

$$F < \frac{1}{2N}, \tag{9.1.2}$$

where $F = \max\limits_{j,k} \max\limits_{\varphi\in[0;1]} f_{jk}(\varphi)$.

2. For $t \in [-\infty; t_0]$, the oscillators produced pulses sparsely such as for all k and p

$$t_k^p - t_k^{p-1} \geq \Theta, \tag{9.1.3}$$

where $\Theta = (1 - 2FN)/\Omega$, $\Omega = \max\limits_{j,k} \omega_j$.

Then, for any given time $t > t_0$ not more than P, recent pulses produced by each oscillator can influence the future dynamics of the network, with P given by

$$P = 1 + \left[\frac{T}{\Theta}\right], \tag{9.1.4}$$

where $T = \max\limits_{j,k} \tau_{jk}$.

Thus, the state of system (9.1.1) can be fully described by the following set of $N(P+1)$ numbers:

1. Phases φ_j of the oscillators.
2. The timing t_j^p of the latest P produced pulses of each oscillator.

For further studying, it is convenient to introduce the state vector

$$\xi(t) = \left(\varphi_1(t), \varphi_2(t), ..., \varphi_N(t), x_1^1, x_1^2, ..., x_1^P, x_2^1, x_2^2, ..., x_2^P, ..., x_N^1, x_N^2, ..., x_N^P\right), \tag{9.1.5}$$

where $x_j^p = t - t_j^p$ is the time which passed from the moment when that jth oscillator emitted his pth pulse. x_j^1 corresponds to the latest produced pulse, x_j^2 corresponds to the previous one, and so on. The state vector ξ fully describes the state of the system (9.1.1) and allows to predict its future dynamics.

Now, we construct the map describing the evolution of the state vector with time. All the components of the vector grow uniformly except certain moments when they undergo stepwise changes. These moments are related to the so-called G-events which are either emissions or receptions of the pulses.

When the phase of the jth oscillator reaches unity, it emits a new pulse with $t_j^p = t + \theta_j$, where

$$\theta_j = \frac{1-\varphi_j}{\omega_j}. \tag{9.1.6}$$

Then, the state vectors change as follows:

$$\begin{aligned}
&\varphi_j(t') = 0,\\
&\varphi_k(t') = \varphi_k(t) + \omega_k\theta_j,\\
&x_j^1(t') = 0,\\
&x_j^p(t') = x_j^{p-1}(t) + \theta_j, \quad p \in [2; P],\\
&x_k^p(t') = x_k^p(t) + \theta_j, \quad p \in [1; P]
\end{aligned} \tag{9.1.7}$$

where $k \neq j$. Denote transformation (9.1.7) as the map $E_j : \xi(t) \mapsto \xi(t')$.

When a pulse produced by the kth oscillators reaches the jth oscillator after the delay, the phase of the latter oscillator instantly shifts. For the given (j,k) pair, this will happen at the moment $t' = t + \vartheta_{jk}$, where

$$\vartheta_{jk} = \tau_{jk} - x_q^k, \tag{9.1.8}$$

where $q = \max\{p | x_k^p < \tau_{jk}\}$. The state vector changes as follows:

$$\begin{aligned}
&\varphi_j(t') = \varphi_j(t) + \omega_j\vartheta_{jk} + f_{jk}\left(\varphi_j(t) + \omega_j\vartheta_{jk}\right),\\
&\varphi_m(t') = \varphi_m(t) + \omega_m\vartheta_{jk}, \quad p \in [1; P]
\end{aligned} \tag{9.1.9}$$

$$x_j^p(t') = x_j^p(t) + \vartheta_{jk}, \quad p \in [1; P]$$
$$x_m^p(t') = x_m^p(t) + \vartheta_{jk}, \quad p \in [1; P] \tag{9.1.10}$$

where $m \neq j$. Denote transformation (9.1.9) as the map $F_{jk} : \xi(t) \mapsto \xi(t')$.

To determine the nearest G-event, one should find the minimum value $\delta_{\min}$ of the values θ_j and ϑ_{jk} for all j and k. The system state between the subsequent G-events changes according to the map

$$G : \xi(t) \mapsto \xi(t') = \begin{cases} E_k, & \delta_{\min} = \theta_k, \\ F_{mk}, & \delta_{\min} = \vartheta_{mk}. \end{cases} \tag{9.1.11}$$

If any two or more G-events coincide, one must sequentially apply the corresponding transformations in arbitrary order.

We have shown that under certain conditions, system (9.1.1) can be described by state vector (9.1.5) and its dynamics is governed by the map (9.1.11). Further, we will utilize these findings to study networks of particular configuration.

9.2 Jittering Regimes of Single Oscillator with Feedback

In this section, we consider a single oscillator with pulsatile delayed feedback [60, 61]. The study on this basic and very common "motif" [62] is important for understanding the behavior of larger delay-coupled networks [63]. For instance, a loop consisting of one excitatory and one inhibitory neuron with delayed connection shows similar behavior to a neuron with delayed self-feedback [64–66], and also, the behavior of rings of several neurons is, in some cases, related to the behavior of a single neuron with delayed feedback [67–69]. In fact, a larger neuronal feedback delay might firstly arise due to a chained propagation of action potentials along a ring of neurons.

It turns out that an oscillatory system with delayed pulsatile feedback may generically exhibit a very surprising phenomenon. Under some conditions, a periodical regime of regular spiking destabilizes in a degenerate manner such that several multipliers (Lyapunov exponents) become critical at once. The number of the critical multipliers is proportional to the feedback delay and can be arbitrary large. Thus, the dimension of the unstable manifold of the regular spiking solution changes abruptly from zero to an arbitrary large value, which we call the "dimension explosion" phenomenon. As a result of such a bifurcation, we show that there appear multiple coexistent periodic solutions with larger periods, characterized by distinct ISIs. Remarkably, the numerous jittering regimes emerge at once at the bifurcation point which leads us to adopt the name "multi-jitter" bifurcation. We prove that the number of the emergent jittering solutions grows exponentially with the delay.

We consider an oscillator with delayed pulsatile feedback of the form [22, 26, 39, 60, 70–72]:

$$\frac{d\varphi}{dt} = 1 + Z(\varphi) \sum_{t_j} \delta(t - t_j - \tau). \tag{9.2.1}$$

The oscillator is described by its phase φ, which changes on the circle $[0, 1]$ with $\varphi = 0$ and $\varphi = 1$ identified. In the case without delayed feedback, the phase grows uniformly with normalized frequency $\omega = 1$. When the phase reaches unity, the oscillator is assumed to emit a pulse. The instants when the pulses are emitted are denoted by $t_j, j = 1, 2, \ldots$. The emitted pulses propagate along the feedback line and affect the oscillator after the delay τ at the time instants $t_j^* = t_j + \tau$. When a pulse is received, the phase of the oscillator undergoes an instantaneous, discontinuous shift and changes its value to the new value $\varphi(t_j^* + 0) = \varphi + Z(\varphi)$, where $\varphi = \varphi(t_j^* - 0)$ and the function $Z(\varphi)$ is the PRC [71, 73, 74]. For numerical illustrations, we consider the PRC

$$Z(\varphi) = \kappa \times (\sin(\pi\varphi))^q, \tag{9.2.2}$$

Here, $\kappa > 0$ is the feedback strength, and $q > 1$ is a parameter that controls the steepness of the PRC, which is the crucial quantity for the dynamical phenomena reported in this paper.

Following the approach from the previous section, we derive a map governing the dynamics of (9.2.1). It is convenient to write it the ISIs $T_j = t_j - t_{j-1}$:

$$T_{j+1} = 1 - Z\left(\tau - \sum_{k=j-P+1}^{j} T_k\right). \tag{9.2.3}$$

This form is valid under the assumption that exactly one spike arrives per ISI. Here, P is the number of ISIs between the emission time and the arrival time of each pulse.

The basic dynamical regime of the oscillator is regular spiking when the it emits pulses periodically with $T_j = T$. These solutions correspond to a fixed point of (9.2.3), and therefore, all possible periods T are given as solutions to

$$T = 1 - Z(\tau - PT) \tag{9.2.4}$$

where $P = [\tau/T]$ is the number of full periods within one-delay interval ($[\cdot]$ denotes the integer part). Thus, $\tau = PT + \psi$ with $\psi := \tau \mod T$.

Let us analyze the linear stability of the RS solutions. For this purpose, we introduce small perturbations δ_j to the initial conditions such that $T_j = T + \delta_j$, and study whether the perturbations are damped or amplified with time. Since small perturbations do not violate the property that only one spike occurs within each interval $[t_j, t_{j+1}]$, the map (9.2.3) can be used to study their evolution relevant to the stability of the corresponding RS solution. We substitute $T_j = T + \delta_j$ into (9.2.3), linearize the obtained expression and arrive to the characteristic equation

$$\chi_{P,\alpha}(\lambda) = \lambda^P - \alpha \sum_{k=0}^{P-1} \lambda^k = 0 \tag{9.2.5}$$

where $\alpha := Z'(\psi)$. If Eq. (9.2.5) has only multipliers with $|\lambda| < 1$, the corresponding RS regime is locally stable. The following statements summarize properties of the multipliers:

(A) For $-1 < \alpha < 1/P$, all multipliers have absolute values less than one. As a result, the RS solution is asymptotically stable.
(B) At $\alpha = 1/P$, one critical multiplier crosses the unit circle at $\lambda = 1$. For $\alpha > 1/P$, this multiplier remains unstable.
(C) At $\alpha = -1$, there are P critical multipliers $\lambda_k = e^{i2\pi k/(P+1)}$, $k = 1, \ldots, P$, crossing $|\lambda| = 1$ simultaneously. For $\alpha < -1$, there are P unstable multipliers with $|\lambda_k| > 1, k = 1, \ldots, P$.

The most remarkable destabilization scenario is related to the transition at the parameter value $\alpha = -1$, where P multipliers become unstable simultaneously if α is decreased. At this point, the dimension of the unstable manifold increases abruptly from 0 (stable RS solution) to P, which can be arbitrary large depending on the size of the delay τ. Although this "dimension explosion" seems to be very degenerate, it occurs generically within our setup. In the following, we study this surprising bifurcation.

A bifurcation diagrams in Fig. 9.1 illustrates the dimension explosion. It depicts the observed ISIs of the system for continuously varying delay τ and $q = 28$. For each value of the delay τ, we simulated the system 20 times starting from random initial conditions (initial ISIs were drawn from a uniform distribution in [0.9, 1.0]). For each simulation, all different values of ISIs T_j, which could be observed after a transient, were saved and plotted by red dots. Note that $q = 28$ is the case close to criticality with $\alpha_{\min} \approx -1.017 < -1$. The panels Fig. 9.1b–d show enlarged neighborhoods of the intervals near the bifurcation for $P = 1, 3, 4$.

For the regular spiking, there is only one ISI for each delay τ. However, two points $\psi_{A,B} \in (0, 1)$ exist for which $Z'(\psi_{A,B}) = -1$. This means that when $\psi = \tau \bmod T$ equals either to ψ_A or ψ_B, the dimension explosion takes place. This happens for the following two values of the delay for each $P \in \mathbb{N}$:

$$\tau^P_{A,B} = P(1 - Z(\psi_{A,B})) + \psi_{A,B}, \tag{9.2.6}$$

for which the dimension of the unstable manifold of the regular spiking solution explodes from 0 to P.

Note that for the case $P = 1$, the only multiplier $\lambda = -1$ crosses the unit circle at the bifurcation points. In this case, the bifurcation is a supercritical period doubling giving birth to a stable period-2 solution. For this solution, the spiking regime is "jittering": the ISIs T_j are not equal anymore, but they form an alternating sequence with $T_{2j+1} = T_1$ and $T_{2j} = T_2$, with $T_1 \neq T_2$. The temporal dynamics of the ISIs for the period-2 solution is illustrated in Fig. 9.1e together with a corresponding cobweb

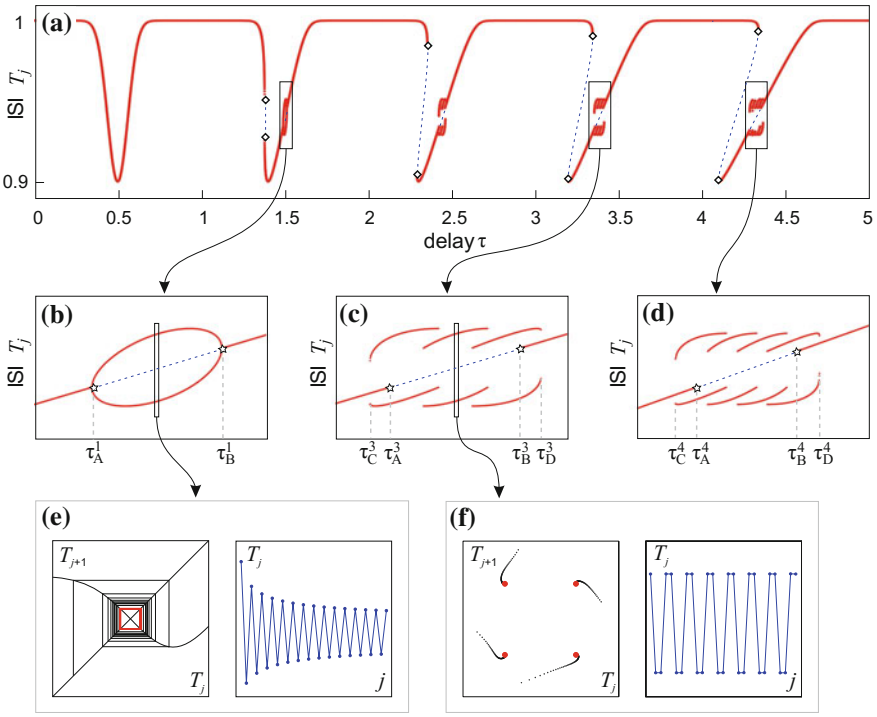

Fig. 9.1 (Color online) **a** Numerical bifurcation diagram for (9.2.1) with PRC (9.2.2) where $q = 28$. The delay τ is varied in the range [0, 5]. *Red dots* correspond to ISIs observed in direct simulations; the *blue dashed lines* corresponds to unstable RS; *squares* indicate fold bifurcations. **b–d** are zooms into regions of **a** where irregular spiking occurs; *stars* indicate multi-jitter bifurcations. **e** *Left panel* one-dimensional map describing the dynamics of ISIs for $P = 1$ ($\tau = 1.5$), together with a cobweb diagram for a trajectory converging to the stable period-2 solution. *Right panel* temporal dynamics, ISIs T_j versus time. **f** Bipartite period-4 solution $(\overline{T_1, T_1, T_2, T_2})$ for $P = 3$ ($\tau = 3.38$). *Left panel* a trajectory converging to this solution in the (T_{j+1}, T_j)-plane; *Right panel* temporal dynamics

diagram. In the bifurcation diagram, Fig. 9.1a, a period-2 solution corresponds to a pair of points (τ, T_1) and (τ, T_2).

For $P \geq 2$, bifurcations take place, where P multipliers simultaneously becoming unstable at $\tau = \tau_{A,B}^P$. The regular spiking solution loses its stability inside the interval $\tau \in \left[\tau_A^P, \tau_B^P\right]$, and various stable "jittering" regimes with nonequal ISIs appear. In numerical studies, we observe that the emerging solutions have period $(P + 1)$. However, a consistent property of these period-$(P + 1)$ solutions is that their ISIs consist of only two (or less often three) different values of T_j. An example of such a period-4 solution at $P = 3$ is given in Fig. 9.1f.

It turns out that a large number of "jittering" solutions, i.e., solutions with different ISIs, emerges in the dimension explosion bifurcation, which allows to adopt the name "multi-jitter" bifurcation also. To show this, consider the equation

$$1 - T = Z(T - \theta), \tag{9.2.7}$$

where $\theta > 0$ is a constant and $T \in [\theta, \theta + 1]$. It is easy to show that when this equation has several different solutions, one can construct an arbitrary $(P + 1)$-periodic sequence $(T_1, T_2, ..., T_{P+1})$ where each T_j is a solution to (9.2.7), and this sequence will be a solution of the map (9.2.3) for

$$\tau = \left(\sum_{j=1}^{P+1} T_j \right) - \theta. \tag{9.2.8}$$

This statement is readily confirmed by a direct check. When $Z(\varphi)$ has parts with slope < -1, (9.2.7) can have up to three different solutions, which allows to construct "jittering" solutions with distinct ISIs. The solutions consisting of two distinct ISIs we call bipartite, and of three tripartite. A series of the solution branches obtained in this way is shown in Fig. 9.2 for $q = 28$ and $P = 1, ..., 4$, and $P = 10$. The obtained stable solutions coincide with the attractors from the bifurcation diagrams in Fig. 9.1b–d and complement the diagrams by parts which are difficult to obtain by direct simulation.

The stability of the jittering solutions requires a separate study. After carrying it out it can be shown that each bipartite solution has its interval of stability. It is easy to estimate the number of different bipartite solutions which exist for a given P. It is equal to the number of (nontrivial) binary sequences of the length $P + 1$ which can be estimated as

$$\#\{\text{bipartite solutions for } P\} \geq \left(2^{P+1} - 2\right)/(P + 1). \tag{9.2.9}$$

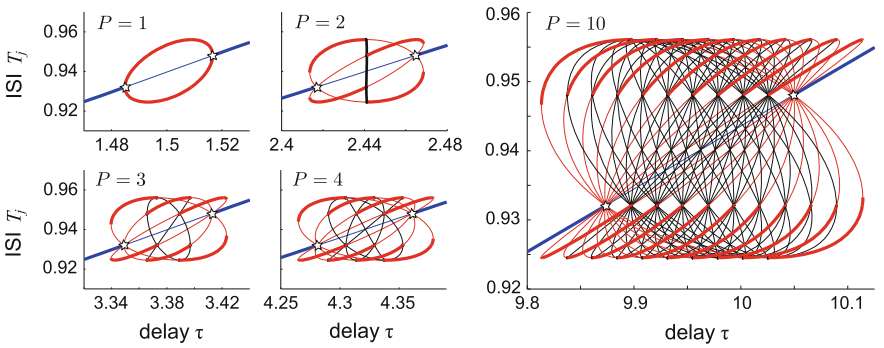

Fig. 9.2 (Color online) **a–d** Branches of RS (*blue* or *light gray*), bipartite (*red* or *dark gray*), and tripartite (*black*) solutions in system (9.2.1) with PRC (9.2.2) and $q = 28$, for different values of P as indicated in the plots. Stable parts of the branches are shown by *thick* and unstable by *thin lines*; *stars* indicate multi-jitter bifurcations

Thus, the number of the emerging solutions grows exponentially with P. So we have shown that the "dimension explosion" of the unstable manifold, which takes place at the multi-jitter bifurcation of the RS regime, is also a "solution explosion." In this bifurcation, numerous bipartite solutions branch off, and the number of the emergent solution grows exponentially with the delay τ. Since each of these solutions corresponds to a jittering regime, we adopt the term "multi-jitter bifurcation." Each multi-jitter bifurcation is accompanied by the emergence of numerous "jittering" periodic solutions with distinct ISIs. Thus, when the delay is increased, the number of different solutions grows combinatorially causing high multi-stability and extremely complex structure of the system's phase space.

9.3 Jittering Waves in Rings of Oscillators

In this section, we investigate unidirectional rings of phase oscillators with pulse delayed coupling [75, 76]. A feed-forward ring is one of the fundamental network motifs that often appears in nature [77–81]. It is a natural extension of one oscillator with the feedback loop considered in the previous section. We start with an analytical study of rotating waves and demonstrate that they may destabilize through the multi-jitter bifurcation. Subsequent numerical and experimental study shows that jittering waves with distinct ISIs are born at the bifurcation points. The period of these regimes is proportional to the delay, and their number grows exponentially. The most interesting distinctive feature is that in rings, the jittering regimes appear at much shorter delays than in a single oscillator with delayed feedback.

The ring of N oscillators with pulse delayed coupling is governed by the equations

$$\frac{d\varphi_j}{dt} = \omega_j + Z(\varphi_j) \sum_{t_s^{j-1}} \delta(t - t_s^{j-1} - \tau_j). \tag{9.3.1}$$

Here, $j = 1, ..., N$ is the oscillator number, and each oscillator is described by its phase $\varphi_j \in \mathbb{S}^1$. Without coupling, the phase grows uniformly with $d\varphi_j/dt = \omega_j$. When the phase reaches unity, it resets to zero and the oscillator emits a spike. The instants when this happens are denoted by t_s^j, $s \in \mathbb{Z}$. Each jth oscillator receives input from its previous neighbor, the $(j-1)$st oscillator (the first one receives input from the last one, so we identify 0 and N). This means that each spike produced by the $(j-1)$-st oscillator at t_s^{j-1} results in a pulse arriving to the jth one after the delay τ_j. When the oscillator receives a pulse, its phase instantly changes to the new value: $\varphi_j \mapsto \varphi_j + Z\left(\varphi_j\right)$, where the function $Z(\varphi)$ is the phase resetting curve (PRC) [71]. We consider identical oscillators with $\omega_j = 1$.

The basic dynamical regimes observed in rings of unidirectionally coupled oscillators are rotating waves [72, 82, 83]. Such waves are characterized by the same dynamical profile of all oscillators that is shifted by a constant time lag between the

neighbors, i.e., $\varphi_j(t) = \varphi_{j-1}(t + \Delta)$. Suppose that system (9.3.1) demonstrates such a regime with the period T and the lag Δ. Then, each oscillator receives one pulse per period at phase $\psi = (\tau - \Delta) \mod T$, which allows to determine the period as $T = 1 - Z(\psi)$, which is the time between the consecutive spikes of one oscillator. The total time lag over the whole ring must be a multiple of the period, i.e., $\Delta = RT/N$, where $R = 0, ..., N - 1$ is the wavenumber which characterizes the type of the rotation wave. Taking this into account, the equations for the rotating waves can be written as

$$T = 1 - Z(\psi), \ \Delta = RT/N, \ \tau = PT + \Delta + \psi. \tag{9.3.2}$$

Here, $\psi \in [0, 1]$ is the phase at which oscillators receive input. The wavenumber $R = 0$ corresponds to a complete synchronization, $R = 1$ to the splay state, etc. P is the integer number controlling the value of the delay or, more exactly, the number of full periods in the delay τ.

Further, we study the local stability of the rotating waves. For this, we consider a perturbed solution with spiking times $t_s^j = sT + j\Delta + \delta_s^j$, where $\delta_s^j \ll T$ are deviations from the periodic regime. Let k be the wavenumber of the perturbation (not to be confused with R) $\delta_s^j \sim \exp(ikj)$, then the stability of this kth mode can be found from the ansatz $\delta_s^j = \lambda(k)^s \exp(ikj)$, where λ is the multiplier of the rotating wave corresponding to the spatial perturbation mode $\exp(ikj)$. We obtain the characteristic equation

$$\lambda^{P+1}(k) - (1 + \alpha)\lambda^P(k) + \alpha e^{-ik} = 0. \tag{9.3.3}$$

The properties of (9.3.3) can be summarized as follows. Its spectrum has the form $\Lambda \cup \{1\}$, where $\lambda(0) = 1$ is the trivial multiplier corresponding to the neutral stability along the phase shift. Stability of the limit cycle is defined by the set Λ, which includes critical multipliers only in the following cases:

– $\alpha = 1/P$: one critical multiplier $\lambda(0) = 1$ for $k = 0$.
– $\alpha = 0$: $(N - 1)$ critical multipliers $\lambda(k) = 1$ for $k = 2\pi n/N$, $n = 1, ..., N - 1$.
– $\alpha = -1$: $N(P + 1) - 1$ critical multipliers $\lambda_m(k) = \exp(-ik + i2\pi m/(P + 1))$, where $m = 0, ..., P$ for $k \neq 0$ and $m = 1, ..., P$ for $k = 0$.

Thus, the rotating wave may change its stability only at the parameter values $\alpha \in \{-1, 0, 1/P\}$. The more remarkable scenario is observed again at $\alpha = -1$ where *all* multipliers become critical at once. The rotating wave loses its stability, and the so-called jittering waves or regimes with distinct inter-spike intervals emerge. Because of the coexistence of a big number of these solutions, the corresponding scenario is called a "multi-jitter bifurcation", see also [60, 61].

For the numerical illustration, we chose the PRC in the form [39]

$$Z(\varphi) = \frac{\kappa}{2}\left(1 - \cos(2\pi\varphi^2)\right) \tag{9.3.4}$$

Here, $\kappa = 0.185$ is the coupling strength and controls both the magnitude and slope of the PRC.

We varied the delay and simulated system (9.3.1) directly for $N = 6$ starting from 20 different initial conditions for each value of τ. For each trial, the initial phases of the oscillators at $t = 0$ were chosen randomly with a uniform distribution, and it was assumed that no spikes were produced by any of the oscillators for $t < 0$. The obtained numerical results are depicted in Fig. 9.3a by dots. The color of each dot corresponds to the wavenumber of the established regime (see the legend). Gray dots correspond to asymmetric regimes. The branches obtained theoretically are plotted by thin dashed lines. The points of the stability loss are marked by circles (for $\alpha = 0$) and stars (for $\alpha = -1$). One can see that the numerically obtained dots coincide with the stable parts of the theoretical branches. There are also several branches of asymmetric regimes, but, most importantly, the jittering wave regimes are observed, which emerge from the multi-jitter bifurcations (stars).

Jittering waves are characterized by distinct inter-spike intervals, and they emerge from the rotating wave at the multi-jitter bifurcation, see Fig. 9.3b–e. Each such solution is close to the rotating wave from which it is born. However, the intervals between the consecutive spikes of each oscillator are not constant anymore, but constitute a periodic sequence of two distinct ISIs. We use this property to encode the jittering regimes by binary sequences, where 0 corresponds to the shorter and 1 to the longer interval. For example, a regime when oscillators produce two long and then one short ISIs periodically is encoded as 110 (see Fig. 9.3b). The other regimes shown are 1100 (c), 1110000 (d), and 1110010 (e). Note that in Fig. 9.3, the plots of the ISIs for different oscillators are shifted along the vertical axis.

We have shown that rotating waves in rings of oscillators may destabilize in the multi-jitter bifurcation. In such a scenario, all the multipliers of the corresponding limit cycle become critical simultaneously. When the rotating wave destabilizes, it gives rise to the so-called jittering wave regimes with distinct ISIs. In the jittering regime, each oscillator produces a periodic sequence of long and short ISIs. These sequences are the same for all oscillators although shifted in phase. A lot of common features are shared by the multi-jitter bifurcations observed in a single oscillator with delayed feedback and in a ring of oscillators considered here. First, the condition for the bifurcation is exactly the same for the both systems. Namely, the slope of the PRC at the phase at which the oscillator is simulated must be equal -1. Secondly, the properties of the emergent jittering regimes are quite similar. The most surprising feature also observed in the both cases is the following: For an arbitrary binary sequence of a given period, the parameter interval does exist where the corresponding jittering regime is present and stable.

Multi-jitter bifurcation in rings still has an important distinction from that in one oscillator with feedback. For one oscillator, the value of the delay must be large compared to the oscillator's natural period. The period of jittering regimes is roughly the delay divided over the natural period. Thus, to obtain jittering regimes with long periods, one needs delays several times larger than the natural period. For rings, the situation is different. The period of the emergent jittering solutions is roughly proportional to the delay times the number of oscillators or the total delay along the ring. As a consequence, even short coupling delays may result in higher-periodical jittering regimes if the number of oscillators is large enough.

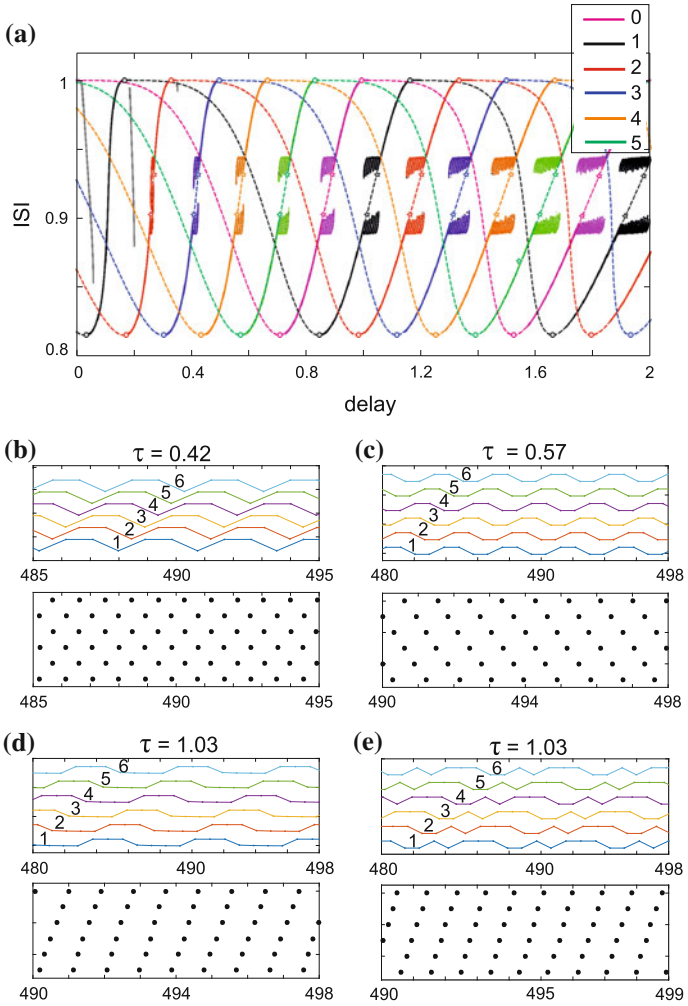

Fig. 9.3 Periodic rotating waves and jittering wave regimes in a ring of $N = 6$ oscillators. **a** The bifurcation diagram, the observed inter-spike intervals versus the delay. Different colors correspond to the different wavenumbers, see the legend. *Thin dashed* and *thick lines* correspond to unstable and stable rotating waves, respectively. *Stars* denote the multi-jitter bifurcations. Jittering regimes are characterized by several distinct ISIs for the same value of delay. **b–e** Examples of jittering regimes. In the *top* of each panel, the ISI demonstrated by each oscillator is plotted versus time. The plots are shifted along the vertical axis for the convenience. In the *bottom* of each panel, the time instants of the spikes emission are depicted by *dots*. Note that the firing patterns are close to the rotating waves, and the deviations are visible only after a careful examination or a zoom

9.4 Synchronization of Two Oscillators with Pulse Delayed Coupling

In the present section, we consider a system of two oscillators with pulse time-delayed coupling [41]. We show that nonidentical oscillators can be synchronized with arbitrary large coupling delay. The same type of coupling may lead to in-phase, antiphase or out-of-phase synchronization. The system of delay-coupled oscillators can manifest multi-stability that consists of either coexistence of different synchronous regimes or both synchronous and asynchronous regimes.

Let us consider a pair of pulse oscillators with time-delay coupling and different intrinsic frequencies $\omega_1 \neq \omega_2$ and time delay τ. The dynamics of the system is governed by the following equations:

$$\frac{d\varphi_k(t)}{dt} = \omega_k + \sum_{j=1}^{\infty} \delta(t - (t_j^m + \tau_j)) f(\varphi_k(t)), \tag{9.4.1}$$

where $k, m = \overline{1,2}$, $k \neq m$, $\delta(t)$ is the Dirac delta-function, t_j^m are the times of the mth unit firing, and $\varphi_m(t_j^m) = 1$. For the sake of certainty, we consider the case of symmetric coupling, so that $\tau_1 = \tau_2 = \tau$. However, generalization to the case of distinct delays is straightforward [84]. Thus, $t_j^m + \tau$ are the instants of time when pulses from the mth unit come to the kth unit. The phase φ_k instantly changes at these times.

A map describing changes of the state vector (9.1.5) can be constructed as (9.1.11). Using this map, we consider the mutual synchronization of the oscillators. We understand the term "synchronization" periodically firing of both units with the same period. To study synchronization, we introduce the Poincare section $\varphi_2 = x_1^2 = 0$ and examine how the state of the system changes during one period between the two instants of the second unit firing t_j^2 and t_{j+1}^2. During this time, the G-events may occur in different order. Taking into account all possible cases, we get the map

$$H: \begin{cases} \overline{\varphi_1} &= \omega_1(T - \Delta) + a, \\ \overline{x_1^1} &= T - \Delta, \\ \overline{x_j^{1,2}} &= x_{j-1}^{1,2} + T, \quad j \in [2; M], \end{cases} \tag{9.4.2}$$

where

$$\Delta = \frac{1 - \varphi_1 - b}{\omega_1},$$
$$T = \frac{1 - c}{\omega_2},$$
$$a = (1 - \alpha) f\left(\omega_1(\tau - \Delta - x_{n_2}^2)\right),$$

$$
\begin{aligned}
b &= \alpha f\left(\varphi_1 + \omega_1(\tau - x^2_{n_2})\right),\\
c &= f\left(\omega_2(\tau - x^1_{n_1})\right),\\
n_1 &= \left[\frac{\tau+\Delta}{T}\right],\\
n_2 &= \left[\frac{\tau}{T}\right] + 1,\\
\alpha &= \begin{cases} 0, & \Delta < \tau \bmod T,\\ 1, & \Delta > \tau \bmod T; \end{cases}
\end{aligned}
$$

if $n_1 = 0$, we take $x^1_0 \equiv -\Delta$.

Synchronous regimes of the system correspond to fixed points of map (9.4.2) defined as

$$
\begin{aligned}
x^1_j &= jT - \Delta, \quad j = \overline{1, M}\\
x^2_j &= (j-1)T, \quad j = \overline{2, M}\\
\varphi_1 &= \omega_1(T - \Delta) + a.
\end{aligned}
\tag{9.4.3}
$$

This fixed point corresponds to the periodic solution of system (9.4.1). The values T and Δ have simple physical sense: T is the period of unit firing, and Δ is the time interval between the instants of first and second unit firing, or interspike lag. Using (9.4.3), we obtain the following equations for T and Δ:

$$
\begin{aligned}
f\left(\omega_1\left((\tau - \Delta) \bmod T\right)\right) &= 1 - \omega_1 T,\\
f\left(\omega_2\left((\tau + \Delta) \bmod T\right)\right) &= 1 - \omega_2 T.
\end{aligned}
\tag{9.4.4}
$$

By solving these equations, we can get the expressions for the values of T and Δ that fully characterize the synchronous regime. To study its stability, we linearize map (9.4.2) near its fixed point (9.4.3).

For numerical illustrations, we use $f(\varphi) = -\mu \sin 2\pi\varphi$. The diagrams in Fig. 9.4 represent the solutions of (9.4.4). We plot the value of the relative interspike lag Δ/T versus the coupling time delay τ. Black lines correspond to stable solutions, and gray lines correspond to unstable ones. The coupling strength $\mu = 0.1$ is a constant for all the diagrams, and the intrinsic frequency of the first unit $\omega_1 = 1$ is a constant too, while the intrinsic frequency of the second unit increases from (a) to (c).

Figure 9.4a represents synchronous regimes for a pair of identical pulse oscillators. One can see that for different values of coupling delay τ, in-phase or antiphase synchronization is possible. In Fig. 9.4b, c, synchronous regimes of nonidentical oscillators are illustrated. For any nonzero value of frequency mismatch $\zeta = \omega_2 - \omega_1$ system (9.4.1) has a number of periodic solutions that exist in the corresponding intervals of delay τ. In each interval, there is a pair of stable and unstable solutions

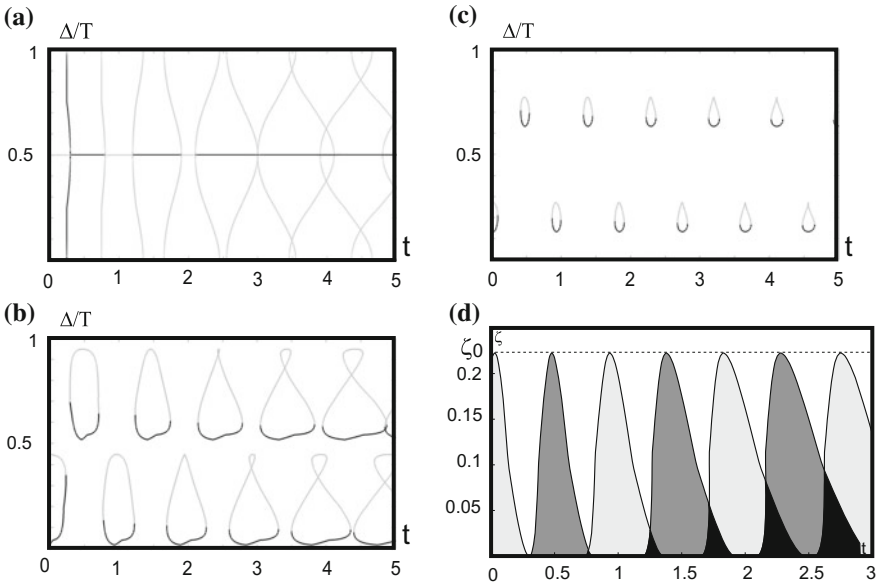

Fig. 9.4 **a**–**c** Periodic solutions of (9.4.1): relative interspike lag Δ/T versus the coupling delay τ. The parameters $\mu = 0.1$ and $\omega_1 = 1$ are constant, while ω_2 increases from **a** to **c**: **a** $\omega_2 = 1$, **b** $\omega_2 = 1.05$, **c** $\omega_2 = 1.2$. **d** Bifurcation diagram for $\mu = 0.1$, and $\omega_1 = 1$. Synchronization zones. *Light gray* corresponds to the in-phase synchronization, while *dark gray* corresponds to the antiphase one. *Black* overlap areas correspond to multi-stability

that appear and disappear through saddle-node bifurcation of periodic points. Synchronization occurs inside these intervals; therefore, we call them *synchronization intervals*. The interspike lag Δ between the oscillators strongly differs from one synchronization interval to another. Depending on the relative interspike lag Δ/T, we differ 'in-phase" and "antiphase" synchronization. For nonidentical oscillators, these terms are used not in strict sense, because Δ is not equal exactly 0 or $T/2$. Notice that the intervals corresponding to in-phase and antiphase synchronization alternate while τ grows. The width of synchronization intervals decreases with growth of the frequency mismatch ζ (compare Fig. 9.4b, c). Synchronization occurs for frequency mismatches

$$\zeta \leq \zeta_0 = \frac{2\mu\omega_1}{1-\mu}.$$

Outside the synchronization intervals, system (9.4.1) does not have any periodic solutions: The units oscillate with different periods, and phase locking does not occur.

In Fig. 9.4d, we plot a bifurcation diagram on the parameter plane $\tau - \zeta$. Here, we see a set of the so-called *synchronization zones*, in which periodic solutions of (9.4.1) exist and synchronization takes place. These zones correspond to synchronization intervals in the previous figures. Light gray-colored zones correspond to the in-phase

synchronization, and dark gray zones correspond to the antiphase synchronization. The width of each zone along τ decreases with growth of ζ; for $\zeta > \zeta_0$, the zones disappear. Let us draw your attention to the fact that different zones may overlap. The overlaps are colored black and correspond to the parameter areas where the system is multi-stable. Outside the synchronization zones, there is no periodic solutions of the system and the oscillators have different periods of firing.

One of the most interesting points is that synchronization of oscillators is observed for arbitrary large values of coupling delay. Thus, two *nonidentical* oscillators can be synchronized even if they interact with time delay which is much larger than their native periods. Other specific properties of coupling with large delay are as follows: (1) increasing of synchronization zones size in parameter space with delay growth; (2) appearance of multi-stability as a consequence; (3) quick growth of the transient time (as τ^3). All this shows that the case of large coupling delays appeared to be interesting and providing new dynamical effects.

9.5 Cross-Frequency Synchronization of Two Oscillators

In this section, we investigate the case of cross-frequency, or harmonic synchronization of two oscillators which is observed for large frequency mismatch [9]. Cross-frequency synchronization is a periodical regime when the frequencies of the individual oscillators are locked and relate as small integer numbers. For a pair of coupled oscillators, this means a relation $f_1 : f_2 = m : n$, which regime is called $m : n$ synchronization. Cross-frequency synchronization of oscillators of various nature was in a focus of some previous works [85], but the influence of the delays has not been explored sufficiently. In our study, we consider two oscillators with time-delayed pulsatile coupling. We systematically study $m : n$ synchronization of the oscillators and obtain analytical criteria for existence of these regimes in the limit of weak coupling. In order to confirm the obtained theoretical results, we developed an electronic circuit implementing the system and explored its dynamics experimentally.

The basic model considered in this section is (9.4.1). We also assume without loss of generality $\omega_1 = 1$, and denote $\omega \equiv \omega_2$. We define $m : n$ synchronization as a periodical regime when the first oscillator emits m pulses per period and the second one emits n pulses per period, where m and n are incommensurable (further, we suppose $m \geq n$). For $m = n = 1$, this means phase locking in the ordinary sense, otherwise it is cross-frequency synchronization. The ratio $m : n$ is also called the rotation number ρ.

Let us study solutions of system (9.4.1) corresponding to $m : n$ synchronization. We consider the case of weak coupling and replace the PRC $f(\varphi)$ by $\varepsilon f(\varphi)$ where $\varepsilon \ll 1$. Suppose that $\varphi_1(t = 0) = 0$ and $\varphi_2(t = 0) = \eta$, and the period of the sought-for solution is P. This means that the first (second) oscillator emitted m (n) pulses for $t \in [0; P)$ Denote $t_1^1, t_1^2, ..., t_1^m$ the moments when the first oscillator produces pulses, and $t_2^1, t_2^2, ..., t_2^n$ the moments when the second one does. Then, the moments when the oscillators receive input pulses equal $(t_2^p + \tau) \mod P$, $p = 1, 2, ..., n$

for the first oscillator, and $(t_1^p + \tau) \mod P$, $p = 1, 2, ..., m$ for the second one. Denote the values of the phases just before the moments of the pulses arrival as $\varphi_1^p = \varphi_1\left(t = (t_2^p + \tau) \mod P\right)$ and $\varphi_2^p = \varphi_2\left(t = (t_1^p + \tau) \mod P\right)$. Then, the values of the phase shifts caused by the pulses equal $\Delta\varphi_j^p = \varepsilon\omega_j f(\varphi_j^p)$. This means that the values of the phases for $t = P$ equal

$$\varphi_1(P) = \left(P + \varepsilon\sum_{p=1}^{n} f(\varphi_1^p)\right) \mod 1 = P + \varepsilon\sum_{p=1}^{n} f(\varphi_1^p) - m,$$

$$\varphi_2(P) = \left(\eta + \omega P + \omega\varepsilon\sum_{p=1}^{m} f(\varphi_2^p)\right) \mod 1 = \eta + \omega P + \omega\varepsilon\sum_{p=1}^{m} f(\varphi_2^p) - n.$$

Provided $\varphi_1(P) = 0$, one may obtain an equation for the period P:

$$P = m - \varepsilon\sum_{p=1}^{n} f(\varphi_1^p),$$

and calculate the new phase difference $\overline{\eta} = \varphi_2(P) - \varphi_1(P)$:

$$\overline{\eta} = \eta + \omega m - n + \omega\varepsilon\left(\sum_{p=1}^{m} f(\varphi_2^p) - \sum_{p=1}^{n} f(\varphi_1^p)\right). \tag{9.5.1}$$

This equation is a Poincare map governing dynamics of the phase difference η in vicinity of the periodical solution. The regime of $m : n$ synchronization corresponds to a stable fixed point of the map (9.5.1). Let us study the map (9.5.1) for small $\varepsilon \to 0$. It is easy to see that for $\varepsilon = 0$

$$t_1^p = p,$$

$$t_2^p = \frac{p - \eta}{\omega_2},$$

$$\varphi_1^p = t_2^p + \tau = \frac{p - \eta}{\omega} + \tau, \tag{9.5.2}$$

$$\varphi_2^p = \eta + \omega(t_1^p + \tau) = \eta + \omega(p + \tau) \tag{9.5.3}$$

The map (9.5.1) reduces to

$$\overline{\eta} = \eta + \omega m - n,$$

which has a (neutrally) stable fixed point for $\omega = n/m$. For $0 < \varepsilon \ll 1$, variations of φ_j^p with respect to the values (9.5.2)–(9.5.3) are of the order of ε, and the map (9.5.1) transforms into

$$\overline{\eta} = \eta + \omega m - n + \omega\varepsilon \left(\sum_{p=1}^{m} f\left(\eta + \omega(p+\tau)\right) - \sum_{p=1}^{n} f\left(\frac{p-\eta}{\omega} + \tau\right) \right) + O(\varepsilon^2),$$

which implies $\omega = n/m + O(\varepsilon)$ and allows further simplification:

$$\overline{\eta} = \eta + \omega m - n + \varepsilon\omega S_{\tau}^{mn}(\eta), \tag{9.5.4}$$

where

$$S_{\tau}^{mn}(\eta) = \sum_{p=1}^{m} f\left(\eta + \frac{n}{m}(p+\tau)\right) - \sum_{p=1}^{n} f\left(\frac{m}{n}(p-\eta) + \tau\right),$$

the terms $O\left(\varepsilon^2\right)$ omitted. The shape of the function $S_{\tau}^{mn}(\eta)$ depends on the shape of the PRC $f(\varphi)$, as well as the values of m, n, and the delay τ. The synchronization is possible when at least one stable fixed point exists which implies the following condition:

$$\frac{m}{n} + \frac{\varepsilon A_{\tau}^{mn}}{n} \le \mu \le \frac{m}{n} + \frac{\varepsilon B_{\tau}^{mn}}{n}, \tag{9.5.5}$$

where $\mu \equiv 1/\omega$ is the autonomous period of the second oscillator, $A_{\tau}^{mn} := \sup_{\eta\in(0,1)} S_{\tau}^{mn}(\eta)$ and $B_{\tau}^{mn} := \inf_{\eta\in(0,1)} S_{\tau}^{mn}(\eta)$. The double inequality (9.5.5) defines the so-called synchronization zone—the area in the parameter space inside which $m:n$ synchronization is observed.

For the illustration purposes, we choose $f(\varphi) = -\sin(2\pi\varphi)$. The synchronization zones for such the PRC are depicted in Fig. 9.5.

The most interesting fact about the synchronization zones is that they last to infinity along the τ axis. This means that synchronization with arbitrary rotation number is possible for arbitrary large coupling delays. Moreover, the width of the

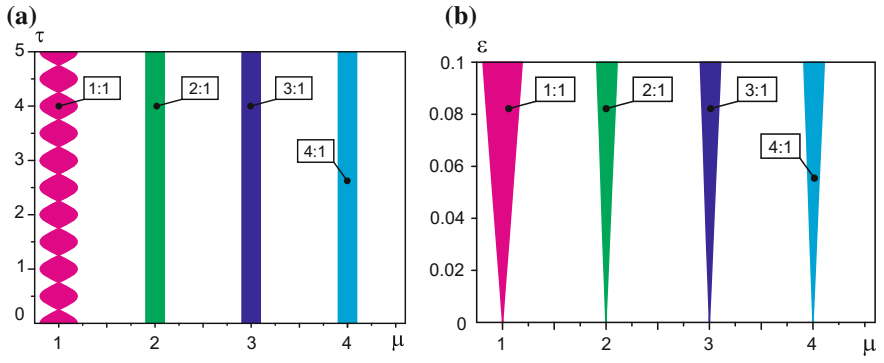

Fig. 9.5 (Color online) Synchronization zones for the sinusoid PRC $f(\varphi) = -\sin(2\pi\varphi)$. The rotation numbers of the zones are given in the *bars*. **a** The plane $\mu - \tau$ for the fixed value of $\varepsilon = 0.1$. **b** The plane $\mu - \varepsilon$ for the fixed value of τ=0.5

synchronization zone is a periodical function of the delay. For a special case of the sinusoid PRC, this width is constant for $m > n = 1$ and very small ($O(\varepsilon^2)$) for $m > n > 1$. For nonsinusoid PRCs, all the zones have width of the order of ε, and the borders if all the zones are periodical with respect to τ.

9.6 Phase Patterns in a Small Network with Heterogeneous Delays

Even small networks of oscillators may possess rich variety of different structures and demonstrate diverse dynamics [86]. In this section, we illustrate this diversity by the study of phase patterns emerging in a small network of just four oscillators with heterogeneous delays. We consider a network of four globally coupled oscillator (neurons) which is depicted in Fig. 9.6a. Four neurons are located in corners of a square, delays between neighboring neurons equal $\tau/2$, and delays between diagonal neurons equal τ. The PRC for each connection is given as $f(\varphi) = -\mu \sin 2\pi\varphi$, and the coupling strength equals $\mu = 0.1$. Frequencies ω_j have Gaussian distribution with the mean $\omega = 1$ and dispersion $\sigma = 0.01$. We set them not identical to study the influence of possible parameters varying and make sure that the regimes we obtain are not sensible to them.

Studying of the network showed that depending on the delay parameter τ it may produce a number of various rhythmic patterns. We mark these patterns with sets of four numbers $(\varphi_1, \varphi_2, \varphi_3, \varphi_4)$, where φ_j means the phase lag between the first and the jth neurons firing. The most typical are the following patterns: (i) the pattern (0, 0, 0, 0) of global synchronization, when all the units fire simultaneously in the same phase; (ii) the pattern (0, 0.5, 0, 0.5) or partial pairwise synchronization, when the first unit fires in phase with the third one, and the second unit fires sin phase with the fourth one, while these pairs fire in antiphase; (iii) the pattern (0, 0.25, 0.5, 0.75) of sequential firing, when all the units fire one after another with the quarter-period lag.

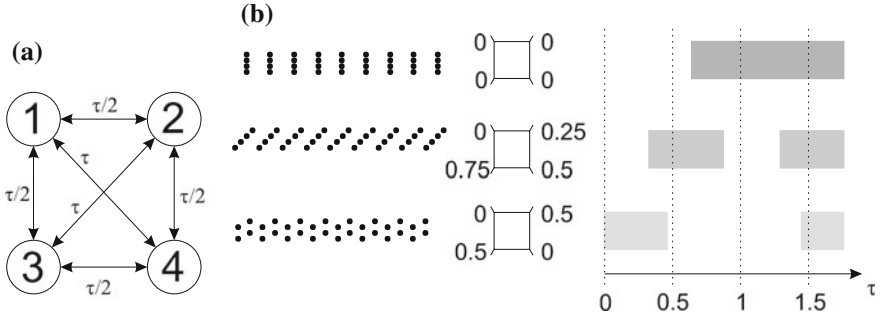

Fig. 9.6 **a** CPG consisting of four neurons with delayed coupling. **b** Possible output rhythmic patterns and τ intervals inside which they exist. Sequences of *black dots* determine series of pulses emitted by the oscillators

Each of these three patterns exists in definite interval of delay coefficient τ. These intervals are depicted in Fig. 9.6b. One can see that the key features of the system dynamics are similar as in the case of two units. Slow increasing of the parameter τ results in sequential switching between the patterns. For $\tau = 0$, the only pattern (0, 0.5, 0, 0.5) exists. When $\tau = \tau_1 \approx 0.37$ the second pattern (0, 0.25, 0.5, 0.75) appears. And for $\tau = \tau_2 \approx 0.61$ the third pattern (0, 0, 0, 0) appears. The switching between the patterns is concerned with hysteresis which comes from the system instability near the points in which new patterns are born. For example, the pattern (0, 0.25, 0.5, 0.75) appears for $\tau = \tau_1$, but the pattern (0, 0.5, 0, 0.5) disappears only for $\tau = \tau_1' \approx 0.48$. This means that when τ increases the switching (0, 0.5, 0, 0.5)→(0, 0.25, 0.5, 0.75) takes place for $\tau = \tau_1'$. But when the τ decreases the opposite switching takes place only for $\tau = \tau_1$.

Our results show that coupling delays may be an instrument for control of rhythmic patterns of small oscillatory networks, for example central pattern generators. Varying delays in a small network of coupled oscillatory neurons allows to change phase relationships between the units. In the previous papers, it was shown that special tuning of the oscillators parameters can be used to establish the certain phase relations [87–91]. Here, we show that switching of the patterns may occur when only one parameter, the delay, is changed.

9.7 Global Synchronization of All-to-All Coupled Networks

In the last section, we study the dynamics of large all-to-all connected networks with pulse delayed coupling [92]. The dynamical regime we focus on is the global synchronization when all the oscillators produce spikes simultaneously. In neuroscience, the synchronization of neuron populations plays an important role and might even lead to pathological effects [93]. In an ensemble of all-to-all pulse-coupled oscillators without delays, the global synchronization is destabilized via the emergence of various two-cluster states [39]. Here, we study how coupling delays influence this scenario.

A network of globally pulse-coupled oscillators with time-delayed coupling is governed by the following dynamical system:

$$\dot{\varphi}_j(t) = 1 + \zeta\left(\varphi_j(t)\right) \sum_{k=1}^{N} \sum_{t_k^p} \delta(t - t_k^s - \tau), \quad j = 1, ..., N. \tag{9.7.1}$$

Here, $\varphi_j \in [0; 1]$ are the phases of the oscillators. When the phase φ_j reaches unity the jth oscillator produces a pulse and its phase resets to zero. The instants when this happens are denoted as t_j^s. Each emitted pulse reaches all the oscillators (including the one which produced it) after the time delay τ. When a pulse reaches an oscillator, its phase shifts instantly by a certain amount $\Delta\varphi$. This phase shift depends on the phase value before the pulse arrival: $\Delta\varphi = \zeta(\varphi(t - 0))$, where $\zeta(\varphi)$ is the phase

resetting curve. In the rest of the paper, we scale the PRC with the network size, so that $\zeta(\varphi) = \frac{\varkappa}{N} Z(\varphi)$, where $\varkappa$ is the coupling coefficient. Thus, after a pulse arrival the oscillator's phase is changed so that $\varphi(t+0) = \mu(\varphi(t-0))$, where

$$\mu(\varphi) = \varphi + \frac{\varkappa}{N} Z(\varphi). \tag{9.7.2}$$

If several, say m, pulses happen to arrive simultaneously, the map (9.7.2) is applied m times, so that $\varphi(t+0) = \mu^m(\varphi(t-0))$.

Consider the regime of global synchronization when all the oscillators produce pulses simultaneously with the same period T. In this regime, the instants $t_j^s = sT$ and the pulses produced at $t = sT$ are received by all the oscillators simultaneously at $t = sT + \tau$. Before the arrival of this burst of pulses, the phases of the oscillators equal $\psi = \tau - PT = \tau \mod T$, where $P = [\tau/T]$. After reception of the pulses, the phases of the oscillators change to the value $\mu^N(\psi)$. Hence, the period T must satisfy the equation

$$\tau \mod T + 1 - \mu^N(\tau \mod T) = T. \tag{9.7.3}$$

To study the stability of the regular spiking solution, we introduce perturbations so that $t_j^s = sT + \delta_j^s$ and explore dynamics of the perturbations δ_j^s. It is rather complicated to study the network dynamics for an arbitrary perturbation, so we first introduce some specific classes of perturbations. Consider a regime when the units of the network are split into two clusters: The first cluster of size M includes the nodes from 1 to M, and the second one of the size $N - M$ includes the rest of the network. The oscillators of each cluster fire in synchrony. The described regimes form a subset

$$\Pi_M := \{\delta_j^s = \delta_1^s,\ 1 < j \le M\} \cap \{\delta_j^s = \delta_N^s,\ M \le j < N\}.$$

Note that the subset Π_M is invariant: Since the oscillators of each cluster receive the same input, they will stay synchronous. Let us now study the dynamics of the network in this invariant subspace. The bursts of pulses produced by the clusters at t_1^{s-P} and t_N^{s-P} and are received by the network at between the instants at $t_1^* = t_1^{s-P} + \tau$ and $t_N^* = t_N^{s-P} + \tau$, respectively. Assume that the first cluster fires first, i.e., $t_N^s > t_1^s$. Then, if the perturbations are small, the sequence of the events is as follows: $t_1^s < t_N^s < t_1^* < t_N^* < t_1^{s+1} < t_N^{s+1}$. Denote the intercluster distance $\Delta^s = t_N^s - t_1^s$, then one can calculate Δ^{s+1} as follows:

$$\Delta^{s+1} = \mu^{N-M}\left(\mu^M\left(\psi + \delta_1^{s-P} - \delta_N^s\right) + \Delta^{s-P}\right) - \mu^{N-M}\left(\mu^M\left(\psi + \delta_1^{s-P} - \delta_1^s\right) + \Delta^{s-P}\right).$$

Linearization of () leads to

$$\Delta^{s+1} = \left(\mu^{N-M}\right)'\left(\mu^M(\psi)\right) \times \left(\mu^M\right)'(\psi) \times \left(\delta_N^s - \delta_1^s\right) = \beta\Delta^s,$$

where $\beta = \left(\mu^N\right)'(\psi)$. The linearized map () describes dynamics of the intercluster distance for perturbations from the subset Π_M. For $|\beta| < 1$, this distance converges to zero which means that the perturbation converges to the subset Π_0 for which the phases of all the oscillators are equal.

Notice now that an arbitrary perturbation $\overrightarrow{\delta}$ of (9.7.1) that preserves the phase order can be represented as a superposition of perturbations $\overrightarrow{\delta_M} \in \Pi_M$ for $M = 0, 1, ..., N-1$. If $|\beta| < 1$, all these perturbations converge to the subset Π_0. Thus, the stability of the regular spiking is determined by the dynamics of perturbations from this subset. Note that in this subset, the networks behaves like a single oscillator with delayed feedback. As was shown in Sect. 9.2, the stability of the regular spiking is given by the condition $-1 < \alpha < 1/P$, where $\alpha = \beta - 1$.

For weak coupling iterative, the map $\mu^N(\varphi)$ can be approximated as

$$\mu^N(\varphi) \approx \varphi + \kappa Z(\varphi),$$

and $\alpha \approx \kappa Z'(\psi)$. Taking into account that $T \approx 1$, the condition for the global synchronization stability can be written as

$$-1 < f'(\tau \mod 1) < 0, \tag{9.7.4}$$

where $f(\tau) \equiv Z(\tau \mod 1)$ is the PRC.

To illustrate the results of the theoretical analysis, we have performed a series of numerical simulations of the ensembles for the sin-shape phase reset curve $f(\varphi) = -\sin 2\pi\varphi$, which corresponds to the isochronal clock model [26]. The stability criterion (9.7.4) for this case says that the global synchronization is stable for

$$(\tau \mod 1) < \frac{1}{4} \quad \text{and} \quad (\tau \mod 1) > \frac{3}{4}, \tag{9.7.5}$$

and is unstable for the other values of τ.

The results of the numerical simulations are given in Fig. 9.7 which represents the bifurcation diagram for $N = 10$. The horizontal axis is the coupling delay, and the vertical axis is the coupling strength. The condition (9.7.4) defines a series of vertical stripes in this plane which are plotted by light gray. The areas in which the regime of global synchronization is observed in numerical simulations are plotted by dark gray. For weak coupling, these areas coincide with the areas predicted analytically, but when the coupling strength grow they widen. This widening is more pronounced for large delays. The other feature of the strong coupling appearance of the bistability areas plotted by black. In these areas, the global synchronization is observed for some initial conditions and does not occur for the others. The rest of the plane is colored white and corresponds to the asynchronous states.

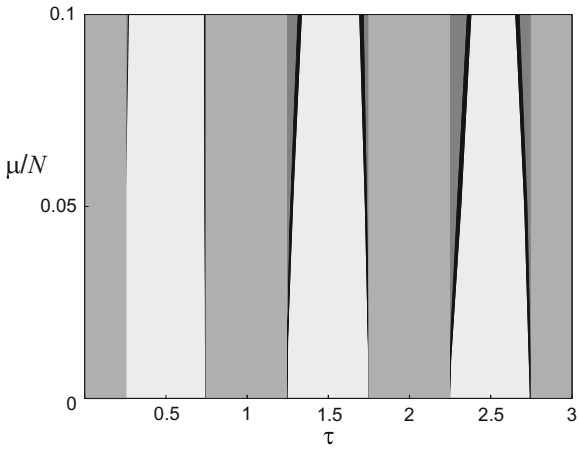

Fig. 9.7 The bifurcation diagram for the ensemble of $N = 10$ units for the sin-shape phase reset curve. *Gray* are the areas of the global synchronization (*light gray* – analytical estimates, *dark gray* – numerical results), *black* are the multi-stable areas, *white* are the areas without synchronous state

9.8 Conclusions

We have presented the results of the study of the influence of the coupling delays on the dynamics of networks of pulse-coupled oscillators. For all the network configurations considered this influence is significant. For large networks of all-to-all coupled oscillators, the delay controls the global synchronization. For smaller networks, it may switch the phase patterns established. For two coupled oscillators, the delay defines in-phase, antiphase, out-of-phase, and cross-frequency synchronization. For the cross-frequency synchronization, the synchronization zones of the higher orders do not depend on the delay only for the particular case of harmonical coupling function. For the PRC containing more than one Fourier harmonic, the synchronization zones do depend on the delay.

Probably, the most interesting and unexpected example of the delay-induced effect was observed in the most simple configuration of a single oscillator with feedback. In this case, the introduction of a sufficiently large delay leads to the emergence of a completely new type of behavior. The regular spiking changes to irregular "jittering" regimes with distinct inter-spike intervals. The larger is the delay, the longer is the periods of the jittering regimes.

One of the common properties of dynamical systems with delays is their multi-stability. A typical mechanism for the emergence of multi-stability for large delays is the so-called reappearance of periodical solutions [43]. This mechanism leads to the linear growth of the number of coexisting regimes with the delay. However, in oscillators and rings with delayed feedback, we have reported a new combinatorial mechanism due to which the multi-stability develops exponentially.

References

1. Yuste, R., MacLean, J.N., Smith, J., Lansner, A.: The cortex as a central pattern generator. Nat. Rev. Neurosci. **6**, 477–483 (2005)
2. Kunysz, A.M., Shrier, A., Glass, L.: Bursting behavior during fixed-delay stimulation of spontaneously beating chick heart cell aggregates. Am. J. Physiol. Cell Physiol. **273**(1), C331–C346 (1997)
3. Winfree, A.T.: The Geometry of Biological Time. Springer, Berlin (2001)
4. Buck, J.: Synchronous rhythmic flashing of fireflies. II. Q. Rev. Biol. **63**, 265–289 (1988)
5. Mirollo, R.E., Strogatz, S.H.: Synchronization of pulse-coupled biological oscillators. SIAM J. Appl. Math. **50**, 1645–1662 (1990)
6. Brzeski, P., Kapitaniak, T., Perlikowski, P.: Experimental verification of the hybrid dynamical model of the church bell. Int. J. Impact Eng. **80**, 177–184 (2015)
7. Lopera, A., Buldú, J.M., Torrent, M.C., Chialvo, D.R., García-Ojalvo, J.: Ghost stochastic resonance with distributed inputs in pulse-coupled electronic neurons. Phys. Rev. E **73**, 021101 (2006)
8. Rosin, D.P., Rontani, D., Gauthier, D.J., Schöll, E.: Control of synchronization patterns in neural-like boolean networks. Phys. Rev. Lett. **110**, 104102 (2013)
9. Klinshov, V.V., Shchapin, D.S., Nekorkin, V.I.: Cross-frequency synchronization of oscillators with time-delayed coupling. Phys. Rev. E **90**, 042923 (2014)
10. Shchapin, D.S.: Dynamics of two neuronlike elements with inhibitory feedback. J. Commun. Technol. Electron. **54**(2), 175–184 (2009)
11. Colet, P., Roy, R.: Digital communication with synchronized chaotic lasers. Opt. Lett. **19**(24), 2056–2058 (1994)
12. Boyd, R.W., Gauthier, D.J.: Controlling the velocity of light pulses. Science **326**(5956), 1074–1077 (2009)
13. Otto, C., Lüdge, K., Vladimirov, A.G., Wolfrum, M., Schöll, E.: Delay-induced dynamics and jitter reduction of passively mode-locked semiconductor lasers subject to optical feedback. New J. Phys. **14**(11), 113033 (2012)
14. de la Iglesia, H.O., Cambras, T., Schwartz, W.J., Diez-Noguera, A.: Forced desynchronization of dual circadian oscillators within the rat suprachiasmatic nucleus. Curr. Biol. **14**, 796–800 (2004)
15. Peskin, C.S.: Mathematical Aspects of Heart Physiology New York. Courant Institute of Mathematical Sciences, New York (1975) (New York University)
16. Michaels, D.C., Matyas, E.P., Jalife, J.: A mathematical model of the effects of acetylcholine pulses on sinoatrial pacemaker activity. Circ. Res. **55**(1), 89–101 (1984)
17. Dokos, S., Celler, B.G., Lovell, N.H.: Vagal control of sinoatrial rhythm: a mathematical model. J. Theor. Biol. **182**(1), 21–44 (7 Sep 1996)
18. Tsalikakis, D.G., Fotiadis, D.I., Michalis, L.K., Kremmydas, G.P.: Phase resetting in one-dimensional model of the sinoatrial node. IEEE Trans. Biomed. Eng. **54**(9), 1710–1714 (2007)
19. Lewis, J., Bachoo, M., Glass, L., Polosa, C.: Complex dynamics resulting from repeated stimulation of nonlinear oscillators at a fixed phase. Phys. Lett. A **125**(2–3), 119–122 (1987)
20. Lewis, J.E., Glass, L., Bachoo, M., Polosa, C.: Phase resetting and fixed-delay stimulation of a simple model of respiratory rhythm generation. J. Theor. Biol. **159**(4), 491–506 (1992)
21. Minors, D.S., Waterhouse, J.M., Wirz-Justice, A.: A human phase-response curve to light. Neurosci. Lett. **133**(1), 36–40 (1991)
22. Achuthan, S., Canavier, C.C.: Phase-resetting curves determine synchronization, phase locking, and clustering in networks of neural oscillators. J. Neurosci. **29**, 5218–5233 (2009)
23. Canavier, C.C., Butera, R.J., Dror, R.O., Baxter, D.A., Clark, J.W., et al.: Phase response characteristics of model neurons determine which patterns are expressed in a ring circuit model of gait generation. Biol. Cybern. **77**, 367–380 (1997)
24. Canavier, C.C., Kazanci, F.G., Prinz, A.A.: Phase resetting curves allow for simple and accurate prediction of robust N:1 phase locking for strongly coupled neural oscillators. Biophys. J. **97**, 59–73 (2009)

25. Glass, L., Mackey, M.C.: From Clocks to Chaos: The Rhythms of Life. Princeton University Press, Princeton (1988)
26. Goel, P., Ermentrout, B.: Synchrony, stability, and firing patterns in pulse-coupled oscillators. Phys. D: Nonlinear Phenom. **163**, 191–216 (2002)
27. Oprisan, S.A., Prinz, A.A., Canavier, C.C.: Phase resetting and phase locking in hybrid circuits of one model and one biological neuron. Biophys. J. **87**, 2283–2298 (2004)
28. Foss, J., Milton, J.: Multistability in recurrent neural loops arising from delay. J. Neurophysiol. **84**, 975–985 (2000)
29. Glass, L., Guevara, M.R., Belair, J., Shrier, A.: Global bifurcations of a periodically forced biological oscillator. Phys. Rev. A **29**, 1348–1357 (1984)
30. Anumonwo, J.M., Delmar, M., Vinet, A., Michaels, D.C., Jalife, J.: Phase resetting and entrainment of pacemaker activity in single sinus nodal cells. Circ. Res. **68**(4), 1138–1153 (1991)
31. Galán, R.F., Ermentrout, G.B., Urban, N.N.: Efficient estimation of phase-resetting curves in real neurons and its significance for neural-network modeling. Phys. Rev. Lett. **94**, 158101 (2005)
32. Ermentrout, G.B., Beverlin II, B., Troyer, T., Netoff, T.I.: The variance of phase-resetting curves. J. Comput. Neurosci. **31**(2), 185–197 (2011)
33. Ernst, U., Pawelzik, K., Geisel, T.: Delay-induced multistable synchronization of biological oscillators. Phys. Rev. E **57**, 2150–2162 (1998)
34. Tsodyks, M., Mitkov, I., Sompolinsky, H.: Pattern of synchrony in inhomogeneous networks of oscillators with pulse interactions. Phys. Rev. Lett. **71**(8), 1280–1283 (1993)
35. Bottani, S.: Pulse-coupled relaxation oscillators: from biological synchronization to self-organized criticality. Phys. Rev. Lett. **74**, 4189–4192 (1995)
36. Abbott, L.F., van Vreeswijk, C.: Asynchronous states in networks of pulse-coupled oscillators. Phys. Rev. E **48**(2), 1483–1490 (1993)
37. Ernst, U., Pawelzik, K., Geisel, T.: Synchronization induced by temporal delays in pulse-coupled oscillators. Phys. Rev. Lett. **74**, 1570–1573 (1995)
38. van Vreeswijk, C.: Partial synchronization in populations of pulse-coupled oscillators. Phys. Rev. E **54**(5), 5522–5537 (1996)
39. Lücken, L., Yanchuk, S.: Two-cluster bifurcations in systems of globally pulse-coupled oscillators. Phys. D: Nonlinear Phenom. **241**, 350–359 (2012)
40. Zillmer, R., Livi, R., Politi, A., Torcini, A.: Stability of the splay state in pulse-coupled networks. Phys. Rev. E **76**(4), 046102 (2007)
41. Klinshov, V.V., Nekorkin, V.I.: Synchronization of time-delay coupled pulse oscillators. Chaos Solitons Fractals **44**, 98–107 (2011)
42. Schuster, H.G., Wagner, P.: Mutual entrainment of two limit cycle oscillators with time delayed coupling. Prog. Theor. Phys. **81**, 939 (1989)
43. Yanchuk, S., Perlikowski, P.: Delay and periodicity. Phys. Rev. E **79**(4), 046221 (2009)
44. Reddy, D.V.R., Sen, A., Johnston, G.L.: Time delay induced death in coupled limit cycle oscillators. Phys. Rev. Lett. **80**, 5109 (1998)
45. Heiligenthal, S., Dahms, T., Yanchuk, S., Jüngling, T., Flunkert, V., Kanter, I., Schöll, E., Kinzel, W.: Strong and weak chaos in nonlinear networks with time-delayed couplings. Phys. Rev. Lett. **107**, 234102 (2011)
46. Izhikevich, E.M.: Polychronization: computation with spikes. Neural Comput. **18**, 245–282 (2006)
47. Popovych, O.V., Yanchuk, S., Tass, P.A.: Delay- and coupling-induced firing patterns in oscillatory neural loops. Phys. Rev. Lett. **107**, 228102 (2011)
48. Erneux, T.: Applied Delay Differential Equations, vol. 3. Springer, Berlin (2009)
49. Soriano, M.C., Garcia-Ojalvo, J., Mirasso, C.R., Fischer, I.: Complex photonics: dynamics and applications of delay-coupled semiconductors lasers. Rev. Mod. Phys. **85**, 421–470 (2013)
50. Kantner, M., Schöll, E., Yanchuk, S.: Delay-induced patterns in a two-dimensional lattice of coupled oscillators. Sci. Rep. **5**, 8522 (2015)
51. Singer, W.: Annu. Rev. Phys. **55**, 349 (1993); Neuron **69**, 1991 (2011)

52. Gray, C.M., König, P., Engel, A.K., Singer, W.: Oscillatory responses in cat visual cortex exhibit inter-columnar synchronization which reflects global stimulus properties. Nature **338**, 334–337 (1989)
53. Sarnthein, J., Petsche, H., Rappelsberger, P., Shaw, G.L., Von Stein, A.: Proc. Natl. Acad. Sci. U.S.A. **95**, 7092 (1998); Int. J. Psychophysiol. **24**, 61 (1996)
54. Kazantsev, V.B., Nekorkin, V.I., Makarenko, V.I., Llinás, R.: Self-referential phase reset based on inferior olive oscillator dynamics. Proc. Natl. Acad. Sci. **101**(52), 18183–18188 (2004)
55. Hammond, C., Bergman, H., Brown, P.: Trends Neurosci. **30**, 357 (2007); Singer, W.: Nat. Rev. Neurosci. **11**, 100 (2010)
56. Canavier, C.C., Baxter, D.A., Clark, J.W., Byrne, J.H.: Control of multistability in ring circuits of oscillators. Biol. Cybern. **80**, 87–102 (1999)
57. Dror, R.O., Canavier, C.C., Butera, R.J., Clark, J.W., Byrne, J.H.: A mathematical criterion based on phase response curves for stability in a ring of coupled oscillators. Biol. Cybern. **80**, 11–23 (1999)
58. Netoff, T.I., Banks, M.I., Dorval, A.D., Acker, C.D., Haas, J.S., et al.: Synchronization in hybrid neuronal networks of the hippocampal formation. J. Neurophysiol. **93**, 1197–1208 (2005)
59. Klinshov, V.V., Nekorkin, V.I.: The map with no predetermined firing order for the network of oscillators with time-delayed pulsatile coupling. Commun. Nonlinear Sci. Numer. Simul. **18**(4), 973–977 (2013)
60. Klinshov, V., Lücken, L., Shchapin, D., Nekorkin, V., Yanchuk, S.: Multistable jittering in oscillators with pulsatile delayed feedback. Phys. Rev. Lett. **114**, 178103 (2015)
61. Klinshov, V.V., Lücken, L., Shchapin, D.S., Nekorkin, V.I., Yanchuk, S.: Emergence and combinatorial accumulation of jittering regimes in spiking oscillators with delayed feedback. Phys. Rev. E. **92**, 042914 (2015)
62. Ramón y Cajal, S.: Histology of the Nervous System of Man and Vertebrates. Oxford University Press, Oxford (1995)
63. Milo, R., Shen-Orr, S., Itzkovitz, S., Kashtan, N., Chklovskii, D., Alon, U.: Network motifs: simple building blocks of complex networks. Science **298**(5594), 824–827 (2002)
64. Ma, J., Wu, J.: Multistability in spiking neuron models of delayed recurrent inhibitory loops. Neural Comput. **19**(8), 2124–2148 (2007)
65. Ma, J., Wu, J.: Patterns, memory and periodicity in two-neuron delayed recurrent inhibitory loops. Math. Model. Nat. Phenom. **5**, 67–99, 1 (2010)
66. Hashemi, M., Valizadeh, A., Azizi, Y.: Effect of duration of synaptic activity on spike rate of a Hodgkin-Huxley neuron with delayed feedback. Phys. Rev. E **85**, 021917 (2012)
67. Van der Sande, G., Soriano, M.C., Fischer, I., Mirasso, C.R.: Dynamics, correlation scaling, and synchronization behavior in rings of delay-coupled oscillators. Phys. Rev. E **77**, 055202 (2008)
68. Kantner, M., Yanchuk, S.: Bifurcation analysis of delay-induced patterns in a ring of Hodgkin-Huxley neurons. Philos. Trans. R. Soc. A **371**, 20120470 (2013)
69. Yanchuk, S., Perlikowski, P., Popovych, O.V., Tass, P.A.: Variability of spatio-temporal patterns in non-homogeneous rings of spiking neurons. Chaos **21**, 047511 (2011)
70. Lücken, L., Yanchuk, S., Popovych, O.V., Tass, P.A.: Desynchronization boost by non-uniform coordinated reset stimulation in ensembles of pulse-coupled neurons. Front. Comput. Neurosci. **7**, 63 (2013)
71. Canavier, C.C., Achuthan, S.: Pulse coupled oscillators and the phase resetting curve. Math. Biosci. **226**(2), 77–96 (2010)
72. Ermentrout, B., Kopell, N.: Multiple pulse interactions and averaging in systems of coupled neural oscillators. J. Math. Biol. **29**, 195–217 (1991)
73. Tsubo, Y., Takada, M., Reyes, A.D., Fukai, T.: Layer and frequency dependencies of phase response properties of pyramidal neurons in rat motor cortex. Eur. J. Neurosci. **25**(11), 3429–3441 (2007)
74. Schultheiss, N.W., Edgerton, J.R., Jaeger, D.: Phase response curve analysis of a full morphological globus pallidus neuron model reveals distinct perisomatic and dendritic modes of synaptic integration. J. Neurosci. Off. J. Soc. Neurosci. **30**(7), 2767–2782 (2010). doi:10.1523/JNEUROSCI.3959-09.2010. ISSN 0270-6474

75. Klinshov, V.V., Maslennikov, O.V., Nekorkin, V.I.: Jittering regimes of two spiking oscillators with delayed coupling. Appl. Math. Nonlinear Sci. **1**, 197 (2016)
76. Klinshov, V., Shchapin, D., Yanchuk, S., Nekorkin, V.: Jittering waves in rings of pulse oscillators. Phys. Rev. E **94**, 012206 (2016)
77. Bressloff, P.C., Coombes, S., de Souza, B.: Dynamics of a ring of pulse-coupled oscillators: group-theoretic approach. Phys. Rev. Lett. **79**(15), 2791–2794 (1997)
78. Alexander, G.E., Delong, M.R., Strick, P.L.: Parallel organization of functionally segregated circuits linking basal ganglia and cortex. Annu. Rev. Neurosci. **9**, 357–381 (1986)
79. Courtemanche, M., Glass, L., Keener, J.P.: Instabilities of a propagating pulse in a ring of excitable media. Phys. Rev. Lett. **70**, 2182–2185 (1993)
80. Ben-Yishai, R., Hansel, D., Sompolinsky, H.: Traveling waves and the processing of weakly tuned inputs in a cortical network module. J. Comput. Neurosci. **4**, 57–77 (1997)
81. Elowitz, M.B., Leibler, S.: A synthetic oscillatory network of transcriptional regulators. Nature **403**, 335–338 (2000)
82. Matias, M.A., Guemez, J.: Phys. Rev. Lett. **81**, 4124 (1998)
83. Perlikowski, P., Yanchuk, S., Popovych, O.V., Tass, P.A.: Periodic patterns in a ring of delay-coupled oscillators. Phys. Rev. E. **82**, 036208 (2010)
84. Lücken, L., Pade, J.P., Knauer, K., Yanchuk, S.: Reduction of interaction delays in networks. Europhys. Lett. **103**, 10006 (2013)
85. Glass, L., Sun, J.: Phys. Rev. E **50**, 5077 (1994); Coombes, S., Bressloff, P.C.: Phys. Rev. E. **60**, 2086 (1999); Kuznetsov, A.P., Stankevich, N.V., Tyuryukina, L.V.: Tech. Phys. Lett. **32**, 343 (2006); Kuznetsov, A.P., Stankevich, N.V., Turukina, L.V.: Phys. D Nonlinear Phenom. **238**, 1203 (2009)
86. Klinshov, V.V., Nekorkin, V.I.: Synchronization in networks of pulse oscillators with time-delay coupling. Cybern. Phys. **1**(2), 106–112 (2012)
87. Collins, J., Stewart, I.N.: Coupled nonlinear oscillators and the symmetries of animal gaits. J. Nonlinear Sci. **3**, 349–392 (1993)
88. Collins, J., Richmond, S.A.: Hard-wired central pattern generators for quadrupedal locomotion. Biol. Cybern. **71**, 375–385 (1994)
89. Abarbanel, H.D.I., Rabinovich, M.I., Selverston, A., Bazhenov, M.V., Huerta, R., Sushchik, M.M., Rubchinskii, L.L.: Synchronization in neural networks. Physics-Uspekhi **39**, 337–362 (1996)
90. Kimura, H., Akiyama, S., Sakurama, K.: Realization of dynamic walking and running of the quadruped using neural oscillator. Auton. Robot. **7**, 247–258 (1999)
91. Shinkichi, I., Yuasa, Y., Suzuki, T., Arai, T.: Wave CPG model for autonomous decentralized multi-legged robot: gait generation and walking speed control. Robot. Auton. Syst. **54**, 118–126 (2006)
92. Klinshov, V.V., Nekorkin, V.I.: Global synchronization of large ensembles of pulse oscillators with time-delay coupling. Discontinuity Nonlinearity Complex. **1**, 253–261 (2012)
93. Tass, P.: Phase Resetting in Medicine and Biology. Stochastic Modelling and Data Analysis. Springer Series in Synergetics. Springer, Berlin (1999)

Chapter 10
Bifurcation Trees of Period-3 Motions to Chaos in a Time-Delayed Duffing Oscillator

Albert C.J. Luo and Siyuan Xing

The time-delayed Duffing oscillator is extensively applied in engineering and particle physics. Determination of periodic motions in such a system is significant. Thus, here in, period-1 motions in the time-delayed Duffing oscillator are discussed through a semi-analytical method. The semi-analytical method is based on the implicit mappings constructed by discretization of the corresponding differential equation. Complex period-3 motions are predicted, and the corresponding stability and bifurcation analysis are completed. From predictions, complex periodic motions are simulated numerically, and the harmonic amplitudes and phases are presented. Through this study, the complexity of periodic motions in the time-delayed Duffing oscillator can be better understood. This chapter is dedicated to Professor Valentin Afraimoich's 70th birthday.

10.1 Introduction

In recent decades, time-delay nonlinear systems have received great attentions. Periodic solutions in nonlinear dynamical systems have been of great interest for a long time. However, one still cannot obtain adequate solutions of periodic motions to chaos in nonlinear dynamical systems.

In 1788, Lagrange [1] investigated periodic motions of three-body problem through a perturbation of the two-body problem with the method of averaging. In the end of 19th century, Poincare [2] developed the perturbation theory for periodic

A.C. Luo (✉) · S. Xing
Department of Mechanical and Industrial Engineering, Southern Illinois University Edwardsville, Edwardsville, IL 62026-1805, USA
e-mail: aluo@siue.edu

D. Volchenkov and X. Leoncini (eds.), *Regularity and Stochasticity of Nonlinear Dynamical Systems*, Nonlinear Systems and Complexity 21,
DOI 10.1007/978-3-319-58062-3_10

motions of celestial bodies. In 1920, van der Pol [3] employed the method of averaging for the periodic solutions of oscillation systems in circuits. Until 1928, the asymptotic validity of the method of averaging was not proved. Fatou [4] gave the proof of the asymptotic validity through the solution existence theorems of differential equations. In 1935, Krylov and Bogoliubov [5] further developed the method of averaging for nonlinear oscillations in nonlinear vibration systems. Since then, one extensively used the perturbation method to investigate periodic solutions in nonlinear dynamical systems. In 2012, Luo [6] developed an analytical method for analytical solutions of periodic motions in nonlinear dynamical systems. Luo and Huang [7] applied such a method to the Duffing oscillator for approximate solutions of periodic motions, and Luo and Huang [8] gave the analytical bifurcation trees of period-m motions to chaos in the Duffing oscillator (also see, Luo and Huang [9, 10]).

The approximate solutions of periodic motion in the time-delayed nonlinear oscillators were investigated by the method of multiple scales (e.g., Hu et al. [11], Wang and Hu [12]). The harmonic balance method was also employed for approximate solutions of periodic motions in time-delayed nonlinear oscillators (e.g., MacDonald [13]; Liu and Kalmar-Nagy [14]; Lueng and Guo [15]). However, these methods are not accurate enough to give reliable results. For instance, the multiple scale method can only be applied to dynamical systems with weak nonlinear terms. The harmonic balance method is based on one or two harmonic terms. In 2013, Luo [16] systematically presented an analytical method for periodic motions in time-delayed, nonlinear dynamical systems. Luo and Jin [17] applied such an analytical method to the time-delayed, quadratic nonlinear oscillator, and the analytical bifurcation trees of period-1 motions to chaos were obtained. In Luo and Jin [18], complex period-1 motions of the periodically forced Duffing oscillator with a time-delayed displacement were investigated, which cannot be obtained from the traditional harmonic balance and perturbation methods. In Luo and Jin [19], the period-m motions of the time-delayed Duffing oscillator were investigated analytically, and complex period-m motions were observed in such a time-delayed Duffing oscillator. The bifurcation trees of period-1 motion to chaos were also discussed.

To determine stability of time-varying coefficient systems with time-delay, Insperger and Sepan [20] developed the semi-discretization method, and the detailed description of such a method can be found in Insperger and Sepan [21]. In 2011, based on the ideas of finite element method, Khasawneh and Mann [22] developed the spectral element approach for stability of delayed systems. In 2016, Lehotzsky, Insperger, and Stepan [23] extended this idea for time-periodic delayed, differential equations with multiple and distributed delay. Such a method cannot be applied to periodic motions in nonlinear time-delay systems. In 2015, Luo [24] developed a semi-analytical method to determine periodic motions in nonlinear dynamical systems with/without time-delay through discrete implicit maps. Luo [25] systematically discussed the discretization methods of continuous dynamical systems with/ without time-delay. Luo and Guo [26] applied such an approach to investigate bifurcation trees of the Duffing oscillator, and nonlinear frequency-amplitude characteristics of periodic motion to chaos.

This semi-analytical method for time-delayed, nonlinear dynamical systems is different from the aforementioned semi-analytical method for non-time-delayed nonlinear dynamical systems. Thus, for a periodically forced, time-delayed, hardening Duffing nonlinear oscillator, the different semi-analytical method was adopted in Luo and Xing [27] for determining complex symmetric and asymmetric period-1 motions. With decreasing excitation frequency, symmetric and asymmetric period-1 motions become very complicated. From the asymmetric period-1 motions, the corresponding period-doubling bifurcations were observed. Thus, period-2 motions should be discovered. If the period-doubling bifurcations of period-2 motions exist, the period-4 motions will be discovered. In Luo and Xing [28], the bifurcation trees of periodic motions to chaos in the hardening Duffing oscillator were discussed. The double-well Duffing oscillators extensively exist in engineering and physical systems, and one often used displacement feedback to control periodic motions in such a twin-well Duffing oscillator. Thus, the bifurcation trees of periodic motions to chaos in such a time-delayed Duffing oscillator are of great interest for a better understanding of global pictures of periodic motions switching and complexity. Before determining bifurcation trees, period-3 motions should be determined first.

In this chapter, the semi-analytical method will be used to investigate period-3 motions in a periodically forced Duffing oscillator with time-delay. This time-delay is caused by the displacement feedback. The analytical predictions of period-3 motions will be completed, and the corresponding stability and bifurcation will be carried out through the eigenvalue analysis. To understand the motion complexity, the numerical simulations will be completed and harmonic amplitudes and phases will be presented.

10.2 Discrete Mappings

Consider a time-delayed, Duffing oscillator

$$\ddot{x} + \delta\dot{x} + \alpha_1 x - \alpha_2 x^\tau + \beta x^3 = Q_0 \cos \Omega t \tag{10.1}$$

where $x = x(t)$ and $x^\tau = x(t - \tau)$. In state space, the above equation becomes

$$\begin{aligned} \dot{x} &= y, \\ \dot{y} &= Q_0 \cos \Omega t - \delta y - \alpha_1 x + \alpha_2 x^\tau - \beta x^3. \end{aligned} \tag{10.2}$$

Let $\mathbf{x} = (x, y)^{\mathrm{T}}$ and $\mathbf{x}^\tau = (x^\tau, y^\tau)^{\mathrm{T}}$. For discrete time $t_k = kh$ $(k = 0, 1, 2, \ldots)$, $\mathbf{x}_k = (x_k, y_k)^{\mathrm{T}}$ and $\mathbf{x}_k^\tau = (x_k^\tau, y_k^\tau)^{\mathrm{T}}$. Using a midpoint scheme for the time interval $t \in [t_{k-1}, t_k]$ $(k = 1, 2, \ldots)$, the foregoing differential equation is discretized to form an implicit map P_k:

$$\begin{array}{l} P_k : (\mathbf{x}_{k-1}^{(m)}, \mathbf{x}_{k-1}^{\tau(m)}) \to (\mathbf{x}_k^{(m)}, \mathbf{x}_k^{\tau(m)}) \\ \Rightarrow (\mathbf{x}_k^{(m)}, \mathbf{x}_k^{\tau(m)}) = P_k(\mathbf{x}_{k-1}^{(m)}, \mathbf{x}_{k-1}^{\tau(m)}) \end{array} \tag{10.3}$$

The corresponding implicit relations for the implicit map are

$$\begin{array}{l} x_k = x_{k-1} + \frac{1}{2}h(y_k + y_{k-1}), \\ y_k = y_{k-1} + h[Q_0 \cos\Omega(t_{k-1} + \frac{h}{2}) - \frac{1}{2}\delta(y_k + y_{k-1}) \\ \quad -\frac{1}{2}\alpha_1(x_k + x_{k-1}) + \frac{1}{2}\alpha_2(x_k^\tau + x_{k-1}^\tau) - \frac{1}{8}\beta(x_k + x_{k-1})^3]. \end{array} \tag{10.4}$$

The time-delay node $\mathbf{x}_k^\tau \approx \mathbf{x}(t_{k-\tau})$ of $\mathbf{x}_k \approx \mathbf{x}(t_k)$ lies between $\mathbf{x}_{k-l_k}$ and $\mathbf{x}_{k-l_k-1}$ ($l_k = \text{int}(\tau/h)$). The time-delay nodes can be expressed by an interpolation function of two points $\mathbf{x}_{k-l_k}$ and $\mathbf{x}_{k-l_k-1}$. For a time-delay node $\mathbf{x}_j^\tau$ ($j = k-1, k$), we have

$$\mathbf{x}_j^\tau = \mathbf{h}_j(\mathbf{x}_{r_j-1}, \mathbf{x}_{r_j}, \theta_{r_j}) \text{ for } r_j = j - l_j. \tag{10.5}$$

For instance, the time-delay discrete node $\mathbf{x}_j^\tau$ is determined by the simple Lagrange interpolation, i.e.,

$$\begin{array}{l} x_j^\tau = x_{j-l_j-1} + (1 - \frac{\tau}{h} + l_j)(x_{j-l_j} - x_{j-l_j-1}), \\ y_j^\tau = y_{j-l_j-1} + (1 - \frac{\tau}{h} + l_j)(y_{j-l_j} - y_{j-l_j-1}). \end{array} \tag{10.6}$$

Thus, the time-delay nodes are expressed by non-time-delay nodes. The discretization of differential equation for the time-delayed Duffing oscillator is completed. In the next section, the discrete mapping will be used to determine period-3 motions in the time-delayed Duffing oscillator.

10.3 Period-m Motions and Stability

To represent the period-m motion in such a Duffing oscillator, a discrete mapping structure, presented in Luo [20], is constructed as

$$P = \underbrace{P_{mN} \circ P_{mN-1} \circ \cdots \circ P_2 \circ P_1}_{mN-\text{actions}} : (\mathbf{x}_0^{(m)}, \mathbf{x}_0^{\tau(m)}) \to (\mathbf{x}_N^{(m)}, \mathbf{x}_N^{\tau(m)}) \tag{10.7}$$

with

$$\begin{array}{l} P_k : (\mathbf{x}_{k-1}^{(m)}, \mathbf{x}_{k-1}^{\tau(m)}) \to (\mathbf{x}_k^{(m)}, \mathbf{x}_k^{\tau(m)}) \\ (k = 1, 2, \cdots, mN). \end{array} \tag{10.8}$$

By applying a midpoint scheme discretization, the corresponding algebraic equations of P_k are obtained as follows:

$$P_k : \begin{cases} x_k^{(m)} = x_{k-1}^{(m)} + \frac{1}{2}h(y_k^{(m)} + y_{k-1}^{(m)}), \\ y_k^{(m)} = y_{k-1}^{(m)} + h[Q_0 cos\omega(t + \frac{1}{2}h) - \frac{1}{2}\delta(y_k^{(m)} + y_{k-1}^{(m)}) \\ \quad -\frac{1}{2}\alpha_1(x_k^{(m)} + x_{k-1}^{(m)}) + \frac{1}{2}\alpha_2(x_k^{\tau(m)} + x_{k-1}^{\tau(m)}) \\ \quad -\frac{1}{8}\beta(x_k^{(m)} + x_{k-1}^{(m)})^3] \\ \quad (k = 1, 2, \cdots, mN). \end{cases} \tag{10.9}$$

Application of the simple Lagrange interpolation, the time-delay node $\mathbf{x}_j^{\tau} = \mathbf{h}_j(\mathbf{x}_{r_j-1}, \mathbf{x}_{r_j}, \theta_{rj})$ is expressed as

$$\begin{aligned} x_k^{\tau(m)} &= x_{k-l_k-1}^{(m)} + (1 - \tfrac{\tau}{h} + l_k)(x_{k-l_k}^{(m)} - x_{k-l_k-1}^{(m)}), \\ y_k^{\tau(m)} &= y_{k-l_k-1}^{(m)} + (1 - \tfrac{\tau}{h} + l_k)(y_{k-l_k}^{(m)} - y_{k-l_k-1}^{(m)}). \end{aligned} \tag{10.10}$$

Then, the set of points on the periodic motion are computed by

$$\left.\begin{array}{l} \mathbf{g}_k(\mathbf{x}_{k-1}^{(m)*}, \mathbf{x}_k^{(m)*}; \mathbf{x}_{k-1}^{\tau(m)*}, \mathbf{x}_k^{\tau(m)*}, \mathbf{p}) = \mathbf{0} \\ \mathbf{x}_j^{\tau(m)*} = \mathbf{h}_j(\mathbf{x}_{r_j-1}^{(m)*}, \mathbf{x}_{r_j}^{(m)*}, \theta_{rj}),\ j = k, k-1 \\ \mathbf{x}_0^{(m)*} = \mathbf{x}_{mN}^{(m)*}\ and\ \mathbf{x}_0^{\tau(m)*} = \mathbf{x}_{mN}^{\tau(m)*} \end{array}\right\} (k = 1, 2, \cdots, mN) \tag{10.11}$$

Once the node points $\mathbf{x}_k^{(m)*}$ $(k = 1, 2, \cdots, mN)$ of the period-m motion are obtained, the stability of period-m motion can be discussed through the eigenvalue analysis of the corresponding Jacobian matrix.

$$\begin{aligned} &\sum_{j=k-1}^{k} \frac{\partial \mathbf{g}_k}{\partial \mathbf{x}_j^{(m)}} \Delta \mathbf{x}_j^{(m)} + \frac{\partial \mathbf{g}_k}{\partial \mathbf{x}_j^{\tau(m)}} \left(\frac{\partial \mathbf{x}_j^{\tau(m)}}{\partial \mathbf{x}_{r_j}^{\tau(m)}} \Delta \mathbf{x}_{r_j}^{\tau(m)} + \frac{\partial \mathbf{x}_j^{\tau(m)}}{\partial \mathbf{x}_{r_j-1}^{\tau(m)}} \Delta \mathbf{x}_{r_j-1}^{\tau(m)}\right) = \mathbf{0} \\ &\text{with } r_j = j - l_j,\ j = k-1, k;\ (k = 1, 2, \cdots, mN). \end{aligned} \tag{10.12}$$

As in Luo [20], new vectors are introduced as

$$\begin{aligned} \mathbf{y}_k^{(m)} &= (\mathbf{x}_k^{(m)}, \mathbf{x}_{k-1}^{(m)}, \cdots, \mathbf{x}_{r_{k-1}}^{(m)})^{\mathrm{T}}, \\ \mathbf{y}_{k-1}^{(m)} &= (\mathbf{x}_{k-1}^{(m)}, \mathbf{x}_{k-2}^{(m)}, \cdots, \mathbf{x}_{r_{k-1}-1}^{(m)})^{\mathrm{T}}, \\ \Delta\mathbf{y}_k^{(m)} &= (\Delta\mathbf{x}_k^{(m)}, \Delta\mathbf{x}_{k-1}^{(m)}, \cdots, \Delta\mathbf{x}_{r_{k-1}}^{(m)})^{\mathrm{T}}, \\ \Delta\mathbf{y}_{k-1}^{(m)} &= (\Delta\mathbf{x}_{k-1}^{(m)}, \Delta\mathbf{x}_{k-2}^{(m)}, \cdots, \Delta\mathbf{x}_{r_{k-1}-1}^{(m)})^{\mathrm{T}}. \end{aligned} \tag{10.13}$$

The resultant Jacobian matrices of the periodic motions are

$$DP = DP_{mN(mN-1)\cdots 1} = \left[\frac{\partial \mathbf{y}_{mN}^{(m)}}{\partial \mathbf{y}_0^{(m)}}\right] = \mathbf{A}_{mN}\mathbf{A}_{mN-1}\cdots\mathbf{A}_1 \tag{10.14}$$

with

$$\Delta\mathbf{y}_k^{(m)} = \mathbf{A}_k^{(m)}\Delta\mathbf{y}_{k-1}^{(m)},\ \mathbf{A}_k^{(m)} \equiv \left[\frac{\partial \mathbf{y}_k^{(m)}}{\partial \mathbf{y}_{k-1}^{(m)}}\right]_{(\mathbf{y}_{k-1}^{(m)*}, \mathbf{y}_k^{(m)*})} \tag{10.15}$$

and

$$\begin{aligned}
&\mathbf{A}_k^{(m)} = \begin{bmatrix} \mathbf{B}_k^{(m)} & (\mathbf{a}_{k(r_{k-1}-1)}^{(m)})_{2\times 2} \\ \mathbf{I}_k^{(m)} & \mathbf{0}_k^{(m)} \end{bmatrix}_{2(s+1)\times 2(s+1)}, s = 1 + l_{k-1} \\
&\mathbf{B}_k^{(m)} = [(\mathbf{a}_{k(k-1)}^{(m)})_{2\times 2}, \mathbf{0}_{2\times 2}, \cdots, (\mathbf{a}_{k(r_k-1)}^{(m)})_{2\times 2}], \\
&\mathbf{I}_k^{(m)} = diag(\mathbf{I}_{2\times 2}, \mathbf{I}_{2\times 2}, \cdots, \mathbf{I}_{2\times 2})_{2s\times 2s}, \\
&\mathbf{0}_k^{(m)} = (\underbrace{\mathbf{0}_{2\times 2}, \mathbf{0}_{2\times 2}, \cdots, \mathbf{0}_{2\times 2}}_{s})^{\mathrm{T}};
\end{aligned} \tag{10.16}$$

$$\begin{aligned}
&\mathbf{a}_{kj}^{(m)} = [\tfrac{\partial \mathbf{g}_k}{\partial \mathbf{x}_k^{(m)}}]^{-1} \tfrac{\partial \mathbf{g}_k}{\partial \mathbf{x}_j^{(m)}}, \\
&\mathbf{a}_{kr_j}^{(m)} = [\tfrac{\partial \mathbf{g}_k}{\partial \mathbf{x}_k^{(m)}}]^{-1} \tfrac{\partial \mathbf{g}_k}{\partial \mathbf{x}_j^{(m)\tau}} \tfrac{\partial \mathbf{x}_j^{(m)\tau}}{\partial \mathbf{x}_{r_j}^{(m)\tau}}, \\
&\mathbf{a}_{k(r_j-1)}^{(m)} = [\tfrac{\partial \mathbf{g}_k}{\partial \mathbf{x}_k^{(m)}}]^{-1} \tfrac{\partial \mathbf{g}_k}{\partial \mathbf{x}_j^{(m)\tau}} \tfrac{\partial \mathbf{x}_j^{(m)\tau}}{\partial \mathbf{x}_{r_j-1}^{(m)\tau}} \\
&\text{with } r_j = j - l_j,\ j = k-1, k;
\end{aligned} \tag{10.17}$$

$$\begin{aligned}
&\frac{\partial \mathbf{g}_k}{\partial \mathbf{x}_{k-1}^{(m)}} = \begin{bmatrix} -1 & -\frac{1}{2}h \\ \Delta & \frac{1}{2}\delta h - 1 \end{bmatrix}, \quad \frac{\partial \mathbf{g}_k}{\partial \mathbf{x}_{k1}^{(m)}} = \begin{bmatrix} 1 & -\frac{1}{2}h \\ \Delta & \frac{1}{2}\delta h + 1 \end{bmatrix}, \\
&\frac{\partial \mathbf{g}_j^{\tau(m)}}{\partial \mathbf{x}_{r_j-1}^{(m)}} = \begin{bmatrix} 0 & 0 \\ \frac{\tau}{h} - l_j & 0 \end{bmatrix}, \quad \frac{\partial \mathbf{g}_j^{\tau(m)}}{\partial \mathbf{x}_{r_j}^{(m)}} = \begin{bmatrix} 0 & 0 \\ 1 - \frac{\tau}{h} + l_j & 0 \end{bmatrix}, \\
&\frac{\partial \mathbf{g}_k}{\partial \mathbf{x}_j^{\tau(m)}} = \begin{bmatrix} 0 & 0 \\ 0 & -\frac{1}{2}h\alpha_2 \end{bmatrix}, \\
&\Delta = \tfrac{1}{2}h[\alpha_1 + \beta(x_k + x_{k-1})].
\end{aligned} \tag{10.18}$$

The eigenvalues of DP for such periodic flow are determined by

$$|DP - \lambda \mathbf{I}_{2(s+1)\times 2(s+1)}| = 0. \tag{10.19}$$

(i) If the magnitudes of all eigenvalues of DP are less than one (i.e., $|\lambda_i| < 1, i, 1, 2, \cdots, 2(s+1)$), the approximate periodic solution is stable.
(ii) If at least the magnitude of one eigenvalue of DP is greater than one (i.e., $|\lambda_i| > 1, i \in \{1, 2, \cdots, n(s+1)\}$), the approximate periodic solution is unstable.
(iii) The boundaries between stable and unstable periodic flow with higher-order singularity give bifurcation and stability conditions with higher-order singularity.

The bifurcation conditions are given as follows.

(1) If $\lambda_i = 1$ with $|\lambda_j| < 1 (i, j \in \{1, 2, \cdots, 2(s+1)\}$ and $i \neq j)$, the saddle-node bifurcation (SN) occurs.

(2) If $\lambda_i = -1$ with $|\lambda_j| < 1 (i, j \in \{1, 2, \cdots, 2(s+1)\}$ and $i \neq j)$, the period-doubling bifurcation (PD) occurs.
(3) If $|\lambda_{i,j}| = 1$ with $|\lambda_l| < 1 (i, j, l \in \{1, 2, \cdots, 2(s+1)\}$ and $\lambda_i = \bar{\lambda}_j \quad l \neq i, j)$, Neimark bifurcation (NB) occurs.

10.4 Frequency-Amplitude Analysis

From the node points of period-m motions in the time-delayed Duffing oscillator, $\mathbf{x}_k^{(m)} = (x_k^{(m)}, y_k^{(m)})^{\mathrm{T}}$ $(k = 0, 1, 2, \cdots, mN)$, the period-$m$ motions can be approximately expressed by the Fourier series, i.e.,

$$\mathbf{x}^{(m)}(t) \approx \mathbf{a}_0^{(m)} + \sum_{j=1}^{M} \mathbf{b}_{j/m} \cos(\frac{k}{m}\Omega t) + \mathbf{c}_{j/m} \sin(\frac{k}{m}\Omega t) \tag{10.20}$$

The $(2M+1)$ unknown vector coefficients of $\mathbf{a}_0^{(m)}$, $\mathbf{b}_{j/m}$, $\mathbf{c}_{j/m}$ should be determined from discrete nodes $\mathbf{x}_k^{(m)} (k = 0, 1, 2, \cdots, mN)$ with $mN + 1 \geq 2M + 1$. For $M = mN/2$, the node points $\mathbf{x}_k^{(m)}$ on the period-m motion can be expressed for $t_k \in [0, mT]$

$$\begin{aligned} \mathbf{x}^{(m)}(t_k) \equiv \mathbf{x}_k^{(m)} &= \mathbf{a}_0^{(m)} + \sum_{j=1}^{mN/2} \mathbf{b}_{j/m} \cos(\frac{j}{m}\Omega t_k) + \mathbf{c}_{j/m} \sin(\frac{j}{m}\Omega t_k) \\ &= \mathbf{a}_0^{(m)} + \sum_{j=1}^{mN/2} \mathbf{b}_{j/m} \cos(\frac{j}{m}\frac{2k\pi}{N}) + \mathbf{c}_{j/m} \sin(\frac{j}{m}\frac{2k\pi}{N}) \\ &(k = 0, 1, \cdots, mN-1) \end{aligned} \tag{10.21}$$

where

$$\left.\begin{aligned} &T = \tfrac{2\pi}{\Omega} = N\Delta t;\ \Omega t_k = \Omega k \Delta t = \tfrac{2k\pi}{N} \\ &\mathbf{a}_0^{(m)} = \tfrac{1}{N}\textstyle\sum_{k=0}^{mN-1} \mathbf{x}_k^{(m)}, \\ &\mathbf{b}_{j/m} = \frac{2}{mN} \sum_{k=1}^{mN-1} \mathbf{x}_k^{(m)} \cos(k\frac{2j\pi}{mN}), \\ &\mathbf{c}_{j/m} = \frac{2}{mN} \sum_{k=1}^{mN-1} \mathbf{x}_k^{(m)} \sin(k\frac{2j\pi}{mN}) \end{aligned}\right\} (j = 1, 2, \cdots, mN/2) \tag{10.22}$$

and

$$\mathbf{a}_0^{(m)} = (a_{01}^{(m)}, a_{02}^{(m)})^{\mathrm{T}}, \mathbf{b}_{j/m} = (b_{j/m1}, b_{j/m2})^{\mathrm{T}}, \mathbf{c}_{j/m} = (c_{j/m1}, c_{j/m2})^{\mathrm{T}}. \tag{10.23}$$

The harmonic amplitudes and phases for the period-m motions are expressed by

$$\begin{aligned} A_{j/m1} &= \sqrt{b_{j/m1}^2 + c_{j/m1}^2},\ \varphi_{j/m1} = \arctan\tfrac{c_{j/m1}}{b_{j/m1}}, \\ A_{j/m2} &= \sqrt{b_{j/m2}^2 + c_{j/m2}^2},\ \varphi_{j/m2} = \arctan\tfrac{c_{j/m2}}{b_{j/m2}}. \end{aligned} \tag{10.24}$$

Thus, the approximate expression of period-m motions in Eq. (10.20) can be given as

$$\mathbf{x}^{(m)}(t) \approx \mathbf{a}_0^{(m)} + \sum_{j=1}^{mN/2} \mathbf{b}_{j/m} \cos(\frac{k}{m}\Omega t) + \mathbf{c}_{j/m} \sin(\frac{k}{m}\Omega t). \tag{10.25}$$

For the time-delayed Duffing oscillator,

$$\left\{ \begin{matrix} x^{(m)}(t) \\ y^{(m)}(t) \end{matrix} \right\} \equiv \left\{ \begin{matrix} x_1^{(m)}(t) \\ x_2^{(m)}(t) \end{matrix} \right\} \approx \left\{ \begin{matrix} a_{01}^{(m)} \\ a_{02}^{(m)} \end{matrix} \right\} + \sum_{j=1}^{mN/2} \left\{ \begin{matrix} A_{j/m1} \cos(\frac{k}{m}\Omega t - \varphi_{j/m1}) \\ A_{j/m1} \cos(\frac{k}{m}\Omega t - \varphi_{j/m2}) \end{matrix} \right\}. \tag{10.26}$$

To reduce illustrations, only frequency-amplitude curves of displacement $x^{(m)}(t)$ for period-m motions are presented. However, the frequency-amplitudes for velocity $y^{(m)}(t)$ can also be done in a similar fashion. Thus, the displacement for period-m motion is given by

$$x^{(m)}(t) \approx a_0^{(m)} + \sum_{j=1}^{mN/2} b_{j/m} \cos(\frac{k}{m}\Omega t) + c_{j/m} \sin(\frac{k}{m}\Omega t) \tag{10.27}$$

or

$$x^{(m)}(t) \approx a_0^{(m)} + \sum_{j=1}^{mN/2} A_{j/m} \cos(\frac{k}{m}\Omega t - \varphi_{j/m}) \tag{10.28}$$

where

$$A_{j/m} = \sqrt{b_{j/m}^2 + c_{j/m}^2},\ \varphi_{j/m} = \arctan\frac{c_{j/m}}{b_{j/m}}. \tag{10.29}$$

10.5 Bifurcation Trees of Period-3 to Period-6 Motions

In this section, a complete picture of P-3 motions and bifurcation trees of P-3 to P-6 motions will be presented. The corresponding stability and bifurcation will be investigated through eigenvalue analysis. Consider a set of parameters under strong excitation as

$$\alpha_1 = 2.0, \alpha_2 = 1.0,\ \beta = 4.0, \delta = 0.2,\ Q_0 = 100.0 \tag{10.30}$$

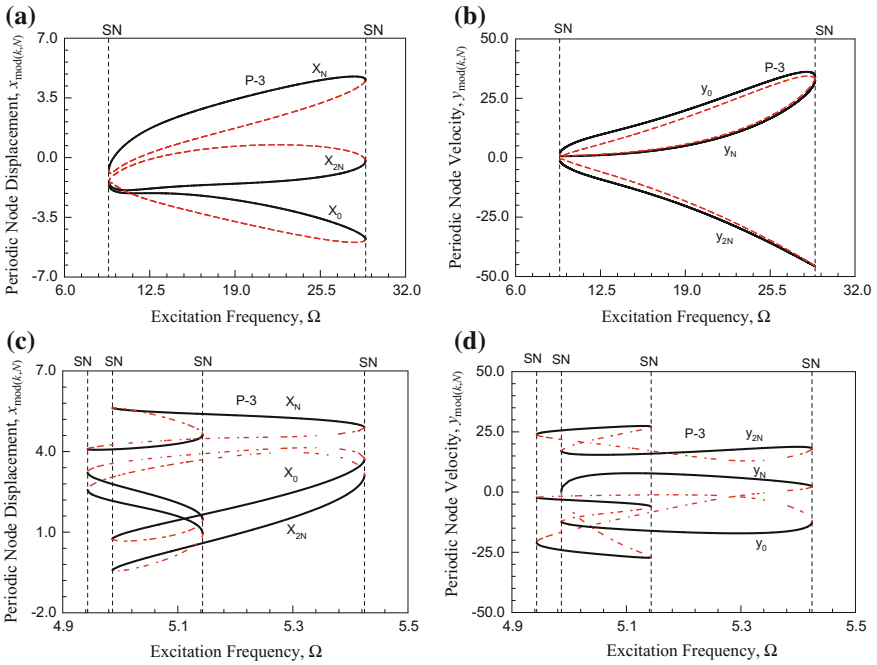

Fig. 10.1 Period-3 motions **a** displacement, **b** velocity for $\Omega \in (9.385, 28.943)$, **c** displacement, **d** velocity for $\Omega \in (4.987, 5.425)$

and the time-delay term $\tau = T/4$ where $T = 2\pi/\Omega$.

Two branches of simple symmetric period-3 motions and another two branches of period-3 to period-6 motions are presented in Figs. 10.1 and 10.2, respectively. For each branch of periodic motions, the displacement and velocity of periodic nodes $x_{mod(x,N)}$ and $y_{mod(x,N)}$ for $\text{mod}(x, N) = 0$ are presented. Two simple symmetric period-3 motions exist in $\Omega \in (9.385, 28.943)$ and $\Omega \in (4.987, 5.425)$, while two period-3 to period-6 motions exist in $\Omega \in (2.812, 3.352)$ and $\Omega \in (2.277, 2.762)$. The acronyms 'SN' and 'PD' denote saddle-node bifurcation and period-doubling bifurcation, respectively. The letters 'A' and 'S' are for asymmetric and symmetric motions, respectively. The black solid curve is for the stable periodic motions while the red-curve for the unstable periodic motions. For the first branch of period-3 motion, two saddle-node bifurcations are observed at $\Omega \approx 9.385$ and $\Omega \approx 28.943$. For the second branch of period-3 motion, four saddle-node bifurcations are observed at $\Omega \approx 4.987$, $\Omega \approx 4.943$, $\Omega \approx 5.143$, and $\Omega \approx 5.452$, respectively. Two of them where $\Omega \approx 4.987$ and $\Omega \approx 5.143$ are for jump phenomena. No period-doubling bifurcation is observed in these two branches of period-3 motions. Thus, no higher periodic motions appear. For the first period-3 to period-6 motions, two saddle-node bifurcations for jump phenomena are observed at $\Omega \approx 3.352$ *and* $\Omega \approx 3.289$. Two saddle-node bifurcations for symmetric to asymmetric period-3 motions occur at $\Omega \approx 2.880$ and $\Omega \approx 3.180$. Two period-doubling bifurcations for period-3 to

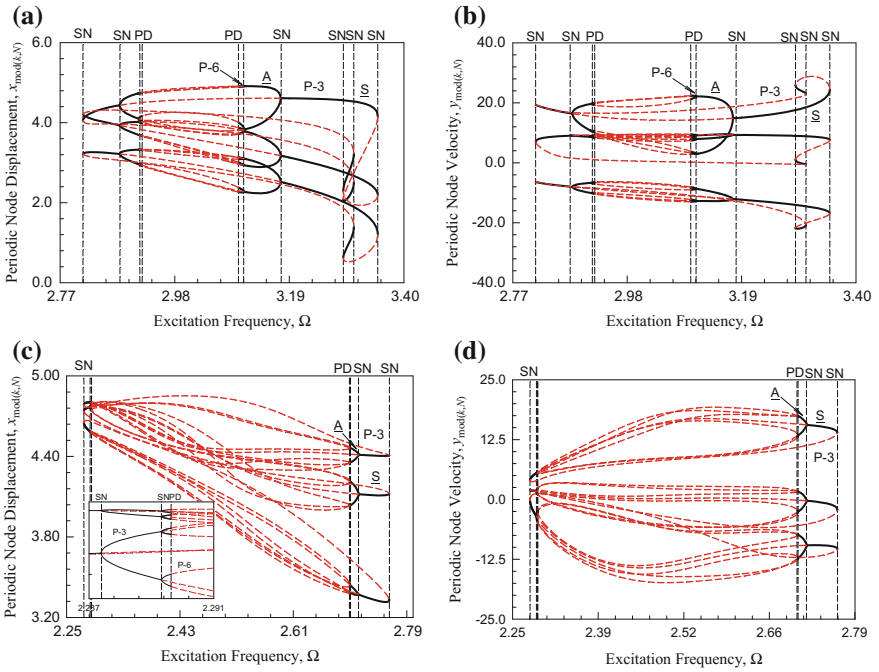

Fig. 10.2 Bifurcation trees of period-3 to period-6 motions **a** displacement, **b** velocity for $\Omega \in (2.812, 3.352)$; **c** displacement, **d** velocity for $\Omega \in (2.277, 2.762)$

period-6 motions appear at $\Omega \approx 2.916$ and $\Omega \approx 3.106$. Two period-doubling bifurcations for period-6 to period-12 motions emerge at $\Omega \approx 3.097$ and $\Omega \approx 2.920$. For the second period-3 to period-6 motions, no saddle-node bifurcations for jump phenomena are observed. Saddle-node bifurcations for symmetric to asymmetric period-3 motions appear at $\Omega \approx 2.287$ and $\Omega \approx 2.714$. Period-doubling bifurcations occur at $\Omega \approx 2.289$ and $\Omega \approx 2.701$ for period-3 to period-6 motions and at $\Omega \approx 2.290$ and $\Omega \approx 2.699$ for period-6 to period-12 motions.

10.6 Numerical Illustrations

The analytical prediction of period-3 to period-6 motions was predicted analytically for the bifurcation trees of period-3 to period-6 motions. To illustrate complexity of periodic motions in the time-delayed Duffing oscillator, initial conditions from the analytical prediction will be used for numerical simulations of period-3 to period-6 motions in the bifurcation trees, and the corresponding harmonic amplitudes of periodic motions will be presented to show harmonic terms effects on periodic motions. The system parameters in Eq. (10.30) are used. Numerical and analytical results

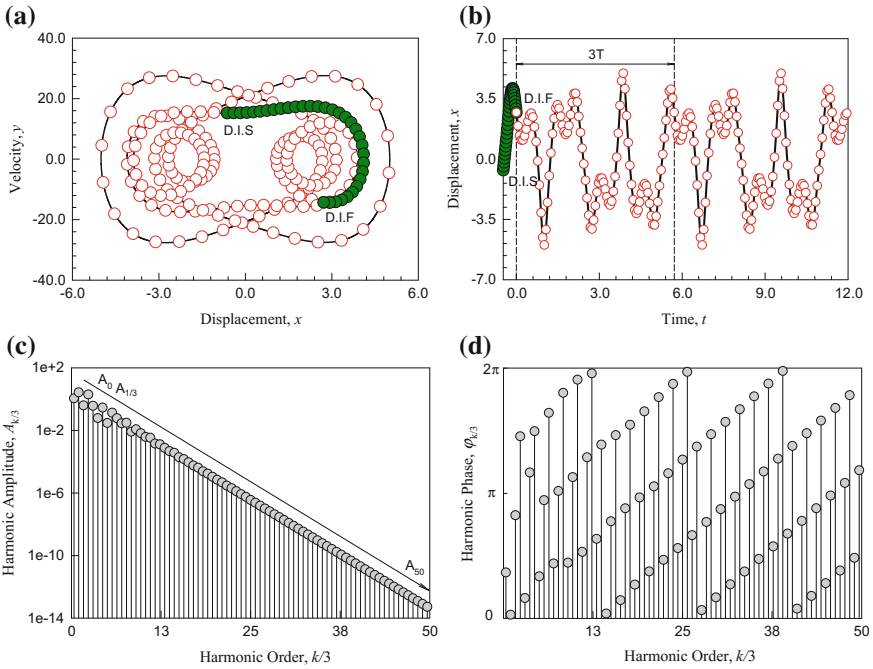

Fig. 10.3 A stable symmetric period-3 motion for $\Omega = 3.3$. **a** trajectory, **b** displacement versus time, **c** harmonic amplitude spectrum, **d** harmonic phase spectrum with initial conditions $(x_0, \dot{x}_0) \approx (2.714985, -14.294936)$ $(\alpha_1 = -10.0, \alpha_2 = 5.0, \beta = 10.0, \delta = 0.5, Q_0 = 100.0, \tau = T/4)$

are presented by solid curves and symbols, respectively. The initial time-delay is presented through blue circular symbols. The delay-initial starting and delay-initial finishing points are 'D.I.S' and 'D.I.F,' respectively.

Consider a stable symmetric period-3 motion of $\Omega = 3.3$, and the initial condition $(x_0, \dot{x}_0) \approx (2.714985, -14.294936)$ is computed from the analytical prediction. Trajectory and displacement for such a simple symmetric period-3 motion are presented in Fig. 10.3a, b, respectively. The initial time-delay is presented by green symbols. The numerical solution of the stable period-3 motion is presented by solid curves, and the analytical prediction is depicted by red symbols. The corresponding harmonic amplitudes and phases are presented in Fig. 10.3c, d, respectively. The harmonic terms $A_{n/3} = 0 (n = 0, 2, 4, 6, \ldots)$. The main harmonic amplitudes are $A_{1/3} = 1.1264$, $A_1 = 2.7333$, $A_{5/3} = 0.4010$, $A_{7/3} = 2.0006$, $A_3 = 0.3755$, $A_{11/3}$=0.0621, $A_{13/3}$=0.2879, A_5=0.0300, $A_{17/3}$=0.1362, $A_{19/3}$=0.0607, $A_7 = 0.0288$, $A_{23/3} = 0.0288$, $A_{25/3} = 8.3549$e-3, and $A_9 = 0.0119$. Other harmonic amplitudes lie in $A_{(2l-1)/3} \in (10^{-15}, 10^{-3})$ $(l = 15, 16, \cdots, 80)$, and 6.2469e-15. For such a period-3 motion, one can use 150 harmonic terms to approximate exact solution.

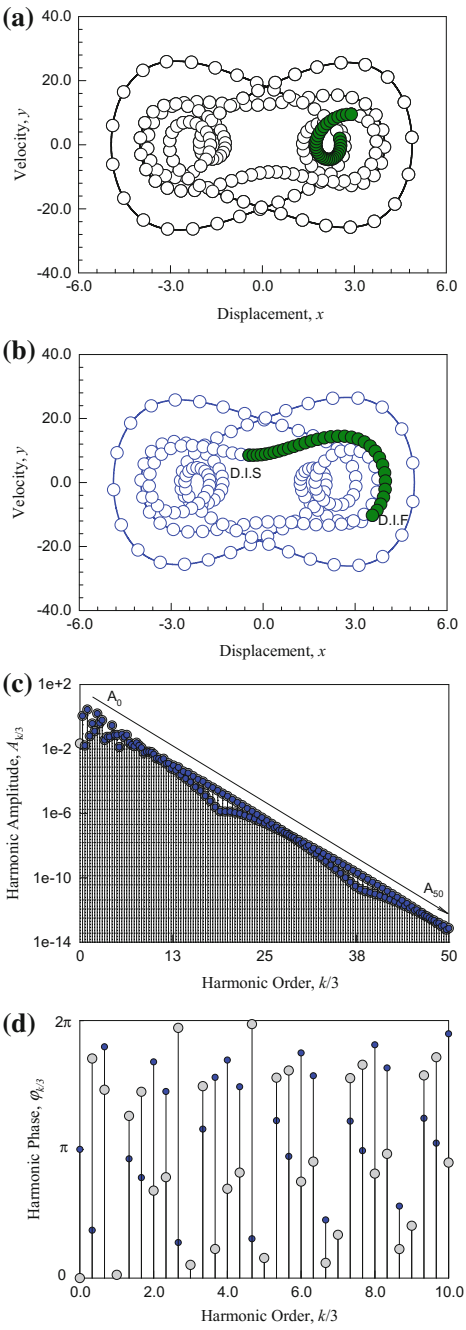

Fig. 10.4 A pair of stable asymmetric period-3 motion for $\Omega = 3.15$. **a**, **b** trajectory, **c** harmonic amplitude spectrum, **d** harmonic phase spectrum with initial conditions **a** $(x_0, \dot{x}_0) \approx (3.567230, -10.284055)$ and **b** $(x_0, \dot{x}_0) \approx (2.899588, 9.507185)$ $(\alpha_1 = -10.0, \alpha_2 = 5.0, \beta = 10.0, \delta = 0.5, Q_0 = 100.0, \tau = T/4)$

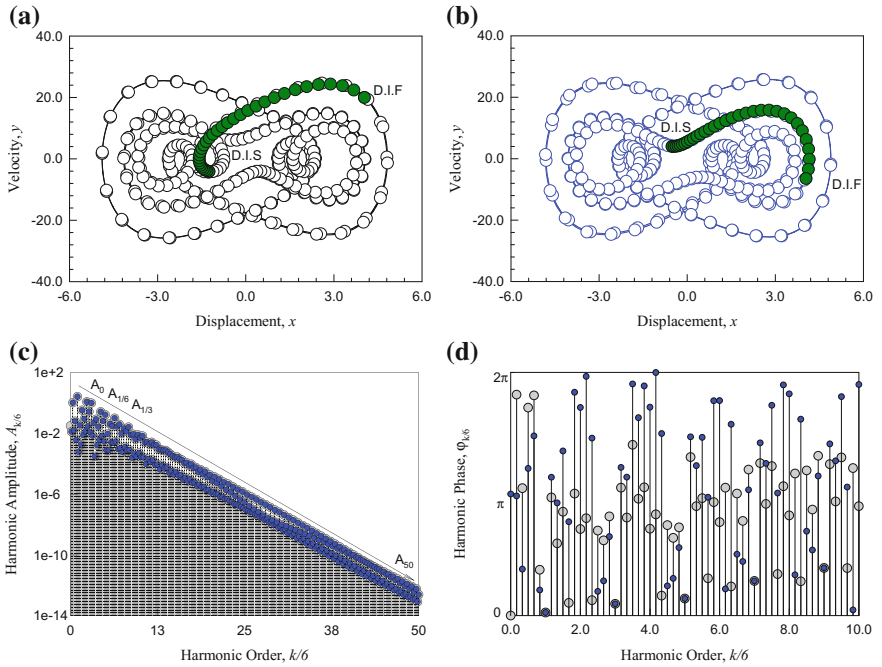

Fig. 10.5 A pair of stable asymmetric period-6 motion for $\Omega = 3.10$. **a**, **b** trajectory, **c** harmonic amplitude spectrum, d) harmonic phase spectrum with initial 0 conditions **a** $(x_0, \dot{x}_0) \approx (4.039509, 19.992432)$ and **b** $(x_0, \dot{x}_0) \approx (4.044199, -6.483031)$ $(\alpha_1 = -10.0, \alpha_2 = 5.0, \beta = 10.0, \delta = 0.5, Q_0 = 100.0, \tau = T/4)$

Consider a pair of asymmetric period-1 motions at $\Omega = 3.15$, as shown in Fig. 10.4. The initial conditions are obtained from the analytical prediction. $x_0 \approx 3.567230$ and $\dot{x}_0 \approx -10.284055$ are for the asymmetric period-3 motion in Fig. 10.4a and $x_0 \approx 2.899588$ and $\dot{x}_0 \approx 9.507185$ are for the asymmetric period-3 motion in Fig. 10.4b. The harmonic amplitudes and phases are presented in Fig. 10.3c, d, respectively. The center of the trajectory is far away from the origin compared to the previous symmetric period-3 motion. That is, $a_0^{black} = -a_0^{blue} = A_0 = 0.0220$.

The main harmonic amplitudes for the two asymmetric period-3 motions are $A_{1/3} \approx 1.1178$, $A_{2/3} \approx 0.0161$, $A_1 \approx 2.7884$, $A_{4/3} \approx 0.0625$, $A_{5/3} \approx 0.3811$, $A_2 \approx 0.1265$, $A_{7/3} \approx 1.5774$, $A_{8/3} \approx 0.4019$, $A_3 \approx 0.6085$, $A_{10/3} \approx 0.0360$, $A_{11/3} \approx 0.0561$, $A_4 \approx 0.0560$, $A_{13/3} \approx 0.2871$, $A_{14/3} \approx 0.0725$, $A_5 \approx 0.0738$, $A_{16/3} \approx 0.0131$, $A_{17/3} \approx 0.0820$, $A_6 \approx 0.0542$, $A_{19/3} \approx 0.0737$, $A_{20/3} \approx 0.0253$, $A_7 \approx 0.0185$, $A_{22/3} \approx 0.0149$, $A_{23/3} \approx 0.0241$, $A_8 \approx 0.0164$, $A_{25/3} \approx 0.0120$. Other harmonic amplitudes lie in $A_{l/3} \in (10^{-14}, 10^{-3})$ $(l = 26, 27, \cdots, 150)$ and $A_{50} \approx 7.2626\text{e-}14$. The two asymmetric period-3 motions need about 150 harmonic terms in the finite Fourier series for an approximate analytical expression. The first and third harmonic terms play very important roles on such symmetric period-3 motions. Because harmonic amplitude of even terms is relatively small, such harmonic terms make the two

asymmetric period-3 motions be close to asymmetric period-3 motions. In addition, harmonic phase distribution varying with harmonic orders is clearly presented. The gray circular symbols are for the harmonic phases of the upper asymmetric period-3 motion and the red symbols are for the harmonic phases of the lower asymmetric period-3 motion. The harmonic phase relations between the two asymmetric period-3 motions are $\varphi^{black}_{k/(2^l m)} = \mathrm{mod}(\varphi^{blue}_{k/(2^l m)} + ((m+2r)k/(2^l m)+1))\pi, 2\pi)$ for $l = 0, m = 3, r = 1$ and $t_0 = rT$ with $r \in \{0, 1, \cdots, 2^l m - 1\}$.

Consider a pair of asymmetric period-6 motions at $\Omega = 3.10$, as shown in Fig. 10.5. The initial conditions are obtained from the analytical prediction. $x_0 \approx 4.039509$ and $\dot{x}_0 \approx 19.992432$ are for the asymmetric period-6 motion in Fig. 10.5a and $x_0 \approx 4.044199$ and $\dot{x}_0 \approx -6.483031$ are for the asymmetric period-6 motion in Fig. 10.5b. The harmonic amplitudes and phases are presented in Fig. 10.5c, d, respectively. The center of the trajectory is far away from the origin compared to the previous asymmetric period-3 motion. That is, $a_0^{black} = -a_0^{blue} = A_0 = 0.0319$. The main harmonic amplitudes for the two asymmetric period-1 motions are $A_{1/6} \approx 0.0131$, $A_{1/3} \approx 1.0622$, $A_{1/2} \approx 0.0160$, $A_{2/3} \approx 0.0646$, $A_{5/6} \approx 3.7917\text{e-}3$, $A_1 \approx 2.6545$, $A_{7/6} \approx 6.2608\text{e-}4$, $A_{4/3} \approx 0.0345$, $A_{3/2} \approx 1.8623\text{e-}3$, $A_{5/3} \approx 0.3432$, $A_{11/6} \approx 7.8357\text{e-}3$, $A_2 \approx 0.0910$, $A_{13/6} \approx 0.0139$, $A_{7/3} \approx 1.2285$, $A_{5/2} \approx 0.0305$, $A_{8/3} \approx 0.2763$, $A_{17/6} \approx 0.0124$, $A_3 \approx 1.0138$, $A_{19/6} \approx 7.2666\text{e-}3$, $A_{10/3} \approx 0.0509$, $A_{7/2} \approx 3.1323\text{e-}4$, $A_{11/3} \approx 0.0866$, $A_{23/6} \approx 1.6868\text{e-}3$, $A_4 \approx 0.0.0280$, and $A_{25/6} \approx 3.7414\text{e-}3$, $A_{13/3} \approx 0.0.2680$, $A_{9/2} \approx 6.9915\text{e-}3$, $A_{14/3} \approx 0.0667$, $A_{29/6} \approx 2.9448\text{e-}3$, $A_5 \approx 0.1699$, $A_{31/6} \approx 8.1422\text{e-}4$, $A_{16/3} \approx 0.0.2680$, $A_{11/2} \approx 7.9530\text{e-}4$, $A_{17/3} \approx 0.0433$, $A_{35/6} \approx 2.6005\text{e-}3$, $A_6 \approx 0.0306$, $A_{37/6} \approx 2.8367\text{e-}3$, $A_{19/3} \approx 0.1016$, $A_{13/2} \approx 3.0073\text{e-}3$, $A_{20/3} \approx 0.0285$, $A_{41/6} \approx 9.4470\text{e-}4$, $A_7 \approx 0.0398$, $A_{43/6} \approx 1.0742\text{e-}3$, $A_{22/3} \approx 9.9107\text{e-}3$, $A_{15/2} \approx 5.8637\text{e-}3$, $A_{23/3} \approx 0.0217$, $A_{47/6} \approx 1.3083\text{e-}3$, $A_8 \approx 0.0139$, $A_{49/6} \approx 8.0876\text{e-}4$, $A_{25/3} \approx 0.0264$. Other harmonic amplitudes lie in $A_{l/6} \in (10^{-14}, 10^{-3})$ $(l = 51, 52, \cdots, 300)$, and $A_{50} \approx 2.4131\text{e-}13$. The two asymmetric period-6 motions need about 300 harmonic terms in the finite Fourier series for an approximate analytical expression. The first and third harmonic terms play very important roles on such asymmetric period-6 motions. Because harmonic amplitude of even terms is relatively small, such harmonic terms make the two asymmetric period-6 motions be close to asymmetric period-3 motions. In addition, harmonic phase distribution varying with harmonic orders is clearly presented. The gray circular symbols are for the harmonic phases of the upper asymmetric period-6 motion, and the blue symbols are for the harmonic phases of the lower asymmetric period-6 motion. The harmonic phase relations between the two asymmetric period-6 motions are for $\varphi^{blue}_{k/(2^l m)} = \mathrm{mod}(\varphi^{black}_{k/(2^l m)} + ((m+2r)k/(2^l m)(2^l m)+1))\pi, 2\pi)$ for $l = 1, m = 3, r = 5$ and $t_0 = rT$ with $r \in \{0, 1, \cdots, 2^l m - 1\}$.

10.7 Conclusions

The symmetric and asymmetric period-3 motions in the time-delayed, double-well Duffing oscillator were predicted through the semi-analytical method. The semi-analytical method is based on the implicit mappings constructed by discretization of the corresponding differential equation. The corresponding stability and bifurcation analysis were studied. From the analytical predictions, numerical simulations of complex periodic motions were presented, and the harmonic amplitudes and phases were presented. The harmonic effects on period-3 motions can be clearly observed.

References

1. Lagrange, J.L.: Mecanique Analytique, vol. 2 (1788) (edition Albert Balnchard: Paris 1965)
2. Poincare, H.: Methodes Nouvelles de la Mecanique Celeste, vol. 3. Gauthier-Villars, Paris (1899)
3. Van der Pol, B.: A theory of the amplitude of free and forced triode vibrations. Radio Rev. **1**, 701–710, 754–762 (1920)
4. Fatou, P.: Sur le mouvement d'un systeme soumis à des forces a courte periode. Bull. Soc. Math. **56**, 98–139 (1928)
5. Krylov, N.M., Bogolyubov, N.N.: Methodes approchees de la mecanique non-lineaire dans leurs application a l'Aeetude de la perturbation des mouvements periodiques de divers phenomenes de resonance s'y rapportant, Academie des Sciences d'Ukraine:Kiev (1935) (in French)
6. Luo, A.C.J.: Continuous Dynamical Systems. HEP/L&H Scientific, Beijing/Glen Carbon (2012)
7. Luo, A.C.J., Huang, J.Z.: Approximate solutions of periodic motions in nonlinear systems via a generalized harmonic balance. J. Vib. Control **18**, 1661–1871 (2012)
8. Luo, A.C.J., Huang, J.Z.: Analytical dynamics of period-m flows and chaos in nonlinear systems. Int. J. Bifurc. Chaos **22** (2012). Article No. 1250093 (29 p)
9. Luo, A.C.J., Huang, J.Z.: Analytical routines of period-1 motions to chaos in a periodically forced Duffing oscillator with twin-well potential. J. Appl. Nonlinear Dyn. **1**, 73–108 (2012)
10. Luo, A.C.J., Huang, J.Z.: Unstable and stable period-m motions in a twin-well potential Duffing oscillator. Discont. Nonlinearity Complex. **1**, 113–145 (2012)
11. Hu, H.Y., Dowell, E.H., Virgin, L.N.: Resonance of harmonically forced Duffing oscillator with time-delay state feedback. Nonlinear Dyn. **15**(4), 311–327 (1998)
12. Hu, H.Y., Wang, Z.H.: Dynmaics of Controlled Mechanical Systems with Delayed Feedback. Springer, Berlin (2002)
13. MacDonald, N.: Harmonic balance in delay-differential equations. J. Sounds Vib. **186**(4), 649–656 (1995)
14. Leung, A.Y.T., Guo, Z.: Bifurcation of the periodic motions in nonlinear delayed oscillators. J. Vib. Control **20**, 501–517 (2014)
15. Liu, L., Kalmar-Nagy, T.: High-dimensional harmonic balance analysis for second-order delay-differential equations. J. Vib. Control **16**(7–8), 1189–1208 (2010)
16. Luo, A.C.J.: Analytical solutions of periodic motions in dynamical systems with/without time-delay. Int. J. Dyn. Control **1**, 330–359 (2013)
17. Luo, A.C.J., Jin, H.X.: Bifurcation trees of period-m motion to chaos in a time-delayed, quadratic nonlinear oscillator under a periodic excitation. Discont. Nonlinearity Complex. **3**, 87–107 (2014)
18. Luo, A.C.J., Jin, H.X.: Complex period-1 motions of a periodically forced Duffing oscillator with a time-delay feedback. Int. J. Dyn. Control (2014, in press)

19. Luo, A.C.J., Jin, H.X.: Period-m motions to chaos in a periodically forced Duffing oscillator with a time-delay feedback. Int. J. Bifurc. Chaos **24**(10) (2014). Article no: 1450126 (20 p)
20. Insperger, T., Stepan, G.: Semi-discretization of delayed dynamical systems. Int. J. Numer. Methods Eng. **55**(5), 503–518 (2002)
21. Insperger, T., Stepan, G.: Semi-Discretization of Time-Delay Systems. Springer, New York (2002)
22. Khasawneh, F.A., Mann, B.P.: A spectral element approach for the stability of delay system. Int. J. Numer. Methods Eng. **87**, 566–592 (2011)
23. Lehotzky, D., Insperger, T., Stepan, G.: Extension of the spectral element method for stability analysis of time-periodic delay-diferential equations with multiple and distributed delays. Commun. Nonlinear Sci. Numer. Simul. **35**, 177–189 (2016)
24. Luo, A.C.J.: Periodic flows in nonlinear dynamical systems based on discrete implicit maps. Int. J. Bifurc. Chaos **25**(3) (2015). Article No: 1550044 (62 p)
25. Luo, A.C.J.: Discretization and Implicit Mapping Dynamics. HEP/Springer, Beijing/Dordrecht (2015)
26. Luo, A.C.J., Guo, Y.: A semi-analytical prediction of periodic motions in Duffing oscillator through mapping structures. Discont. Nonlinearity Complex. **4**(2), 121–150 (2015)
27. Luo, A.C.J., Xing, S.Y.: Symmetric and asymmetric period-1 motions in a periodically forced, time-delayed, hardening Duffing oscillator. Nonlinear Dyn. **85**(2), 1141–1166 (2016)
28. Luo, A.C.J., Xing, S.Y.: Multiple bifurcation trees of period-1 motions to chaos in a periodically forced, time-delayed, hardening Duffing oscillator. Chaos Soliton Fractals. **89**, 405–434 (2016)

Chapter 11
Travelable Period-1 Motions to Chaos in a Periodically Excited Pendulum

Yu Guo and Albert C.J. Luo

In this chapter, the analytical bifurcation trees of travelable period-1 motions to chaos in a periodically excited pendulum are presented with varying excitation amplitude. The analytical prediction of bifurcation trees of periodic motions is based on the implicit discrete maps obtained from the midpoint scheme of the corresponding differential equation. Using the discrete maps, mapping structures are developed for various periodic motions, and analytical bifurcation trees of periodic motions to chaos can be obtained. The corresponding eigenvalue analysis provides the stability and bifurcation conditions. Finally, numerical illustrations of periodic motions on the bifurcation trees are presented in verification of the analytical prediction. This chapter is dedicated to Professor Valentin Afraimovich's 70th birthday for his contributions in nonlinear dynamics.

11.1 Introduction

A periodically driven pendulum is one of the typical nonlinear oscillators that possesses complicated dynamical behaviors. The periodic solutions and bifurcation analysis of such a nonlinear oscillator have been of great interests to researchers for a long time. The history of investigations on periodic motions in nonlinear systems

Y. Guo (✉)
McCoy School of Engineering, Midwestern State University, Wichita Falls, TX 76308, USA
e-mail: yu.guo@mwsu.edu

A.C.J. Luo
Department of Mechanical and Industrial Engineering, Southern Illinois University Edwardsville, Edwardsville, IL 62026-1805, USA
e-mail: aluo@siue.edu

D. Volchenkov and X. Leoncini (eds.), *Regularity and Stochasticity of Nonlinear Dynamical Systems*, Nonlinear Systems and Complexity 21,
DOI 10.1007/978-3-319-58062-3_11

can be chase back to as early as seventeenth century, when Lagrange [10] introduced the method of averaging to investigate the three-body problems as a perturbation of the two-body problems. Poincare [17] further developed such a perturbation theory and applied it on the investigation of the motions of celestial bodies. Since then, researchers started to show interest on the perturbation theory to approximate the analytical periodic solutions of nonlinear systems. van der Pol [19] used the method of averaging to determine the periodic solutions of an oscillator circuits. Fatou [4] proved the asymptotic validity of such a perturbation method. Krylov and Bogolyubov [9] further developed the method of averaging. Hayashi [8] presented the perturbation methods including averaging method and principle of harmonic balance. Barkham and Soudack [1, 2] extended the Krylov–Bogoliubov to approximate the solutions of nonlinear autonomous second-order differential equations. Rand and Armbruster [18] used the perturbation method and bifurcation theory to determine the stability of periodic solutions; at the same time, Garcia-Margallo and Bejarano [7] determined the approximated solutions of nonlinear oscillations with strong nonlinearity using a generalized harmonic balance approach. Yuste and Bejarano [20–22] used the elliptic functions rather than trigonometric functions to improve the Krylov–Bogoliubov method. Coppola and Rand [3] obtained approximation of limit cycle using the averaging method with elliptic functions.

On the other hand, one was also interested in chaotic behavior in such a nonlinear pendulum systems. Zaslavsky and Chirikov [23] discussed the resonance overlap and the stochastic (chaotic) instability of nonlinear oscillation based on a periodically excited pendulum. Luo and Han [14] presented a more accurate method to predict the resonance and stochastic layer of a periodically driven pendulum. Luo [11] developed an analytical method for obtaining approximate analytical solutions of periodic motions in nonlinear dynamical systems based on the generalized harmonic balance method. Then, Luo and Guo [13] applied such a method on Duffing oscillator to obtain approximate analytical solutions of periodic motions. In addition, Luo and Huang [16] also provided the bifurcation trees of period-m motions to chaos in such a nonlinear oscillatory system.

Although the aforementioned method in Luo [11] was very successful on some nonlinear systems, it cannot be applied for nonlinear dynamical systems with non-polynomial functions such as the pendulum system. Thus, Luo [12] developed a semi-analytical method based on implicit mappings between discrete nodes in order to obtain predictions in complicated nonlinear dynamical systems. The mapping structures developed from such implicit mapping can be used to describe different periodic motions. To verify this semi-analytical method, Guo and Luo [5] applied such a method to predict bifurcation trees of periodic motions to chaos in the Duffing oscillators as compared to the approximated analytical solutions obtained in Luo and Huang [15]. The two methods give the same solutions of periodic motions to chaos in the Duffing oscillators. More prediction results are presented in Guo and Luo [6].

Thus, herein the aforementioned approach in Luo [12] will be applied to investigate the rich nonlinear dynamical behaviors in a periodically excited pendulum. The discrete implicit maps between two discrete nodes will be developed. Based on the implicit maps, mapping structures will be constructed. Analytical predictions of

bifurcation trees from travelable period-1 motions to chaos will be presented. The corresponding stability and bifurcation conditions will be determined from eigenvalues using the theory of discrete dynamical systems. Finally, numerical illustrations of periodic motions on the bifurcation trees will be demonstrated.

11.2 Method

In this section, a semi-analytical method for periodic motions in the periodically excited pendulum will be presented through the corresponding implicit discrete mappings under specific computational accuracy. The mapping structures of periodic motions will be employed, and the corresponding stability and bifurcation will be discussed.

11.2.1 Discrete Mappings

A periodically driven pendulum system is described as

$$\ddot{x} + \delta\dot{x} + \alpha \sin x = Q_0 \cos \Omega t \tag{11.1}$$

where δ is the damping coefficient, α is stiffness, Q_0 and Ω are excitation amplitude and frequency, respectively. In phase space, such a system can be rewritten as

$$\begin{aligned} \dot{x} &= y, \\ \dot{y} &= Q_0 \cos(\Omega t) - \delta\dot{x} + \alpha \sin x. \end{aligned} \tag{11.2}$$

Using a midpoint scheme for the time interval $t \in [t_{k-1}, t_k]$, the above system can be discretized to form an implicit map P_k $(k = 0, 1, 2, ...)$ as

$$P_k : (x_{k-1}, y_{k-1}) \to (x_k, y_k) \Rightarrow (x_k, y_k) = P_k(x_{k-1}, y_{k-1}) \tag{11.3}$$

with the implicit relations

$$\begin{aligned} x_k &= x_{k-1} + \frac{1}{2}h(y_{k-1} + y_k), \\ y_k &= y_{k-1} + h\{Q_0 \cos \Omega (t_{k-1} + \frac{1}{2}h) - \frac{1}{2}\delta(y_{k-1} + y_k) - \alpha \sin[\frac{1}{2}(x_{k-1} + x_k)]\}. \end{aligned} \tag{11.4}$$

The above discretization experiences an accuracy of $O(h^3)$ for each step. To keep computational accuracy less than 10^{-9}, $h < 10^{-3}$ needs to be maintained.

11.2.2 Periodic Motions

In general, a period-m periodic motion in the periodically excited pendulum system can be represented by a discrete mapping structure, i.e.,

$$P = \underbrace{P_{mN} \circ P_{mN-1} \circ \cdots \circ P_2 \circ P_1}_{mN-\text{actions}} : (x_0^{(m)}, y_0^{(m)}) \to (x_{mN}^{(m)}, y_{mN}^{(m)}) \tag{11.5}$$

with

$$\begin{array}{l} P_k : (x_{k-1}^{(m)}, y_{k-1}^{(m)}) \to (x_k^{(m)}, y_k^{(m)}) \\ \Rightarrow (x_k^{(m)}, y_k^{(m)}) = P_k(x_{k-1}^{(m)}, y_{k-1}^{(m)}) \\ (k = 1, 2, \cdots, mN). \end{array} \tag{11.6}$$

From Eq. (11.4), the corresponding algebraic equations can be obtained by

$$\left.\begin{array}{l} x_k^{(m)} = x_{k-1}^{(m)} + \frac{1}{2}h(y_{k-1}^{(m)} + y_k^{(m)}), \\ y_k^{(m)} = y_{k-1}^{(m)} + h\{Q_0 \cos\Omega(t_{k-1} + \frac{1}{2}h) \\ \quad -\frac{1}{2}\delta(y_{k-1}^{(m)} + y_k^{(m)}) - \alpha \sin[\frac{1}{2}(x_{k-1}^{(m)} + x_k^{(m)})]\} \end{array}\right\} \text{ for } P_k. \tag{11.7}$$
$$(k = 1, 2, \cdots, mN)$$

The corresponding periodicity conditions are given as

$$(x_{mN}^{(m)}, y_{mN}^{(m)}) = (x_0^{(m)} + 2l\pi, y_0^{(m)}),\ l = 0, \pm 1, \pm 2, \cdots; m = 1, 2, \cdots \tag{11.8}$$

From Eqs. (11.6) and (11.8), nodes at the discretized Duffing oscillator can be determined by $2(mN + 1)$ equations. Once the node points $\mathbf{x}_k^{(m)*}$ $(k = 1, 2, \cdots, mN)$ of the period-m motion are obtained, the corresponding stability and bifurcation of period-m motion can be discussed by the corresponding Jacobian matrix. For a small perturbation in vicinity of $\mathbf{x}_k^{(m)*}$, $\mathbf{x}_k^{(m)} = \mathbf{x}_k^{(m)*} + \Delta\mathbf{x}_k^{(m)}$, $(k = 0, 1, 2, \cdots, mN)$,

$$\Delta\mathbf{x}_{mN} = DP\Delta\mathbf{x}_0^{(m)} = \underbrace{DP_{mN} \cdot DP_{mN-1} \cdot \ldots \cdot DP_2 \cdot DP_1}_{mN-\text{multiplication}} \Delta\mathbf{x}_0^{(m)}. \tag{11.9}$$

with

$$\begin{array}{l} \Delta\mathbf{x}_k^{(m)} = DP_k\Delta\mathbf{x}_{k-1}^{(m)} \equiv \left[\frac{\partial\mathbf{x}_k^{(m)}}{\partial\mathbf{x}_{k-1}^{(m)}}\right]_{(\mathbf{x}_k^{(m)*}, \mathbf{x}_{k-1}^{(m)*})} \Delta\mathbf{x}_{k-1}^{(m)}, \\ (k = 1, 2, \cdots, mN) \end{array} \tag{11.10}$$

where

$$DP_k = \left[\frac{\partial\mathbf{x}_k^{(m)}}{\partial\mathbf{x}_{k-1}^{(m)}}\right]_{(\mathbf{x}_k^{(m)*}, \mathbf{x}_{k-1}^{(m)*})} = \left[\begin{array}{cc} \frac{\partial x_k^{(m)}}{\partial x_{k-1}^{(m)}} & \frac{\partial x_k^{(m)}}{\partial y_{k-1}^{(m)}} \\ \frac{\partial y_k^{(m)}}{\partial x_{k-1}^{(m)}} & \frac{\partial y_k^{(m)}}{\partial y_{k-1}^{(m)}} \end{array}\right]_{(\mathbf{x}_k^{(m)*}, \mathbf{x}_{k-1}^{(m)*})} \tag{11.11}$$

for $k = 1, 2, \cdots, mN$.

The corresponding eigenvalues are computed by

$$|DP - \lambda \mathbf{I}| = 0 \tag{11.12}$$

where

$$DP = \prod_{k=mN}^{1} \left[\frac{\partial \mathbf{x}_k^{(m)}}{\partial \mathbf{x}_k^{(m)}} \right]_{(\mathbf{x}_k^{(m)*}, \mathbf{x}_{k-1}^{(m)*})}. \tag{11.13}$$

For stability analysis, if all $|\lambda_i| < 1$ for$(i = 1, 2)$, the periodic motion is stable; if one of $|\lambda_i| > 1$ for $(i \in \{1, 2\})$, the periodic motion is unstable. As one of $\lambda_i = -1$ and $|\lambda_j| < 1$ for $(i, j \in \{1, 2\}$ and $j \neq i)$, the period-doubling bifurcation of periodic motion occurs. As one of $\lambda_i = -1$ and $|\lambda_j| > 1$ for $(i, j \in \{1, 2\}$ and $j \neq i)$, the unstable period-doubling bifurcation of periodic motion occurs. As one of $\lambda_i = 1$ and $|\lambda_j| < 1$ for $(i, j \in \{1, 2\}$ and $j \neq i)$, the saddle-node bifurcation of the periodic motion occurs. As one of $\lambda_i = 1$ and $|\lambda_j| > 1$ for $(i, j \in \{1, 2\}$ and $j \neq i)$, the unstable saddle-node bifurcation of the periodic motion occurs. When $|\lambda_{1,2}| = 1$ is a pair of complex eigenvalues, the Neimark bifurcation of the periodic motion occurs.

11.3 Frequency-Amplitude Characteristics

From the node points of period-m motions in periodically forced pendulum, $\mathbf{x}_k^{(m)} = (x_k^{(m)}, y_k^{(m)})^{\mathrm{T}}$ $(k = 0, 1, 2, \cdots, mN)$, the period-m motions can be approximately expressed by the Fourier series, i.e.,

$$\mathbf{x}^{(m)}(t) \approx \mathbf{a}_0^{(m)} + \sum_{j=1}^{M} \mathbf{b}_{j/m} \cos(\frac{k}{m}\Omega t) + \mathbf{c}_{j/m} \sin(\frac{k}{m}\Omega t). \tag{11.14}$$

The $(2M + 1)$ unknown vector coefficients of $\mathbf{a}_0^{(m)}$, $\mathbf{b}_{j/m}$, $\mathbf{c}_{j/m}$ should be determined from discrete nodes $\mathbf{x}_k^{(m)}(k = 0, 1, 2, \cdots, mN)$ with $mN + 1 \geq 2M + 1$. For $M = mN/2$, the node points $\mathbf{x}_k^{(m)}$ on the period-m motion can be expressed for $t_k \in [0, mT]$

$$\begin{aligned} \mathbf{x}^{(m)}(t_k) \equiv \mathbf{x}_k^{(m)} &= \mathbf{a}_0^{(m)} + \sum_{j=1}^{mN/2} \mathbf{b}_{j/m} \cos(\frac{j}{m}\Omega t_k) + \mathbf{c}_{j/m} \sin(\frac{j}{m}\Omega t_k) \\ &= \mathbf{a}_0^{(m)} + \sum_{j=1}^{mN/2} \mathbf{b}_{j/m} \cos(\frac{j}{m}\frac{2k\pi}{N}) + \mathbf{c}_{j/m} \sin(\frac{j}{m}\frac{2k\pi}{N}) \\ (k &= 0, 1, \cdots, mN - 1) \end{aligned} \tag{11.15}$$

where

$$\left.\begin{aligned} T &= \frac{2\pi}{\Omega} = N\Delta t;\ \Omega t_k = \Omega k\Delta t = \frac{2k\pi}{N} \\ \mathbf{a}_0^{(m)} &= \frac{1}{N}\sum_{k=0}^{mN-1}\mathbf{x}_k^{(m)}, \\ \mathbf{b}_{j/m} &= \frac{2}{mN}\sum_{k=1}^{mN-1}\mathbf{x}_k^{(m)}\cos(k\frac{2j\pi}{mN}), \\ \mathbf{c}_{j/m} &= \frac{2}{mN}\sum_{k=1}^{mN-1}\mathbf{x}_k^{(m)}\sin(k\frac{2j\pi}{mN}) \end{aligned}\right\}\ (j = 1, 2, \cdots, mN/2) \tag{11.16}$$

and

$$\mathbf{a}_0^{(m)} = (a_{01}^{(m)}, a_{02}^{(m)})^{\mathrm{T}}, \mathbf{b}_{j/m} = (b_{j/m1}, b_{j/m2})^{\mathrm{T}}, \mathbf{c}_{j/m} = (c_{j/m1}, c_{j/m2})^{\mathrm{T}}. \tag{11.17}$$

The harmonic amplitudes and phases for the period-m motions are expressed by

$$\begin{aligned} A_{j/m1} &= \sqrt{b_{j/m1}^2 + c_{j/m1}^2},\ \varphi_{j/m1} = \arctan\tfrac{c_{j/m1}}{b_{j/m1}}, \\ A_{j/m2} &= \sqrt{b_{j/m2}^2 + c_{j/m2}^2},\ \varphi_{j/m2} = \arctan\tfrac{c_{j/m2}}{b_{j/m2}}. \end{aligned} \tag{11.18}$$

Thus, the approximate expression of period-m motions in Eq. (11.14) becomes

$$\mathbf{x}^{(m)}(t) \approx \mathbf{a}_0^{(m)} + \sum_{j=1}^{mN/2}\mathbf{b}_{j/m}\cos(\frac{k}{m}\Omega t) + \mathbf{c}_{j/m}\sin(\frac{k}{m}\Omega t). \tag{11.19}$$

For the periodically forced pendulum, we have

$$\left\{\begin{matrix} x^{(m)}(t) \\ y^{(m)}(t) \end{matrix}\right\} \equiv \left\{\begin{matrix} x_1^{(m)}(t) \\ x_2^{(m)}(t) \end{matrix}\right\} \approx \left\{\begin{matrix} a_{01}^{(m)} \\ a_{02}^{(m)} \end{matrix}\right\} + \sum_{j=1}^{mN/2}\left\{\begin{matrix} A_{j/m1}\cos(\frac{k}{m}\Omega t - \varphi_{j/m1}) \\ A_{j/m2}\cos(\frac{k}{m}\Omega t - \varphi_{j/m2}) \end{matrix}\right\}. \tag{11.20}$$

To reduce illustrations, only frequency-amplitude curves of velocity $y^{(m)}(t)$ for period-m motions are presented. However, the frequency-amplitudes for displacement $x^{(m)}(t)$ can also be done in a similar fashion. Thus, the velocity for period-m motion is given by

$$y^{(m)}(t) \approx a_0^{(m)} + \sum_{j=1}^{mN/2} b_{j/m}\cos(\frac{k}{m}\Omega t) + c_{j/m}\sin(\frac{k}{m}\Omega t) \tag{11.21}$$

or

$$y^{(m)}(t) \approx a_0^{(m)} + \sum_{j=1}^{mN/2} A_{j/m} \cos(\frac{k}{m}\Omega t - \varphi_{j/m}) \tag{11.22}$$

where

$$A_{j/m} = \sqrt{b_{j/m}^2 + c_{j/m}^2}, \varphi_{j/m} = \arctan \frac{c_{j/m}}{b_{j/m}}. \tag{11.23}$$

11.4 Bifurcation Trees

In this section, bifurcation trees are presented to show analytical predictions of the travelable period-1 motions to chaos in the periodically excited pendulum. The eigenvalue analysis will be illustrated to demonstrate stability and bifurcation conditions. The solid and dashed curves represent the stable and unstable motions, respectively. The black and red colors indicate pairs of asymmetric motions, respectively. The acronyms 'SN,' 'PD,' and 'USN' represent the saddle-node, period-doubling, and unstable saddle-node bifurcations, respectively. The symmetric and asymmetric periodic motions are labeled by 'S' and 'A,' respectively. The following parameters are considered for such a periodically excited pendulum.

$$\alpha = 4.0, \delta = 0.1, \Omega = 2.0. \tag{11.24}$$

The bifurcation trees of travelable period-1 motions to chaos will be presented through the analytical predictions of period-1 to period-2/period-4 motions. An overview of analytical bifurcation trees is illustrated in Fig. 11.1 with varying excitation amplitude Q_0. Figure 11.1a, b present the predictions of displacement and velocity of the periodic nodes $\text{mod}(x_{\text{mod}(k,N)}, 2\pi)$ and $y_{\text{mod}(k,N)}$ for $\text{mod}(k, N) = 0$, respectively. The period-1, period-2, and period-4 motions are labeled by P-1, P-2, and P-4, respectively. There are totally four different branches of bifurcation trees shown in Fig. 11.1. Each of them are indicated by 'B1,' 'B2,' 'B3,' and 'B4,' respectively. Different branches could have overlap in the range of existing, but the motions do not interfere with each other. For all four branches, no symmetric motions exist. Thus, in the bifurcation trees, the asymmetric period-1 motions are independent of symmetric period-1 motions. Such asymmetric period-1 motions form a closed loop with itself in the same branch through jumping phenomenon. The period-2 motions appear from period-doubling bifurcations of the asymmetric period-1 motions, and period-4 motions appear from period-doubling bifurcations of the period-2 motion. Such period-doubling bifurcations corresponds to either stable- or unstable saddle-node bifurcations of period-1 or period-2 motions. In addition, the period-2 and period-4 motions are asymmetric. The cascaded period-doubling bifurcations continue thereafter, introducing period-8, period-16 motions, and so on, which eventually go to chaos. The real part, imaginary parts, and magnitudes of eigenvalues for all

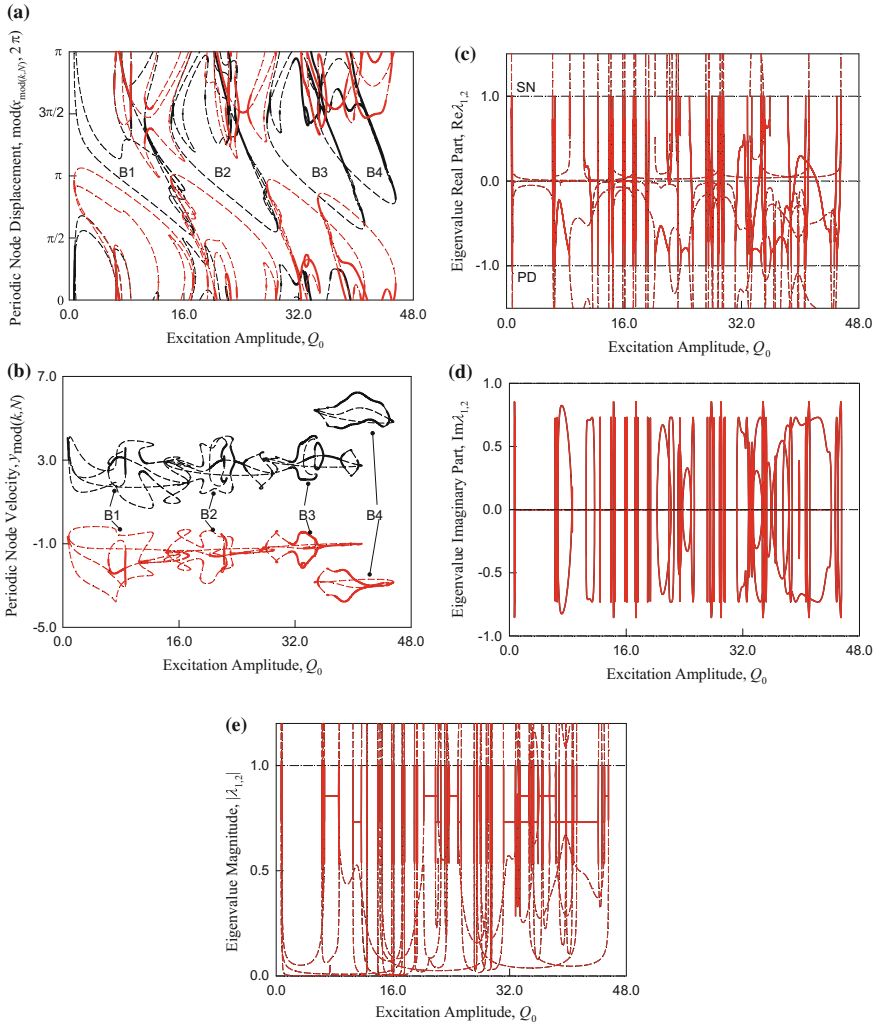

Fig. 11.1 Bifurcation tree of travelable period-1 to period-4 motions varying with excitation amplitude Q_0. **a** Node displacement $x_{\text{mod }(k,N)}$, **b** node velocity $y_{\text{mod }(k,N)}$, **c** real part of eigenvalues, **d** imaginary part of eigenvalues, **e** eigenvalue magnitudes ($\alpha = 4.0$, $\delta = 0.1$, $\Omega = 2.0$)

periodic motions are illustrated in Fig. 11.1c–e, respectively. For a better illustration of these bifurcations trees, the separated view of each of the branches in the windows of $Q_0 \in$ (0.0, 18.0), (14.0, 30.0), (26.0, 42.0), and (34.0, 46.0) is shown in Figs. 11.2, 11.3, 11.4, and 11.5, respectively. The corresponding bifurcation points for each of the branches are tabulated in Tables 11.1, 11.2, 11.3, and 11.4, respectively. In Tables 11.1, 11.2, 11.3, and 11.4, the acronyms 'SN,' 'PD,' and 'USN' indicates saddle-node, period-doubling, and unstable saddle-node bifurcations, respectively. In the parentheses, the acronym 'J' indicates the bifurcation points associated with

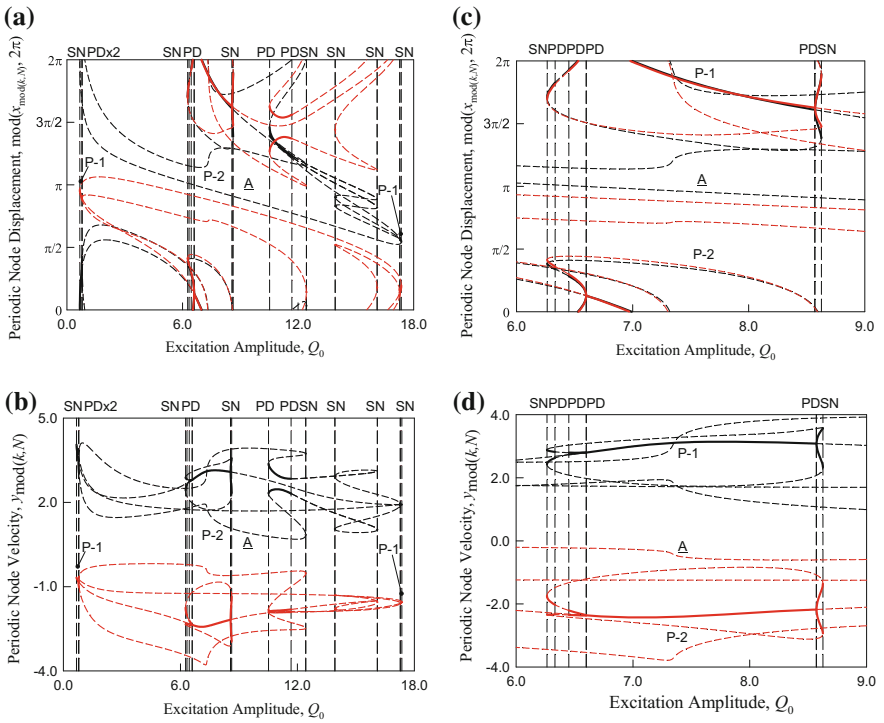

Fig. 11.2 Branch1 separated view. **a** Periodic node displacement mod $(x_{\text{mod}\,(k,N)}, 2\pi)$, **b** periodic node velocity $y_{\text{mod}\,(k,N)}$, **c**, **d** zoomed view for $Q_0 \in (6.0, 9.0)$: $(\alpha = 4.0, \delta = 0.1, \Omega = 2.0)$. mod $(k, N) = 0$

jumping phenomenon; and the acronym 'P_m' with $m = 1,\ 2,\ 3$ ... indicates the bifurcation point is transiting to period-m motions.

The first branch ('B1') of the bifurcation trees exists for the range of $Q_0 \in (0.6663, 17.3588)$, as presented in Fig. 11.2. The asymmetric period-1 motions are stable for the ranges of $Q_0 \in (0.6663,\ 0.7684)$, $(6.5996,\ 8.5712)$, and $(17.2820,\ 17.3588)$. These stable period-1 motions are connected together by the unstable period-1 motions for $Q_0 \in (0.7684,\ 6.5996)$ and $(8.5712,\ 17.2820)$. In addition, these period-1 motions encounter SN bifurcations associated with jumping phenomena at $Q_0 \approx 0.6663$ and 17.3588. The introduced unstable period-1 motion connects the two SN bifurcation points together, which forms a closed loop of the period-1 motions. Furthermore, the asymmetric period-1 motions experience two pairs of PD bifurcations for $Q_0 \approx 0.7684,\ 17.2820$ and $Q_0 \approx 6.5996,\ 8.5712$, which also correspond to SN bifurcations of period-2 motions. Each pair of the PD bifurcations encloses a period-2 motion. The period-2 motions in the range of $Q_0 \in (0.7684,\ 17.2820)$ experience three pairs of PD bifurcations that introduce period-4 motions and further cascaded period doublings to chaos. These three pairs of PD bifurcations exist at locations of $Q_0 \approx 0.7937,\ 12.4310$, $Q_0 \approx 11.6760,\ 16.1026$,

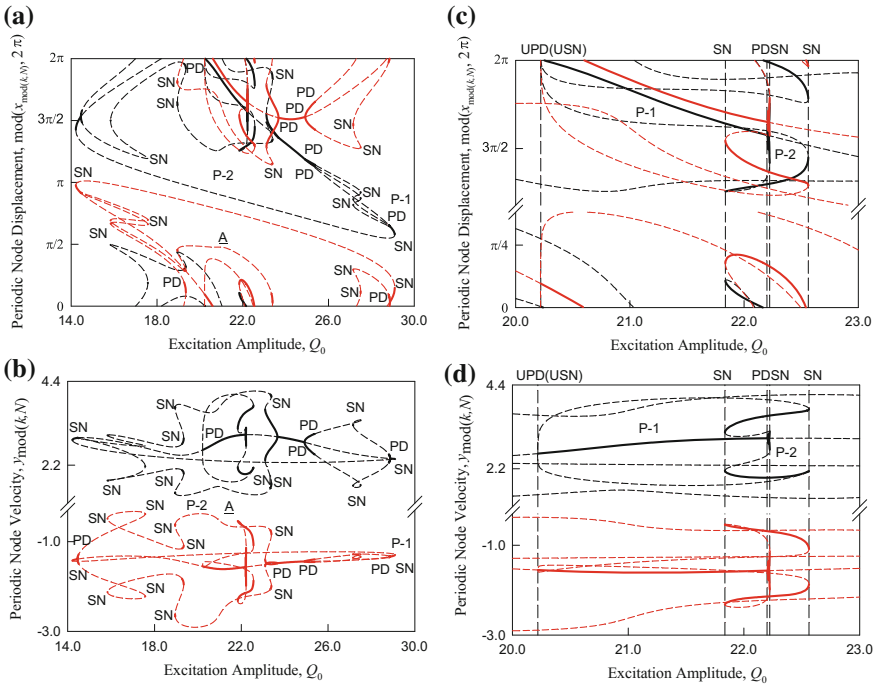

Fig. 11.3 Branch2 separated view for $Q_0 \in (14.0,\ 30.0)$. **a** Periodic node displacement mod $(x_{\text{mod}\,(k,N)}, 2\pi)$, **b** periodic node velocity $y_{\text{mod}\,(k,N)}$, **c**, **d** zoomed view for $Q_0 \in (20.0, 23.0)$: $(\alpha = 4.0, \delta = 0.1, \Omega = 2.0)$. $\text{mod}(k, N) = 0$

and $Q_0 \approx 13.9267,\ 17.2819$, respectively. The same period-2 motions in the range of $Q_0 \in (0.7684,\ 17.2820)$ also experience two pairs of SN bifurcations associated with jumping phenomena, at $Q_0 \approx 10.5220,\ 12.4314$ and $Q_0 \approx 13.9266,\ 16.1026$, respectively. The other period-2 motions exist for $Q_0 \in (6.2636,\ 8.6264)$, which are introduced by the PD bifurcations of period-1 motions at $Q_0 \approx 6.5996,\ 8.5712$. This period-2 motion encounters one pair of PD bifurcations at $Q_0 \approx 6.3320,\ 6.4500$, introducing period-4 motions and further cascaded period doublings to chaos. In addition, it experiences a pair of SN bifurcations associated with jumping phenomena at $Q_0 \approx 6.2636,\ 8.6264$. A detailed view for the range of $Q_0 \in (6.0,\ 9.0)$ is provided in Fig. 11.2c, d for a better illustration.

The second branch ('B2') of the bifurcation trees exists for the range of $Q_0 \in (14.2157, 29.0904)$ as presented in Fig. 11.3. The asymmetric period-1 motions are stable for $Q_0 \in (14.2157,\ 14.4494)$, $(20.2191,\ 22.2001)$, $(23.6701,\ 24.9181)$, and $(28.8655,\ 29.0904)$. These stable period-1 motions are connected together by the unstable period-1 motions for $Q_0 \in (14.4494,\ 20.2191)$, $(22.2001,\ 23.6701)$, and $(24.9181,\ 28.8655)$. In addition, these period-1 motions encounter SN bifurcations associated with jumping phenomena at $Q_0 \approx 14.2157$ and 29.0904. The induced unstable period-1 motion connects the two SN bifurcation points together, which

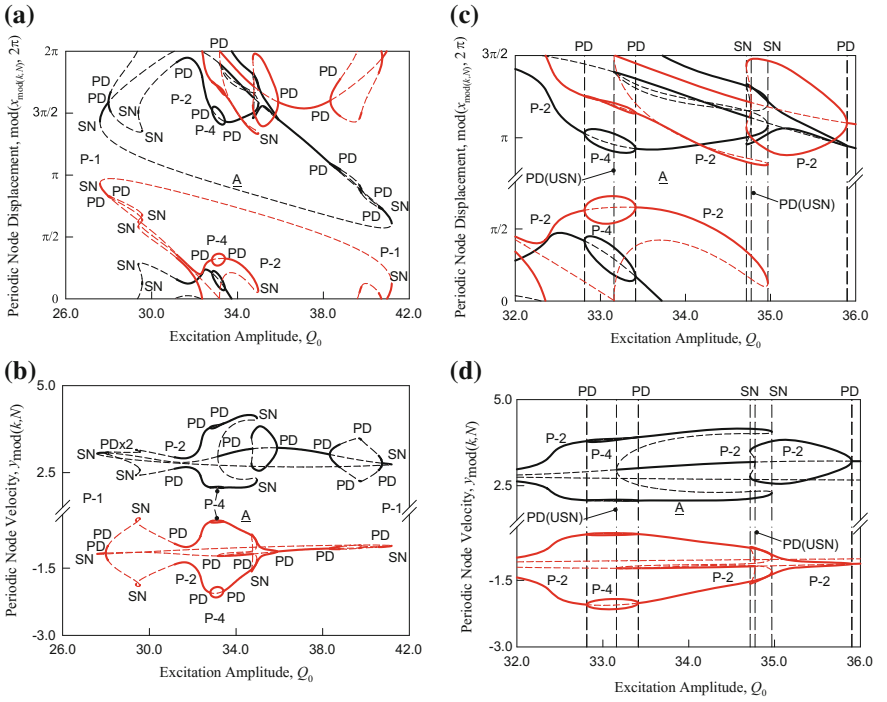

Fig. 11.4 Branch3 separated view for $Q_0 \in (26.0,\ 42.0)$. **a** Periodic node displacement mod $(x_{\text{mod}\,(k,N)}, 2\pi)$, **b** periodic node velocity $y_{\text{mod}\,(k,N)}$, **c**, **d** zoomed view for $Q_0 \in (32.0, 36.0)$: $(\alpha = 4.0, \delta = 0.1, \Omega = 2.0)$. $\text{mod}(k, N) = 0$

forms a closed loop of the period-1 motions. Furthermore, the asymmetric period-1 motions experience three pairs of PD bifurcations for $Q_0 \approx 14.4494,\ 23.6701$, $Q_0 \approx 20.2191,\ 22.2001$, and $Q_0 \approx 24.9181,\ 28.8655$. The PD bifurcation at $Q_0 \approx$

Table 11.1 Bifurcation points of Branch1 motions $(Q_0 \in (0.0, 18.0),\ \alpha = 4.0,\ \delta = 0.1,\ \Omega = 2.0)$

	Period-doubling bifurcations			Saddle-node bifurcations		
	Q_0	Left	Right	Q_0	Left	Right
P_1	(0.7684, 17.2820)	PD (P_2)	PD (P_2)	(0.6663, 17.3588)	SN (J)	SN (J)
	(6.5996, 8.5712)	PD (P_2)	PD (P_2)	–	–	–
P_2	(0.7937, 12.4310)	PD (P_4)	PD (P_4)	(0.7684, 17.2820)	SN (P_1)	SN (P_1)
	(6.3320, 6.4500)	PD (P_4)	PD (P_4)	(6.2636, 8.6264)	SN (J)	SN (J)
	(11.6760, 16.1026)	PD (P_4)	PD (P_4)	(6.5996, 8.5712)	SN (P_1)	SN (P_1)
	(13.9267, 17.2819)	PD (P_4)	PD (P_4)	(10.5220, 12.4314)	SN (J)	SN (J)
	–	–	–	(13.9266, 16.1026)	SN (J)	SN (J)

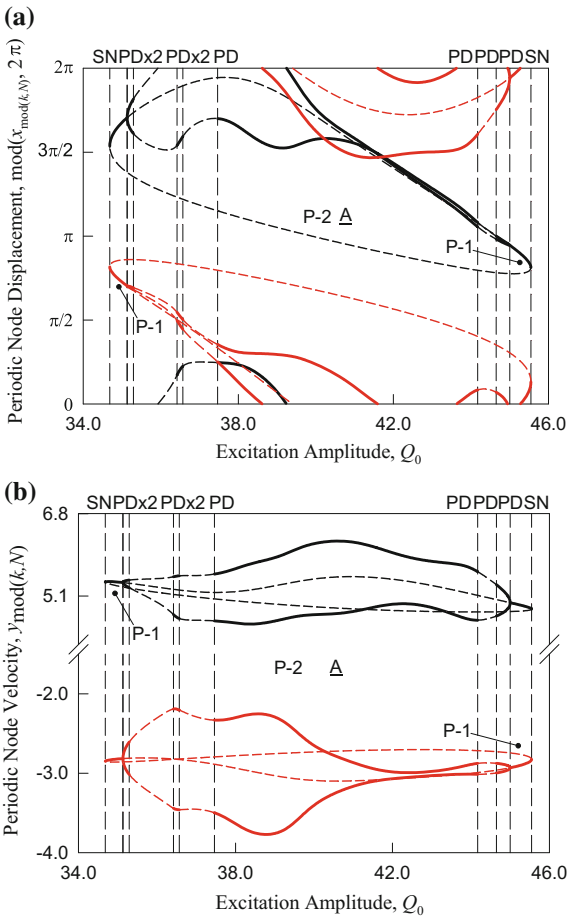

Fig. 11.5 Branch4 separated view for $Q_0 \in (34.0,\ 46.0)$. **a** Periodic node displacement $\mathrm{mod}(x_{\mathrm{mod}\,(k,N)}, 2\pi)$, **b** periodic node velocity $y_{\mathrm{mod}\,(k,N)}$. ($\alpha = 4.0$, $\delta = 0.1$, $\Omega = 2.0$). $\mathrm{mod}(k, N) = 0$

20.2191 corresponds to the USN bifurcation of period-2 motions. The rest of the PD bifurcations all correspond to SN bifurcations of the period-2 motions, which lead to stable period-2 motions. There are total of three pieces of period-2 motions introduced. The first period-2 motions in $Q_0 \in (14.4494,\ 23.6701)$ experience three pairs of PD bifurcations that introduce period-4 motions and further cascaded period doublings to chaos. The three pairs of PD bifurcations exist at $Q_0 \approx 14.5039,\ 17.5725$, $Q_0 \approx 15.8362,\ 19.2654$, and $Q_0 \approx 18.9544,\ 23.3417$, respectively. These period-2 motions also experience three pairs of SN bifurcations associated with jumping phenomena, existing at $Q_0 \approx 15.8361,\ 17.5726$, $Q_0 \approx 18.9481,\ 19.3433$, and $Q_0 \approx 23.1041,\ 23.3912$, respectively. The second piece of period-2 motions exist for $Q_0 \in (20.2191,\ 22.5622)$, which are introduced by the PD bifurcations of period-1 motions at $Q_0 \approx 20.2191,\ 22.2001$. As mentioned before, the PD bifurcation at $Q_0 \approx 20.2191$ corresponds to the USN bifurcation

Table 11.2 Bifurcation points of Branch2 motions ($Q_0 \in (14.0, 30.0)$, $\alpha = 4.0$, $\delta = 0.1$, $\Omega = 2.0$)

	Period-doubling bifurcations			Saddle-node bifurcations		
	Q_0	Left	Right	Q_0	Left	Right
P_1	(14.4494, 23.6701)	PD (P_2)	PD (P_2)	(14.2157, 29.0904)	SN (J)	SN (J)
	(20.2191, 22.2001)	PD (P_2)	PD (P_2)	–	–	–
	(24.9181, 28.8655)	PD (P_2)	PD (P_2)	–	–	–
P_2	(14.5039, 17.5725)	PD (P_4)	PD (P_4)	(15.8361, 17.5726)	SN (J)	SN (J)
	(15.8362, 19.2654)	PD (P_4)	PD (P_4)	(18.9481, 19.3433)	SN (J)	SN (J)
	(18.9544, 23.3417)	PD (P_4)	PD (P_4)	(20.2191, 22.2001)	USN (P_1)	SN (P_1)
	(25.3770, 27.4937)	PD (P_4)	PD (P_4)	(20.2191, 22.5622)	USN (P_1)	SN (J)
	(27.1549, 28.8023)	PD (P_4)	PD (P_4)	(21.8361, 22.2236)	SN (J)	SN (J)
	–	–	–	(23.1041, 23.3912)	SN (J)	SN (J)
	–	–	–	(27.1548, 27.5008)	SN (J)	SN (J)

Table 11.3 Bifurcation points of Branch3 motions ($Q_0 \in (26.0, 42.0)$, $\alpha = 4.0$, $\delta = 0.1$, $\Omega = 2.0$)

	Period-doubling bifurcations			Saddle-node bifurcations		
	Q_0	Left	Right	Q_0	Left	Right
P_1	(27.9872, 33.1591)	PD (P_2)	PD (P_2)	(27.5912, 41.1842)	SN (J)	SN (J)
	(34.7730, 35.9030)	PD (P_2)	PD (P_2)	–	–	–
	(38.3290, 40.7450)	PD (P_2)	PD (P_2)	–	–	–
P_2	(28.0910, 29.5565)	PD (P_4)	PD (P_4)	(29.3783, 29.5614)	SN (J)	SN (J)
	(29.3835, 31.1640)	PD (P_4)	PD (P_4)	(27.9872, 33.1591)	SN (P_1)	USN (P_1)
	(32.8132, 33.4130)	PD (P_4)	PD (P_4)	(33.1591, 34.9693)	USN (P_1)	SN (J)
	(38.7920, 39.6830)	PD (P_4)	PD (P_4)	(34.7160, 34.7730)	SN (J)	USN (P_1)
	(39.7760, 40.5837)	PD (P_4)	PD (P_4)	(34.7730, 35.9030)	USN (P_1)	SN (P_1)
	–	–	–	(38.3290, 40.7450)	SN (P_1)	SN (P_1)

of period-2 motions, which means it introduces unstable period-2 motions instead of stable ones. Thus, these period-2 motions start at $Q_0 \approx 20.2191$ as unstable ones and end at $Q_0 \approx 22.2001$ as stable ones. No PD bifurcations are observed. Thus, no period-4 motions and further cascaded period doublings to chaos exist. Instead, these period-2 motions experience two jumping phenomena. The first jumping phenomenon is enclosed by the USN and SN bifurcations at $Q_0 \approx 20.2191$ and 22.5622, and the other one is enclosed by a pair of SN bifurcations at $Q_0 \approx 21.8361,\ 22.2236$. A detailed view for $Q_0 \in (20.0,\ 23.0)$ is in Fig. 11.3c, d for a better illustration. Finally, the third piece of period-2 motions exist for $Q_0 \in (24.9181,\ 28.8655)$, which is introduced by the pair of PD bifurcations at $Q_0 \approx 24.9181,\ 28.8655$. These period-2 motions experience two pairs of PD bifurcations at $Q_0 \approx 25.3770,\ 27.4937$ and $Q_0 \approx 27.1549,\ 28.8023$, which introduce period-4 motions and further cascaded

Table 11.4 Bifurcation points of Branch4 motions ($Q_0 \in (34.0, 46.0)$, $\alpha = 4.0$, $\delta = 0.1$, $\Omega = 2.0$)

	Period-doubling bifurcations			Saddle-node bifurcations		
	Q_0	Left	Right	Q_0	Left	Right
P_1	(35.1315, 45.0020)	PD (P_2)	PD (P_2)	(34.6814, 45.5469)	SN (J)	SN (J)
P_2	(35.2908, 36.4180)	PD (P_4)	PD (P_4)	(35.1315, 45.0020)	SN (P_1)	SN (P_1)
	(36.5660, 37.4640)	PD (P_4)	PD (P_4)	–	–	–
	(44.1730, 44.6500)	PD (P_4)	PD (P_4)	–	–	–

period z-4 to chaos. In addition, they also encounter a pair of SN bifurcations associated with jumping phenomena at $Q_0 \approx 27.1548,\ 27.5008$.

The third branch ('B3') of the bifurcation trees exists for the range of $Q_0 \in (27.5912, 41.1842)$ as presented in Fig. 11.4. The asymmetric period-1 motions are stable for the ranges of $Q_0 \in (27.5912,\ 27.9872)$, $(33.1591,\ 34.7730)$, $(35.9030,\ 38.3290)$, and $(40.7450,\ 41.1842)$. These stable period-1 motions are connected together by the unstable period-1 motions for $Q_0 \in (27.9872,\ 33.1591)$, $(34.7730,\ 35.9030)$, and $(38.3290,\ 40.7450)$. In addition, these period-1 motions encounter SN bifurcations associated with jumping phenomena at $Q_0 \approx 27.5912$ and 41.1842. The introduced unstable period-1 motion connects the two SN bifurcation points together, which forms a closed loop of the period-1 motions. Furthermore, the asymmetric period-1 motions experience three pairs of PD bifurcations for $Q_0 \approx 27.9872,\ 33.1591,\ Q_0 \approx 34.7730,\ 35.9030$, and $Q_0 \approx 38.3290,\ 40.7450$. The PD bifurcations at $Q_0 \approx 33.1591$ and 34.7730 correspond to the USN bifurcations of period-2 motions, which introduce unstable period-2 motions instead of stable ones. The rest of the PD bifurcations all correspond to SN bifurcations of the period-2 motions, which lead to stable period-2 motions. There are total of three pieces of period-2 motions introduced. The first period-2 motions in the range of $Q_0 \in (27.9872,\ 34.9693)$ experience three pairs of PD bifurcations that introduce period-4 motions and further cascaded period doublings to chaos. These three pairs of PD bifurcations exist at $Q_0 \approx 28.0910,\ 29.5565,\ Q_0 \approx 29.3835,\ 31.1640$, and $Q_0 \approx 32.7320,\ 33.4130$, respectively. These period-2 motions also experience two jumping phenomena. The first jumping phenomenon is enclosed by a pair of SN bifurcations at $Q_0 \approx 29.3783,\ 29.5614$; and the other one is enclosed by a USN bifurcation and a SN bifurcation at $Q_0 \approx 33.1591$ and 34.9693, respectively. The second piece of period-2 motions exist for $Q_0 \in (34.7160,\ 35.9030)$, which are introduced by the PD bifurcations of period-1 motions at $Q_0 \approx 34.7730,\ 35.9030$. No PD bifurcations are observed. Thus, no period-4 motions and further cascaded period doublings to chaos exist. Instead, these period-2 motions experience a jumping phenomenon, which is enclosed by the SN and USN bifurcations at $Q_0 \approx 34.7160$ and 34.7730. A detailed view for the range of $Q_0 \in (32.0,\ 36.0)$ is provided in Fig. 11.4c, d for a better illustration of the USN bifurcations and jumping phenomenon. Finally, the third piece of period-2 motions exist for the range of $Q_0 \in (38.3290,\ 40.7450)$,

which is introduced by the pair of PD bifurcations at $Q_0 \approx 38.3290,\ 40.7450$. These period-2 motions experience two pairs of PD bifurcations at $Q_0 \approx 38.7920,\ 39.6830$ and $Q_0 \approx 39.7760,\ 40.5837$, which introduce period-4 motions and further cascaded period doublings to chaos. In addition, they also encounter a pair of SN bifurcations associated with jumping phenomena at $Q_0 \approx 38.3290,\ 40.7450$.

The fourth branch ('B4') of the bifurcation trees existing in the range of $Q_0 \in (34.6814, 45.5469)$ is relatively simply, as presented in Fig. 11.5. The asymmetric period-1 motions are stable for the ranges of $Q_0 \in (34.6814,\ 35.1315)$ and $(45.0020,\ 45.5469)$. These stable period-1 motions are connected together by the unstable period-1 motions for $Q_0 \in (35.1315,\ 45.0020)$. Such period-1 motions encounter SN bifurcations associated with jumping phenomena at $Q_0 \approx 34.6814$ and 45.5469. The introduced unstable period-1 motion connects the two SN bifurcation points together, forming a closed loop. Only one pair of PD bifurcations exist for such period-1 motions at $Q_0 \approx 35.1315,\ 45.0020$. The enclosed period-2 motions experience three pairs of PD bifurcations that introduce period-4 motions and further cascaded period doublings to chaos. These three pairs of PD bifurcations exist at $Q_0 \approx 35.2908,\ 36.4180,\ Q_0 \approx 36.5660,\ 37.4640$, and $Q_0 \approx 44.1730,\ 44.6500$, respectively. No jumping phenomena are observed.

11.5 Simulation and Illustrations

Using the same parameters in Eq. (11.24), different excitation amplitudes Q_0 will be selected from the bifurcation trees to demonstrate different travelable periodic motions. For such travelable periodic motions, the displacement does not return to the initial point. Instead, it always returns to a point that is $2N\pi,\ N = 1, 2, 3...$ away from the initial point, which still indicates same position of the pendulum. On the other hand, the velocity of such travelable periodic motions is purely periodic. In these illustrations, time histories of displacement and velocity, trajectories and harmonic amplitudes, and phases of velocity will be presented from numerical and analytical results. The numerical and analytical results will be presented by solid curves and hollow circles, respectively. The initial points and periodic nodes are indicated by green circles. For asymmetric motions, the black and red colors indicate the motions are on black and red branches on the bifurcation trees, respectively. 'IC' indicates the initial conditions. For travelable periodic motions of pendulum, no Fourier series expression displacements of periodic motions exists. Herein, the harmonic amplitudes and phases of velocity for travelable periodic motions will be presented. The travelable periodic motions of pendulum possess $x_0 = \mathrm{mod}(x_{mT}, 2\pi)$ but $x_0 \neq x_{mT}$. Physical motion is indeed a closed periodic motion. However, the periodic solution of displacement for the pendulum is not closed. So, the Fourier series of displacement does not exist.

In Fig. 11.6, a pair of travelable asymmetric period-1 motions are presented for $Q_0 = 7.0$. The initial time is $t_0 = 0.0$. The initial conditions are $x_0 \approx 6.2751$, $\dot{x}_0 \approx 2.9956$ for the black branch and $x_0 \approx 6.2541$, $\dot{x}_0 \approx -2.4295$ for the red branch.

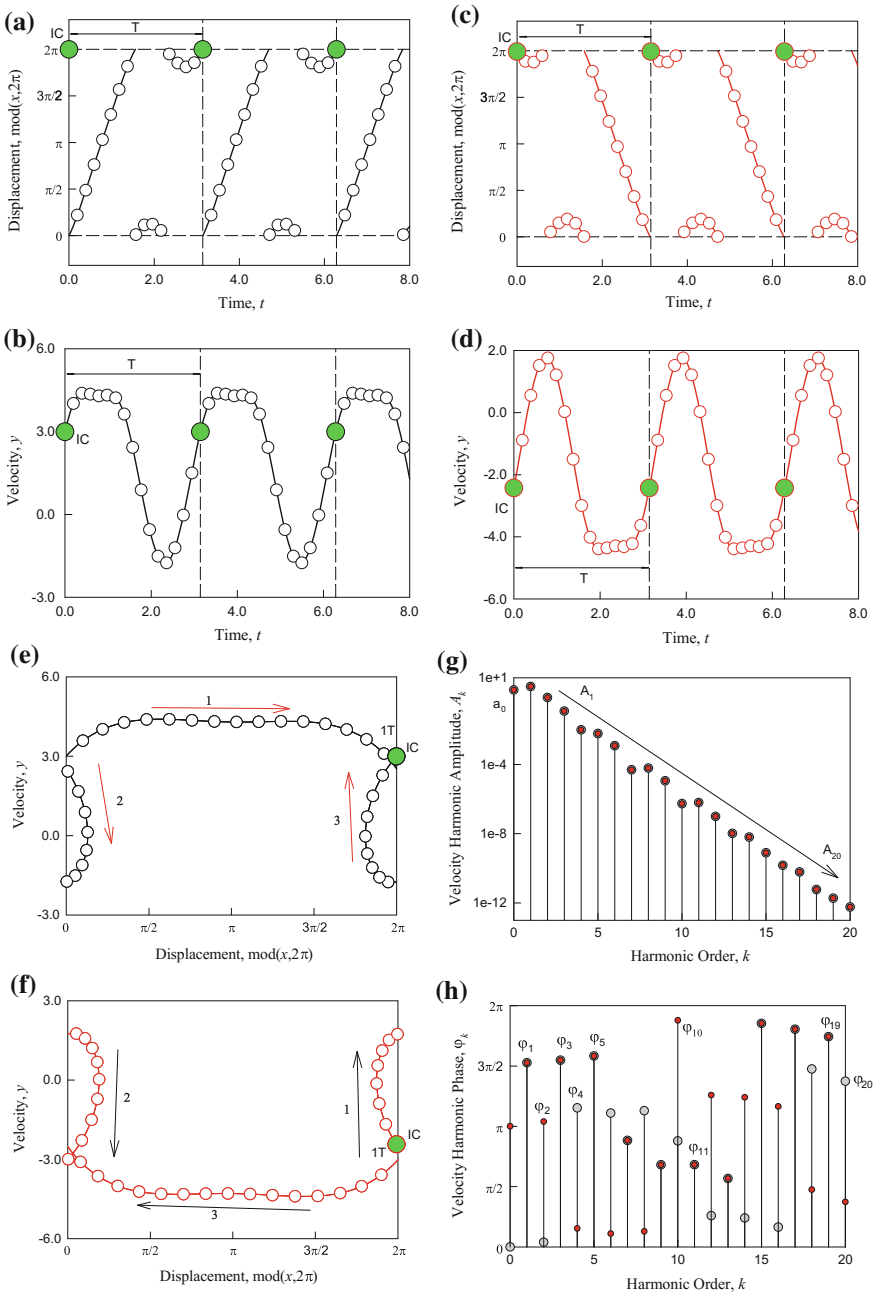

Fig. 11.6 Asymmetric period-1 motion ($Q_0 = 7.0$): **a**, **b** displacement and velocity (*black*), **c**, **d** displacement and velocity (*red*), **e**, **f** trajectories, **g**, **h** harmonic amplitudes and phases. IC: $t_0 = 0.0$, *Black branch* ($x_0 \approx 6.2751$, $\dot{x}_0 \approx 2.9956$), *Red branch* ($x_0 \approx 6.2541$, $\dot{x}_0 \approx -2.4295$). ($\alpha = 4.0$, $\delta = 0.1$, $\Omega = 2.0$)

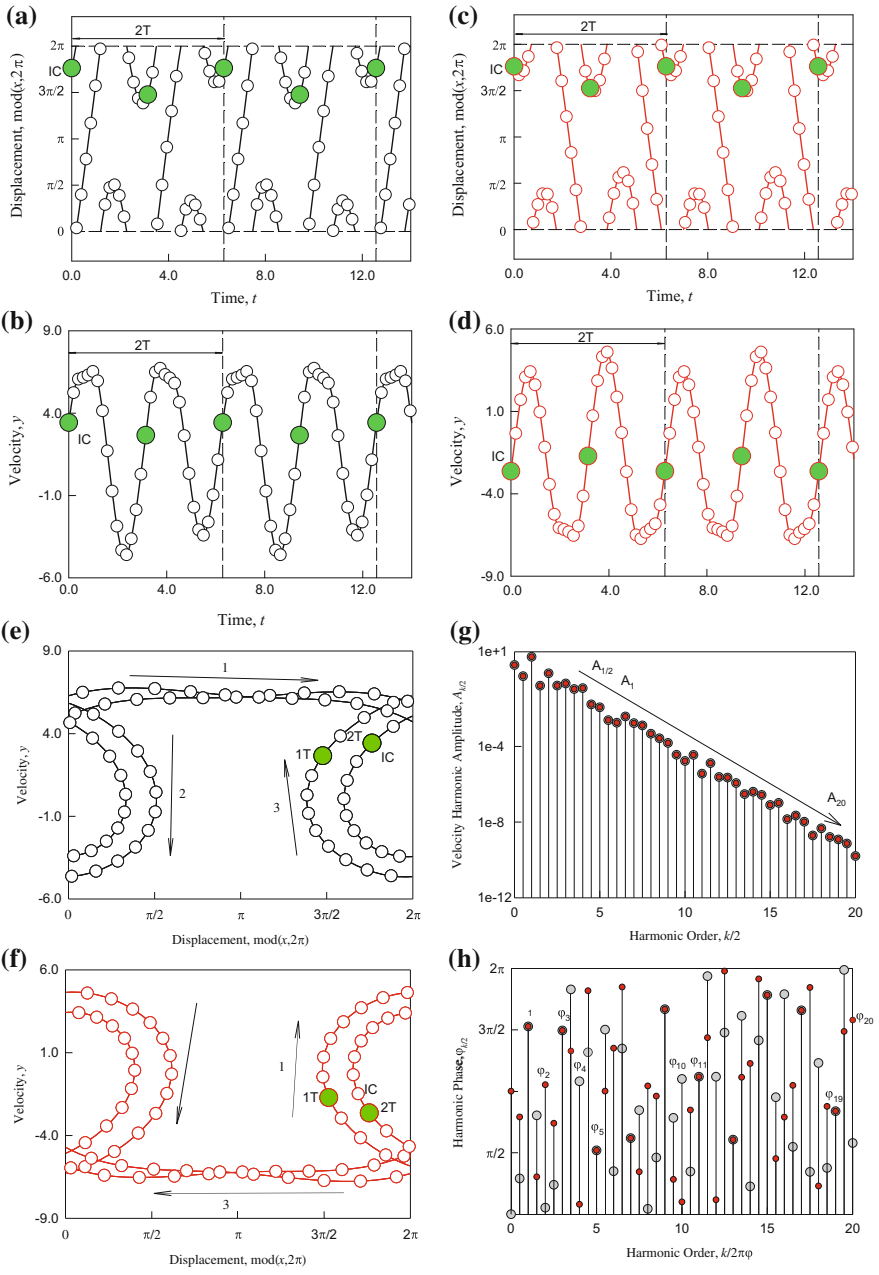

Fig. 11.7 Asymmetric period-2 motion ($Q_0 = 8.6$): **a**, **b** displacement, velocity of the *black branch*, **c**, **d** displacement, velocity of the *red branch*, **e**, **f** trajectories, **g**, **h** harmonic amplitudes and phases. IC: $t_0 = 0.0$, *Black branch* ($x_0 \approx 5.5369$, $\dot{x}_0 \approx 3.4309$), *Red branch* ($x_0 \approx 5.5315$, $\dot{x}_0 \approx -2.6347$). ($\alpha = 4.0$, $\delta = 0.1$, $\Omega = 2.0$)

These initial conditions are obtained from the analytical predictions. The time histories of displacement and velocity are presented in Fig. 11.6a, b for the black branch and in Fig. 11.6c, d for the red branch, respectively. Figure 11.6e, f present the trajectories of periodic motions on the black and red branches, respectively. In Fig. 11.6g, h, the harmonic amplitudes and phases of velocity for the periodic motions are presented. In all plots, displacements of pendulum are presented with a modulus to 2π. From the figures, the periodic motion on the black branch starts at a little bit less than 2π. The pendulum motion goes through one full rotation counterclockwise to 4π and swings back and forth once around 4π to complete one period. The velocities at ending point and initial point are exactly the same, while the displacement at ending point is 2π away from the initial point. The motion of the red branch also starts at a little bit lower than 2π. It first swings back and forth once around 2π and then goes through one full rotation clockwise to a little bit lower than 0 to complete two periods. Thus, the velocities at ending point and initial point are exactly the same, while the displacement at ending point is -2π away from the initial point. From two trajectories, the motion on the black and red branches is of the skew symmetry to each other according to the point $(\pi,\ 0)$. From the harmonic amplitudes of velocity, $a_0^R = -a_0^B = -2.0$. The main harmonic amplitudes are $A_1 \approx 3.1491$, $A_2 \approx 0.7280$, $A_3 \approx 0.1199$, and $A_4 \approx 0.0100$. The other velocity harmonic amplitudes are $A_k \in (10^{-13}, 10^{-2})$. The harmonic phases of velocity are $\varphi_k^R = \mathrm{mod}(\varphi_k^B + (k+1)\pi, 2\pi)$ for $k = 0, 1, 2, \cdots$. $x_T - x_0 = 2\pi$ for the black branch and $x_T - x_0 = -2\pi$ for the red branch.

As mentioned previously in the bifurcation trees, such asymmetric period-1 motions encounter a PD bifurcation at $Q_0 \approx 8.5712$, introducing period-2 motions. Thus, at $Q_0 = 8.6$, a pair of travelable asymmetric period-2 motions are presented in Fig. 11.7. The initial time is $t_0 = 0.0$. The initial conditions are $x_0 \approx 5.5369$, $\dot{x}_0 \approx 3.4309$ for the black branch and $x_0 \approx 5.5315$, $\dot{x}_0 \approx -2.6347$ for the red branch. Again, these initial conditions are obtained from the analytical predictions. The time histories of displacement and velocity are presented in Fig. 11.7a, b for the black branch and Fig. 11.7c, d for the red branch, respectively. Figure 11.7e, f present the trajectories of the black and red branches, respectively. In all figures, the displacement of pendulum is presented with a modulus to 2π. The periodic motion on the black branch starts at a little bit less than 2π. It first goes through one full rotation counterclockwise to 4π and swings back and forth once around 4π. Then, the motion goes through another full rotation counterclockwise to 6π and swings back and forth once again around 6π to complete two periods. The velocities at ending point and initial point are exactly the same, while the displacement at ending point is 4π away from the initial point. The periodic motion of the red branch also starts at a little bit lower than 2π. It first swings back and forth once around 2π and goes through one full rotation clockwise to zero. Then, it swings back and forth once again around zero and goes through one more full rotation clockwise to a little bit lower than -2π to complete two periods. Thus, the velocities at ending and initial points are exactly the same, while the displacement at ending point is -4π away from the initial point. Furthermore, from trajectories, motions on the black and red branch are of skew symmetry to each other according to the point $(\pi,\ 0)$. From the harmonic amplitudes of velocity, $a_0^{(2)R} = -a_0^{(2)B} = -2.0$. The main

harmonic amplitudes are $A_{1/2} \approx 0.5136$, $A_1 \approx 5.4078$, $A_{1/2} \approx 0.1609$, $A_2 \approx 0.7335$, $A_{3/2} \approx 0.1643$, $A_3 \approx 0.2115$, $A_{7/2} \approx 0.1072$, $A_4 \approx 0.1201$, $A_{9/2} \approx 0.0166$, and $A_5 \approx 0.0116$. The other velocity harmonic amplitudes are $A_k \in (10^{-13}, 10^{-2})$. The harmonic phases of velocity are $\varphi^R_{k/2} = \text{mod}(\varphi^B_{k/2} + ((1+2r)k/2+1)\pi, 2\pi)$ for $k = 0, 1, 2, \cdots$ and $r = 0$. $t_0 = rT \quad r \in \{0, 1\}$. $x_{2T} - x_0 = 4\pi$ for the black branch and $x_{2T} - x_0 = -4\pi$ for the red branch.

11.6 Conclusions

In this chapter, the travelable period-1 motions to chaos of a periodically excited pendulum were presented. The implicit discrete maps were obtained from the mid-point scheme of the corresponding differential equation of such a periodically excited pendulum. Using the discrete maps, mapping structures were developed for various periodic motions, from which analytical bifurcation trees of periodic motions to chaos can be obtained. The complete bifurcation trees of travelable periodic motions in the system were obtained from analytical prediction with varying excitation amplitude. The corresponding stability and bifurcation conditions were achieved through eigenvalue analysis of discrete dynamical system. Finally, numerical illustrations of periodic motions on the bifurcation trees were presented in verification of the analytical prediction.

References

1. Barkham, P.G.D., Soudack, A.C.: An extension to the method of Krylov and Bogoliubov. Int. J. Control **10**, 377–392 (1969)
2. Barkham, P.G.D., Soudack, A.C.: Approximate solutions of nonlinear, non-autonomous second-order differential equations. Int. J. Control **11**, 763–767 (1970)
3. Coppola, V.T., Rand, R.H.: Averaging using elliptic functions: approximation of limit cycle. Acta Mechanica **81**, 125–142 (1990)
4. Fatou, P.: Sur le mouvement d'un systeme soumis 'a des forces a courte periode. Bull. Soc. Math. **56**, 98–139 (1928)
5. Guo, Y., Luo, A.C.J.: On complex periodic motions and bifurcations in a periodically forced, damped, hardening Duffing oscillator. Chaos Solitons Fractals **81**(2015), 378–399 (2015)
6. Guo, Y., Luo, A.C.J.: Periodic motions in a double-well Duffing oscillator under periodic excitation through discrete implicit mappings. Int. J. Dyn. Control (2015). doi:10.1007/s40435-015-0161-6
7. Garcia-Margallo, J., Bejarano, J.D.: A generalization of the method of harmonic balance. J. Sound Vib. **116**, 591–595 (1987)
8. Hayashi, C.: Nonlinear Oscillations in Physical Systems. McGraw-Hill Book Company, New York (1964)
9. Krylov, N.M., Bogolyubov, N.N.: Methodes approchees de la mecanique non-lineaire dans leurs application a l'Aeetude de la perturbation des mouvements periodiques de divers phenomenes de resonance s'y rapportant, Academie des Sciences d'Ukraine:Kiev. (in French) (1935)
10. Lagrange, J.L.: Mecanique Analytique, vol. 2 (edition Albert Balnchard: Paris, 1965) (1788)
11. Luo, A.C.J.: Continuous Dynamical Systems. HEP/L&H Scientific, Beijing/Glen Carbon (2012)

12. Luo, A.C.J.: Periodic flows to chaos based on discrete implicit mappings of continuous nonlinear systems. Int. J. Bifurc. Chaos **25**(3), Article No. 1550044 (62 p) (2015)
13. Luo, A.C.J., Guo, Y.: A semi-analytical prediction of periodic motions in Duffing oscillator through mapping structures. Discontinuity Nonlinearity Complex. **4**(2), 13–44 (2015)
14. Luo, A.C.J., Han, R.P.S.: The dynamics of stochastic and resonant layers in a periodically driven pendulum. Chaos Solitons Fractals **11**, 2349–2359 (2000)
15. Luo, A.C.J., Huang, J.Z.: Approximate solutions of periodic motions in nonlinear systems via a generalized harmonic balance. J. Vib. Control **18**, 1661–1871 (2012)
16. Luo, A.C.J., Huang, J.Z.: Analytical dynamics of period-m flows and chaos in nonlinear systems. Int. J. Bifurc. Chaos **22**, Article No. 1250093 (29 p) (2012)
17. Poincare, H.: Methodes Nouvelles de la Mecanique Celeste, vol. 3. Gauthier-Villars, Paris (1899)
18. Rand, R.H., Armbruster, D.: Perturbation Methods, Bifurcation Theory, and Computer Algebra. Applied Mathematical Sciences, vol. 65. Springer, New York (1987)
19. van der Pol, B.: A theory of the amplitude of free and forced triode vibrations. Radio Rev. **1**(701–710), 754–762 (1920)
20. Yuste, S.B., Bejarano, J.D.: Construction of approximate analytical solutions to a new class of non-linear oscillator equations. J. Sound Vib. **110**(2), 347–350 (1986)
21. Yuste, S.B., Bejarano, J.D.: Extension and improvement to the Krylov-Bogoliubov method that use elliptic functions. Int. J. Control **49**, 1127–1141 (1989)
22. Yuste, S.B., Bejarano, J.D.: Improvement of a Krylov-Bogoliubov method that uses Jacobi elliptic functions. J. Sound Vib. **139**(1), 151–163 (1990)
23. Zaslavsky, G.M., Chirikov, B.V.: Stochastic instability of nonlinear oscillations. Sov. Phys. USP **14**(5), 549–672 (1972)

Chapter 12
Automorphic Systems and Differential-Invariant Solutions

A.A. Talyshev

12.1 Introduction

Further, we use following notations: $X = R^n$ is a space of independent variables, $Y = Y_0 = R^m$ is a space of depended variables, $Z_k = X \times Y_0 \times \cdots \times Y_k$, $k = 0, 1, \ldots$, where $Y_k = R^m \otimes S^k R^n$, $k = 1, \ldots$ are prolonged spaces. The vectors of the spaces Y_k are denoted by $\underset{k}{y}$ and their components is denoted by y_α, where $\alpha = (\alpha_1, \ldots, \alpha_n)$ are multi-indexes and $|\alpha| = \alpha_1 + \cdots + \alpha_n = k$. Dimension of the space Z_k is denoted by ν_k, i.e.

$$\nu_k = \dim(Z_k) = n + m\binom{n+k}{n}.$$

By ρ_k^{k+1}, denote the canonical projection Z_{k+1} onto Z_k:

$$\rho_k^{k+1}(x, y, \underset{1}{y}, \ldots, \underset{k}{y}, \underset{k+1}{y}) = (x, y, \underset{1}{y}, \ldots, \underset{k}{y}).$$

The total derivative operators are denoted by D_j, i.e.

$$D_j = \partial_{x_j} + \sum_{|\alpha| \geqslant 0} y_{\alpha+\gamma_j} \partial_{y_\alpha} \quad j = 1, \ldots, n,$$

where $|\gamma_j| = 1$ and the jth component of the multi-index γ_j is equal to 1.

A.A. Talyshev (✉)
Novosibirsk State University, Pirogova st. 2, Novosibirsk, Russia
e-mail: tal@academ.org

D. Volchenkov and X. Leoncini (eds.), *Regularity and Stochasticity of Nonlinear Dynamical Systems*, Nonlinear Systems and Complexity 21,
DOI 10.1007/978-3-319-58062-3_12

12.2 Symmetries of Prolonged Systems

The algorithm for calculation of admitted Lie group of point transformations described, for example, in the paper [7, Sect. 5]; in general, itself is applicable to any set of differential equations, even if the set of solutions of this system is empty.

The classic property involutiveness [2, 11] ensures that the prolongation of involutive system is always an involution and that any system of a finite number of prolongations given to the involutive or algebraically contradictory system.

The paper [12] shows that in the class of tangent transformations (on the solutions of the system), group Lie admitted involutive system is equal to group Lie admitted prolongation of this system.

In this section, present study establishes that under certain conditions the shape of the recording system of differential equations each of its point symmetry admitted of the prolonged system. It follows that at the points of general position, involutive system resulting from prolonged not loosing none from the point symmetry of the original system. The example of isobaric gas motions demonstrates that the group may extends after actuation system to involutive form (see the paper [13]).

In this section, we consider differential equations in the form

$$\begin{aligned} &\Phi(x, u, \partial_x u, \ldots, \partial_x^k u) = 0, \\ &x \in X = R^n, \quad u\colon R^n \to Y_0, \quad Y_0 = R^m, \\ &\partial_x^i u\colon X \to Y_i, \quad Y_i = R^m \otimes S^i R^n, \quad i = 1, \ldots, k, \\ &\Phi\colon Z_k \to R^s, \quad Z_i = X \times Y_0 \times \cdots \times Y_i, \quad i = 0, 1 \ldots \end{aligned} \tag{12.1}$$

Group analysis of differential equations using geometric representation of differential equations and their solutions as finite-dimensional manifolds in the space Z_k. This approach imposes a condition on the shape of the recording system. This condition means that together with all the algebraic consequence $\phi = 0$ of order $l < k$, algebraic consequences are equations whose left sides are all derivative from the ϕ to the independent variables to the order $k - l$ inclusive. For example, the Navier–Stokes equations must be added four more obtained by differentiating the equation $\operatorname{div} \mathbf{u} = u_x + v_y + w_z = 0$ all the independent variables. It is assumed that this agreement on the form of the recording system (12.1) is satisfied. It also assumes that from (12.1) should not be any relationships linking variables x and u, i.e.

$$\dim \rho_0^k \left(\{z \in Z_k : \Phi(z) = 0\}\right) = n + m. \tag{12.2}$$

In this section, we consider the point transformations, i.e. transformations of the dependent and independent variables for the needs of the differential equations prolonged to the space Z_k.

One-parameter local Lie group of point transformations completely determines infinitesimal operator

$$L = \sum_{i=1}^{n} \xi^i(x,u)\partial_{x_i} + \sum_{j=1}^{m} \zeta^j(x,u)\partial_{u^j}. \tag{12.3}$$

The prolongation of L on the space Z_k is written as

$$L^k = L + \sum_{|\alpha|>0}^{|\alpha|\leqslant k} \zeta_\alpha \partial_{u_\alpha},$$

where

$$\zeta_{\alpha+\gamma_j} = D_j\zeta_\alpha - \sum_{i=1}^{n} u_{\alpha+\gamma_i} D_j\xi^i, \quad j = 1,\ldots,n. \tag{12.4}$$

System (12.1) admits operator (12.3) if and only if the following condition be satisfied

$$L^k\Phi\big|_{\Phi=0} = 0. \tag{12.5}$$

It follows from formulas (12.4) that

$$L^\infty D_j = D_j L^\infty - \sum_{i=1}^{n} D_j(\xi^i)D_i, \quad j = 1,\ldots,n. \tag{12.6}$$

In the paper [7, Sect. 4.9], formulas (12.6) named lemma on commutator.

Lemma 12.1 *An prolonged system of partial differential equations admits each symmetry of an original system.*

Proof To prove the lemma is needed to establish that

$$L^{k+1} D_j\Phi\big|_{\Phi=0,\Phi_1=0} = 0, \quad j = 1,\ldots,n \tag{12.7}$$

follows from (12.5), where $\Phi_1 = \{D_1\Phi,\ldots,D_n\Phi\}$.

Operators L^k and L^{k+1} in the expressions (12.5) and (12.7) can be replaced by the infinity prolonged operator L^∞. After this substitution, the formulas (12.6) allow to move the left-hand of expression (12.7) as

$$L^{\infty}D_j\Phi\big|_{\Phi=0,\Phi_1=0} = \left(D_jL^{\infty}\Phi - \sum_{i=1}^{n} D_j(\xi^i)D_i\Phi\right)\Bigg|_{\Phi=0,\Phi_1=0} =$$
$$= D_jL^{\infty}\Phi\big|_{\Phi=0,\Phi_1=0}, \quad j = 1,\ldots,n. \tag{12.8}$$

Expression (12.8), in general, is not required zero. But it follows from the theorem on the representation of a non-singular invariant manifold (see [7, Sect. 18.7]) that allows to select as a mapping Φ in (12.1) invariant of the operator L^k in the space Z_k. Indeed, by condition (12.2) it follows that manifold (12.1) is non-singular invariant manifold under any one-parametric group Lie admitted by system (12.1). □

Corollary 12.1 *The manifold*

$$\Theta = p_k^{k+1}(\{z \in Z_{k+1} : \Phi(p_k^{k+1}(z)) = 0, \Phi_1(z) = 0\})$$

is invariance under any Lie symmetry admitted by system (12.1).

Proof Obviously, that $\Theta \subseteq F = \{z \in Z_k : \Phi(z) = 0\}$. If the manifold Θ is empty or is equal to F, then statement of Lemma is true. If $\Theta \subset F$, then there exits the mapping $\varphi : Z_k \to R^{s_1}$ such that $\Theta = \{z \in Z_k : \Phi(z) = 0,\ \varphi(z) = 0\}$.

For any infinitesimal operator L, the set of equations

$$(L^{\infty}\Phi, L^{\infty}\Phi_1)\big|_{\Phi=0,\Phi_1=0} = 0$$

is equal the set of equations

$$(L^{\infty}\Phi, L^{\infty}\varphi, L^{\infty}\Phi_1)\big|_{\Phi=0,\varphi=0,\Phi_1=0} = 0.$$

Last set is equal to the union of two next sets of equations:

$$\begin{aligned}(L^{\infty}\Phi, L^{\infty}\varphi)\big|_{\Phi=0,\varphi=0} &= 0,\\ (L^{\infty}\Phi_1)\big|_{\Phi=0,\Phi_1=0} &= 0.\end{aligned} \tag{12.9}$$

If system (12.1) admits the operator L, then by Lemma 12.1 it follows that (12.9) is true. But the set of Eq. (12.9) is not equal the set of Eq. (12.5), firstly because of reduced number of variables over which the splitting Eq. (12.5) and secondly because of the addition of the new equations $\varphi = 0$ in the system. So it is possible the emergence of the new symmetries of the system $\Phi = 0$, $\varphi = 0$. Isobaric gas motion example demonstrates such an extension group [13]. □

Bringing the system to involutive form carried out by means of prolongations. Any system of partial differential equations is a finite number of prolongations to the involutive form or contradictory system [11, Sect. 63]. So, if the system can

be brought to mind involutive finite number of prolongations, is a finite number of applications of Lemma 12.1 and Corollary 12.1 establish the validity the following statement.

Corollary 12.2 *The system of differential equations reduced to involutive form admits all point symmetry of the original system at the points of general position.*

12.3 Automorphic Systems

Definition 12.1 If any solution of a system of differential equations is obtained from one fixed solutions by means of action of the group transformations G, then this system is called automorphic with respect to the group G [7, Sect. 25.1].

We consider the Lie group $G^r(h)$ of the finite dimension r generated by the mapping $h : Z \times B \to Z$, where $B = R^r$. There exists unique prolongation of the mapping h on the space Z_k for all $k > 0$. Here, this prolongation is written in the form

$$\underset{k}{h} : Z_k \times B \to Z_k.$$

Starting with some k the general rank r_k of the group G^r on the space Z_k is equal to r. Here, this value of k is denoted by k_1.

The mapping $u : X \to Y$ for every $k \geqslant 0$ determines the manifold in the space Z_k ('graph of mapping')

$$\underset{k}{U} = \left\{ x, y_\alpha = \frac{\partial^{|\alpha|} u}{\partial x_1^{\alpha_1} \dots \partial x_n^{\alpha_n}}, \quad 0 \leqslant |\alpha| \leqslant k \right\}. \tag{12.10}$$

The result of the action of the group G^r on the manifold (12.10) is called an orbit of the manifold and is denoted by $\underset{k}{h}(\underset{k}{U}, O)$, where O is a neighbourhood 0 in the space B. Dimension of the orbit d_k satisfies inequalities

$$\max\{n, r_k\} \leqslant d_k = \dim \underset{k}{h}(\underset{k}{U}, O) \leqslant \min\{n + r_k, \nu_k\}. \tag{12.11}$$

It is obvious that for all $k \geqslant 0$

$$\rho_k^{k+1}\left(\underset{k+1}{h}(\underset{k+1}{U}, O)\right) = \underset{k}{h}(\underset{k}{U}, O). \tag{12.12}$$

Obviously, there exists $k_2 \geqslant k_1$ (k_2 depends of the mapping u) such that the orbit is a own manifold of the space Z_k for all $k \geqslant k_2$. When $k \geqslant k_2$ there exist mappings $\psi_k : Z_k \to R^{s_k}$ such that

$$\underset{k}{h}(\underset{k}{U}, O) = \{z_k \in Z_k : \psi_k(z_k) = 0\},$$

where $s_k = \nu_k - d_k$. Due to (12.12) the mappings ψ_k can be chosen such that the set of the mappings ψ_{k+1} for every k is an expansion of the set of the mapping ψ_k.

The relations

$$\psi_k(z) = 0, \quad z \in Z_k \tag{12.13}$$

give a system of differential equations of the order k on m functions of n variables and mapping u is the solution of this system.

The system

$$p(\psi_k)(z) = \{\psi_k(\rho_k^{k+1}(z)), (D_1\psi_k)(z), \ldots, (D_n\psi_k)(z)\} = 0, \quad z \in Z_{k+1}$$

is called the first prolongation of the system (12.13). Accordingly, the manifold

$$p(\underset{k}{h}(\underset{k}{U}, O)) = \{z \in Z_{k+1} : p(\psi_k)(z) = 0\}$$

is called the first prolongation of the orbit $\underset{k}{h}(\underset{k}{U}, O)$.

Lemma 12.2 *The following relation holds for every $k \geqslant k_2$:*

$$p(\underset{k}{h}(\underset{k}{U}, O)) \supseteq \underset{k+1}{h}(\underset{k+1}{U}, O). \tag{12.14}$$

Proof By Lemma 12.1, it follows that an prolonged system of partial differential equations admits each symmetry of an original system. Hence, prolonged system $p(\psi_k(z)) = 0$ admits the group G^r and the mapping u is the solution of this system. Therefore, the prolongation of the orbit u from the space Z_k contains the orbit of the solution u in the space Z_{k+1}. □

Lemma 12.3 *The following equality holds for every $k \geqslant k_2$:*

$$\rho_k^{k+1}(p(\underset{k}{h}(\underset{k}{U}, O))) = \underset{k}{h}(\underset{k}{U}, O).$$

Proof On the one hand, the obvious embedding holds

$$\rho_k^{k+1}(p(\underset{k}{h}(\underset{k}{U}, O)) \subseteq \underset{k}{h}(\underset{k}{U}, O).$$

On the other hand, applying the projection ρ_k^{k+1} to both sides of the relation (12.14) and using equality (12.12) provides the reverse embedding. □

Restriction of the Pfaff system

$$dy_\alpha - \sum_{j=1}^{n} y_{\alpha+\gamma_j} dx_j = 0, \quad 0 \leqslant |\alpha| < k$$

on the manifold $\underset{k}{h}(\underset{k}{U}, O))$ provides the Pfaff system with the given independent variables x. This system is equivalent to the system of differential equations (12.13). The opposite also holds: every Pfaff system with given independent variables corresponds to an equivalent system of differential equations. The equivalence in this case is understood as the fact that there is a bijection between integral manifolds of the system of exterior equations and solutions of the system of differential equations. In terms of this equivalence, a system of differential equations is called here completely integrable if the equivalent Pfaff system is completely integrable. Further forms of the Pfaff system equivalent to the system (12.13) are denoted by $\omega(\psi_k)$.

Theorem 12.1 *There exits $k_3 \geqslant k_2$ such that for every $k \geqslant k_3$ the system (12.13) is completely integrable.*

Proof Due to the right-hand inequalities (12.11), there exists k_3 such that

$$d_{k_3-1} = d_{k_3} < \nu_{k_3-1}.$$

It follows that

$$\operatorname{rank} \frac{\partial \psi_{k_3}}{\partial_{\underset{k_3}{y}}} = \nu_{k_3} - \nu_{k_3-1} = \dim Y_{k_3},$$

i.e. the system of differential equations $\psi_{k_3} = 0$ can be solved with respect to all higher derivatives. Therefore, the system $p(\psi_{k_3}) = 0$ is also solvable with respect to all higher derivatives and, consequently,

$$\dim p(\underset{k_3}{h}(\underset{k_3}{U}, O)) = \dim \underset{k_3}{h}(\underset{k_3}{U}, O) = d_{k_3}. \tag{12.15}$$

Therefore, by Lemma 12.2, it follows that $d_k = d_{k_3}$ for all $k > k_3$.

It follows from Lemma 12.3 that for all $k \geqslant k_3$ the ideal generated by the system $\omega(\psi_k) = 0$ is closed with respect to the operation of the exterior differentiation. Hence, the statement of the Lemma follows from the Frobenius theorem. □

Theorem 12.2 *The system (12.13) is automorphic for every $k \geqslant k_3$.*

Proof The system of exterior equations $\omega(\psi_k)$ with $k \geqslant k_3$ is completely integrable, i.e. the unique integral manifold passes through every point of the orbit $\underset{k}{h}(\underset{k}{U}, O)$ (see the paper [11]). On the other hand, for any point $z' \in \underset{k}{h}(\underset{k}{U}, O)$ there exist a transformation $g \in G^r$ and a point $z \in \underset{k}{U}$ such that the transformation g maps the point z into the point z'. Therefore, this unique integral manifold coincides with the image of the manifold $\underset{k}{U}$ under the action of the transformation g. □

Remark 12.1 It follows from the Eq. (12.15), in particular, that the system $\psi_{k+1}(z) = 0$ for every $k \geqslant k_3$ is the first prolongation of the system $\psi_k(z) = 0$. Consequently, all the systems $\psi_k(z) = 0$ are prolongations of the system $\psi_{k_3}(z) = 0$

when $k > k_3$. The system $\psi_{k_3}(z) = 0$, as Example 1 (variant 7) shows, is not always the prolongation of the system $\psi_{k_3-1}(z) = 0$.

Remark 12.2 Lemmas 12.2 and 12.3 also hold for the infinite-dimensional Lie groups if there exists the finite k_2. If the mapping u is the solution of the system of differential equations, admitting a group, then the finite k_2 exists and does not exceed the order of the system.

12.4 Construction of Automorphic Systems

To construct automorphic systems, one uses according to the paper [7, Sect. 25.3], the Theorem on representation of a non-singular invariant manifold. Due to this Theorem, one can choose the invariant of the group G^r of the corresponding dimension as ψ_{k_3}. This invariant is expressed via the universal invariant $\underset{k_3}{J}$ of the order k_3, i.e.

$$\psi_{k_3}(z) = \Psi(\underset{k_3}{J}(z)) = 0. \tag{12.16}$$

The requirement of complete integrability of this system imposes conditions on the mapping Ψ. These conditions give a system of differential equations on the mapping Ψ, this system is called the 'resolving system' (see the paper [7, Sect. 26.1]).

The algorithm of construction of all the automorphic systems of the given group consists in investigating all possible dimensions of orbits determined by the inequalities (12.11). One and the same dimension of the orbit, at least from the point of view of the inequalities (12.11), can be obtained for different values k_3. The number of these different values is finite. Therefore, up to the operation of prolongation, there is a finite number of different automorphic systems. But not all the variants admitted by the inequalities (12.11) are realized.

It is stated in the paper [7, Sect. 25.4] that for given n, m, and r the type of the automorphic system is completely determined by one parameter: rank, defect, or dimension of the orbit (these three values quantities are uniquely expressed via each other). As shown in Example 1 (variants 6 and 7), apart from defect the value k_3, i.e. the order of the automorphic system is also important.

The system (12.16) is written, as a rule, in the solved form with respect to the part of invariants. The relations (12.12) allows to write the system (12.16) in the form

$$J'' = \varphi(J'), \tag{12.17}$$

$$J''' = \psi(J'), \tag{12.18}$$

where the order of the invariants J' and J'' is lower then k_3 and all invariants of the order k_3 are denoted by J'''. Dividing the invariants into J' and J'' is not always unique and 'the branching' of the process is possible. 'The branching' is also possible for further calculations.

In addition to the inequalities (12.11), there is one more restriction on the dimension of the orbit. This restriction is connected with consideration of orbits of 'graphs' of the mappings $u : X \to Y$. Therefore, the equations of orbits should not impose restrictions on variables of the space X, i.e. the following inequality should hold

$$\nu_k - d_k \leqslant \operatorname{rank}\left(\partial_v \underset{k}{J}\right), \qquad v = (y, \underset{1}{y}, \ldots, \underset{k}{y}), \quad k = k_3 - 1. \tag{12.19}$$

The set of invariants J'' should be chosen such that $\partial_v J'' \geqslant \nu_{k_3-1} - d_{k_3-1}$.

If u is not an arbitrary mapping but a solution of a system of differential equations E admitting a group G^r, then the following condition is imposed on the functions φ and ψ from (12.17), (12.18): the system E should be a differential-algebraic corollary of the Eqs. (12.17), (12.18). If the order of the system E does not exceed k_3, then it is expedient to include the system E, written via invariants of the group, into the system (12.17), (12.18).

12.5 Invariant and Partially Invariant Solutions

Invariant and partially invariant solutions [7, Sect. 19, 22] are solutions of corresponding automorphic systems. For invariant solutions, $k_3 = 1$.

Invariant solutions exist when the inequality (12.19) holds. So the Eq. (12.17) is solvable with respect to the variables y and the Eq. (12.18); due to Lemma 12.3 and Theorem 12.1, simply provides expressions for the functions ψ. Therefore, there is no need to calculate invariants of the first order and the resolving system is obtained after substitution of expressions of the variables y into the initial system of differential equations. That is the technology of construction of invariant solutions with the use of the notion of automorphic systems does not differ from that described in the paper [7, Sect. 19].

To construct partially invariant solution with the use of automorphic systems, one needs differential invariants of the first or, possibly, a higher order. This complicates the algorithm as compared to the one described in the paper [7, Sect. 22]. But there is no need to use the notion of 'redundant' functions.

12.6 On 'Simple' Solutions

When $r \geqslant n$, the minimal possible dimension of the orbit is equal to r. In case of this minimal dimension $s_{k_3} = \nu_{k_3} - r$, i.e. it coincides with the dimension of the space of invariants. Therefore, the set of invariants J' from (12.17), (12.18) is empty and the functions φ and ψ are constants. The resolving system in this case is the system of algebraic equations for these constants. For the case $r = n$, such automorphic systems provide invariant solutions, which are called in the paper [10] 'simple'. By

analogy, solutions of such automorphic systems can be also called 'simple' even when $r > n$. We use this term up to the end of this section.

If H is a subgroup of the group G^r, then every 'simple' solution with respect to the subgroup H is a 'simple' solution with respect to the group G^r. Indeed, every differential invariant of the group G^r is a differential invariant of the subgroup H and the subgroup H also has other invariants. Therefore, the system (12.17), (12.18) for the subgroup H is an expansion of a similar system for the group G^r.

12.7 Example 1

Equations of one-dimensional dynamics of polytropic gas

$$u_t + uu_x + \rho^{-1} p_x = 0, \quad \rho_t + u\rho_x + \rho u_x = 0, \quad p_t + up_x + \gamma p u_x = 0, \tag{12.20}$$

admit the group with the Lie algebra

$$\partial_t, \quad \partial_x, \quad t\partial_x + \partial_u, \quad t\partial_t + x\partial_x, \quad t\partial_t - u\partial_u + 2\rho\partial_\rho, \quad p\partial_p + \rho\partial_\rho. \tag{12.21}$$

Differential invariants of the first order can be chosen in the form

$$J_1 = \frac{\rho(u_t + uu_x)}{p_x}, \quad J_2 = \frac{\rho_t + u\rho_x}{\rho u_x}, \quad J_3 = \frac{p_t + up_x}{pu_x},$$

$$J_4 = \frac{p_x}{u_x\sqrt{\rho p}}, \quad J_5 = \frac{\rho_x\sqrt{p}}{u_x\sqrt{\rho^3}}.$$

The given set of invariants forms a basis, i.e. any invariant can be obtained from this set by means of algebraic operations and actions of the operators of the invariant differentiation

$$\Lambda_1 = \frac{1}{u_x} D_t + \frac{u}{u_x} D_x, \quad \Lambda_2 = \frac{u_t + uu_x}{u_x^2} D_x.$$

Below, we use the following set of differential invariants of the second order:

$$J_{21} = \frac{p_{tt} + 2up_{tx} + u^2 p_{xx}}{pu_x^2}, \quad J_{22} = \frac{(p_{tx} + up_{xx})p_x}{\rho p u_x^3}, \quad J_{23} = \frac{p_{xx} p_x^2}{\rho^2 p u_x^4},$$

$$J_{24} = \frac{(\rho_{tt} + 2u\rho_{tx} + u^2\rho_{xx})p_x^2}{\rho^2 p u_x^4}, \quad J_{25} = \frac{(\rho_{tx} + u\rho_{xx})p_x^3}{\rho^3 p u_x^5}, \quad J_{26} = \frac{\rho_{xx} p_x^4}{\rho^4 p u_x^6},$$

$$J_{27} = \frac{(u_{tt} + 2uu_{tx} + u^2 u_{xx})\rho}{p_x u_x}, \quad J_{28} = \frac{u_{tx} + uu_{xx}}{u_x^2}, \quad J_{29} = \frac{u_{xx} p_x}{\rho u_x^3}.$$

The system (12.20) is written in the space of invariants in the form

$$J_1 = -1, \quad J_2 = -1, \quad J_3 = -\gamma. \tag{12.22}$$

The inequalities (12.11) admit the following variants of automorphic systems for the Eq. (12.20):

No.	d_1	d_2	d_3	d_4	k_3	δ
1	6	6	6	6	2	4
2	6	7	7	7	3	5
3	6	7	8	8	4	6
4	6	8	8	8	3	6
5	7	7	7	7	2	5
6	7	8	8	8	3	6
7	8	8	8	8	2	6

Here $\delta = d_{k_3} - n$ is the defect of invariance. Further, we construct the systems (12.17), (12.18) for every variant from the table and investigate the resolving system for some of them.

For variants 1–4, the dimension $d_1 = 6$, i.e. $s_1 = \nu_1 - d_1 = 5$ and coincides with the number of the invariants of the first order. Therefore, all invariants of the first order should be equal to constants, i.e. the Eq. (12.22) should be supplemented by the equations

$$J_4 = c_4, \quad J_5 = c_5, \tag{12.23}$$

where c_4 and c_5 are some constants.

Since the complete set of invariants of a higher order can be obtained by the action of operators of invariant differentiation on the invariants of the first order, the invariants of a higher order should be equal to zero. Therefore, the arbitrary way in construction of the system (12.17), (12.18) for variants 1–4 does not exceed two constants.

The system (12.22), (12.23) is compatible if $c_5 = (c_4^2 - \gamma + 1)/c_4$ and the first prolongation of these equations is completely integrable under the condition $c_4^2 \neq \gamma$. Under these conditions and when $\gamma \neq 1$ the solution of the system (12.22), (12.23) has the form

$$u = ax + u_1(t), \quad \rho = \rho_1 p^{\alpha}, \quad p = (p_1(t) + 0.5(1-\alpha)c_4 a\sqrt{\rho_1}x)^{2/(1-\alpha)},$$

where

$$\alpha = (c_4^2 - \gamma + 1)/c_4^2, \quad a = 1/(c_6 + 0.5(1+\gamma)t), \quad \rho_1 = c_7(c_6 + 0.5(1+\gamma)t)^{2/(1+\gamma)},$$

c_6, c_7 are constants and the functions $u_1(t)$ and $p_1(t)$ satisfy the linear system of ordinary differential equations

$$\frac{du_1}{dt} = -a\left(u_1 + \frac{c_4}{\sqrt{\rho_1}}p_1\right), \quad \frac{dp_1}{dt} = -\frac{\gamma - 1}{2c_4^2}a(c_4\sqrt{\rho_1}u_1 + \gamma p_1).$$

If $c_4^2 = \gamma$, then system (12.22), (12.23) is involutive and none of its prolongations is completely integrable. Hence, in particular, there are no automorphic systems of variants 2, 3, 4 for the system (12.20).

For variant 5, the Eqs. (12.17), (12.18) consist of the Eq. (12.22) and one of the following systems of equations

$$J_4 = \varphi(J_5), \quad J_{2i} = \psi_i(J_5), \quad i = 1, \ldots, 9,$$

$$J_5 = c_5, \quad J_{2i} = \psi_i(J_4), \quad i = 1, \ldots, 9.$$

For variant 6, the Eqs. (12.17), (12.18) consist of the Eq. (12.22) and one of the following system of equations

$$J_4 = \varphi_0(J_5), \quad J_{2i} = \varphi_i(J_5, J_{26}), \quad i \in \{1, \ldots, 9\},\ i \neq 6, \quad \Lambda_2 J_{26} = \psi(J_5, J_{26}),$$

$$J_5 = c_5, \quad J_{2i} = \varphi_i(J_4, J_{23}), \quad i \in \{1, \ldots, 9\},\ i \neq 3, \quad \Lambda_2 J_{23} = \psi(J_4, J_{23}). \tag{12.24}$$

The condition of complete integrability of the system (12.22), (12.24) gives the following equations for determining the functions φ_i:

$$\varphi_{21} = (\gamma^2 J_4^2 + \gamma J_{23} + \gamma J_4^2 + J_4^4)/J_4^2, \quad \varphi_{22} = -J_4^2(\gamma + 1), \quad \varphi_{24} = J_{23} + 2J_4^2,$$

$$\varphi_{25} = \varphi_{26} = \varphi_{29} = 0, \quad \varphi_{27} = \gamma + 1, \quad \varphi_{28} = -(J_{23} + J_4^2)/J_4^2,$$

$c_5 = 0$ and $\psi = \theta(J_{23}/J_4^4)J_4^6$, where θ is an arbitrary function of one argument.

For variant 7 the Eq. (12.17) coincide with the Eq. (12.22) and the Eq. (12.18) are written in the form

$$J_{2i} = \psi_i(J_4, J_5), \quad i = 1, \ldots, 9. \tag{12.25}$$

Six of the functions ψ_i are determined from the condition of complete integrability of the system (12.22), (12.25) by the equations

$$\begin{aligned}
\psi_1 &= (\gamma^2 J_4^2 - \gamma J_4^3 J_5 + \gamma J_4^2 + \gamma\psi_3 + J_4^4)J_4^{-2},\\
\psi_2 &= -(\gamma J_4^2 + \gamma\psi_9 + J_4^2),\\
\psi_4 &= 2J_4^2 + \psi_3,\\
\psi_5 &= -J_4^2(2J_4J_5 + \psi_9),\\
\psi_7 &= (\gamma J_4^2 + \gamma\psi_9 + J_4^2)J_4^{-2},\\
\psi_8 &= (J_4^3 J_5 - J_4^2 - \psi_3)J_4^{-2},
\end{aligned}$$

and the rest of them satisfy the system of quasi-linear equations

$$
\begin{aligned}
&J_4^3 A\psi_9 + B\psi_3 + 2J_4(\gamma J_4^4\psi_9 + \gamma J_4^2\psi_9^2 + 2J_4^6 J_5^2 + 3J_4^5 J_5\psi_9 + \\
&+J_4^4\psi_3 + J_4^2\psi_9\psi_3 - J_4^2\psi_6 - 2\psi_3^2) = 0, \\
&\gamma B\psi_9 + J_4 A\psi_3 + 2J_4(2\gamma J_4^4\psi_9 + \gamma J_4^3 J_5\psi_9 + 3\gamma J_4^2\psi_9^2 + 2\gamma J_4^2\psi_3 + \\
&+\gamma\psi_9\psi_3 + J_4^4\psi_9 + 4J_4^3 J_5\psi_3 - 2J_4^2\psi_3 - 4\psi_3^2) = 0, \\
&J_4 B\psi_9 + A\psi_6 + 2(3\gamma J_4^2\psi_6 + 4\gamma\psi_9\psi_6 + 4J_4^5 J_5\psi_9 + 3J_4^4\psi_9^2 + \\
&6J_4^3 J_5\psi_6 - J_4^2\psi_9\psi_3 - 3J_4^2\psi_6 - 6\psi_6\psi_3) = 0,
\end{aligned}
$$

where

$$
A = J_4\alpha_1\frac{\partial}{\partial J_4} + \alpha_2\frac{\partial}{\partial J_5}, \quad B = J_4^2\alpha_3\frac{\partial}{\partial J_4} + \alpha_4\frac{\partial}{\partial J_5},
$$

$$
\begin{aligned}
\alpha_1 &= -\gamma J_4^2 - 2\gamma\psi_9 - 2J_4^3 J_5 + J_4^2 + 2\psi_3, \\
\alpha_2 &= -\gamma J_4^2 J_5 - 2J_4^3 J_5^2 + J_4^2 J_5 - 2J_4\psi_9 + 2J_5\psi_3, \\
\alpha_3 &= -J_4^4 - J_4^3 J_5 - 2J_4^2\psi_9 + 2\psi_3, \\
\alpha_4 &= J_4^5 J_5 - 3J_4^4 J_5^2 - 2J_4^3 J_5\psi_9 + 2\psi_6.
\end{aligned}
$$

12.8 Example 2

The example of the present section demonstrates that the automorphic system of the infinite-dimensional Lie group is not necessarily completely integrable.

Group foliation for the Karman–Guderley equation

$$
-\varphi_x\varphi_{xx} + \varphi_{yy} + \varphi_{zz} = 0 \tag{12.26}
$$

was constructed in the paper [3] with respect to the infinite-dimensional group with the infinitesimal operator $f(y, z)\partial_\varphi$, where $f(y, z)$ is an arbitrary harmonic function. This operator determines the transformation $\varphi \to \varphi + f(y, z)$.

Group foliation of the Eq. (12.26) is given, as shown in the paper [3], by the automorphic system

$$
\varphi_x = a, \quad \varphi_{yy} + \varphi_{zz} = aa_x \tag{12.27}
$$

and the resolving equation

$$
-aa_{xx} - a_x^2 + a_{yy} + a_{zz} = 0.
$$

The difference of any two solutions of the system (12.27) is a harmonic function of variables y, z and does not depend on the variable x. Therefore, the system (12.27)

is in fact automorphic. The system (12.27), where a satisfies the resolving equation, is involutive but not completely integrable.

Remark 12.3 If the system of differential equations E admits the finite-dimensional Lie group G^r, then any solution of the system E is the solution of some automorphic system of the group G^r. An automorphic system is relatively simply integrable, but the resolving system can be significantly more complex than the initial system E. Example 1 (variant 7) demonstrates it. An exception is provided by automorphic systems of a minimal defect. In this case, the resolving system is a system of algebraic equations for the totality of constants.

The fact that an automorphic system should be completely integrable allows to write representation of the system of a given type (or several representations like in variants 5 and 6 of Example 1) immediately. There is no need to write all the equations of the system (12.18) for definite calculations.

12.9 On Integration of Automorphic Systems of Finite-Dimensional Lie Group

In the present section for completely integrable Pfaff systems, we prove theorems on order reducing for the system admitting Lie symmetry, on a sequential order reducing for the system admitting more than one-parametric Lie symmetries, and on the integrating factor for one-dimensional systems.

The first and the third theorems are direct generalization of similar theorems for ordinary differential equations described in the paper [7, Sect. 8.5]. Other ways of employing an admitted Lie symmetry for the order reducing of ordinary differential equations are described in the papers [4–6].

Generally speaking, the calculation of admitted group for completely integrable Pfaff system (as for a system of ordinary differential equations) is not simple than integrating the original system. But the automorphic system of a finite-dimensional Lie group G admits a Lie group which is given 'for free': this group is the restriction of group G on the manifold determined by the system.

12.9.1 Symmetries for Pfaff System

We consider the completely integrable Pfaff system

$$\omega = dy - \varphi^1(x, y)\, dx^1 - \cdots - \varphi^n(x, y)\, dx^n = 0, \quad x \in R^n, \quad y \in R^m. \quad (12.28)$$

System (12.28) is called completely integrable in some domain of space $R^n \times R^m$ if for each point of this domain an n-dimensional integral surface of system (12.28) passes through (in this case for each point just one surface passes through)

[11, Sect. 23]. In accordance with Frobenius theorem [11, Sect. 26], system (12.28) is completely integrable if and only if the external derivatives $d\omega$ belongs to the ideal generated by forms ω. The latter is true if and only if $d\omega|_{\omega=0} = 0$. And this condition is equivalent to the expressions

$$[D_i, D_j] = 0, \quad i, j = 1, \ldots, n, \tag{12.29}$$

where

$$D_i = \partial_{x^i} + \varphi^i \cdot \partial_y, \quad i = 1, \ldots, n. \tag{12.30}$$

Indeed,

$$d\omega|_{\omega=0} = -\sum_{i,j} D_j\varphi^i\, dx^j \wedge dx^i = -\sum_{j>i} (D_j\varphi^i - D_i\varphi^j)\, dx^j \wedge dx^i.$$

The one-parametric group with the infinitesimal operator

$$L = \xi(x, y) \cdot \partial_x + \eta(x, y) \cdot \partial_y \tag{12.31}$$

is admitted by system (12.28) if and only if

$$[\tilde{L}, D_i] = 0, \quad i = 1, \ldots, n, \tag{12.32}$$

where

$$\tilde{L} = L - \xi^1 D_1 - \cdots - \xi^n D_n = (\eta - \xi^1\varphi^1 - \cdots - \xi^n\varphi^n) \cdot \partial_y = \tilde{\eta} \cdot \partial_y. \tag{12.33}$$

This fact can be established straightforwardly or one can employ a similar statement for the generalized symmetries in the papers [6, Lemma 5.12], [1]. The matter is that the generalized symmetries of system (12.28) coincide with point ones.

It follows from relations (12.32) and (12.33) that, in particular, each linear combination of operators (12.30) with coefficients depending on variables x, y is admitted by system (12.28), and these linear combinations form an ideal of the algebra admitted by system (12.28). It is also clear that component ξ of field L is an arbitrary vector-function of variables x, y.

12.9.2 Order Reducing for Pfaff System

Theorem 12.3 *Suppose Pfaff system (12.28) is completely integrable and admits the one-parametric Lie group with operator (12.31). Then, once $m > 1$, the knowing of the universal invariant for operator (12.33) allows us to reduce the dimension of system (12.28) by one.*

Proof Universal invariant of operator (12.33) can be chosen as

$$x^1, \ldots, x^n, \quad J^1(x, y), \ldots, J^{m-1}(x, y).$$

If an one-dimensional mapping $\psi(x, y)$ is so that $\tilde{L}\psi = 1$, then rank $\partial(J, \psi)/\partial y = m$ [7, Sect. 8.5], and hence, for each x the mapping

$$y' = J(x, y) = (J^1(x, y), \ldots, J^{m-1}(x, y)), \quad y'' = \psi(x, y) \tag{12.34}$$

is a local transformation of space R^m. By (12.32), operators (12.30) are the operators of invariant differentiation for the algebra generated by the operator (12.33). Therefore, the mapping DJ is an invariant of this algebra and is expressed by its universal invariant, i.e. there exists a mapping θ such that $DJ = \theta(x, J)$. In view of this fact, in terms of variables x, y', y'' system (12.28) is written as

$$dy' = J_x dx + J_y dy = DJ dx = \theta(x, y')dx, \tag{12.35}$$

$$dy'' = D\psi dx = \vartheta(x, y', y'')dx. \tag{12.36}$$

System (12.35) consists of $m - 1$ equations for $m - 1$ functions. Equation (12.36) should be integrated after the integration of system (12.35). □

Remark 12.4 If function ψ satisfies additional conditions

$$D_i\psi = 0, \quad i = 1, \ldots, n, \tag{12.37}$$

then Eq. (12.36) casts into the form $dy'' = 0$, i.e. it can be written as the relation $y'' = \text{const}$. It is clear that there always exists a function ψ satisfying conditions (12.37). The question is just how to find its analytic representation. But the same concerns the universal invariant.

The requirement $\tilde{L}\psi = 1$ is not always convenient and can be replaced by $\tilde{L}\psi \neq 0$.

12.9.3 Further Reduction of Order

Lemma 12.4 *Let the operators $L_1 = \xi_1 \cdot \partial_z$, $L_2 = \xi_2 \cdot \partial_z$, $D = \eta \cdot \partial_z$ acts in space R^k and satisfy the conditions*

$$[L_1, D] = 0, \quad [L_2, D] = 0.$$

Let also the mappings $\phi : R^k \to R^{k-1}$ obey the conditions

$$L_1\phi = 0, \quad L_1\psi = 1, \quad D\psi = 0, \quad \partial\phi/\partial x = k - 1.$$

Then,

$$[L_2|_M, D|_M] = [L_2, D]|_M = 0,$$

where $M = \{z \in R^k : \psi(z) = 0\}$.

Proof After the change of variables

$$z' = \phi(z), \quad z'' = \psi(z)$$

operators L_2 and D are written as

$$L_2' = \xi_2'(z', z'')\partial_{z'} + \xi_2''(z', z'')\partial_{z''}, \quad D' = \eta'(z')\partial_{z'}.$$

Indeed, $D\phi$ is the invariant of operator L_1, and thus, it is expressed in terms of universal invariant ϕ. Then,

$$[L_2', D']\big|_M = ((\eta_{z'}'\xi_2'(z', z'') - \xi_{2z'}'(z', z'')\eta') \cdot \partial_{z'} + (\dots)\partial_{z''})|_M =$$

$$= (\eta_{z'}'\xi_2'(z', 0) - \xi_{2z'}'(z', 0)\eta') \cdot \partial_{z'} = [L_2'\big|_M, D'\big|_M].$$

It is clear that $[L_2', D'] = 0$, and therefore, the restriction of this commutator on manifold M vanishes. □

Lemma 12.4 implies the theorem which allows one to reduce sequentially the order of the system once the group is wide enough.

Theorem 12.4 *Each symmetry of system (12.28) transformed by (12.34) and restricted then to the space of variables* (x, y') *is admitted by system (12.35).*

12.9.4 First Order ($m = 1$)

Theorem 12.5 *Suppose that Pfaff system (12.28) is completely integrable, admits one-parametric Lie group with infinitesimal operator (12.31) and* $m = 1$, *i.e. we are given one Pfaff equation. Then,* $\mu = 1/\tilde{\eta}$ *is an integrating factor for this Pfaff equation.*

Proof To prove the theorem, we need to establish the existence of a function $u(x, y)$ such that

$$\frac{\partial u}{\partial y} = \frac{1}{\tilde{\eta}}, \quad \frac{\partial u}{\partial x_i} = -\frac{\varphi^i}{\tilde{\eta}}, \quad i = 1, \dots, n.$$

In its turn, such function u exists if

$$\frac{\partial}{\partial x_i}\frac{1}{\tilde{\eta}} + \frac{\partial}{\partial y}\frac{\varphi^i}{\tilde{\eta}} = 0, \quad \frac{\partial}{\partial x_j}\frac{\varphi^i}{\tilde{\eta}} - \frac{\partial}{\partial x_i}\frac{\varphi^j}{\tilde{\eta}} = 0, \quad i, j = 1, \dots, n. \tag{12.38}$$

These conditions are satisfied by virtue of (12.29), (12.32). Indeed, the left-hand side of the former expression in (12.38) after the differentiation is written as $\tilde{\eta}^{-2}(\tilde{\eta}_{x_i} + \tilde{\eta}_y \varphi^i - \varphi^i_y \tilde{\eta})$ and up to a factor it coincides with the left-hand side of expression (12.32). The left-hand side of the latter expression (12.38) after the differentiation is written as $\tilde{\eta}^{-2}(\varphi^i_{x_j}\tilde{\eta} - \varphi^i \tilde{\eta}_{x_j} - \varphi^j_{x_i}\tilde{\eta} + \varphi^j \tilde{\eta}_{x_i})$. And substituting then in this expression the $\tilde{\eta}_{x_i}$, $\tilde{\eta}_{x_j}$ from (12.32) and $\varphi^i_{x_j}$ from (12.29), we see that it vanishes. □

12.9.5 Automorphic Systems

The restriction of Pfaff system

$$dy_\alpha - \sum_{j=1}^{n} y_{\alpha+\gamma_j} dx_j = 0, \quad 0 \leqslant |\alpha| < k$$

on the manifold determined by an automorphic (with respect to r-parametric Lie group G^r) system of order k gives completely integrable Pfaff system. Here, $\alpha = (\alpha_1, \ldots, \alpha_n)$ are multi-indexes, $|\alpha| = \alpha_1 + \cdots + \alpha_n$, $|\gamma_j| = 1$ and the jth component of the multi-index γ_j is equal to 1.

The restriction of kth prolongation of group G^r on the manifold determined by an automorphic system is obviously admitted by Pfaff system. Application of Theorems 12.3–12.5 allows us to reduce the order of Pfaff system or completely integrate under the sufficient rank of the group.

12.10 Example 3

Pfaff system

$$\begin{aligned} du &= -\left(u + c\sqrt{p/\rho}\right) u_1 dt + u_1 dx, \\ d\rho &= -\left(\rho + u(c^2 - \gamma + 1)/c\sqrt{\rho^3/p}\right) u_1 dt + \\ &\quad + (c^2 - \gamma + 1)/c\sqrt{\rho^3/p}\, u_1 dx, \\ dp &= -\left(\gamma p + uc\sqrt{\rho p}\right) u_1 dt + c\sqrt{\rho p} u_1 dx, \\ du_1 &= -(\gamma + 1)/2 u_1^2 dt \end{aligned} \tag{12.39}$$

is equivalent to the automorphic system

$$\begin{aligned} &u_t + uu_x + \rho^{-1} p_x = 0, \quad \rho_t + u\rho_x + \rho u_x = 0, \quad p_t + up_x + \gamma p u_x = 0, \\ &p_x = c\sqrt{\rho p}\, u_x, \quad \rho_x = (c^2 - \gamma + 1)/c\sqrt{\rho^3/p}\, u_x, \quad u_{xx} = 0 \end{aligned}$$

from Example 1 (12.22), (12.23). Here, constant c_4 ($c_4^2 \neq \gamma$) is replaced by constant c. Below we treat the case $\gamma \neq 1$.

The restrictions of first prolongation of the operators (12.21) on the manifold determined by the system (12.39) is written as

$$L_1 = \partial_t, \quad L_2 = \partial_x, \quad L_3 = t\partial_x + \partial_u, \quad L_4 = t\partial_t + x\partial_x - u_1\partial_{u_1},$$
$$L_5 = t\partial_t - u\partial_u + 2\rho\partial_\rho - u_1\partial_{u_1}, \quad L_6 = p\partial_p + \rho\partial_\rho.$$

In what follows, for the order reducing of the system we employ sequentially operators L_6, L_3 and L_2. In each step we indicate the universal invariant, function ψ, new representations of operators D_t, D_x, and remained operators $\tilde{L}$. New representation for the Pfaff system is not written since it is completely determined by operators D_t, D_x. The superscript indicates the step. While writing out the universal invariant, we introduce the notations for new variables. In each step, function ψ obeys condition (12.37).

First step (operator $\tilde{L}_6$). Universal invariant is $t, x, u, u_1, p_1 = p/\rho$.

$$\psi^1 = \ln\rho - 2(c^2 - \gamma + 1)/(\gamma - 1)\ln\left(2c\sqrt{p/\rho}\right) + 2(c^2 - \gamma)/(\gamma + 1)\ln u_1,$$
$$D_t^1 = \partial_t - u_1(c\sqrt{p_1} + u)\partial_u - u_1^2(\gamma + 1)/2\partial_{u_1} + p_1u_1(1 - \gamma)(1 + u/(c\sqrt{p_1}))\partial_{p_1},$$
$$D_x^1 = \partial_x + u_1\partial_u + p_1u_1(\gamma - 1)/(c\sqrt{p_1})\partial_{p_1},$$
$$\tilde{L}_3^1 = (1 - tu_1)\partial_u + (p_1tu_1(1 - \gamma))/(c\sqrt{p_1})\partial_{p_1},$$
$$\tilde{L}_2^1 = -u_1\partial_u - p_1u_1(\gamma - 1)/(c\sqrt{p_1})\partial_{p_1}.$$

Second step (operator $\tilde{L}_3^1$). Universal invariant is $t, x, u_1, p_2 = 2\sqrt{p_1} - tuu_1$ $(\gamma - 1)/(c(tu_1 - 1))$.

$$\psi^2 = u - 2c\sqrt{p_1}/(\gamma - 1),$$
$$D_t^2 = \partial_t - u_1^2(\gamma + 1))/2\partial_{u_1} + (p_2u_1(\gamma - 1))/(2(tu_1 - 1))\partial_{p_2},$$
$$D_x^2 = \partial_x + (u_1(-\gamma + 1))/(c(tu_1 - 1))\partial_{p_2},$$
$$\tilde{L}_2^2 = (u_1(\gamma - 1))/(c(tu_1 - 1))\partial_{p_2}.$$

Third step (operator $\tilde{L}_6$). Universal invariant is t, x, u_1.

$$\psi^3 = (2cp_2tu_1 - 2cp_2 - \gamma^2tu_1 + 2\gamma u_1x + 2\gamma + tu_1 - 2u_1x - 2)/(2u_1(\gamma - 1)),$$
$$D_t^3 = \partial_t - u_1^2(\gamma + 1)/2\partial_{u_1},$$
$$D_x^3 = \partial_x.$$

Finally, we obtain one-dimensional Pfaff system

$$du_1 + u_1^2(\gamma + 1)/2\,dt = 0,$$

which is easily integrated $u_1 = 2/((\gamma + 1)t + c_4)$, where c_4 is some constant.

Returning back to the original variables and employing the expressions for the invariants and relations $\psi^i = c_i$, $i = 1, 2, 3$, where c_i are some constants, we obtain the general solution of system (12.39):

$$u = (c_2(\gamma - 1)t + 2x + c_4 - 2c_3 + c_2c_4)/((\gamma + 1)t + c_4),$$

$$\rho = c_1(4c^2p_1)^{c^2/(\gamma-1)-1}u_1^{2(\gamma-c^2)/(\gamma+1)}, \quad p = p_1\rho, \quad u_1 = 2/((\gamma + 1)t + c_4),$$

where $p_1 = (\gamma - 1)^2(x - c_2t + c_4/2 - c_3)^2/(c(c_4 + (\gamma + 1)t))^2$.

12.11 Example 4

In the paper [3], there was found an admitted group and there was constructed a group foliation for the Karman–Gooderley equation

$$-u_xu_{xx} + u_{yy} + u_{zz} = 0 \tag{12.40}$$

with respect to the infinite-dimensional part of the admitted group. To construct the automorphic system, here there was used a finite-dimensional subgroup of the admitted group generated by the operators

$$\begin{gathered} L_1 = \partial_x, \quad L_2 = \partial_y, \quad L_3 = \partial_z, \quad L_4 = z\partial_y - y\partial_z, \\ L_5 = y\partial_y + z\partial_z - 2u\partial_u, \quad L_6 = x\partial_x + 3u\partial_u. \end{gathered} \tag{12.41}$$

The solutions to Eq. (12.40) which form six-dimensional orbits in the prolonged spaces under the action of the group generated by operators (12.41) satisfy one of two following automorphic systems:

$$\begin{aligned} &u_x = (3/2)^{2/3}(u_y^2 + u_z^2)^{1/3}, \quad u_{xx} = (3/2)^{1/3}(u_y^2 + u_z^2)^{2/3}/u, \\ &u_{xy} = (3/2)^{2/3}(u_y^2 + u_z^2)^{1/3}u_y/u, \quad u_{yy} = 3/2\,u_y^2/u, \\ &u_{xz} = (3/2)^{2/3}(u_y^2 + u_z^2)^{1/3}u_z/u, \quad u_{yz} = 3/2\,u_yu_z/u, \quad u_{zz} = 3/2\,u_z^2/u; \end{aligned} \tag{12.42}$$

$$\begin{aligned} &u_x = (3/2)^{1/3}(u_y^2 + u_z^2)^{1/3}, \quad u_{xx} = (3/2)^{-1/3}(u_y^2 + u_z^2)^{2/3}/u, \\ &u_{xy} = (3/2)^{1/3}(u_y^2 + u_z^2)^{1/3}u_y)/u, \quad u_{yy} = (3u_y^2 - u_z^2)/(2u), \\ &u_{xz} = (3/2)^{1/3}(u_y^2 + u_z^2)^{1/3}u_z/u, \; u_{yz} = (2u_yu_z)/u, \; u_{zz} = (-u_y^2 + 3u_z^2)/(2u). \end{aligned} \tag{12.43}$$

In what follows, to reduce the order of automorphic system (12.42), we employ sequentially operators L_2, L_4. Pfaff system equivalent to system (12.42) can be written as

$$
\begin{aligned}
&du - (3/2)^{2/3}(v^2+w^2)^{1/3}dx - vdy - wdz = 0,\\
&dv - (3/2)^{2/3}(v^2+w^2)^{1/3}vdx - 3/(2u)v^2dy - 3/(2u)vwdz = 0,\\
&dw - (3/2)^{2/3}(^2{+}w^2)^{1/3}wdx - 3/(2u)vwdy - 3/(2u)w^2dz = 0.
\end{aligned}
$$

Then, the restrictions of first prolongation of operators L_2, L_4 on the manifold determined by system (12.42) followed by the factorization with respect to the ideal are written as follows

$$
\begin{aligned}
\tilde{L}_2 &= -v\partial_u - 3/(2u)(v^2\partial_v + vw\partial_w),\\
\tilde{L}_4 &= (-vz+wy)\partial_u + (2uw - 3v^2z + 3vwy)/(2u)\partial_v +\\
&\quad + (-2uv - 3vwz + 3w^2y)/(2u)\partial_w.
\end{aligned}
$$

First step (operator $\tilde{L}_2$). The universal invariant is $x, y, z, v_1 = v/u^{3/2}, w_1 = w/u^{3/2}$.

$$
\begin{aligned}
&\psi^1 = 2u/v + y + zw/v,\\
&D_x^1 = \partial_x + (3/2)^{2/3}(v_1^2+w_1^2)^{1/3}(\partial_u + v_1\partial_{v_1} + w_1\partial_{w_1}),\\
&D_y^1 = \partial_y, \quad D_z^1 = \partial_z, \quad \tilde{L}_4^1 = w_1\partial_{v_1} - v_1\partial_{w_1}.
\end{aligned}
$$

Second step (operator $\tilde{L}_4^1$). The universal invariant is $x, y, z, v_2 = \sqrt{v_1^2+w_1^2}$.

$$
\begin{aligned}
&\psi^2 = \arctan(v_1/w_1) + 3^{2/3}2^{-5/3}x - 3/2(v_1^2+w_1^2)^{-1/3},\\
&D_x^2 = \partial_x - (3/2)^{2/3}/2v_2^{5/3}\partial_{v_2}, \quad D_y^2 = \partial_y, \quad D_z^2 = \partial_z.
\end{aligned}
$$

As a result, we get one-dimensional Pfaff system $dv_2 + (3/2)^{2/3}/2v_2^{5/3}dx = 0$, which can be easily integrated $v_2 = (x/\sqrt[3]{12} + c_3)^{-3/2}$. Returning back to the original variables and employing the expressions for the invariants and relations $\psi^i = c_i$, $i = 1, 2$, where c_i are some constants, we obtain the general solution to system (12.42):

$$
u = 4(x/\sqrt[3]{12} + c_3)^3/(y\sin(c_2) + z\cos(c_2) + c_1)^2. \tag{12.44}
$$

In the same way, one can obtain the general solution to system (12.43):

$$
u = 2/9(x+c_1)^3/((y+c_2)^2 + (z+c_3)^2). \tag{12.45}
$$

Remark 12.5 The above examples of solutions demonstrate application of the results of the Sect. 12.9 and we do not claim that other known methods can not be applied here. In particular, solutions (12.44), (12.45) as $c_1 = c_2 = c_3 = 0$ equal $2/9x^3/(y^2 + z^2)$, respectively, and they are self-similar solutions to Eq. (12.40). Hence, solutions (12.44), (12.45) can be obtained from self-similar solutions by means of translations and rotations.

12.12 Example 5

An example, this section shows that undecidability Lie algebra does not prevent a decrease of the order ordinary differential equation on the value of algebra dimension.

Consider a system of differential equations

$$\frac{d^2x}{dt^2} = xg(r), \quad \frac{d^2y}{dt^2} = yg(r), \quad \frac{d^2z}{dt^2} = zg(r), \quad r = x^2 + y^2 + z^2, \tag{12.46}$$

where g is some function of one argument. The system (12.46) admit undecidable Lie algebra with operators:

$$M_1 = y\partial_z - z\partial_y, \quad M_2 = x\partial_z - z\partial_x, \quad M_3 = x\partial_y - y\partial_x. \tag{12.47}$$

System (12.46) is equivalent to the following Pfaff system:

$$\begin{aligned} &dx - udt = 0, \quad du - xgdt = 0,\\ &dy - vdt = 0, \quad dv - ygdt = 0,\\ &dz - wdt = 0, \quad dw - zgdt = 0. \end{aligned} \tag{12.48}$$

Prolongation of the operators (12.47) are

$$\begin{aligned} M_1 &= y\partial_z - z\partial_y + v\partial_w - w\partial_v,\\ M_2 &= x\partial_z - z\partial_x + u\partial_w - w\partial_u,\\ M_3 &= x\partial_y - y\partial_x + u\partial_v - v\partial_u. \end{aligned} \tag{12.49}$$

The total derivative operator of the system (12.48) is

$$D_t = \partial_t + u\partial_x + v\partial_y + w\partial_z + xg\partial_u + yg\partial_v + zg\partial_w.$$

The system (12.48) admit operators (12.49), then

$$[D_t, M_j] = 0, \quad j = 1, 2, 3.$$

Invariants of the operator M_3

$$t_1 = t, \quad x_1 = \sqrt{x^2 + y^2}, \quad z_1 = z, \quad w_1 = w,$$

$$u_1 = (ux + vy)/\sqrt{x^2 + y^2}, \quad v_1 = (vx - uy)/\sqrt{x^2 + y^2},$$

and function

$$\psi_1 = \arctan\left(\frac{y}{x}\right) - \arctan\left(\frac{uyz - vxz}{uxz + vyz - wx^2 - wy^2}\right),$$

$$M_3\psi_1 = 1, \quad D_t\psi_1 = 0$$

may be select as new variables. Operator D_t in this variables is written as

$$D_t^1 = \partial_t + u_1\partial_{x_1} + w_1\partial_{z_1} + (g_1x_1^2 + v_1^2)/x_1\partial_{u_1} + (-u_1v_1)/x_1\partial_{v_1} + g_1z_1\partial_{w_1}.$$

Pfaff system (12.48) is written as

$$\begin{aligned} &dx_1 - u_1dt = 0, \quad && du_1 - (g_1x_1^2 + v_1^2)/x_1dt = 0, \\ & && dv_1 - (-u_1v_1)/x_1dt = 0, \\ &dz_1 - w_1dt = 0, \quad && dw_1 - z_1g_1dt = 0. \end{aligned} \tag{12.50}$$

Here,

$$g_1 = g(x_1^2 + z_1^2).$$

Operators M_1 and M_2 in this variables and restricted to manifold $\psi_1 = 0$ is written as

$$\begin{aligned} \bar{M}_1^1 &= \rho^{-1}(v_1z_1^2\partial_{x_1} - v_1x_1z_1\partial_{z_1} + v_1z_1(-u_1z_1 + 2w_1x_1)x_1^{-1}\partial_{u_1} + \\ &+ (u_1^2z_1^2 - 2u_1w_1x_1z_1 + w_1^2x_1^2)x_1^{-1}\partial_{v_1} - v_1w_1x_1\partial_{w_1}), \\ \bar{M}_2^1 &= \rho^{-1}(z_1(-u_1z_1 + w_1x_1)\partial_{x_1} + x_1(u_1z_1 - w_1x_1)\partial_{z_1} + \\ &+ (-u_1w_1x_1z_1 - v_1^2z_1^2 + w_1^2x_1^2)x_1^{-1}\partial_{u_1} + \\ &+ v_1z_1(u_1z_1 - w_1x_1)x_1^{-1}\partial_{v_1} + (u_1^2z_1 - u_1w_1x_1 + v_1^2z_1)\partial_{w_1}), \end{aligned}$$

where

$$\rho = \sqrt{(u_1z_1 - w_1x_1)^2 + v_1^2z_1^2}.$$

Let $M_1^1 = \rho\bar{M}_1^1$ and $M_2^1 = \rho\bar{M}_2^1$, then

$$[D_t^1, \bar{M}_j^1] = 0, \ [D_t^1, M_j^1] = 0, \ j = 1, 2 \quad [\bar{M}_1^1, \bar{M}_2^1] \neq 0, \ [M_1^1, M_2^1] = 0,$$

$$[D_t^1, M_1^1] = 0, \quad [D_t^1, M_2^1] = 0, \quad [\rho M_1^1, \rho M_2^1] = 0.$$

Invariants of the operator M_1^1

$$t_2 = t, \quad x_2 = \sqrt{x_1^2 + z_1^2}, \quad u_2 = (2u_1x_1z_1 - w_1x_1^2 + w_1z_1^2)/(2z_1\sqrt{x_1^2 + z_1^2}),$$

$$v_2 = (u_1^2z_1^2 - 2u_1w_1x_1z_1 + v_1^2z_1^2 + w_1^2x_1^2)/z_1^2, \quad w_2 = w_1\sqrt{x_1^2 + z_1^2}/z_1,$$

and function

$$\psi_2 = -\arctan\left(\frac{\sqrt{u_1^2z_1^2 - 2u_1w_1x_1z_1 + v_1^2z_1^2 + w_1^2x_1^2}}{v_1x_1}\right),$$

$$D_t^1\psi_2 = 0, \quad M_1^1\psi_2 \neq 0$$

may be select as new variables. Operator D_t^1 in this variables is written as

$$D_t^2 = \partial_t + (2u_2 + w_2)/2\partial_{x_2} + (gx_2^2 - 2u_2^2 + u_2w_2 + 2v_2)/(2x_2)\partial_{u_2} +$$

$$+(-2v_2w_2)/x_2\partial_{v_2} + (2gx_2^2 + 2u_2w_2 - w_2^2)/(2x_2)\partial_{w_2}.$$

Pfaff system (12.50) is written as

$$\begin{aligned} &dx_2 - (2u_2 + w_2)/2dt = 0,\\ &du_2 - (g_2x_2^2 - 2u_2^2 + u_2w_2 + 2v_2)/(2x_2)dt = 0,\\ &dv_2 - (-2v_2w_2)/x_2dt = 0,\\ &dw_2 - (2g_2x_2^2 + 2u_2w_2 - w_2^2)/(2x_2)dt = 0. \end{aligned} \tag{12.51}$$

Here, $g_2 = g(x_2^2)$. Operator M_2^1 in this variables and restricted to manifold $\psi_2 = 0$ is written as

$$M_2^2 = v_2x_2(-1/2\partial_{u_2} + (w_2 - 2u_2)\partial_{v_2} + \partial_{w_2}),$$

$$[D_t^2, M_2^2] = 0.$$

Invariants of the operator M_2^2 are

$$t_3 = t, \quad x_3 = x_2, \quad u_3 = u_2 + w_2/2, \quad v_3 = v_2 + 2u_2w_2.$$

Operator D_t^2 in the space of invariants is written as

$$D_t^3 = \partial_t + u_3\partial_{x_3} + (g_3x_3^2 - u_3^2 + v_3)/x_3\partial_{u_3} + 2g_3u_3x_3\partial_{v_3}.$$

Finally, Pfaff system (12.51) is written as

$$\begin{aligned}\frac{dx_3}{dt} &= u_3,\\ \frac{du_3}{dt} &= \frac{g_3x_3^2 - u_3^2 + v_3}{x_3},\\ \frac{dv_3}{dt} &= 2g_3u_3x_3,\end{aligned}$$

where $g_3 = g(x_3)$.

12.13 Differential-Invariant Solutions

Automorphic system of maximal rank take part in the group foliation [7, Sect. 26.1]. A solution of automorphic systems of lower rank is named differential-invariant solutions.

In recent years, the efforts of a number of researchers, and above all L.V. Ovsyannikov, managed to restore some order in the set of invariant and partially invariant solutions. This is due to the concept of an optimal system of subalgebras [8], the reduction theorem [7, Sect. 22.7], Lemma LOT [9].

Naturally, there is a desire to impose some order in a set of differential-invariant solutions. But the task is complicated by the fact that any solution of a system of differential equations is some differential-invariant solution regarding any subgroup of the admitted group (in fact, not necessarily admitted).

Acknowledgements I wish to thank organizers and participants of the conferences MOGRAN. Many useful discussions on MOGRAN conferences stimulated the author to those described in this chapter of the study.

For bulky calculations we employed system of analytic calculations 'Reduce (Free CSL version)' (http://reduce-algebra.sourseforge.net).

References

1. Bluman, G.W., Cheviakov, A.F., Anco, S.C.: Applications of Symmetry Methods to Partial Differential Equations. Applied Mathimatical Sciences, vol. 168. Springer, New York (2010)
2. Cartan, E.: Les systèmes différential extèrior et leurs applications scietifiques – Herman (1946)
3. Golovin, S.V.: Group stratification and exact solutions of the equation of transonic gas motions. Prikl. mekh. tekh. fiz. **44**(3), 51–63 (2003) (in Russian); English transl.: [J. Appl. Mech. Tech. Phys. **44**(3), 344–354 (2003).]
4. Ibragimov, N.Kh.: An ABC of Group Analysis, vol. 8. Znanie, Moscow (1989) (in Russian)
5. Ibragimov, N.Kh.: The Experience of Group Analysis of Ordinary Differential Equations, vol. 7. Znanie, Moscow (1991) (in Russian)

6. Olver, P.J.: Applications of Lie Groups to Differential Equations. Springer, New York (1986)
7. Ovsyannikov, L.V.: Group Analysis of Differential Equations, 400 p. Nauka, Moskow (1978) (in Russian); English transl.: [Academic Press, New York (1982)]
8. Ovsyannikov, L.V.: Programm submodels. Gas dynamics. Applied Mathematic and Mechanics. **58**(4), 30–55 (1994) (in Russian)
9. Ovsyannikov, L.V.: On hierarchy of invariant submodels of differential equations. DAN **361**(6), 740–742 (1998) (in Russian)
10. Ovsyannikov, L.V.: On 'simple' solutions of equations of dynamics of polytropic gas. Prikl. mekh. tekh. fiz. **40**(2), 5–12 (1999) (in Russian)
11. Rashevskii, P.K.: Geometry theory of partial differential equation. – M.: Gostexizdat (1947) (in Russian)
12. Talyshev, A.A.: On high order tangent transforms of systems of partial differential equation. Dyn. Solid Mediu. **54**, 142–152 (1982) (in Russian)
13. Talyshev, A.A.: On symmetries of isobaric motion gaz. Ufimskij matem. zhurn. **2**(3), 106–110 (2010) (in Russian)
14. Talyshev, A.A.: On symmetries of non-involutive systems. In: Proceedings of the International Conference "Modern Problems of Applied Mathematics and Mechanics: Theory, Experiment and Practice", Dedicated to the 90th Anniversary of N.N. Yanenko (Novosibirsk, Russia, 30 May–4 June 2011) (2011). http://conf.nsc.ru/files/conferences/niknik-90/fulltext/39591/46771/talyshev_2011.pdf (in Russian)
15. Talyshev, A.A.: On automorphic systems of finite-dimensional Lie groups. Ufimskij matem. zhurn. **4**, 130–138 (2012) (in Russian); English transl.: [Ufa Math. J. **4**, 127–134 2012]
16. Talyshev, A.A. (2014). *On integration of automorphic systems of finite-dimensional Lie groups.* Ufimskij matem. zhurn. **6**(1), 107–113 (in Russian); English transl.: [Ufa Math. J. **6**(1), 104–110 (2014)]

Index

D. Volchenkov and X. Leoncini (eds.), *Regularity and Stochasticity of Nonlinear Dynamical Systems*, Nonlinear Systems and Complexity 21,
DOI 10.1007/978-3-319-58062-3